



Leonardo Simões de Abreu Carneiro

**Arylation of carbonyl compounds via
photoredox catalysis**

Tese de Doutorado

Thesis presented to the Programa de Pós-graduação em Química of PUC-Rio in partial fulfillment of the requirements for the degree of Doutor em Ciências - Química.

Advisor: Prof. Camilla Djenne Buarque Muller

Rio de Janeiro
September 2020



Leonardo Simões de Abreu Carneiro

**Arylation of carbonyl compounds via photoredox
catalysis**

Thesis presented to the Programa de Pós-graduação em Química of PUC-Rio in partial fulfillment of the requirements for the degree of Doutor em Ciências - Química. Approved by the Examination Committee:

Prof. Camilla Djenne Buarque Muller

Advisor

Departamento de Química – PUC-Rio

Prof. Giovanni Wilson Amarante

UFRJ

Prof. Fernanda Gadini Finelli

UFRJ

Prof. Rodrigo Octavio Mendonça Alves de Souza

UFRJ

Prof. Jones Limberger

Departamento de Química – PUC-Rio

Prof. Nicolás Adrian Rey

Departamento de Química – PUC-Rio

Rio de Janeiro, September 18th, 2020.

All rights reserved

Leonardo Simões de Abreu Carneiro

Graduated in Chemistry at Pontifical Catholic University of Rio de Janeiro (PUC-Rio) in 2014 and obtained his M.Sc. Degree in Chemistry from PUC-Rio in 2016.

Bibliographic data

Carneiro, Leonardo Simões de Abreu

Arylation of carbonyl compounds via photoredox catalysis / Leonardo Simões de Abreu Carneiro ; advisor: Camilla Djenne Buarque Muller. – 2020.

297 f. : il. color. ; 30 cm

Tese (doutorado)–Pontifícia Universidade Católica do Rio de Janeiro, Departamento de Química, 2020.

Inclui bibliografia

1. Química – Teses. 2. Catálise fotoredox. 3. Arilação. 4. Cumarina. 5. Enol acetato. 6. Tetralona. I. Muller, Camilla Djenne Buarque. II. Pontifícia Universidade Católica do Rio de Janeiro. Departamento de Química. III. Título.

CDD: 540

Acknowledgements

To my parents, Rita and Antonio, and family members, I am thankful for the strong support during this journey. A special gratitude to my godparents, Paulo and Rosa, not only for the support, but for the example of professionals and human beings whom I am inspired by.

To my advisor, Dr. Camilla Buarque. We've been working together since 2013; this is a long journey. There were so many ideas, discussions, stories and great moments that I can say, with no doubt, that I cannot imagine myself having a different advisor. This Dissertation shall not be the end of this partnership!

To all the LabSint family, but especially to Verônica, my "scientific sister", and to my "scientific children": Yanne, Rachel, Leticia, Francisco, Bruno, Pedro, Rodrigo, Eduardo, Felipe, Alessandra and Bianca. All of you were important in creating a relaxed atmosphere of joy at work in the most difficult moments.

To Dr. Pierre Esteves, my deep gratitude for all the lessons and advices during this journey. At this Dissertation I am especially grateful for the support and discussions of the theoretical calculations. I also deeply thank all the Interlab friends, especially Geisa, Renata, Sunny and Felipe, for the friendship.

To Dr. Corey Stephenson, from The University of Michigan, for kindly accepting me in his group for a 10 months internship. My vision of the meaning of Science changed entirely after that time in his lab. To all the group members, but in special to my bay colleages, Alexandra, James, Rory and Anthony, and Ted, my sincere appreciation for all the support given to make my stay more pleasant.

To Dr. Denise Perdomo, my dear professor at IFRJ, my main example of how to be a teacher and, nowadays, a dear friend.

To my dear friends outside the lab: Vanessa, Leila, Joseany, André and Guilherme, my thanks for the friendship and moments of joy and fun.

To Fatima and, more recently, Marlene for the support during my time as a Graduate student; also to all the technicians, Álvaro, Bia, Sulamita, Rodrigo, Douglas and Maurício, who helped me during my work.

To Dr. Ricardo Aucélio, at whose lab I worked for 6 months, my first experience in a lab at PUC; and for allowing me to use his lab's spectrofluorimeter for this dissertation. I must thank him for all the lessons - not only chemical.

To CNPq, for the funding and authorization for the internship at the University of Michigan.

This study was financed in part by the Coordenação de Aperfeiçoamento de Pessoal de Nível Superior - Brasil (CAPES) - Finance Code 001.

Abstract

Carneiro, Leonardo Simões de Abreu; Muller, Camilla Djenne Buarque (Advisor). **Arylation of carbonyl compounds via photoredox catalysis**. Rio de Janeiro, 2020. 201p. Tese de Doutorado - Departamento de Química, Pontifícia Universidade Católica do Rio de Janeiro

The advent of photoredox catalysis allowed the development of a series of new C-C bond formation reactions using visible light and photocatalysts to generate organic radicals. It allows methodologies to be developed at room temperature and within short periods of time. Arylation reactions, which involve the insertion of aryl groups, can be performed using diazonium salts as source of aryl radicals. The aim of this dissertation was to study α -arylation reactions of carbonyl compounds using photoredox catalysis. This dissertation is divided into four chapters, being the General Introduction the first one. In the second chapter, a coumarin arylation methodology was developed, based on König's Arylation, to obtain 4-(*N*-phenyl)amino-3-phenylcoumarins. These compounds were obtained in up to 95% yield. The reaction mechanism was studied from trapping experiments with TEMPO and Stern-Volmer correlation. The obtained coumarins had their biological activities evaluated, and three of them showed promising results as antileishmaniasis candidates. Finally, one of the coumarins was used for the synthesis of azacoumestan, a nitrogenous analog of the natural product coumestan. In the third chapter of the thesis, a theoretical study via Density Functional Theory (DFT) was carried out to study the α -arylation of enols acetates to obtain aryl ketones. Previous studies have shown that these reactions perform better when electron withdrawing groups are present in diazonium salts. The use of the Fischer-Radom model allowed us to verify that polar effects are more prominent than enthalpic effects. The origin of these effects was verified as field effects and not resonance effect, since the SOMO orbital in phenyl radicals is orthogonal to the π system. Finally, the effect of substituents on enol acetates was studied by Taft and Charton correlations. In the fourth and last chapter, attempts were made to α -arylate cyclic ketones combining photoredox catalysis with organocatalysis, work developed during the internship period at the University of Michigan. Several

methodologies were tried, however none allowed the formation of the desired product. Studies via DFT showed that the combination of ketone nucleophilicity and steric effects prevented this reaction from being carried out. Therefore, a new methodology was tested using isonitriles of alkyl halides. After extensive optimization, it was possible to obtain a nickel-catalyzed tosylation methodology.

Keywords

Photoredox catalysis, arylation, coumarin, enol acetate, tetralone.

Resumo

Carneiro, Leonardo Simões de Abreu; Muller, Camilla Djenne Buarque (Advisor). **Arilação de compostos carbonílicos via catálise fotorredox**. Rio de Janeiro, 2020. 201p. Tese de Doutorado - Departamento de Química, Pontifícia Universidade Católica do Rio de Janeiro

O advento da catálise fotorredox permitiu o desenvolvimento de uma série de novas reações de formação de ligação C-C utilizando luz visível e catalisadores para gerar radicais orgânicos. Isso permite que metodologias sejam desenvolvidas à temperatura ambiente e com curtos períodos de tempo. Reações de arilação, que envolvem a inserção de grupos aril, podem ser realizadas utilizando sais de diazônio como fontes de radicais arila. O objetivo dessa tese foi estudar reações de α -arilação de compostos carbonílicos usando catálise fotorredox. A tese é dividida em quatro capítulos, sendo o primeiro, a Introdução Geral. No segundo, foi desenvolvida uma metodologia de arilação de cumarinas, baseada na Arilação de König, para obtenção de compostos do tipo 4-(*N*-fenil)amino-3-fenilcumarina. Esses compostos foram obtidos em rendimentos de até 95%. O mecanismo da reação foi estudado a partir de experimentos de trapeamento com TEMPO e correlação de Stern-Volmer. As cumarinas obtidas tiveram suas atividades biológicas avaliadas, e três delas mostraram-se promissoras como fármacos contra leishmaniose. Por fim, uma das cumarinas foi utilizada para a síntese do azacumestano, análogo nitrogenado do produto natural cumestano. No terceiro capítulo da tese, um estudo teórico via Teoria do Funcional da Densidade (DFT) foi realizado para estudar a α -arilação de enóis acetatos para obtenção de aril-cetonas. Estudos previamente realizados mostraram que essas reações têm melhor performance quando grupos retiradores de elétrons estão presentes nos sais de diazônio. O uso do modelo de Fischer-Radom permitiu verificar que efeitos polares são mais proeminentes do que efeitos entálpicos. A origem desses efeitos foi verificada como partindo de efeitos de campo e não de efeito de ressonância, uma vez que o orbital SOMO em radicais fenila é ortogonal ao sistema π . Finalmente, o efeito de substituintes nos enóis acetatos foi estudado a partir das correlações de Taft e Charton. Finalmente, no quarto capítulo foram

abordadas as tentativas de α -arilação de cetonas cíclicas combinando-se catálise fotoredox com organocatálise, trabalho esse desenvolvido durante período sanduíche na Universidade de Michigan. Diversas metodologias foram testadas, entretanto nenhuma permitiu a formação do produto desejado. Estudos via DFT mostraram que a combinação da nucleofilicidade das cetonas e efeitos estéricos impediram que essa reação pudesse ser realizada. Sendo assim, uma nova metodologia foi testada a partir do uso de isonitrilas de haletos de alquila. Após extensa otimização, foi possível obter uma metodologia de tosilação catalisada por níquel.

Palavras-chave

Catálise fotorredox, arilação, cumarina, enol acetato, tetralona.

Table of contents

1. General Introduction	24
1.1. Photoredox catalysis – general aspects	24
1.2. Radical addition to C=C bonds	34
1.3. Photoredox α -arylation of carbonyl compounds	60
2. Synthesis of 3-aryl-4-(<i>N</i>-aryl)aminocoumarins via photoredox catalysis	74
2.1. 3-Arylcoumarins: a privileged scaffold	74
2.2. Objectives	86
2.3. Synthetic plan to the synthesis of 3-arylcoumarins and azacoumestan	86
2.4. Results and discussion	87
2.5. Conclusion and future perspectives	109
2.6. Experimental procedures	110
3. Reactivity of phenyl radicals toward enol acetates: a theoretical study	122
3.1. Introduction	122
3.2. Objectives	124
3.3. Results and discussion	124
3.4. Conclusion	139
3.5. Experimental procedures	140
4. Synthesis of α-aryl-1-tetralones by photoredox catalysis	141
4.1. α -aryl-1-tetralones as analogues of isoflavanones	141
4.2. α -Arylation of cyclic ketones	144
4.3. Objectives	148
4.4. Results and discussion	148
4.5. Conclusion and future perspectives	173
4.6. Experimental procedures	177
5. Bibliographic references	176

Appendix 1: NMR spectra 206

Appendix 2: Cartesian coordinates of the optimized structures 234

List of Abbreviations

¹³C NMR	¹³ C Nuclear Magnetic Resonance Spectroscopy
¹H NMR	¹ H Nuclear Magnetic Resonance Spectroscopy
Ac	Acetyl group
ADME	Adsorption, Distribution, Metabolism, and Excretion properties
AGE	Advanced Glycation End-products
AIBN	Azobisisobutyronitrile
AMB	Amphotericin B
APT	Attached proton test
Aqmoc	Anthraquinon-2-ylmethoxycarbonyl group
B3LYP	Becke, 3-parameter, Lee–Yang–Parr
BHandHLYP	Becke-Half-and-Half-LYP
BHT	Butylhydroxytoluene
Bn	Benzyl group
Boc	<i>t</i> -Butyloxycarbonyl group
BOM	Benzyloxymethyl acetal group
Bz	Benzoyl group
Cbz	Carboxybenzyl group
CDC	Cross Dehydrogenative Coupling
CDFT	Conceptual Density Functional Theory
DABCO	1,4-diazabicyclo[2.2.2]octane
DCM	Dichloromethane
DFT	Density Functional Theory
DIPEA	<i>N,N</i> -Diisopropylethylamine
Dmb	2,4-Dimethoxybenzyl group
DMF	<i>N,N</i> -Dimethylformamide
DMN	2,3-Dimethylmaleimide group
DMSO	Dimethylsulfoxide
DOX	Doxorubicine
DPMS	Diphenylmethylsilyl group

DPTBOS	<i>t</i> -Butoxydiphenylsilyl group
Ds	Dansyl group
DTBMS	Di- <i>t</i> -butylmethylsilyl group
EDG	Electron-donating group
EWG	Electron-withdrawing group
FMO	Frontier molecular orbital
Fmoc	Fluorenylmethoxycarbonyl group
GC-MS	Gas chromatography-mass spectrometry
HCV	Hepatitis C virus
HIV	Human Immunodeficiency Virus
HLY	Hu-Lu-Yang charges
HOMO	Highest Occupied Molecular Orbital
IC	Internal Conversion
ISC	Intersystem Crossing
LFER	Linear Free Energy Relationships
LUMO	Lowest Unoccupied Molecular Orbital
MLCT	Metal-Ligand Charge Transfer
MO	Molecular Orbital
MOM	Methoxymethyl group
Moz	<i>p</i> -Methoxybenzyl carbonyl group
MP2	Second order Møller–Plesset calculation
MPM	Methoxybenzyl group
MPO	Myeloperoxidase
MS	Molecular sieves
Ms	Mesyl group
NBO	Natural Bond Orbitals
NP	No product observed
NR	No reaction
Ns	Nosyl group
PC	Photocatalyst
PCM	Polarizable Continuum Model
PCTE	Proton Coupled electron Transfer
Pic	2-Picolyl group
PIFA	(Bis(trifluoroacetoxy)iodo)benzene

Piv	Pivaloyl group
PMP	<i>p</i> -Methoxyphenyl
PNP	<i>p</i> -Nitrophenyl
PNZ	<i>p</i> -Nitrobenzyl carbonyl group
PTH	10-Phenylphenothiazine
S₀	Ground state energy
S₁	First excited singlet state
SAR	Structure-activity relationship
SET	Single-electron transfer
SOC	Spin-orbital coupling
SOMO	Single Occupied Molecular Orbital
T₁	First excited triplet state
TBDMS	<i>t</i> -Butyldimethylsilyl group
TBDPS	<i>t</i> -Butyldiphenylsilyl group
TBMPs	<i>t</i> -Butylmethoxyphenylsilyl group
TEMPO	(2,2,6,6-Tetramethylpiperidin-1-yl)oxyl
TES	Triethylsilyl group
Tf	Trifluoromethanesulfonyl group
TFA	Trifluoroacetic acid
TFAA	Trifluoroacetic anhydride
TFE	2,2,2-Trifluoroethanol
THF	Tetrahydrofuran
THP	Tetrahydropyranyl ether group
TIPS	Triisopropylsilyl group
TLC	Thin layer chromatography
TMS	Trimethylsilyl group
TPS	Triphenylsilyl group
Troc	Trichloroethyl chloroformate group
TS	Transition State
Ts	Tosyl group
TTMSS	Tris(trimethylsilyl)silane
UPLC	Ultra Performance Liquid Chromatography

List of Figures

Figure 1: Jablonski diagram.	24
Figure 2: The MLCT process at $[\text{Ru}(\text{bpy})_3]^{2+}$.	25
Figure 3: The photoredox catalysis cycles.	25
Figure 4: Electrochemical data of the most used photocatalysts.	27
Figure 5: Main types of radical reactions.	35
Figure 6: Energy profile of a reaction with early transition state.	36
Figure 7: Linear combination of the two main valence-bond contribution to R-X bond.	39
Figure 8: Configuration mixing for radical addition to alkene.	42
Figure 9: The excitation of diazonium salt promoted by $[\text{CuCl}_4]^{2-}$ as a spin catalysis followed by formation of phenyl radical.	47
Figure 10: Selected reduction potentials of aryl halides.	51
Figure 11: The d-p orbital interaction at Sn-X bond.	53
Figure 12: Alkenes and phenyl radicals studied by Skoultchi et al.	58
Figure 13: Alkenes studied by Pryor and Fiske.	59
Figure 14: Alkenes and 4-nitrophenyl radical used in Scaiano and Stewart work.	59
Figure 15: The possible positions of aryl radical attack onto carbonyl compounds.	60
Figure 16: Reduction potential of some aryl sulfonyl chlorides and diaryliodonium salts. ^{61,115}	66
Figure 17: High reducing photocatalysts.	68
Figure 18: Pharmacophoric groups of coumarin and its numbering.	74
Figure 19: 3-Arylcoumarins with anti-HIV activity.	75
Figure 20: 3-Arylcoumarins with anti-HIV activity.	75
Figure 21: 3-Arylcoumarins and their anticancer activities (IC_{50} in μM).	76
Figure 22: 3-Arylcoumarins and their anticancer activities (IC_{50} in μM).	77
Figure 23: 3-arylcoumarins and IC_{50} (μM) for α -glucosidase and AGEs inhibition.	78
Figure 24: 3-arylcoumarins and IC_{50} (nM) for hMAO-B inhibition.	78
Figure 25: Structure of the coumestan and the azacoumestan.	79
Figure 26: Reactivity parameters (in eV) of 262 , 351 and 356 calculated at (U)B3LYP/6-31+G(d) level of theory.	89

Figure 27: Scales of nucleophilicity and electrophilicity.	89
Figure 28: The stabilization of diazo coupling products 357 and 358 by intramolecular hydrogen bond.	89
Figure 29: Evaluation of the diazonium salt scope.	95
Figure 30: Optimized structures of 354a , 354b , 354i , 354j and 354l at M06-2X/6-311++G(d,p) level of theory.	97
Figure 31: Evaluation of the coumarin scope.	99
Figure 32: Stern-Volmer analysis for 216 and 353 as quenchers of [Ru(bpy) ₃] ²⁺ .	102
Figure 33: Mechanism proposed to the photoredox arylation of 4-(N-aryl)aminocoumarin.	103
Figure 34: Coumarins with activity against L. major promastigotes.	106
Figure 35: Coumarins with activity against MDA-MB-231 cells (breast cancer).	107
Figure 36: Photoredox reaction setup.	115
Figure 37: The proposed mechanism for the arylation of enol acetates by photoredox catalysis.	123
Figure 38: Energy profile diagram calculated at UBHandHLYP/6-311G** level of theory. The approximation distance is expressed in Angstroms (Å).	126
Figure 39: Plots of (a) transition state enthalpy (ΔH^\ddagger) against reaction enthalpy (ΔH_{rxn}) and (b) SOMO energy against ΔH_{rxn} .	128
Figure 40: (a) Frontier molecular orbital diagram describing the possible MO interactions; (b) NBO involved at phenyl radical addition TS.	129
Figure 41: IRC calculated for the phenyl radical addition to the acetone-based enol acetate.	130
Figure 42: Plots of $\log k_{rel}$ and ΔG^\ddagger against (a) Hammett σ_p , (b) σ_p^+ , (c) σ^\bullet , (d) Field effect (F) and (e) Resonance effect (R) for para-substituted phenyl radical additions to acetone-based enol acetate at UBHandHLYP/6-311G** level of theory.	131
Figure 43: Plots of $\log k_{rel}$ and ΔG^\ddagger against (a) Hammett σ_p , (b) σ_p^+ , (c) σ^\bullet , (d) Field effect (F) and (e) Resonance effect (R) for para-substituted phenyl radical additions to acetone-based enol acetate at PCM(DMF)/UBHandHLYP/6-311++G**//UBHandHLYP/6-311G** level of theory.	132
Figure 44: Plots of transition state enthalpy (ΔH^\ddagger) against reaction enthalpy (ΔH_{rxn}) and (b) HOMO energy for the addition of p-nitrophenyl radical towards α -alkyl enol acetates.	135

Figure 45: LFER plots with (a) Taft ($-E_s$) and (b) Charton constants (ν) for the addition of p-nitrophenyl radical towards α -alkyl enol acetates.	136
Figure 46: Plots of $\log k_{rel}$ and ΔG^\ddagger against (a) Hammett σ_p , (b) σ_p^+ , (c) σ^\bullet , (d) Field effect (F) and (e) Resonance effect (R) for substituted p-nitrophenyl radical addition to acetophenone-based enol acetates.	138
Figure 47: Examples of naturally occurring isoflavanones.	142
Figure 48: Optimized structures of 430 and 431 at B3LYP/6-311++G(d,p) level of theory: (a) the iminium 430 in front view, (b) the iminium 430 in side view, (c) the enamine 431 in front view and (d) the enamine 431 in side view.	154
Figure 49: The energy of stabilization $E(2)$ and the parameter F_{ij} as a function of the [C1'-N-C1-C2] dihedral angle.	156
Figure 50: Transition states for the addition of the phenyl radical to 431 (left) and 425 (right) calculated at UBHandHLYP/6-311G** level of theory.	158
Figure 51: Energy profile diagram for the phenyl radical addition to 425 and 431 , calculated at UBHandHLYP/6-311G** level of theory.	159
Figure 52: Cyclic voltammetry of 440 .	160
Figure 53: Chromatogram of the reduction of 440 in the presence of [Ir(ppy) ₂ (dtbbpy)]PF ₆ and DIPEA as additive.	162
Figure 54: ¹ H NMR of the compound 450 .	164
Figure 55: ¹³ C NMR of the compound 450 .	165
Figure 56: APT spectra of the compound 450 .	165

List of Tables

Table 1: Reduction potentials of substituted diazonium salts in sulfolane. ⁵⁹	50
Table 2: Relative kinetic constants for phenyl and p-chlorophenyl radical addition to different alkenes.	57
Table 3: Relative rate constants for phenyl radical additions at 25 and 60 °C obtained by Bevington and Ito.	58
Table 4: Relative rate constants of phenyl radical addition obtained by Pryor and Fiske.	59
Table 5: Global chemical potential (μ^0/eV), global hardness (η^0/eV), global electrophilicity (ω^0/eV) and global nucleophilicity (N^0/eV) of protected 4-hydroxycoumarins.	90
Table 6: Global chemical potential (μ^0/eV), global hardness (η^0/eV), global electrophilicity (ω^0/eV) and global nucleophilicity (N^0/eV) of protected 4-aminocoumarins calculated at B3LYP/6-31+G(d) level of theory.	93
Table 7: Optimization studies on the arylation of 368a by photoredox catalysis.	94
Table 8: Global chemical potential (μ^0/eV), global hardness (η^0/eV), global electrophilicity (ω^0/eV) and global nucleophilicity (N^0/eV) of the phenyl radicals calculated at UB3LYP/6-31+G(d) level of theory	96
Table 9: Structural parameters of some optimized 3-arylcoumarins calculated at M06-2X/6-311++G(d,p) level of theory.	98
Table 10: Global chemical potential (μ^0/eV), global hardness (η^0/eV), global electrophilicity (ω^0/eV) and global nucleophilicity (N^0/eV) of 4-(N-aryl)coumarins calculated at B3LYP/6-31+G(d) level of theory	100
Table 11: Optimization of the intramolecular oxidative amination of the coumarin 354a .	104
Table 12: The IC_{50} ($\mu\text{mol L}^{-1}$) against promastigotes of <i>L. amazonensis</i> and MCF-7 and MDA-MB-231 cells after 24 h of treatment.	105
Table 13: Classification of the toxicity as a function of the ToxPot calculated at the OpenVirtualToxLab software.	107
Table 14: Calculated ToxPot at the OpenVirtualToxLab software for the synthesized coumarins and azacoumestan.	108

Table 15: Calculated IC ₅₀ (μmol L ⁻¹) for compounds 354d , 354h , 354s and 354x at 16 proteins using OpenVirtualToxLab software.	109
Table 16: Calculated transition state Gibbs free energy (ΔG [‡] / kcal mol ⁻¹) and enthalpy (ΔH [‡] / kcal mol ⁻¹), reaction Gibbs free energy (ΔG _{rxn} / kcal mol ⁻¹) and enthalpy (ΔH _{rxn} / kcal mol ⁻¹) at UBHandHLYP/6-311G** level of theory.	127
Table 17: Calculated radical SOMO levels (eV), at UMP2/6-31G** level of theory.	128
Table 18: Calculated transition state Gibbs free energy (ΔG [‡] / kcal mol ⁻¹) and enthalpy (ΔH [‡] / kcal mol ⁻¹), reaction Gibbs free energy (ΔG _{rxn} / kcal mol ⁻¹) and enthalpy (ΔH _{rxn} / kcal mol ⁻¹) at UBHandHLYP/6-311G** level of theory for p-nitrophenyl radical addition to α-alkyl enol acetates.	134
Table 19: Taft (-E _s) and Charton (ν) constants and log k _{rel} for different alkyl groups.	135
Table 20: Approximation distante (r _{CC} / Å) and angle (θ / °) calculated at transition states of p-nitrophenyl addition to enol acetates.	136
Table 21: Hammett constants (σ _p and σ _p ⁺), Creary constant (σ [•]), field effect (F) and resonance effect (R) constants and the energy barrier ΔG [‡] (kcal mol ⁻¹) and the log k _{rel} for the p-nitrophenyl radical addition to the acetophenone-based enol acetates.	137
Table 22: Attempts on the arylation of cyclohexanone by photoredox catalysis and organocatalysis.	149
Table 23: Attempts on the arylation of 6-methoxy-1-tetralone by photoredox catalysis and organocatalysis.	150
Table 24: Attempts on the arylation of 6-methoxy-1-tetralone with 248 by photoredox catalysis and organocatalysis.	150
Table 25: Attempts on the arylation of 6-methoxy-1-tetralone with different phenyl radical sources and chiral phosphoric acid as organocatalyst.	152
Table 26: Attempts on the arylation of the 6-methoxy-1-tetralone derived enol acetate with different phenyl radical sources and chiral phosphoric acid as organocatalyst.	153
Table 27: Conceptual DFT parameters calculated for enamines and enol acetates at B3LYP/6-31+G(d).	157
Table 28: Thermodynamic parameters for the phenyl radical addition to pyrrolidine-derived enamines, calculated at UBHandHLYP/6-311G**.	159
Table 29: Attempts on the reduction of 440 using photoredox catalysis.	161

Table 30: Attempts on the formation of the desired imine by photoredox catalysis using commercially available isonitriles.	163
Table 31: Merging photoredox catalysis with nickel coupling to obtain the tosylated compound 450 .	164
Table 32: Control experiments to evaluate the photoredox or the nickel catalysis.	166
Table 33: Optimization of the catalyst, ligand and solvent at the tosylation of 448 .	167
Table 34: Optimization of the base, additive and temperature at the tosylation of 448 .	169
Table 35: Control experiments for the tosylation of 448 .	170
Table 36: Evaluation of the water and reactants content on the tosylation of 448 .	171

List of Schemes

Scheme 1: Photoredox version of the Pschorr reaction.....	28
Scheme 2: Yoon's [2+2] cycloaddition of enones.	29
Scheme 3: MacMillan's enantioselective α -alkylation of aldehydes.	30
Scheme 4: Stephenson's reductive dehalogenation.....	31
Scheme 5: Total synthesis of (+)-batrachotoxinin A.	32
Scheme 6: Total synthesis of (+)-actinophyllic acid.....	33
Scheme 7: Total synthesis of aspergillide A.	34
Scheme 8: Mechanism of radical polymerization.	35
Scheme 9: Addition of alkyl radicals to styrenes and ρ constants.....	38
Scheme 10: (a) Methyl radical addition to substituted alkenes. (b) Alkyl radical addition to methyl acrylate.....	41
Scheme 11: Meerwein arylation and selected examples.	43
Scheme 12: First proposed mechanism of the Meerwein arylation.....	44
Scheme 13: Selected examples of the different products obtained by the Meerwein reaction as a function of the alkene.....	45
Scheme 14: Mechanism of the Meerwein arylation based on the formation of diazoacetate species.	45
Scheme 15: Mechanism of the Meerwein arylation based on the Cu(I) as the active species of the catalysis.	46
Scheme 16: Mechanism of the Meerwein arylation based on spin-orbital couple.	47
Scheme 17: Intramolecular 5-exo-trig cyclizations catalysed by Fe(II).	49
Scheme 18: Possible mechanisms to reduction of aryl halides to phenyl radical.	51
Scheme 19: General mechanism of phenyl radical formation by tin hydrides.....	52
Scheme 20: Synthesis of 142 by intramolecular cyclization using $\text{Me}_3\text{SnPPh}_2$	53
Scheme 21: Synthesis of 147 by intramolecular cyclization with $(\text{Bu}_3\text{Sn})_2$ as intermediate of the synthesis of acutumine	54
Scheme 22: Total synthesis of a gelsemine analogue.....	55
Scheme 23: The use of TTMSS in the reductive dehalogenation of aryl halides.	56
Scheme 24: Synthesis of the tetracycle 174	56
Scheme 25: Xia's direct arylation of carbonyl compounds.....	61

Scheme 26: β -arylation of carbonyl compounds.....	62
Scheme 27: Photoredox arylations with diazonium salts.....	63
Scheme 28: Photoredox arylations of alkenes and alkynes followed by intramolecular cyclizations.	64
Scheme 29: Arylation of phenylpyridines with diazonium salts merging photoredox catalysis and cross-coupling reaction.....	65
Scheme 30: Photoredox arylation merged with palladium and gold catalysis.	66
Scheme 31: Photoredox arylations using (A,B) hypervalent iodines and (C,D) sulfonyl chlorides.	67
Scheme 32: Reductive dehalogenation of aryl halides using PTH as photocatalyst.	68
Scheme 33: König's arylation of coumarin.	69
Scheme 34: Photoredox arylation of coumarins using porphyrin-based photocatalysts.	70
Scheme 35: Photoredox arylation of enol acetates.	70
Scheme 36: Photoredox arylation combined with micellar catalysis.	71
Scheme 37: Synthesis of isoflavones by photoredox arylation of enamines followed by intramolecular cyclization.	71
Scheme 38: Li's carboarylation of alkenes.	72
Scheme 39: Synthesis of arylketones by oxidative arylation of styrenes.	73
Scheme 40: Synthesis of acrylonitriles by oxidative arylation of styrenes.....	73
Scheme 41: Synthetic strategies to achieve coumestans.....	79
Scheme 42: Synthetic strategies to achieve azacoumestans.	80
Scheme 43: Synthesis of azacoumestan by intramolecular Heck cyclization of 323	81
Scheme 44: Synthesis of azacoumestan by cross dehydrogenative coupling of 324	81
Scheme 45: Synthesis of azacoumestan by intramolecular cyclization of azides. ...	82
Scheme 46: Synthesis of azacoumestan by Cadogan-Sundberg reaction.	83
Scheme 47: Arylation of coumarins by Suzuki cross-coupling reaction.	84
Scheme 48: Arylation of coumarins by decarboxylative coupling with aryl iodides. .	84
Scheme 49: Arylation of coumarins with no functionalization of the C3 position.....	85
Scheme 50: Arylation of coumarins promoted by KMnO_4	86
Scheme 51: Proposed retrosynthesis of N-arylazacoumestan 355	87
Scheme 52: Synthesis of the 4-aminocoumarin 356	87

Scheme 53: Diazo coupling between diazonium salt (216) and 4-hydroxy (351) and 4-aminocoumarins (356).	88
Scheme 54: Attempts on the arylation of protected 4-hydroxycoumarins.	92
Scheme 55: Control experiments and radical-trapping reaction with TEMPO.....	101
Scheme 56: The radical addition step of the enol acetate arylation.....	124
Scheme 57: Costa's α -arylation of 1-tetralones by Buchwald-Hartwig-Myura reaction.	143
Scheme 58: Costa's synthesis of carbapterocarpens.	143
Scheme 59: Costa's modified synthesis of carbapterocarpens through 1-tetralones.	144
Scheme 60: Synthesis of cephalotaxinone by intramolecular arylation of 402 with Ni(0).....	144
Scheme 61: Arylation of cyclohexanone combining organotin and palladium catalysis.	145
Scheme 62: Arylation of cyclic ketones using diphenyliodonium triflates.....	145
Scheme 63: Direct arylation of cyclohexanone by palladium catalysis.	145
Scheme 64: Arylation of cyclopentanones merging cross-coupling and organocatalysis.	146
Scheme 65: Arylation of 418 with chlorobenzene using 419 in subcatalytic amounts.	146
Scheme 66: arylation of 1-tetralone with 421 by nickel catalysis.	147
Scheme 67: Arylation of cyclic ketones with nitrobenzenes by nucleophilic aromatic substitution.	147
Scheme 68: Attempt on the arylation of 425 by photoredox catalysis.....	151
Scheme 69: Mechanism of the non-catalyzed formation of the enamine 431	153
Scheme 70: Proposed synthesis of α -aryl-1-tetralones using isonitriles.	160
Scheme 71: Synthesis of the organozinc species 451 and its tosylation with TosMIC.	172
Scheme 72: Proposed mechanism for the tosylation of 448 with TosMIC catalysed by nickel.	173

1

General Introduction

1.1.

Photoredox catalysis – general aspects

Organic photochemistry is the area that studies the effects of light on organic compounds. When a compound is irradiated and absorbs energy, it is excited from the ground state (S_0) to a high energy state (usually S_1). Jablonski diagram summarizes the physical processes that can occur after the excitation (Figure 1). Two processes are related to relaxation of S_1 state: internal conversion (IC), where the emitted energy is equal to the absorbed one, and vibrational relaxation followed by fluorescence, in which there is emission of photons.¹

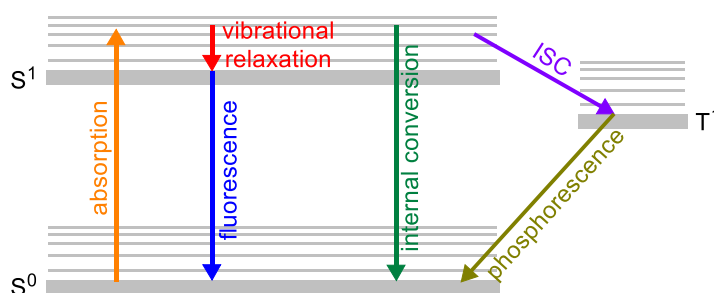


Figure 1: Jablonski diagram.

As there is no spin change, which is quantum mechanically prohibited, the first excited state is singlet as the ground state. However, some species can have their spin changed migrating to a triplet state (T_1) by a process called intersystem crossing (ISC). In such case, the route back to the ground state can have photon emission as a phosphorescence process.² Some organometallic compounds of ruthenium and iridium can generate triplet excited states with high lifetime. In such cases, these species are prone to make oxidations or reductions to generate radicals in the reaction media.³ The methodology that employs these compounds as catalysts is called photoredox catalysis.

The most important ruthenium complex used in photoredox catalysis is $[\text{Ru}(\text{bpy})_3]\text{Cl}_2$. Its excited state has a lifetime of 1100 ns in acetonitrile¹² and 580 ns in water¹³, which is long enough to be prone to bimolecular SET reactions. After the excitation irradiating it with the white or blue light source, one electron of ruthenium t_{2g} orbital is promoted to $\text{bpy } \pi^*$ orbital with spin change. This process is called metal-ligand charge transfer (MLCT) (Figure 2). The maximum absorbance of light is around 450 nm, that is, at visible-light region, and corresponds to MLCT.¹⁴

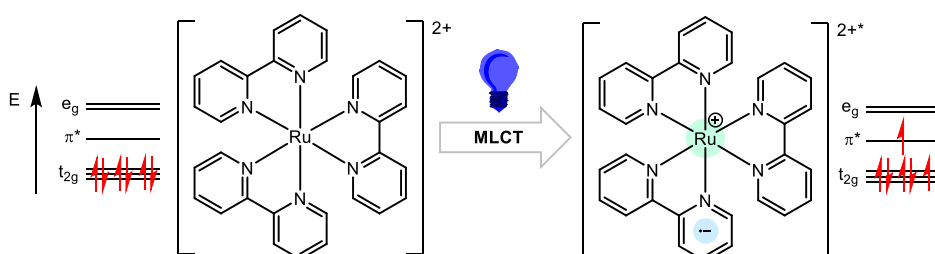


Figure 2: The MLCT process at $[\text{Ru}(\text{bpy})_3]^{2+}$.

Once the excited photocatalyst (PC), $^*[\text{Ru}(\text{bpy})_3]^{2+}$, is generated in the reaction media, it can donate or accept one electron by outer-sphere single electron transfer (SET) mechanism, changing its formal charge and returning to the ground state (Figure 3). If it is quenched by an acceptor species (A), it donates an electron, oxidizing itself, and is converted to a Ru(III) species. A second SET occurs with a donor species (D) to recover the photocatalyst. This mechanism is called the reductive quenching cycle. On the other hand, the first SET can also be done against a donor species. In this case, ruthenium is reduced to Ru(I) and the second SET occurs with an acceptor species. This pathway is called the oxidative quenching cycle.

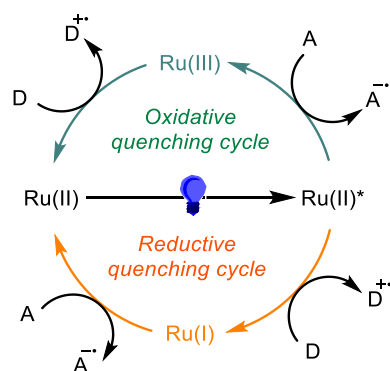


Figure 3: The photoredox catalysis cycles.

As the transformations are based on redox reactions, the redox potentials ($E_{1/2}$) must be evaluated. Organometallic photocatalysts are influenced by the nature of the ligands.¹⁵ The PC that possesses electron-rich substituents tends to be more reducing. The presence of electron-poor substituents increases its oxidizing power. The notation used in this Dissertation for redox potentials is $E_{1/2}(\text{PC}^+/\text{PC}^*)$, which means that this is the potential to transform PC^* to PC^+ , for example. A set of electrochemical data is shown in Figure 4.^{16,17}

To preview the suitability of a certain PC^* to be quenched by a substrate, the redox potential of the other chemicals must be known. In the case of no data available, cyclic voltammetry is the recommended technique to obtain the redox potential. For an electrochemical transformation to be spontaneous, its Gibbs free energy must be negative (Equation 1). The energy of the system, defined as the difference of donor and acceptor potentials, must be positive (Equation 2).

$$\Delta G_{\text{SET}} = -nFE_{\text{system}} \quad (1)$$

$$E_{\text{system}} = E_{1/2}(\text{donor}) - E_{1/2}(\text{acceptor}) \quad (2)$$

One of the first reports of a reaction that involves this approach was proposed by Cano-Yelo and Deronzier.⁴ The authors showed the formation of phenanthrenes by a photocatalytic version of Pschorr reaction (Scheme 1A). The diazonium salt **1** would quench the ruthenium salt in the excited state generating a phenyl radical (Scheme 1B). After a homolytic aromatic substitution, the desired product **2** was achieved in quantitative yield. The same substrate was submitted to direct photolysis, but the product was formed in 20% yield. In such case, **3** was observed as byproduct in 80% yield (Scheme 1C).

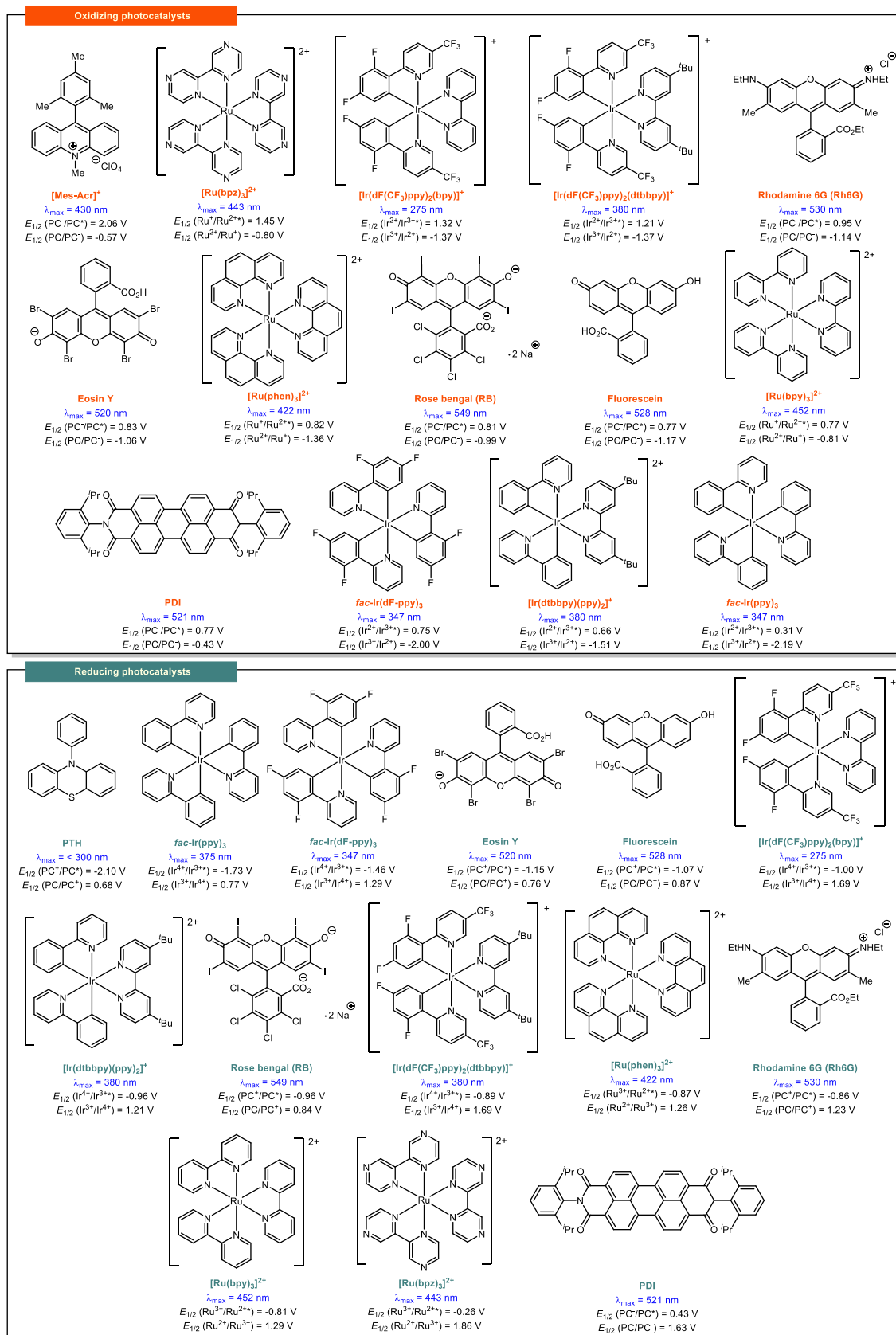
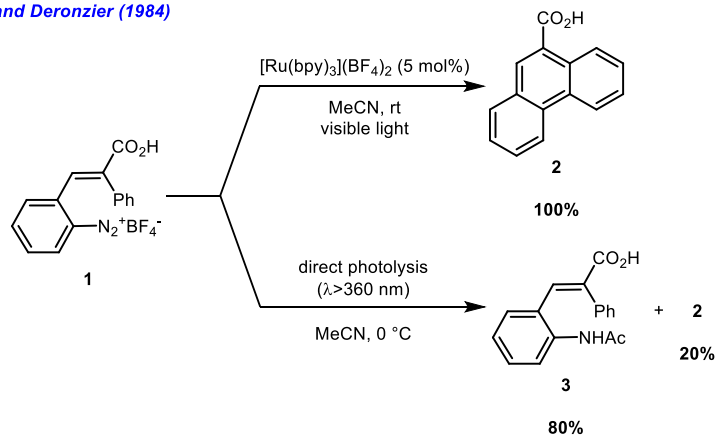
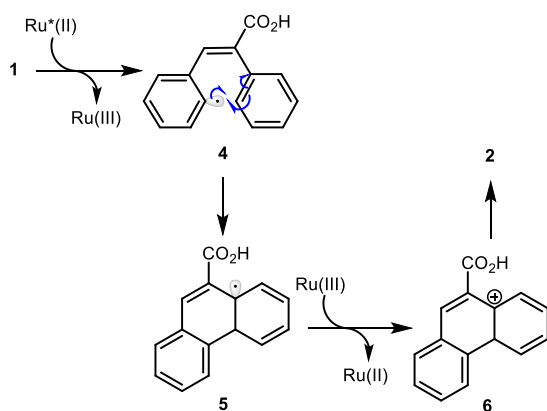
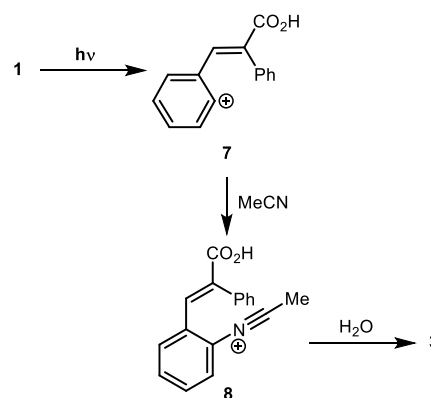


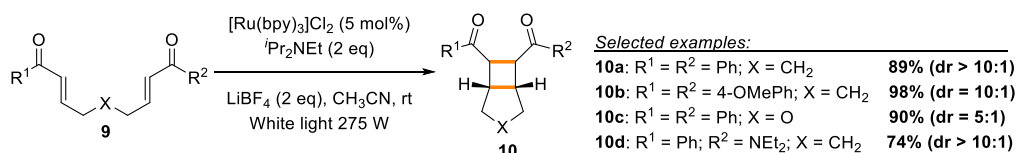
Figure 4: Electrochemical data of the most used photocatalysts.

A) *Cano-Yelo and Deronzier (1984)*B) *Photocatalytic Pschorr reaction*C) *Formation of 3 by direct photolysis of 1*

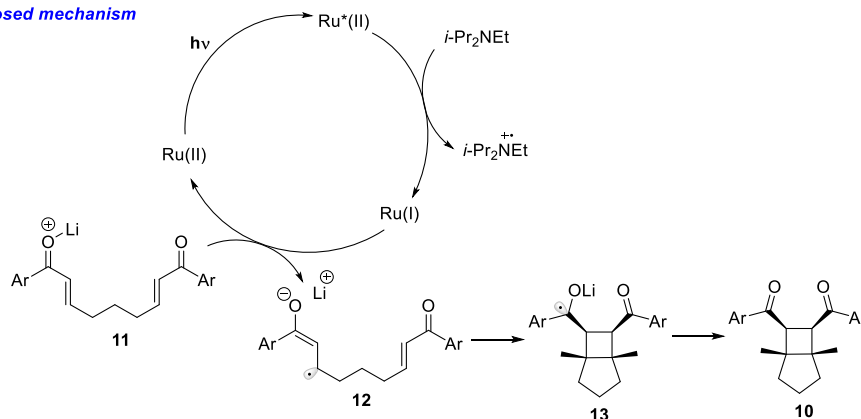
Scheme 1: Photoredox version of the Pschorr reaction.

At the beginning of this century, three different works revisited this Chemistry introducing a milestone to Photoredox Catalysis. In 2008, Yoon et al reported the photocatalytic [2+2] cycloaddition of enone **9** with high diastereoselectivity (Scheme 2).⁵ The authors proposed that, after reduction of $\text{Ru}^*(\text{II})$ to $\text{Ru}(\text{I})$, the activated enone **11**, where Li acts as a Lewis acid, is reduced to **12** by the photocatalyst, as described by Krische in reactions catalyzed by cobalt^{6,7} and copper⁸. A control reaction with no $^i\text{Pr}_2\text{NEt}$ gave no product, which corroborates the purpose that $\text{Ru}(\text{I})$ is the species that reduces the enone. Once **12** is formed, an intramolecular cycloaddition gives the product **10**.

A) Yoon's [2+2] cycloaddition of enones

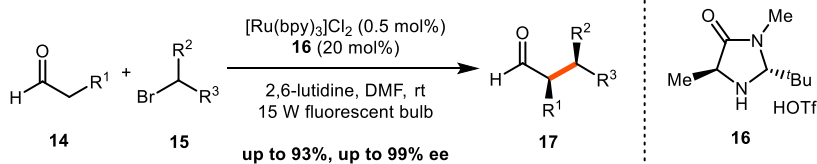


B) Proposed mechanism

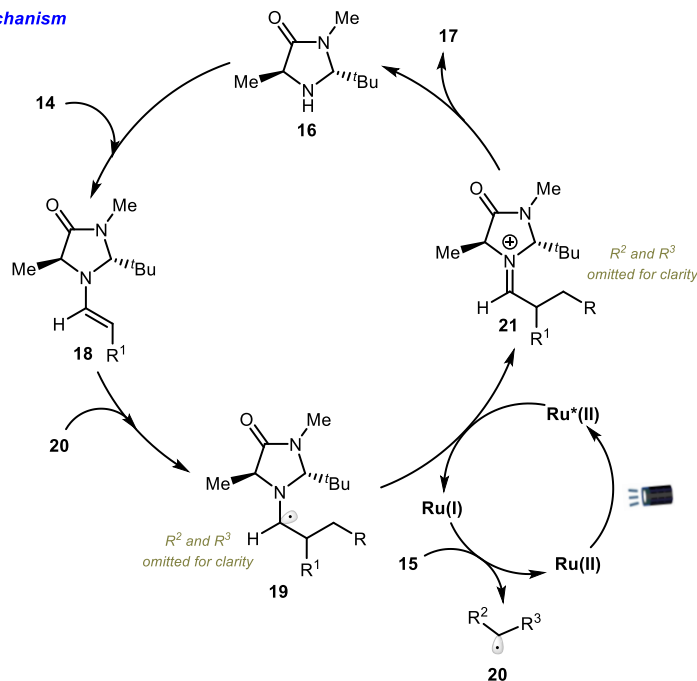


Scheme 2: Yoon's [2+2] cycloaddition of enones.

In the same year, Nicewicz and MacMillan combined photoredox catalysis with organocatalysis to promote enantioselective α -alkylation of aldehydes (Scheme 3).⁹ The organocatalysts **16** reacts with the aldehyde **14** to make a SOMOphilic enamine **18**. The photoredox cycle initiates by sacrificing part of the amine to reduce $\text{Ru}^*(\text{II})$ to $\text{Ru}(\text{I})$. Then, the alkyl bromide **15** is reduced to the alkyl radical **20**. Finally, it couples with **16** through the *Si* face to give the radical **19**, which by SET with $\text{Ru}^*(\text{II})$, gives **21** and then the desired product **17**, in high enantioselectivity.

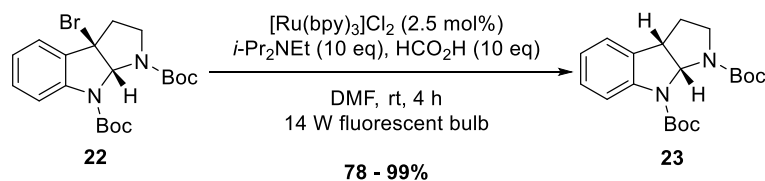
A) MacMillan's enantioselective α -alkylation of aldehydes

B) Proposed mechanism

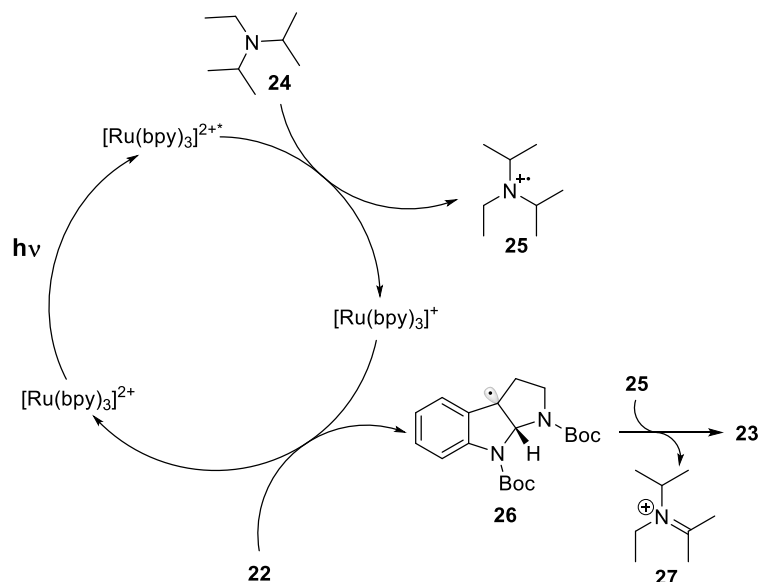
Scheme 3: MacMillan's enantioselective α -alkylation of aldehydes.

Finally, Stephenson et al proposed the reductive dehalogenation of alkanes like **22** (Scheme 4).¹⁰ Usually, this kind of reaction is carried out by using a huge variety of metals, most of them toxic such as tin, as demonstrated by Yus et al.¹¹ As well as Yoon's cycloaddition and MacMillan's alkylation, a tertiary amine was used to generate a $\text{Ru}(\text{I})$ species as reducing agent; it was essential to reaction, affording trace amounts of the product after 48 h without it. The radical **26** abstracts the hydrogen from **25** to give the product **23**. An alternative abstraction was proposed, in which formic acid would be the hydrogen source. However, such path might be minor.

A) *Stephenson's reductive dehalogenation*



B) *Proposed mechanism*



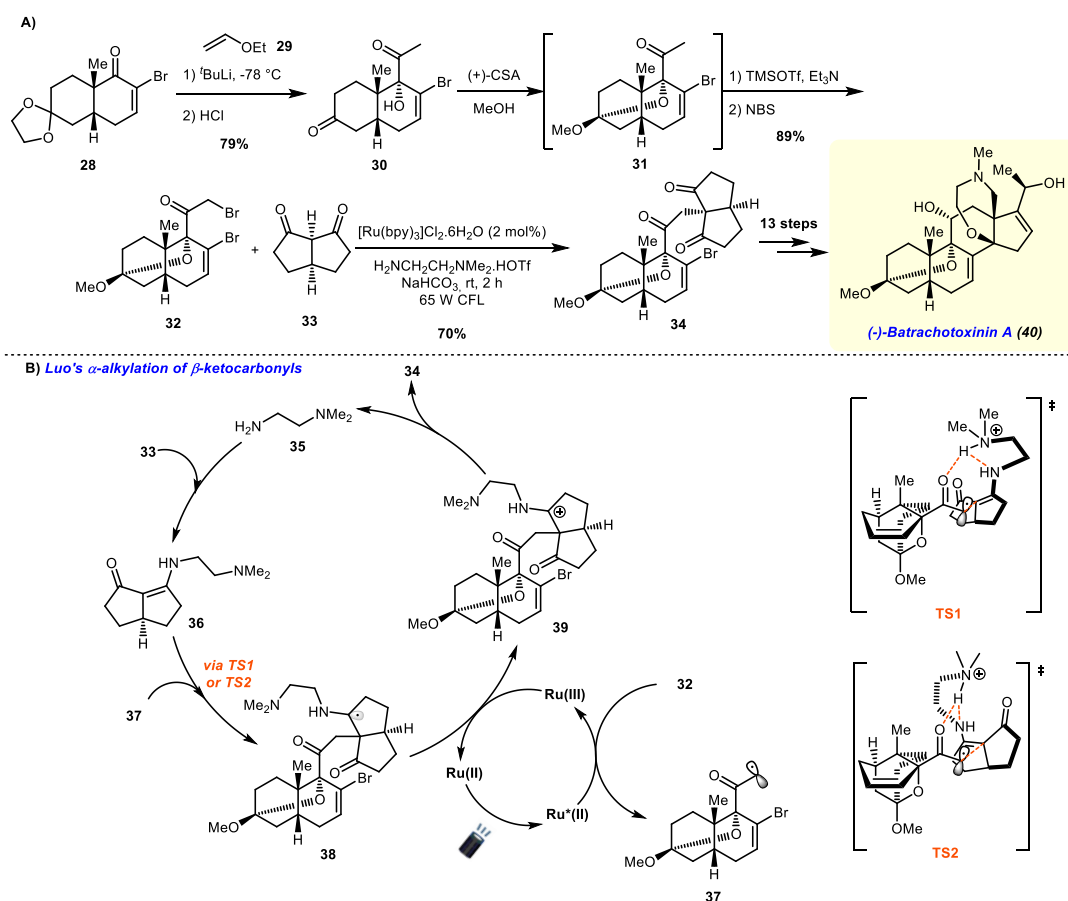
Scheme 4: Stephenson's reductive dehalogenation.

1.1.1. Applications in natural products synthesis

The use of photoredox catalysis in Organic Synthesis has gained attention because of its advantages as compared to classical methodologies like cross-coupling reactions. The possibility of metal-free photocatalysts, room temperature reactions, use of visible-light and formation of new and unique radical species are some reasons why this methodology might be considered when a synthesis is planned. Some reviews reported its use in the synthesis of complex natural products. In this subsection, some recent examples are presented.

Luo et al (2020) showed the total synthesis of (-)-batrachotoxinin A (Scheme 5A).¹⁸ This alkaloid was first extracted from the skin of *Phyllobates* sp., a poison-dark frog.¹⁹ In their route, a coupling between **32** and **33** was planned as one of the key steps. The intermediate **32** was prepared from an attack of vinyl ether to **29** to **28** followed by hydrolysis and α -bromination in high yields. The desired substitution was carried out as a S_N2 reaction; however, the attempts were not successful because of

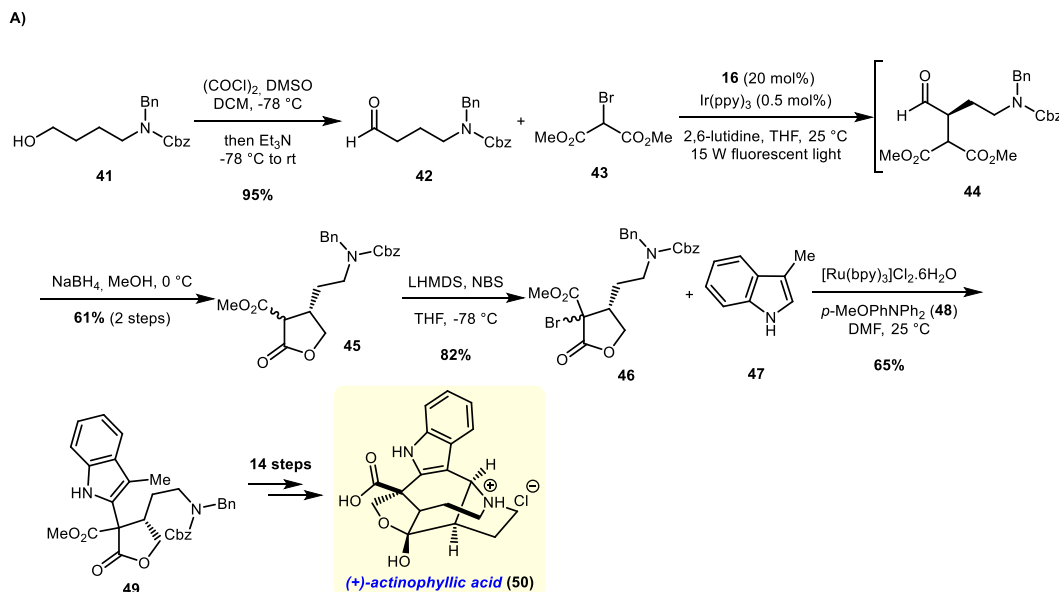
steric and stereoelectronic effects. It was decided to employ Luo's α -alkylation of β -ketocarboxyls using primary amines as organocatalysts.²⁰ This reaction is based on the coupling of radical **37**, formed from the reduction of α -bromoketone, with enamine **36** (Scheme 5B) through two possible transition states, **TS1** and **TS2**. The reaction was successfully done in 70% yield. After more 13 steps, (-)-batrachotoxinin A (**40**) was achieved.



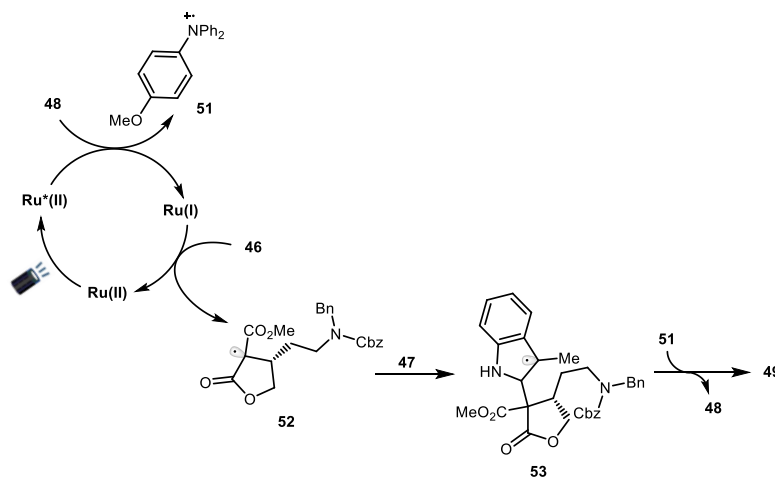
Scheme 5: Total synthesis of (+)-batrachotoxinin A.

Qin et al proposed the total synthesis of (+)-actinophyllic acid (Scheme 6A).²¹ These compounds were isolated in 2005 from the aqueous extract of *Alstonia actinophylla* leaves and showed great activity as carboxypeptidase U inhibitor.²² The first key step of their plan was based on asymmetric α -alkylation of the aldehyde **42** with **43**, obtained after Swern oxidation of the commercially available alcohol **41**. The combined photoredox organocatalytic methodology proposed by MacMillan et al⁹ was modified and followed by reduction with NaBH_4 to achieve **45** in 61% yield and 92% ee. The authors increased the scale to 10 g with no loss of yield and enantioselectivity.

After its bromination to make **46**, another photoredox step was employed: to couple the indole nucleus, they used Stephenson's methodology of reductive dehalogenation¹⁰ (Scheme 6B), trapping the formed radical with indole to achieve **49** in 65% yield. After more 14 steps, (+)-actinophyllic acid (**50**) was obtained.



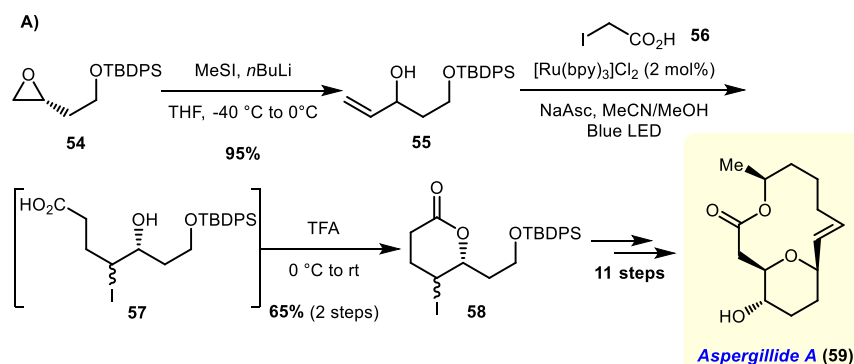
B) Stephenson's reductive dehalogenation applied to synthesis of #



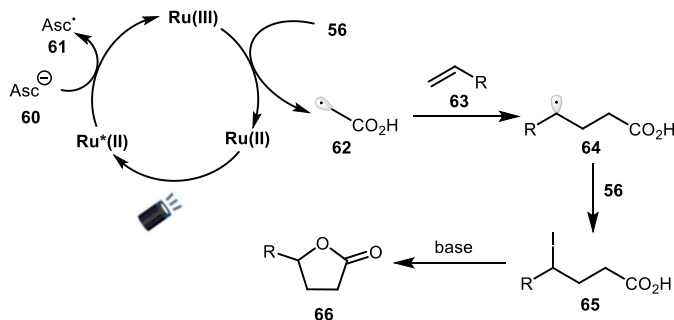
Scheme 6: Total synthesis of (+)-actinophyllic acid.

Mateus-Ruiz and Cordero-Vargas worked in the total synthesis of aspergillide A (Scheme 7A), a natural product extracted from the marine fungus *Aspergillus ostianus*.^{23,24} Starting from the epoxide **54**, it was treated with Me_3SI and $n\text{-BuLi}$ to achieve **55**. Then, the desired transformation was the lactonization with **56** to make the intermediate **57**. The application of Kokotos's photoredox lactonization²⁵ was employed to achieve **58** in 65% yield. The proposed mechanism (Scheme 7B) is based

on the reduction of α -iodoacetic acid to make the radical **62**. Then, it adds to an alkene, like **63**, forming **64** that, iodinated from **56**, gives **65**. After deprotonation and intramolecular nucleophilic substitution, the lactone **66** is formed. Another methodology was tried, but the photoredox reaction was easier to be purified and scaled up. Finally, aspergillide A (**59**) was obtained after more 11 steps.



B) Kokoto's lactonization



Scheme 7: Total synthesis of aspergillide A.

1.2.

Radical addition to C=C bonds

The advent of photoredox catalysis was an important step in radical chemistry. After the formation of such radicals in the reaction media, they proceeded with the main types of reactions (Figure 5): combination, abstraction of atoms, fragmentation, and addition to multiple bonds. The latter is one of the most used in photoredox methodologies and allows the formation of new σ bonds. The chemistry behind this class of reactions was built up based on industrial applications of radical-induced polymeric reactions. One example of this reaction is the synthesis of polystyrene (Scheme 8). Benzoyl peroxide (**67**), used as the initiator, fragments in two radicals **68**

when heated, which, after decarboxylation, are converted to phenyl radicals **69**. Then, they are added to styrene (**70**) to produce the radical intermediate **71**. After successive additions to **70**, the chain grows up and a polymer **73** is formed. Finally, the termination step can be fulfilled by a combination of two **73** to set the desired polymer **74**.

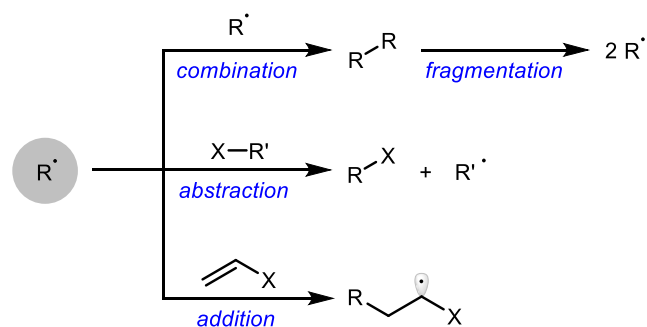
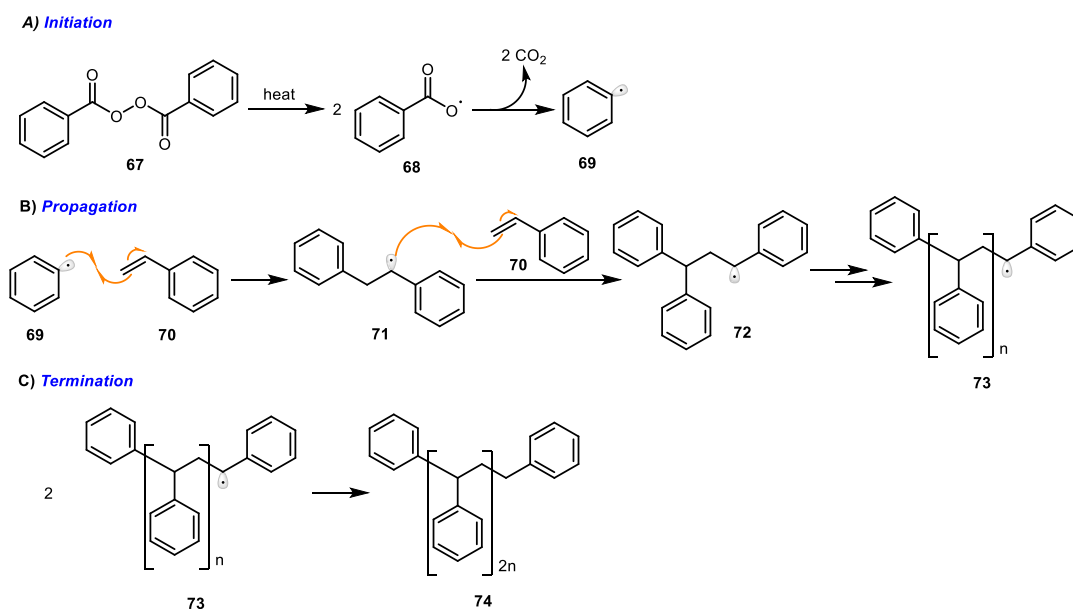


Figure 5: Main types of radical reactions.



Scheme 8: Mechanism of radical polymerization.

The reactivity and regioselectivity of radical addition to $C=C$ bonds were extensively studied, and some models were developed. The first was introduced by Giese and Tedder and tries to qualitatively explain the influence of substituents at the alkene. The variables that would be controlled are expressed as two effects: enthalpic and polar effects.²⁶⁻²⁸ Giese proposed that the rates are influenced by substitution at radical and both atoms of $C=C$ alkene bond.^{29,30}

Enthalpic effects are related to the relative strength of the bonds broken and formed among the reaction. In a general view, addition reactions are based on the break of a $\pi_{C=C}$ bond and formation of a σ_{C-C} one. Such bonds are stronger (81 kcal/mol compared to 67 kcal/mol of π bond).³¹ Hence, the reaction is exothermic ($\Delta H < 0$) and the radical adduct formed is thermodynamically more stable than the starting materials. This fact has direct influence on the transition state. Tedder proposed the First Law of free radical reactions based on the exothermicity.²⁷

If the heat of reaction ΔH of a free radical process is large and negative, the transition state is early and the reaction will be fast and unselective; if ΔH is large and positive the transition state will be late and the reaction slow and selective: but if ΔH is small (positive or negative) the relative rate and selectivity will depend on other factors, especially polarity. (TEDDER, 1982)

Clearly, this is the contextualization of Hammond Postulate to radical additions. According to this principle, the transition state of a reaction that produces high stabilized product needs less reorganization energy of reactants; in other words, the transition state is more reactant-like than product-like (Figure 6).³²

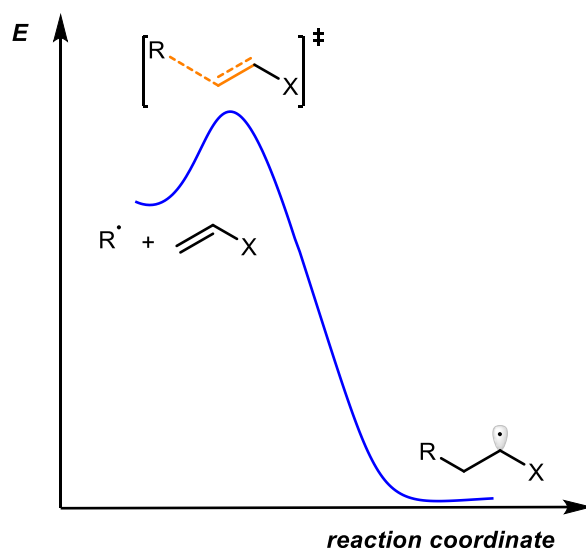


Figure 6: Energy profile of a reaction with early transition state.

The electronic nature of radical and alkene can also influence the addition reaction rates. It can be explained in terms of frontier molecular orbitals (FMO). The interaction between the SOMO of the radical and the HOMO or LUMO of the alkene

dictates which one is the nucleophile or the electrophile. This is known as a polar effect.

The Klopman-Salem equation (Equation 3) describes the change of energy of two approaching chemical species, in terms of their molecular orbitals, based on a Taylor expansion of the total energy (perturbation theory).³³ The first term is related to the interaction between filled orbitals. The second term computes the Coulombic interactions (repulsion or attraction). The third term of this equation is the second-order perturbation, which comes from the interaction between filled/unfilled orbitals. In terms of radical additions, the second-order perturbation is related to SOMO-HOMO and SOMO-LUMO interactions. Mathematically, two orbitals closer in energy contribute more to the interaction energy. The equation can summarize the phenomenon that happens when two molecules approach each other to react at the orbital level. Besides the repulsion of filled orbitals, filled and unfilled orbitals interact causing the attraction of the molecules.

$$\Delta E = \pm \sum_{ab} (q_a + q_b) \beta_{ab} S_{ab} + \sum_{k < l} \frac{Q_k Q_l}{\epsilon R_{kl}} + \sum_r^{\text{occ}} \sum_s^{\text{unocc}} \pm \sum_r^{\text{occ}} \sum_s^{\text{unocc}} \frac{2(\sum_{ab} c_{ra} c_{sb} \beta_{ab})^2}{E_r \pm E_s} \quad (3)$$

- q_a and q_b : electron populations at atomic orbitals a and b .
- β_{ab} : resonance integral between atoms a and b .
- S_{ab} : overlap integral between atoms a and b .
- Q_k and Q_l : total charges at atoms k and l .
- R_{kl} : distance between atoms k and l .
- c_{ra} and c_{sb} : coefficient of atomic orbital a at molecular orbital r and atomic orbital b at molecular orbital s .
- E_r and E_s : energy of molecular orbitals r and s .

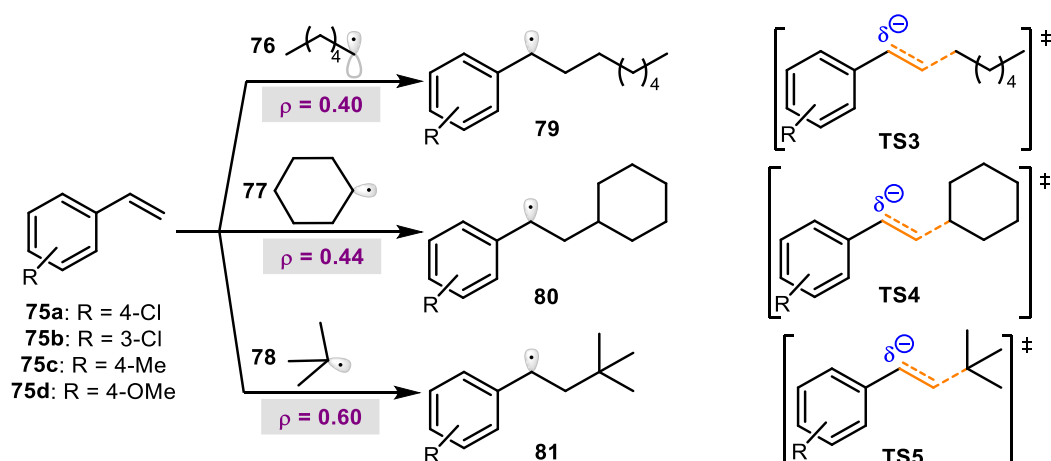
The Natural Bond Orbitals (NBO) are a description of the localized Lewis structure.³⁴ As two orbitals get closer, delocalization occurs due to their interaction. According to NBO analysis, such interaction is described as a second-order perturbation ($E(2)$, Equation 4).³⁵ As at Klopman-Salem equation, $E(2)$ relates the perturbation and the energy difference between the orbitals in the same manner: the preferred perturbation will be the one with higher energy, which gives the closest approximation.

$$E(2) = -n \frac{F_{ij}^2}{\Delta E} \quad (4)$$

- n : population of the donor orbital.
- F_{ij} : Fock matrix element between orbitals i and j .
- ΔE : energy difference between orbitals i and j .

According to Giese, substituents will influence the orbital levels depending on the nature of the polar effect.^{29,30} The interaction SOMO-LUMO indicates that alkene acts as the electrophile. Then, substitutions at C=C would have a higher impact on the reaction rate. Electron withdrawing groups (EWG) lower the LUMO energy at both carbons, but more strongly at the not attacked one. In the interaction SOMO-HOMO, the alkene acts as the nucleophile. On the other hand, substitutions at the radical would impact the rate. The presence of EWG groups lower the SOMO level, and such interaction gets stronger, thus increasing the rate.

To exemplify this approach, Giese and Meister studied the addition of different alkyl radicals (**76** – **78**) to substituted styrenes (**75a** – **d**) (Scheme 9).³⁶ The Hammett plot at -56 °C indicated a linear relation with good correlation and positive ρ constants. It means that at the not attacked carbon there is the formation of negative partial charge. Thus, the alkyl radicals act as the nucleophiles, while the styrenes act as electrophiles.



Scheme 9: Addition of alkyl radicals to styrenes and ρ constants.

1.2.1. The Fischer-Radom model

Both polar and enthalpic factors interfere with kinetics. Methyl radical addition was used over the years as a good model to study radical additions to alkenes. Its low size reduces sterics and allows the evaluation of those effects. Despite the contribution of Giese and Tedder work, no quantitative relation was expressed in terms of kinetic or thermodynamics. To overcome it, Fischer and Radom combined their kinetic data

set with computational insights to propose a model that could explain the influence of alkene structure.

The origin of this model is the Pross and Shaik approach to organic reactivity. Two radicals R^\bullet and X^\bullet are considered to combine, forming a R-X bond. The two main valence-bond contributions for R-X are represented in the energy diagram of Heitler-London (Figure 7): $[R^\bullet \bullet X]$, in which each electron of the bond is associated to R and X, and $[R^+ :X^-]$; in this configuration, both electrons are associated to X, generating a zwitterionic form. In solution, the solvation effect to stabilize R^+ and X^- minimizes their energy and, hence, the curves cross each other. Taking a linear combination of the contributions, both wavefunctions mix in a manner to generate R-X bond in the ground state (S_0) and in the first excited state (S_1). The effect of the crossing curves is observed at the S_0 R-X bond (red dotted line). As R-X is stretched, its energy increases until reaching the crossing point, where the energy of covalent and ionic configurations is the same. After this point, the most stable configuration is the ionic one, indicating that through a SET from R to X, $[R^\bullet \bullet X]$ switched to $[R^+ :X^-]$.

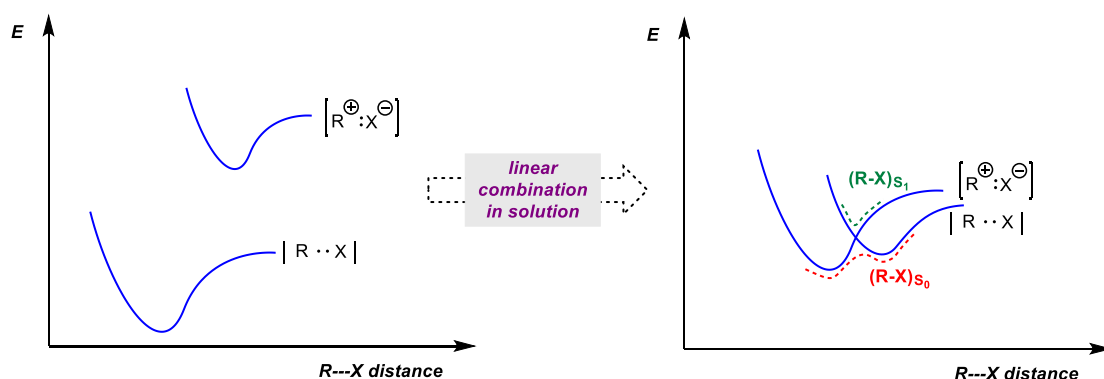


Figure 7: Linear combination of the two main valence-bond contribution to R-X bond.

Fischer and Radom proposed that four configurations are possible in a radical addition to alkenes: the ground state approximation of radical and alkene $[R^\bullet + C=C^1]$, the radical approximation to triplet state alkene $[R^\bullet + C=C^3]$, and two charge-transfer configurations - $[R^+ + C=C^-]$ and $[R^- + C=C^+]$ (Figure 8). The energy of $[R^\bullet + C=C^1]$ increases as R^\bullet approaches to $C=C$ and no bond is formed because $C=C$ bond stretches and crosses the excited state configuration. This mixing is the key factor to describe the reaction barrier energy. On the other hand, the charge-transfer contributions are stabilized as both charges approach, as described by Coulomb Law.

The higher is this stabilization, the more influence these configurations have: the minimum gets closer to the crossing point and influences the barrier.

The evaluation of this diagram can predict how energy parameters control the reaction. When such contributions are deciphered, quantitative approaches can be used to rationalize the reactivity. The enthalpic effect will be the major contribution when the charge-transfer configurations have low or no influence. In such a case, the energy barrier is related to the exothermicity of the reaction. The Evans-Polanyi equation dictates this relation (Equation 3): there is a linear relationship between activation energy and the enthalpy of the reaction, where α is a constant that varies between 0 and 1 and E_0 is the barrier at 0 K.³⁷

$$E_a = E_0 + \alpha \Delta H \quad (3)$$

Carbon-centered radical additions to alkenes are usually governed by enthalpic effects. Radom et al studied the addition of methyl radical **82** to substituted alkenes and **83** calculated the activation energy and reaction enthalpy (Scheme 10A).^{38,39} The extreme barriers were calculated to be 8.4 kcal/mol for the non-substituted alkene and 4.9 kcal/mol for the one CN substituted. The enthalpy was observed to have the opposite trend: higher barrier was related to lower exothermicity (-22.0 kcal/mol), while the lower barrier was defined by higher reaction enthalpy (-30.4 kcal/mol). A good correlation between these values ($r^2 = 0.973$) indicated that exothermicity governs the reactivity of such alkenes. Fouassier et al worked on the addition of different radicals to methyl acrylate (Scheme 10B). Except for aminoalkyl (**87-90**) and dialkylketyl radicals (**91** and **92**), the activation energy of the other alkyl radicals correlates with enthalpy according to Evans-Polanyi relation, which means that the transition state structure is controlled by an enthalpic effect.

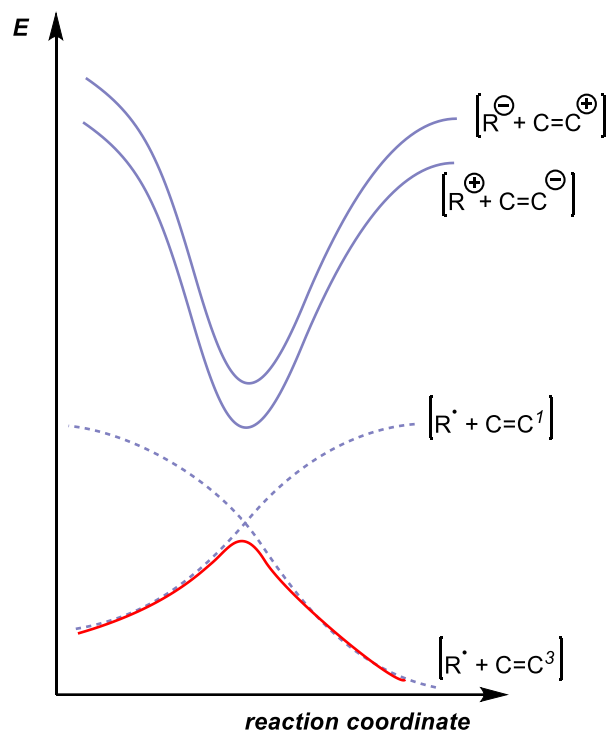


Figure 8: Configuration mixing for radical addition to alkene.

If the charge-transfer configurations contribute significantly, polar effects are observed. The energy of such configurations is expressed in terms of activation energy (AE) and ionization potential (IP) of radical and alkene (Equations 4 and 5). Due to the electrostatic behavior of this interaction, a coulombic contribution C is depicted, but often neglected.

$$E ([R^{\oplus} + C=C^{\ominus}]) = IP_R - AE_{C=C} - C \quad (4)$$

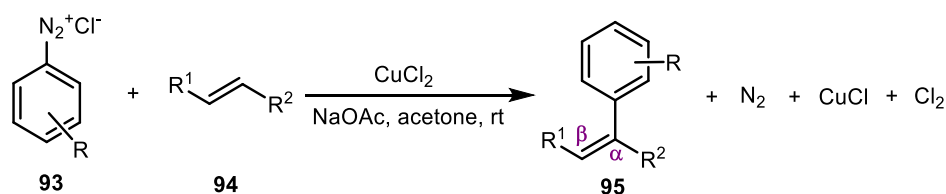
$$E ([R^{\ominus} + C=C^{\oplus}]) = IP_{C=C} - AE_R - C \quad (5)$$

A consequence of these relations is the characterization of the radicals as nucleophilic or electrophilic relative to the alkene. If $E ([R^{\ominus} + C=C^{\oplus}]) > E ([R^{\oplus} + C=C^{\ominus}])$ the latter configuration is more stabilized than the former, which means that the radical has nucleophilic behavior and the alkene acts as the electrophile. The opposite analysis is true: when $E ([R^{\ominus} + C=C^{\oplus}]) < E ([R^{\oplus} + C=C^{\ominus}])$, the radical is the nucleophile and alkene the electrophile.

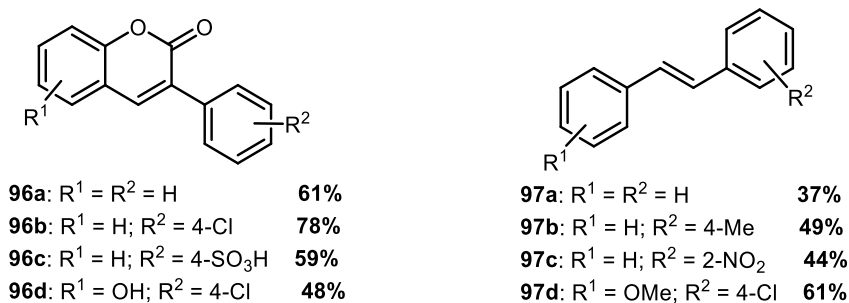
1.2.2. The Meerwein arylation reaction

The use of radicals to promote arylations is studied since 1939 when Meerwein et al reported the arylation of unsaturated compounds **94** using diazonium salts **93** in the presence of CuCl_2 in acid buffer at room temperature (Scheme 11).⁴¹ A large scope of unsaturated compounds and diazonium salts were employed. As examples, the arylation of coumarin (**96a-d**) showed the insertion of aryl group at position C3 in reasonable yields and styrenes were arylated at β carbon (**97a-b**).

A) Meerwein arylation (1939)

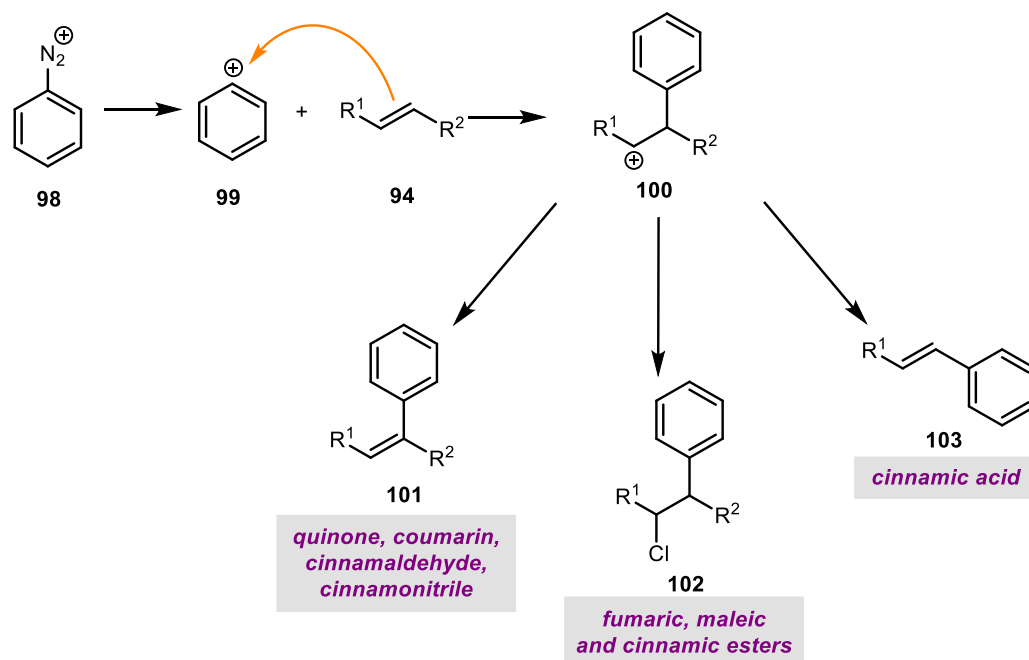


B) Selected examples



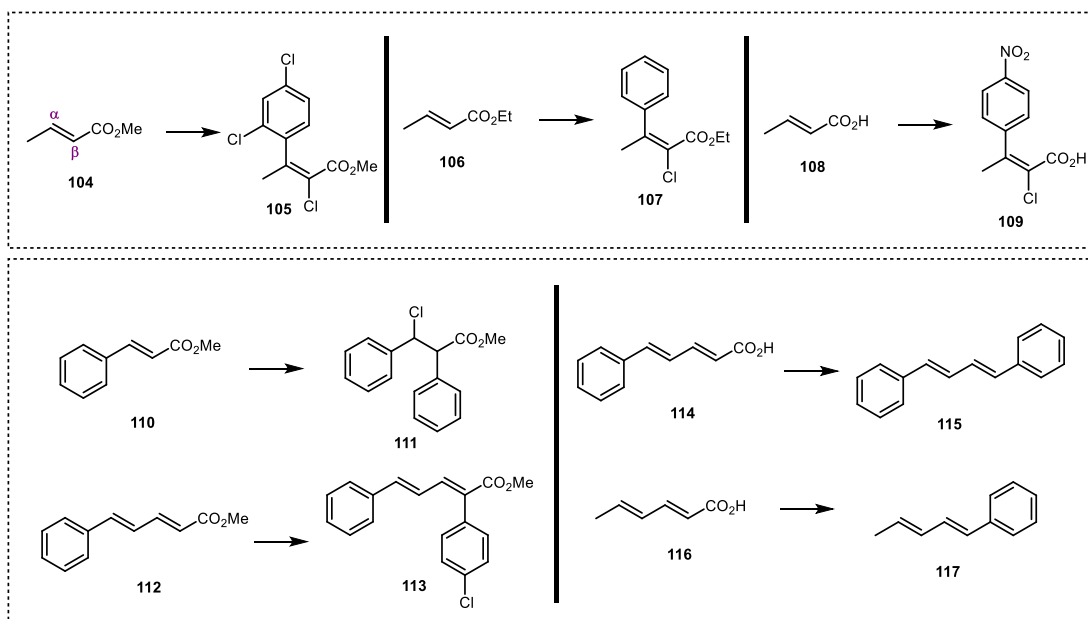
Scheme 11: Meerwein arylation and selected examples.

The authors proposed that diazonium salt decomposes to form phenyl cation **99**. Then, $\text{C}=\text{C}$ bond attacks **99** generating the intermediate **100**. This cation can undergo different mechanisms depending on the nature of the alkene. Quinones, coumarins, cinnamaldehydes and cinnamonnitriles suffer elimination to give a product like **101**. Fumaric, maleic and cinnamic esters generate the product **102**, where chloride anion, the counterion of diazonium salt, attacks the carbon that is the positive charge center. Finally, when cinnamic acid is used, the product **103** is observed; in this case, the carboxylate anion attacks the positive carbon followed by elimination of CO_2 (Scheme 12).



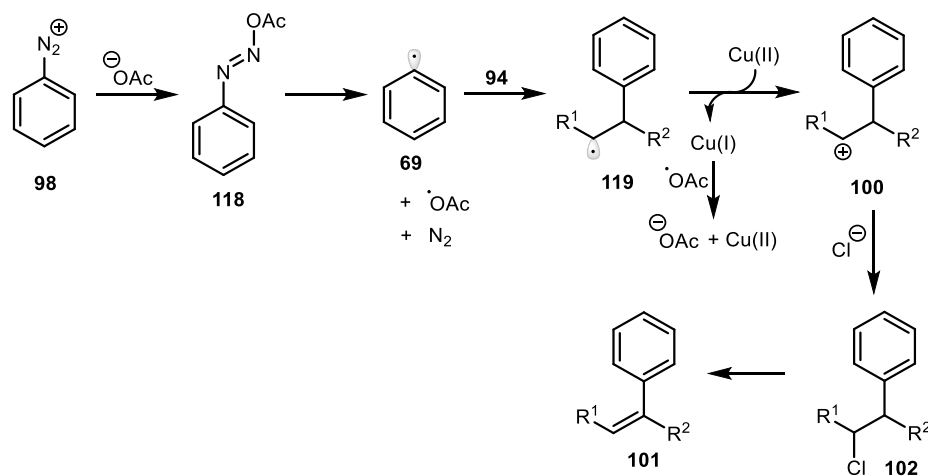
Scheme 12: First proposed mechanism of the Meerwein arylation.

According to Rondestvedt, this mechanistic proposal fails at one point. Alkenes with EWG at the attacked carbon gave the best results; however, these compounds are low reactive towards electrophilic additions.⁴² Koelsch and Boekelheide carried out Meerwein conditions to a large scope of α,β -unsaturated compounds.⁴³ They observed the same trend of Meerwein: when the phenyl group bonds to the α -carbon (**104**, **106** and **108**), the chloride anion bonds to the β -carbon (**105**, **107** and **109**). The phenyl group bonds to the β -carbon when there is a Ph group (**110**) or dienes (**112**, **114** and **116**). The former produces **111**, where the double bond was not formed. As for the dienes cases, two situations were possible: if an ester was bonded to β -carbon this group was maintained in the product **113**; however, when a carboxylic acid was bonded, there was a decarboxylation, forming the conjugated alkenes **115** and **117**.



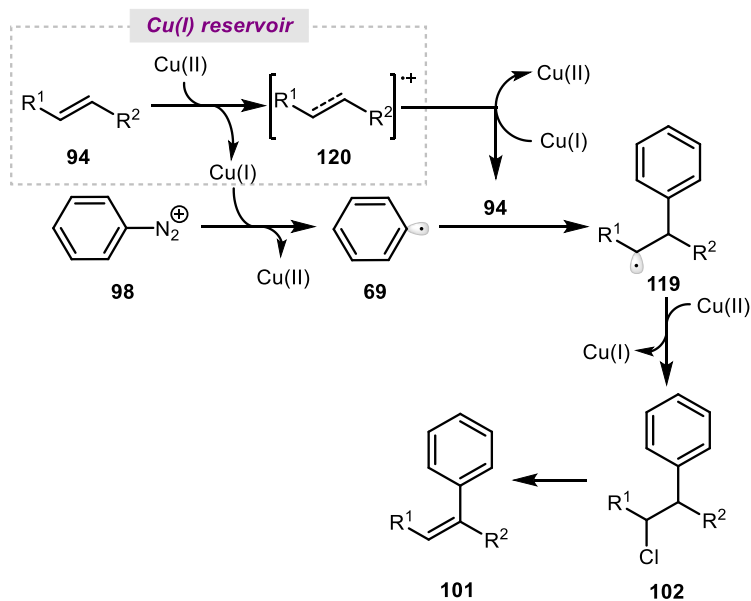
Scheme 13: Selected examples of the different products obtained by the Meerwein reaction as a function of the alkene.

The authors proposed that diazonium salt **98** cannot decompose by itself; it needs to react with acetate anion to make a diazoacetate species **118** that is prone to cleave the C-N bond into phenyl radical **69** and acetoxy radical. The next step is the radical attack to **94**. It was observed that **69** prefers to attack the carbon in which the intermediate is better stabilized by resonance. The role of the copper catalyst is to oxidize **119** to afford the cation **100**. Anion chloride attacks the positive carbon, generating **102**, and gives the product **101** after elimination (Scheme 14).



Scheme 14: Mechanism of the Meerwein arylation based on the formation of diazoacetate species.

Obushak et al suggested a third mechanism to Meerwein's arylation (Scheme 15).⁴⁴ The authors proposed that Cu(I) is the active species that reduces the diazonium salt to phenyl radical, although the reaction setup needs a Cu(II) salt as catalyst. They believe that the excess of alkene would act as a reservoir of Cu(I) species by donating an electron to Cu(II) and forming the radical cation **120**, which could be recovered by reduction of Cu(I). Once **69** is formed, the radical addition is followed as it is known.



Scheme 15: Mechanism of the Meerwein arylation based on the Cu(I) as the active species of the catalysis.

However, Bondarchuk and Minaev say that decomposition of diazonium salt to phenyl radical is impossible at the ground state.⁴⁵ They calculated, by Hartree-Fock (HF) theory, that LUMO of **98** is located at C-N bond ($\sigma_{\text{C-N}}^*$), suggesting that excitation would stretch this bond. The $S_0 \rightarrow T_1$ transition is prohibited and the organic species needs, initially, $S_0 \rightarrow S_1$ so that $S_1 \rightarrow T_1$ occurs by ISC. However, they found that S_1 level of diazonium salt is so high that this transition is neglectable.

The reaction needs water to work. In aqueous media with an excess of Cl⁻, Cu(II) exist as $[\text{CuCl}_4]^{2+}$, a tetrahedral complex with split 3d orbital.⁴⁶ The electronic configuration $[\text{Ar}]3d^94s^0$ suggests that an unpaired electron is at d_{xy} orbital. The approximation of diazonium salt to $[\text{CuCl}_4]^{2+}$ would cause a metal-to-ligand donation where an electron at HOMO orbital of **98** is donated to 4s orbital of $[\text{CuCl}_4]^{2+}$ at the same time that the unpaired electron of t_2 level is donated to LUMO (Figure 9). Then,

the electron at 4s orbital relaxes to t_2 . The magnetic moment is conserved and diazonium salt is promoted to triplet state without passing through any excited singlet state. After the excitation, the Cu(I) species promotes the fragmentation, generating the phenyl radical.

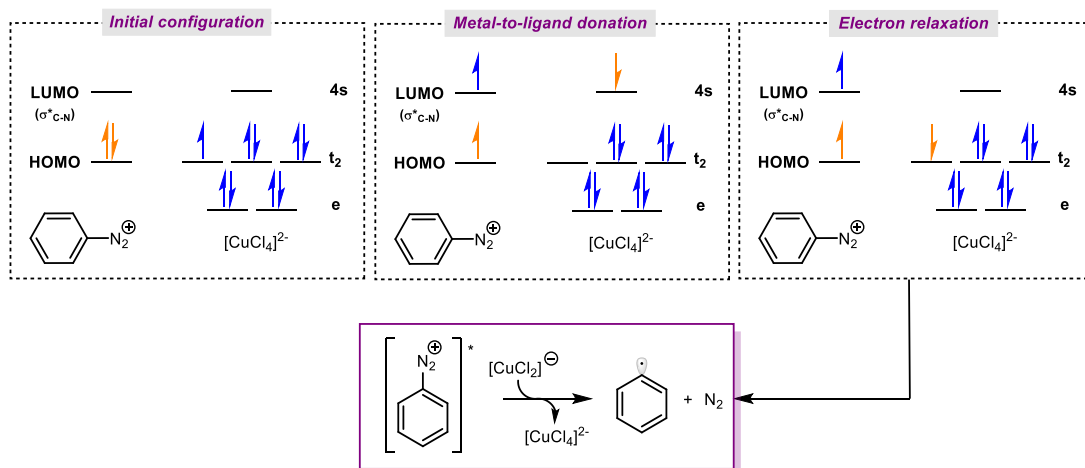
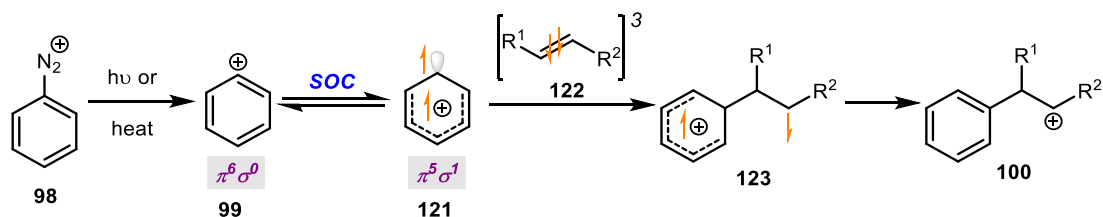


Figure 9: The excitation of diazonium salt promoted by $[\text{CuCl}_4]^{2+}$ as a spin catalyst followed by formation of phenyl radical.

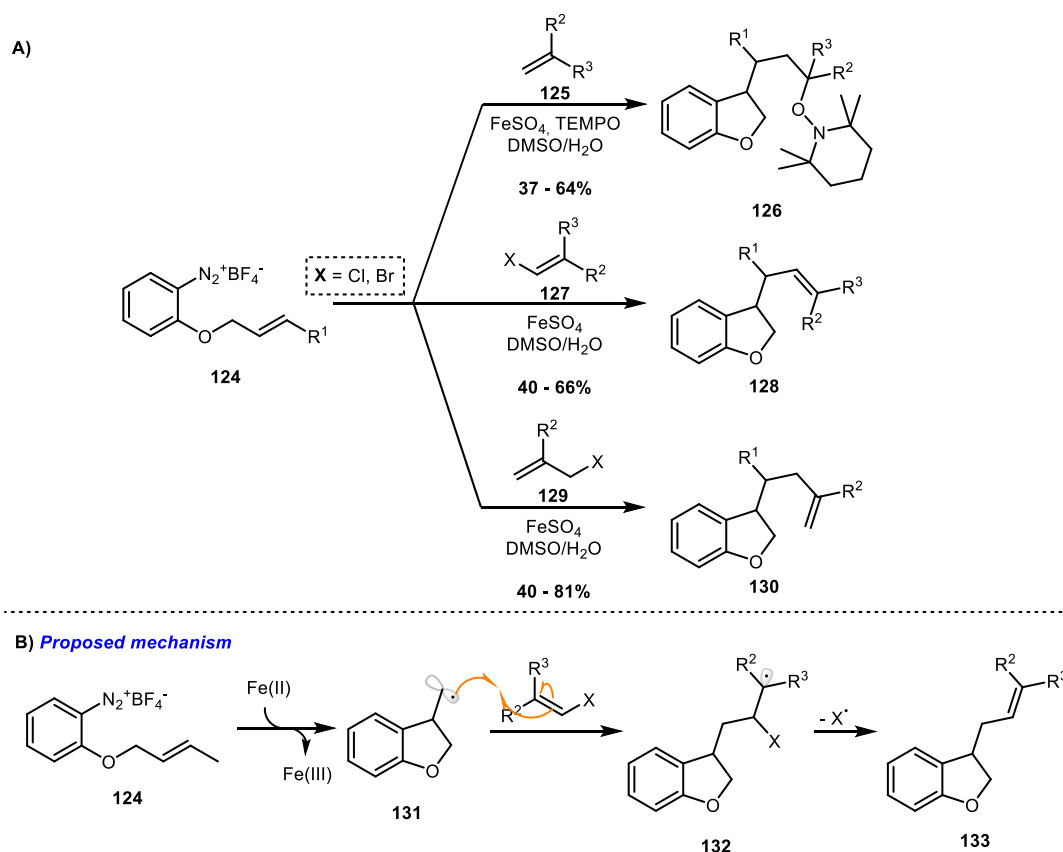
The Obushak's mechanism and the above triplet excitation model have a fail: several reports show that Meerwein reaction can work with no catalyst.^{44–47} Bondarchuk and Minaev again turned their attention to this reaction to understand the mechanism with no copper salt (Scheme 16).⁴⁸ They believe that light or heating could break C-N bond to make **99**. This species can undergo spin-orbital couple (SOC) to generate a triplet $\sigma\pi$ cation **121**. It happens because triplet state of aryl cations is low energy and $S \rightarrow T$ transition is allowed.^{49,50} This reactive intermediate causes $S \rightarrow T$ transition of an alkene to give **122**; they react to give the excited singlet diradical cation **123** and, finally, are transformed into the carbocation **100**. The mechanism proceeds as previous approaches.



Scheme 16: Mechanism of the Meerwein arylation based on spin-orbital couple.

A drawback of the Meerwein arylation is the limited scope. As pointed by the seminal paper, this reaction works only with alkenes with EWG⁴¹, but this arylation is still important and deserves more research. In a recent review, Kindt and Heinrich highlight the actual directions in this area.⁵¹ The discovery of new aryl radical sources and reaction conditions are popular, but increasing the substrate scope is also important.

Heinrich et al showed that **124** can undergo intramolecular *5-exo-trig* cyclizations in the presence of stoichiometric amounts of FeSO₄ which act as a reducing agent (Scheme 17A).⁵² Substituted 2,3-dihydrobenzofurans (**126**, **128** and **130**) were obtained in moderate yields. The authors proposed that, after the reduction of diazonium salt by Fe(II) salt and cyclization, the intermediate **131** attacks the alkene to form **132** (Scheme 17B). Then, the liberation of a halogen radical occurs after elimination. This radical is quickly reduced to form halide anion, preventing undesired side reactions. Trapping **132** with TEMPO to obtain the class of products **126** was also used by Studer et al.⁵³ Later, they also reported that diazonium salts can be generated *in situ* by adding MeSO₃H and isoamyl nitrite in the reaction media.⁵⁴



Scheme 17: Intramolecular 5-exo-trig cyclizations catalysed by Fe(II).

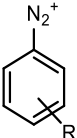
1.2.3. Obtention of phenyl radicals

Phenyl radicals have an important role in many areas and not exclusively in organic synthesis. In Biochemistry, for example, the metabolism of aniline in the human body generates phenyl radical by the action of myeloperoxidase (MPO).⁵⁵ This radical attacks MPO, generating MPO• at neutrophils, which causes its depletion (agranulocytosis). Such side reaction is associated with toxic side-effects of aniline containing drugs. Siraki et al showed that polyunsaturated fatty acids can trap such radicals preventing the reaction with MPO and, hence, agranulocytosis.⁵⁶

It is remarkable that Meerwein reaction was used as a model to study phenyl radical additions to alkenes. Besides Meerwein mechanism that proposed the formation of a phenyl cation, all other proposals have in common the formation of phenyl radicals, a reactive intermediate that could explain the reactivity discussed above. Galli in his review details the timeline of the radical approach.⁵⁷ The advantage of using phenyl radicals in arylation reactions is the adoption of mild conditions.⁵⁸

Diazonium salts are good candidates to generate them because they are easy to make, stable when BF_4^- and PF_6^- are the counterions, and easy to be reduced based on their reduction potentials (Table 1). The positive values indicate that they are good oxidants and, in other words, prone to be reduced. EWG increase the potentials, while EDG decreases them. This trend was confirmed by the linear fit between $E_{1/2}$ and Hammett σ^+ constants with positive slope ($\rho = 0.229$).⁵⁹

Table 1: Reduction potentials of substituted diazonium salts in sulfolane.⁵⁹

	R	$E_{1/2}$ vs. SCE (V)	R	$E_{1/2}$ vs. SCE (V)
		4-NO ₂	0.450	4-Me
	4-CN	0.433	4-OMe	0.140
	4-Cl	0.350	4-NMe ₂	-0.095
	4-Br	0.383	3-Cl	0.410
	4-I	0.383	3-Me	0.285
	4-CO ₂ ⁻	0.328	2-Cl	0.410
	H	0.295	2-OMe	0.153

Besides the use of such compounds as sources of phenyl radicals, other compounds were used to generate them. Aryl halides are good candidates for this proposal. They are commercially available, ready to be used, bench-stable in reactions, and inexpensive. The drawback of these compounds is related to their high reduction potentials (Figure 10).⁶⁰⁻⁶²

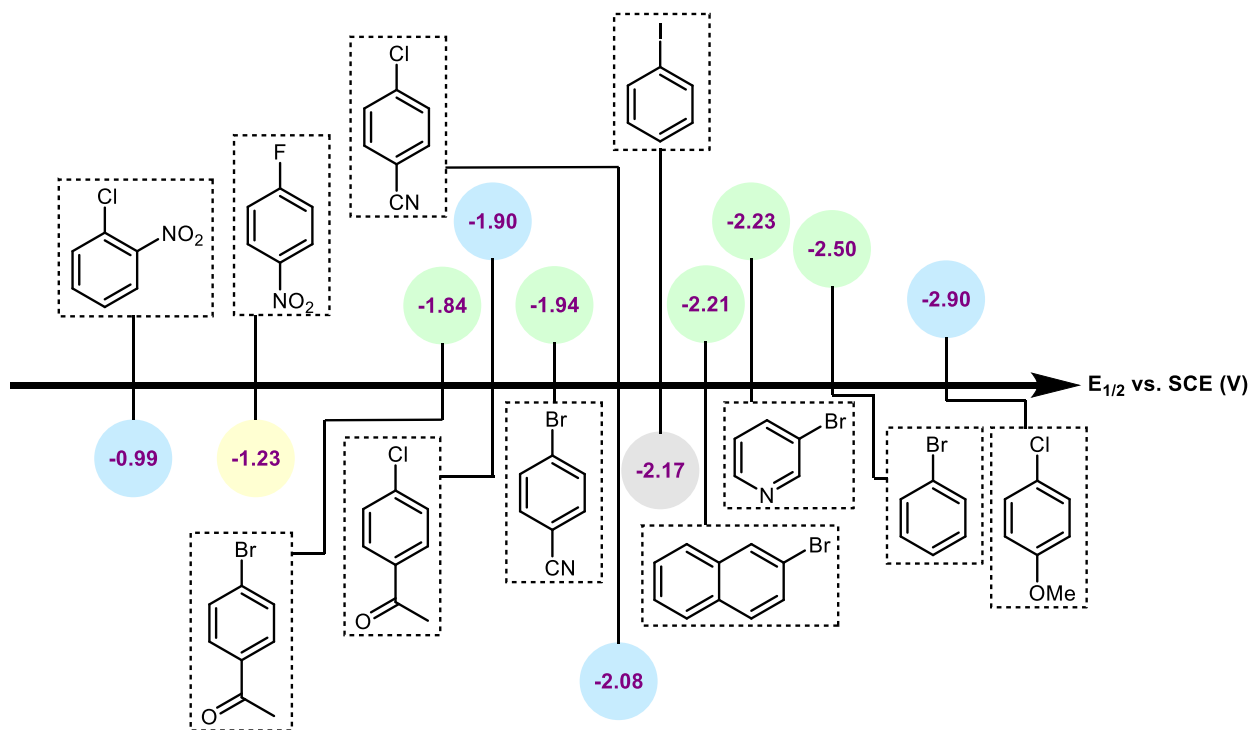
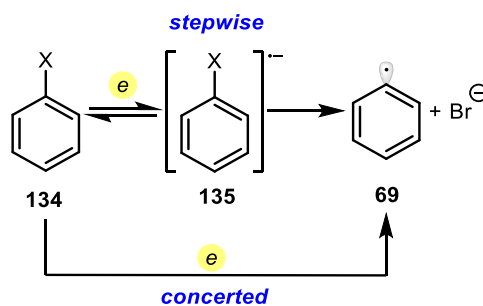


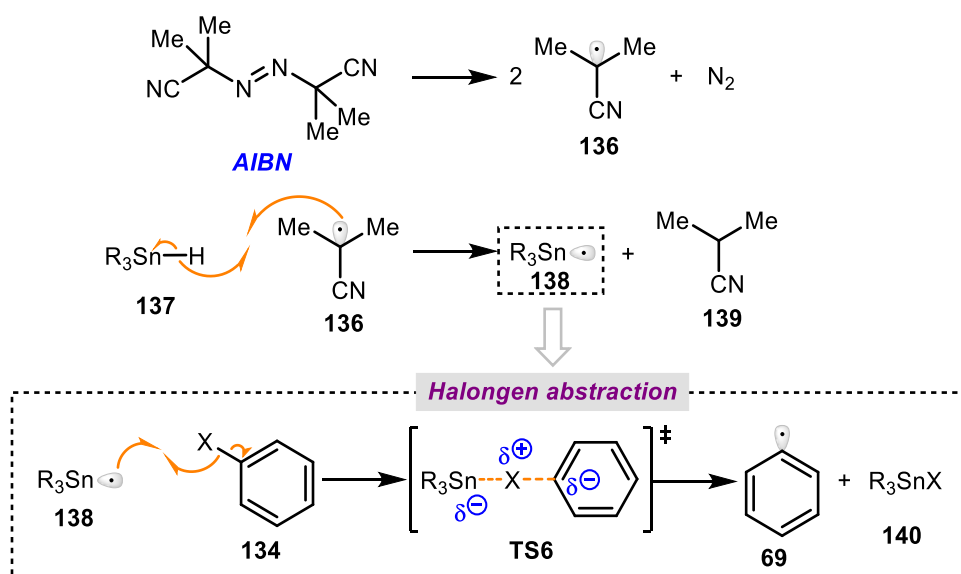
Figure 10: Selected reduction potentials of aryl halides.

Two possible mechanisms are proposed to reduction of **134** (Scheme 18).⁶³ The first is based on reduction to form a radical anion **135**, which undergoes fragmentation to afford **69** and halide anion. A concerted mechanism could also be plausible. For bromo- and chlorobenzene, the stepwise mechanism is preferred due to the large bond dissociation energy of C-Cl and C-Br bonds and a low-level π^* orbital able to accommodate foreign electrons. Iodobenzene is a borderline case and the mechanism is apparently a transition between concerted and stepwise, where increasing the temperature favors the former.



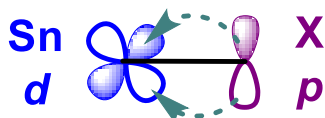
Scheme 18: Possible mechanisms to reduction of aryl halides to phenyl radical.

Many types of methodologies were developed to generate phenyl radicals from aryl halides. One of the most popular is the use of tin hydrides.⁶⁴ Tributylstannane ($n\text{Bu}_3\text{SnH}$) is widely used as a source of $n\text{Bu}_3\text{Sn}^\bullet$ radical, which can make homolytic halogen abstractions to generate carbon-centered radicals.⁶⁵ Therefore, to generate the tin radical, an initiator, like azobisisobutyronitrile (AIBN), must be used to abstract the hydride (Scheme 19). AIBN decomposes into the radical **136** and abstracts the hydride **137** forming **139**. Once in the reaction media, **139** can undergo halogen abstraction. The driving force of this transformation is that tin radicals have higher nucleophilic character than carbon-centered ones, so polar factors stabilize **TS6** and the reaction works.⁶⁶ The Hammett correlation of chloride abstraction to generate benzylic radicals with tributylstannane have a positive slope ($\rho = 0.81$), confirming that tin radical is nucleophilic.⁶⁷

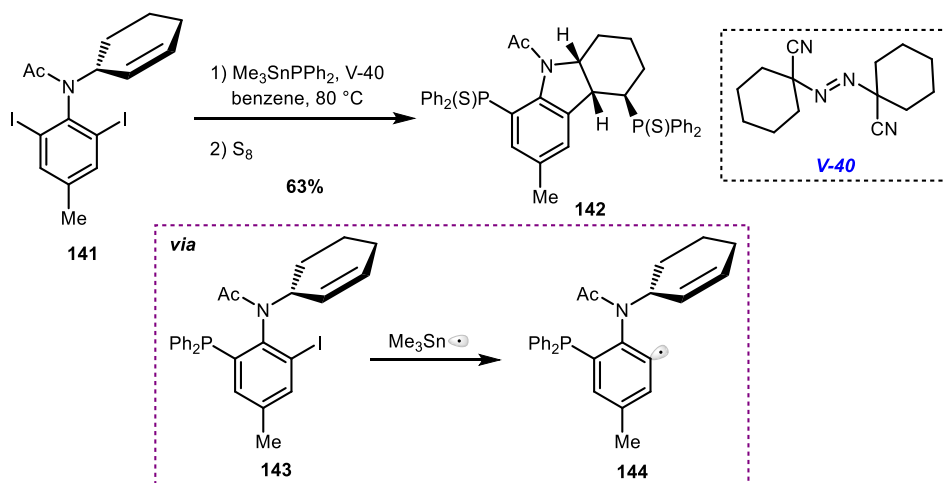


Scheme 19: General mechanism of phenyl radical formation by tin hydrides.

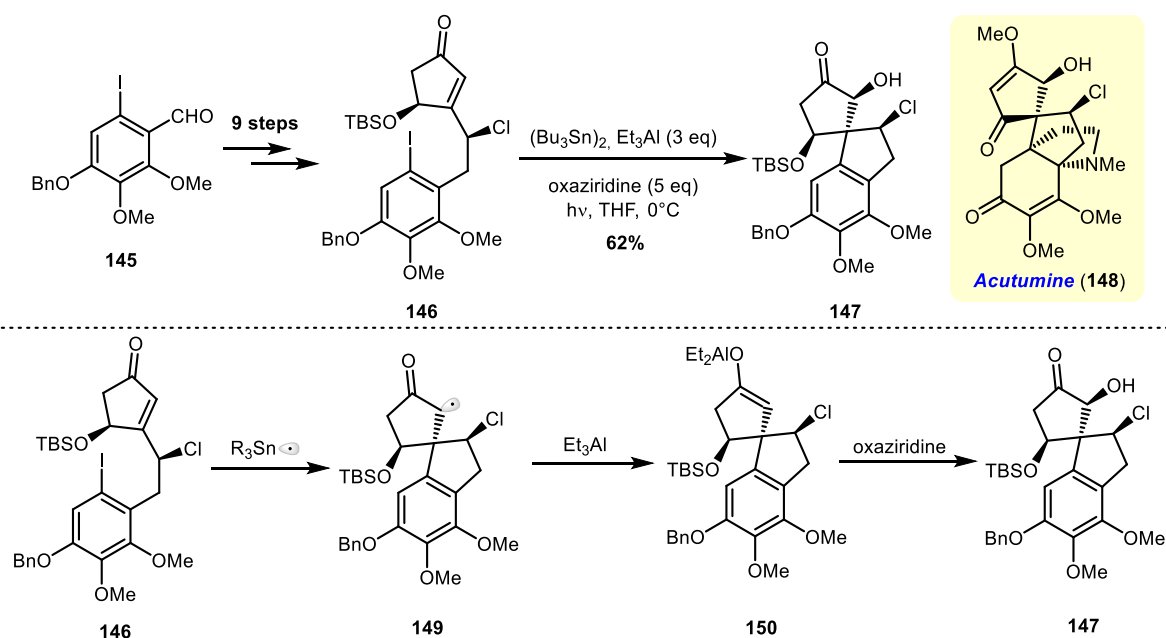
The “halophylic” character of tin radicals can be explained in terms of Molecular Orbital (MO) Theory.⁶⁸ Sn-X bonds are weaker than C-X bonds, which could be a drawback to such transformation. However, halogens can donate their lone pairs at p orbitals to tin through its *d* empty orbitals (Figure 11). Such interaction is not possible at C-X bonds, as carbon does not have empty *d* orbitals available.

Figure 11: The *d-p* orbital interaction at Sn-X bond.

The intramolecular version of this approach was widely used in the synthesis of cyclic compounds. Curran et al treated **141** with 6 equivalents of $\text{Me}_3\text{SnPPh}_2$ in the presence of V-40 as initiator (Scheme 20).⁶⁹ The first iodine atom is replaced by PPh_2 group to give **143**, while the second is responsible to generate the radical **144** that attacks the C=C bond of cyclohexenyl ring. After treatment with S_8 the product **142** was achieved in 63% yield.

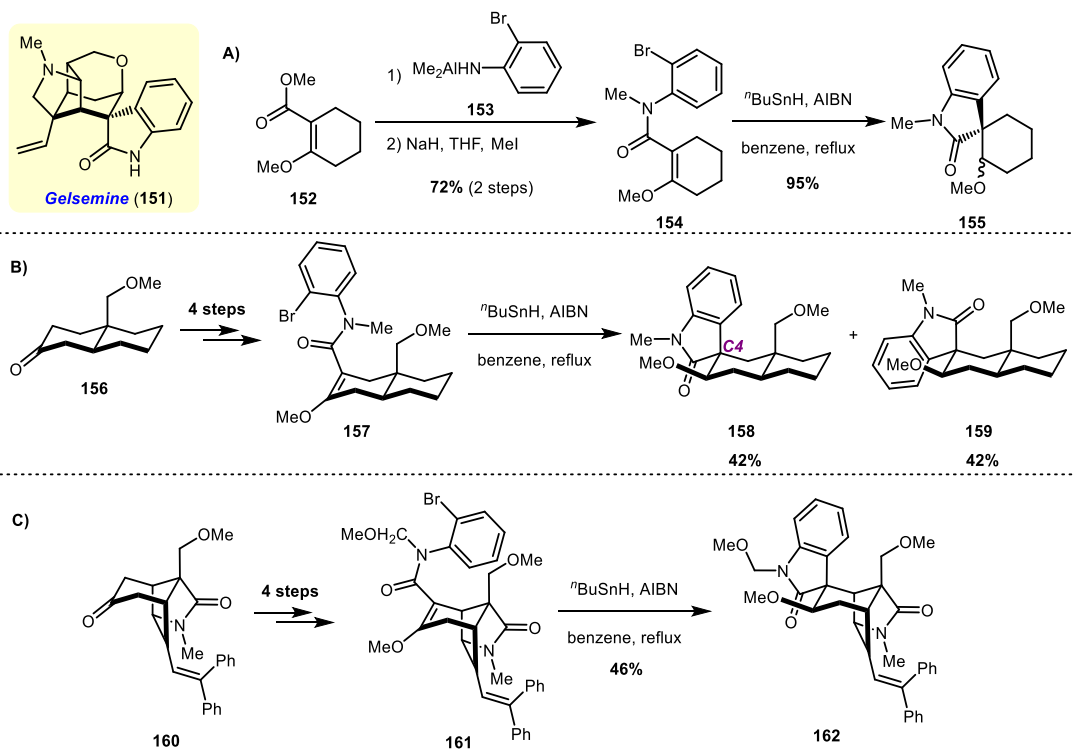
Scheme 20: Synthesis of **142** by intramolecular cyclization using $\text{Me}_3\text{SnPPh}_2$.

Li and Castle synthesized the spirocycle analogous of acutumine (**148**) (Scheme 21), an alkaloid isolated from *Menispermum dauricum*, isolated from an Asian vine.⁷⁰ Starting from **145**, after 9 steps the intermediate **146** was obtained, the precursor of spirocycle. The authors used $(\text{Bu}_3\text{Sn})_2$ as an initiator to make the radical **149**, which attack the C=C bond in a 5-*exo-trig* cyclization. At the same pot, a radical-polar crossover was achieved using Et_3Al to give **150** followed by hydroxylation with oxaziridine to afford **147**. The spirocyclization was afforded in 62% yield.



Scheme 21: Synthesis of **147** by intramolecular cyclization with $(\text{Bu}_3\text{Sn})_2$ as intermediate of the synthesis of acutumine

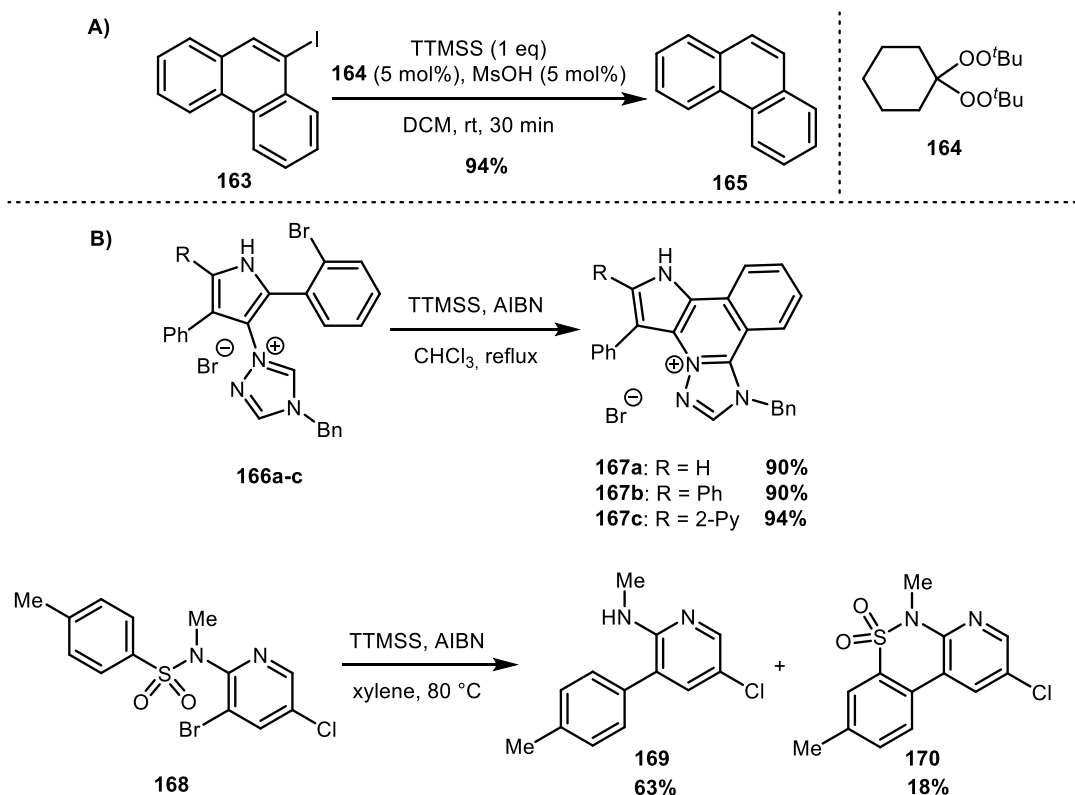
Hart and Wu were interested in the synthesis of gelsemine (**151**).⁷¹ Starting from **152**, they obtained the intermediate **154**, after treatment with dialkylaluminum **153** followed by amide methylation, in 72% yield (Scheme 22). Then, the use of $n\text{BuSnH}$ combined with AIBN allowed the spirocyclization to achieve **155** in 95% in equal amounts of diastereomers. These reactions were used as a model to the synthesis of **151**. Compound **156** was used as starting material and, after 4 steps, **157** was prepared. Treatment with tin hydride and AIBN gave **158** and **159** in 42% each. If the alkyl group bonded to the amide nitrogen is bulkier, it would induce the formation of the right stereochemistry at C4. So then they tried a new route starting with the available **160** and, after 4 steps, submitted **161** to radical arylation and obtained **162** in 46% as a gelsemine analogue.



Scheme 22: Total synthesis of a gelsemine analogue.

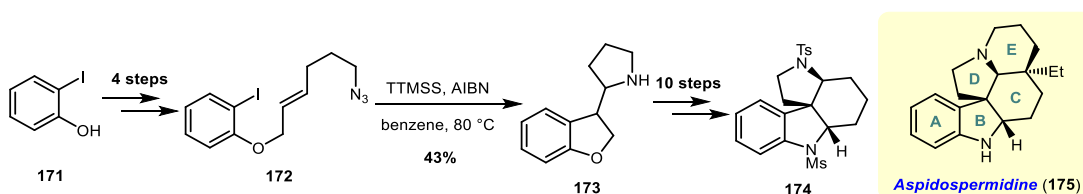
Silicon would be expected to have similar properties as tin. They are elements of group IV and Si also has available *d* orbitals to interact with halogens making Si-X bonds.⁶⁸ Silane compounds are the ones that have Si-H bonds. Compounds like $(\text{TMS})_3\text{Si-H}$, called as supersilane or TTMSS, have Si-H bonds weaker compared to $\text{Me}_3\text{Si-H}$ according to their bond dissociation energy (83.7 and 94.6 kcal/mol, respectively).^{72,73} The radical $(\text{TMS})_3\text{Si}^\bullet$ is more stable than $\text{Me}_3\text{Si}^\bullet$ and more capable of abstracting halogens.^{72,74}

The mechanism associated with halogen abstraction to generate phenyl radicals is like stannanes. AIBN can be used as an initiator to generate $(\text{TMS})_3\text{Si}^\bullet$.^{75,76} Reports show the reductive dehalogenation of **163** to give phenanthrene **165**⁷⁷ (Scheme 23A) and generation of phenyl and heterophenyl radicals followed by radical trapping to make C-C bonds (Scheme 23B).^{78,79}



Scheme 23: The use of TTMSS in the reductive dehalogenation of aryl halides.

Kizil and Murphy used TTMSS approach in a step of synthesis of a tetracycle found in indole alkaloids like aspidofermidine (**175**) (Scheme 24).⁸⁰ Starting from **171**, the intermediate **172** was obtained after 4 steps. The treatment with TTMSS in the presence of AIBN afforded **173** in 43% yield. After 10 steps, the desired tetracycle **174** was achieved.



Scheme 24: Synthesis of the tetracycle **174**.

1.2.4. Kinetics of phenyl radical addition to C=C bonds

The study of kinetics provides some information about the reaction mechanism, which is useful for synthetic purposes. The evaluation of rate constants

was a popular field of study in Organic Chemistry in the 70's and 80's. Techniques like laser flash photolysis and time resolved measurements are used to photogenerate radicals in the presence of a substrate to trap it. The former technique is based on the absorption of photons with specific wavelength emitted from a pulse laser. In the desired reaction, the C-X bond is photochemically broken to generate phenyl radicals. This approach can measure rate constants for the radical addition step. For this, the following mechanism is considered:

Initiation



Phenyl radical addition



Once the radical is formed, the aryl radical addition step dictates the reactivity, *i.e.*, the radical addition to the unsaturated compound is the rate-determining step, as previously reported.⁸¹⁻⁸³ Phenyl radicals can either promote hydrogen atom abstractions or additions to π -systems, with the latter tending to be faster. The work of Skoutchi et al was one of the first reports to study phenyl radical additions to olefins.⁸⁴ The authors tried to use kinetic data to understand the mechanism of Meerwein reaction. The reactions were carried out mixing excess of the alkene with diazonium salt at room temperature under nitrogen atmosphere. The complete data set is shown at Table 2.

Table 2: Relative kinetic constants for phenyl and *p*-chlorophenyl radical addition to different alkenes.

Alkene	69		181
	k_d/k_{177}	k_d/k_{179}	k_d/k_{177}
70	0.86±0.02	0.74±0.02	1.47±0.03
176	0.79±0.03	0.69±0.02	0.97±0.04
177	1.00	---	1.00
178	1.07±0.01	0.93±0.06	1.52±0.06
179	---	1.00	---

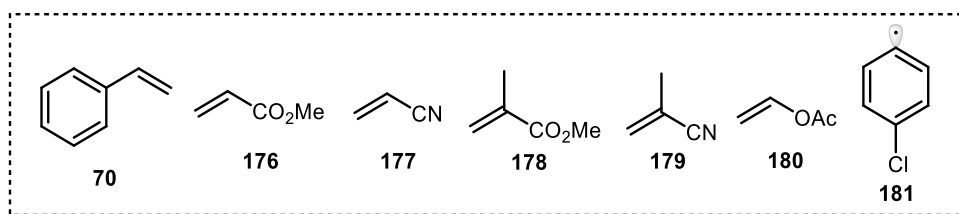


Figure 12: Alkenes and phenyl radicals studied by Skoultchi et al.

Styrene (**70**) showed a significant change in reactivity when a chlorine atom is present at phenyl radical. Its reactivity increased, which evidenced the presence of polar effects acting on phenyl radical. As chlorine is an EWG, it makes the radical more electrophilic and **70** would act as a nucleophile. The same trend was observed to the other alkenes. Methyl acrylate (**176**) was less reactive than acrylonitrile (**177**), which suggests that the CN group tends to stabilize more the radical adduct formed. However, when a methyl group is bonded to the not attacked carbon (**178**), k_{rel} increases compared to **176**, suggesting that the reactivity also increases.

The reactivity under polymerization conditions was investigated by Bevington and Ito.⁸⁵ Benzoyl peroxide was used as phenyl radical source and the reactions were carried out in the presence of DMF at 60°C. The authors observed that addition to styrene is almost 12 to 20 times faster than hydrogen abstraction. As shown above, **178** is more reactive than **70** and the rise in temperature increases the reactivity difference (Table 3). On the other hand, vinyl acetate (**180**) is much less reactive than **70**. It clearly indicates that EWG-activated alkenes react faster than the deactivated vinyl acetate.

Table 3: Relative rate constants for phenyl radical additions at 25 and 60 °C obtained by Bevington and Ito.

Temperature (°C)	70	178	180
60	1.0	1.7	0.08
25 ⁽⁸⁴⁾	1.0	1.2	---

Pryor and Fiske observed the same kind of results of Bevington and Ito (Table 4).⁸⁶ It is clear that the activation of alkene increases the reactivity. Compounds **180** and **182** were 3.4 and 1.7 times, respectively, less reactive than **176**. Adding substituents at the not attacked carbon increased reactivity, as reported previously by Skoultchi et al. Surprisingly, **185** was 2.17 times more reactive than styrene. The attack promotes the formation of a radical adduct stabilized by resonance, but the

presence of a heteroatom increased such stability. Kirschstein et al. showed that addition to **182** is 10 times slower than addition to ethyl acrylate.⁸⁷

Table 4: Relative rate constants of phenyl radical addition obtained by Pryor and Fiske.

Alkene	k_x/k_{64}	Alkene	k_x/k_{64}
70	1.0	184	1.24
180	0.23	178	1.78
182	0.46	185	2.17
176	0.78	178	2.46
183	0.79		

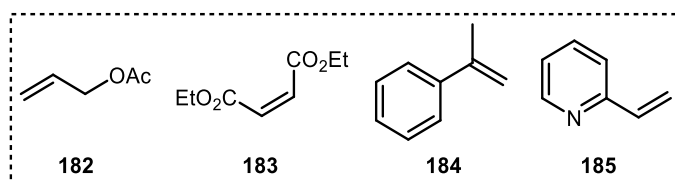


Figure 13: Alkenes studied by Pryor and Fiske.

These three works above reported relative rate constants. Until that moment, no absolute data was published. Scaiano and Stewart obtained absolute rate constants for a series of phenyl radical reactions. The addition to **70**, **186** and **176** are considered fast processes, with rate constants ranging from 10^7 to 10^8 $M^{-1} s^{-1}$.⁸⁸ Preidel and Zellner found slower additions to **187**, **188** and **189** ($k = 1.2 \times 10^4$, 1.6×10^4 and 4.8×10^5 $M^{-1} s^{-1}$, respectively).⁸⁹ It proves that substituents that stabilize in a certain way the radical adduct increase the reaction rate.

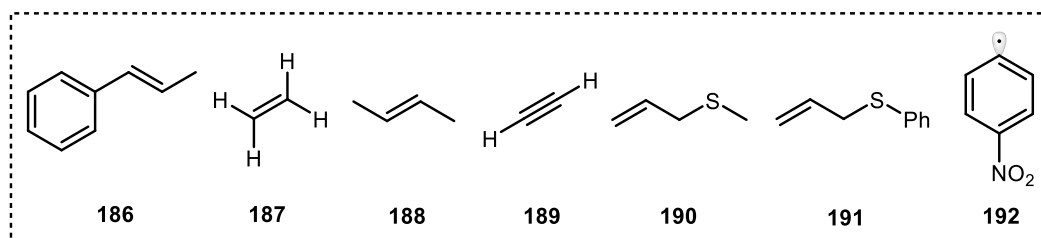


Figure 14: Alkenes and 4-nitrophenyl radical used in Scaiano and Stewart work.

The presence of EWG substituents at phenyl radical tends to increase the rate. Kosugi *et al.* observed that *p*-nitrophenyl radical (**192**) adds 10.7 times faster to allyl methyl sulfide (**190**) and 15.4 times faster to allyl phenyl sulfide (**191**).⁹⁰ Vismara *et al.* pointed that reaction of *p*-chlorophenyl radical to α,β -unsaturated carbonyl compounds

prefer the addition to α -carbon with rate constants ranging from 1.77×10^7 to 1.33×10^8 $\text{M}^{-1}\text{s}^{-1}$.⁹¹ DFT analysis, at B3LYP/6-311++G(d,p) level of theory, of the addition of phenyl radical to **176** revealed that phenyl radical had no remarkable nucleophilic or electrophilic character.⁹² Zhao *et al.* estimated that addition of *p*-chlorophenyl radical to vinyl acetate has $k = 2.7 \times 10^6$ $\text{M}^{-1}\text{s}^{-1}$.⁹³

Finally, the influence of solvent polarity was also evaluated for addition to **178** relative to **70** at 60 °C. Solomon *et al.*⁹⁴ observed that at apolar solvents like benzene and toluene the rates are similar ($k_{\text{rel}} = 1.00$ and 1.03, respectively). At polar solvents **70** tends to be less reactive ($k_{\text{rel}} = 1.22$ and 1.14 for acetone and butan-2-one, respectively).

1.3.

Photoredox α -arylation of carbonyl compounds

As shown above, radical arylations gained attention after the development of the Meerwein arylation. During the 80's and 90's, the use of tin hydrides to generate aryl radicals was desired as an efficient methodology. However, the use of tin complexes, which are highly toxic, is a disadvantage. Alternatives to generate such radicals are being researched. In this section, the use of photoredox catalysis is discussed as a platform for the α -arylation of carbonyl compounds. Such compounds have three preferential positions to be attacked by radicals (Figure 15).

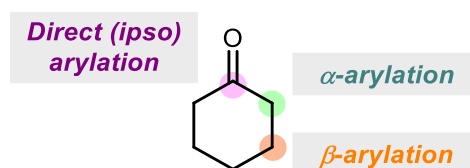
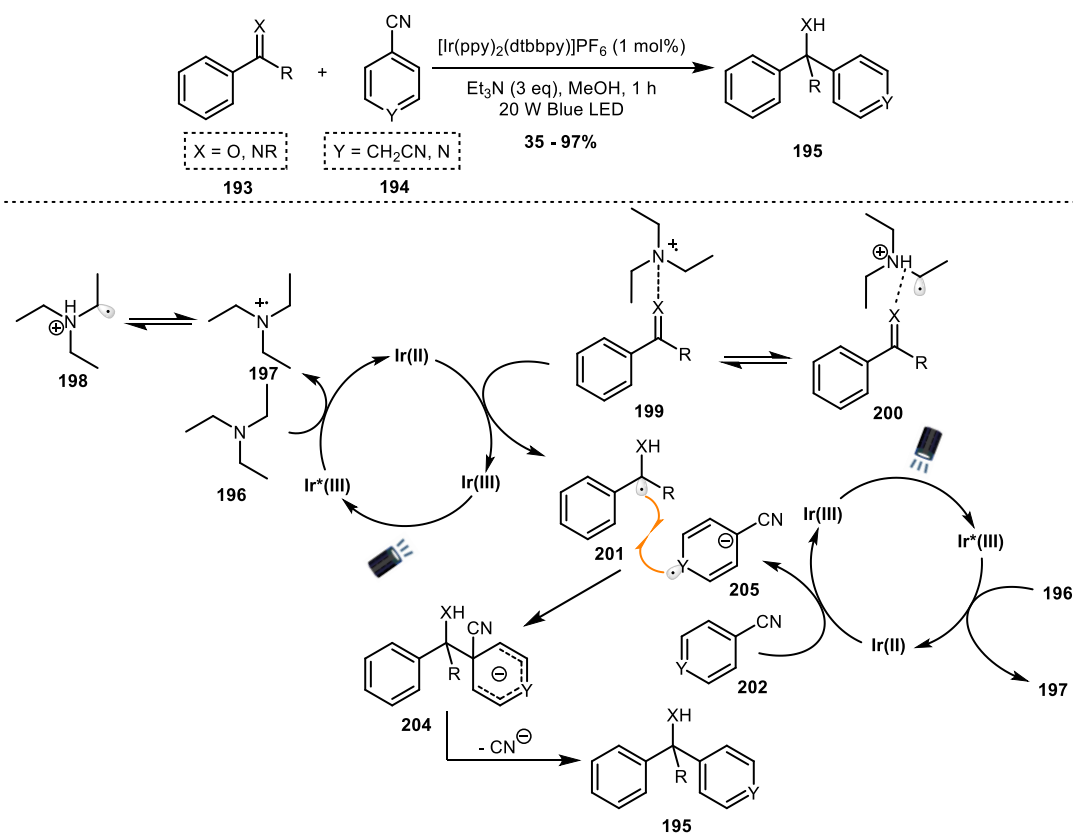


Figure 15: The possible positions of aryl radical attack onto carbonyl compounds.

The first direct arylation of carbonyl compounds was developed by Xia *et al.* (Scheme 25).⁹⁵ The reduction of $\text{C}=\text{O}$ and $\text{C}=\text{NR}$ bonds is a challenge and proton-coupled electron transfer (PCTE) showed great advances to this proposal.^{96,97} The authors suggested two photocatalytic cycles, each one generating a radical to combine and form the product. In both cases, Et_3N was used as a photocatalyst reducing agent. The radical cation **197** can act as Lewis acid (**199**) or its tautomer can

be a hydrogen bond donor (**200**). A PCTE reaction carries out to generate the radical **201**. The second cycle is responsible to generate the aryl radical reducing **202** to **203**. After radical combination (**204**) and loss of cyanide, the product **195** is achieved. This approach was supported by other kinds of ipso-functionalization.^{98–101}

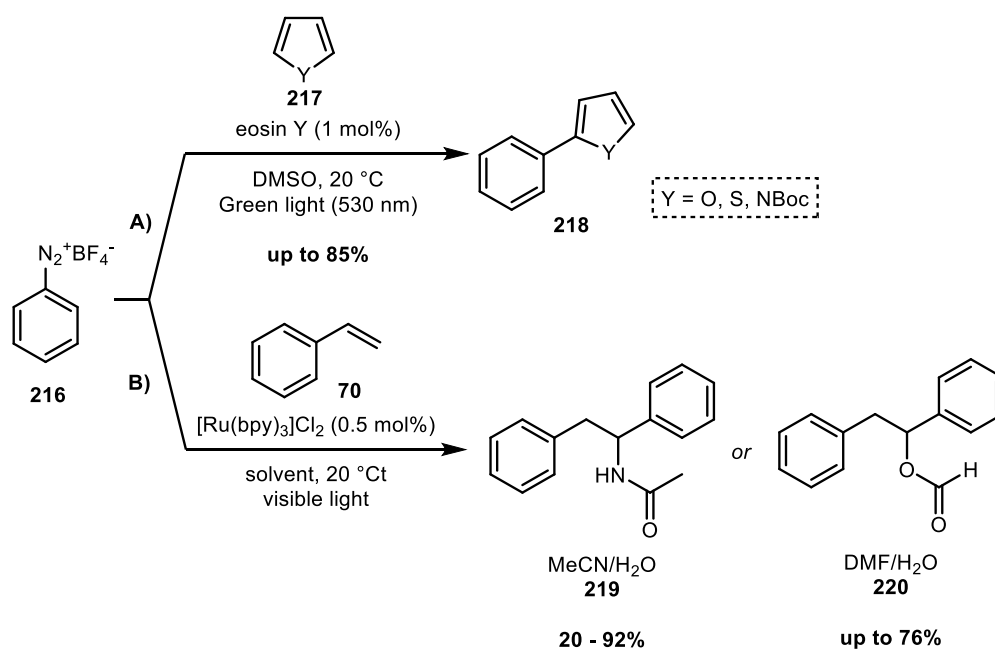


Scheme 25: Xia's direct arylation of carbonyl compounds.

The β -arylation was established by MacMillan et al based on the activation of enamides (Scheme 26).¹⁰² This methodology was an important advance in β -carbonyl functionalization, as usually such reaction is achieved by addition of soft nucleophiles to α,β -unsaturated carbonyls. The key step is the formation of the β -enaminy radical (**214**). The authors supposed that β C-H bond of radical cation **213** is weak and prone to ease deprotonation. The generated $5\pi e$ species **214** was able to couple with the radical anion **203** to give the intermediate **215** and, finally, the product **211**. The functionalization of β -position was further expanded to other kinds of radicals.^{103,104}

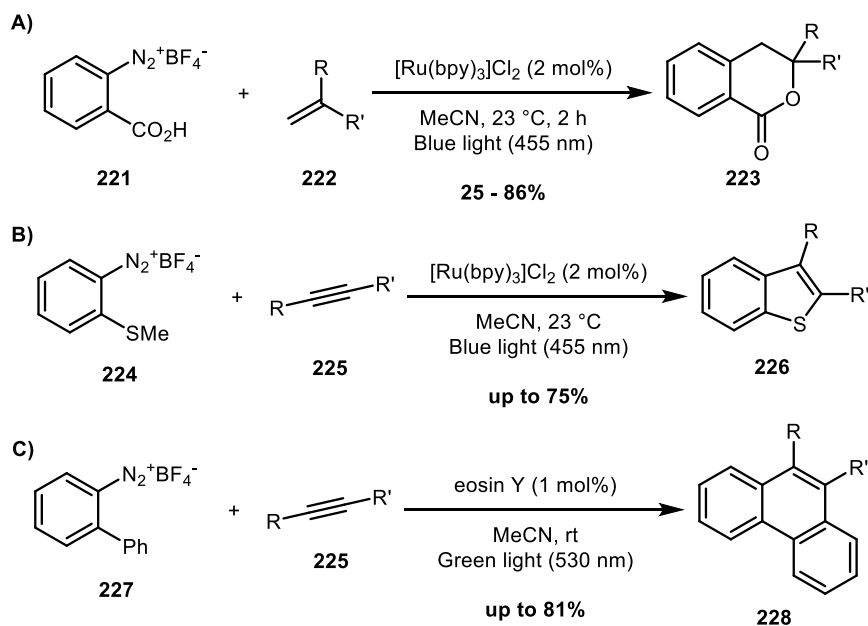
sources were presented: diazonium salts and aryl halides. Such compounds are extreme in a range of aryl radical sources based on reduction potentials. Diazonium salts have $E_{1/2} > 0$ V and are easy to be reduced. On the other hand, aryl halides have stronger C-X bonds and $E_{1/2} < -1.0$ V. Two extensive reviews discuss the use of these compounds and others as phenyl radical sources in photoredox catalysis.^{105,106}

As pointed out in the first photoredox reaction (Scheme 1), $[\text{Ru}(\text{bpy})_3]^{2+}$ can reduce diazonium salts by SET mechanism. The group of Prof. Burkhard König extensively used diazonium salts in arylations of heteroarenes (**217**) (Scheme 28A) and in Meerwein-like additions (Scheme 28B).



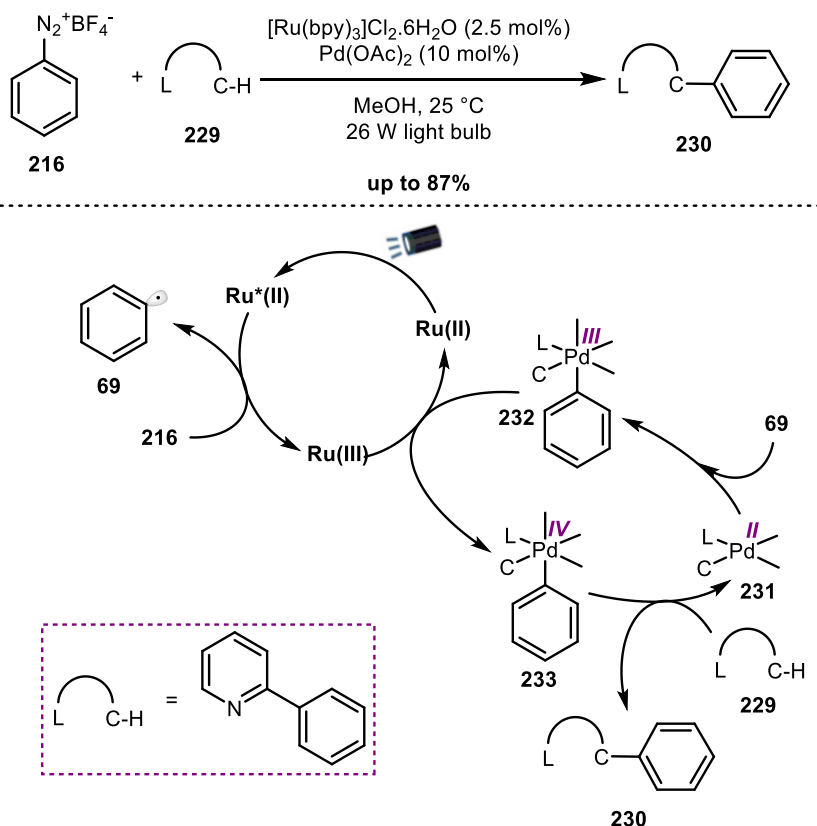
Scheme 27: Photoredox arylations with diazonium salts.

Additions with **221**, derived from anthranilic acid, could afford isochromanones and isochromenones (**223**) (Scheme 28A). Alkynes were also used to make benzothiophenes (**226**) (Scheme 28B) and phenanthrenes (**228**) in a Pschorr-like reaction (Scheme 28C).



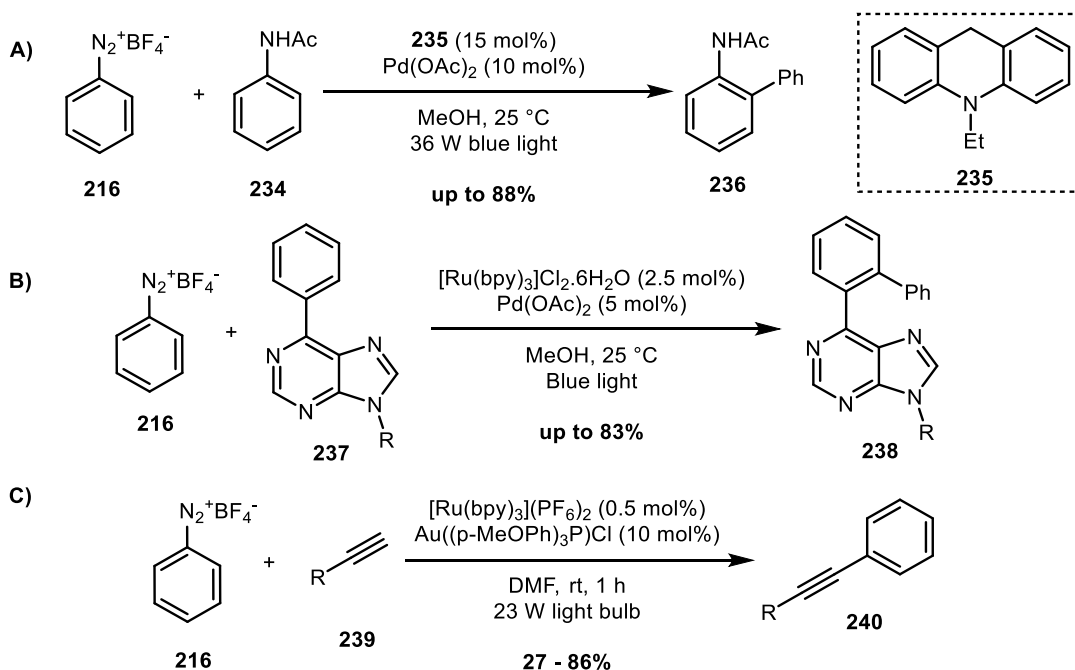
Scheme 28: Photoredox arylations of alkenes and alkynes followed by intramolecular cyclizations.

The arylation of heteroarenes can also be carried out by merging photoredox with other metals and cross-coupling reactions. Sanford et al developed ligand directed C-H arylations using $\text{Pd}(\text{OAc})_2$ (Scheme 29).¹⁰⁷ The reaction starts generating the radical **69** in the photoredox cycle. It coordinates to **231** thus forming a Pd(III) species **232** that is oxidized to Pd(IV) (**233**) by Ru(III) and the reductive elimination step gives the desired product **230**.



Scheme 29: Arylation of phenylpyridines with diazonium salts merging photoredox catalysis and cross-coupling reaction.

The combination of cross-coupling and photoredox catalysis as a dual catalysis approach became popular after Sanford's work. Xu et al prepared biphenyls (**236**) merging acridines as photocatalyst and Pd(OAc)₂ (Scheme 30A).¹⁰⁸ According to mechanistic experiments, they proposed that a palladacycle is generated *in situ* with starting acetanilides. Guo et al promoted selective arylation of 6-arylpurine nucleosides (**237**) with tolerance to a large range of functional groups (Scheme 30B).¹⁰⁹ Other metals such as gold can also be combined^{110–113}, especially when coupling with alkynes is desired¹¹⁴ (Scheme 30C).



Scheme 30: Photoredox arylation merged with palladium and gold catalysis.

Aryl sulfonyl chlorides (**241-243**) and diaryliodonium salts (**244**) are other classes of compounds that are used as phenyl radical sources. They have lower reduction potentials as compared to diazonium salts (Figure 16).¹⁰⁵

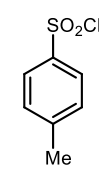
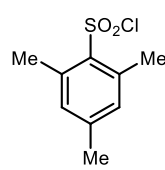
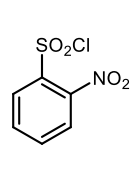
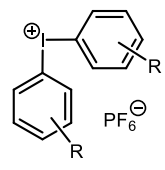
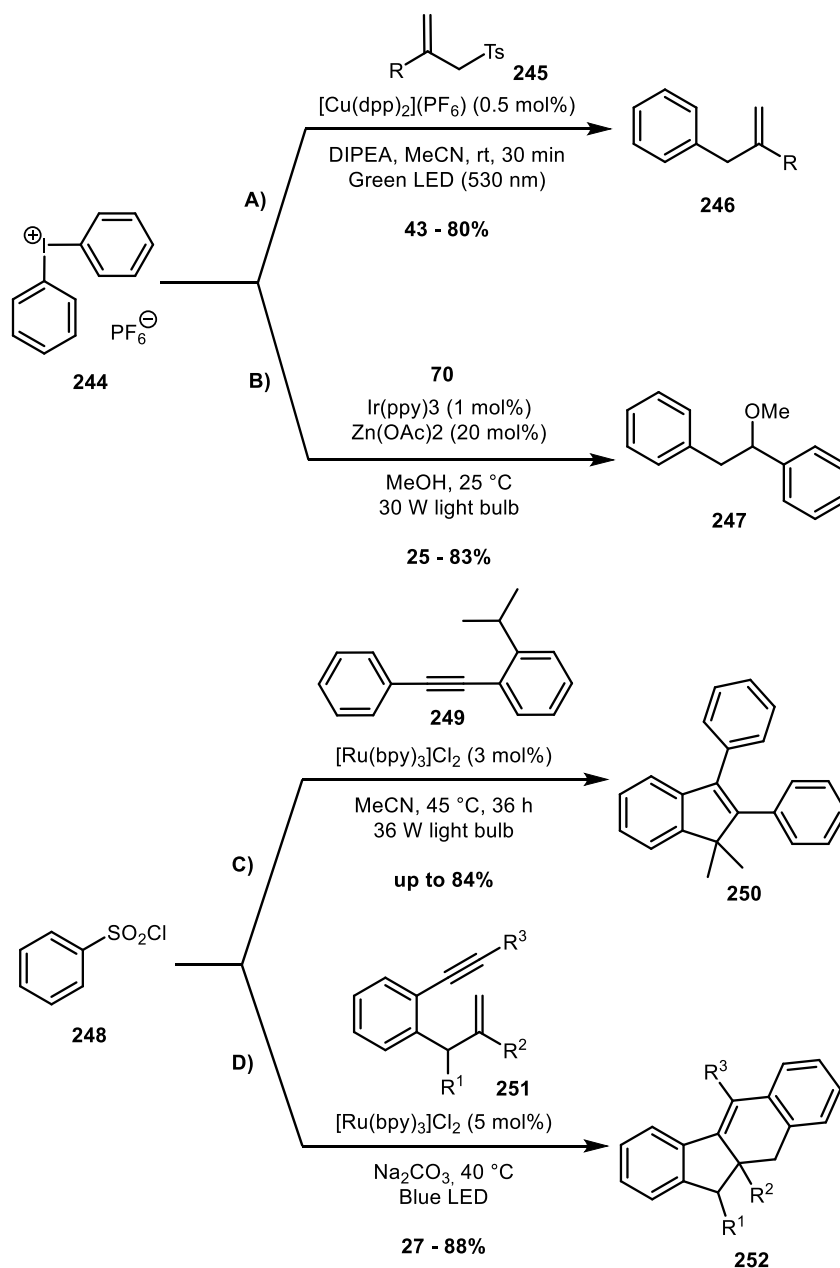
				$E_{1/2}$ vs. SCE (V)
$E_{1/2}$ vs. SCE (V)	-1.37	-1.45		-0.51

Figure 16: Reduction potential of some aryl sulfonyl chlorides and diaryliodonium salts.^{61,115}

Ollivier et al obtained aryl radicals from **244** to carry out arylation in allyl sulfones (**245**), where the Ts is a leaving group, to obtain **246** (Scheme 31A).¹¹⁶ Greaney et al used the same phenyl radical source to obtain **247** (Scheme 31B).¹¹⁷ The methoxy group came from the solvent acting as a nucleophile. The use of sulfonyl chlorides (**248**) usually requires low heating to eliminate SO₂ as observed by Reiser

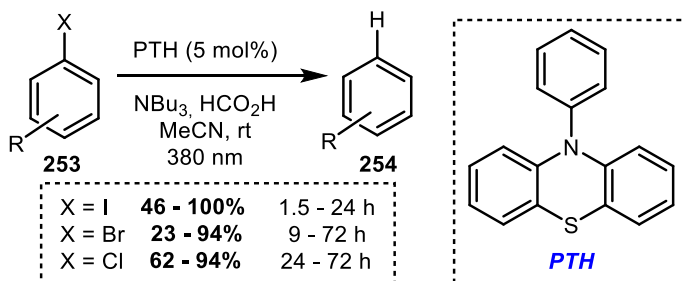
et al that temperature is a key factor if C-S or C-C bond formation is desired.¹¹⁸ Li et al designed the synthesis of 1*H*-indenes moieties (**250**) using a photoredox step (Scheme 31C).¹¹⁹ The same group used a similar approach to make the cycle **252** (Scheme 31D).¹²⁰



Scheme 31: Photoredox arylations using (A,B) hypervalent iodines and (C,D) sulfonyl chlorides.

The last class of phenyl radicals sources is the aryl halides (**253**). Due to the difficulty of having reducing agents, many approaches are based on merging

photoredox with cross-coupling reactions.^{121,122} As the traditional photocatalysts are not prone to do it, some groups direct their efforts to design new high reducing agents. The most successful one was developed by de Alaniz et al: PTH has $E_{1/2}$ (PC⁺/PC^{*}) = -2.1 V and is able to make phenyl radicals from iodobenzene and bromobenzene, the former being reduced in 1 h (Scheme 32).¹²³ The reduction of chlorobenzenes was also achieved in the presence of EWG.



Scheme 32: Reductive dehalogenation of aryl halides using PTH as photocatalyst.

Since this report, other compounds were obtained with higher reducing power (Figure 17). Miyake et al introduced diaryl dihydrophenazines (**256** - **259**) with $E_{1/2}$ up to -2.24 V to applications in atom transfer radical polymerizations (ATRP).¹²⁴ The same group investigated 18 phenoxazines and surprisingly the simplest one, **260**, was the most reducing with $E_{1/2} = -2.11$ V.¹²⁵ Recently, Nicewicz et al discovered that acridinium radical **261**, when excited at 390 nm, has its *N*-phenyl ring rotated, which allows twisted intramolecular charge-transfer (TICT).¹²⁶ They showed that, when this compound was irradiated at such wavelength, it could reduce not only aryl bromides but also aryl chlorides in good yields after 16 h.

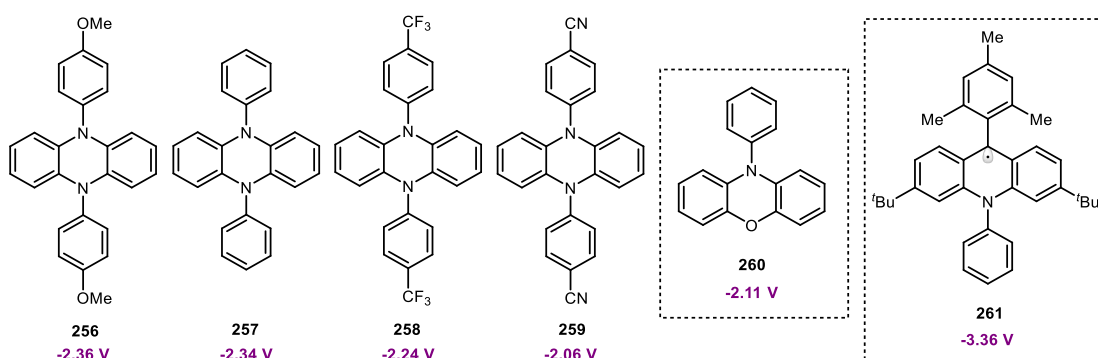
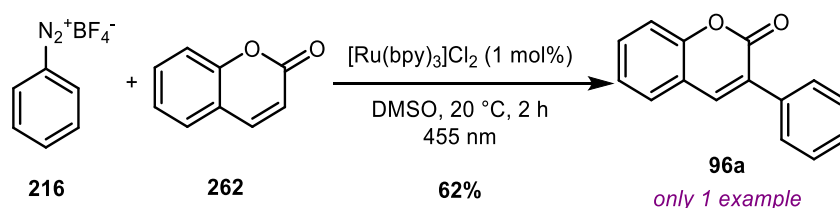


Figure 17: High reducing photocatalysts.

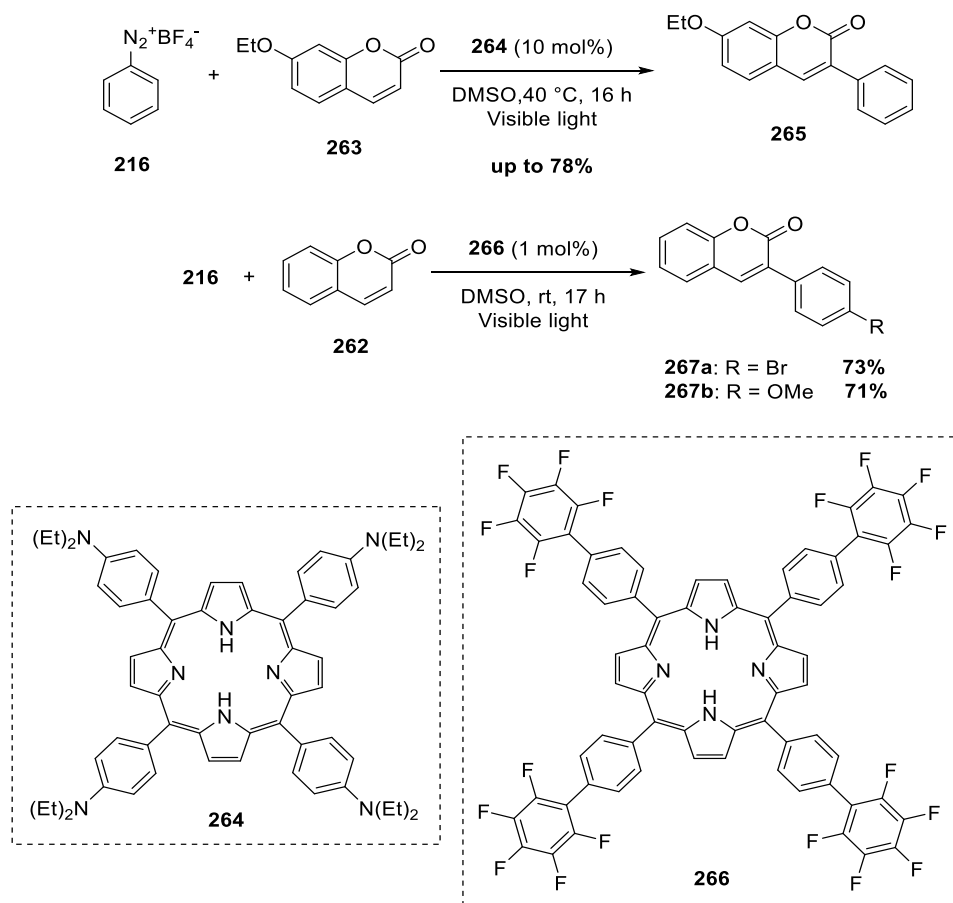
1.3.2. Photoredox Meerwein reaction as a platform to α -arylations

The generation of the phenyl radicals by photoredox catalysis was an important step to the development of new Meerwein protocols. One of the substrates used by Meerwein was coumarin (**262**), as pointed out previously. König et al showed that **96a** could be achieved in 62% yield (Scheme 33).¹²⁷ The proposed mechanism was similar to the Pschorr reaction (Scheme 1B). Benzoquinone and cinnamic acid were also arylated in 89 and 49% yield, respectively. The latter was decarboxylated as expected.



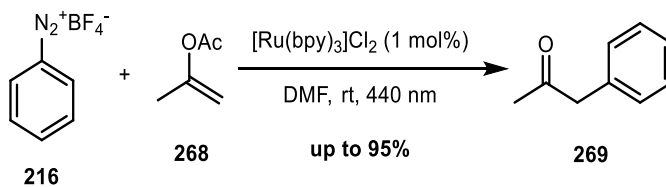
Scheme 33: König's arylation of coumarin.

This work opened doors to α -arylations based on the photoredox methodologies. Kanai et al proposed the arylation of 7-ethoxycoumarin (**263**) through new porphyrins (**264** and **266**) as photocatalyst (Scheme 34).¹²⁸ Yields up to 78% were achieved. Compared to the König's arylation, Kanai's one needed higher temperature (40 °C) and reaction time. The catalyst must be synthesized in poor yields. Gryko et al also obtained another porphyrin photocatalyst and showed the synthesis of **267a** and **267b** in 73 and 71% yield, respectively.¹²⁹



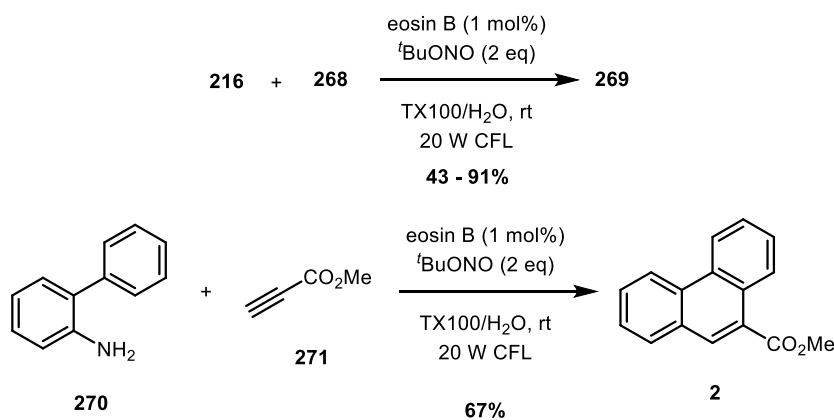
Scheme 34: Photoredox arylation of coumarins using porphyrin-based photocatalysts.

α -Arylation of ketones was achieved by König et al by using enol acetates **268** as substrates followed by hydrolysis (Scheme 35).¹³⁰ Great yields of **269** were obtained with EWG substituents at diazonium **216**. The authors observed that the arylation of enol acetates derived from aldehydes gave trace to poor yields due to competition with parallel aldol reactions. Oliveira et al carried out the same reaction catalyzed by porphyrin in a continuous flow approach, thus obtaining reasonable yields and multi-gram scale reactions.¹³¹



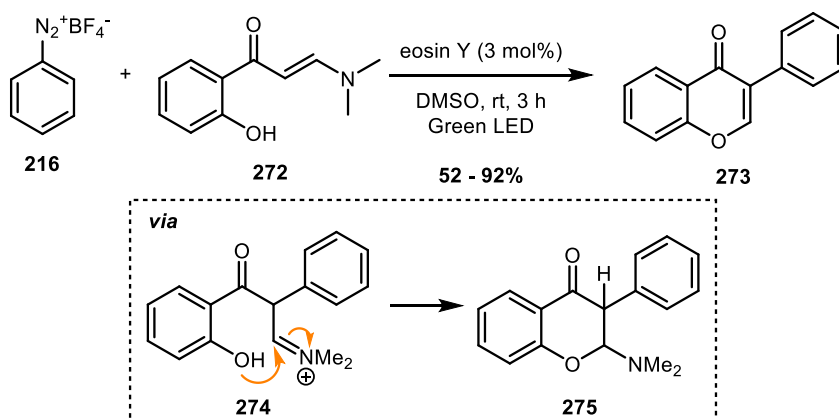
Scheme 35: Photoredox arylation of enol acetates.

Cai et al proposed the combination of photoredox and micellar catalysis.¹³² The addition of a surfactant, such as the Triton X-100, was able to proceed with arylations producing diazonium salts *in situ* in water as solvent (Scheme 36). The authors got arylations of the enol acetates in 43 to 91% yield and addition of **270** in **271** to make **2** in 67% yield.



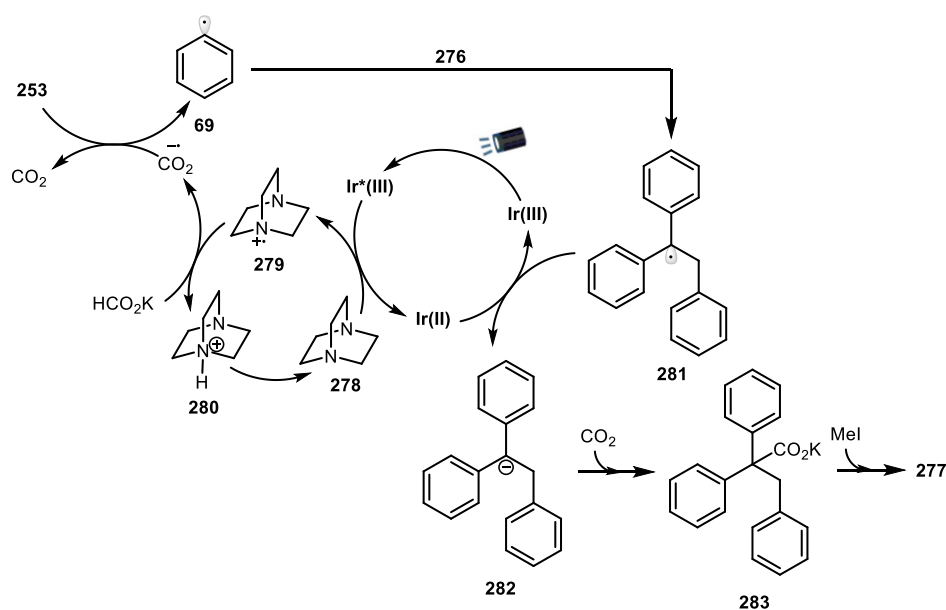
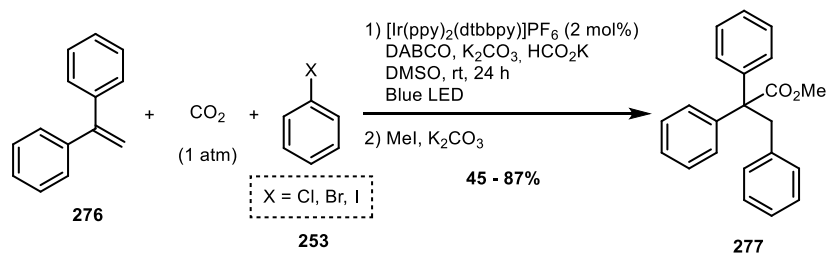
Scheme 36: Photoredox arylation combined with micellar catalysis.

Mkrtchyan and Laroshenko obtained the isoflavones (**273**) by α -arylation of enaminones (**272**) followed by intramolecular cyclization (Scheme 37).¹³³ After the photoredox arylation, the *o*-hydroxy group attacks the iminium carbon (**274**) to afford the intermediate **275**, which after elimination is converted to the isoflavone. Diaryliodonium triflates were also used as phenyl radical sources with $[\text{Ru}(\text{bpy})_3]\text{Cl}_2$ as the photocatalyst in good yields.



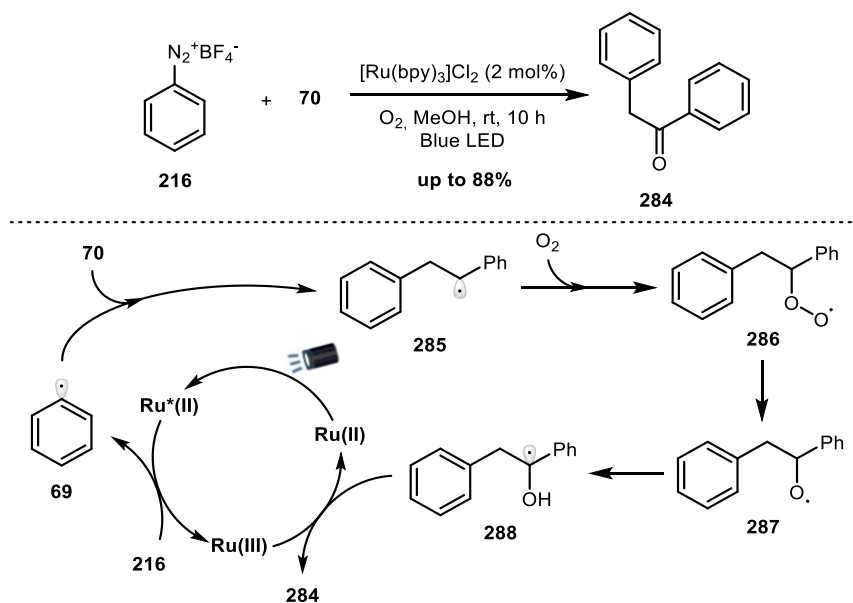
Scheme 37: Synthesis of isoflavones by photoredox arylation of enaminones followed by intramolecular cyclization.

Li et al used Meerwein's approach to carry out alkene carboarylation with CO₂ to give **277** in yields ranging from 45 to 87% (Scheme 38).¹³⁴ The excited photocatalyst oxidize DABCO (**278**) into the radical cation **279**, which reacts with HCO₂K to generate CO₂^{•-}. This radical anion reduces **253** and then **69** reacts with **276** to form the radical **281**. After its reduction to **282**, the carbanion reacts with CO₂ to give **283** followed by methylation to achieve the desired product **277**.



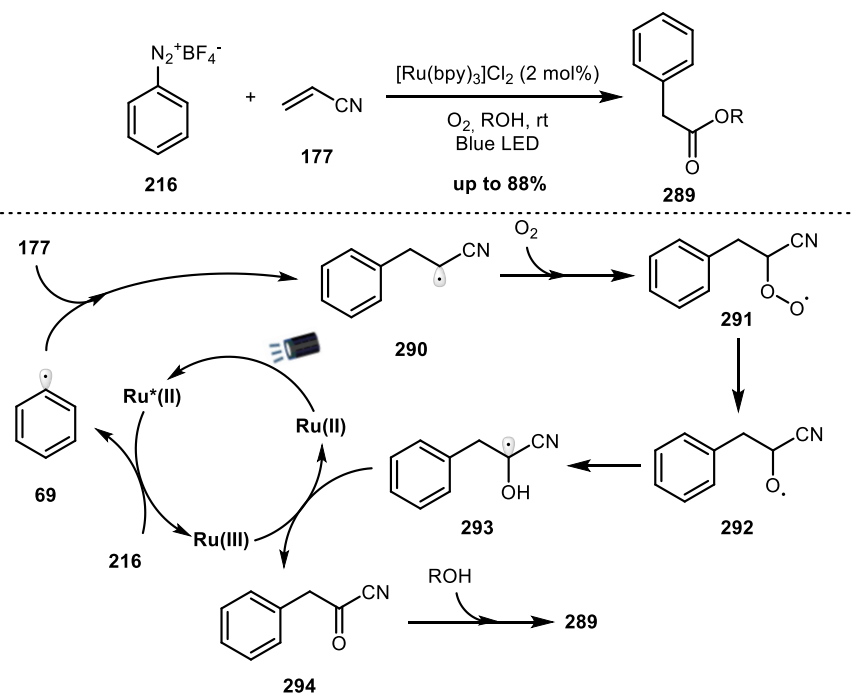
Scheme 38: Li's carboarylation of alkenes.

Meerwein reaction in styrenes can also be used to make ketones. Molecular oxygen can react with carbon-centered radicals and after several transformations produces alkoxy radicals. Such transformations were used by Cai et al to make α -aryl ketones in up to 90% yield (Scheme 39).¹³⁵ The reaction was based on Meerwein addition to **70** followed by reaction with O₂ to give the peroxy radical **286** and the alkoxy radical **287**. Then, a 1,2-hydrogen shift occurs to give **288**, which after SET forms the desired product **284**.



Scheme 39: Synthesis of arylketones by oxidative arylation of styrenes.

Jiang et al used a similar fashion to develop a new strategy for the synthesis of α -aryl esters starting from acrylonitriles (Scheme 40).¹³⁶ The ester formation was achieved in up to 88% yield. The proposed mechanism is like Cai's aryl ketone synthesis, however a nucleophilic substitution at formed **294** allowed the ester formation.



Scheme 40: Synthesis of acrylonitriles by oxidative arylation of styrenes.

2

Synthesis of 3-aryl-4-(*N*-aryl)aminocoumarins via photoredox catalysis

2.1.

3-Arylcoumarins: a privileged scaffold

Coumarins are usually used as a prototype of new drug candidates, such as anticancer^{137–140}, antiviruses^{141–143}, antimicrobial^{144–146} and antioxidant^{147–149}. Their structures have two pharmacophoric groups: the aromatic ring, that can promote hydrophobic interactions, such as π -interactions, and the lactone group, that is a hydrogen bond acceptor with receptors and enzymes (Figure 18).¹⁵⁰ More than 1300 kinds of coumarins were discovered and typify a huge class of natural products, usually obtained as secondary metabolites of plants, bacteria and fungi. Most of them have oxygenated substituents at positions C5, C6, C7 and C8.^{151,152}

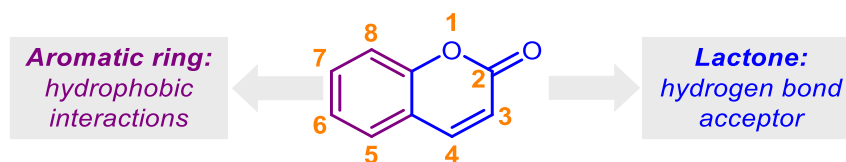


Figure 18: Pharmacophoric groups of coumarin and its numbering.

The presence of a phenyl ring at position C3 gives to coumarin extra functionalization possibilities; it was explored in the synthesis of new drug candidates. Coumarins **295** and **296**, commonly named as isoglycycomarin and licoarylcoumarin, have an aryl group at position C3 (Figure 19). These compounds showed great activity for HIV TPA promoter-suppressive effects.¹⁵³ Based on this fact, Olmedo et al proposed new 3-arylcoumarins as candidates for HIV inhibitors. Compound **298** was the most potent to inhibit the virus replication. Despite **297** having lower activity, experiments showed that the mechanism related to the biological activity is different from **298**. HeLa-Tat-luc and HeLa-Tat-ON essays pointed that **299** had specific inhibition to such targets, besides the reasonable activity.

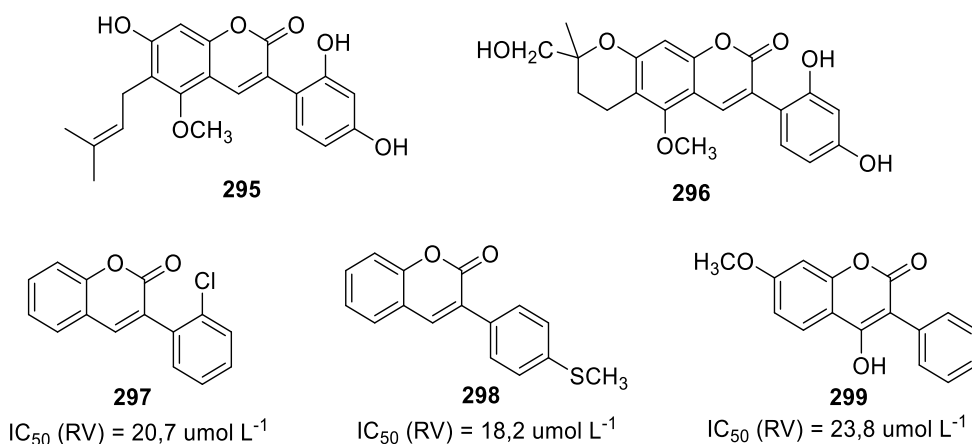


Figure 19: 3-Arylcoumarins with anti-HIV activity.

Ong et al studied the structure-activity relationship (SAR) against inhibition of viral protein R (Vpr) of HIV-1.¹⁵⁴ Compound **300** was used as prototype for new synthetic coumarins (Figure 20). The authors observed that the OMe group at position 5' of ring C and the presence of a carbamate group are essential for the inhibition of Vpr. Based on these results, they synthesized **301** and **302**, called as vipirinine. They found out that such compounds probably bind the target protein in the hydrophobic region about residues Glu-25 and Gln-65.

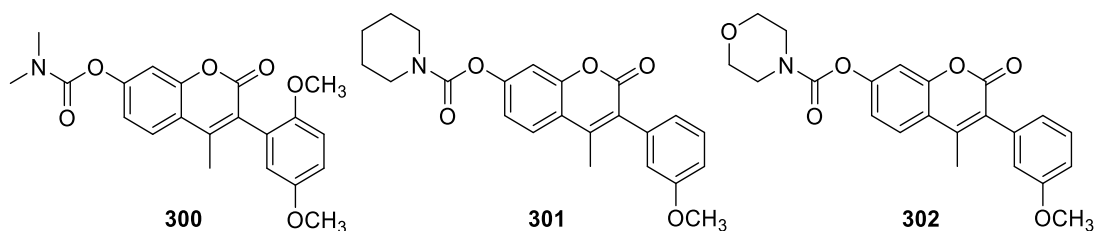


Figure 20: 3-Arylcoumarins with anti-HIV activity.

In the treatment of cancer, many studies show that 3-aryl coumarins are promising scaffolds (Figure 21). Li et al obtained **303** inspired by the osthole (**304**), a natural product obtained from *Cnidium monnieri* (L.) *Cusson*, a plant used in traditional Chinese medicine.¹⁵⁵ Their synthetic coumarin had greater activity against MCF-7 and MDA-MB-231 cells (breast cancer). Preliminary SAR studies pointed out that the 7-OMe and the 3-phenyl group are essential for the biological activities. Compounds **305** and **306** showed *in vitro* activity against human gastric cancer SGC7901 cells (11.15 and 12.60 μM , respectively) and cervical cancer HeLa cells (7.00 and 7.68 μM).¹⁵⁶

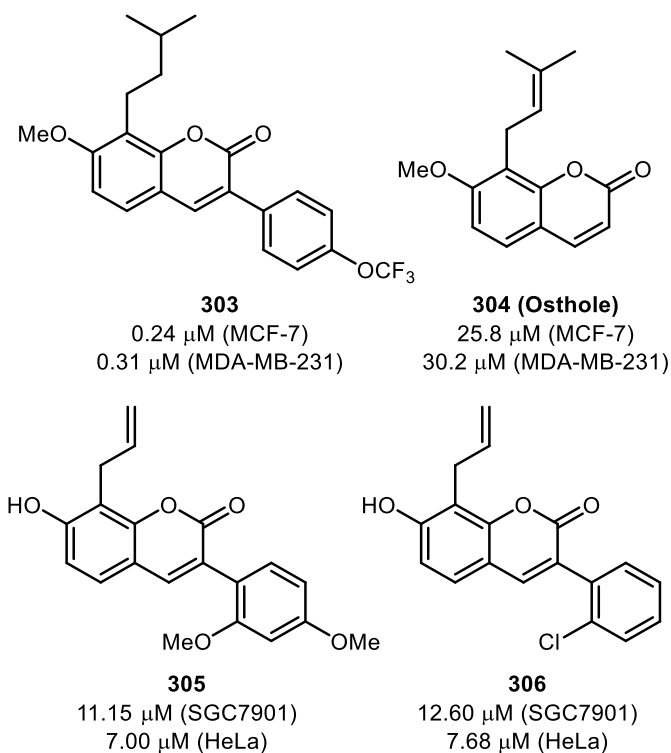


Figure 21: 3-Arylcoumarins and their anticancer activities (IC_{50} in μM).

A series of 3-(4-nitrophenyl)coumarins were evaluated in tumor cell lines. Compound **307** showed cytotoxicity to human lung cancer A549 cells ($12.2 \pm 1.85 \mu\text{M}$), MDA-MB-231 cells ($27.6 \pm 3.4 \mu\text{M}$) and prostate cancer PC3 cells ($18.2 \pm 0.2 \mu\text{M}$).^{157–159} The presence of OAc groups at positions C7 and C8 was responsible for the observed cytotoxicity. Detsi et al obtained 3-arylcoumarins with substitution at position C5.¹⁶⁰ Compounds **308** and **309** showed $\text{IC}_{50} = 1.8$ and $6.1 \mu\text{M}$ against HeLa cells, respectively, and **310** showed $\text{IC}_{50} = 9.7 \mu\text{M}$ for human neuroblastoma SK-N-SH cells. Finally, Blagg et al showed that these coumarins are Hsp90 inhibitors. Compounds **311** and **312**, which have a methyl group at position C8, exhibited $\text{IC}_{50} = 4.51 \pm 0.42$ and $4.94 \pm 0.03 \mu\text{M}$, respectively, for estrogen receptor negative, Her2 overexpressing breast cancer cells (SKBr3) and 1.65 ± 0.16 and $1.24 \pm 0.06 \mu\text{M}$ for MCF-7. Compounds **313** to **315** had better activities for SKBr3 (Figure 22).

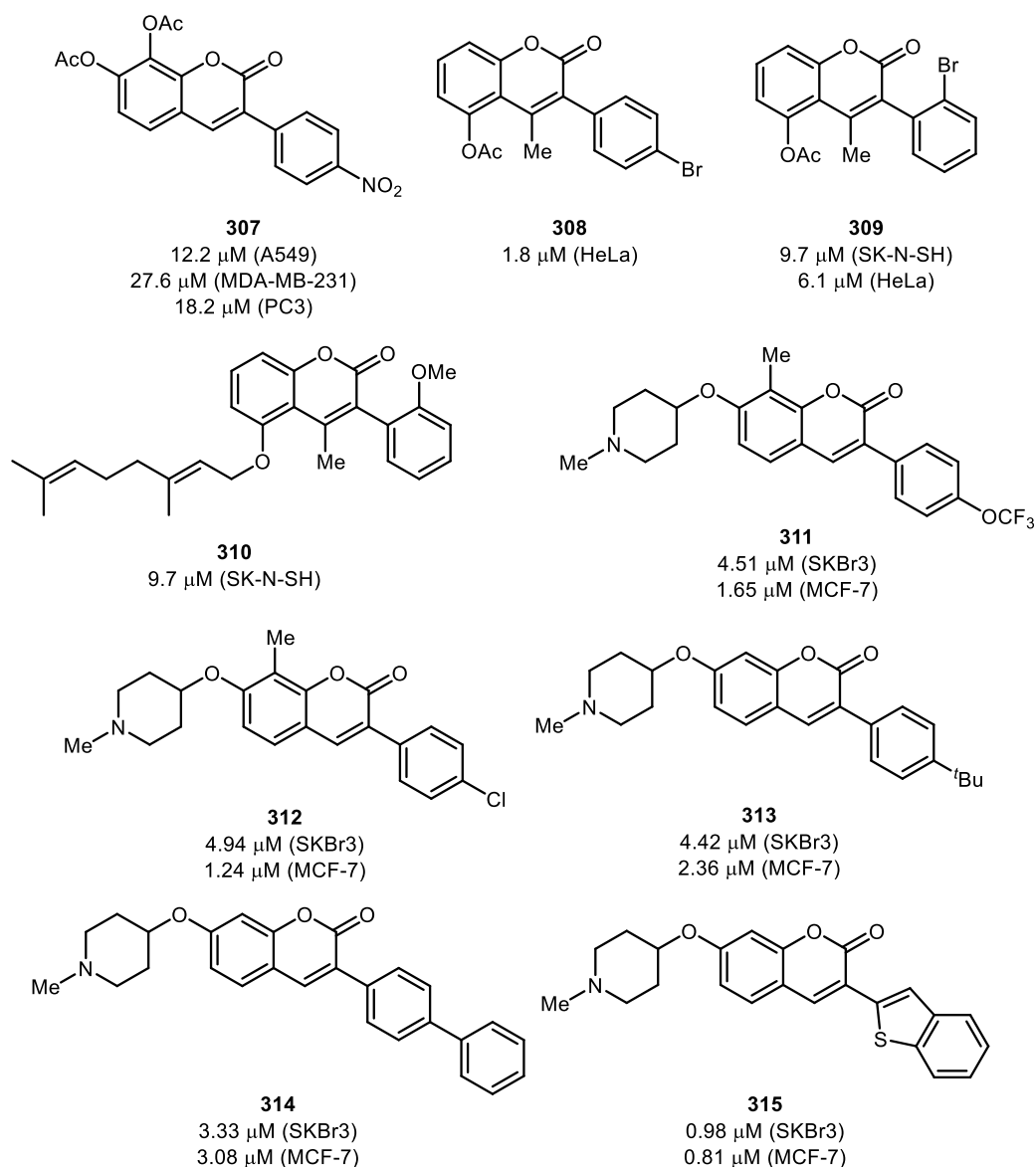
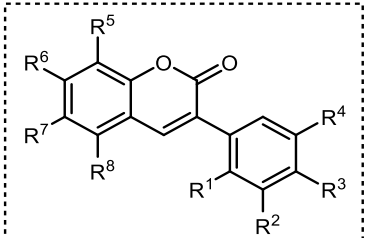


Figure 22: 3-Arylcoumarins and their anticancer activities (IC₅₀ in μM).

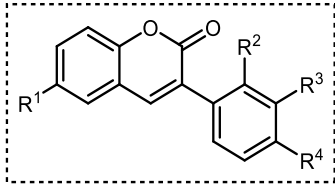
Studies reported that isoflavones showed activity as binding peroxisome proliferator-activated receptors, which appeared to be candidates for obesity and type II diabetes drugs.^{161,162} Based on this, Wang et al proposed 3-aryl- and 4-arylcoumarins as α -glucosidase and advanced glycation end-products (AGE) formation inhibitors due to the structure similarity to isoflavones (Figure 23).¹⁶³ Compounds **316b**, **316e** and **316f** showed the best results for both biological activities. Analysis *in vivo* showed that **316c** and **316f** had equipotent results as compared to glibenclamide, the positive control.



	α -glucosidase inhibitory activity	AGEs inhibitory activity
316a : R ¹ = Me; R ⁶ = OH	16.39	>1000
316b : R ³ = R ⁶ = OH	19.91	1.42
316c : R ³ = OH; R ⁷ = OH	11.54	24.68
316d : R ³ = Me; R ⁶ = R ⁸ = OH	11.49	45.75
316e : R ³ = OH; R ⁶ = R ⁸ = OH	1.37	2.52
316f : R ³ = OMe; R ⁶ = R ⁸ = OH	10.81	5.21
316g : R ² = R ³ = R ⁵ = R ⁶ = OH	247.34	14.16

Figure 23: 3-arylcoumarins and IC₅₀ (μ M) for α -glucosidase and AGEs inhibition.

Viña et al synthesized 3-arylcoumarins to evaluate the affinity with human monoamine oxidase B (hMAO-B) as candidates for treating neurodegenerative diseases (Figure 24).¹⁶⁴ The authors observed compounds with IC₅₀ at picomolar range. The best compound, **317e**, had the IC₅₀ = 134±0.009 pM, more active than the selegiline, the reference compound. An extensive SAR was carried out through molecular docking calculations and showed that R¹ might be a small group to better interact with the protein. Bromine at R³ and R⁴ positions allows better fit in the cavity. Other studies supported that this scaffold has a potential to be a drug for neurodegenerative diseases.^{165–169}



	IC ₅₀ (nM)
317a : R ¹ = Me; R ⁴ = Me	0.31±0.02
317b : R ¹ = Me; R ³ = OMe	0.80±0.05
317c : R ¹ = Me; R ³ = Br; R ⁴ = OMe	0.74±0.02
317d : R ¹ = Me; R ⁴ = Br	0.387±0.026
317e : R ¹ = Me; R ³ = Br	0.134±0.009
317f : R ¹ = OMe; R ⁴ = Br	0.320±0.017
317g : R ¹ = OMe; R ³ = Br	0.650±0.035

Figure 24: 3-arylcoumarins and IC₅₀ (nM) for hMAO-B inhibition.

2.1.1. Synthetic value of 3-arylcoumarins

The 3-arylcoumarins compounds have important value as intermediates of the coumestans synthesis. Coumestans are a class of natural products based on coumarin nucleus with a fused benzofuran ring (Figure 25). They have a great number of bioactive applications, such as antiophidic^{170–172}, anticancer^{173–182}, anti-HCV¹⁸³, antitubercular^{184,185}, osteogenesis promoter^{186,187} and adipogenesis inhibitor¹⁸⁶ and antiobesity and other metabolic disorders¹⁸⁸. Replacing benzofuran by an indole ring

gives the nitrogen analogue, azacoumestan or indole[3,2-*c*]coumarin. On the other hand, such analogues have few descriptions of their biological actions, including three patents and an *in silico* study of only one azacoumestan.^{189–192} The presence of the nitrogen atom is interesting due to the possibility of functionalization at this position. Our group has shown that the presence of the *N*-tosyl group in the carbapterocarpan LQB-223 is important for its anticancer activity.¹⁹³

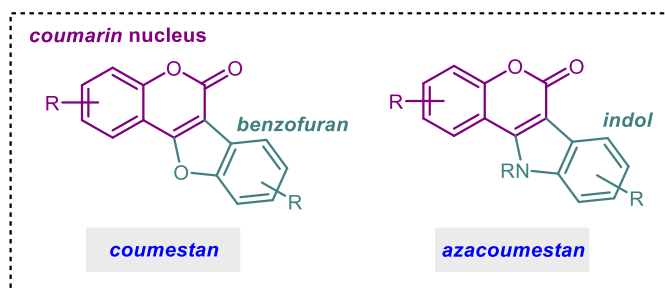
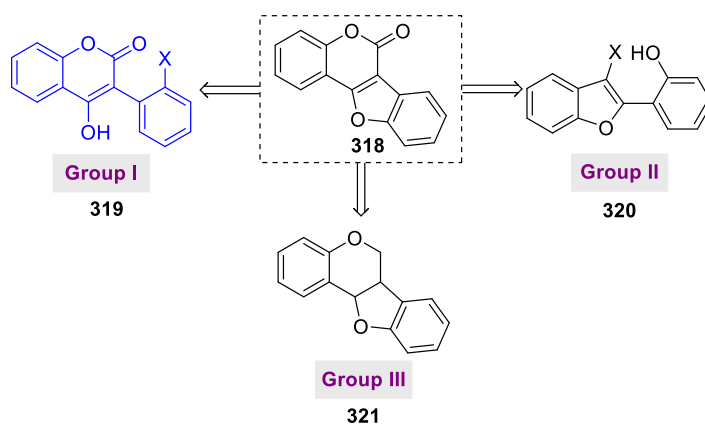


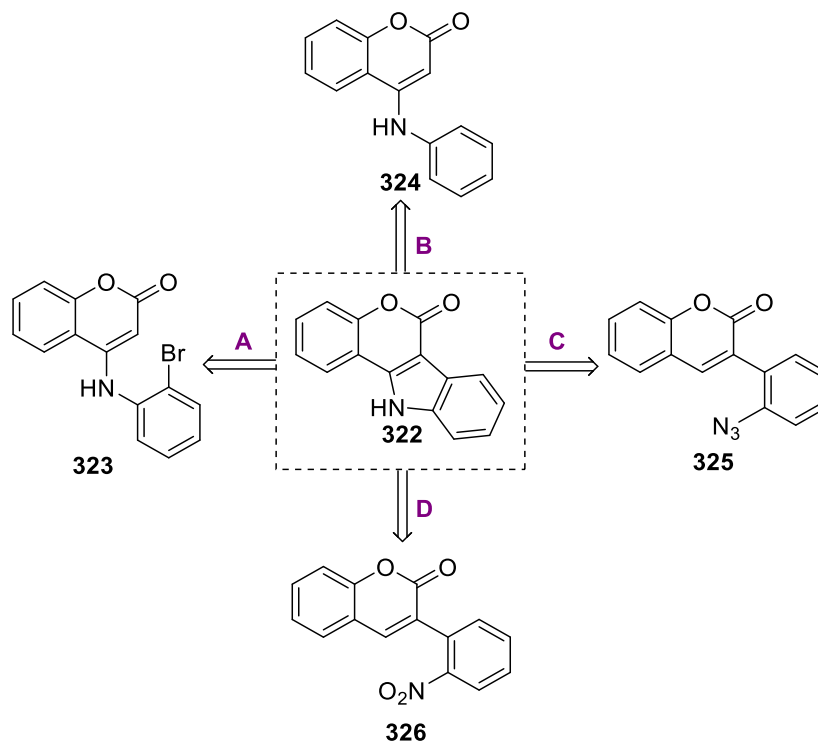
Figure 25: Structure of the coumestan and the azacoumestan.

The coumestans (**318**) synthesis can be divided in three groups (Scheme 41).¹⁹⁴ The Group I is based on the formation of the C-O bond at **319** with the presence of a leaving group at the phenyl ring at the C3 position. This is the most developed method in the literature, however it is common to adopt the use of expensive catalysts, such as palladium salts and enzymes, harsh reaction conditions, and the use of starting materials that need more than one step to be prepared.^{195–198} Group II is a similar approach, however an α -pyrone intermediate (**320**) is required. Finally, group 3 is based on the oxidation of pterocarpan like **321**.



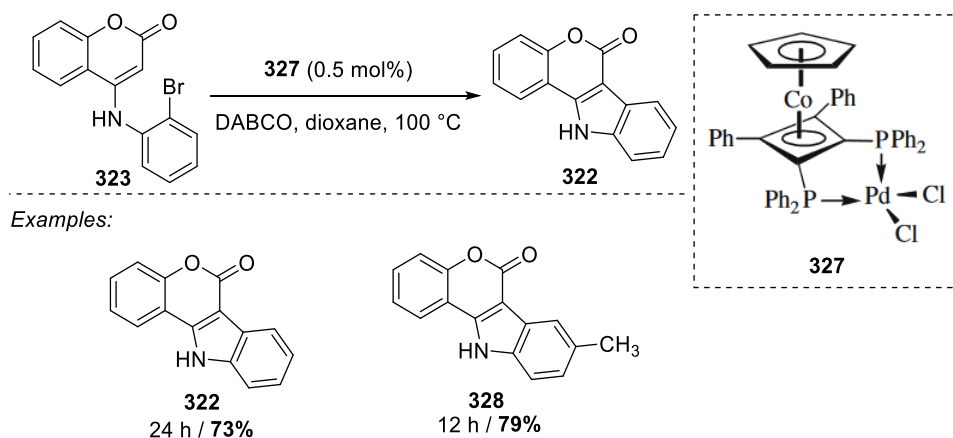
Scheme 41: Synthetic strategies to achieve coumestans.

The nitrogen coumestans analogues, azacoumestans (**322**), on the other hand, have more synthetic approaches (Scheme 42). Starting from the coumarin scaffold, four different methods were rationalized to make these compounds.



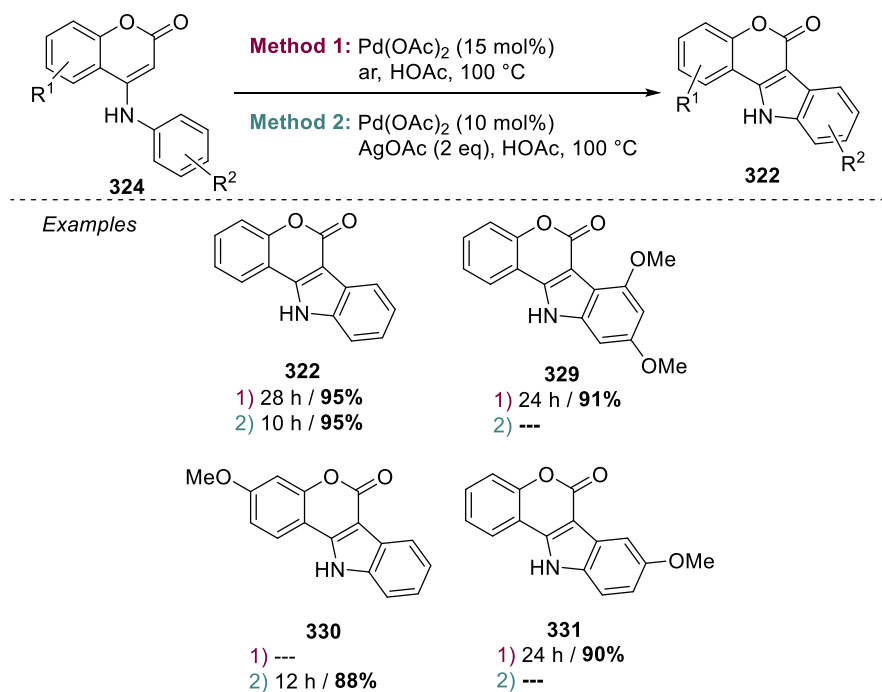
Scheme 42: Synthetic strategies to achieve azacoumestans.

Route A was based on an intramolecular Heck cyclization of **323** (Scheme 43). The authors developed a new palladium/cobalt bimetal catalyst (**327**) and obtained **322** and **328** in 73 and 79% yield, respectively.¹⁹⁹ The catalyst requires a two step synthesis with high cost reactants and the small scope of the work were limitations for the use of this methodology.



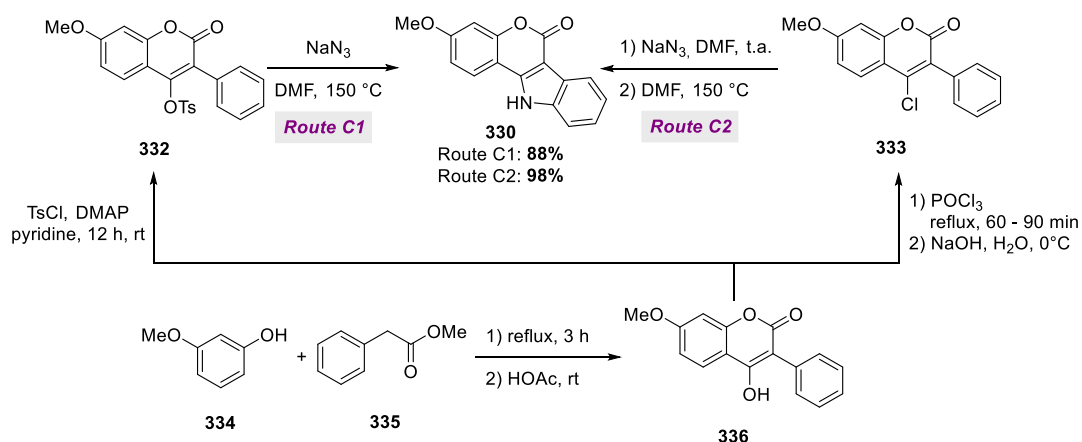
Scheme 43: Synthesis of azacoumestan by intramolecular Heck cyclization of **323**.

Route B proposed by McGlacken et al was initially planned to coumestans synthesis (Scheme 44).²⁰⁰ The authors observed that azacoumestans could also be obtained from **324** by the two proposed methods in yields in the range from 88 to 95%. The intended cross dehydrogenative coupling (CDC) required the use of $\text{Pd}(\text{OAc})_2$ as catalyst, and air or AgOAc as oxidants; however, the latter reduces the reaction time. Besides the intramolecular coupling, secondary enaminolactones and the presence of electron-withdrawing groups at both aromatic rings were not evaluated.



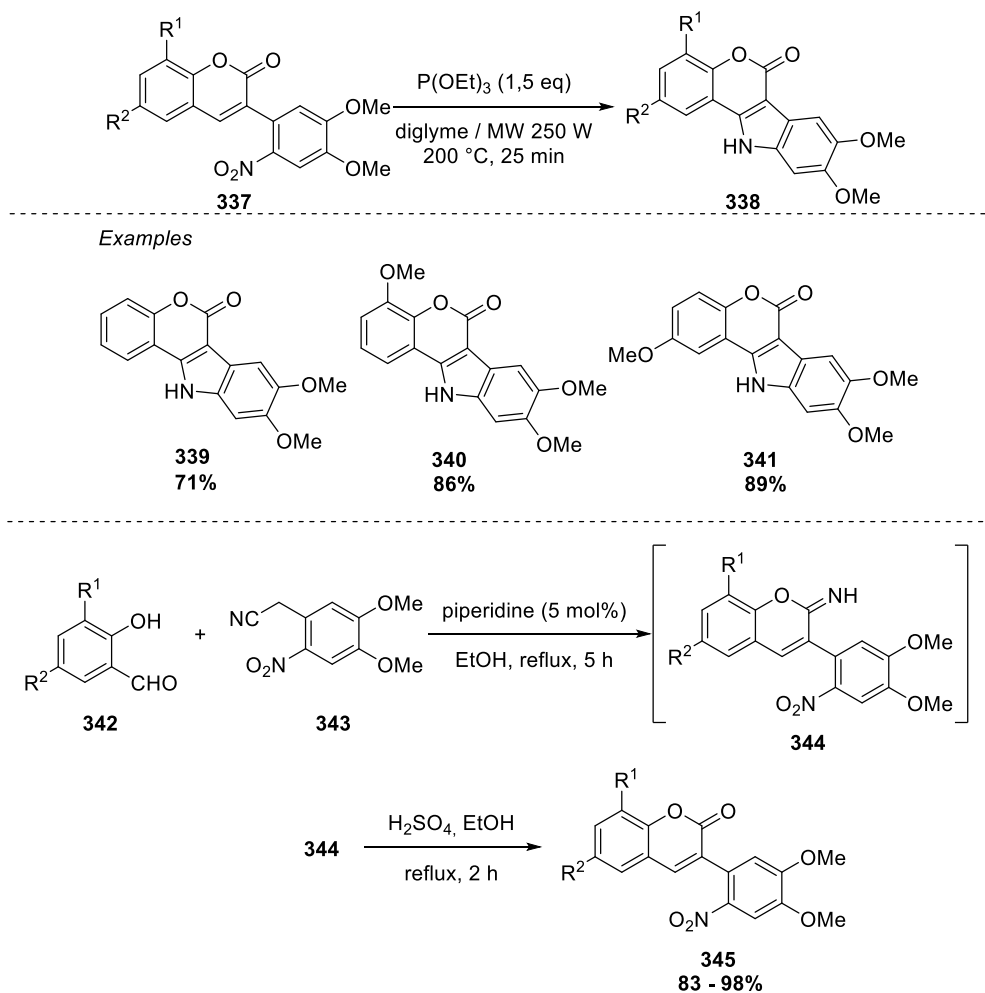
Scheme 44: Synthesis of azacoumestan by cross dehydrogenative coupling of **324**.

Route C was conducted by Kappe et al and was based on the substitution of the OTs group at **332** or the Cl at **333** by azide, followed by the intramolecular cyclization with loss of N₂ (Scheme 45).²⁰¹ The azacoumestan **330** was achieved in excellent yields. Compounds **332** and **333** were obtained from **336**, which was synthesized from the Pechmann condensation of **334** and **335**.²⁰² Only two examples were given, with high yields, and they were not able to evaluate the tolerance of the methodology against functional groups and sterics, for example.



Scheme 45: Synthesis of azacoumestan by intramolecular cyclization of azides.

Finally, route D was developed by Charushin et al and was inspired at the reductive cyclization of **326** by the Cadogan-Sundberg reaction under microwaves (Scheme 46).²⁰³ The authors reported that the synthesis of the starting material **337** was achieved after failed attempts of the Pechmann condensation, even when strong bases like KO^tBu were employed. For this purpose, the salicylaldehydes **342** were reacted with the nitrated homoveratronitrile **343** in the presence of piperidine. The intermediate pyranimines **344** were further treated with H₂SO₄ in ethanol, to achieve the desired coumarins. The NO₂ group at *ortho* position of the C3 phenyl ring was reduced *in situ* by the presence of P(OEt)₃ and followed by the cyclization. The access to this phosphite can be difficult as this chemical is controlled by the Brazilian Army. When it was changed to PPh₃, some of the reactions did not work, which suggests that strongly nucleophilic phosphines are necessary.



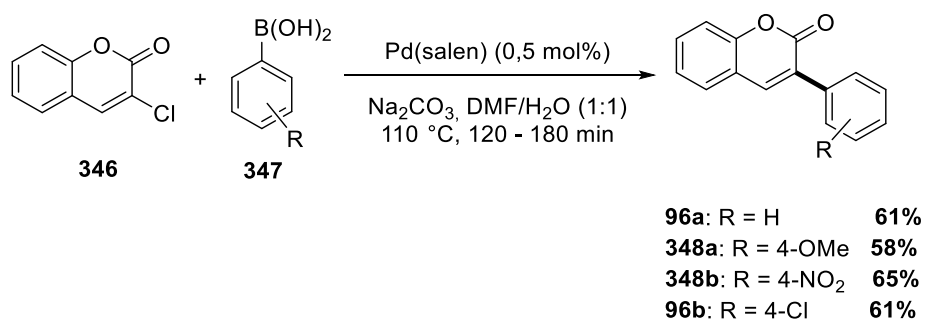
Scheme 46: Synthesis of azacoumestan by Cadogan-Sundberg reaction.

2.1.2. Synthesis of 3-arylcoumarins by cross-coupling reactions

The 3-arylcoumarins can be synthesized in two different approaches. The first one is based on building the coumarin scaffold already having the aryl group present at the starting materials through condensation reactions, such as Pechmann^{204,205}, Perkin^{157,206–210} or Knoevenagel^{211,212}, catalyzed condensation by *N*-heterocyclic carbenes, carbonylative annulation between phenols and alkynes²¹³ and mediated synthesis by cyanuric chloride²¹⁴.

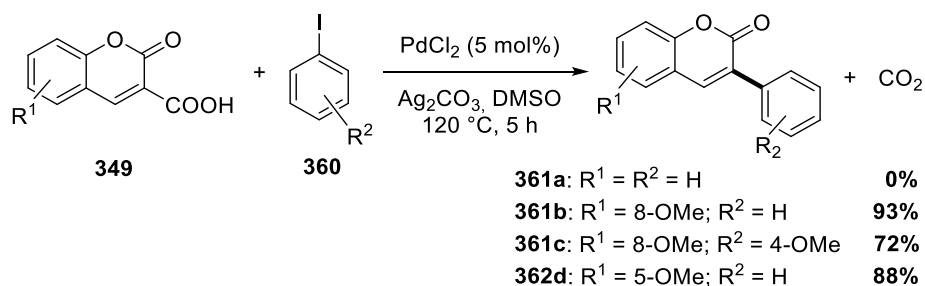
Conversely, though, the second approach is found on direct arylation of the coumarin nucleus. One of the possible strategies is using cross-coupling reactions with palladium catalysts. Matos et al obtained 3-arylcoumarins reacting **346** with boronic acids (**347**) in the presence of Pd(salen) as pre-catalyst in 55 – 65% yields

(Scheme 47).²¹⁵ The presence of EDG or EWG did not influence the yields significantly. The authors highlight that the 3-chlorocoumarin **346** is commercially available, differently from the bromine and iodine analogues, which should be synthesized prior to be used. Despite this fact, the substitution at the coumarin aromatic ring was not evaluated and such compounds are not available.



Scheme 47: Arylation of coumarins by Suzuki cross-coupling reaction.

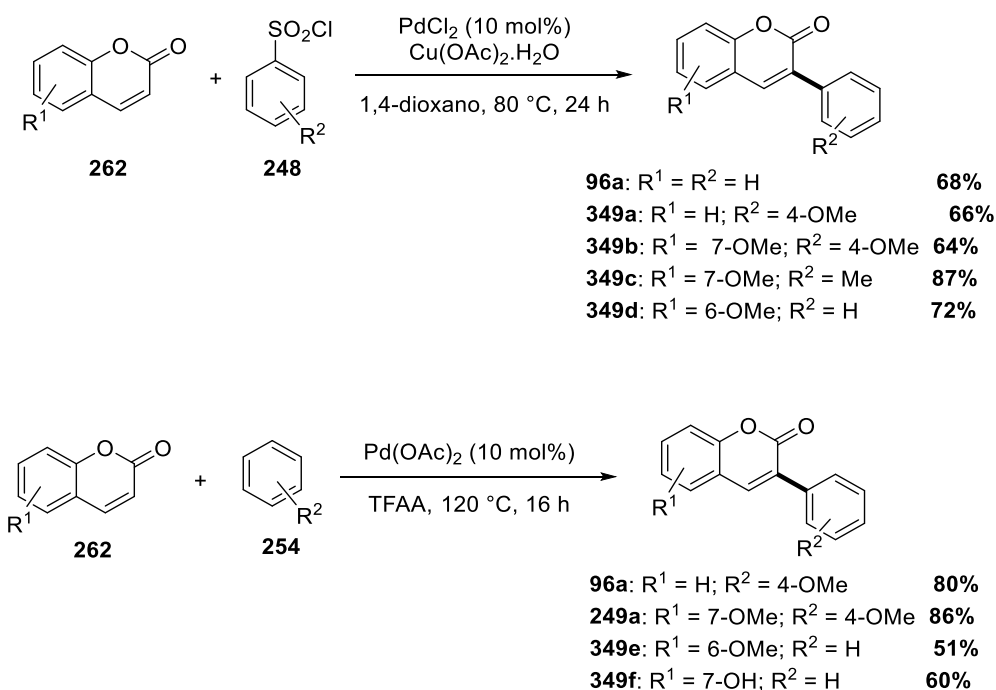
Jafapour et al promoted decarboxylation of **349** to make the desired coumarins in the presence of Ag₂CO₃ as the base and high temperature (Scheme 48).²¹⁶ Yields up to 93% were achieved. The use of ligands, surprisingly, reduced the reaction performance. The starting coumarin **349** was obtained from the condensation of salicylaldehyde with Meldrum's acid.



Scheme 48: Arylation of coumarins by decarboxylative coupling with aryl iodides.

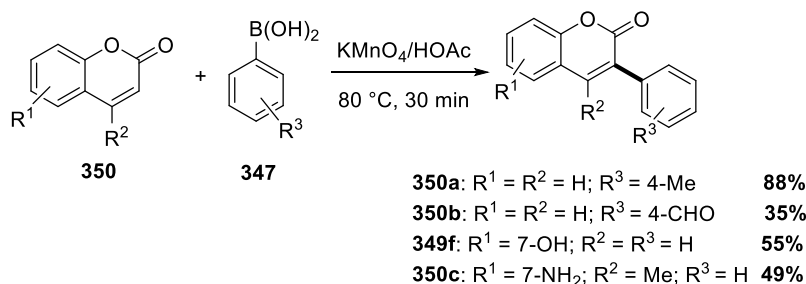
The same group explored two other methodologies with no functionalization of the position C3 (Scheme 49). The first was based on the use of arylsulfonyl chlorides **248** with **262**, with no functionalization at C3 position.²¹⁷ The copper salt was used as oxidant in 1.0 equivalent, but the author did not conclude its real role in the mechanism. Yields up to 87% were achieved, however the methodology was not tolerant to the

presence of electron-withdrawing groups at the coumarin ring. The latter used non activated arenes (**245**) with Pd(OAc)₂, using trifluoroacetic anhydride as solvent.²¹⁸ The authors suggested that the trifluoroacetic anhydride (TFAA) would react with Pd(OAc)₂ to form Pd(TFA)₂ which is, then, transformed into [Pd(OCOCF₃)]⁺, the catalytic active species. As the previous method, the reaction was not tolerant to EWG, with high recovering of the starting materials. Substitution at the **254** with EDG increased the yields. The formation of biphenyls as subproducts was observed.



Scheme 49: Arylation of coumarins with no functionalization of the C3 position.

To overcome the use of palladium catalysts, Yuan et al proposed the use of KMnO₄/HOAc with **347** to promote the desired arylation (Scheme 50).²¹⁹ The presence of EWG at **347** harshly reduced the yields, and the protection of the C3 position induced the arylation at the C4 position. The reaction also showed tolerance to the use of quinolinones instead of coumarins. The authors observed that the reaction in the presence of TEMPO and BHT gave trace amounts of the product, which indicated the presence of radicals in the mechanism. Finally, it was proposed that KMnO₄ would react with AcOH to form a Mn(III) species, which would oxidize **347** to form a phenyl radical.

Scheme 50: Arylation of coumarins promoted by KMnO₄.

2.2.

Objectives

Having pointed out the biological and synthetic values of 3-arylcoumarins, the objective of this work is the synthesis of this class of compounds by photoredox catalysis. Thus, the following specific objectives can be set out:

- Development of a methodology to arylation of 4-hydroxy- or 4-aminocoumarin by photoredox catalysis.
- Determination of viable protecting groups for 4-hydroxy- and 4-aminocoumarin by calculations based on the reactivity parameters of the Conceptual Density Functional Theory (CDFT).
- Optimization and study of the mechanism of the arylation of 4-(*N*-phenyl)aminocoumarin with diazonium salts by photoredox catalysis.
- Obtention of the *N*-phenyl-azacoumestan by intramolecular oxidative amination with hypervalent iodine.
- Study of the leishmanial and anti-cancer activities of the synthesized compounds.

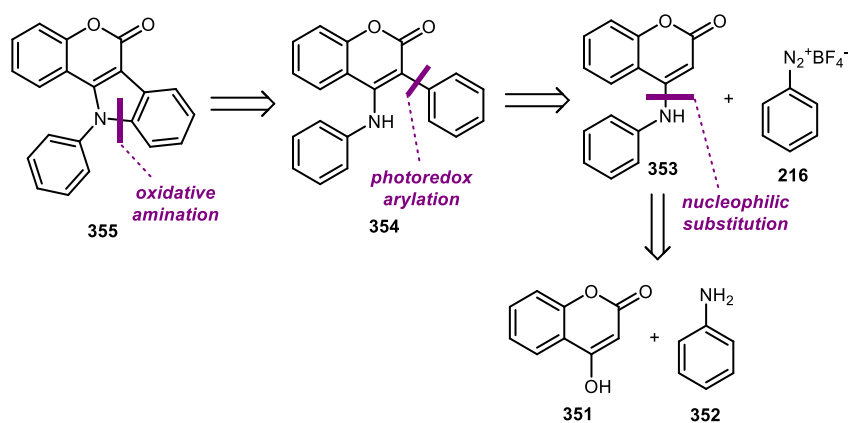
2.3.

Synthetic plan to synthesize 3-arylcoumarins and azacoumestan

As shown previously, the main reactions to obtain 3-arylcoumarins are based on the use of cross-coupling reactions. These methods requires the use of palladium salts and harsh reaction conditions, such as high temperatures and reaction times. Besides that, oxidants must be necessary for the reaction to work. The photoredox

catalysis showed potential to be a method to overcome these drawbacks but was not explored with coumarins with higher structural complexity.

The synthesis of 3-aryl-4-(*N*-aryl)coumarins (**354**) was planned to be a key step for the synthesis of azacoumestans such as **355** (Scheme 51). For this propose, the synthetic plan was based on the oxidative amination of **354**, which would be obtained from the arylation of **353** with **216**. Finally, compound **353** would be synthesized from nucleophilic substitution on **351** with **352**.



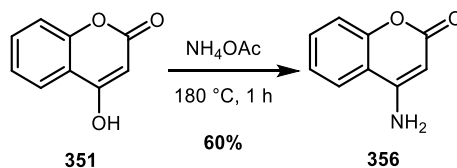
Scheme 51: Proposed retrosynthesis of *N*-arylazacoumestan **355**.

2.4.

Results and discussion

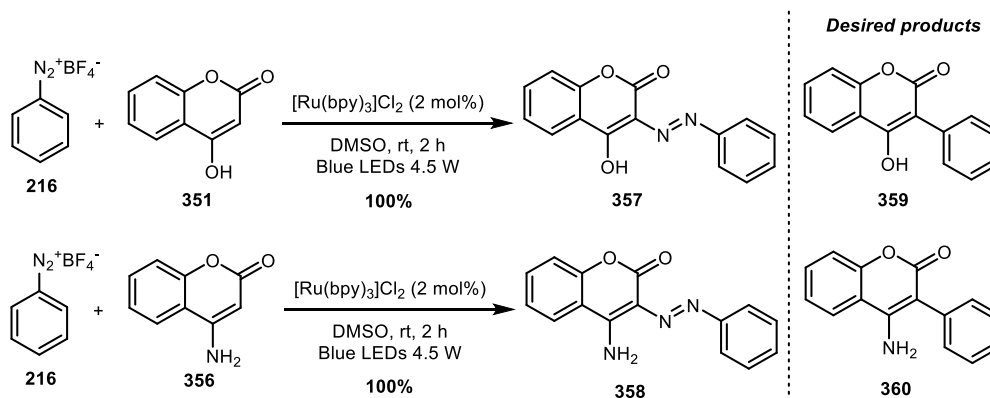
2.4.1. Choice of protecting group

The first attempts of photoredox arylation were tried on **351**, commercially available, and **356**, obtained from reaction of **351** with NH_4OAc at $180\text{ }^\circ\text{C}$. The compound **356** was obtained in 60% yield (Scheme 52).



Scheme 52: Synthesis of the 4-aminocoumarin **356**.

The arylations of **351** and **356** did not produce the desired products **359** and **360**, respectively. On the other hand, the diazo coupling products **357** and **358** were obtained in quantitative yields (Scheme 53).



Scheme 53: Diazo coupling between diazonium salt (**216**) and 4-hydroxy (**351**) and 4-aminocoumarins (**356**).

To investigate why these reactions did not work, the reactivity parameters from Conceptual Density Functional Theory were calculated at B3LYP/6-31+G(d) level of theory (Figure 26). The complete description of the equations used to calculate these parameters is presented at the *Experimental Procedures* section. The three evaluated coumarins have lower global chemical potential (μ^0) than the phenyl radical, so the latter must act as the nucleophile of the reaction and the coumarins, as the electrophiles. Hence, the analysis of their electrophilicity is necessary. The global electrophilicity (ω^0) indicates that **262** and **356** have similar behaviors (2.26 and 2.21 eV, respectively) and **351** is smaller (2.04 eV). The nucleophilicity scale proposed by Domingo et al (Figure 27) indicates that phenyl radical would be a weak nucleophile, which could be a reason for its lower reactivity towards these coumarins.²²⁰

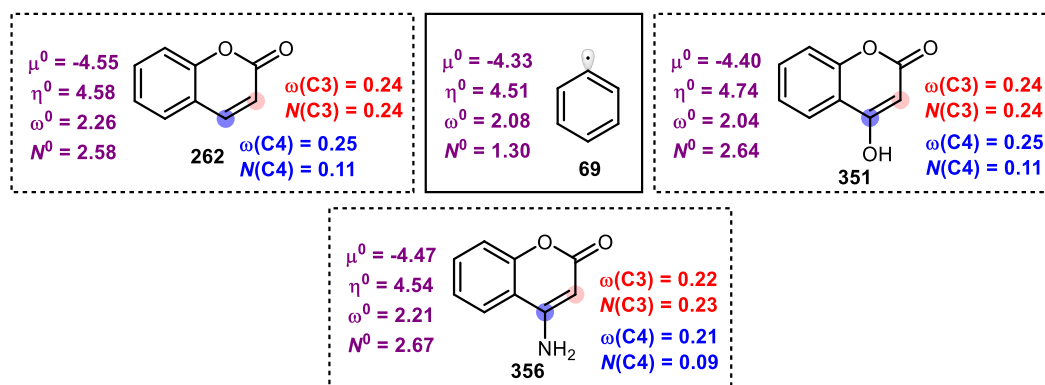


Figure 26: Reactivity parameters (in eV) of **262**, **351** and **356** calculated at (U)B3LYP/6-31+G(d) level of theory.

Nucleophilicity scale	Electrophilicity scale
$N^0 \geq 3.00$ eV - strong nucleophile	$\omega^0 \geq 1.50$ eV - strong electrophile
$2.00 < N^0 < 3.00$ eV - moderate nucleophile	$0.80 < \omega^0 < 1.50$ eV - moderate electrophile
$N^0 \leq 2.00$ eV - weak nucleophile	$\omega^0 \leq 1.50$ eV - weak electrophile

Figure 27: Scales of nucleophilicity and electrophilicity.

The analysis of the local parameters (ω_k and N_k), using the Mulliken atomic spin density analysis, showed that OH and NH₂ groups did not change significantly the electrophilicity and nucleophilicity of C3 position, which was expected to be the reactive site. Thus, the reason for diazo coupling being majority in relation to photoredox arylation might be related to the intramolecular hydrogen bond that would stabilize the diazo product by a 6-membered ring intermediate (Figure 28), as shown by Zollinger.²²¹

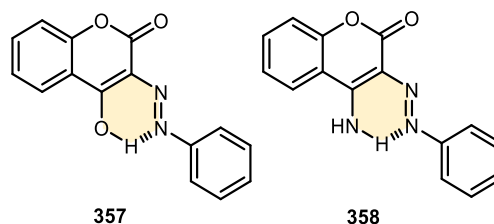


Figure 28: The stabilization of diazo coupling products **357** and **358** by intramolecular hydrogen bond.

Based on these facts, both groups should be protected. The choice of such a protecting group might be followed up by the increase of chemical potential and,

hence, the coumarins' character changing to nucleophilic. The evaluation of the protecting groups of the OH was carried out by the global reactivity parameters of the Conceptual DFT (Table 5). Alkyl groups (**361a-e**), PMP (**361f**) and benzylic groups **361h** and **361i** increase the chemical potential in such a way that the coumarins would act as the nucleophiles. Silyl groups (**361l-t**) also exhibited the same tendency. These groups have moderate nucleophilicity according to the calculations, which means that probably such reactions would not work or give low yields. Surprisingly, the dansyl group (**361am**) was the only sulfonyl protecting group that increased the chemical potential and would exhibit a strong behavior, probably due to the presence of the NMe₂ group, a strong EDG. Its little commercial availability and high price was a drawback to the usefulness of this protecting group.

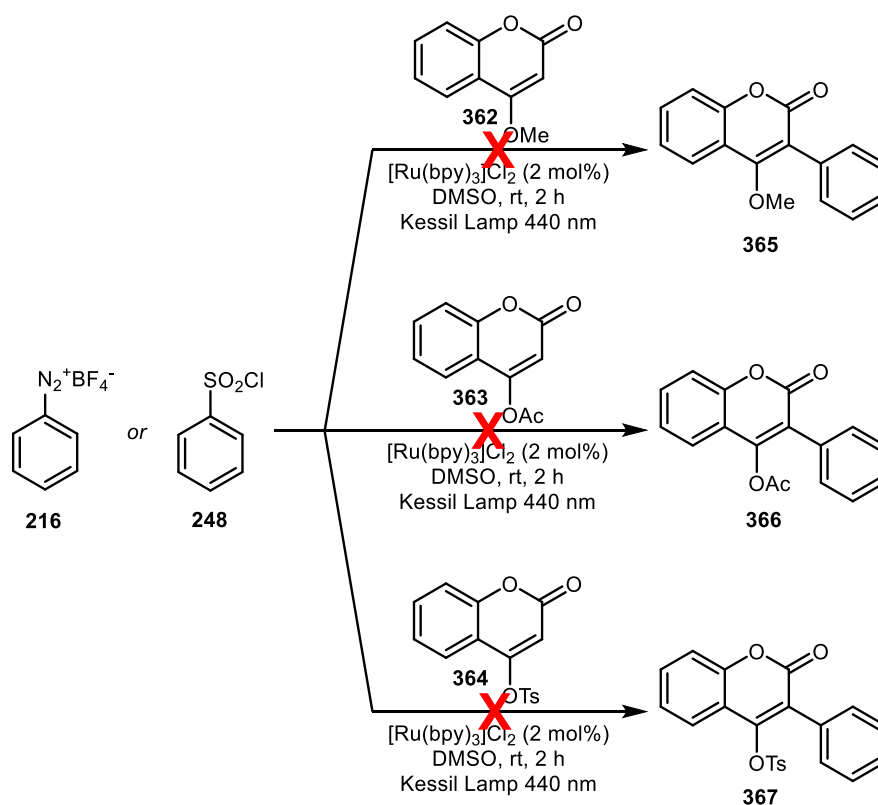
Table 5: Global chemical potential (μ^0/eV), global hardness (η^0/eV), global electrophilicity (ω^0/eV) and global nucleophilicity (N^0/eV) of protected 4-hydroxycoumarins.

Compound	R	μ^0	η^0	ω^0 ^a	N^0 ^a
361a	Me	-4.27	4.80	1.90	2.74
361b	MOM	-4.26	4.74	1.91	2.78
361c	BOM	-4.23	4.74	1.89	2.80
361d	THP	-4.17	4.74	1.83	2.87
361e	^t Bu	-4.14	4.78	1.79	2.88
361f	PMP	-4.28	4.75	1.93	2.76
361g	PNP	-5.09	3.77	3.44	2.43
361h	Bn	-4.22	4.80	1.85	2.79
361i	4-OMeBn	-4.16	4.80	1.81	2.85
361j	4-NO ₂ Bn	-5.05	3.61	3.53	2.56
361k	TMS	-4.66	3.96	2.74	2.77
361l	TES	-4.14	4.73	1.82	2.90
361m	TIPS	-4.14	4.72	1.82	2.91
361n	TBDMS	-4.16	4.72	1.83	2.89
361o	TBDPS	-4.12	4.70	1.81	2.94
361p	TPS	-4.14	4.69	1.82	2.93
361q	DPMS	-4.14	4.71	1.82	2.91
361r	DTBMS	-4.16	4.71	1.83	2.90
361s	TBMPs	-4.21	4.68	1.89	2.86
361t	DPTBOS	-4.13	4.69	1.82	2.93

361u	Ac	-4.54	4.60	2.25	2.57
361v	C(O)CH ₂ Cl	-4.73	4.57	2.45	2.39
361w	C(O)CHCl ₂	-4.82	3.70	3.13	2.74
361x	TFA	-5.01	4.35	2.88	2.23
361y	C(O)CH ₂ OMe	-4.57	4.60	2.27	2.54
361z	Piv	-4.50	4.60	2.20	2.60
361aa	Bz	-4.61	4.35	2.45	2.62
361ab	4-NO ₂ Bz	-5.35	3.40	4.21	2.36
361ac	Pic	-4.67	4.07	2.69	2.70
361ad	CO ₂ Et	-4.47	4.65	2.16	2.61
361ae	Boc	-4.41	4.66	2.09	2.67
361af	Troc	-4.66	4.61	2.36	2.44
361ag	Fmoc	-4.45	3.77	2.62	3.08
361ah	Aqmoc	-5.16	3.40	3.91	2.55
361ai	Ms	-4.58	4.65	2.26	2.50
361aj	Tf	-4.98	4.48	2.77	2.19
361ak	Ts	-4.66	4.40	2.46	2.55
361al	Ns	-4.90	3.59	3.34	2.71
361am	Ds	-4.18	3.95	2.22	3.26

^a Legend of colors: good; moderate and weak nucleophile/electrophile.

To validate these calculations, reactions were carried out with some of the calculated coumarins. The photoredox arylations were carried out using **216** and **248** as phenyl radicals' sources with **362**, **363** and **364** (Scheme 54). As expected, the desired products (**365**, **366** and **367**) were not observed neither diazo coupling when diazonium salt was used, suggesting that the usefulness of reactivity parameters could be a reasonable analysis to predict if the arylation would work or not as a function of the protecting group. When **248** was used, the total consumption of the starting material was observed by TLC after 1 h of reaction, but no product was formed after 24 h, which was further confirmed by GC-MS.



Scheme 54: Attempts on the arylation of protected 4-hydroxycoumarins.

Then, the analysis of protected 4-aminocoumarins was carried out (Table 6). Besides the typical protecting groups, phenyl group (**368a**) and alkyl groups (**368b-d**) were also analysed. Such groups were considered based on their synthetic value and possibilities of post-functionalization. The compounds **368a-d** and **368f-h** exhibited higher μ^0 than the phenyl radical, indicating that such groups would be useful to the arylation. Turning the attention to the nucleophilicity values, **368p** and **368r** are moderate nucleophiles and would not form product if used in the desired reaction. To continue with this study, compound **368a** was chosen to optimize the photoredox arylation.

Table 6: Global chemical potential (μ^0 /eV), global hardness (η^0 /eV), global electrophilicity (ω^0 /eV) and global nucleophilicity (N^0 /eV) of protected 4-aminocoumarins calculated at B3LYP/6-31+G(d) level of theory.

Compound	R	μ^0	η^0	ω^0	N^0
368a	Ph	-3.72	4.30	1.61	3.54
368b	Me	-3.68	4.58	1.73	3.14
368c	ⁿ Bu	-3.96	4.58	1.72	3.16
368d	MOM	-4.10	4.59	1.83	3.02
368e	CH ₂ CN	-4.41	4.65	2.09	2.68
368f	Bn	-3.98	4.58	1.73	3.14
368g	MPM	-3.92	4.57	1.68	3.20
368h	Dmb	-3.81	4.57	1.59	3.31
368i	CHO	-4.61	4.49	2.37	2.55
368j	Ac	-4.48	4.51	2.22	2.67
368k	C(O)CH ₂ Cl	-4.61	4.48	2.37	2.56
368l	C(O)CCl ₃	-4.82	4.34	2.68	2.42
368m	TFA	-4.92	4.37	2.77	2.31
368n	Bz	-4.51	4.35	2.34	2.73
368o	CO ₂ Me	-4.41	4.56	2.13	2.72
368p	Boc	-4.32	4.56	2.05	2.81
368q	Cbz	-4.37	4.56	2.09	2.76
368r	Moz	-4.32	4.54	2.05	2.82
368s	PNZ	-5.04	3.59	3.53	2.58
368t	Fmoc	-4.25	4.22	2.14	3.05
368u	Ms	-4.59	4.62	2.28	2.51
368v	Tf	-4.87	4.53	2.62	2.27
368w	Ts	-4.49	4.53	2.22	2.66
368x	Phthalimide	-4.92	3.87	3.12	2.55
368y	DMN	-4.93	3.80	3.20	2.58

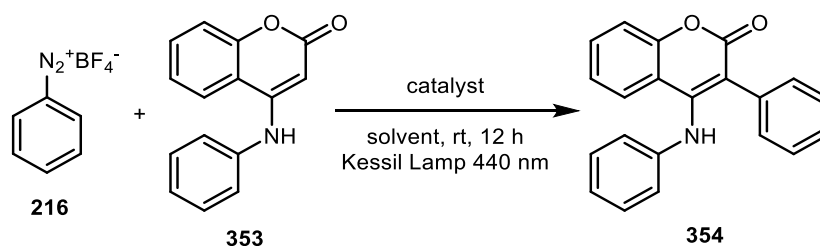
^a Legend of colors: good; moderate and weak nucleophile/electrophile.

2.4.2. Optimization of photoredox arylation

Based on the theoretical calculations of the protecting groups, compound **368a** was chosen to optimize the photoredox arylation (Table 7). In this reaction only two

variables must be optimized: catalyst and solvent. Due to iridium complexes are more expensive, this study was carried out with more “cost-friendly” catalysts. The photocatalyst $[\text{Ru}(\text{bpy})_3]\text{Cl}_2$ in 1.0 mol% (Entry 1) gave 53% yield, while metal-free photocatalysts (Entries 2, 3 and 4) gave lower yields (30 – 33%).

Table 7: Optimization studies on the arylation of **368a** by photoredox catalysis.



Entry	Catalyst (mol%)	Solvent	Yield ^a (%)
1	$[\text{Ru}(\text{bpy})_3]\text{Cl}_2$ (1.0)	DMSO	53 (50 ^b)
2	Eosin Y (2.0)	DMSO	33
3	Rose Bengal (2.0)	DMSO	32
4	PDI (2.0)	DMSO	30
5	$[\text{Ru}(\text{bpy})_3]\text{Cl}_2$ (1.0)	DMF	NP
6	$[\text{Ru}(\text{bpy})_3]\text{Cl}_2$ (1.0)	MeCN	NP
7	$[\text{Ru}(\text{bpy})_3]\text{Cl}_2$ (1.0)	DMSO ^c	21

General reaction conditions: 0.2 mmol of **216**, 1.0 mmol of **368a**, 2.5 mL of solvent, 1.0 mol% of the catalyst and irradiation with Kessil Lamp 440 nm. ^a Yields determined after work up by ¹H-NMR using 1,3,5-trimethoxybenzene or 1,4-dimethoxybenzene as internal standard. ^b Isolated yield after column chromatography. ^c DMSO used directly from the bottle with no drying procedure.

The solvent optimization was done evaluating DMF and MeCN (Entries 5 and 6). No product was observed in both reactions, which suggests that the DMSO participates in the reaction mechanism. These reactions were used after drying procedures. When DMSO was used with no drying (Entry 7) the yield decreased to 21%, which means that the presence of water in the reaction media reduces its performance. It is important to point out that these reactions were carried out in 0.08 mol L⁻¹ of **368a** in the solvents. This coumarin showed poor solubility in all the solvents and required higher amount of them to solubilize it entirely. Because of the more diluted starting materials, the optimizations were carried out in 12 h.

2.4.3. Diazonium salt scope

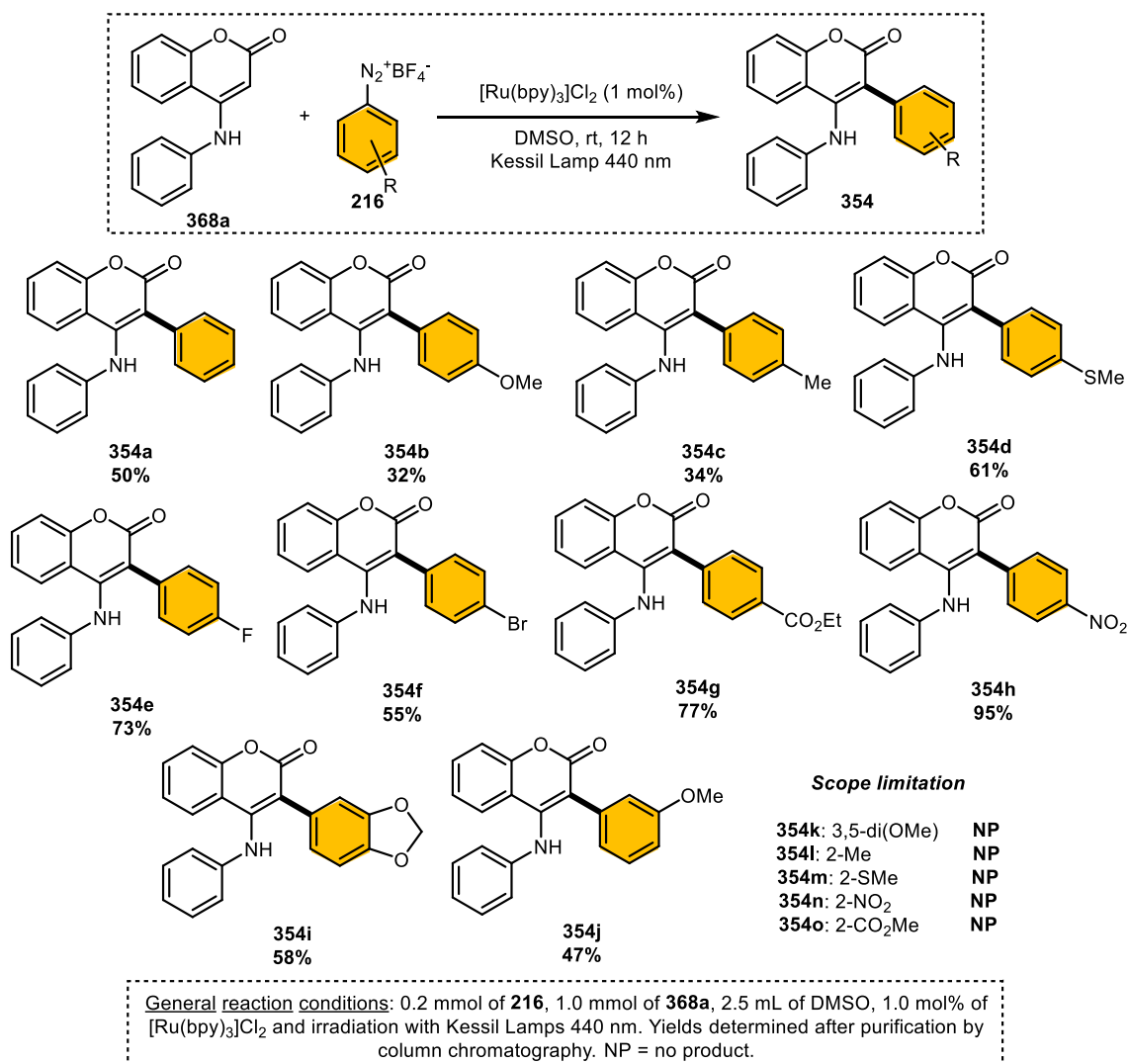


Figure 29: Evaluation of the diazonium salt scope.

The next step was the evaluation of the diazonium salt scope to evaluate the optimized methodology (Figure 29). The reactions with phenyl diazonium salts with groups at *para*-position are suitable. The presence of stronger donating groups at **354b** and **354c** reduces the yield to 32 and 34%, respectively. A neutral group (**354d**, 61% yield) and halogens (**354e** and **354f**, 73 and 55% yield, respectively) have improved performance compared to the product with no substituents. Electron withdrawing groups improved the reaction to achieve good yields, as in **354g** (77% yield) and **354h** (95% yield). The presence of a dioxazole group (**354i**) gave the

product in 58% yield. The presence of only one substituent at *meta*-position was suitable as in **354j** (47% yield). When a second group at *meta*-position is present, no product is formed. The use of *ortho*-substituted diazonium salts (**354l** to **354o**) tolerated.

These results clearly indicate the electronic demand at the diazonium salts. The reactivity parameters were calculated for the radicals used in the photoredox arylations (Table 8). Coumarin **354a** has the $\mu^0 = -3.72$ eV, which is higher than all the calculated radicals. It indicates that for all the reactions the coumarin is the nucleophile and the phenyl radical is the electrophile. The ω^0 calculated showed that these phenyl radicals are good electrophiles and the electrophilicity increases as the group is more electron withdrawing.

Table 8: Global chemical potential (μ^0 /eV), global hardness (η^0 /eV), global electrophilicity (ω^0 /eV) and global nucleophilicity (N^0 /eV) of the phenyl radicals calculated at UB3LYP/6-31+G(d) level of theory

Compound	R	μ^0	η^0	ω^0	N^0
69a	H	-4.33	4.51	2.08	1.30
69b	4-OMe	-3.99	4.07	1.96	1.86
69c	4-Me	-4.19	4.46	1.97	1.47
69d	4-SMe	-4.21	3.95	2.25	1.70
69e	4-F	-4.54	4.55	2.27	1.07
69f	4-Br	-4.57	4.35	2.40	1.14
69g	4-CO ₂ Et	-4.54	4.50	2.29	1.10
69h	4-NO ₂	-5.00	4.52	2.77	0.63
69i	dioxazole	-4.32	3.41	2.74	1.86
69j	3-OMe	-4.40	3.84	2.53	1.57

^a Legend of colors: good; moderate and weak nucleophile/electrophile.

These calculations are in consonance with the expectations. The presence of EWG, such as NO₂ and CO₂Et, in the phenyl radical reduces the electronic density and make these radicals more electrophilic. In terms of FMO, these groups would lower the SOMO level of these radicals. On the other hand, the presence of EDG would increase the electronic density at the carbon-centered radical making it less electrophilic and, hence, being less reactive toward the coumarins.

The choice of the diazonium salts could also be explained based on the synthetic value of the substituents planning future functionalizations. The methoxy

group at **354b** can be converted to phenol and then, to other, and more complex, ethers. The thiomethyl group at **354d** can be oxidized to sulfoxides and sulfones groups. The presence of halogen as in **354f** can undergo coupling reactions to allow new C-C bonds. The ester group as in **354g** can be transesterified to other esters and hydrolyzed to acids to, then, be covered to other functions like amides and anhydrides. Finally, the nitro group at **354h** can be reduced to amino.

To understand the scope limitations, the structures of the compounds **354a**, **354b**, **354i**, **354j** and **354l** were optimized at M06-2X/6-311++G(d,p) level of theory (Figure 30). The 3-phenyl ring in all the structures is twisted. Two geometrical parameters were taken into account to understand such compounds: the C3-C1' bond length ($R_{C3-C1'}$) and the torsion angle (θ), represented by the dihedral angle between atoms C2-C3-C1'-C2' (Table 9). There was no difference in the $R_{C3-C1'}$ distance but when there was a substituent at *ortho*-position, the torsion angle increased around 10° . The presence of the OMe group near the carbonyl or the *N*-phenyl-amino group increases the steric hindrance and can explain why *ortho* substituted compounds are not tolerated.

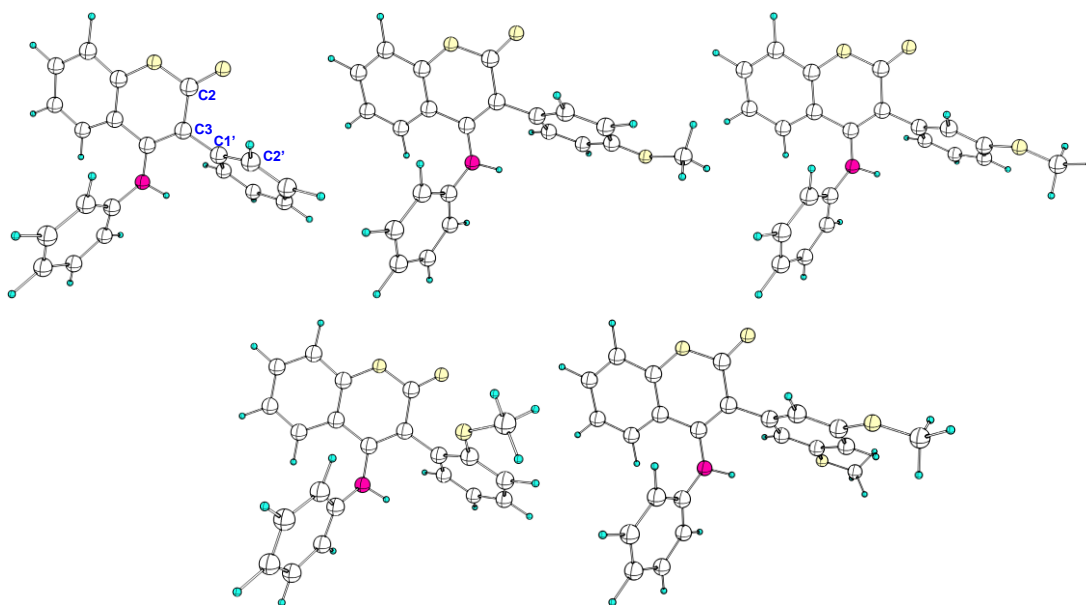


Figure 30: Optimized structures of **354a**, **354b**, **354i**, **354j** and **354l** at M06-2X/6-311++G(d,p) level of theory.

Table 9: Structural parameters of some optimized 3-arylcoumarins calculated at M06-2X/6-311++G(d,p) level of theory.

Compound	R _{C3-C1'} (Å)	θ (°)
354a	1.485	57.4
354b	1.483	55.9
354j	1.486	59.8
354k	1.486	60.2
354l	1.482	67.5

2.4.4. Coumarin scope

The presence of substituents at the *N*-aryl-amino group was also evaluated. The use of anilines to make 4-aminocoumarins allowed the obtation of five new functionalizable positions, which were further explored in the biological activities' tests. The inversion of the reactivity was observed (Figure 31). The strongest donating group OMe (**354p**) increased the yield to 66%. Weaker donating groups (**354q**, 54% yield) and halogens (**354r** and **354s**, 53 and 50% yield, respectively) did not influence significantly. The use of withdrawing groups decreased the yield to 42% (**354t**) and a stronger group such as NO₂ did not give product (**354y**). The presence of substituents at *ortho*- and *meta*-position (**354u** and **354v**) and at both rings (**354w** and **354x**) were also tolerated.

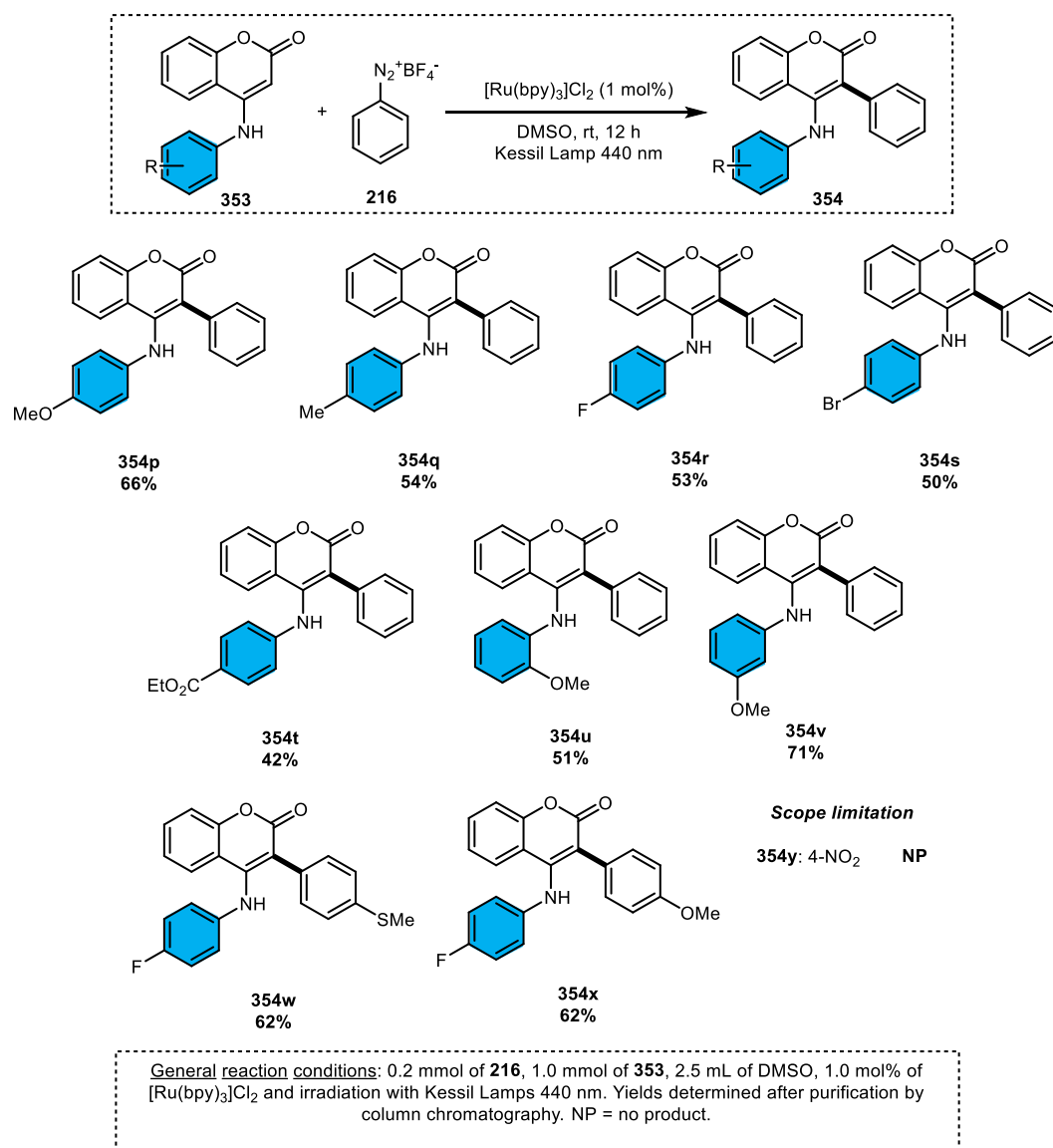


Figure 31: Evaluation of the coumarin scope.

The substitution at *N*-aryl ring pointed out the inverted the electronic demands. The presence of EDG increased the yields, while EWD decreased. The former groups would increase the electronic density at the C3 position, turning the coumarin more nucleophilic. This effect is observed at the global nucleophilicity, that decreases as more withdrawing is the group attached to the *N*-aryl group (Table 10). The nitro group reduced the N^0 of **353g** to 2.99 eV, which is a value related to moderate nucleophiles, suggesting that this reaction needs good nucleophiles reacting with the phenyl radicals to work. This is in consonance with the expected reduction of the electronic density at the C3 position due to the withdrawing effect of this group.

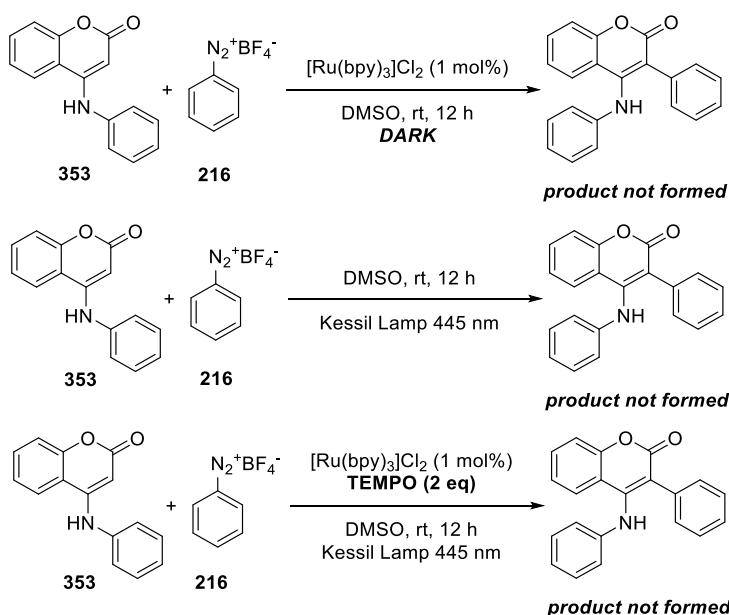
Table 10: Global chemical potential (μ^0/eV), global hardness (η^0/eV), global electrophilicity (ω^0/eV) and global nucleophilicity (N^0/eV) of 4-(*N*-aryl)coumarins calculated at B3LYP/6-31+G(d) level of theory

Compound	R	μ^0	η^0	ω^0	N^0
353a	H	-3.72	4.30	1.61	3.54
353b	4-OMe	-3.52	4.16	1.49	3.81
353c	4-Me	-3.64	4.26	1.56	3.64
353d	4-F	-3.77	4.32	1.65	3.48
353e	4-Br	-3.86	4.26	1.75	3.42
353f	4-CO ₂ Et	-3.95	4.19	1.86	3.36
353g	4-NO ₂	-4.49	3.86	2.61	2.99

^a Legend of colors: good; moderate and weak nucleophile/electrophile.

2.4.5. Mechanistic studies

Control experiments were carried out to confirm the photoredox behavior of the reaction (Scheme 55). The reactions with no light and no catalyst did not give the desired product. It confirms that both are required in the reaction and suggests a photoredox mechanism. Thus, the generation of radicals was investigated adding 2 equivalents of TEMPO in the reaction. No product was observed, suggesting the formation of radical species during the reaction. Unfortunately, no trapped radical species were identified.



Scheme 55: Control experiments and radical-trapping reaction with TEMPO.

Stern-Volmer experiments were done to identify the specie that quenches the photocatalyst in the excited state (Figure 32), once secondary amines are prone to quench $Ru(II)^*$ to generate nitrogen-centered radical cation species.^{222,223} A solution of $[Ru(bpy)_3]Cl_2$ was prepared in anhydrous DMSO ($[Ru(II)] = 10^{-4} \text{ mol L}^{-1}$), excited at 453 nm and the emitted luminescence at 600 nm recorded. Aliquots of stock solutions of **216** and **353** were added in separated experiments under argon atmosphere. The addition of **353** did not quench the photoluminescence, however, **216** quenched. It suggests that **216** reacts with $Ru(II)^*$ via SET to generate the phenyl radical and **69** is involved in further steps.

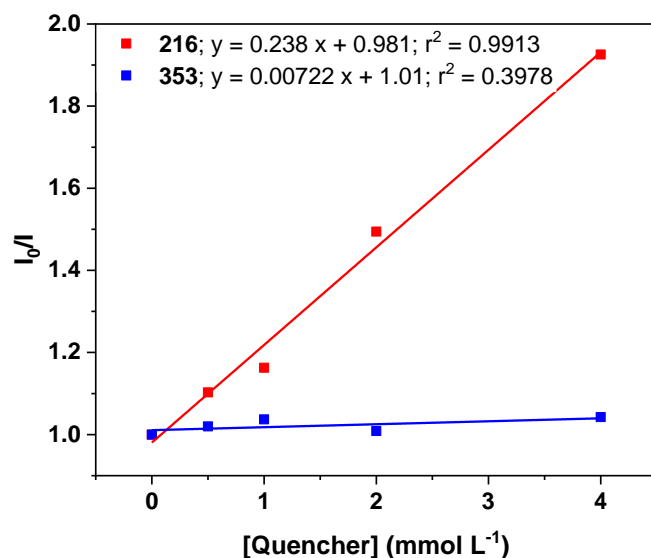


Figure 32: Stern-Volmer analysis for **216** and **353** as quenchers of $[\text{Ru}(\text{bpy})_3]^{2+}$.

The linear fitting obtained from the **216** quenching data showed good correlation with $r^2 = 0.9913$. The slope is considered as the Stern-Volmer constant (K_{SV}) which is equal to 0.238. The kinetic of this process is dictated by the Stern-Volmer relationship (Equation 6). The quenching rate constant k_q was calculated from the linear fitting as $2.18 \times 10^5 \text{ M}^{-1} \text{ s}^{-1}$. The quenching fraction of $Q = 0.81$ (equation 7) indicates that 81% of the photons absorbed by the photocatalyst induce an electron transfer process to generate phenyl radicals.

$$\frac{I_0}{I} = 1 + k_q \tau_0 [\text{Quencher}] \quad (6)$$

- I_0 : intensity of the emitted luminescence in the absence of a quencher.
- I : intensity of the emitted luminescence in the presence of a quencher.
- k_q : quenching rate constant.
- τ_0 : excited state lifetime.

$$Q = \frac{k_{q,216}[\mathbf{216}]}{\tau_0^{-1} + k_{q,216}[\mathbf{216}] + k_{q,353}[\mathbf{353}]} \quad (7)$$

- $k_{q,216}$ and $k_{q,353}$: quenching rate constants of **216** and **353**, respectively.
- **[216]** and **[353]**: concentration of the quenchers **216** and **353**, respectively.

Based on these results, a plausible mechanism could be proposed in an oxidative quenching cycle (Figure 33). After the excitation of the $[\text{Ru}(\text{bpy})_3]^{2+}$ by the

blue light to $[\text{Ru}(\text{bpy})_3]^{2+*}$, it carries out a SET reaction with **98** to generate the phenyl radical **69**. Then, the radical is added to the coumarin **353** to make the adduct **369**, which, via SET, donates an electron to the Ru(III) to regenerate the photocatalyst and to achieve the intermediate cation **370**. Finally, an elimination step of **370** gives the desired product **354**.

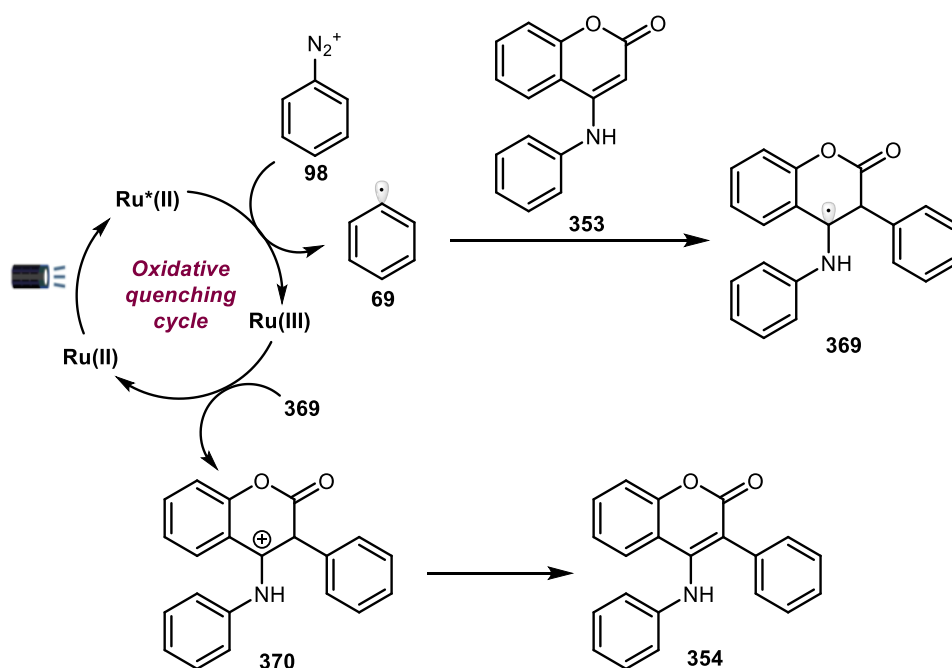
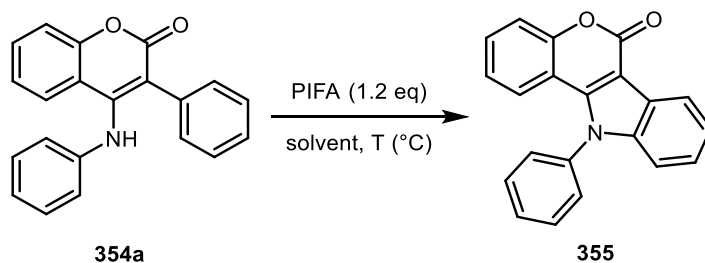


Figure 33: Mechanism proposed to the photoredox arylation of 4-(*N*-aryl)aminocoumarin.

2.4.6. Azacoumestan synthesis

Once the compound **354a** was obtained, attempts were carried out to make the indole ring, characteristic of the azacoumestans. Zhao et al proposed the intramolecular C-N bond formation from enamines using the hypervalent iodine specie PIFA as oxidizing agent.²²⁴ Starting from PIFA, the cyclizations were carried out using different solvents (Table 11).

Table 11: Optimization of the intramolecular oxidative amination of the coumarin **354a**.

Entry	Solvent	Temperature (°C)	Time (h)	Yield (%)
1	DCM	rt	1	32
2	DCM	rt	24	35
3	EtOAc	rt	1	42
4	MeCN	rt	1	48
5	MeCN	reflux	24	NP
6	TFE	rt	1	86

Initially, the reaction was done with the same reaction conditions from Zhao et al, using DCM as solvent (Entry 1 and 2). The reaction needed 1 h to achieve the product in 32% yield. Increasing the reaction time to 24 h did not increase the amount of formed product (35% yield) and the total consumption of the starting material was not observed. Then, the solvent was changed to EtOAc (Entry 4) and MeCN (Entry 5), observing that the yield increased to 42% and 48%, respectively. At both conditions, the starting material was not consumed totally. Increasing the reaction temperature to reflux decomposed the PIFA and no product was observed. Finally, the reaction was carried out using trifluoroethanol (TFE) as solvent (Entry 6). It is known that fluorinated solvents increase the reaction performance of hypervalent iodines.²²⁵ Using this condition, the conversion was observed to be 100% and the desired azacoumestan was achieved in 86% yield.

2.4.7. Biological studies – antileishmanial and anti-cancer activity

The obtained coumarins were evaluated as potential antileishmanial and anti-cancer drug candidates. The *in vitro* activity was measured in terms of the inhibitory concentration (IC₅₀) against promastigotes of *Leishmania amazonensis* and MCF-7 and MDA-MB-231 cells of breast cancer (Table 12). The evaluated compounds were

compared to the reference drugs miltefosine and amphotericin B (AMB) for leishmaniasis and doxorubicin (DOX) for cancer cells.

Table 12: The IC₅₀ (μmol L⁻¹) against promastigotes of *L. amazonensis* and MCF-7 and MDA-MB-231 cells after 24 h of treatment.

Compound	IC ₅₀ (μmol L ⁻¹)		
	<i>L. amazonensis</i>	MCF-7	MDA-MB-231
354a	>300	492.08±4.37	>600
354b	>300	>600	>600
354c	>300	466.42±4.51	>600
354d	5.96±3.21	178.05±4.35	>600
354e	>300	266.76±4.00	>600
354f	>300	437.47±3.91	>600
354g	>300	193.24±3.97	>600
354h	>300	416.25±5.87	336.6±4.3
354i	>300	273.33±3.822	>600
354j	>300	>600	>600
354p	>300	>600	>600
354q	>300	>600	>600
354r	>300	>600	>600
354s	9.05±2.86	267.86±3.59	>600
354t	>300	>600	>600
354u	>300	>600	>600
354v	>300	420.52±3.96	>600
354w	>300	229.15±3.94	>600
354x	5.65±2.08	267.86±3.59	>600
355	>300	>600	>600
Miltefosine	8.56±0.70	---	---
AMB	0.41±0.13	---	---
DOX	---	3.03±1.14	289.4±2.5

The compounds **354d**, **354s** and **354x** showed great *in vitro* activity against *L. amazonensis* with IC₅₀ of 5.96±3.21, 9.05±2.86 and 5.65±2.08 μmol L⁻¹, respectively, after 24 h of treatment. These results are lower than IC₅₀ = 0.14±0.13 μmol L⁻¹ for

amphotericin B. On the other hand, these activities were comparable to the miltefosine ($IC_{50} = 8.56 \pm 0.70 \mu\text{mol L}^{-1}$), which is the drug used in the oral treatment of leishmaniasis.²²⁶ These compounds have higher activity as compared to 4-phenylcoumarins synthesized by Santos et al.²²⁷ Singh et al obtained five coumarins with the group 1,3-benzodioxole at position C3 after an extensive *in silico* screening. The compounds **371** and **372** showed the $IC_{50} = 223$ and $524 \mu\text{mol L}^{-1}$ after 48 h of treatment of *L. major* promastigotes (Figure 34).²²⁸ The coumarin obtained by this work with the same group at position C3 (**354i**) did not show activity.

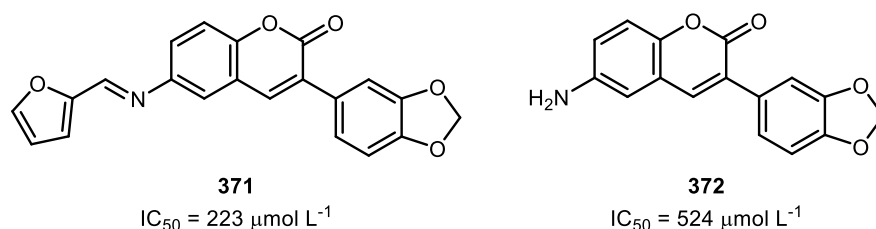


Figure 34: Coumarins with activity against *L. major* promastigotes.

The synthesized coumarins were also evaluated as potential anti-cancer candidates. The high values of IC_{50} indicated that these compounds did not have similar efficiency for inhibiting MCF-7 cells growth as compared to DOX. For MDA-MB-231 cells, only **354h** exhibited activity with $IC_{50} = 336.6 \pm 4.3 \mu\text{mol L}^{-1}$, however still lower than DOX ($IC_{50} = 289.4 \pm 2.5 \mu\text{mol L}^{-1}$). Gdadebo et al obtained coumarins analogue to **354h** (Figure 35). The cytotoxicity evaluated as the CC_{50} value showed that the presence of the 4-nitrophenyl group at position C3 is not responsible for the activity against MDA-MB-231 cells after 48 h of treatment, but OAc groups at C7 and C8 positions (**307**) caused the death of the cells with $CC_{50} = 17.1 \pm 1.1 \mu\text{mol L}^{-1}$. This report indicates that functionalization of **354h** at ring A could increase its activity.

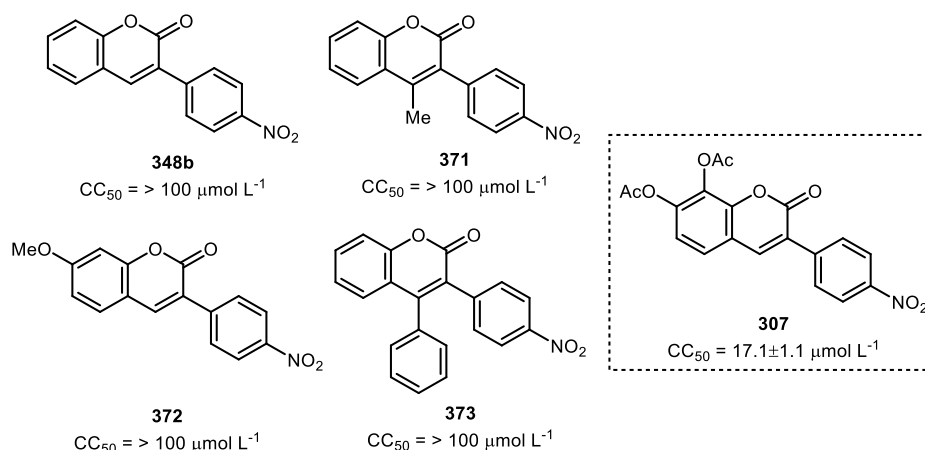


Figure 35: Coumarins with activity against MDA-MB-231 cells (breast cancer).

The *in silico* toxicity was calculated using the *OpenVirtualToxLab* software.²²⁹ It simulates the binding affinities of the desired compound in 16 proteins, which are suspected to be involved in side effects: 10 nuclear receptors (androgen, estrogen α , estrogen β , thyroid α , thyroid β , glucocorticoid, liver X, mineralocorticoid, progesterone and peroxisome proliferator-activated receptor γ), 4 members of the cytochrome P450 enzyme family (1A2, 2C9, 2D6 and 3A4), the aryl hydrocarbon receptor, and the potassium ion channel hERG. These interactions are converted in the ToxPot, a value between 0.0 (none) and 1.0 (extreme) that measures the toxicity potential of a molecule (Table 13). According to González-Laredo et al, the algorithm used by this software is based only in thermodynamics properties and, because of this, ADME properties (adsorption, distribution, metabolism and elimination) should be analyzed in parallel to have a better evaluation.²³⁰

Table 13: Classification of the toxicity as a function of the ToxPot calculated at the *OpenVirtualToxLab* software.

Class	ToxPot	Classification
	≤ 0.3	None
0	$0.3 < \text{ToxPot} \leq 0.4$	Low
	$0.4 < \text{ToxPot} \leq 0.5$	Moderate
I	$0.5 < \text{ToxPot} \leq 0.6$	Elevated
II	$0.6 < \text{ToxPot} \leq 0.7$	High
III	$0.7 < \text{ToxPot} \leq 0.8$	Very high
IV	> 0.8	Extreme

The synthesized coumarins and azacoumestan were submitted to the calculations and miltefosine; AMB and DOX were used as references (Table 14). Unfortunately, the calculation with AMB failed due to its high molecular weight, which is not accepted by the software. The estimated ToxPot for DOX was 0.690, which is considered as a high toxic compound. The simulations showed moderate binding to the enzyme CYP1A4 ($0.169 \mu\text{mol L}^{-1}$) and the mineralocorticoid receptor (MR, $0.806 \mu\text{M}$), and strong binding to hERG (715 pmol L^{-1}). DOX binds weakly to ER β ($26.2 \mu\text{mol L}^{-1}$), PPAR γ ($41.4 \mu\text{mol L}^{-1}$) and TR β ($48.2 \mu\text{mol L}^{-1}$). To the other proteins, the affinity was higher than $100 \mu\text{mol L}^{-1}$, which, according to the software, is considered as “not binding”.

Table 14: Calculated ToxPot at the *OpenVirtualToxLab* software for the synthesized coumarins and azacoumestan.

Compound	ToxPot	Compound	ToxPot
354a	0.375	354q	0.472
354b	0.401	354r	0.474
354c	0.404	354s	0.408
354d	0.428	354t	0.392
354e	0.408	354u	0.522
354f	0.419	354v	0.441
354g	0.421	354w	0.383
354h	0.468	354x	0.390
354i	0.505	355	0.456
354j	0.504	AMB	NA
354p	0.340	DOX	0.690

The ToxPot calculated to all the synthesized compounds ranged from 0.375 to 0.505 (Table 14), which means that they have lower probability of being more toxic than DOX. Comparing to **354a**, the presence of substituents increased the ToxPot. A closer look at the compounds **354d**, **354h**, **354s** and **354x** showed binding to more proteins than DOX. These coumarins interacted to AhR from weak to moderate (from 9.89 to $0.919 \mu\text{M}$), while DOX did not interact with this protein. Important interactions with AR, PPAR γ , TR α and TR β were also observed. The strong binding mode to hERG

observed with DOX was also calculated for the coumarins, but in weak to moderate fashion.

Table 15: Calculated IC₅₀ (μmol L⁻¹) for compounds **354d**, **354h**, **354s** and **354x** at 16 proteins using *OpenVirtualToxLab* software.

	354d	354h	354s	354x	DOX
AR	0.928	0.220	8.84	1.30	NB
AhR	0.531	0.824	0.789	1.65	NB
CYP1A2	NB	94.8	NB	60.6	NB
CYP2C9	NB	64.8	34.0	NB	0.169
CYP2D6	NB	7.59	99.2	89.8	NB
CYP3A4	98.8	22.7	81.3	NB	NB
ERα	17.2	12.9	7.26	25.2	NB
ERβ	1.92	NB	32.0	NB	26.2
GR	17.4	0.533	15.0	50.9	NB
hERG	4.05	3.16	4.97	3.51	0.000715
LXR	24.3	53.1	48.1	29.1	NB
MR	28.9	92.3	12.7	12.8	0.806
PPARγ	24.3	8.12	4.74	3.07	41.4
PR	63.7	6.66	4.69	9.46	NB
TRα	51.9	10.4	1.72	8.89	NB
TRβ	43.0	4.55	3.03	21.0	48.2

NB = not binding

2.5.

Conclusion and future perspectives

With an optimized photoredox arylation it was possible to obtain 4-(*N*-aryl)amino-3-arylcoumarins in yields up to 95%. The methodology showed tolerant to many functional groups, while *ortho*- or *dimetha*-substitution at the diazonium salt and the presence of strong EWG at the 4-(*N*-aryl)amino ring were the limitations. The electronic demands were evaluated with the Conceptual DFT, which showed that electron-withdrawing groups make the phenyl radicals more electrophilic, which was important to increase the yields, since according to the chemical potentials, the

coumarins are the nucleophiles. When electron-withdrawing groups are at the 4-(*N*-aryl) ring, it decreases the nucleophilicity and could explain why these groups tend to reduce the yields. Three of the obtained coumarins showed good activity against *L. amazonensis* promastigotes, which means that these compounds are candidates for new anti-leishmaniasis drugs.

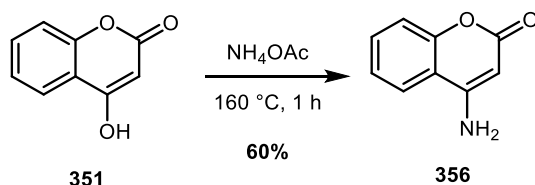
The amastigote cells are being tested for the coumarins and the mechanism related to the mode of action. With these results, it will be possible to plan better substitutions and new coumarins will be synthesized. Further, the optimization of the azacoumestan synthesis will be carried out in terms of new hypervalent iodines that would be useful for the oxidative amination and also evaluate the behaviour of the methodology in the presence of different functional groups at both analyzed rings.

2.6.

Experimental procedures

All reagents were bought from Sigma-Aldrich, Oakwood Chemicals or Isolar and used as received. DMSO, DMF and acetonitrile were dried refluxing overnight over CaH₂, followed by distillation (vacuum one for DMSO and DMF), and stored in molecular sieves. Dioxane was dried over sodium followed by distillation and stored in molecular sieves. Pyridine was dried over CaH₂ overnight and used after distillation. Phenyl diazonium salts were obtained according to the literature procedures.^{127,130} Acetone and THF were dried over molecular sieves overnight. Reactions were monitored by thin layer chromatography using Merck TLC Silica gel 60 F254. The chromatographic columns were performed over Merck Silica gel 60 Å (particle size: 0.040–0.063 mm, 230–400 mesh ASTM) treated with triethylamine before use when needed. The columns were run at Biotage® Isolera One instrument. ¹H NMR and ¹³C NMR spectra were recorded on a Bruker Avance III spectrometer, operating at 400 MHz for ¹H NMR and 100 MHz for ¹³C NMR (¹H-decoupled) using CDCl₃ or DMSO-*d*₆ as solvents. The chemical shifts (δ) were given in parts per million (ppm) and tetramethylsilane was used as internal standard. The multiplicities were reported as s = singlet, d = doublet, t = triplet, q = quartet, m = multiplet and br = broad signal. All coupling constants (*J* values) were given in Hz. The biological essays were carried out at Fundação Oswaldo Cruz (FIOCRUZ) and conducted by Dr. Fernando Almeida.

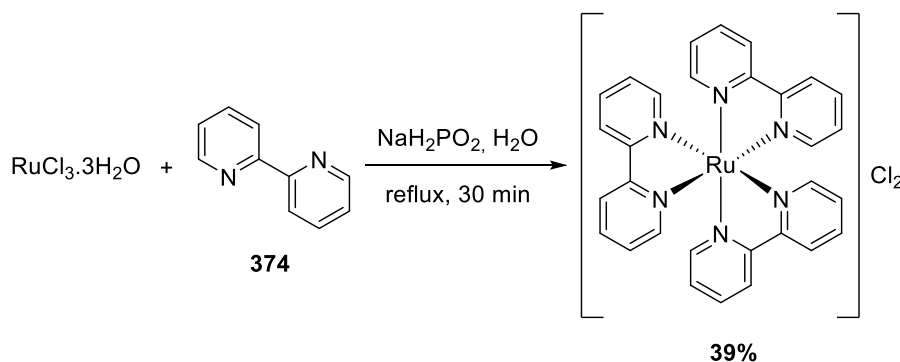
2.6.1. Synthesis of 4-aminocoumarin



The reaction was carried out according to the literature.²³¹ In an opened flask, 2.0322 g (12.3 mmol) of **351** and 9.5539 g (124 mmol) of NH_4OAc were stirred at 160 °C for 1 h. After this time, the reaction was cooled to room temperature and water was added. This mixture was stirred at 60 °C for 30 min and filtered. The obtained solid was washed with water. The product **356** was oven dried overnight and used with no further purification.

Compound **356**. White solid (1.1622 g, 60%). $^1\text{H NMR}$ (400 MHz, $\text{DMSO-}d_6$): δ 7.98 (d, 7.9 Hz, 1H), 7.62 – 7.55 (m, 1H), 7.38 (br, 2H), 7.33 – 7.26 (m, 2H), 5.22 (s, 1H).

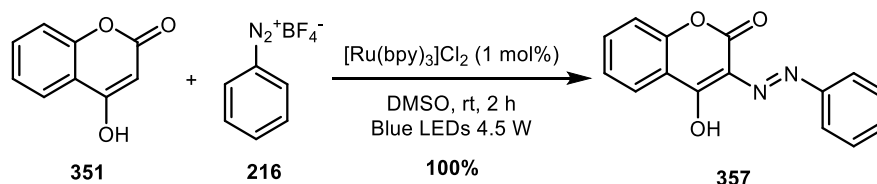
2.6.2. Synthesis of the photocatalyst $[\text{Ru}(\text{bpy})_3]\text{Cl}_2$



A 50 mL becher was charged with 101.4 mg (0.5 mmol) of $\text{RuCl}_3 \cdot x\text{H}_2\text{O}$, 0.2361 g (1.5 mmol) of **374**, 10 mL of water and 0.55 mL of an aqueous solution 6.0 mol L^{-1} of NaH_2PO_4 . The mixture was stirred at reflux for 30 min. The color changed from black to red. The reaction was cooled to room temperature and heated again to dissolve the solids. Finally, the flask was cooled in ice bath and the solid was filtered, washed with cold water and dried to achieve the desired photocatalyst.

Red solid (146.1 mg, 39%). ^1H NMR (400 MHz, $\text{DMSO}-d_6$): δ 8.85 (d, 8.1 Hz, 1H), 8.21 – 8.11 (m, 1H), 7.75 – 7.69 (m, 1H), 7.56 – 7.49 (m, 1H). ^{13}C NMR (100 MHz): δ 156.6, 151.3, 138.1, 128.0, 124.6.

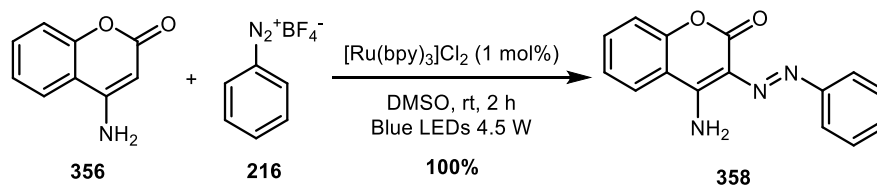
2.6.3. Arylation of the 4-hydroxycoumarin



A 2-dram vial was charged with 38.4 mg (0.2 mmol) of **216**, 162 mg (1.0 mmol) of **351**, 1.5 mg (1 mol%) of $[\text{Ru}(\text{bpy})_3]\text{Cl}_2$ and 1.0 mL of anhydrous DMSO. The reaction was irradiated with blue LEDs at room temperature for 2 h. After this time, the reaction was quenched with brine and extracted with dichloromethane (3X15 mL). The organic phases were dried with Na_2SO_4 and evaporated. The product was purified by column chromatography.

Compound **357**. Orange solid (52.5 mg, 100%). ^1H NMR (400 MHz, CDCl_3): δ 16.38 (br, 1H), 8.07 (dd, 7.8 and 1.5 Hz, 1H), 7.68 – 7.64 (m, 3H), 7.48 (t, 7.9 Hz, 2H), 7.40 – 7.27 (m, 3H).

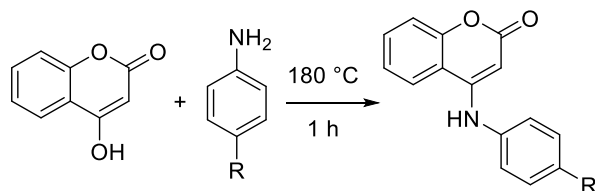
2.6.4. Arylation of the 4-aminocoumarin



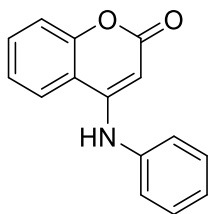
A 2-dram vial was charged with 38.4 mg (0.2 mmol) of **216**, 161 mg (1.0 mmol) of **356**, 1.5 mg (1 mol%) of $[\text{Ru}(\text{bpy})_3]\text{Cl}_2$ and 1.0 mL of anhydrous DMSO. The reaction was irradiated with blue LEDs at room temperature for 2 h. After this time, the reaction was quenched with brine and extracted with dichloromethane (3X15 mL). The organic phases were dried with Na_2SO_4 and evaporated. The product was purified by column chromatography.

Compound **358**. Yellow solid (52.8 mg, 100%). ^1H NMR (400 MHz, CDCl_3): δ 8.10 (d, 6.5 Hz, 1H), 7.70 – 7.65 (m, 3H), 7.49 (t, 7.9 Hz, 2H), 7.39 – 7.28 (m, 3H).

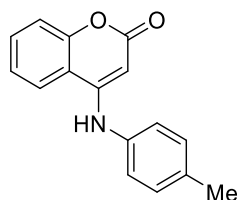
2.6.5. Synthesis of the 4-(N-aryl)aminocoumarins



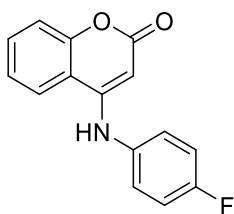
General procedure: a mixture of **351** (1 g, 6.2 mmol) and the respective aniline (2 eq) was heated in a 50 mL becher at 180 °C for 1 h under vigorous stirring. Then, the solid was added to a solution containing 30 mL of hot methanol and 30 mL of aqueous NaOH 1 mol L⁻¹. The mixture was stirred for 30 min at 60 °C and filtered afterwards. The solid was washed with water, dried and used without further purification.



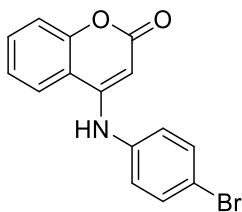
Compound **353a**. Yellow solid (1.1331 g, 80%). ^1H NMR (400 MHz, $\text{DMSO}-d_6$): δ 9.34 (br, 1H), 8.26 (dd, 1.2 and 8.1 Hz, 1H), 7.66 (m, 1H), 7.49 (m, 2H), 7.39 (m, 4H), 7.30 (t, 7.4 Hz, 1H), 5.31 (s, 1H). ^{13}C NMR (100 MHz): δ 161.5, 153.4, 152.5, 138.2, 132.4, 139.6, 126.0, 125.1, 123.6, 122.8, 117.1, 114.5, 84.4.



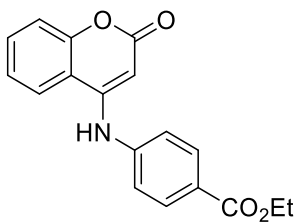
Compound **353c**. Pale yellow solid (1.0245 g, 66%). ^1H NMR (400 MHz, $\text{DMSO}-d_6$): δ 9.26 (br, 1H), 8.24 (dd, 7.1 and 0.9 Hz, 1H), 7.67 – 7.61 (m, 1H), 7.41 – 7.34 (m, 2H), 7.27 (q, 8.4 Hz, 4H), 5.21 (s, 1H), 2.34 (s, 3H). ^{13}C NMR (100 MHz): δ 161.5, 153.4, 152.7, 135.7, 135.3, 132.3, 130.0, 125.2, 123.5, 122.8, 117.0, 114.6, 83.8, 20.6.



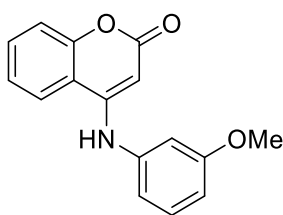
Compound **353d**. Gray solid (1.0333 g, 66%). ^1H NMR (400 MHz, $\text{DMSO}-d_6$): δ 9.30 (br, 1H), 8.22 (dd, 8.0 and 1.2 Hz, 1H), 7.71 – 7.61 (m, 1H), 7.48 – 7.25 (m, 6H), 5.19 (s, 1H). ^{13}C NMR (100 MHz): δ 161.4, 161.2, 158.7, 153.4, 152.8, 134.5, 134.4, 132.4, 127.6, 127.5, 123.6, 122.7, 117.0, 116.5, 116.2, 114.4, 84.3.



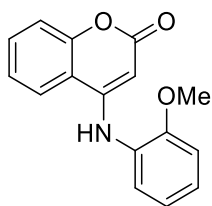
Compound **353e**. Pale yellow solid (1.0441 g, 53%). ^1H NMR (400 MHz, $\text{DMSO}-d_6$): δ 9.33 (br, 1H), 8.21 (dd, 8.0 and 1.1 Hz, 1H), 7.71 – 7.61 (m, 3H), 7.49 – 7.29 (m, 4H), 5.37 (s, 1H). ^{13}C NMR (100 MHz): δ 161.3, 152.0, 137.8, 132.5, 132.4, 126.8, 123.7, 122.8, 117.9, 1117.1, 114.5, 85.1.



Compound **353f**. Yellow solid (0.7811 g, 41%). ^1H NMR (400 MHz, CDCl_3): δ 8.10 (d, 8.5 Hz, 2H), 7.68 (d, 8.0 Hz, 1H), 7.60 (t, 7.6 Hz, 1H), 7.36 (m, 4H), 6.91 (br, 1H), 5.98 (s, 1H), 4.40 (q, 7.1 Hz, 2H), 1.41 (t, 7.1 Hz, 3H). ^{13}C NMR (100 MHz): δ 165.9, 162.8, 154.1, 150.4, 142.1, 132.6, 131.5, 127.7, 124.0, 122.7, 120.4, 118.3, 114.5, 89.3, 61.3.

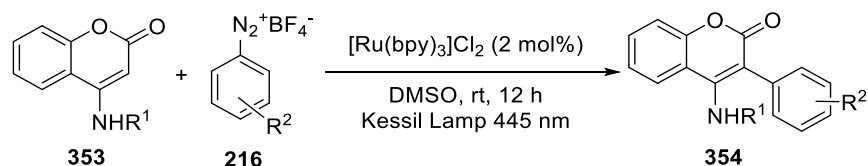


Compound **353h**. Pale yellow solid (1.2891 g, 78%). ^1H NMR (400 MHz, $\text{DMSO}-d_6$): δ 9.30 (br, 1H), 8.22 (dd, 1.2 and 8.0 Hz, 1H), 7.70 – 7.60 (m, 1H), 7.46 – 7.33 (m, 3H), 6.96 (dd, 1.2 and 7.9 Hz, 4H), 6.92 (t, 2.2 Hz, 1H), 6.87 (dd, 2.2 and 8.1 Hz, 1H), 5.37 (s, 1H), 3.78 (s, 3H). ^{13}C NMR (100 MHz): δ 161.7, 160.2, 153.5, 152.5, 139.5, 132.6, 130.5, 130.4, 123.8, 122.9, 117.2, 114.6, 111.6, 110.8, 110.6, 84.8, 55.3.



Compound **353i**. Pale yellow solid (0.7393 g, 45%). ^1H NMR (400 MHz, $\text{DMSO}-d_6$): δ 9.08 (br, 1H), 8.25 (dd, 1.2 and 8.1 Hz, 1H), 7.69 – 7.60 (m, 1H), 7.43 – 7.33 (m, 3H), 7.30 (dd, 1.5 and 7.7 Hz, 1H), 7.21 (dd, 1.0 and 8.3 Hz, 1H), 7.07 (td, 1.2 and 7.6 Hz, 1H), 4.72 (s, 1H), 3.79 (s, 3H). ^{13}C NMR (100 MHz): δ 161.7, 154.7, 153.4, 153.3, 132.4, 128.9, 128.6, 125.9, 123.7, 122.9, 121.0, 117.1, 114.5, 112.7, 84.0, 55.6.

2.6.6. Photoredox arylations



General procedure: an oven dried 2 dram vial was charged with 0.2 mmol of **216**, 1.0 mmol (5 eq) of **353** based compound, 0.004 mmol of $[\text{Ru}(\text{bpy})_3]\text{Cl}_2$, and 2.5 mL of anhydrous DMSO. The vial was purged with argon and the reaction was carried out at room temperature for 12 h under blue light (440 nm) irradiation with a Kessil Lamp. After this time, the reaction was quenched with brine and extracted with dichloromethane (3X30 mL). The organic phases were dried with Na_2SO_4 and evaporated. The product was purified by column chromatography using silica treated with Et_3N prior to use.

Reaction setup:

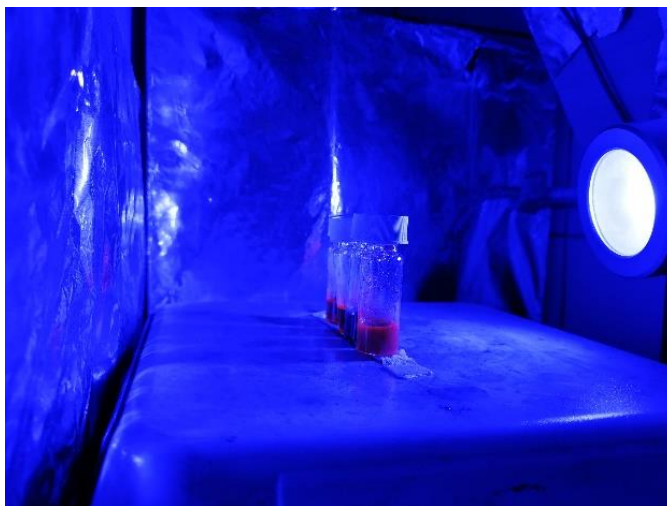
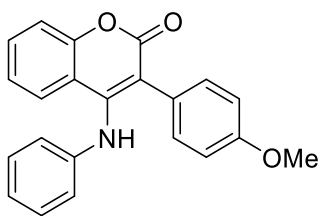


Figure 36: Photoredox reaction setup.

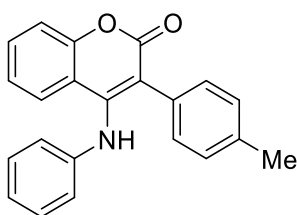


Compound **354a**. Yellow solid (31.6 mg, 50%). ^1H NMR (400 MHz, $\text{DMSO}-d_6$): δ 7.51-7.30 (m, 8H), 7.24 (t, 6.9 Hz, 2H), 7.09 (t, 7.4 Hz, 1H), 7.02 (t, 7.6 Hz, 1H), 6.92 (d, 7.8 Hz, 2H), 6.26 (br, 1H). ^{13}C NMR

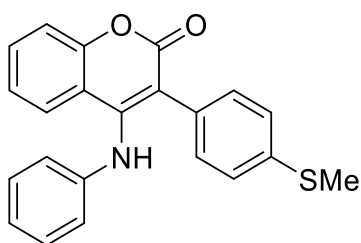
(100 MHz): δ 162.0, 153.5, 148.8, 142.3, 132.3, 132.3, 131.6, 130.3, 129.5, 129.3, 128.6, 126.3, 124.3, 123.3, 121.9, 117.4, 115.6, 111.9.



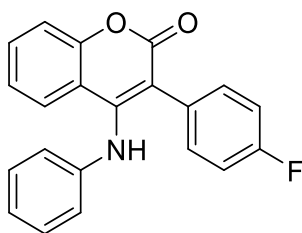
Compound **354b**. Yellow solid (21.4 mg, 32%). ^1H NMR (400 MHz, $\text{DMSO-}d_6$): δ 7.48 (t, 7.7 Hz, 1H), 7.41-7.32 (m, 4H), 7.30-7.24 (m, 2H), 7.11 (t, 7.4 Hz, 1H), 7.04 (t, 7.6 Hz, 1H), 6.96 (m, 4H), 6.25 (br, 1H), 3.83 (s, 3H). ^{13}C NMR (100 MHz): δ 162.2, 159.8, 153.4, 148.7, 142.5, 131.6, 131.4, 129.5, 126.3, 124.2, 124.2, 123.2, 121.7, 117.4, 115.7, 115.7, 114.9, 112.0, 55.4.



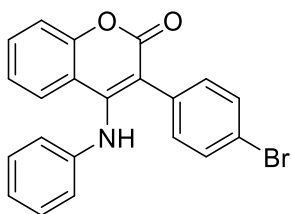
Compound **354c**. Yellow solid (22.1 mg, 34%). ^1H NMR (400 MHz, $\text{DMSO-}d_6$): δ 7.48-7.43 (m, 1H), 7.38 (8.1 Hz, 1H), 7.34-7.22 (m, 7H), 7.10 (t, 7.4 Hz, 1H), 7.01 (t, 7.6 Hz, 1H), 6.93 (d, 7.9 Hz, 2H), 6.20 (br, 1H), 2.37 (s, 3H). ^{13}C NMR (100 MHz): δ 162.1, 153.6, 148.8, 142.6, 138.7, 131.5, 130.2, 130.1, 129.6, 129.1, 26.5, 124.3, 123.2, 121.8, 117.4, 115.6, 112.4, 21.5.



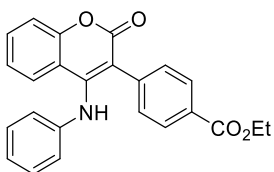
Compound **354d**. Brown solid (43.4 mg, 61%). ^1H NMR (400 MHz, $\text{DMSO-}d_6$): δ 7.49-7.43 (m, 1H), 7.38 (d, 8.2 Hz, 1H), 7.32 (t, 6.7 Hz, 4H), 7.29-7.22 (m, 4H), 7.10 (t, 7.4 Hz, 1H), 7.03 (t, 7.6 Hz, 1H), 6.92 (d, 7.9 Hz, 2H), 6.19 (br, 1H), 2.48 (s, 3H). ^{13}C NMR (100 MHz): δ 162.0, 153.6, 148.8, 142.4, 139.5, 131.6, 130.7, 129.6, 128.7, 127.1, 126.3, 124.4, 123.3, 123.3, 121.8, 117.5, 115.6, 111.7, 15.6.



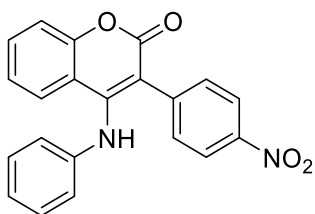
Compound **354e**. Yellow solid (48.6 mg, 73%). ^1H NMR (400 MHz, $\text{DMSO-}d_6$): δ 7.49 (m, 1H), 7.36 (m, 4H), 7.24 (m, 2H), 7.06 (m, 4H), 6.91 (d, 7.9 Hz, 2H), 6.20 (br, 1H). ^{13}C NMR (100 MHz): δ 164.0, 162.0, 161.5, 153.5, 148.8, 142.0, 132.4, 132.3, 131.7, 129.5, 123.4, 121.9, 117.5, 116.4, 116.2, 115.6, 110.6.



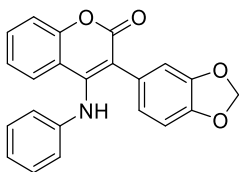
Compound **354f**. Yellow solid (43.2 mg, 55%). ^1H NMR (400 MHz, $\text{DMSO-}d_6$): δ 7.54-7.45 (m, 3H), 7.37 (d, 9.1 Hz, 2H), 7.28-7.21 (m, 4H), 7.13-7.02 (m, 2H), 6.90 (d, 7.8 Hz, 2H), 6.25 (br, 1H). ^{13}C NMR (100 MHz): δ 161.8, 153.5, 148.8, 141.9, 132.4, 132.1, 131.8, 129.5, 126.0, 124.6, 123.5, 122.8, 121.9, 117.5, 115.5, 110.3.



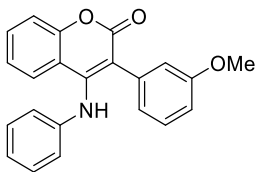
Compound **354g**. Yellow solid (59.4 mg, 77%). ^1H NMR (400 MHz, $\text{DMSO-}d_6$): δ 8.03 (d, 8.2 Hz, 1H), 7.53-7.43 (m, 3H), 7.42-7.36 (m, 2H), 7.22 (t, 7.8 Hz, 2H), 7.07 (t, 7.6 Hz, 2H), 6.90 (d, 7.8 Hz, 2H), 6.33 (br, 1H), 4.35 (q, 7.1 Hz, 2H), 1.37 (t, 7.1 Hz, 3H). ^{13}C NMR (100 MHz): δ 166.2, 161.7, 153.6, 148.9, 141.8, 137.4, 131.9, 130.5, 130.2, 129.5, 125.9, 124.5, 123.5, 121.9, 117.5, 115.6, 110.3, 61.2, 14.4.



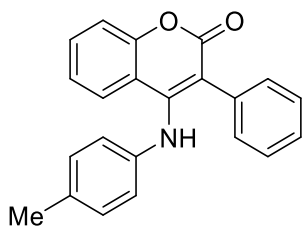
Compound **354h**. Yellow solid (67.9 mg, 95%). ^1H NMR (400 MHz, $\text{DMSO-}d_6$): δ 8.14 (d, 8.6 Hz, 2H), 7.53 (m, 4H), 7.42 (d, 8.2 Hz, 1H), 7.17 (m, 3H), 7.04 (t, 7.2 Hz, 1H), 6.88 (7.9 Hz, 2H), 6.35 (br, 1H). ^{13}C NMR (100 MHz): δ 161.5, 153.6, 148.6, 147.3, 140.7, 140.2, 132.5, 131.7, 129.5, 125.1, 124.8, 123.9, 122.2, 117.8, 115.6, 107.5.



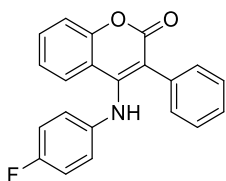
Compound **354i**. Yellow solid (41.4 mg, 58%). ^1H NMR (400 MHz, $\text{DMSO-}d_6$): δ 7.49 – 7.43 (m, 1H), 7.37 (d, 7.5 Hz, 1H), 7.33 – 7.23 (m, 3H), 7.10 (t, 7.4 Hz, 1H), 7.05 – 6.99 (m, 1H), 6.93 (d, 7.8 Hz, 2H), 6.88 – 6.83 (m, 3H), 6.27 (br, 1H), 5.97 (s, 2H). ^{13}C NMR (100 MHz): δ 162.1, 153.5, 149.0, 148.5, 148.0, 142.3, 131.6, 129.6, 126.3, 125.6, 124.5, 123.8, 123.3, 122.1, 117.5, 115.5, 111.5, 110.9, 109.3, 101.5.



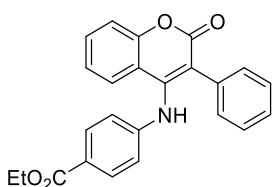
Compound **354j**. Yellow solid (32.1 mg, 47%). ^1H NMR (400 MHz, CDCl_3): δ 7.50 – 7.44 (m, 1H), 7.41 – 7.36 (m, 2H), 7.35 – 7.30 (m, 2H), 7.29 – 7.23 (m, 1H), 7.10 (t, 7.5 Hz, 1H), 7.05 – 6.96 (m, 2H), 6.95 – 6.90 (m, 4H), 6.23 (br, 1H), 3.77 (s, 3H). ^{13}C NMR (100 MHz): δ 160.3, 153.7, 149.0, 142.5, 133.6, 131.6, 130.6, 129.6, 126.5, 124.5, 122.1, 117.5, 115.8, 115.6, 112.0, 55.4.



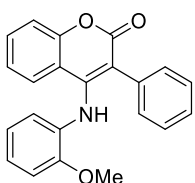
Compound **354q**. Yellow solid (35.0 mg, 54%). $^1\text{H NMR}$ (400 MHz, $\text{DMSO-}d_6$): δ 7.43-7.31 (m, 8H), 7.14 (d, 8.4 Hz, 2H), 7.05 (t, 7.7 Hz, 1H), 6.85 (d, 8.4 Hz, 2H), 6.21 (br, 1H), 2.45 (s, 3H). $^{13}\text{C NMR}$ (100 MHz): δ 162.0, 153.5, 148.7, 139.8, 134.1, 132.2, 131.6, 130.3, 129.3, 128.7, 128.1, 126.2, 123.3, 122.5, 117.4, 115.5, 111.8, 16.5.



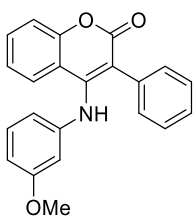
Compound **354r**. Yellow solid (35.2 mg, 53%). $^1\text{H NMR}$ (400 MHz, $\text{DMSO-}d_6$): δ 7.55-7.34 (m, 7H), 7.34-7.27 (m, 1H), 7.12-7.04 (m, 1H), 7.01-6.89 (m, 4H), 6.21 (br, 1H). $^{13}\text{C NMR}$ (100 MHz): δ 162.0, 161.1, 158.6, 153.6, 148.8, 138.3, 138.2, 131.6, 130.4, 129.4, 126.0, 124.0, 123.9, 117.6, 116.4, 116.2, 115.4, 111.4.



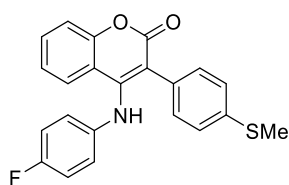
Compound **354t**. Yellow solid (31.9 mg, 42%). $^1\text{H NMR}$ (400 MHz, $\text{DMSO-}d_6$): δ 7.91 (d, 8.5 Hz, 2H), 7.52 (t, 7.4 Hz, 1H), 7.45-7.31 (m, 7H), 7.10 (t, 7.5 Hz, 1H), 6.84 (d, 8.5 Hz, 2H), 6.28 (br, 1H), 4.35 (q, 7.1 Hz, 2H), 1.37 (t, 7.1 Hz, 3H). $^{13}\text{C NMR}$ (100 MHz): δ 166.2, 161.8, 153.4, 147.4, 146.8, 132.0, 131.9, 131.2, 130.1, 129.2, 128.9, 126.0, 125.1, 123.7, 119.3, 117.5, 115.8, 115.2, 61.0, 14.5.



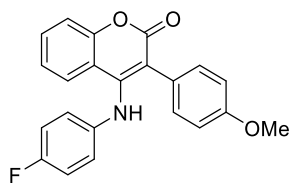
Compound **354u**. Yellow solid (35.0 mg, 51%). $^1\text{H NMR}$ (400 MHz, $\text{DMSO-}d_6$): δ 7.51 – 7.42 (m, 3H), 7.40 – 7.36 (m, 5H), 7.11 – 7.05 (m, 1H), 7.02 – 6.95 (m, 2H), 6.85 (d, 8.0 Hz, 1H), 6.75 – 6.72 (m, 1H), 6.27 (br, 1H), 3.79 (s, 3H). $^{13}\text{C NMR}$ (100 MHz): δ 165.8, 162.2, 153.3, 150.5, 148.5, 132.8, 132.7, 131.6, 131.2, 131.1, 130.4, 129.0, 128.4, 125.6, 124.2, 123.3, 121.1, 120.7, 117.4, 116.2, 111.0, 55.8.



Compound **354v**. Yellow solid (48.9 mg, 71%). $^1\text{H NMR}$ (400 MHz, $\text{DMSO-}d_6$): δ 7.50 – 7.34 (m, 8H), 7.14 (t, 8.1 Hz, 1H), 7.08 -7.02 (m, 1H), 6.64 (dd, 8.3 and 2.1 Hz, 1H), 6.50 (d, 7.9 Hz, 1H), 6.45 (t, 2.0 Hz, 1H), 6.17 (br, 1H), 3.72 (s, 3H). $^{13}\text{C NMR}$ (100 MHz): δ 162.0, 160.6, 153.5, 148.7, 143.7, 132.3, 131.6, 130.3, 129.3, 128.7, 126.4, 123.3, 117.4, 115.7, 114.2, 112.4, 109.7, 107.8, 107.8, 55.5.

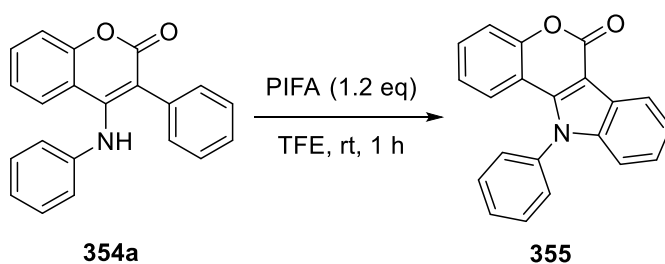


Compound **354w**. Yellow solid (46.1 mg, 62%). ^1H NMR (400 MHz, $\text{DMSO-}d_6$): δ 7.51-7.44 (m, 1H), 7.37 (dd, 8.3 and 1.0 Hz, 1H), 7.32-7.27 (m, 5H), 7.08-7.01 (m, 1H), 6.98-6.87 (m, 4H), 6.19 (br, 1H), 2.48 (s, 3H). ^{13}C NMR (100 MHz): δ 161.9, 161.1, 158.6, 153.6, 148.8, 139.5, 138.2, 131.7, 130.7, 128.7, 127.1, 125.9, 123.9, 123.8, 123.4, 117.6, 116.5, 116.2, 115.4, 110.9, 15.6.



Compound **354x**. Yellow solid (44.5 mg, 62%). ^1H NMR (400 MHz, $\text{DMSO-}d_6$): δ 7.50-7.44 (m, 1H), 7.37 (d, 8.1 Hz, 1H), 7.35-7.25 (m, 3H), 7.04 (t, 7.6 Hz, 1H), 6.99-6.87 (m, 6H), 6.18 (br, 1H), 3.82 (s, 3H). ^{13}C NMR (100 MHz): δ 162.2, 161.0, 159.8, 158.6, 153.5, 148.8, 138.5, 138.4, 131.6, 131.5, 126.0, 124.1, 123.8, 123.7, 123.3, 117.5, 116.4, 116.2, 115.4, 114.9, 111.4, 55.5.

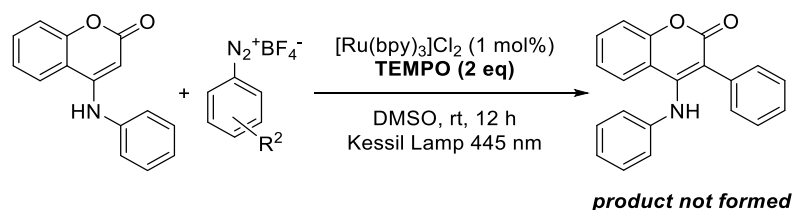
2.6.7. Azacoumestan synthesis



A 2-dram vial was charged with 31.5 mg (0.1 mmol) of **354a** and 0.5 mL of TFE. The mixture was cooled to 0 °C and 51.8 mg (0.12 mmol) of PIFA was added in portions. The reaction was stirred at room temperature for 1 h. After this time, it was quenched with brine and extracted with dichloromethane (3X10 mL). The organic phase was dried with Na_2SO_4 and evaporated. The product was purified by column chromatography.

Compound **355**. Yellow solid (26.1 mg, 86%). ^1H NMR (400 MHz, CDCl_3): δ 8.41 (d, 7.8 Hz, 1H), 7.75 – 7.64 (m, 3H), 7.56 – 7.48 (m, 3H), 7.47 – 7.40 (m, 2H), 7.39 – 7.33 (m, 1H), 7.08 (d, 8.1 Hz, 1H), 6.99 (t, 7.6 Hz, 1H), 6.90 (d, 8.1 Hz, 1H). ^{13}C NMR (100 MHz): δ 159.0, 153.7, 141.2, 141.1, 137.2, 130.7, 130.3, 128.7, 125.4, 124.2, 123.5, 121.7, 118.2, 113.6, 110.9, 102.7.

2.6.8. Mechanistic studies - radical trapping experiment with TEMPO



A typical photoredox procedure was carried out as described in section 2.6.6, but this time 62.4 mg (0.4 mmol, 2 eq) of TEMPO were added to the reaction. After 12 h, TLC and GC-MS analysis showed that no product was formed, indicating the formation of radicals as reactive intermediates.

2.6.9. Mechanistic studies – Stern-Volmer experiments

A solution of 10^{-4} mol L⁻¹ of [Ru(bpy)₃]Cl₂ in DMSO was placed in a quartz cuvette, sparged with argon, quickly capped and sealed with parafilm. The solutions were irradiated at 453 nm and the luminescence was measured at 600 nm. For each quencher concentration, three scans were taken, and the average was calculated for each I₀/I. Each experiment was made in triplicate.

2.6.10. Computational details

All computational calculations were carried out with Gaussian 03 software.²³² The geometries of phenyl radicals and coumarins were fully optimized using Density Functional Theory (DFT) with the B3LYP hybrid functional (unrestricted for phenyl radicals) and 6-31+G(d) basis set. Based on these results some reactivity parameters can be calculated, as described below.

Global chemical potential (μ^0):

$$\mu^0 = \frac{\partial E}{\partial N} \Big|_v \approx \frac{E_{\text{HOMO}} + E_{\text{LUMO}}}{2}$$

Global chemical hardness (η^0):

$$\eta^0 = \left. \frac{\partial \mu}{\partial N} \right|_v = \left. \frac{\partial^2 E}{\partial N^2} \right|_v \approx E_{\text{LUMO}} - E_{\text{HOMO}}$$

Global electrophilicity (ω^0):

$$\omega^0 = \frac{\mu^2}{2\eta}$$

Global nucleophilicity (N^0) – referred to tetracyanoethylene (TCE):

$$N^0 = E_{\text{HOMO}} - E_{\text{HOMO}}(\text{TCE})$$

Fukui function (f):

$$f(\mathbf{r}) = \left. \frac{\partial \rho(\mathbf{r})}{\partial N} \right|_v$$

The Fukui function is obtained by the Mulliken index of each atom in the neutral, cationic and anionic form of the desired molecule. They are, respectively, f_k^0 , f_k^+ and f_k^- , where k is the k atom of the molecule. With these values, local parameters can be calculated.

Local electrophilicity (ω_k):

$$\omega_k = \omega^0 f_k^+$$

Local nucleophilicity (N_k):

$$N_k = N^0 f_k^-$$

3

Reactivity of phenyl radicals toward enol acetates: a theoretical study

3.1.

Introduction

As shown at the previous sections, the visible-light excitation of the photocatalyst allows the formation of aryl radicals via single electron transfer (SET) reactions.¹⁰⁵ The functionalization of ketones was possible to be carried out in mild conditions with König's arylation of enol acetates (**268**) (Figure 37). The proposed mechanism shows that, after the formation of the phenyl radical **69**, it is added to the **268**, generating a radical adduct **375**. This species can donate an electron to the photocatalyst or to another diazonium salt (chain propagation), thus generating a cationic intermediate **376**, which undergoes elimination to provide the desired product **269**. Substituent groups at König's arylation seem to influence the reaction yields. Electron withdrawing groups (EWG) at diazonium salts afford the best yields, while electron donating groups (EDG) result in moderate yields. The authors try to explain these findings by supporting their arguments on the redox potentials of the ArN_2^+ . Diazonium salts substituted with electron withdrawing groups (EWG) have higher oxidation potentials, being considered easier to be reduced to the elusive anion radical, which, by N_2 loss, leads to the phenyl radicals. Later, Oliveira et al used porphyrines combined with continuous flow setup to run the same reactions, observing a similar trend on reactivity.

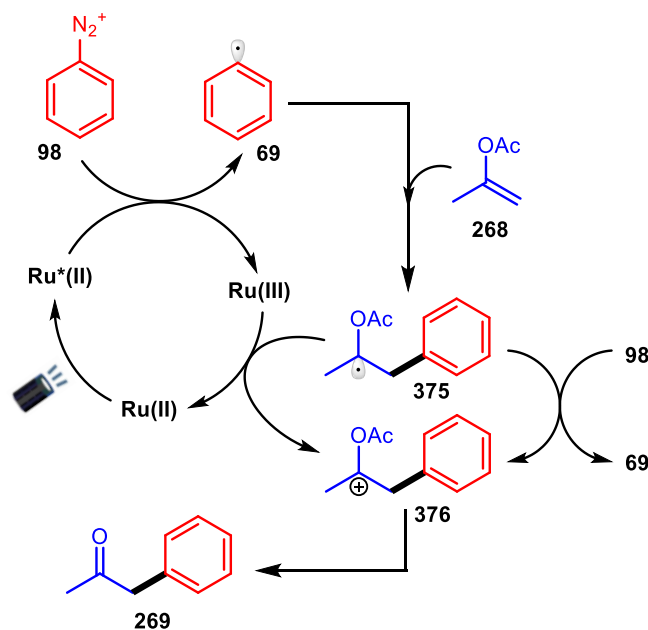


Figure 37: The proposed mechanism for the arylation of enol acetates by photoredox catalysis.

Conversely to the general belief, one could alternatively interpret those results as the following: once the radical is formed, the aryl radical addition step dictates the reactivity, *i.e.*, the radical addition to the unsaturated compound is the rate-determining step, as previously reported.^{81–83} Some reports of photoredox methodologies show the same tendency.^{16,17} Kinetic isotope effect experiments conducted by Yoon et al confirmed that α -amino radical addition to methyl vinyl ketone in the absence of Brønsted acid is rate-determining.²³³ The formation of radicals at photoredox catalysis can be close to diffusional-controlled limit.^{233,236} Deronzier et al showed that quenching of $[\text{Ru}(\text{bpy})_3]^{2+}$ by **216** as an electron transfer process is $3.4 \pm (0.2) \times 10^9 \text{ M}^{-1} \text{ s}^{-1}$ in acetonitrile, suggesting that diazonium salt quenches the photocatalyst in a very fast process.²³⁷ These facts are in contrast with König's assumption that reactivity of arylation of **268** is dictated by the redox potential of the diazonium salts and, conversely, the reduction step would be the rate-determining step.¹³⁰

It could be a common sense that polar effects would influence the reactivity of phenyl radicals toward addition reactions. However, based on the mechanistic models reported by Tedder, Giese, Fischer and Radom, enthalpic and sterics effects can also be relevant and more important to the reactivity than the polar ones. No study was developed with phenyl radicals.

3.2.

Objectives

Due to the lack of consensus about the photoredox version of the Meerwein arylation mechanism, the present contribution aims to investigate the radical addition to enol acetates, using DFT calculations, to elucidate the role of substitutions in the reactivity. Specific objectives of this study can be enumerated:

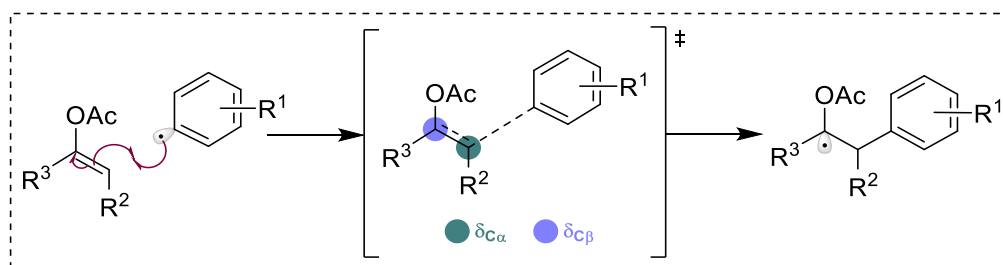
- Calculation of the theoretical barrier heights for the addition of substituted phenyl radicals to enol acetates to evaluate the influence of enthalpic and polar effects.
- Characterization of the frontier molecular orbital interactions as a model to identify the nucleophile and the electrophile of the studied reactions.
- Evaluation of the steric hindrance influence of alkyl groups at enol acetates by LFER parameters.
- Evaluation of the electronic demands at both reactants by LFER relationships.

3.3.

Results and discussion

This work was developed in collaboration with Prof. Pierre Esteves from Universidade Federal do Rio de Janeiro.

The observation of the substituent effects on the reaction kinetics can be interpreted as how the two carbon atoms of the double bonds in the enol acetate are electronically demanded on the rate-controlling transition state (Scheme 56).



Scheme 56: The radical addition step of the enol acetate arylation.

The change of substituent R^1 monitors the sensitivity of the reaction mainly at carbon C_α while C_β can be more directly evaluated by varying substituents R^2 and R^3 . This work was divided into three approaches, each one aiming to understand the influence of these substituents on the reaction kinetics. In the first approach, the role of substituents R^1 at *para*-substituted phenyl radicals attacking the enol acetate derived from acetone ($R^2 = H$ and $R^3 = Me$) was investigated. In a second approach, the influence of alkyl groups at α -carbon of the enol acetate on its reaction with the *p*-nitrophenyl radicals was investigated (influence of R^2). Finally, the third approach analyzed the role of substituents on different acetophenones reacting with *p*-nitrophenyl radicals (R^3). These calculations would allow a better comprehension of the electronic demand on both carbons of the $C=C$ of the enol acetate. The choice of these systems is related to the main factors that affect radical additions to alkenes: enthalpic, polar, and steric effects.

The UBHandHLYP/6-311G** level of theory was chosen to describe our systems.²³⁸ This level is often employed in reactions involving organic radical studies successfully.^{239–241} The geometries were fully optimized for reactants (substituted radical intermediate and enol acetates), the transition state (TS) for the addition at α -carbon, as well as the corresponding adducts. Vibrational analysis at the optimized geometries confirmed that the structures correspond to minimum at the potential energy surface (PES), by the absence of imaginary frequencies. On the other hand, first-order transition states were characterized by the existence of a single imaginary frequency, which, when animated, indicated the expected reaction coordinates. Additionally, the intrinsic reaction coordinate (IRC) calculations were carried out to confirm that the transition state connects the expected reactants to the products of this elementary step. At the optimized geometries of the TS, single-point energy calculations were carried out to perform natural bond order (NBO),²⁴² charge variation to the reactants and FMO analysis. This will allow evaluating how the structural parameters are influencing the reaction rate.

The Figure 38 shows a typical transition state for the addition of the phenyl radical to the enol acetate, with selected geometric parameters. The angle of approximation (107.2°) of the reactants at the TS follows the geometry proposed by Bürgi and Dunitz,²⁴³ and by the distance r_{CC} of about 2.4 \AA indicates an early TS. The reaction is exergonic, which was found for all cases. This means that the substituent

effects at TS should be more alike to the ones in reactants than to the products, according to the Hammond postulate.³²

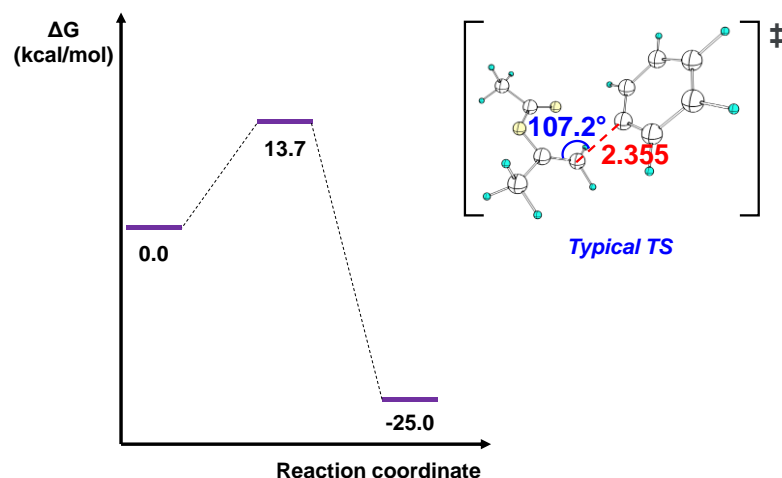
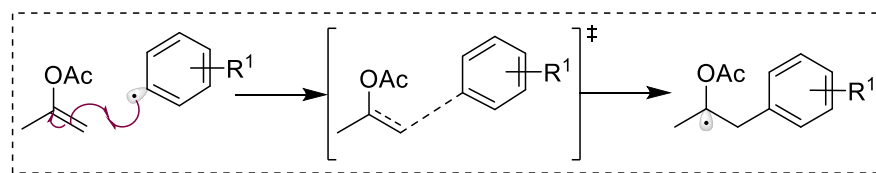


Figure 38: Energy profile diagram calculated at UBHandHLYP/6-311G** level of theory. The approximation distance is expressed in Angstroms (Å).

Aiming at investigating the influence of polar and enthalpic effects, the transition states bearing different groups at the *para* position of phenyl radical were optimized, as well as the reactants. This allowed calculating the TS Gibbs free energy (ΔG^\ddagger) and enthalpy (ΔH^\ddagger), the reaction Gibbs free energy (ΔG_{rxn}) and enthalpy (ΔH_{rxn}), shown in Table 16. All phenyl radical additions are exothermic with ΔH_{rxn} ranging from -37.3 to -40.0 kcal mol⁻¹. They are all exergonic with ΔG_{rxn} , varying from -25.3 to -26.7 kcal mol⁻¹. The analysis of thermodynamic quantities for TS showed small activation barriers, which is consistent with the early TS found by IRC calculation and supported by Hammond's postulate. Electron-withdrawing substituents decrease the energy barrier, although there is a poor correlation between this quantity and the reaction enthalpy.

Table 16: Calculated transition state Gibbs free energy (ΔG^\ddagger / kcal mol⁻¹) and enthalpy (ΔH^\ddagger / kcal mol⁻¹), reaction Gibbs free energy (ΔG_{rxn} / kcal mol⁻¹) and enthalpy (ΔH_{rxn} / kcal mol⁻¹) at UBHandHLYP/6-311G** level of theory.



R ¹	ΔG^\ddagger	ΔH^\ddagger	ΔG_{rxn}	ΔH_{rxn}
H	13.7	2.3	-25.0	-37.3
OMe	12.9	0.7	-26.4	-40.0
Me	13.8	2.8	-25.3	-37.6
^t Bu	13.7	2.8	-25.5	-37.7
SiMe ₃	13.6	2.8	-25.1	-37.3
F	13.1	2.1	-25.6	-38.9
Cl	13.0	1.9	-25.9	-38.2
Br	13.0	2.0	-26.7	-38.9
CF ₃	12.5	2.6	-25.8	-38.1
CN	12.3	2.4	-26.3	-37.6
NO ₂	12.0	2.2	-26.3	-38.6

Figure 39a presents the Arrhenius activation energy, calculated from $E_a = \Delta H^\ddagger + RT$, as a function of ΔH_{rxn} , which may be related to the position of the transition state along the reaction coordinate (α) within the Evans-Polanyi principle framework. A poor correlation ($r^2 = 0.743$) is found with slope of $\alpha = 0.375$, which, being less than 0.5, indicates an early TS, considering that $0 \leq \alpha \leq 1$.³⁷ This shows that, although the enthalpic effect has some influence on the reaction rate, the exothermicity of the reaction has only a small effect on the activation energy for the present case. Fouassier et al showed that the alkyl radicals addition to the methyl acrylate double bond has a strong influence on the enthalpic factor.⁹² In the same work, however, it was observed that the aminoalkyl and the dialkylketyl radicals also present poor correlation. These cases were studied by the same authors and the polar effects were pointed out as the driving force to such reaction.²⁴⁴ They led this work to investigate how the polar effects induce the observed reactivity. The radical SOMO energies (Table 17) were calculated in the framework of the Molecular Orbital (MO) theory using the Hartree-Fock part of the UMP2/6-31G** level of theory calculation. These energies

correlate well with ΔG^\ddagger ($r^2 = 0.890$, Figure 39b). As the SOMO energy becomes more negative, the reaction barrier becomes lower, meaning that a more electrophilic aryl radical is beneficial to the reaction rate. This also suggests that the enol acetate is serving as a nucleophile and the radical seems to be playing the electrophile role in this reaction.

Table 17: Calculated radical SOMO levels (eV), at UMP2/6-31G** level of theory.

R ¹	E _{SOMO}	R ¹	E _{SOMO}	R ¹	E _{SOMO}
H	-9.58	SiMe ₃	-9.52	CF ₃	-10.18
OMe	-9.68	F	-10.02	CN	-10.34
Me	-9.55	Cl	-9.97	NO ₂	-10.49
^t Bu	-9.49	Br	-9.79		

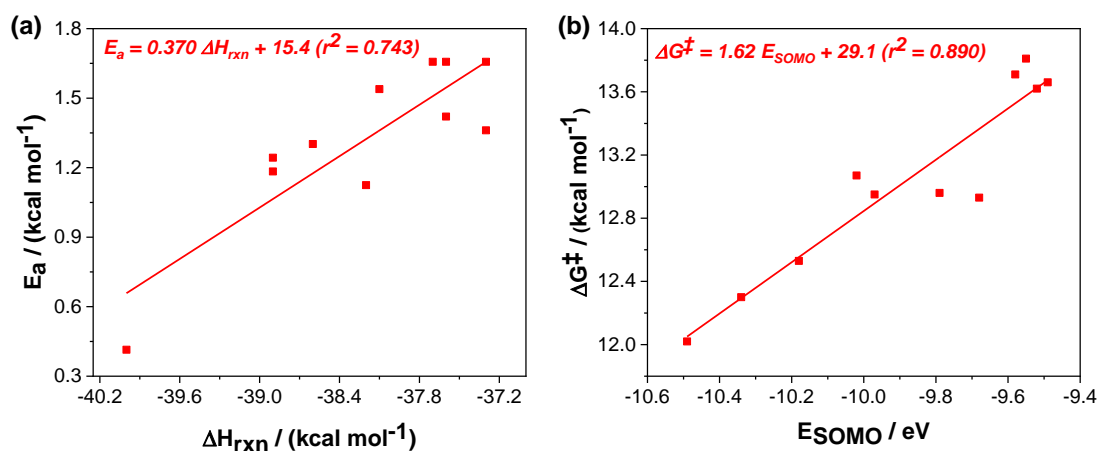


Figure 39: Plots of (a) transition state enthalpy (ΔH^\ddagger) against reaction enthalpy (ΔH_{rxn}) and (b) SOMO energy against ΔH_{rxn} .

The Klopman-Salem equation^{33,245} describes the change of total energy involved in the process of two chemical species approaching each other, in terms of their individual overlapping molecular orbitals, based on a Taylor expansion of the total energy (perturbation theory). The third term of this equation is the second-order perturbation, which comes from the interaction between filled/unfilled orbitals. In terms of the desired reaction, the second-order perturbation is related to SOMO-HOMO_{enol} and SOMO-LUMO_{enol} interactions. Mathematically, two orbitals closer in energy contribute more to the interaction energy. From this perspective, the HOMO level of

enol acetate ($[\text{HOMO}]_{\text{enol}}$) is closer to the SOMO of the radical ($[\text{SOMO}]_{\text{Rad}}$) than does the LUMO (Figure 40a). This fact points out that enol acetate acts as the nucleophile and phenyl radical, as the electrophile. Natural Bond Orbital (NBO) analysis (Figure 40b), carried out using the Hartree-Fock part of the UMP2/6-31G** level of theory, reveals the same kind of interactions: $\text{SOMO} \rightarrow \pi^*_{\text{C=C}}$ at α spin-set and $\pi_{\text{C=C}} \rightarrow \text{SOMO}$ at β spin-set. The stabilization contribution to the energies of the $\text{SOMO} \rightarrow \pi^*_{\text{C=C}}$ was calculated to be 21.3 kcal/mol and the $\pi_{\text{C=C}} \rightarrow \text{SOMO}$ is 29.1 kcal/mol. This analysis confirms that the main contribution comes from the interaction $\pi_{\text{C=C}} \rightarrow \text{SOMO}$, *i.e.*, an electrophilic aryl radical attacking the nucleophilic enol acetate.

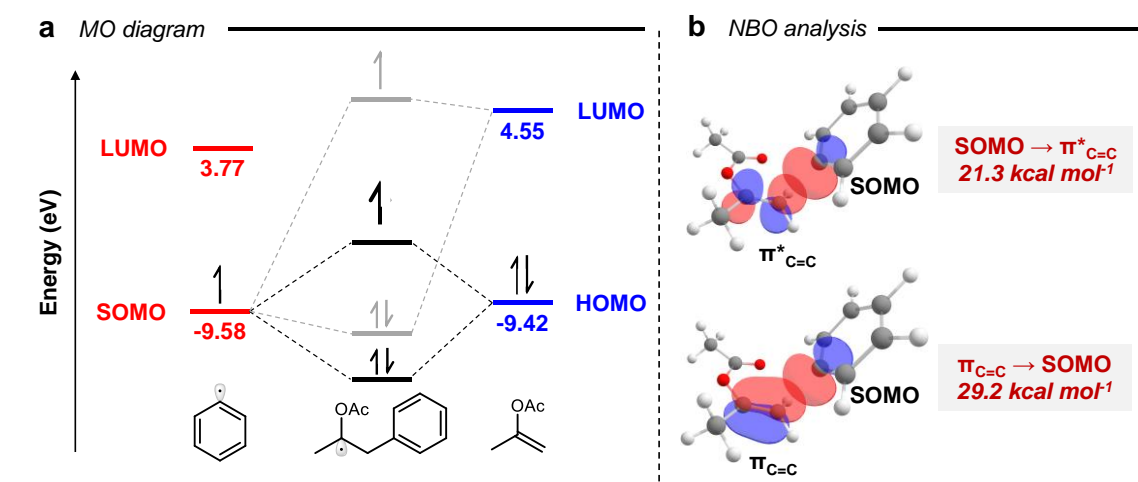


Figure 40: (a) Frontier molecular orbital diagram describing the possible MO interactions; (b) NBO involved at phenyl radical addition TS.

According to the Intrinsic Reaction Coordinate (IRC) calculations (Figure 41), the phenyl radical addition to enol acetate is an early TS. Based on Hammond's postulate,³² this kind of TS is expected to be reactant-like, which means that stabilizing changes in the starting materials would also have a similar effect on the TS. Free energy relationships (LFER) establish the extent to which bond formation and bond breakage happen in the transition state of a reaction. Thus, these are a good way of evaluating the rate-determining transition state and how several structural effects affect it.

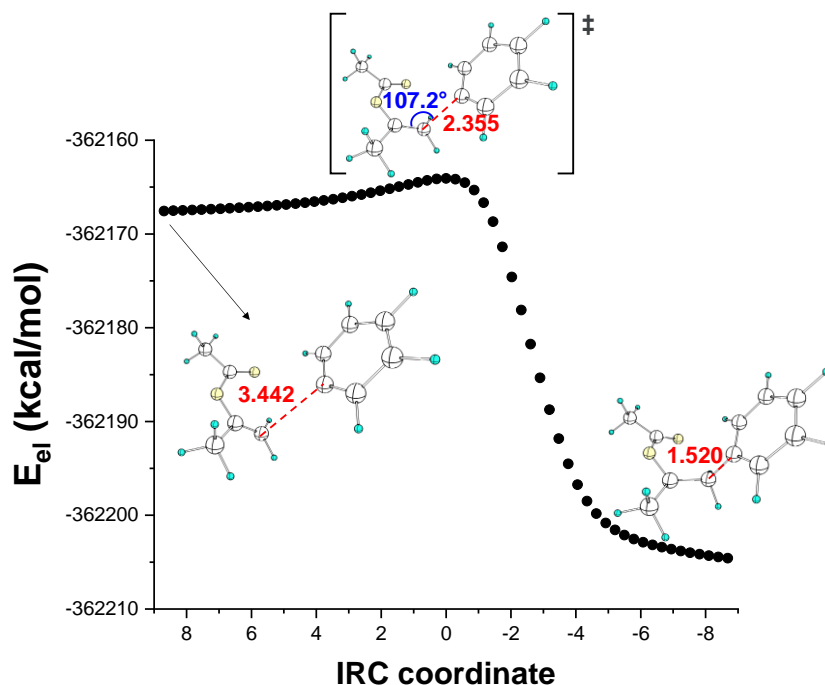


Figure 41: IRC calculated for the phenyl radical addition to the acetone-based enol acetate.

From the values of the reaction barriers (ΔG^\ddagger), it is possible to derive $\log k_{rel}$ once they are formally linearly related. Thus, with these values, correlations with the experimentally derived Hammett parameters (σ) and other LFER related quantities in the traditional way are possible (Figure 42). A correlation of $\log k_{rel}$ with σ_p constants was observed ($r^2 = 0.750$) (Figure 42a). No acceptable correlations were obtained either with σ_p^+ and, surprisingly, with σ^* (Creary scale,²⁴⁶ Figure 42b and c). Swain and Lupton proposed that substituents' effects on the reaction constants can be evaluated independently by their field (F) and resonance (R) effects.²⁴⁷ Figure 42d shows that the relative rates ($\log k_{rel}$) correlate better with the field effect of the substituent (F constants, $r^2 = 0.870$). Conversely, the resonance constant did not correlate in a simple way with the relative rate constants (Figure 42e). The halogens are shown to be outliers. The inclusion of solvent effects and diffuse functions (PCM(DMF)/UBHandHLYP/6-311++G**//UBHandHLYP/6-311G**) results in the same tendency shown before to reaction barriers (Figure 43), suggesting that these factors do not significantly influence the results. Considering that the radical at the phenyl moiety is orthogonal to the π system, it does not allow resonance to occur effectively, the better correlation with F is plausible. Thus, the field effect plays a main role in the polar (*aka* electrostatic, electric field, or field) effect. The stronger one is the

electron-withdrawing effect of the substituent of the aryl radical, the higher one is the reaction rate.

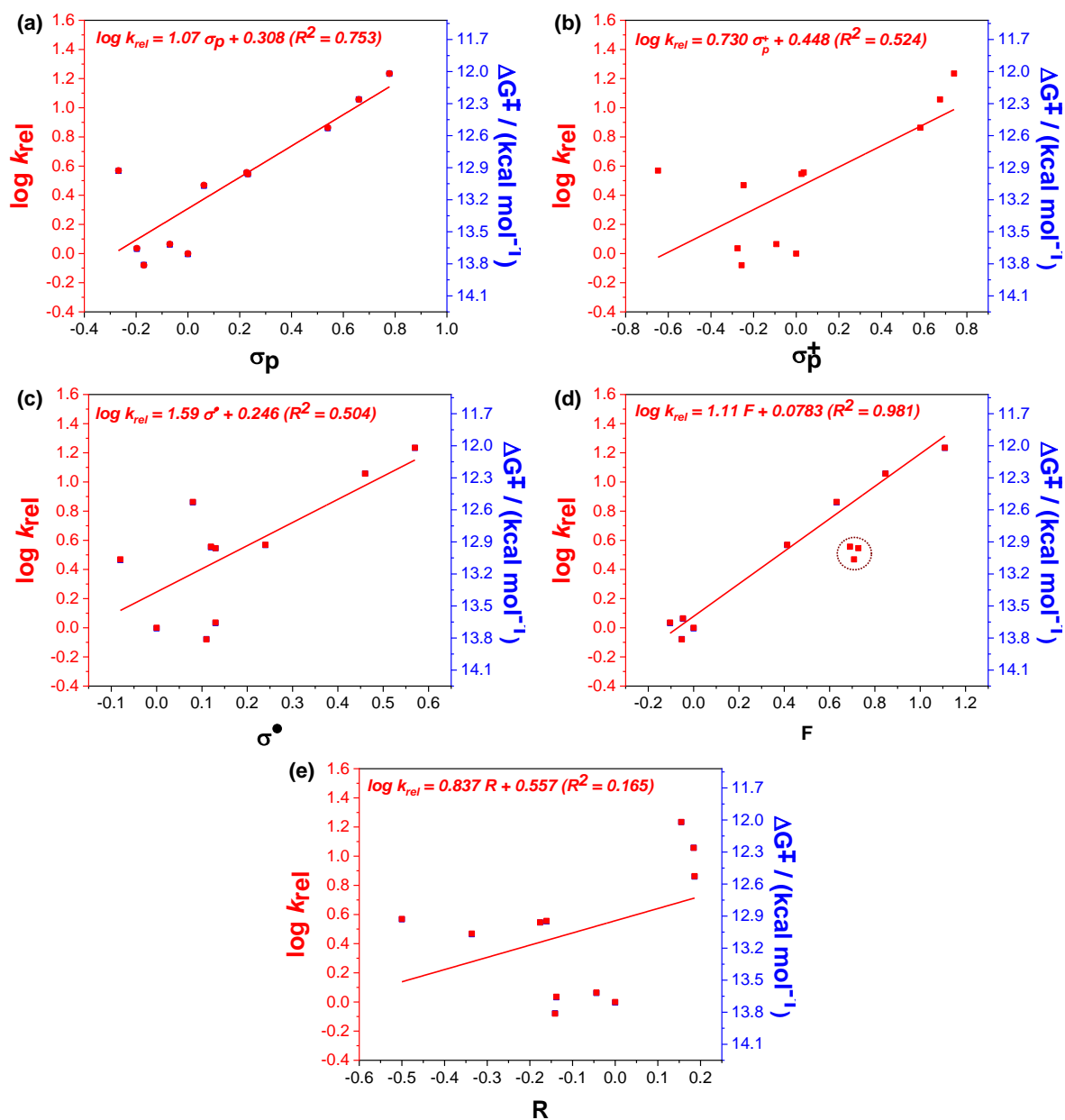


Figure 42: Plots of $\log k_{rel}$ and ΔG^\ddagger against (a) Hammett σ_p , (b) σ_p^+ , (c) σ^* , (d) Field effect (F) and (e) Resonance effect (R) for para-substituted phenyl radical additions to acetone-based enol acetate at UBHandHLYP/6-311G** level of theory.

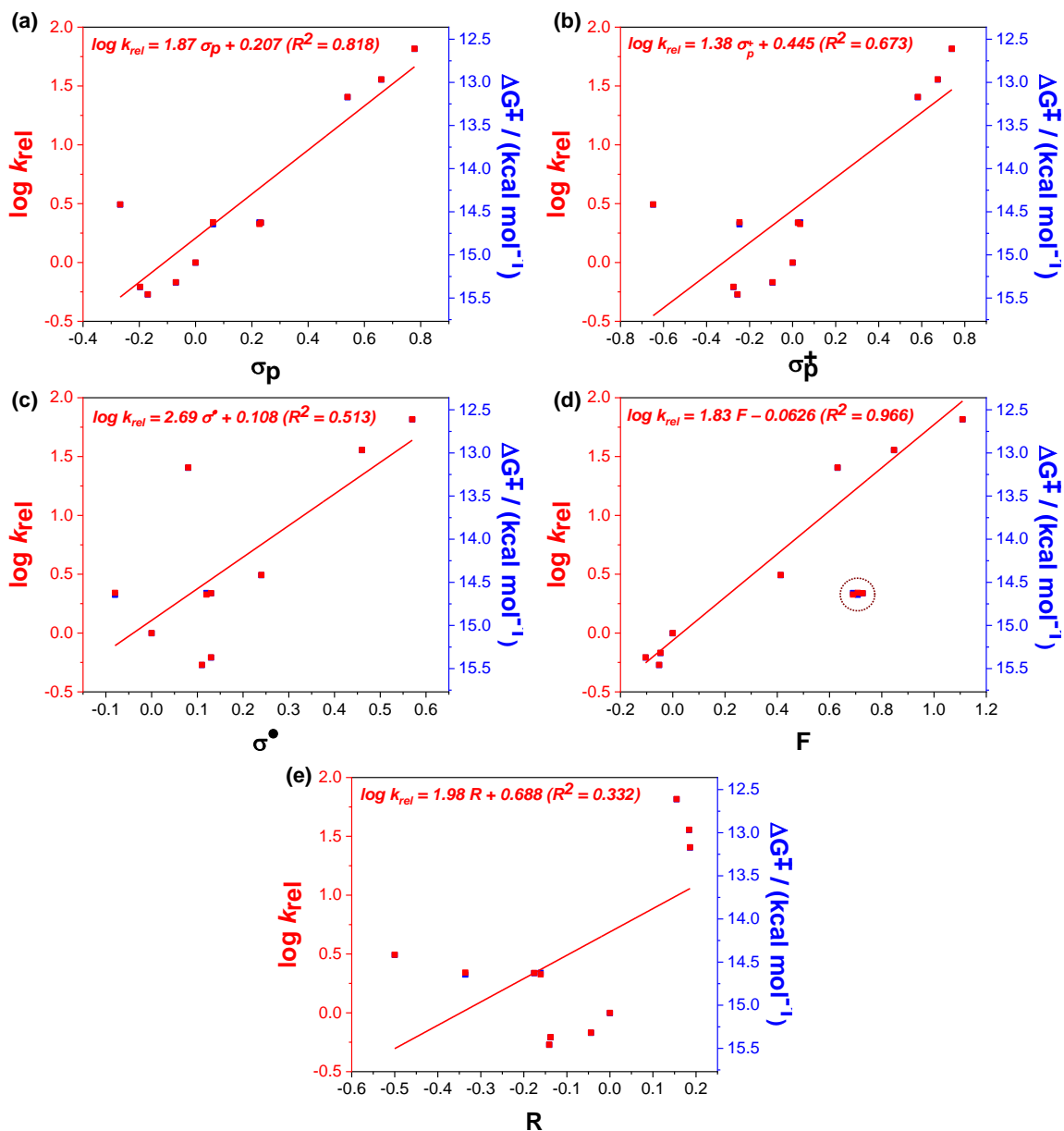


Figure 43: Plots of $\log k_{rel}$ and ΔG^\ddagger against (a) Hammett σ_p , (b) σ_p^+ , (c) σ^* , (d) Field effect (F) and (e) Resonance effect (R) for para-substituted phenyl radical additions to acetone-based enol acetate at PCM(DMF)/UBHandHLYP/6-311++G**//UBHandHLYP/6-311G** level of theory.

The positive slopes (ρ) suggests the formation of a negative partial charge δ^- at its C_α , is being formed in relation to the same atom at the reactant. The atomic charges calculated by Hu, Lu, and Yang (HLY) charge fitting method²⁴⁸ allows the estimation of the charge accumulation at the atom on the TS and in the reactants. Considering that the charge at the C_α , calculated by the HLY method, is $Q_{C_\alpha}(TS) = -0.756e$ in the TS, while it is $Q_{C_\alpha}(enol) = -0.725e$ at the reactant, the charge

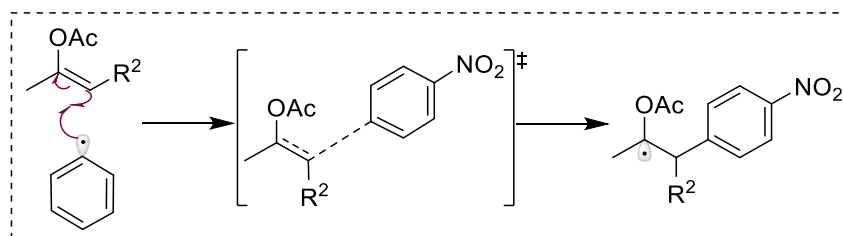
accumulation/depletion (δ) at this carbon in TS can be calculated by $\delta = Q_{C\alpha}(\text{TS}) - Q_{C\alpha}(\text{enol})$, which results in $\delta = -0.031e$. The negative sign confirms the charge accumulation at C_{α} , in agreement with the value (δ^{-}) expected by the positive ρ value from the LFER.

The good correlation with field effect can be explained in terms of radical electrophilicity. Strong electron-withdrawing groups, such as NO_2 , CN and CF_3 , have large dipoles, exerting an electrostatic field (F) which helps to stabilize the accumulation of electron density (δ^{-}) at the reacting center C_{α} . On the other hand, groups that pull electrons, such as alkyl and silyl, tend to have the opposite role.

The arylation of pentan-3-one and cyclohexanone-based enol acetates with *p*- NO_2 substituted phenyl diazonium salt gives yields of 33 and 35%, respectively.¹³⁰ These lower yields, as compared to the unsubstituted case, were attributed to steric demands at α -carbon. To analyze this fact, calculations with alkyl-substituted enol acetate at α -carbon at the TS were carried out. Taft proposed modifying the Hammett equation to include the influence of steric effect.^{249–251} Later, Charton proposed a new scale where the van der Waals radii of different groups were used as reference.^{252–254} These LFERs were employed to evaluate the steric effect at the desired system.

The DFT calculations show that the exothermicity of the reaction is decreased as bulkier the alkyl group is (Table 18), affecting the barrier height. A bulk group such as $t\text{Bu}$ increased the ΔG^{\ddagger} in around 4 kcal mol^{-1} . Cyclic ketones were also evaluated. Cyclohexanone-based enol acetate exhibited similar behavior of *n*-alkyl groups. 1-Tetralone-based enol acetate showed the lowest ΔG^{\ddagger} . As this enol acetate has an aromatic ring fused to a cyclohexanone, the resonance effect would stabilize the adduct formed, which could be observed by the lowest exothermicity.

Table 18: Calculated TS Gibbs free energy (ΔG^\ddagger / kcal mol⁻¹) and enthalpy (ΔH^\ddagger / kcal mol⁻¹), reaction Gibbs free energy (ΔG_{rxn} / kcal mol⁻¹) and enthalpy (ΔH_{rxn} / kcal mol⁻¹) at UBHandHLYP/6-311G** level of theory for p-nitrophenyl radical addition to α -alkyl enol acetates.



R²	ΔG^\ddagger	ΔH^\ddagger	ΔG_{rxn}	ΔH_{rxn}
H	12.0	2.2	-26.3	-38.6
Me	14.0	2.1	-23.7	-37.1
Et	14.5	2.4	-23.5	-37.0
ⁿ Pr	14.6	2.4	-23.4	-36.9
ⁱ Pr	14.3	3.3	-22.5	-35.4
ⁿ Bu	14.7	2.4	-23.4	-36.9
ⁱ Bu	15.9	4.4	-22.0	-34.8
cyclohexanone	13.7	2.6	-22.4	-35.0
1-tetralone	13.1	1.6	-33.1	-46.2

The calculated barrier height showed, excluding the cyclic compounds, poor correlation with the reaction enthalpy ($r^2 = 0.442$, Figure 44a). It means that exothermicity has an influence on the reaction rate to a small degree, as shown by the slope (0.092) close to zero, and therefore it is not the main factor. As shown previously, the enol acetate acts as the nucleophile, so the plot of barrier height against enol acetate HOMO energy was used to evaluate polar effect. No correlation was observed, showing that this effect has a low influence on the energy barrier (Figure 44b).

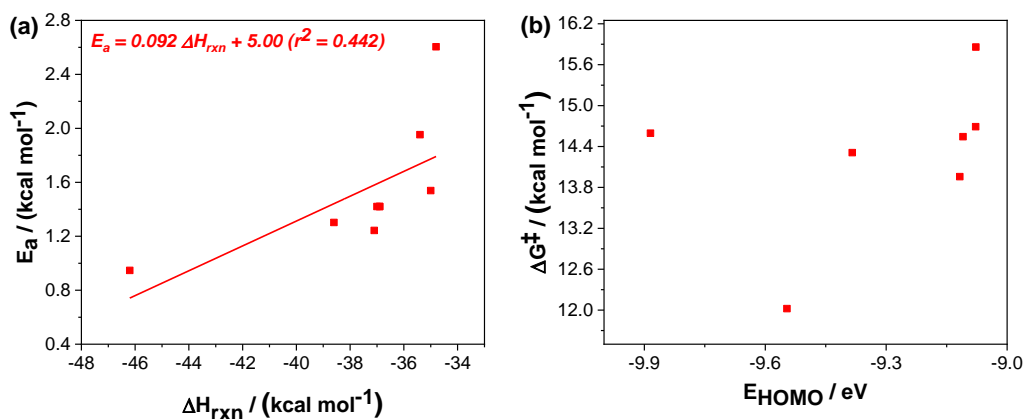


Figure 44: Plots of transition state enthalpy (ΔH^\ddagger) against reaction enthalpy (ΔH_{rxn}) and (b) HOMO energy for the addition of *p*-nitrophenyl radical towards α -alkyl enol acetates.

The Taft and Charton parameters for the evaluated alkyl substituents are showed in Table 19. The plots of $\log k_{rel}$ against steric constants for each showed good correlations: $r^2 = 0.938$ for Taft (Figure 45a) and $r^2 = 0.924$ for Charton (Figure 45b) scales. Due to the methyl group being considered the reference for Taft sterics analysis, the $\log k_{rel}$ for this case was considered as $\log k_X/k_{Me}$, instead of the traditional $\log k_X/k_H$. The $\rho_{Taft} = -1.21$ and $\rho_{Charton} = -2.78$ indicate that steric demands at the α -carbon are particularly important in the reaction.

Table 19: Taft ($-E_s$) and Charton (ν) constants and $\log k_{rel}$ for different alkyl groups.

R^2	$-E_s$	ν	$\log(k_X/k_{Me})$	$\log(k_X/k_H)$
H	-1.24	0	0.19	0
Me	0	0.52	0	-1.42
Et	0.07	0.56	-0.08	-1.85
<i>n</i> -Pr	0.36	0.68	-0.09	-1.89
<i>i</i> -Pr	0.47	0.76	-0.05	-1.68
<i>n</i> -Bu	0.39	0.68	-0.10	-1.96
<i>i</i> -Bu	0.93	0.98	-0.34	-2.81

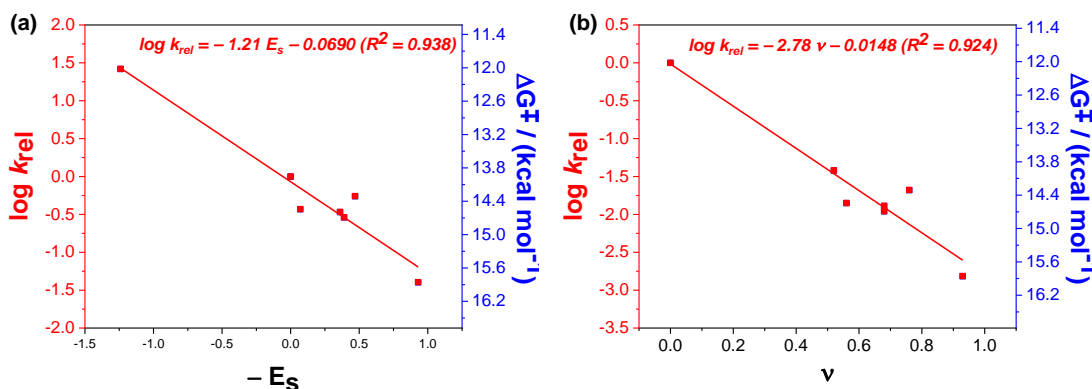


Figure 45: LFER plots with (a) Taft ($-E_s$) and (b) Charton constants (ν) for the addition of *p*-nitrophenyl radical towards α -alkyl enol acetates.

The analysis of structural parameters at transition states can clear what happens in the presence of bulky groups. The approximation distance is reduced up to 0.066 Å but, compared to substituted radicals added to acetone-based enol acetate, these parameters are acceptable. Any other way, the angles of approximation (θ) deviate around -4 to -5° with aliphatic alkyl groups and up to -6.5° in case of cyclic enol acetates, getting far from Bürgi-Dunitz trajectory.

Table 20: Approximation distance (r_{cc} / Å) and angle (θ / °) calculated at transition states of *p*-nitrophenyl addition to enol acetates.

R^2	r_{cc}	θ
H	2.411	105.1
Me	2.368	101.4
Et	2.383	100.0
<i>n</i> -Pr	2.380	100.0
<i>i</i> -Pr	2.345	101.6
<i>n</i> -Bu	2.380	100.0
<i>i</i> -Bu	2.372	100.4
Cyclohexanone	2.384	99.8
1-tetralone	2.406	98.5

Finally, acetophenone-based enol acetates were used to evaluate how substitution at β -carbon (Scheme 1, C_β) influences the rate constants. At König's work, reactions with three substituted acetophenones ($R^3 = \text{OMe}, \text{Br}, \text{H}$) were carried out

and excellent yields were obtained. In such systems, the substitution had no key effect in the reaction yields.

The calculated barrier heights (Table 21) of all the evaluated substituents are close to non-substituted acetophenone. Compared to acetone-based enol acetates, these reactions would be faster with rate constants 10 to 100 times higher. The formation of a new radical species after the addition is stabilized by both phenyl and acetate groups. The plot of the logarithm of the relative rate constants against Hammett constants indicates a good correlation ($r^2 = 0.991$, Figure 46a), but with a smaller slope ($\rho = -0.649$), suggesting little influence on the rate. Correlations with field and resonance effects indicate that both contribute to lower barrier heights. Since the radical formed is coplanar to the π orbitals, the resonance effect would be an expected factor to influence this system (Figure 46e).

Table 21: Hammett constants (σ_p and σ_p^+), Creary constant (σ^*), field effect (F) and resonance effect (R) constants and the energy barrier ΔG^\ddagger (kcal mol $^{-1}$) and the log k_{rel} for the p-nitrophenyl radical addition to the acetophenone-based enol acetates.

R^3	σ_p	σ_p^+	σ^*	F	R	ΔG^\ddagger	log k_{rel}
H	0	0	0	0	0	10.96	0
NH ₂	-0.660	-1.111	---	-0.681	---	10.33	0.466
OMe	-0.268	-0.648	0.24	-0.5	0.24	10.80	0.122
Me	-0.17	-0.256	0.11	-0.141	0.11	10.82	0.102
Br	0.232	0.025	0.13	-0.176	0.13	11.23	-0.197
CN	0.660	0.674	0.46	0.184	0.46	11.53	-0.418
NO ₂	0.778	0.74	0.57	0.155	0.57	11.63	-0.492

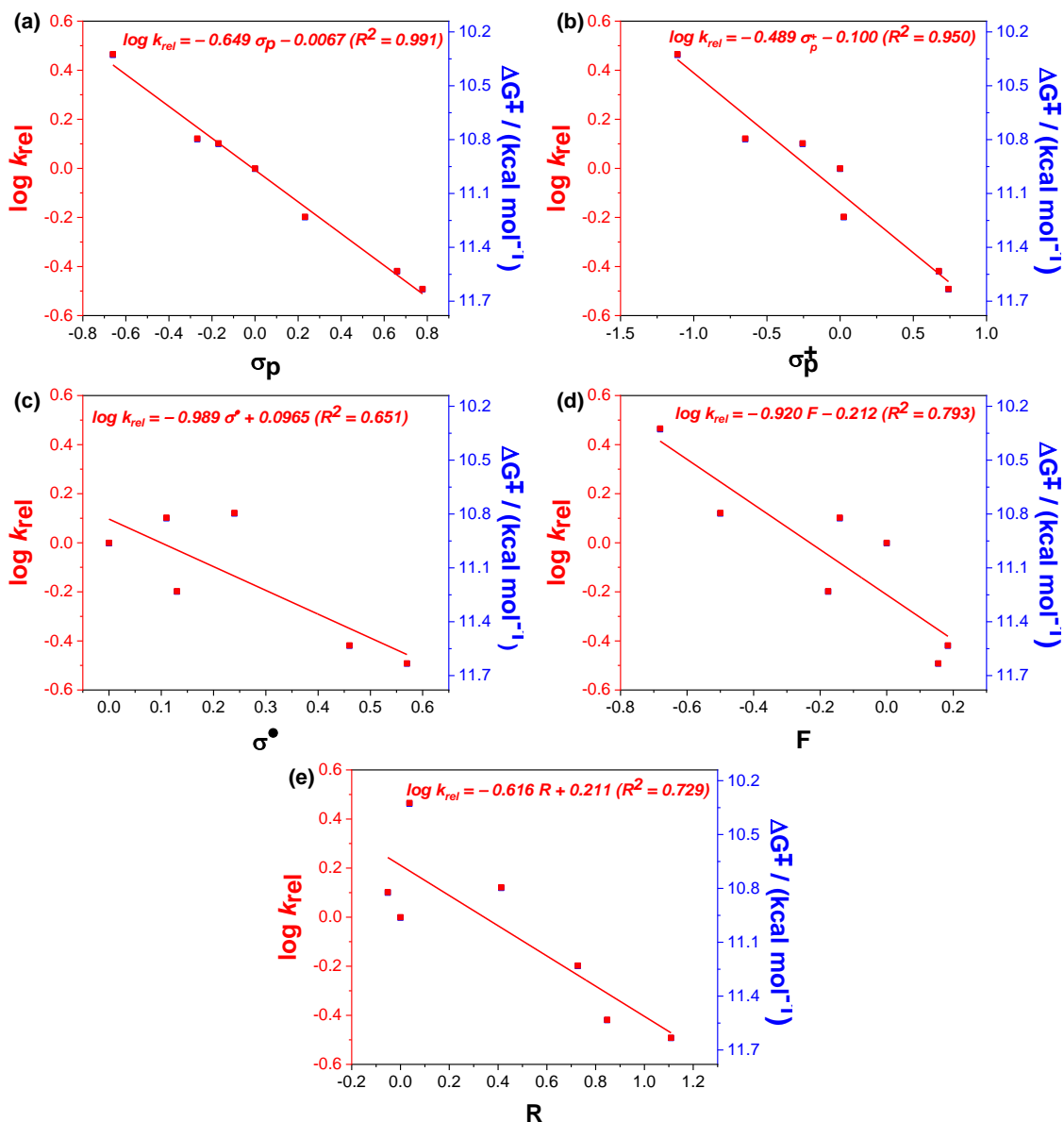


Figure 46: Plots of $\log k_{rel}$ and ΔG^\ddagger against (a) Hammett σ_p , (b) σ_p^+ , (c) σ^\bullet , (d) Field effect (F) and (e) Resonance effect (R) for substituted p-nitrophenyl radical addition to acetophenone-based enol acetates.

The substitution pattern at the aryl ring of acetophenone-based enol acetate monitors the alkene β -carbon. The negative slopes of LFER correlations indicate the electron density depletion or accumulation of positive charge at β -carbon on the TS concerning this atom on the reactants, *i.e.*, $\delta(C_\beta) = \delta^+$. Electron donating groups (EDG) would exhibit higher rates as compared to EWG. The HLY charges were also used for calculating the electron density accumulation/depletion (δ) at the α -carbon, *i.e.*, $\delta = Q_{C_\beta}(\text{TS}) - Q_{C_\beta}(\text{enol})$. Since $Q_{C_\beta}(\text{TS}) = 0.329e$ and $Q_{C_\beta}(\text{enol}) = 0.277e$, this leads to δ

= + 0.052e, which confirms the charge depletion at C_{β} at the TS, in agreement with the value (δ^+) expected by the positive ρ value from the LFER shown in Figure 46a.

Based on this systematic study, we can summarize important features about electronic demand at both aryl radical and enol acetate that affects the photoredox version of the Meerwein arylation, which may work as guidelines for this reaction. These are: 1) Groups that highly pull electronic density by field effect at phenyl radical improve the reaction yields; 2) Electron-donating groups (EDG) directly bonded to the β -carbon of the enol acetate will improve the reaction yields and could be interesting to be in synthetic applications when α -aryl ketones with oxygenated groups, typical of natural products, are desired; 3) Substitution at α -carbon of the enol acetate, such as alkyl groups and cyclic ketones, will decrease the yield.

3.4.

Conclusions

We explored the phenyl radical reactivity in additions to enol acetates. Based on the theoretical calculations and supposing that the addition of the phenyl radicals to the enol acetates would be the step responsible for the reactivity, the polar effects are suggested to dominate the influence by the action of the field effect, which is consistent with the early TS. Based on the theoretical Hammett, HLY charges, and NBO analysis, the accumulation of negative charge at the C_{α} makes the enol acetate the nucleophile of the reaction. The evaluation of the substitutions at the enol acetates showed a strong influence of the substitution at C_{α} by steric effects even reacting with a stronger nucleophile as *p*-nitrophenyl radical. On the other hand, substitution at C_{β} did not show a significant influence on the energy barriers. These results suggest that as the reduction of diazonium salts to phenyl radicals is a very fast process, the influence of substituents would not interfere severely at this step and the addition step is critical to determinate the efficiency of the reaction, different from what was proposed in the literature. To confirm this theoretical evidence, kinetic experiments are suggested in the same systems.

3.5.

Experimental procedures

The computational calculations were carried out by using Gaussian 16 software²⁵⁵. The geometry optimization of reactants and products was performed using BHandHLYP functional²⁵⁶ (unrestricted in case of the radicals) and 6-311G** basis set. Stationary points were characterized as minima with no negative frequencies analyzing harmonic vibrational frequencies at the same theory level as geometry optimization. TS geometries were calculated at the same level of theory and were confirmed by the presence of only one imaginary frequency. Molecular orbitals were calculated from the optimized structure using MP2/6-31G** level of theory (the MO energies were obtained in the Hartree-Fock part of the calculation). NBO calculations were performed within its 3.1 version²⁴² implemented at Gaussian 03 software²³². The cartesian coordinates and energies of the calculated structures are shown in the Appendix 2 of this Thesis.

4

Synthesis of α -aryl-1-tetralones by photoredox catalysis

4.1.

α -Aryl-1-tetralones as analogues of isoflavanones

Isoflavanones (**377**) are a class of isoflavones (**378**) in which the α,β -unsaturation is reduced. These compounds are biosynthetic precursors of isoflavonoids²⁵⁷ and have several biological applications. In Figure 47 some naturally occurring isoflavanones are present. Perbergin (**379**), extracted from the bark of *Dalbergia pervillei*, showed antimicrobial activity against some Gram-positive bacteria, such as *Mycobacterium smegmatis*.²⁵⁸ Sativanone (**380**), extracted from *D. parviflora*, showed moderate activity as MCF-7 and T47D cells proliferation stimulant.²⁵⁹ Saphoronol A (**381**) was obtained from the extract of the roots of *Sophora mollis* and exhibited moderate activity against *Plasmodium falciparum*.²⁶⁰ Cajanol (**382**), extracted from the legume pigeon pea, showed activity against MCF-7 breast cancer cells.²⁶¹ Vestitone (**383**) had antimicrobial activity as compared to streptomycin and was obtained from the extract of *D. odorifera*.²⁶² The isoflavanone **384**, isolated from *Uraria crinite*, exhibited cytotoxicity against KB (mouth epidermal cancer), HepG2 (hepatocellular cancer), Lu (lung cancer) and MCF-7 cells lines.²⁶³ Dothideoisoflavanone (**385**), extracted from *Dothideomyces fungus* CMU-99, showed moderate activity against KB cells.²⁶⁴ Eryvellutinone (**386**) was extracted from the stem bark of *Erythrina vellutina* Willd. No data on its biological activity was presented.²⁶⁵ Ficustikounone A (**387**), isolated from *Ficus tikoua*, but was inactive against A549 (lung cancer), HepG2, MDA231 and SGC7901 (human gastric cancer) cells.²⁶⁶ The kenusanone F 7-methyl ether (**388**) was obtained from the stem bark of *D. melanoxyton* and showed activity against *M. tuberculosis*.²⁶⁷

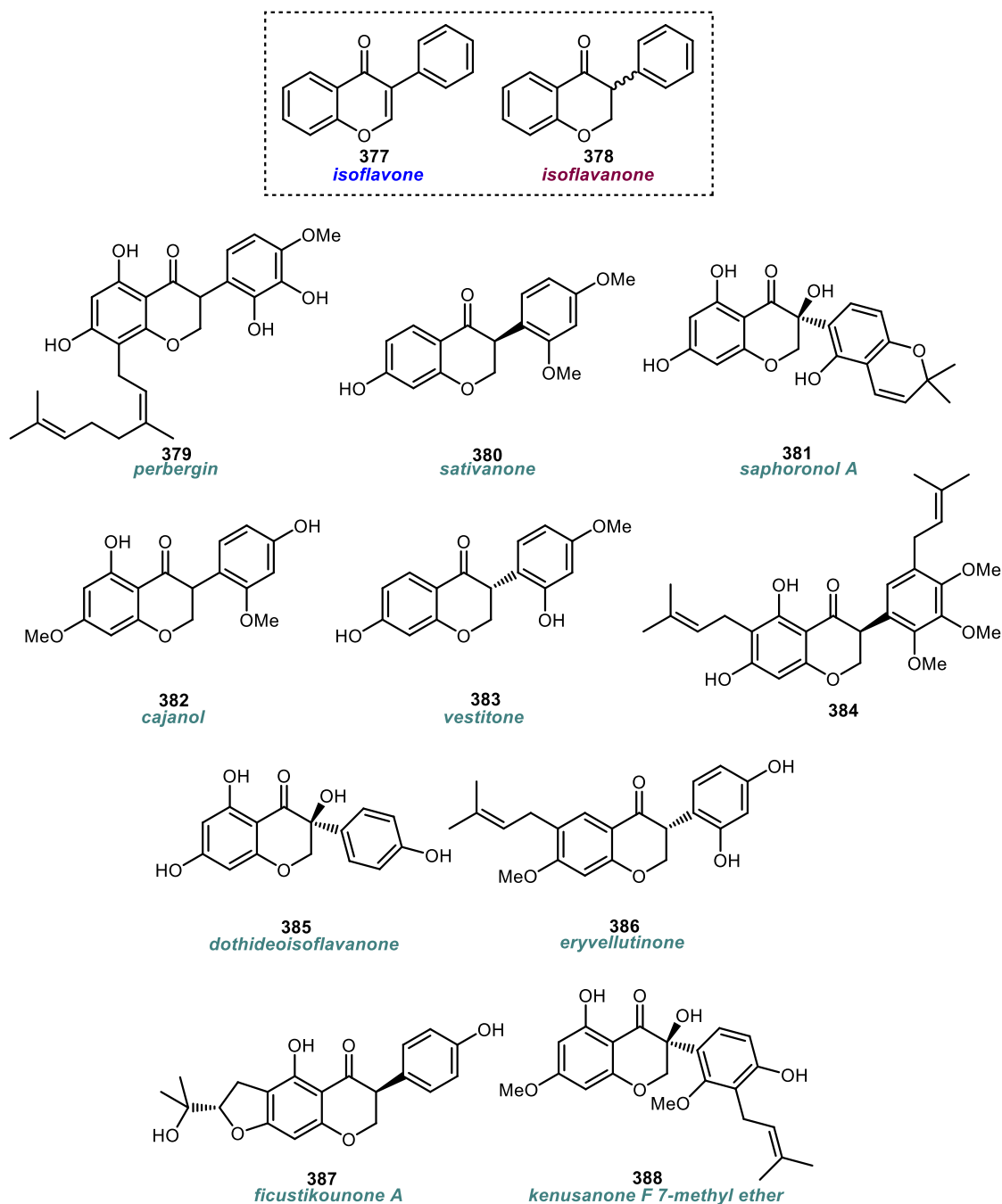
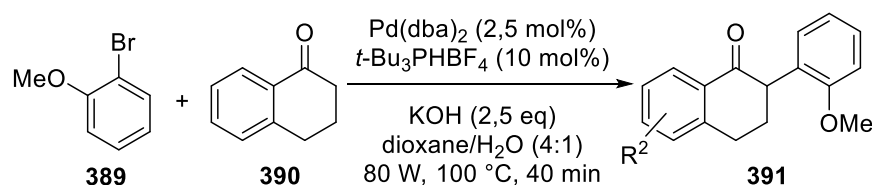


Figure 47: Examples of naturally occurring isoflavanones.

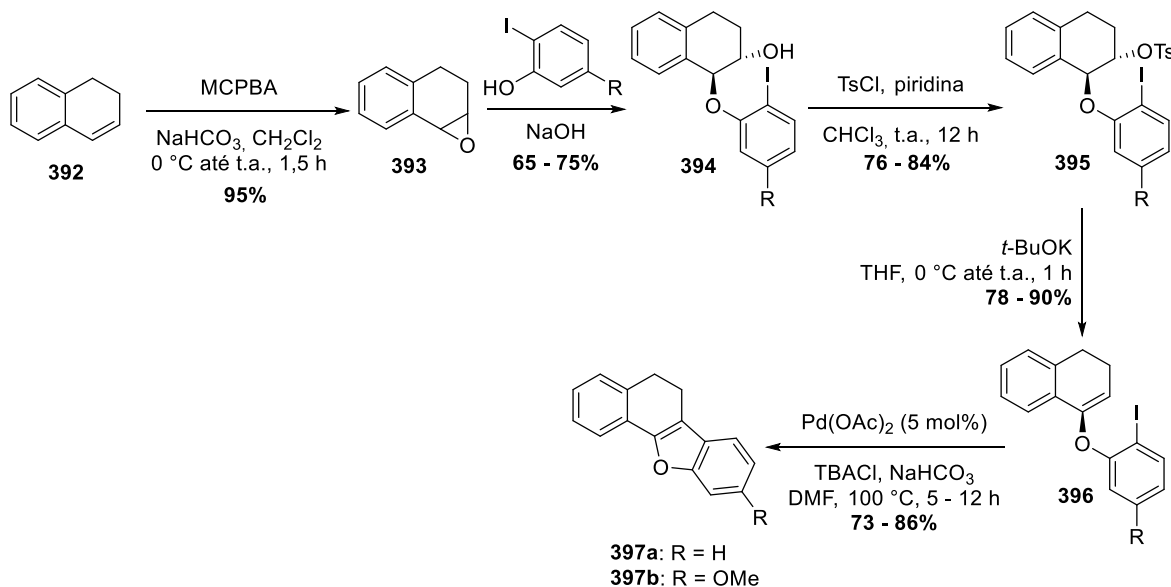
The isosteric change of the oxygen heteroatom to a CH₂ group led to the α -aryl-1-tetralones (like **391**), also known as 1-carbaisoflavanones. These compounds, however, were not extensively investigated for biological applications. Costa et al reported the first use of these compounds as anti-HCV drug candidates.²⁶⁸ The compounds were obtained after the Buchwald-Hartwig-Myura reaction of **389** with **390**

(Scheme 57). Some of the aryl-tetralones showed $EC_{50} < 8 \mu\text{mol L}^{-1}$ against genotype 1a and $< 5 < 8 \mu\text{mol L}^{-1}$ against genotype 2a with high selectivity index.



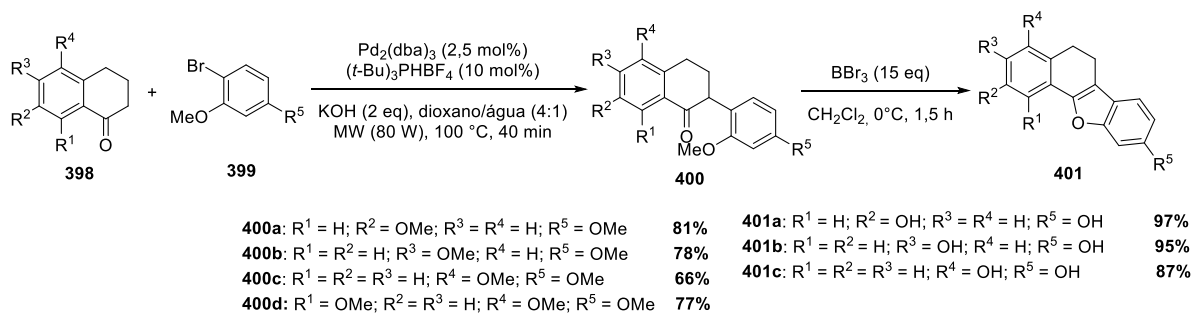
Scheme 57: Costa's α -arylation of 1-tetralones by Buchwald-Hartwig-Myura reaction.

The same group also showed the synthetic value of these compounds as intermediates of the synthesis of carbapterocarpens, which are pterocarpens analogues, a class of natural products that are considered an important class of nonsteroidal antiestrogens for the treatment of hormone-sensitive cancers.²⁶⁹ Costa et al proposed the synthesis of **397a** and its methoxylated version **397b** in a 5-steps synthesis, in which the intermediate **396** undergoes an intramolecular Heck reaction to afford the desired products (Scheme 58).



Scheme 58: Costa's synthesis of carbapterocarpens.

Later, they proposed a shorter route (2 steps) starting from 1-tetralones (**398**) and **399** to obtain the intermediate **400** by Buchwald-Hartwig-Myura reaction followed by the formation of the benzofuran ring to afford **401** in good yields (Scheme 59).

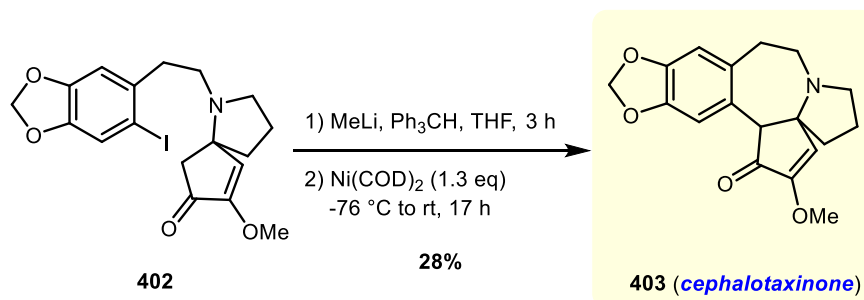


Scheme 59: Costa's modified synthesis of carbapterocarpens through 1-tetralones.

4.2.

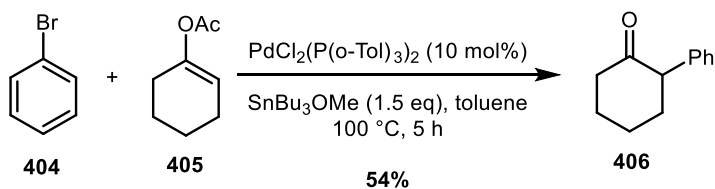
α -Arylation of cyclic ketones

Based on the exposed synthetic and the promising biological values of the α -aryl-1-tetralones, presenting the methodologies for this kind of transformation is required. The most useful strategy to make arylated ketones is the enolization followed by the arylation step. Jones et al proposed the total synthesis of the cephalotaxinone (**403**), an alkaloid isolated from a Japanese plum yew.²⁷⁰ The last step was the ring closure of **402** using stoichiometric amounts of Ni(0) (Scheme 60). The compound **403** was obtained after this arylation in 28% yield.



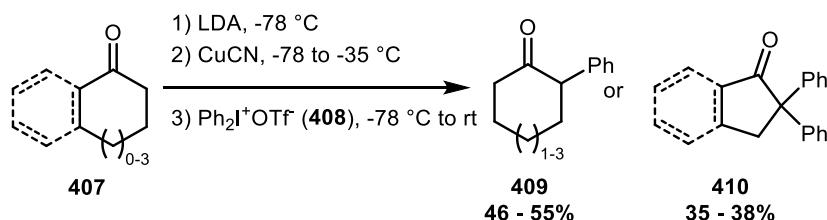
Scheme 60: Synthesis of cephalotaxinone by intramolecular arylation of **402** with Ni(0).

The use of non-catalytic metals was also employed in other works to promote the α -arylation of ketones. Migita et al used bromobenzene as an aryl source to arylations of enol acetates using organotin compounds and palladium catalysis (Scheme 61).²⁷¹ The author proposed the formation of an organotin enolate intermediate. The arylation of **405** with **404** was achieved in 54% yield.



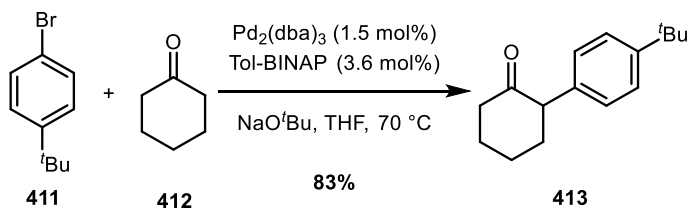
Scheme 61: Arylation of cyclohexanone combining organotin and palladium catalysis.

Ryan and Stang proposed the arylation of cyclic ketones using diphenyliodonium triflate (**408**) (Scheme 62). The authors explained the moderate yields obtained by competing for radical reduction process, assuming that the mechanism is based on radicals. When cyclopentanone and indenone were used, two phenyl groups (**410**) were inserted at the desired position.



Scheme 62: Arylation of cyclic ketones using diphenyliodonium triflates.

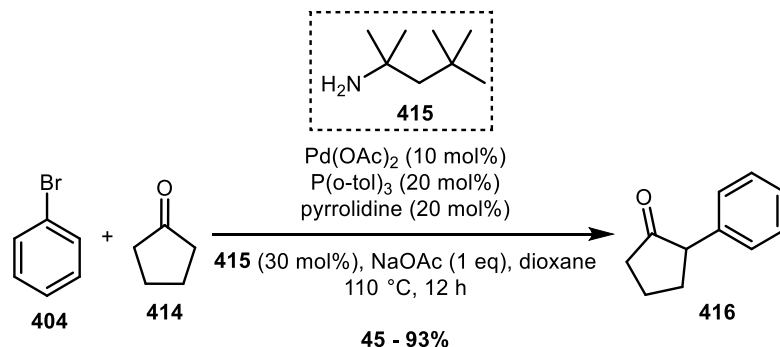
Palucki and Buchwald highlighted that until 1997 the methodologies used to this transformation required stoichiometric amounts of metallic compounds. They proposed a new methodology in which the arylation would work directly, with no need of transformations on **412**. The arylation with **411** was achieved in 83% yield (**413**) when 2 equivalents of the aryl bromide were employed (Scheme 63).²⁷²



Scheme 63: Direct arylation of cyclohexanone by palladium catalysis.

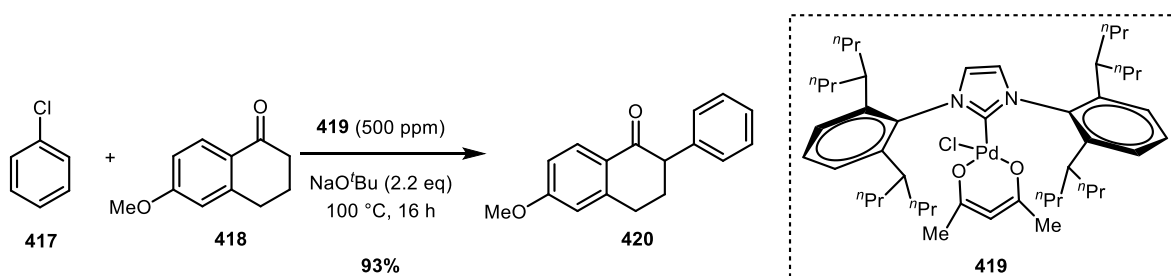
The use of palladium catalysis with organocatalysis was explored by Dong et al. The formation of enamines from **414** and pyrrolidine *in situ* led the generation of

the products like **416** in yields up to 93% (Scheme 64).²⁷³ The methodology showed tolerance to a huge variety of functional groups and to scaling up. However, no other cyclic ketones were evaluated.



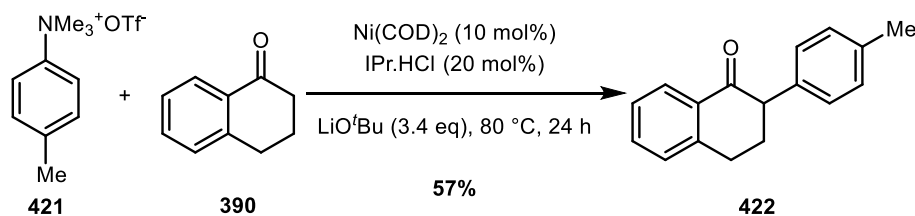
Scheme 64: Arylation of cyclopentanones merging cross-coupling and organocatalysis.

Nolan et al developed a methodology that required sub-catalytic amounts of palladium (Scheme 65). The use of the bench stable pre-catalyst **419** could afford the compound **420** in 93% yield from **417** and **418**, using 500 ppm of **419** in a 0.5 mmol scale.²⁷⁴ The authors highlighted that the proposed protocol does not need glove box or Schlenk techniques, but the yields are improved if they are employed. The compound **420** was obtained inside a glove box.

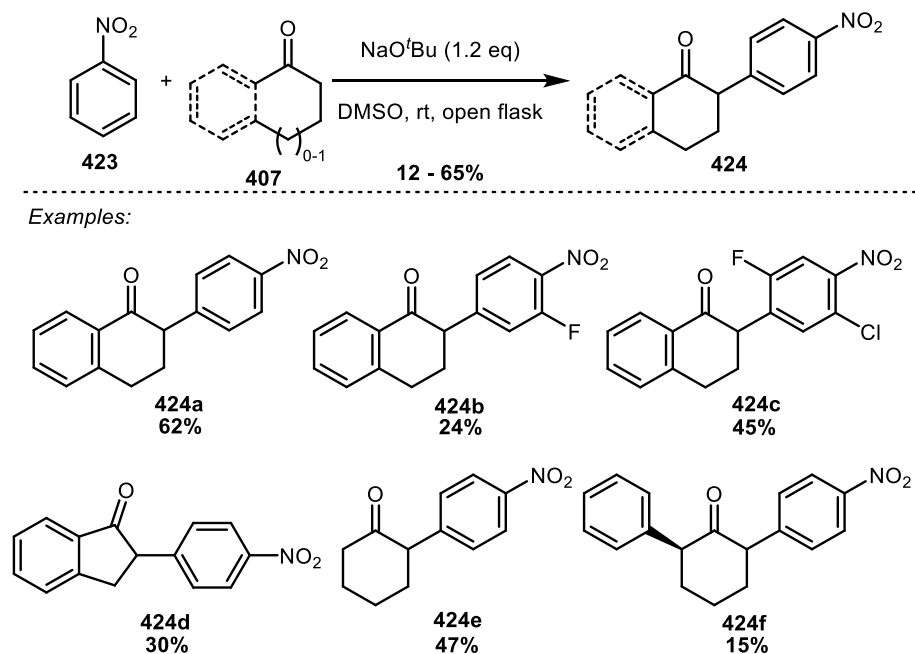


Scheme 65: Arylation of 418 with chlorobenzene using **419** in subcatalytic amounts.

Other metals were also used for this transformation. Li and Wang used nickel to catalyze the α -arylation from aryltrimethylammonium triflates (**421**) (Scheme 66).²⁷⁵ The reaction of **421** with **390** gave the desired product **422** in 57% yield. The mechanism was not elucidated by the authors.

Scheme 66: arylation of 1-tetralone with **421** by nickel catalysis.

Finally, Kürti et al proposed a metal-free reaction to obtain the α -aryl-1-tetralones.²⁷⁶ The use of a strong base like KO^tBu made the arylation with nitroarenes (**423**) possible, while their attempts onto the use of organocatalysis were not successful. Arylated 1-tetralones and 1-indenones were achieved in yields up to 65% (Scheme 67) in a regioselective fashion. When fluorine and chlorine were present as substituents at the nitrobenzene, the yield decreased from 62% (**424a**) to 24% (**424b**) and 45% (**424c**), but the S_NAr product was not observed by the authors. The presence of EDG was not evaluated. The arylation of indenone was achieved in 30% yield (**424d**). Non-aromatic cyclic ketones showed poor yields (**424e**) and when the α -position was already arylated, the arylation occurred at the opposite carbon (**424f**). The formed enolate was nucleophilic enough to promote the attack to the nitrobenzene followed by the C-H oxidation mediated by oxygen.



Scheme 67: Arylation of cyclic ketones with nitrobenzenes by nucleophilic aromatic substitution.

4.3.

Objectives

As pointed out at section 4.1, the α -aryl-1-tetralones showed activity against hepatitis C virus. This result brought our group up the possibility of exploring the use of this class of compounds in other classes of viral diseases, such as zyka and chikungunya. For this purpose, the aim of this work is to develop a new methodology to make α -aryl-1-tetralones by photoredox catalysis. The arylation of these compounds generates a chiral center at the α -position, therefore a methodology to obtain the enantiomeric pure compounds was also studied. For these purposes, four specific objectives are described below.

- Develop a methodology based on merging photoredox catalysis and organocatalysis to obtain chiral α -aryl-1-tetralones.
- Study the reactivity of 1-tetralone derived enamines from pyrrolidine.
- Once the arylation is achieved, develop a methodology to obtain enantiomeric pure α -aryl-1-tetralones.
- Describe the use of isonitriles to obtain 1-tetralones via photoredox catalysis.

4.4.

Results and discussion

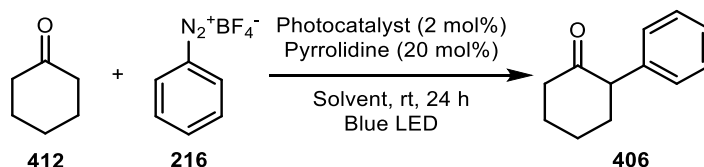
All the results of this work were obtained during the internship at the University of Michigan at the laboratory of Dr. Corey Stephenson.

4.1.1. Organocatalysis approach

To the cyclic ketones, the first attempts were carried out with cyclohexanone (**412**) and diazonium salt **216** in the presence of a photocatalyst and pyrrolidine as organocatalyst (Table 22). As shown in Chapter 2 of this Dissertation, the formation of phenyl radicals is possible with $[\text{Ru}(\text{bpy})_3]\text{Cl}_2$ as photocatalyst. The reactions carried out with this photocatalyst (Entries 1 to 7) did not work, even when the solvent was changed to MeCN and DMF. The other photocatalysts employed (Entries 8 to 11) did

not work, showing that more reducing agents, such as Ir(ppy)₃, and more oxidizing agents, as [Ru(bpz)₃](PF₆)₂, did not affect the reaction.

Table 22: Attempts on the arylation of cyclohexanone by photoredox catalysis and organocatalysis.

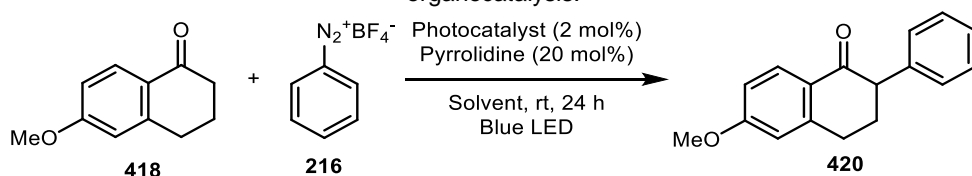


Entry	Photocatalyst	Solvent	Yield ^a
1	[Ru(bpy) ₃]Cl ₂	DMSO	NP
2	[Ru(bpy) ₃]Cl ₂	DMSO ^b	NP
3 ^c	[Ru(bpy) ₃]Cl ₂	DMSO	NP
4 ^c	[Ru(bpy) ₃]Cl ₂	DMSO ^b	NP
5 ^d	[Ru(bpy) ₃]Cl ₂	DMSO	NP
6	[Ru(bpy) ₃]Cl ₂	DMF	NP
7	[Ru(bpy) ₃]Cl ₂	MeCN	NP
8	[Ir(dF(CF ₃)ppy) ₂ (dtbpy)]PF ₆	DMSO	NP
9	[Ir(ppy) ₂ (dtbbpy)]PF ₆	DMSO	NP
10	Ir(ppy) ₃	DMSO	NP
11	[Ru(bpz) ₃](PF ₆) ₂	DMSO	NP

General reaction conditions: **216** (0.1 mmol), **412** (0.5 mmol), photocatalyst (0.002 mmol), pyrrolidine (0.02 mmol), solvent (0.5 mL), rt, 24 h, blue LED irradiation. ^a The reaction was monitored by GC-MS and ¹H NMR. ^b 1.0 mL of solvent; ^c 10 eq of cyclohexanone; ^d 1st step: **412** + pyrrolidine + 0.5 mL DMSO for 18 h, 2nd step: **216** + [Ru] + 0.5 mL DMSO for 6 h. NP = no product observed.

As the reactions with cyclohexanone did not work, the ketone was changed to the 6-methoxy-1-tetralone (**418**) (Table 23). The reaction with the same conditions as above (Entry 1) did not work. The addition of DIPEA did not give the desired product (Entry 2). As pointed out by Cook in his book about the chemistry of enamines,²⁷⁷ the synthesis of enamines from 1-tetralones and pyrrolidine is difficult and strong Lewis acids, such as TiCl₄, are needed. Based on this, MS 4 Å was added to the reaction (Entry 3), but no product was observed. The use of DMF (Entries 4 and 5) and methanol (Entries 6 and 7) did not give the arylated product. Finally, even the use of Ir(ppy)₃ (Entry 8) did not work.

Table 23: Attempts on the arylation of 6-methoxy-1-tetralone by photoredox catalysis and organocatalysis.

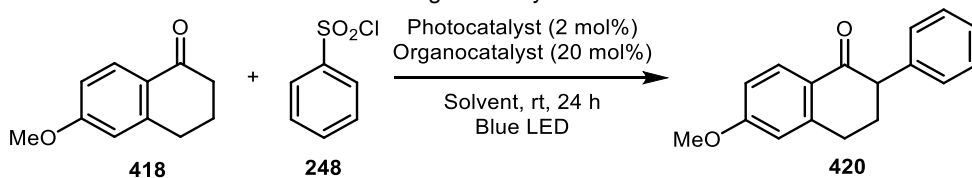


Entry	Photocatalyst	Solvent	Additive	Yield ^a
1	[Ru(bpy) ₃]Cl ₂	DMSO	---	NP
2	[Ru(bpy) ₃]Cl ₂	DMSO	DIPEA (2 eq)	NP
3	[Ru(bpy) ₃]Cl ₂	DMSO	MS 4Å	NP
4	[Ru(bpy) ₃]Cl ₂	DMF	---	NP
5	[Ru(bpy) ₃]Cl ₂	DMF	MS 4Å	NP
6	[Ru(bpy) ₃]Cl ₂	MeOH	---	NP
7	[Ru(bpy) ₃]Cl ₂	MeOH	MS 4Å	NP
8	Ir(ppy) ₃	DMSO	---	NP

General reaction conditions: **216** (0.1 mmol), **418** (0.5 mmol), photocatalyst (0.002 mmol), pyrrolidine (0.02 mmol), solvent (0.5 mL), rt, 24 h, blue LED irradiation.

As it is not possible to monitor the consumption of diazonium salts by TLC or GC-MS, the source of phenyl radical was changed to **248** (Table 24). Using the conditions of the previous attempts (Entries 1 to 6 and 11), the reaction did not give the product, but the full conversion of the sulfonyl chloride was observed. The organocatalysts was changed to morpholine (Entry 8), piperazine (Entry 9) and (*L*)-proline (Entry 10) and **248** was fully converted, but no product obtained.

Table 24: Attempts on the arylation of 6-methoxy-1-tetralone with **248** by photoredox catalysis and organocatalysis.

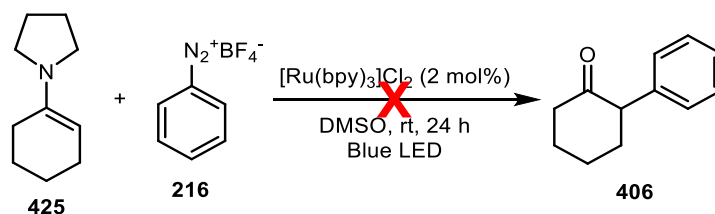


Entry	Photocatalyst	Organocatalyst	Solvent	Additive	Yield ^a
1	[Ru(bpy) ₃]Cl ₂	Pyrrolidine	DMSO	---	NP
2	[Ru(bpy) ₃]Cl ₂	Pyrrolidine	DMSO	MS 4Å	NP
3	[Ru(bpy) ₃]Cl ₂	Pyrrolidine	DMF	---	NP
4	[Ru(bpy) ₃]Cl ₂	Pyrrolidine ^a	DMF	---	NP

5	[Ru(bpy) ₃]Cl ₂	Pyrrolidine	MeOH	---	NP
6	[Ru(bpy) ₃]Cl ₂	Pyrrolidine	MeOH	MS 4Å	NP
7	[Ru(bpy) ₃]Cl ₂	Pyrrolidine	Toluene/DMSO	---	NP
8	[Ru(bpy) ₃]Cl ₂	Morpholine	DMSO	---	NP
9	[Ru(bpy) ₃]Cl ₂	Piperazine	DMSO	---	NP
10	[Ru(bpy) ₃]Cl ₂	(L)-proline	DMSO	---	NP
11	Ir(ppy) ₃	Pyrrolidine	DMSO	---	NP

General reaction conditions: **248** (0.1 mmol), **418** (0.5 mmol), photocatalyst (0.002 mmol), organocatalyst (0.02 mmol), solvent (0.5 mL), rt, 24 h, blue LED irradiation.

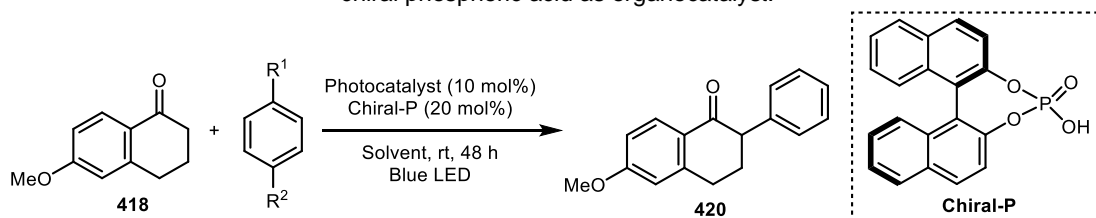
As the phenyl radical source is consumed during the reaction, the addition step to the enamine was investigated. The enamine derived from cyclohexanone and pyrrolidine (**425**) is commercially available and was used in an arylation reaction using the typical conditions showed at Chapter 2 (Scheme 68). The reaction did not work, suggesting that enamines like **425** could not be substrates prone to be arylated by photoredox catalysis.



Scheme 68: Attempt on the arylation of **425** by photoredox catalysis.

The problems related to enamine catalysis and cyclic ketones were showed by Blanchet et al; the authors proposed a complementary approach to enamine catalysis to be used in cases like 1-tetralones.²⁷⁸ The use of chiral phosphoric acids as Brønsted acids can induce the *in situ* formation of enolates. Merging this method with photoredox catalysis (Table 25) could afford the designed product. Initially, aryl bromides were employed as phenyl radical sources using the anthraquinone Aq-OH as photocatalyst (Entries 1 to 3) based on the methodology described by König et al: the reactions did not work.²⁷⁹ Then, 4-bromoacetophenone was used instead of bromobenzene (Entries 4 to 7); different photocatalysts were used; as all the previous attempts, sulfonyl chlorides also did not give the desired product (Entries 8 to 10).

Table 25: Attempts on the arylation of 6-methoxy-1-tetralone with different phenyl radical sources and chiral phosphoric acid as organocatalyst.



Entry	R ¹	R ²	Catalyst	Solvent	Additive	Yield
1	Br	H	Aq-OH	DMSO	DIPEA (3 eq)	NP
2	Br	H	Aq-OH	Toluene	DIPEA (3 eq)	NP
3	Br	H	Aq-OH	Toluene	DIPEA (3 eq)	NP
4	Br	C(O)Me	PDI	DMSO	Et ₃ N (10 eq)	NP
5	Br	C(O)Me	PDI	Toluene	Et ₃ N (10 eq)	NP
6	Br	C(O)Me	Aq-OH	DMSO	Et ₃ N (10 eq)	NP
7	Br	C(O)Me	[Ir(ppy) ₂ (dtbbpy)]PF ₆	DMSO	Et ₃ N (10 eq)	NP
8	SO ₂ Cl	H	Ir(ppy) ₃	Toluene	Et ₃ N (10 eq)	NP
9	SO ₂ Cl	H	Aq-OH	Toluene	Et ₃ N (10 eq)	NP
10	SO ₂ Cl	H	PDI	Toluene	Et ₃ N (10 eq)	NP

The last attempts to arylate the 1-tetralone were carried out with the enol acetate **426** (Table 26). Even with the use of MS 4Å or changing the solvent and the photocatalyst, the reactions did not produce **427**.

The structures of **430** and **431** were optimized at the B3LYP/6-311++G(d,p) level of theory. Despite the steric hindrance pointed out at Scheme 69b, the iminium double bond forces the tetralin conformation in a such way that this steric effect is reduced. However, when the tautomer carries out, the structure of **431** does not allow the half-chair conformation and the steric factor takes place. The DFT calculations showed that the optimized structure has the dihedral angle $[C1'-N-C1-C2] = 29.1^\circ$. It means that the C-N bond is twisted and the orbital overlap at C=C-N bonds is impaired.

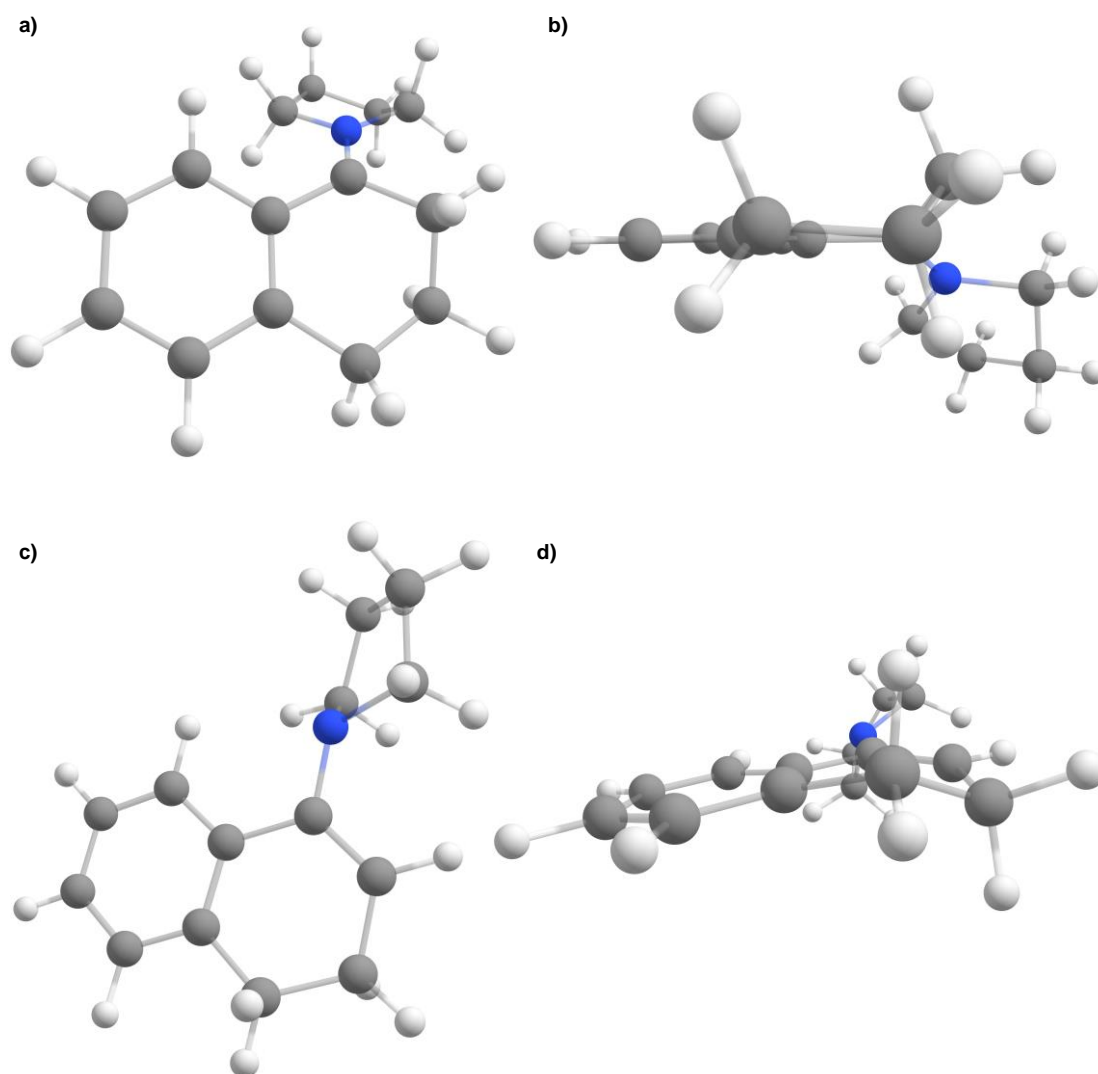


Figure 48: Optimized structures of **430** and **431** at B3LYP/6-311++G(d,p) level of theory: (a) the iminium **430** in front view, (b) the iminium **430** in side view, (c) the enamine **431** in front view and (d) the enamine **431** in side view.

According to the Second Order Perturbation Theory, the energy of the interaction of a pair of orbitals is described by the Equation 8. The smaller the difference of energy between these orbitals is, the bigger will energy of stabilization be. However, this difference is not the only parameter to analyze it. The parameter F_{ij} , which is the Hamiltonian matrix element between the orbitals, is a way to visualize the overlap between two orbitals, and influences the stabilization energy.

$$E(2) = \frac{-q_i |F_{ij}|^2}{E_j - E_i} \quad (8)$$

- $E(2)$: perturbation energy
- q_i : occupancy of the donor orbital (usually = 2)
- F_{ij} : Hamiltonian operator
- E_j and E_i : orbital j energy (acceptor) and orbital i energy (donor)

NBO calculations, carried out at the HF/6-311++G(d,p) level of theory, were conducted to scan the dihedral angles, from 0 to 180°. Both parameters, $E(2)$ and F_{ij} , were calculated as a function of the [C1'-N-C1-C2] dihedral angle (Figure 49). As expected, both parameters have the same tendency. At 0°, in other words, when the pyrrolidine ring is parallel to the tetralin ring, $E(2)$ and F_{ij} have a local maximum value and they decrease as the angle increases. The $E(2)$ is lower than 0.5 kcal mol⁻¹ when the dihedral angle is between 60 and 80°. This means that, at these angles, there is no contribution of the interaction between the enamine N lone pair and $\pi^*_{C=C}$ orbital. The parameters increase until reaching a global maximum value at 150°. The optimized structure does not have the maximum $E(2)$ and F_{ij} values and, based on this scan, it could be clarified as the less hindered structure with higher delocalization.

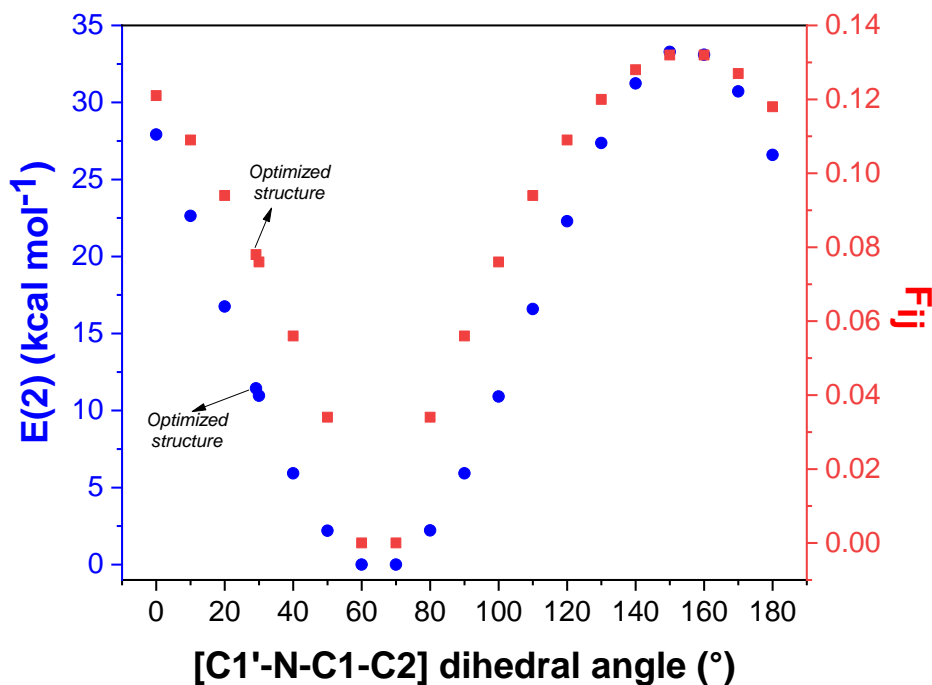
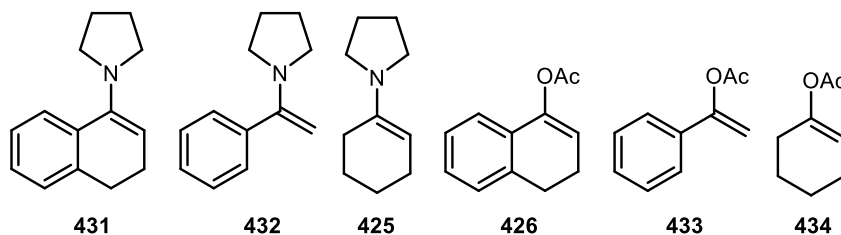


Figure 49: The energy of stabilization $E(2)$ and the parameter F_{ij} as a function of the [C1'-N-C1-C2] dihedral angle.

The second reason would be related to the reactivity of the enamines toward the phenyl radical. As shown in Chapter 3, enol acetates act as nucleophiles when they react with phenyl radicals; it is known that enamines are more nucleophilic than enols.³¹ Studies with Conceptual DFT were conducted to analyze this hypothesis. The reactivity parameters (Table 27) were calculated at B3LYP/6-31+G(d), according to the method described in Chapter 2.

Table 27: Conceptual DFT parameters calculated for enamines and enol acetates at B3LYP/6-31+G(d).



Compound	μ^0	η^0	ω^0	N^0
431	-3.26	4.70	1.13	3.51
432	-3.13	4.83	1.02	3.58
425	-2.43	4.87	0.61	4.26
426	-3.62	4.95	1.32	3.02
433	-3.88	5.17	1.46	2.65
434	-3.46	6.40	0.93	2.47
69	-4.33	4.51	2.08	1.30

Legend of colors: good; moderate and weak nucleophile/electrophile.

For all the structures, the global chemical potential is higher than the one of the phenyl radical. It suggests, as expected, that these compounds would act as the nucleophiles and **69** as the electrophile. The enamines **431**, **432** and **425** are more nucleophilic than the enol acetates **426**, **433** and **434**, so they would be more reactive toward phenyl radical. Based on this analysis, conceptual DFT cannot explain correctly the obtained results.

As pointed out at Chapter 3, sterics influence the phenyl radical addition to enol acetates and the substitution at the C α increases the activation energy. As the approximation of the phenyl radical is out of the plane of the N-C=C bonds, the pyrrolidine ring would hinder the addition and thus increases the activation energy. The TS related to the addition to **431** and **425** was calculated at the UBHandHLYP/6-311G** level of theory (Figure 50). The approximation angles of the phenyl radical to the enamines are close to each other: 103.3° for **431** and 101.6° for **425**. The distances are close too: 2.385 and 2.401 Å for **431** and **425**, respectively. These structural parameters indicate that there is no significant difference for the approximation of the phenyl radical.

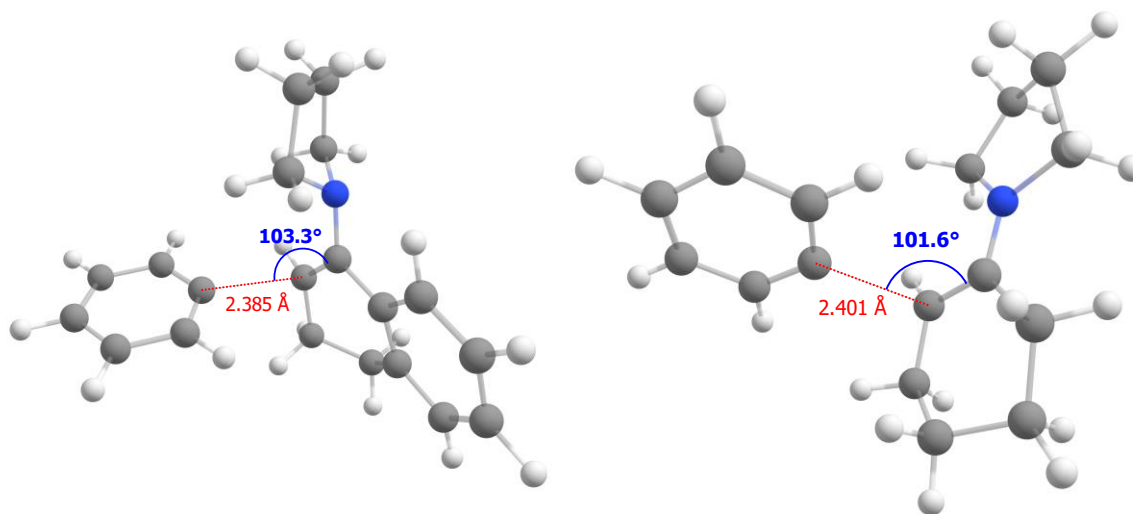


Figure 50: Transition states for the addition of the phenyl radical to **431** (left) and **425** (right) calculated at UBHandHLYP/6-311G** level of theory.

The energy profile diagram (Figure 51) shows that the TS of the addition to the tetralone-derived enamine is higher in energy than the cyclohexanone one. The former has the $\Delta G^\ddagger = 15.7 \text{ kcal mol}^{-1}$, which is a higher energy TS as compared to the additions to the enol acetates. The addition to **425** is lower in energy ($13.0 \text{ kcal mol}^{-1}$) and would be more accessible. Both reactions are exothermic (see

Table 28 for the complete set of thermodynamic parameters) and the adduct **435** is more stable.

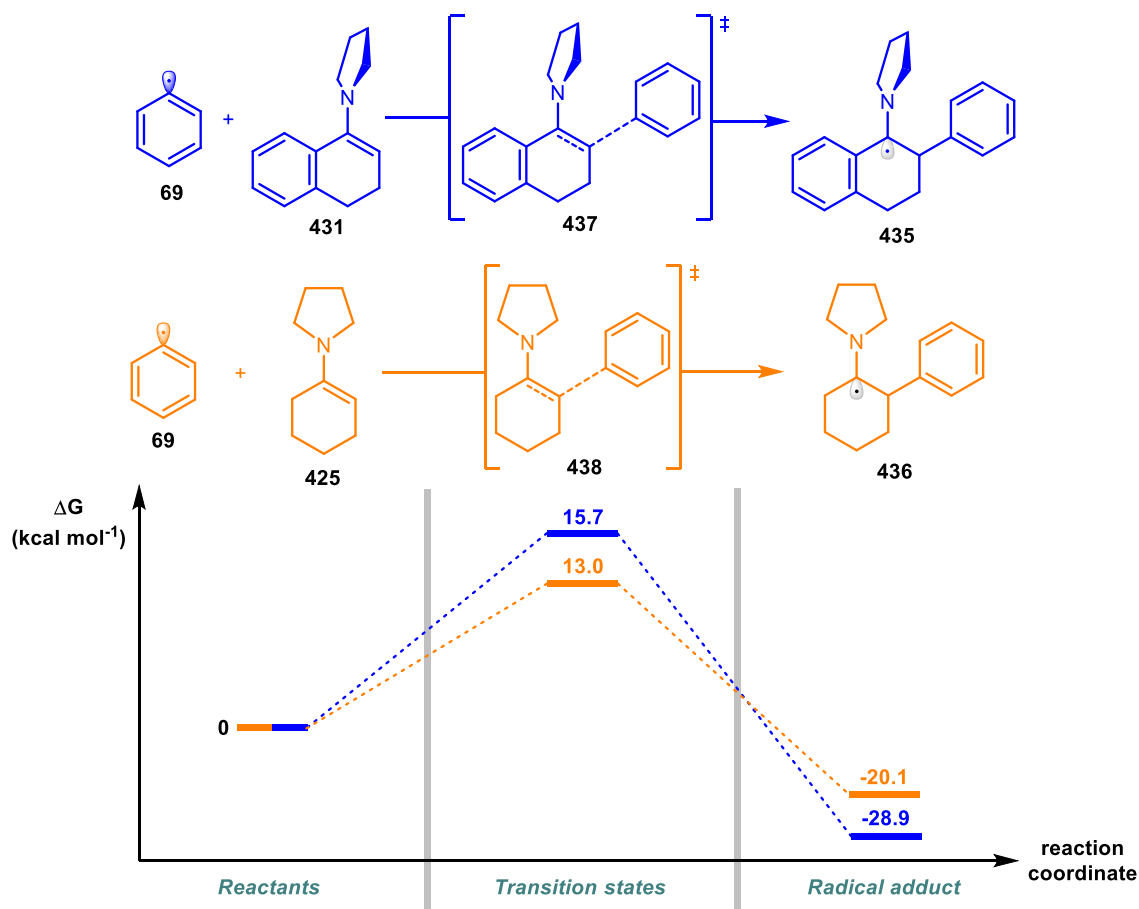


Figure 51: Energy profile diagram for the phenyl radical addition to **425** and **431**, calculated at UBHandHLYP/6-311G** level of theory.

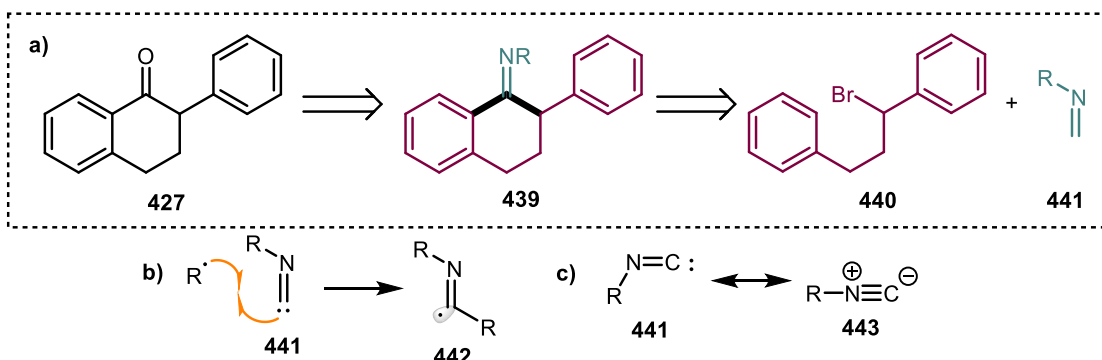
Table 28: Thermodynamic parameters (in kcal/mol) for the phenyl radical addition to pyrrolidine-derived enamines, calculated at UBHandHLYP/6-311G**.

Reaction	ΔG^\ddagger	ΔH^\ddagger	E_a	ΔG_{rxn}	ΔH_{rxn}
69 + 425	13.0	2.1	2.7	-20.1	-30.6
69 + 431	15.7	4.6	5.2	-28.9	-41.3

4.4.2. Isonitrile approach

After the failed attempts of the combination of organocatalysis and photoredox catalysis, a new synthetic approach was designed to obtain **427** (Scheme 70a). This strategy was based on the use of isonitriles **441**, a class of compounds that can react with radicals to form iminyl radical adducts **442** by radical combination (Scheme 70b).

This reaction can occur due to the presence of non-bonding electrons at the carbon atom, as described by the resonance structure **443** (Scheme 70c).



Scheme 70: Proposed synthesis of α -aryl-1-tetralones using isonitriles.

Several works showed the use of isonitriles in the photoredox catalysis context.^{282–286} Its main use is based on a radical combination to obtain an intermediate like **442** followed by radical aromatic substitution. The designed strategy required the formation of a benzylic radical from **440**. To evaluate the photocatalysts that would be prone to reduce **440** and if the alkyl chain would influence the process, the cyclic voltammetry of this compound was carried out (Figure 52). The reduction peak was observed at -1.77 V (vs. SCE), which is consistent with the reduction potential of benzylic bromide (-1.82 V).²⁸⁷

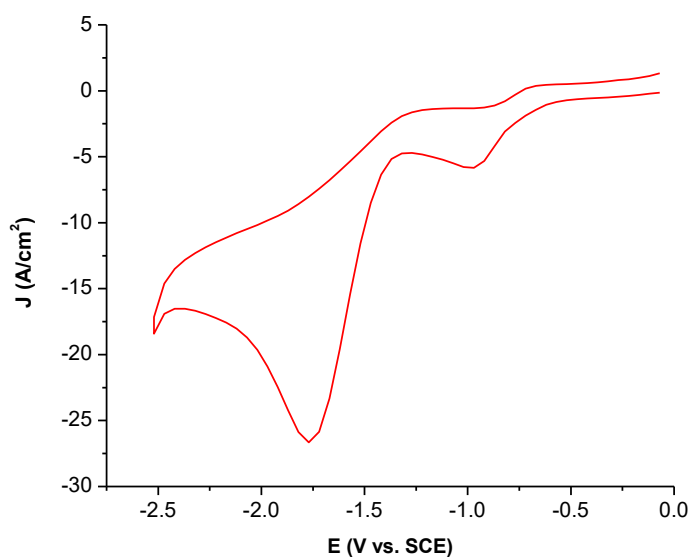
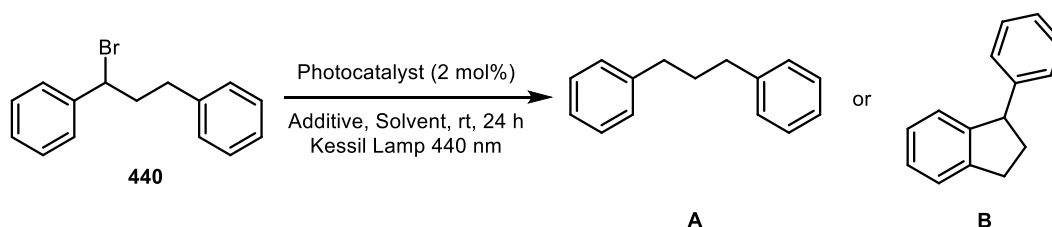


Figure 52: Cyclic voltammetry of **440**.

Then, the compound **440** was submitted to some photoredox conditions to evaluate its reduction (Table 29). The reactions were monitored by GC-MS. Firstly, the reduction was attempted in the presence of $[\text{Ru}(\text{bpy})_3]\text{Cl}_2$ as photocatalyst, and DIPEA and HCO_2H as additives (Entry 1). This method showed effective dehalogenation of α -halocarbonyl compounds,¹⁰ however no reaction was observed and the starting material was recovered. Then, stronger reducing agents were used (entries 2, 3 and 4). The conversion of **440** was sensitive to the kind of additive used. In the presence of $[\text{Ir}(\text{ppy})_2(\text{dtbbpy})]\text{PF}_6$, the reduction was observed when DIPEA was used, instead of Et_3N . In the former, it was observed the formation of two products with $m/z = 196$, which is **440** reduced to the corresponding alkane, and 164 (compound **A**), which suggests the formation of the cyclic compound **B**. When the photocatalyst was changed to $[\text{Ir}(\text{dF}(\text{CF}_3)\text{ppy})_2(\text{dtbpy})]\text{PF}_6$, no reaction was observed.

Table 29: Attempts on the reduction of **440** using photoredox catalysis.



Entry	Photocatalyst	Additive	Solvent	Conversion (%)
1	$[\text{Ru}(\text{bpy})_3]\text{Cl}_2$	DIPEA (10 eq) HCO_2H (10 eq)	DMF	NR
2	$[\text{Ir}(\text{ppy})_2(\text{dtbbpy})]\text{PF}_6$	DIPEA (2.2 eq)	MeCN	100
3	$[\text{Ir}(\text{ppy})_2(\text{dtbbpy})]\text{PF}_6$	Et_3N (2.2 eq)	MeCN	NR
4	$[\text{Ir}(\text{dF}(\text{CF}_3)\text{ppy})_2(\text{dtbpy})]\text{PF}_6$	DIPEA (2.2 eq)	MeCN	NR

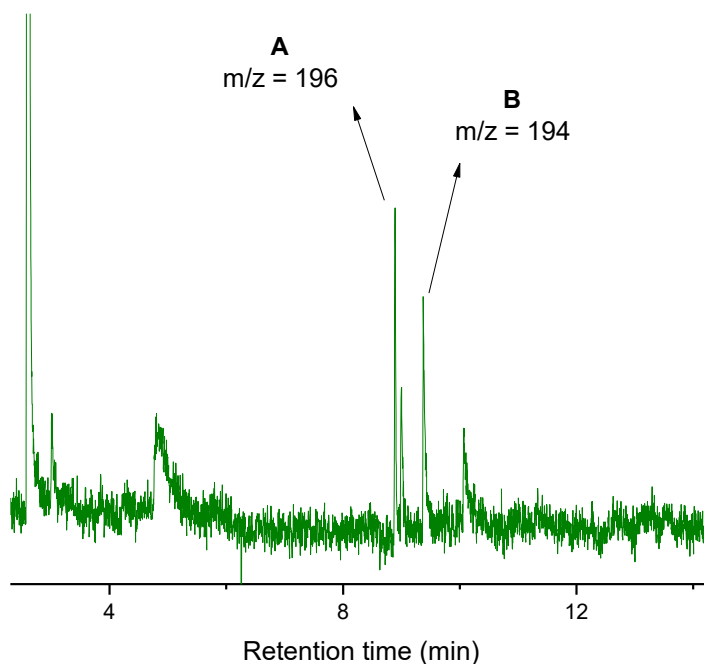
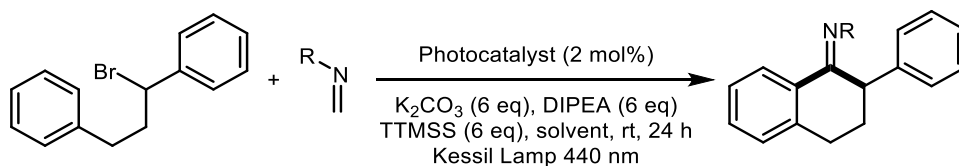


Figure 53: Chromatogram of the reduction of **440** in the presence of $[\text{Ir}(\text{ppy})_2(\text{dtbbpy})]\text{PF}_6$ and DIPEA as additive.

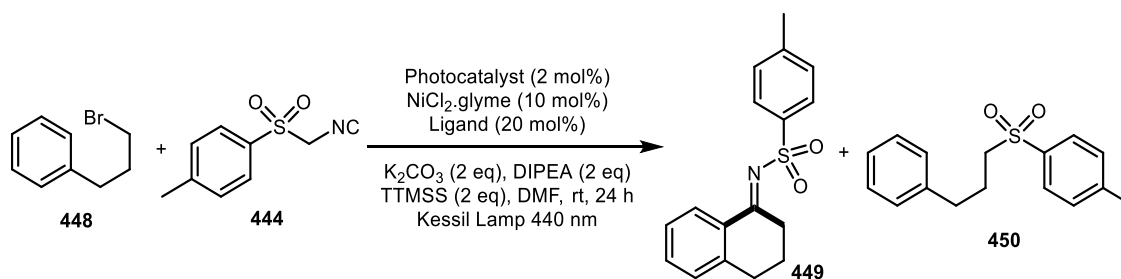
These observations indicated that the reduction is possible and the generated radical would be trappable. The isonitriles were used as trapping agents. Several attempts were tried with commercially available isonitriles (Table 30). To facilitate the reduction of **440**, TTMSS was used as additive. One of the most common isonitrile is the TosMIC (**444**), a cheap and not smelly one. It was employed in the presence of $\text{Ir}(\text{ppy})_3$ or $[\text{Ir}(\text{ppy})_2(\text{dtbbpy})]\text{PF}_6$ as photocatalysts in different solvents (Entries 1 to 14). Despite the consumption of the alkyl bromide, the desired product was not formed. The change of the isonitrile to **445** (Entry 15), **446** (Entry 16) and **447** (Entry 17) did not give the product.

Table 30: Attempts on the formation of the desired imine by photoredox catalysis using commercially available isonitriles.



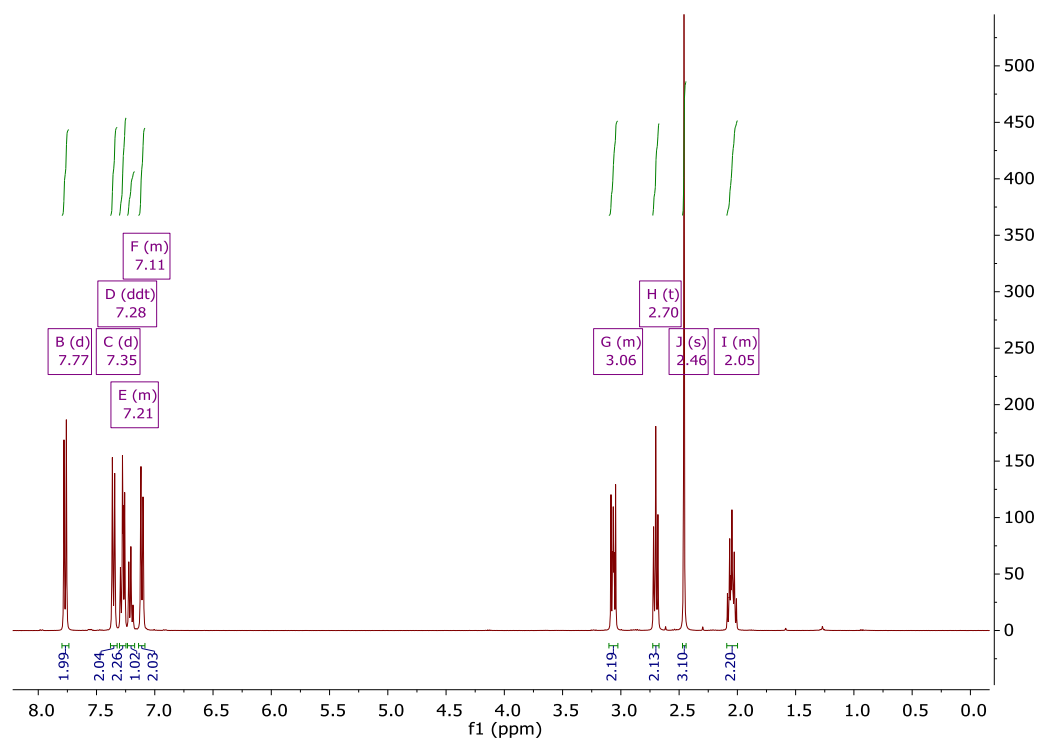
Entry	R	Photocatalyst	Solvent	Yield
1	CH ₂ SO ₂ Tol (TosMIC, 444)	Ir(ppy) ₃	DMSO	NP
2	CH ₂ SO ₂ Tol (TosMIC, 444)	[Ir(ppy) ₂ (dtbbpy)]PF ₆	DMSO	NP
3	CH ₂ SO ₂ Tol (TosMIC, 444)	Ir(ppy) ₃	DMF	NP
4	CH ₂ SO ₂ Tol (TosMIC, 444)	[Ir(ppy) ₂ (dtbbpy)]PF ₆	DMF	NP
5	CH ₂ SO ₂ Tol (TosMIC, 444)	Ir(ppy) ₃	AcOEt	NP
6	CH ₂ SO ₂ Tol (TosMIC, 444)	[Ir(ppy) ₂ (dtbbpy)]PF ₆	AcOEt	NP
7	CH ₂ SO ₂ Tol (TosMIC, 444)	Ir(ppy) ₃	Toluene	NP
8	CH ₂ SO ₂ Tol (TosMIC, 444)	[Ir(ppy) ₂ (dtbbpy)]PF ₆	Toluene	NP
9	CH ₂ SO ₂ Tol (TosMIC, 444)	Ir(ppy) ₃	THF	NP
10	CH ₂ SO ₂ Tol (TosMIC, 444)	[Ir(ppy) ₂ (dtbbpy)]PF ₆	THF	NP
11	CH ₂ SO ₂ Tol (TosMIC, 444)	Ir(ppy) ₃	MeCN	NP
12	CH ₂ SO ₂ Tol (TosMIC, 444)	[Ir(ppy) ₂ (dtbbpy)]PF ₆	MeCN	NP
13	CH ₂ SO ₂ Tol (TosMIC, 444)	Ir(ppy) ₃	DCM	NP
14	CH ₂ SO ₂ Tol (TosMIC, 444)	[Ir(ppy) ₂ (dtbbpy)]PF ₆	DCM	NP
15	4-OMePh (445)	Ir(ppy) ₃	DMSO	NP
16	Ph (446)	Ir(ppy) ₃	DMSO	NP
17	<i>t</i> -Bu (447)	Ir(ppy) ₃	DMSO	NP

As it was observed in the consumption of the alkyl halide, the addition of NiCl₂.glyme was planned to evaluate a photoredox catalysis merged with nickel coupling (Table 31). The supersilane TTMSS was also added. For this purpose, a simpler alkyl halide (**448**) was used. Surprisingly, the desired product **449** was not formed, although a tosylated compound (**450**) was obtained in 20% and 30% in the absence and in the presence of dtbbpy as ligand, respectively.

Table 31: Merging photoredox catalysis with nickel coupling to obtain the tosylated compound **450**.

Entry	Photocatalyst	Ligand	Yield of 449	Yield of 450
1	[Ir(ppy) ₂ (dtbbpy)]PF ₆	---	NP	20%
2	[Ir(ppy) ₂ (dtbbpy)]PF ₆	dtbbpy	NP	30%

The formation of **450** was confirmed by NMR. The ¹H NMR (Figure 54) showed total integration of 18 protons and the absence of a signal at 4.61 ppm (the protons of CH₂ group of TosMIC²⁸⁸) suggested that the CH₂ group of the TosMIC was not incorporated to the product.

Figure 54: ¹H NMR (700 MHz, in CDCl₃) of the compound **450**.

The confirmation of the tosylation came from the ¹³C NMR (Figure 55). The presence of four carbons up to 60 ppm and three of them secondary, as indicated by

the APT spectra (Figure 56), confirmed the tosylation with no incorporation of the CH₂ from TosMIC.

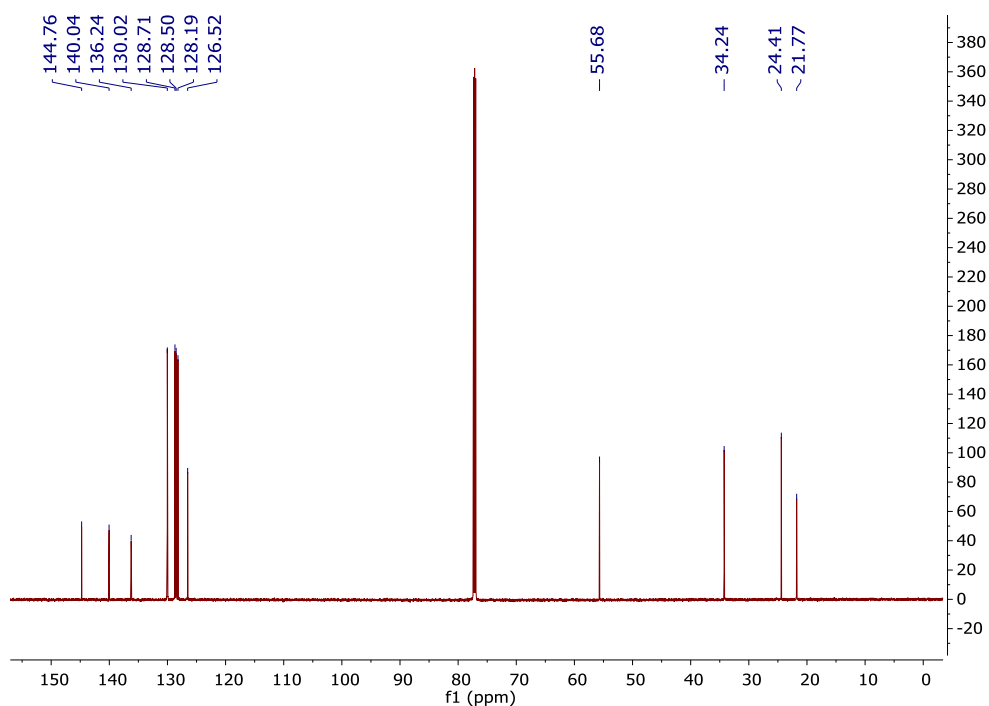


Figure 55: ¹³C NMR (176 MHz, in CDCl₃) of the compound **450**.

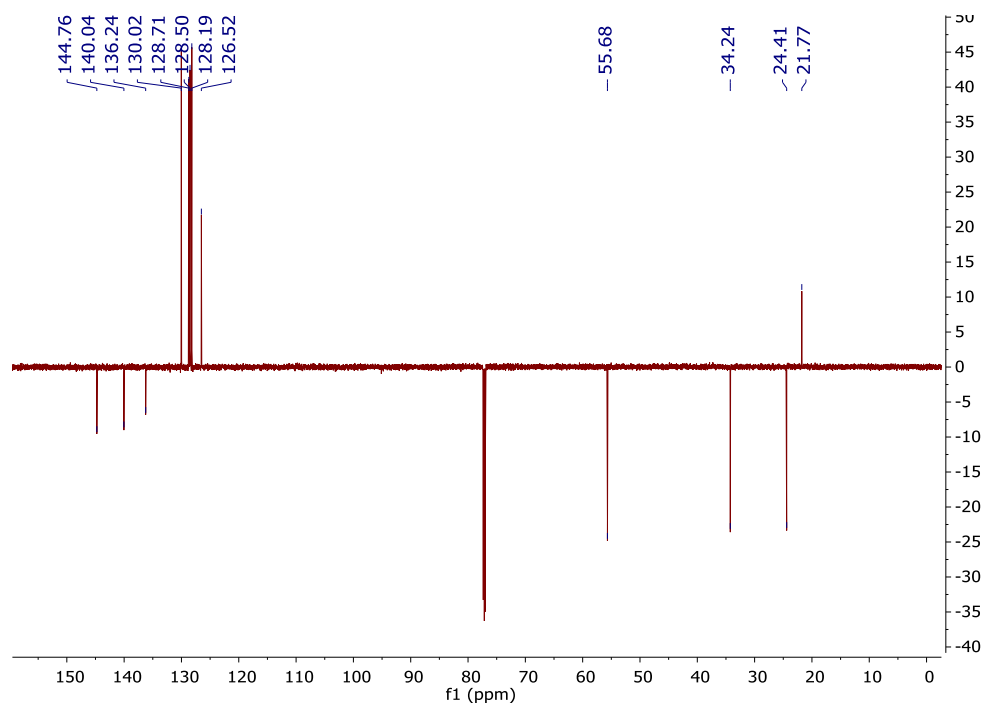
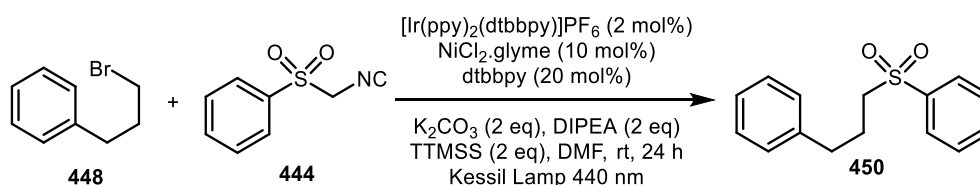


Figure 56: APT (176 MHz, in CDCl₃) spectra of the compound **450**.

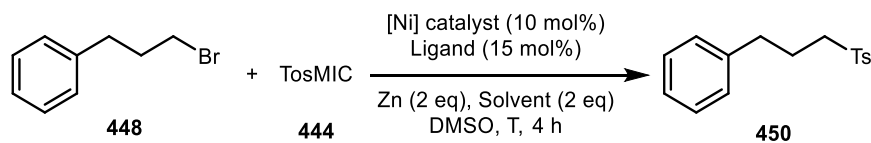
Control experiments were carried out to evaluate if the reaction was a photoredox catalysis (Table 32). Nevertheless, the removal of the photocatalyst (Entry 1) did not stop the reaction, and no product was observed when the nickel catalyst was removed (Entry 2). When TTMSS, DIPEA, or the light were removed (Entry 3 to 5), it did not affect the reaction. When the base was removed (Entry 6), **450** was not formed, suggesting that the combination of nickel catalyst and the base is strictly important to this transformation.

Table 32: Control experiments to evaluate the photoredox or the nickel catalysis.



Entry	Photocatalyst	NiCl ₂ .glyme	TTMSS	DIPEA	K ₂ CO ₃	Light	Yield
1	No	Yes	Yes	Yes	Yes	Yes	30%
2	Yes	No	Yes	Yes	Yes	Yes	NP
3	Yes	Yes	No	Yes	Yes	Yes	32%
4	Yes	Yes	Yes	Yes	Yes	No	41%
5	No	Yes	No	No	Yes	No	30%
6	No	Yes	No	No	No	No	NP

Based on these results, a methodology of tosylation was obtained for alkanes catalyzed by nickel. Usually, reactions with these catalysts require metallic additives, such as zinc.^{289–291} So, it was decided to add the metal to the reaction and proceed to the optimization (Table 33). Two nickel complexes with phosphine ligands were evaluated (Entries 1 and 2) and 14 and 7% yields were obtained, respectively. The use of NiCl₂.glyme with no ligand (Entry 3) produced trace amounts of product. The use of a Ni(0) species like Ni(COD)₂ (Entry 4) gave 22% yield. The use of NiBr₂.glyme with different ligands was employed (Entry 5 to 13). The use of bipyridine ligands showed better performance with yields in the range from 20 to 33%. Each ligand was further evaluated in different solvents. The methoxylated bipyridine (d(OMe)bpy) showed the 53% yield, the highest, in DMSO (Entry 14). When ligands with electron-withdrawing groups were used, the yields harshly decreased (Entries 29 to 36).

Table 33: Optimization of the catalyst, ligand and solvent at the tosylation of **448**.

Entry	[Ni]	Ligand	Solvent	Yield (%)
1	Ni(dppp)Cl ₂	---	DMF	14
2	Ni(PPh ₃) ₂ Cl ₂	---	DMF	7
3	NiCl ₂ .glyme	---	DMF	<5
4	Ni(COD) ₂	---	DMF	22
5	NiBr ₂ .glyme	---	DMF	5
6	NiBr ₂ .glyme	Xantphos	DMF	9
7	NiBr ₂ .glyme	BINAP	DMF	25
8	NiBr ₂ .glyme	phen	DMF	28
9	NiBr ₂ .glyme	Bphen	DMF	11
10	NiBr ₂ .glyme	dtbbpy	DMF	32
11	NiBr ₂ .glyme	bpy	DMF	24
12	NiBr ₂ .glyme	d(Me)bpy	DMF	33
13	NiBr ₂ .glyme	d(OMe)bpy	DMF	20
14	NiBr ₂ .glyme	d(OMe)bpy	DMSO	53
15	NiBr ₂ .glyme	d(OMe)bpy	DMA	31
16	NiBr ₂ .glyme	d(OMe)bpy	NMP	28
17	NiBr ₂ .glyme	d(OMe)bpy	MeCN	15
18	NiBr ₂ .glyme	d(OMe)bpy	PhCF ₃	NR
19	NiBr ₂ .glyme	d(OMe)bpy	Toluene	<5
20	NiBr ₂ .glyme	d(Me)bpy	DMSO	45
21	NiBr ₂ .glyme	d(Me)bpy	DMA	46
22	NiBr ₂ .glyme	d(Me)bpy	NMP	47
23	NiBr ₂ .glyme	d(Me)bpy	MeCN	27
24	NiBr ₂ .glyme	d(Me)bpy	Toluene	<5
25	NiBr ₂ .glyme	dtbbpy	DMSO	37
26	NiBr ₂ .glyme	dtbbpy	DMA	40
27	NiBr ₂ .glyme	dtbbpy	NMP	35
28	NiBr ₂ .glyme	dtbbpy	MeCN	<5

29	NiBr ₂ .glyme	d(CO ₂ Et)bpy	DMF	8
30	NiBr ₂ .glyme	d(CO ₂ Et)bpy	DMSO	13
31	NiBr ₂ .glyme	d(CO ₂ Et)bpy	DMA	14
32	NiBr ₂ .glyme	d(CO ₂ Et)bpy	NMP	12
33	NiBr ₂ .glyme	3,3'-d(CF ₃)bpy	DMF	<5
34	NiBr ₂ .glyme	3,3'-d(CF ₃)bpy	DMSO	11
35	NiBr ₂ .glyme	3,3'-d(CF ₃)bpy	DMA	5
36	NiBr ₂ .glyme	3,3'-d(CF ₃)bpy	NMP	5
37	NiBr ₂ .glyme	bpy	DMSO	45
38	NiBr ₂ .glyme	bpy	DMA	44
39	NiBr ₂ .glyme	bpy	NMP	36

Next, the base, additive and temperature were optimized (Table 34). The change of K₂CO₃ (Entry 1) to other carbonates (Entries 2 and 3) decreased the yields to 27 and 46%. The use of NaHCO₃ (Entry 4) harshly decreased the yield. Other bases like K₃PO₄ and LiOH (Entries 5 and 6) did not improve the reaction. The same effect was observed when organic bases were employed (Entries 7 to 9). When zinc was changed to manganese (Entry 11), the yield was decreased to 37% and when it was removed (Entry 12), the product was obtained in 41% yield. Increases of the temperature to 40 °C reduced the yield (Entry 13), however when the reaction was heated at 60 and 80 °C (Entries 14 and 15), the reaction yields increased to 61 and 69%, respectively, suggesting that at high temperatures a second mechanism takes place. The reaction at 80 °C in argon atmosphere showed a reduction of the yield to 56% (Entry 16). Finally, when the reaction was heated at 100 °C, the performance was decreased to 44% yield (Entry 17).

Table 34: Optimization of the base, additive and temperature at the tosylation of **448**.

Entry	Base	Additive	Temperature (°C)	Yield (%)
1	K ₂ CO ₃	Zn	rt	53
2	Na ₂ CO ₃	Zn	rt	27
3	Cs ₂ CO ₃	Zn	rt	46
4	NaHCO ₃	Zn	rt	<5
5	K ₃ PO ₄	Zn	rt	35
6	LiOH	Zn	rt	26
7	Et ₃ N	Zn	rt	16
8	<i>i</i> -Pr ₂ NH	Zn	rt	26
9	DABCO	Zn	rt	32
10	LiO <i>t</i> -Bu	Zn	rt	33
11	K ₂ CO ₃	Mn	rt	37
12	K ₂ CO ₃	---	rt	41
13	K ₂ CO ₃	Zn	40	34
14	K ₂ CO ₃	Zn	60	61
15	K ₂ CO ₃	Zn	80	69
16 ^a	K ₂ CO ₃	Zn	80	56
17	K ₂ CO ₃	Zn	100	44

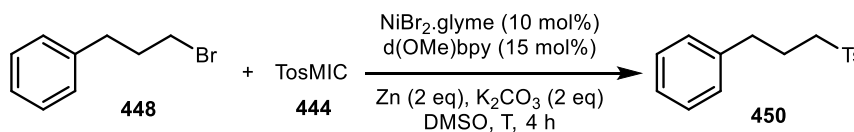
^a Reaction carried out in argon atmosphere.

To evaluate the influence of each reagent, control experiments were carried out at room temperature and at 80 °C (Table 35). The reaction showed to be sensitive to the catalyst removal. However, the yields obtained at 80 °C (16 – 26%) indicated that, at that temperature, part of the product formation is by a second mechanism that does not need the presence of the nickel species. At room temperature, the catalyst was necessary. Zinc was also important to the reaction: its removal at both temperatures (Entries 5 to 7 and 12 to 14) led to small yields at 80 °C or no product formation at room temperature.

Table 35: Control experiments for the tosylation of **448**.

Entry	NiBr ₂ .glyme	d(OMe)bpy	K ₂ CO ₃	Zn	Temp (°C)	Yield (%)
1	No	Yes	Yes	Yes	80	24
2	No	No	Yes	Yes	80	26
3	Yes	Yes	No	Yes	80	39
4	No	No	No	Yes	80	16
5	No	No	No	No	80	4
6	No	No	Yes	No	80	9
7	Yes	Yes	No	No	80	2
8	No	Yes	Yes	Yes	rt	5
9	No	No	Yes	Yes	rt	4
10	Yes	Yes	No	Yes	rt	8
11	No	No	No	Yes	rt	<5
12	No	No	No	No	rt	NR
13	No	No	Yes	No	rt	NR
14	Yes	Yes	No	No	rt	NR

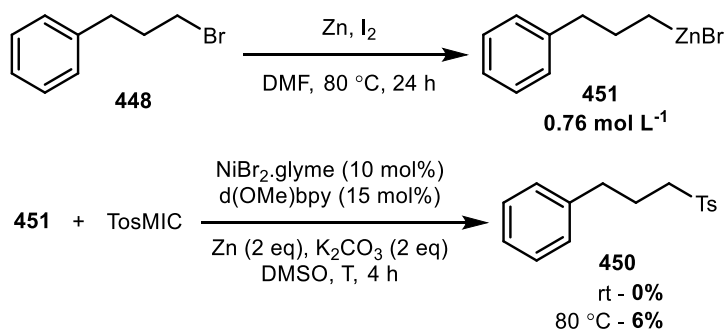
Some modifications were made to evaluate the influence of water and the number of equivalents of the reactants (Table 36). The removal of water drying DMSO with MS 4 Å (Entries 1 and 5) or adding the MS in the reaction media (Entries 2 and 6) reduced the yields. On the other hand, adding water in 3 equivalents (Entries 3 and 7) or 0.1 mL (Entries 4 and 8) had a similar effect on the yields. The use of an excess of TosMIC with 2 or 5 equivalents (Entries 9 to 12) reduced the yield, however when 2 equivalents were used at 80 °C, the decrease was not strong. Large excess of TosMIC impairs the reaction. The excess of **448** had the same tendency (Entries 13 to 19).

Table 36: Evaluation of the water and reactants content on the tosylation of **448**.

Entry	Modification	Temperature (°C)	Yield (%)
1	DMSO in MS 4 Å for 24 h	rt	0
2 ^a	MS 4 Å	rt	13
3	H ₂ O (3 eq)	rt	24
4	H ₂ O (0.1 mL)	rt	18
5	DMSO in MS 4 Å for 24 h	80	48
6	MS 4 Å	80	46
7	H ₂ O (3 eq)	80	64
8	H ₂ O (0.1 mL)	80	50
9	TosMIC in excess 2:1	rt	23
10	TosMIC in excess 5:1	rt	17
11	TosMIC in excess 2:1	80	60
12	TosMIC in excess 5:1	80	23
13	448 in excess 2:1	rt	28
14	448 in excess 3:1	rt	36
15	448 in excess 5:1	rt	14
16	448 in excess 2:1	80	63
17	448 in excess 3:1	80	36
18	448 in excess 4:1	80	34
19	448 in excess 5:1	80	30

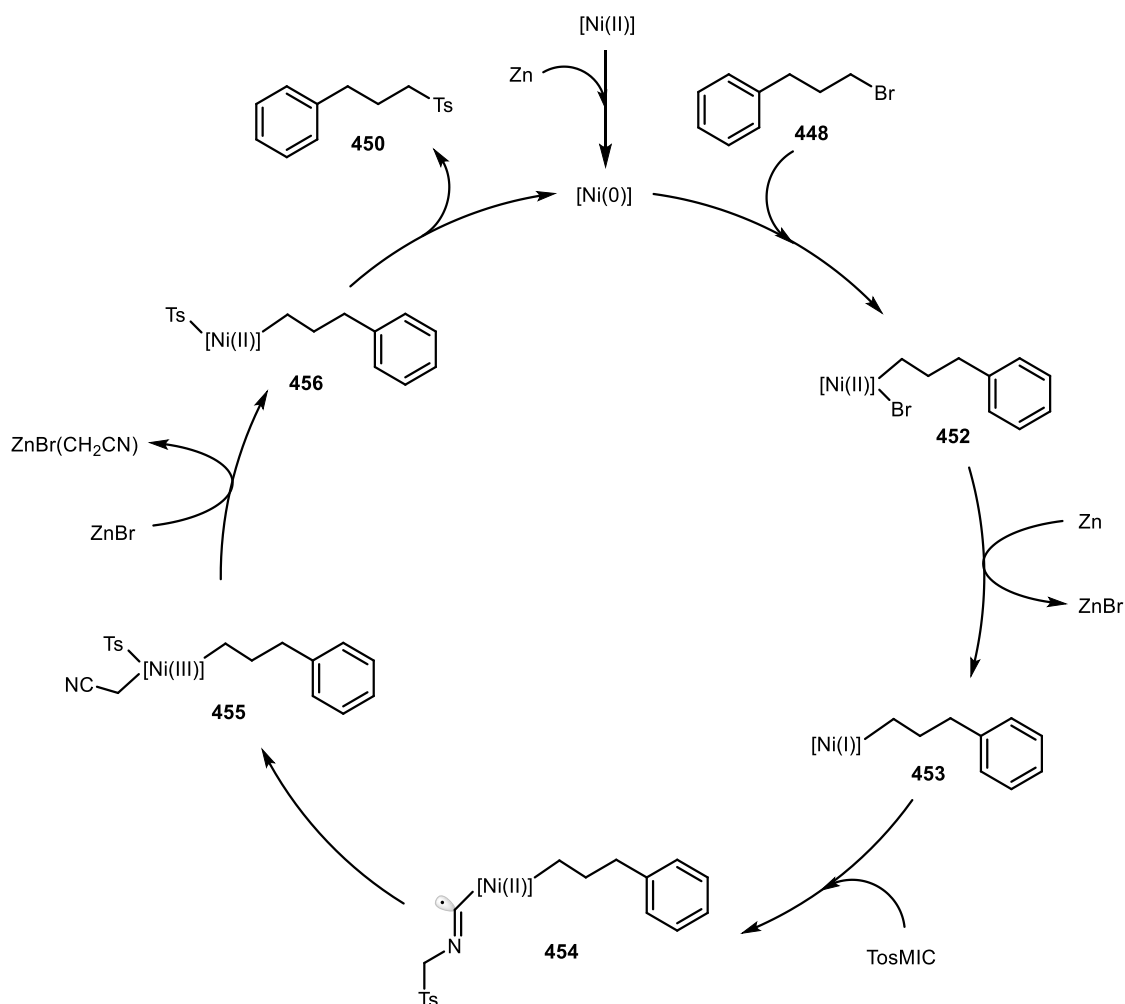
^a 75 mg of MS 4 Å

The role of the zinc in this reaction was evaluated. The formation of an organozinc species was investigated. This intermediate was obtained by the reaction of **448** with Zn in the presence of I₂ in DMF (Scheme 71). The determination of the formed **451** was carried out by titration with LiCl in THF and I₂ (Knochel method²⁹²). The organozinc was formed in the concentration of 0.76 mol L⁻¹. With this solution, the reaction with TosMIC was carried out. No product was obtained at room temperature and 6% yield at 80 °C was observed. It suggested that there is no formation of organozinc species in the reaction.



Scheme 71: Synthesis of the organozinc species **451** and its tosylation with TosMIC.

Based on the control experiments and the organozinc tests, a mechanism for this transformation could be proposed (Scheme 72). Firstly, the Zn acts as reducing agent to generate Ni(0) *in situ*. Then, the oxidative addition of **448** forms the intermediate **452**, which is dehalogenated by Zn to form the Ni(I) species **453**. Next, the TosMIC coordinates **453** to form **454**, which undergoes a rearrangement to generate **455**. After the formation of **456** by the reaction with ZnBr, the reductive elimination takes place to make the desired product **450**.



Scheme 72: Proposed mechanism for the tosylation of **448** with TosMIC catalysed by nickel.

4.5.

Conclusion and future perspectives

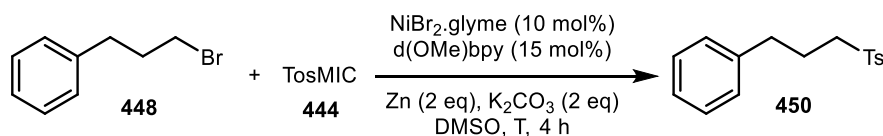
The obtention of 2-aryl-1-tetralones is a key step in the synthesis of pterocarpens and they are intermediates that showed potential biological applications, such as anti-HCV candidates. The synthesis could be achieved by using photoredox catalysis merged with organocatalysis. However, the attempts did not work due to the difficulty of the formation of enamines from 1-tetralone and the high activation energy of the radical addition step. The use of isonitriles did not give the desired product, but when TosMIC was used in the presence of a nickel catalyst, the tosylation by nucleophilic substitution happened. The reaction was optimized and studies are being conducted to evaluate the scope of this reaction.

4.6.

Experimental procedures

All reagents were bought from Sigma-Aldrich, Oakwood Chemicals, Fischer Scientific, Alfa Aesar and TCI Chemicals, and were used as received. The Ni complexes and ligands were stored at a glove box. The solvents were dried at the solvent purification system from Pure Process Technology. Et₃N and DIPEA were distilled prior to use. Reactions were monitored by thin layer chromatography using Merck TLC Silica gel 60 F254. The chromatographic columns were performed over Merck Silica gel 60 Å (particle size: 0.040–0.063 mm, 230–400 mesh ASTM). The columns were run at Biotage® Isolera One instrument. ¹H NMR and ¹³C NMR spectra were recorded on a Varian MR400 spectrometer, operating at 400 MHz for ¹H NMR and 100 MHz for ¹³C NMR (¹H-decoupled), or on a Varian Vnmrs 700, operating at 700 MHz for ¹H NMR and 176 MHz for ¹³C NMR (¹H-decoupled), using CDCl₃ or DMSO-*d*₆ as solvents. The chemical shifts (δ) were given in parts per million (ppm) and the solvent residue was used as reference. The multiplicities were reported as s = singlet, d = doublet, t = triplet, q = quartet, m = multiplet and br = broad signal. All coupling constants (*J* values) were given in Hz. The cyclic voltammetry was conducted at a multipotentiostat from CH Instruments model 100 series. The measurements were performed with a glassy carbon working electrode, Pt auxiliary electrode, and Ag/AgCl reference electrode. The analyte was dissolved in a 0.1 mol L⁻¹ of Bu₄NPF₆ in MeCN as electrolyte ([analyte] = 0.01 mol L⁻¹). The scans were recorded with a sweep rate of 10 mV s⁻¹. The GC-MS analysis were performed at the Shimadzu QP2010 SE equipment with an AOC-20i auto injector. The liquid chromatography analysis were performed at Waters® Acuity H-Class UPLC equipment with an Acquity UPLC BEH C18 column 1.7 μ m 2.1x50 mm and using MeCN/H₂O as mobile phase in gradient mode.

4.6.1. Tosylation with TosMIC



An oven dried 2-dram vial was charged with 17.8 mg (0.09 mmol) of TosMIC, 23 μL (0.15 mmol) of **448**, 3.1 mg (10 mol%) of $\text{NiBr}_2\cdot\text{glyme}$, 3.2 mg (15 mol%) of d(OMe)bpy , 13 mg (0.2 mmol) of Zn powder, 27.6 mg (0.2 mmol) of K_2CO_3 , and 0.5 mL of DMSO. The reaction was stirred at room temperature for 4 h. After this time, the reaction was diluted with dichloromethane (5 mL) and extracted with water (3x5 mL). The organic phase was dried with Na_2SO_4 anhydrous and evaporated. The product was purified by column chromatography.

Compound **450**: colorless solid (13.8 mg, 56%). $^1\text{H NMR}$ (700 MHz, CDCl_3): δ 7.77 (d, 8.2 Hz, 2H), 7.35 (d, 8.0 Hz, 2H), 7.29 – 7.23 (m, 2H), 7.22 – 7.16 (m, 1H), 7.11 (m, 2H), 3.10 – 3.01 (m, 2H), 2.70 (t, 7.5 Hz, 2H), 2.46 (s, 3H), 2.10 – 1.97 (m, 2H). $^{13}\text{C NMR}$ (176 MHz): δ 144.8, 140.0, 136.2, 130.0, 128.7, 128.5, 128.2, 126.5, 55.7, 34.2, 24.4, 21.8.

Bibliographic references

- (1) Hochreiter, B.; Garcia, A. P.; Schmid, J. A. Fluorescent Proteins as Genetically Encoded FRET Biosensors in Life Sciences. *Sensors* **2015**, *15* (10), 26281–26314. <https://doi.org/10.3390/s151026281>.
- (2) Jüstel, T.; Möller, S.; Winkler, H.; Adam, W. Luminescent Materials. In *Ullmann's Encyclopedia of Industrial Chemistry*; 2012; pp 1–75. https://doi.org/10.1007/978-3-319-48933-9_38.
- (3) Shaw, M. H.; Twilton, J.; MacMillan, D. W. C. Photoredox Catalysis in Organic Chemistry. *J. Org. Chem.* **2016**, *81* (16), 6898–6926. <https://doi.org/10.1021/acs.joc.6b01449>.
- (4) Cano-yelo, H.; Deronzier, A. Photocatalysis of the Pschorr Reaction by Tris-(2,2'-Bipyridyl)Ruthenium(II) in the Phenanthrene Series. *J. Chem. Soc., Perkin Trans. 2* **1984**, *2* (6), 1093–1098.
- (5) Ischay, M. A.; Anzovino, M. E.; Du, J.; Yoon, T. P. Efficient Visible Light Photocatalysis of [2+2] Enone Cycloadditions. *J. Am. Chem. Soc.* **2008**, *130* (39), 12886–12887. <https://doi.org/10.1021/ja805387f>.
- (6) Baik, T. G.; Luis, A. L.; Wang, L. C.; Krische, M. J. A Diastereoselective Metal-Catalyzed [2 + 2] Cycloaddition of Bis-Enones [5]. *J. Am. Chem. Soc.* **2001**, *123* (27), 6716–6717. <https://doi.org/10.1021/ja010800p>.
- (7) Wang, L. C.; Jang, H. Y.; Roh, Y.; Lynch, V.; Schultz, A. J.; Wang, X.; Krische, M. J. Diastereoselective Cycloreductions and Cycloadditions Catalyzed by Co(Dpm)₂-Silane (Dpm = 2,2,6,6-Tetramethylheptane-3,5-Dionate): Mechanism and Partitioning of Hydrometallative versus Anion Radical Pathways. *J. Am. Chem. Soc.* **2002**, *124* (32), 9448–9453. <https://doi.org/10.1021/ja020223k>.
- (8) Yang, J.; Cauble, D. F.; Berro, A. J.; Bauld, N. L.; Krische, M. J. Anion Radical [2 + 2] Cycloaddition as a Mechanistic Probe: Stoichiometry- and Concentration-Dependent Partitioning of Electron-Transfer and Alkylation Pathways in the Reaction of the Gilman Reagent Me₂CuLi·LiI with Bis(Enones). *J. Org. Chem.* **2004**, *69* (23), 7979–7984. <https://doi.org/10.1021/jo048499t>.

- (9) Nicewicz, D. A.; MacMillan, D. W. C. Merging Photoredox Catalysis with Organocatalysis: The Direct Asymmetric Alkylation of Aldehydes. *Science* (80-.). **2008**, 322, 77–80. <https://doi.org/10.1126/science.1161976>.
- (10) Narayanam, J. M. R.; Tucker, J. W.; Stephenson, C. R. J. Electron-Transfer Photoredox Catalysis: Development of a Tin-Free Reductive Dehalogenation Reaction. *J. Am. Chem. Soc.* **2009**, 131 (25), 8756–8757. <https://doi.org/10.1021/ja9033582>.
- (11) Alonso, F.; Beletskaya, I. P.; Yus, M. Metal-Mediated Reductive Hydrodehalogenation of Organic Halides. *Chem. Rev.* **2002**, 102 (11), 4009–4091. <https://doi.org/10.1021/cr0102967>.
- (12) Juris, A.; Balzani, V.; Belser, P.; von Zelewsky, A. Characterization of the Excited State Properties of Some New Photosensitizers of the Ruthenium (Polypyridine) Family. *Helv. Chim. Acta* **1981**, 64 (7), 2175–2182. <https://doi.org/10.1002/chin.198212332>.
- (13) McClanahan, S. F.; Kincaid, J. R. 3MLCT Lifetimes of Tris(2,2'-Bipyridine)Ruthenium(II). Position-Dependent Deuterium Effects. *J. Am. Chem. Soc.* **1986**, 108 (13), 3840–3841. <https://doi.org/10.1021/ja00273a055>.
- (14) Kalyanasundaram, K. Photophysics, Photochemistry and Solar Energy Conversion with Tris(Bipyridyl)Ruthenium(II) and Its Analogues. *Coord. Chem. Rev.* **1982**, 46 (C), 159–244. [https://doi.org/10.1016/0010-8545\(82\)85003-0](https://doi.org/10.1016/0010-8545(82)85003-0).
- (15) Tucker, J. W.; Stephenson, C. R. J. Shining Light on Photoredox Catalysis: Theory and Synthetic Applications. *J. Org. Chem.* **2012**, 77 (4), 1617–1622. <https://doi.org/10.1021/jo202538x>.
- (16) Romero, N. A.; Nicewicz, D. A. Organic Photoredox Catalysis. *Chem. Rev.* **2016**, 116 (17), 10075–10166. <https://doi.org/10.1021/acs.chemrev.6b00057>.
- (17) Koike, T.; Akita, M. Visible-Light Radical Reaction Designed by Ru- and Ir-Based Photoredox Catalysis. *Inorg. Chem. Front.* **2014**, 1, 562–576. <https://doi.org/10.1039/c5qi00059a>.
- (18) Guo, Y.; Guo, Z.; Lu, J. T.; Fang, R.; Chen, S. C.; Luo, T. Total Synthesis of (-)-Batrachotoxinin A: A Local-Desymmetrization Approach. *J. Am. Chem. Soc.* **2020**, 142 (8), 3675–3679. <https://doi.org/10.1021/jacs.9b12882>.
- (19) Tokuyama, T.; Daly, J.; Witkop, B. The Structure of Batrachotoxin, a Steroidal Alkaloid from the Colombian Arrow Poison Frog, *Phyllobates Aurotaenia*, and Partial Synthesis of Batrachotoxin and Its Analogs and Homologs. *J. Am.*

- Chem. Soc.* **1969**, *91* (14), 3931–3938. <https://doi.org/10.1021/ja01042a042>.
- (20) Zhu, Y.; Zhang, L.; Luo, S. Asymmetric α -Photoalkylation of β -Ketocarboxyls by Primary Amine Catalysis: Facile Access to Acyclic All-Carbon Quaternary Stereocenters. *J. Am. Chem. Soc.* **2014**, *136* (42), 14642–14645. <https://doi.org/10.1021/ja508605a>.
- (21) Xue, F.; Lu, H.; He, L.; Li, W.; Zhang, D.; Liu, X. Y.; Qin, Y. Formal Total Syntheses of (-)- and (+)-Actinophyllic Acid. *J. Org. Chem.* **2018**, *83* (2), 754–764. <https://doi.org/10.1021/acs.joc.7b02747>.
- (22) Carroll, A. R.; Hyde, E.; Smith, J.; Quinn, R. J.; Guymer, G.; Forster, P. I. Actinophyllic Acid, a Potent Indole Alkaloid Inhibitor of the Coupled Enzyme Assay Carboxypeptidase U/Hippuricase from the Leaves of *Alatonia Actinophylla* (Apocynaceae). *J. Org. Chem.* **2005**, *70* (3), 1096–1099. <https://doi.org/10.1021/jo048439n>.
- (23) Mateus-Ruiz, J. B.; Cordero-Vargas, A. Stereoselective Total Synthesis of Aspergillide A: A Visible Light-Mediated Photoredox Access to the Trisubstituted Tetrahydropyran Core. *J. Org. Chem.* **2019**, *84* (18), 11848–11855. <https://doi.org/10.1021/acs.joc.9b01705>.
- (24) Kito, K.; Ookura, R.; Yoshida, S.; Namikoshi, M.; Ooi, T.; Kusumi, T. New Cytotoxic 14-Membered Macrolides from Marine-Derived Fungus *Aspergillus Ostianus*. *Org. Lett.* **2008**, *10* (2), 225–228. <https://doi.org/10.1021/ol702598q>.
- (25) Triandafillidi, I.; Kokotou, M. G.; Kokotos, C. G. Photocatalytic Synthesis of γ -Lactones from Alkenes: High-Resolution Mass Spectrometry as a Tool to Study Photoredox Reactions. *Org. Lett.* **2018**, *20* (1), 36–39. <https://doi.org/10.1021/acs.orglett.7b03256>.
- (26) Tedder, J. M.; Walton, J. C. Directive Effects in Gas-Phase Radical Addition Reactions. *Adv. Phys. Org. Chem.* **1978**, *16*, 51–86.
- (27) Tedder, J. M. Welche Faktoren Bestimmen Reaktivität Und Regioselektivität Bei Radikalischer Substitution Und Addition? *Angew. Chem.* **1982**, *94* (6), 433–442.
- (28) Tedder, J. M.; Walton, J. C. The Importance of Polarity and Steric Effects in Determining the Rate and Orientation of Free Radical Addition to Olefins: Rules for Determining the Rate and Preferred Orientation. *Tetrahedron* **1980**, *36* (6), 701–707.
- (29) Giese, B. Knüpfung von CC-Bindungen Durch Addition von Radikalen an

- Alkene. *Angew. Chem.* **1983**, *95* (10), 771–782.
- (30) Giese, B. Formation of CC Bonds by Addition of Free Radicals to Alkenes. *Angew. Chemie - Int. Ed.* **1983**, *22* (10), 753–764.
- (31) Lowry, T. H.; Richardson, K. S. *Mechanism and Theory in Organic Chemistry*, 3rd ed.; Harper Collins Publishers: New York, 1997.
- (32) Hammond, G. S. A Correlation of Reaction Rates. *J. Am. Chem. Soc.* **1955**, *77* (2), 334–338.
- (33) Klopman, G. Chemical Reactivity and the Concept of Charge- and Frontier-Controlled Reactions. *J. Am. Chem. Soc.* **1968**, *90* (2), 223–234.
- (34) Weinhold, F.; Landis, C. R. *Discovering Chemistry With Natural Bond Orbitals*, 1st ed.; John Wiley & Sons: Hoboken, NJ, 2012.
- (35) Alabugin, I. V. *Stereoelectronic Effects: A Bridge Between Structure and Reactivity*, 1st ed.; John Wiley & Sons: Hoboken, NJ, 2016.
- (36) Giese, B.; Meister, J. Polar Effects in the Addition of Alkyl Radicals to Olefins. *Angew. Chem. Int. Ed.* **1977**, *16* (3), 178–179. <https://doi.org/10.1002/anie.197701781>.
- (37) Evans, M. G.; Polanyi, M. Further Considerations on the Thermodynamics of Chemical Equilibria and Reaction Rates. *Trans. Faraday Soc.* **1936**, *32*, 1333. <https://doi.org/10.1039/tf9363201333>.
- (38) Wong, M. W.; Pross, A.; Radom, L. Addition of Methyl Radical to Substituted Alkenes: A Theoretical Study of the Reaction Mechanism. *Isr. J. Chem.* **1993**, *33* (4), 415–425. <https://doi.org/10.1002/ijch.199300048>.
- (39) Wong, M. W.; Radom, L.; Pross, A. Are Polar Interactions Important in the Addition of Methyl Radical to Alkenes? *J. Am. Chem. Soc.* **1993**, *115* (23), 11050–11051. <https://doi.org/10.1021/ja00076a097>.
- (40) Pross, A. *Theoretical & Physical Principles of Organic Reactivity*, 1st ed.; John Wiley & Sons: New York, 1995.
- (41) Meerwein, H.; Büchner, E.; van Emster, K. Über Die Einwirkung Aromatischer Diazoverbindungen Auf α,β -Ungesättigte Carbonylverbindungen. *J. für Prakt. Chemie* **1939**, *152* (7–10), 237–266. <https://doi.org/10.1002/prac.19391520705>.
- (42) Rodenstvedt, C. S. Arylation of Unsaturated Compounds by Diazonium Salts (The Meerwein Arylation Reaction). *Org. React.* **1976**, *24*, 225.
- (43) Koelsch, C. F.; Boekelheide, V. The Coupling of α,β -Unsaturated Compounds

- with Diazonium Salts. *J. Am. Chem. Soc.* **1944**, 66 (3), 412–415. <https://doi.org/10.1021/ja01231a031>.
- (44) D.Obushak, M.; B.Lyakhovych, M.; I.Ganushchak, M. Arenediazonium Tetrachlorocuprates(II): Modification of the Meerwein and Sandmeyer Reactions. *Tetrahedron Lett.* **1998**, 39 (51), 9567–9570. [https://doi.org/10.1016/S0040-4039\(98\)02165-0](https://doi.org/10.1016/S0040-4039(98)02165-0).
- (45) Minaev, B. F.; Bondarchuk, S. V. Role of Triplet States of Aryldiazonium Cations in the Meerwein Reaction. *Russ. J. Appl. Chem.* **2009**, 82 (5), 840–845. <https://doi.org/10.1134/S1070427209050176>.
- (46) Rakitin, Y. V.; Kalinnikov, V. T.; Khodasevich, S. G.; Novotortsev, V. M. Structures of the Complex Ions $[\text{CuCl}_4]^{2-}$ and $[\text{CuCl}_5]^{3-}$. *Russ. J. Coord. Chem.* **2007**, 33 (12), 891–895. <https://doi.org/10.1134/S1070328407120044>.
- (47) Lamblin, M.; Naturele, G.; Dessolin, J.; Felpin, F. X. Direct C-H Arylation of Quinones with Anilines. *Synlett* **2012**, 23 (11), 1621–1624. <https://doi.org/10.1055/s-0031-1291163>.
- (48) Bondarchuk, S. V.; Minaev, B. F. About Possibility of the Triplet Mechanism of the Meerwein Reaction. *J. Mol. Struct. THEOCHEM* **2010**, 952 (1–3), 1–7. <https://doi.org/10.1016/j.theochem.2010.04.025>.
- (49) Laali, K. K.; Rasul, G.; Prakash, G. K. S.; Olah, G. A. DFT Study of Substituted and Benzannelated Aryl Cations: Substituent Dependency of Singlet/Triplet Ratio. *J. Org. Chem.* **2002**, 67 (9), 2913–2918. <https://doi.org/10.1021/jo020084p>.
- (50) Aschi, M.; Harvey, J. N. Spin Isomerisation of Para-Substituted Phenyl Cations. *J. Chem. Soc. Perkin Trans. 2* **1999**, No. 6, 1059–1062. <https://doi.org/10.1039/a902279a>.
- (51) Kindt, S.; Heinrich, M. R. Recent Advances in Meerwein Arylation Chemistry. *Synth.* **2016**, 48 (11), 1597–1606. <https://doi.org/10.1055/s-0035-1561586>.
- (52) Jasch, H.; Landais, Y.; Heinrich, M. R. Twofold Carbon-Carbon Bond Formation by Intra- and Intermolecular Radical Reactions of Aryl Diazonium Salts. *Chem. - A Eur. J.* **2013**, 19 (26), 8411–8416. <https://doi.org/10.1002/chem.201300354>.
- (53) Hartmann, M.; Li, Y.; Studer, A. Transition-Metal-Free Oxyarylation of Alkenes with Aryl Diazonium Salts and TEMPONa. *J. Am. Chem. Soc.* **2012**, 134 (40), 16516–16519. <https://doi.org/10.1021/ja307638u>.
- (54) Hartmann, M.; Gerleve, C.; Studer, A. Intramolecular Radical

- Carboaminoxylation of Aryl Amines. *Synlett* **2016**, 27 (5), 724–730. <https://doi.org/10.1055/s-0035-1560770>.
- (55) Siraki, A. G.; Jiang, J.; Mason, R. P. Investigating the Mechanisms of Aromatic Amine-Induced Protein Free Radical Formation by Quantitative Structure-Activity Relationships: Implications for Drug-Induced Agranulocytosis. *Chem. Res. Toxicol.* **2010**, 23 (5), 880–887. <https://doi.org/10.1021/tx900432d>.
- (56) Narwaley, M.; Michail, K.; Arvadia, P.; Siraki, A. G. Drug-Induced Protein Free Radical Formation Is Attenuated by Unsaturated Fatty Acids by Scavenging Drug-Derived Phenyl Radical Metabolites. *Chem. Res. Toxicol.* **2011**, 24 (7), 1031–1039. <https://doi.org/10.1021/tx200016h>.
- (57) Galli, C. Radical Reactions of Arenediazonium Ions: An Easy Entry into the Chemistry of the Aryl Radical. *Chem. Rev.* **1988**, 88 (5), 765–792. <https://doi.org/10.1021/cr00087a004>.
- (58) Vaillard, S. E.; Schulte, B.; Studer, A. Radical - Based Arylation Methods. In *Modern Arylation Methods*; Ackermann, L., Ed.; John Wiley & Sons: Weinheim, 2009; pp 475–511. <https://doi.org/10.1002/9783527627325>.
- (59) Elofson, R. M.; Gadallah, F. F. Substituent Effects in the Polarography of Aromatic Diazonium Salts. *J. Org. Chem.* **1969**, 34 (4), 854–857. <https://doi.org/10.1021/jo01256a016>.
- (60) Poznik, M.; König, B. Fast Colorimetric Screening for Visible Light Photocatalytic Oxidation and Reduction Reactions. *React. Chem. Eng.* **2016**, 1 (5), 494–500. <https://doi.org/10.1039/c6re00117c>.
- (61) Roth, H. G.; Romero, N. A.; Nicewicz, D. A. Experimental and Calculated Electrochemical Potentials of Common Organic Molecules for Applications to Single-Electron Redox Chemistry. *Synlett* **2016**, 27 (5), 714–723. <https://doi.org/10.1055/s-0035-1561297>.
- (62) Kim, H.; Kim, H.; Lambert, T. H.; Lin, S. Reductive Electrophotocatalysis: Merging Electricity and Light to Achieve Extreme Reduction Potentials. *J. Am. Chem. Soc.* **2020**, 142 (5), 2087–2092. <https://doi.org/10.1021/jacs.9b10678>.
- (63) Pause, L.; Robert, M.; Savéant, J. M. Can Single-Electron Transfer Break an Aromatic Carbon - Heteroatom Bond in One Step? A Novel Example of Transition between Stepwise and Concerted Mechanisms in the Reduction of Aromatic Iodides [5]. *J. Am. Chem. Soc.* **1999**, 121 (30), 7158–7159. <https://doi.org/10.1021/ja991365q>.

- (64) Jasch, H.; Heinrich, M. R. *Tin Hydrides and Functional Group Transformations*; 2012. <https://doi.org/10.1002/9781119953678.rad086>.
- (65) RajanBabu, T. V. (Babu); Bulman Page, P. C.; Buckley, B. R. Tri-n-Butylstannane. *Encycl. Reagents Org. Synth.* **2004**, *1* (2), 1–11. <https://doi.org/10.1002/047084289x.rt181.pub2>.
- (66) Kuivila, H. G. Organotin Hydrides and Organic Free Radicals. *Acc. Chem. Res.* **1968**, *1* (10), 299–305. <https://doi.org/10.1021/ar50010a002>.
- (67) Grady, G. L.; Danyliw, T. J.; Rabideux, P. Studies on the Polarity of the Tri-n-Butyltin Radical. *J. Organomet. Chem.* **1977**, *142* (1), 67–70.
- (68) Negishi, E. Organosilicons and Organotins (Silicon, Tin). In *Organometallics in Organic Synthesis - Volume 1*; John Wiley & Sons: New York, 1980; pp 394–400.
- (69) Bruch, A.; Fröhlich, R.; Grimme, S.; Studer, A.; Curran, D. P. One Product, Two Pathways: Initially Divergent Radical Reactions Reconverge to Form a Single Product in High Yield. *J. Am. Chem. Soc.* **2011**, *133* (40), 16270–16276. <https://doi.org/10.1021/ja2070347>.
- (70) Li, F.; Castle, S. L. Synthesis of the Acutumine Spirocycle via a Radical-Polar Crossover Reaction. *Org. Lett.* **2007**, *9* (20), 4033–4036. <https://doi.org/10.1021/ol701757f>.
- (71) Hart, D. J.; Wu, S. C. Intramolecular Addition of Aryl Radicals to Vinylogous Urethanes: Studies Toward Preparation of the Oxindole Portion of Gelsemine. *Tetrahedron Lett.* **1991**, *32* (33), 4099–4102.
- (72) Chatgililoglu, C. *Organosilanes in Radical Chemistry*, 1st ed.; Wiley, 2004. <https://doi.org/10.1002/0470024755>.
- (73) Chatgililoglu, C. Structural and Chemical Properties of Silyl Radicals. *Chem. Rev.* **1995**, *95* (5), 1229–1251. <https://doi.org/10.1021/cr00037a005>.
- (74) Chatgililoglu, C.; Ferreri, C.; Landais, Y.; Timokhin, V. I. Thirty Years of (TMS)₃SiH: A Milestone in Radical-Based Synthetic Chemistry. *Chem. Rev.* **2018**, *118* (14), 6516–6572. <https://doi.org/10.1021/acs.chemrev.8b00109>.
- (75) Curran, D. P.; Keller, A. I. Radical Additions of Aryl Iodides to Arenes Are Facilitated by Oxidative Rearomatization with Dioxxygen. *J. Am. Chem. Soc.* **2006**, *128* (42), 13706–13707. <https://doi.org/10.1021/ja066077q>.
- (76) Wang, M.; Li, M.; Yang, S.; Xue, X. S.; Wu, X.; Zhu, C. Radical-Mediated C-C Cleavage of Unstrained Cycloketones and DFT Study for Unusual

- Regioselectivity. *Nat. Commun.* **2020**, *11* (1), 1–7. <https://doi.org/10.1038/s41467-020-14435-5>.
- (77) Schweitzer-Chaput, B.; Boess, E.; Klussmann, M. Acid-Catalyzed Activation of Peroxyketals: Tunable Radical Initiation at Ambient Temperature and Below. *Org. Lett.* **2016**, *18* (19), 4944–4947. <https://doi.org/10.1021/acs.orglett.6b02419>.
- (78) Funt, L. D.; Tomashenko, O. A.; Mosiagin, I. P.; Novikov, M. S.; Khlebnikov, A. F. Synthesis of Pyrrolotriazoloisoquinoline Frameworks by Intramolecular Cu-Mediated or Free Radical Arylation of Triazoles. *J. Org. Chem.* **2017**, *82* (14), 7583–7594. <https://doi.org/10.1021/acs.joc.7b01341>.
- (79) Sánchez, A.; Núñez, A.; Alvarez-Builla, J.; Burgos, C. Pyridinium N-2'-Pyridylaminide: Synthesis of 3-Aryl-2-Aminopyridines through an Intramolecular Radical Process. *Tetrahedron* **2004**, *60*, 11843–11850. <https://doi.org/10.1016/j.tet.2004.09.099>.
- (80) Kizil, M.; Murphy, J. A. Stereoselective Preparation of the ABCE Tetracycle of Aspidospermidine and Related Alkaloids. *J. Chem. Soc. Chem. Commun.* **1995**, No. 14, 1409. <https://doi.org/10.1039/c39950001409>.
- (81) Baxter, R. D.; Liang, Y.; Hong, X.; Brown, T. A.; Zare, R. N.; Houk, K. N.; Baran, P. S.; Blackmond, D. G. Mechanistic Insights into Two-Phase Radical C-H Arylations. *ACS Cent. Sci.* **2015**, *1* (8), 456–462. <https://doi.org/10.1021/acscentsci.5b00332>.
- (82) Zhang, X. Origins of Regioselectivity in Radical Arylation of Aniline: A Computational Study. *Int. J. Quantum Chem.* **2015**, *115* (23), 1658–1667. <https://doi.org/10.1002/qua.25003>.
- (83) Hofmann, J.; Clark, T.; Heinrich, M. R. Strongly Directing Substituents in the Radical Arylation of Substituted Benzenes. *J. Org. Chem.* **2016**, *81* (20), 9785–9791. <https://doi.org/10.1021/acs.joc.6b01840>.
- (84) Dickerman, S. C.; Megna, I. S.; Skoultchi, M. M. RELATIVE ARYL RADICAL AFFINITIES OF MONOMERS. *J. Am. Chem. Soc.* **1959**, *81* (9), 2270–2271. <https://doi.org/10.1021/ja01518a064>.
- (85) Bevington, J. C.; Ito, T. Reactivities of Monomers towards the Phenyl Radical. *Trans. Faraday Soc.* **1968**, *64*, 1329–1336. <https://doi.org/10.1039/TF9686401329>.
- (86) Pryor, W. A.; Fiske, T. R. Reactivities of Monomers towards the Phenyl Radical;

- a Scale of Phenyl Affinities. *Trans. Faraday Soc.* **1969**, *65*, 1865. <https://doi.org/10.1039/tf9696501865>.
- (87) Heinrich, M. R.; Wetzel, A.; Kirschstein, M. Intermolecular Radical Carboaminohydroxylation of Olefins with Aryl Diazonium Salts and TEMPO. *Org. Lett.* **2007**, *9* (19), 3833–3835. <https://doi.org/10.1021/ol701622d>.
- (88) Scaiano, J. C.; Stewart, L. C. Phenyl Radical Kinetics. *J. Am. Chem. Soc.* **1983**, *105* (11), 3609–3614. <https://doi.org/10.1021/ja00349a043>.
- (89) Preidel, M.; Zellmer, R. A Cw Laser Absorption Study of the Reactions of Phenyl Radicals with NO, NO₂, O₂ and Selected Organics Between 298 - 404 K. *Ber. Bunsenges. Phys. Chem.* **1989**, *93*, 1417–1423.
- (90) Migita, T.; Takayama, K.; Abe, Y.; Kosugi, M. Relative Reactivities of Substituted Phenyl Radicals in Elementary Reactions. *J. Chem. Soc., Perkin Trans. 2* **1979**, 1137–1142. <https://doi.org/10.1017/CBO9781107415324.004>.
- (91) Citterio, A.; Minisci, F.; Vismara, E. Steric, Polar, and Resonance Effects in Reactivity and Regioselectivity of Aryl Radical Addition to α,β -Unsaturated Carbonyl Compounds. *J. Org. Chem.* **1982**, *47* (1), 81–88. <https://doi.org/10.1021/jo00340a017>.
- (92) Lalevée, J.; Allonas, X.; Fouassier, J. P. Reactivity of Carbon-Centered Radicals toward Acrylate Double Bonds: Relative Contribution of Polar vs Enthalpy Effects. *J. Phys. Chem. A* **2004**, *108* (19), 4326–4334. <https://doi.org/10.1021/jp037766g>.
- (93) Minisci, F.; Coppa, F.; Fontana, F.; Pianese, G.; Zhao, L. Polar Effects in Reactions of Carbon-Centered Radicals with Diazonium Salts: Free-Radical Diazo. *J. Org. Chem.* **1992**, *57* (14), 3929–3933. <https://doi.org/10.1021/jo00040a038>.
- (94) Bednarek, D.; Moad, G.; Rizzardo, E.; Solomon, D. H. End Groups of Poly(Methyl Methacrylate-Co-Styrene) Prepared with Tert-Butoxy, Methyl, and/or Phenyl Radical Initiation: Effects of Solvent, Monomer Composition, and Conversion. *Macromolecules* **1988**, *21* (5), 1522–1528. <https://doi.org/10.1021/ma00183a050>.
- (95) Chen, M.; Zhao, X.; Yang, C.; Xia, W. Visible-Light-Triggered Directly Reductive Arylation of Carbonyl/Iminyl Derivatives through Photocatalytic PCET. *Org. Lett.* **2017**, *19* (14), 3807–3810. <https://doi.org/10.1021/acs.orglett.7b01677>.
- (96) Shi, S.; Szostak, R.; Szostak, M. Proton-Coupled Electron Transfer in the

- Reduction of Carbonyls Using SmI₂–H₂O: Implications for the Reductive Coupling of Acyl-Type Ketyl Radicals with SmI₂–H₂O. *Org. Biomol. Chem.* **2016**, *14* (38), 9151–9157. <https://doi.org/10.1039/C6OB01621A>.
- (97) Wang, R.; Ma, M.; Gong, X.; Panetti, G. B.; Fan, X.; Walsh, P. J. Visible-Light-Mediated Umpolung Reactivity of Imines: Ketimine Reductions with Cy₂NMe and Water. *Org. Lett.* **2018**, *20* (8), 2433–2436. <https://doi.org/10.1021/acs.orglett.8b00778>.
- (98) Berger, A. L.; Donabauer, K.; König, B. Photocatalytic Barbier Reaction – Visible-Light Induced Allylation and Benzylolation of Aldehydes and Ketones. *Chem. Sci.* **2018**, *9* (36), 7230–7235. <https://doi.org/10.1039/C8SC02038H>.
- (99) Xia, Q.; Tian, H.; Dong, J.; Qu, Y.; Li, L.; Song, H.; Liu, Y.; Wang, Q. N-Arylamines Coupled with Aldehydes, Ketones, and Imines by Means of Photocatalytic Proton-Coupled Electron Transfer. *Chem. - A Eur. J.* **2018**, *24* (37), 9269–9273. <https://doi.org/10.1002/chem.201801886>.
- (100) Lefebvre, Q.; Porta, R.; Millet, A.; Jia, J.; Rueping, M. One Amine–3 Tasks: Reductive Coupling of Imines with Olefins in Batch and Flow. *Chem. – A Eur. J.* **2020**, *26* (6), 1363–1367. <https://doi.org/10.1002/chem.201904483>.
- (101) Leitch, J. A.; Rossolini, T.; Rogova, T.; Maitland, J. A. P.; Dixon, D. J. α -Amino Radicals via Photocatalytic Single-Electron Reduction of Imine Derivatives. *ACS Catal.* **2020**, *10* (3), 2009–2025. <https://doi.org/10.1021/acscatal.9b05011>.
- (102) Pirnot, M. T.; Rankic, D. A.; Martin, D. B. C.; MacMillan, D. W. C. Photoredox Activation for the Direct α -Arylation of Ketones and Aldehydes. *Science (80-.)*. **2013**, *339* (6127), 1593–1596. <https://doi.org/10.1126/science.1232993>.
- (103) Silvi, M.; Verrier, C.; Rey, Y. P.; Buzzetti, L.; Melchiorre, P. Visible-Light Excitation of Iminium Ions Enables the Enantioselective Catalytic β -Alkylation of Enals. *Nat. Chem.* **2017**, *9* (9), 868–873. <https://doi.org/10.1038/nchem.2748>.
- (104) Anand, D.; Sun, Z.; Zhou, L. Visible-Light-Mediated β -C–H Gem-Difluoroallylation of Aldehydes and Cyclic Ketones through C–F Bond Cleavage of 1-Trifluoromethyl Alkenes. *Org. Lett.* **2020**, *22* (6), 2371–2375. <https://doi.org/10.1021/acs.orglett.0c00568>.
- (105) Ghosh, I.; Marzo, L.; Das, A.; Shaikh, R.; König, B. Visible Light Mediated Photoredox Catalytic Arylation Reactions. *Acc. Chem. Res.* **2016**, *49* (8), 1566–1577. <https://doi.org/10.1021/acs.accounts.6b00229>.

- (106) Wang, C. S.; Dixneuf, P. H.; Soulé, J. F. Photoredox Catalysis for Building C-C Bonds from C(Sp²)-H Bonds. *Chem. Rev.* **2018**, *118* (16), 7532–7585. <https://doi.org/10.1021/acs.chemrev.8b00077>.
- (107) Kalyani, D.; McMurtrey, K. B.; Neufeldt, S. R.; Sanford, M. S. Room-Temperature C–H Arylation: Merger of Pd-Catalyzed C–H Functionalization and Visible-Light Photocatalysis. *J. Am. Chem. Soc.* **2011**, *133* (46), 18566–18569. <https://doi.org/10.1021/ja208068w>.
- (108) Jiang, J.; Zhang, W.-M.; Dai, J.-J.; Xu, J.; Xu, H.-J. Visible-Light-Promoted C–H Arylation by Merging Palladium Catalysis with Organic Photoredox Catalysis. *J. Org. Chem.* **2017**, *82* (7), 3622–3630. <https://doi.org/10.1021/acs.joc.7b00140>.
- (109) Liang, L.; Xie, M.-S.; Wang, H.-X.; Niu, H.-Y.; Qu, G.-R.; Guo, H.-M. Visible-Light-Mediated Monoselective Ortho C–H Arylation of 6-Arylpurine Nucleosides with Diazonium Salts. *J. Org. Chem.* **2017**, *82* (11), 5966–5973. <https://doi.org/10.1021/acs.joc.7b00659>.
- (110) Sahoo, B.; Hopkinson, M. N.; Glorius, F. Combining Gold and Photoredox Catalysis: Visible Light-Mediated Oxy- and Aminoarylation of Alkenes. *J. Am. Chem. Soc.* **2013**, *135* (15), 5505–5508. <https://doi.org/10.1021/ja400311h>.
- (111) Shu, X.; Zhang, M.; He, Y.; Frei, H.; Toste, F. D. Dual Visible Light Photoredox and Gold-Catalyzed Arylative Ring Expansion. *J. Am. Chem. Soc.* **2014**, *136* (16), 5844–5847. <https://doi.org/10.1021/ja500716j>.
- (112) He, Y.; Wu, H.; Toste, F. D. A Dual Catalytic Strategy for Carbon–Phosphorus Cross-Coupling via Gold and Photoredox Catalysis. *Chem. Sci.* **2015**, *6* (2), 1194–1198. <https://doi.org/10.1039/C4SC03092C>.
- (113) Patil, D. V.; Yun, H.; Shin, S. Catalytic Cross-Coupling of Vinyl Golds with Diazonium Salts under Photoredox and Thermal Conditions. *Adv. Synth. Catal.* **2015**, *357* (12), 2622–2628. <https://doi.org/10.1002/adsc.201500525>.
- (114) Tlahuext-Aca, A.; Hopkinson, M. N.; Sahoo, B.; Glorius, F. Dual Gold/Photoredox-Catalyzed C(Sp)–H Arylation of Terminal Alkynes with Diazonium Salts. *Chem. Sci.* **2016**, *7* (1), 89–93. <https://doi.org/10.1039/C5SC02583D>.
- (115) Romańczyk, P. P.; Kurek, S. S. Reliable Reduction Potentials of Diaryliodonium Cations and Aryl Radicals in Acetonitrile from High-Level Ab Initio Computations. *Electrochim. Acta* **2020**, 136404.

<https://doi.org/10.1016/j.electacta.2020.136404>.

- (116) Baralle, A.; Fensterbank, L.; Goddard, J.-P.; Ollivier, C. Aryl Radical Formation by Copper(I) Photocatalyzed Reduction of Diaryliodonium Salts: NMR Evidence for a Cu II /Cu I Mechanism. *Chem. - A Eur. J.* **2013**, *19* (33), 10809–10813. <https://doi.org/10.1002/chem.201301449>.
- (117) Fumagalli, G.; Boyd, S.; Greaney, M. F. Oxyarylation and Aminoarylation of Styrenes Using Photoredox Catalysis. *Org. Lett.* **2013**, *15* (17), 4398–4401. <https://doi.org/10.1021/ol401940c>.
- (118) Pagire, S. K.; Hossain, A.; Reiser, O. Temperature Controlled Selective C–S or C–C Bond Formation: Photocatalytic Sulfonylation versus Arylation of Unactivated Heterocycles Utilizing Aryl Sulfonyl Chlorides. *Org. Lett.* **2018**, *20* (3), 648–651. <https://doi.org/10.1021/acs.orglett.7b03790>.
- (119) Xia, J.-D.; Deng, G.-B.; Zhou, M.-B.; Liu, W.; Xie, P.; Li, J.-H. Reusable Visible Light Photoredox Catalysts; Catalyzed Benzylic C(Sp³)–H Functionalization/Carbocyclization Reactions. *Synlett* **2012**, *23* (18), 2707–2713. <https://doi.org/10.1055/s-0032-1317349>.
- (120) Deng, G.-B.; Wang, Z.-Q.; Xia, J.-D.; Qian, P.-C.; Song, R.-J.; Hu, M.; Gong, L.-B.; Li, J.-H. Tandem Cyclizations of 1,6-Enynes with Arylsulfonyl Chlorides by Using Visible-Light Photoredox Catalysis. *Angew. Chemie Int. Ed.* **2013**, *52* (5), 1535–1538. <https://doi.org/10.1002/anie.201208380>.
- (121) Prier, C. K.; Rankic, D. A.; MacMillan, D. W. C. Visible Light Photoredox Catalysis with Transition Metal Complexes: Applications in Organic Synthesis. *Chem. Rev.* **2013**, *113* (7), 5322–5363. <https://doi.org/10.1021/cr300503r>.
- (122) Wang, C.-S.; Dixneuf, P. H.; Soulé, J.-F. Photoredox Catalysis for Building C–C Bonds from C(Sp²)–H Bonds. *Chem. Rev.* **2018**, *118* (16), 7532–7585. <https://doi.org/10.1021/acs.chemrev.8b00077>.
- (123) Discekici, E. H.; Treat, N. J.; Poelma, S. O.; Mattson, K. M.; Hudson, Z. M.; Luo, Y.; Hawker, C. J.; de Alaniz, J. R. A Highly Reducing Metal-Free Photoredox Catalyst: Design and Application in Radical Dehalogenations. *Chem. Commun.* **2015**, *51* (58), 11705–11708. <https://doi.org/10.1039/C5CC04677G>.
- (124) Theriot, J. C.; Lim, C.-H.; Yang, H.; Ryan, M. D.; Musgrave, C. B.; Miyake, G. M. Organocatalyzed Atom Transfer Radical Polymerization Driven by Visible Light. *Science* (80-.). **2016**, *352* (6289), 1082–1086. <https://doi.org/10.1126/science.aaf3935>.

- (125) McCarthy, B. G.; Pearson, R. M.; Lim, C.-H.; Sartor, S. M.; Damrauer, N. H.; Miyake, G. M. Structure–Property Relationships for Tailoring Phenoxazines as Reducing Photoredox Catalysts. *J. Am. Chem. Soc.* **2018**, *140* (15), 5088–5101. <https://doi.org/10.1021/jacs.7b12074>.
- (126) MacKenzie, I. A.; Wang, L.; Onuska, N. P. R.; Williams, O. F.; Begam, K.; Moran, A. M.; Dunietz, B. D.; Nicewicz, D. A. Discovery and Characterization of an Acridine Radical Photoreductant. *Nature* **2020**, *580* (7801), 76–80. <https://doi.org/10.1038/s41586-020-2131-1>.
- (127) Schroll, P.; Hari, D. P.; König, B. Photocatalytic Arylation of Alkenes, Alkynes and Enones with Diazonium Salts. *ChemistryOpen* **2012**, *1* (3), 130–133. <https://doi.org/10.1002/open.201200011>.
- (128) Kojima, M.; Oisaki, K.; Kanai, M. Metal-Free C(3)-H Arylation of Coumarins Promoted by Catalytic Amounts of 5,10,15,20-Tetrakis(4-Diethylaminophenyl)Porphyrin. *Chem. Commun.* **2015**, *51* (47), 9718–9721. <https://doi.org/10.1039/c5cc02349a>.
- (129) Rybicka-Jasińska, K.; König, B.; Gryko, D. Porphyrin-Catalyzed Photochemical C–H Arylation of Heteroarenes. *European J. Org. Chem.* **2017**, *2017* (15), 2104–2107. <https://doi.org/10.1002/ejoc.201601518>.
- (130) Hering, T.; Hari, D. P.; König, B. Visible-Light-Mediated α -Arylation of Enol Acetates Using Aryl Diazonium Salts. *J. Org. Chem.* **2012**, *77* (22), 10347–10352. <https://doi.org/10.1021/jo301984p>.
- (131) De Souza, A. A. N.; Silva, N. S.; Müller, A. V.; Polo, A. S.; Brocksom, T. J.; De Oliveira, K. T. Porphyrins as Photoredox Catalysts in Csp²-H Arylations: Batch and Continuous Flow Approaches. *J. Org. Chem.* **2018**, *83* (24), 15077–15086. <https://doi.org/10.1021/acs.joc.8b02355>.
- (132) Bu, M.; Lu, G.; Jiang, J.; Cai, C. Merging Visible-Light Photoredox and Micellar Catalysis: Arylation Reactions with Anilines Nitrosated in Situ. *Catal. Sci. Technol.* **2018**, *8* (15), 3728–3732. <https://doi.org/10.1039/C8CY01221K>.
- (133) Mkrtchyan, S.; Iaroshenko, V. O. Visible-Light-Mediated Arylation of Ortho -Hydroxyarylenaminones: Direct Access to Isoflavones. *Chem. Commun.* **2020**, *56* (17), 2606–2609. <https://doi.org/10.1039/C9CC09945J>.
- (134) Wang, H.; Gao, Y.; Zhou, C.; Li, G. Visible-Light-Driven Reductive Carboarylation of Styrenes with CO₂ and Aryl Halides. *J. Am. Chem. Soc.* **2020**, *142* (18), 8122–8129. <https://doi.org/10.1021/jacs.0c03144>.

- (135) Bu, M.; Niu, T. F.; Cai, C. Visible-Light-Mediated Oxidative Arylation of Vinylarenes under Aerobic Conditions. *Catal. Sci. Technol.* **2015**, *5* (2), 830–834. <https://doi.org/10.1039/C4CY01523A>.
- (136) Niu, T.; Li, L.; Ni, B.; Bu, M.; Cai, C.; Jiang, H. Visible-Light-Induced Meerwein Cascade Reactions for the Preparation of α -Aryl Esters. *European J. Org. Chem.* **2015**, *2015* (26), 5775–5780. <https://doi.org/10.1002/ejoc.201500659>.
- (137) Kaur, M.; Kohli, S.; Sandhu, S.; Bansal, Y.; Bansal, G. Coumarin: A Promising Scaffold for Anticancer Agents. *Anticancer. Agents Med. Chem.* **2015**, *15* (8), 1032–1048. <https://doi.org/10.2174/1871520615666150101125503>.
- (138) Morsy, S. A.; Farahat, A. A.; Nasr, M. N. A.; Tantawy, A. S. Synthesis, Molecular Modeling and Anticancer Activity of New Coumarin Containing Compounds. *Saudi Pharm. J.* **2017**, *25* (6), 873–883. <https://doi.org/10.1016/j.jsps.2017.02.003>.
- (139) Garazd, Y.; Garazd, M.; Lesyk, R. Synthesis and Evaluation of Anticancer Activity of 6-Pyrazolinylcoumarin Derivatives. *Saudi Pharm. J.* **2017**, *25* (2), 214–223. <https://doi.org/10.1016/j.jsps.2016.05.005>.
- (140) Hassan, A. Y.; Sarg, M. T.; El Deeb, M. A.; Bayoumi, A. H.; El Rabeb, S. I. Facile Synthesis and Anticancer Activity Study of Novel Series of Substituted and Fused Coumarin Derivatives. *J. Heterocycl. Chem.* **2018**, *55* (6), 1426–1443. <https://doi.org/10.1002/jhet.3179>.
- (141) Hassan, M. Z.; Osman, H.; Ali, M. A.; Ahsan, M. J. Therapeutic Potential of Coumarins as Antiviral Agents. *Eur. J. Med. Chem.* **2016**, *123*, 236–255. <https://doi.org/10.1016/j.ejmech.2016.07.056>.
- (142) Shen, Y.-F.; Liu, L.; Feng, C.-Z.; Hu, Y.; Chen, C.; Wang, G.-X.; Zhu, B. Synthesis and Antiviral Activity of a New Coumarin Derivative against Spring Viraemia of Carp Virus. *Fish Shellfish Immunol.* **2018**, *81*, 57–66. <https://doi.org/10.1016/j.fsi.2018.07.005>.
- (143) Mishra, S.; Pandey, A.; Manvati, S. Coumarin: An Emerging Antiviral Agent. *Heliyon* **2020**, *6* (1), e03217. <https://doi.org/10.1016/j.heliyon.2020.e03217>.
- (144) Souza, S. M. de; Monache, F. D.; Smânia, A. Antibacterial Activity of Coumarins. *Zeitschrift für Naturforsch. C* **2005**, *60* (9–10), 693–700. <https://doi.org/10.1515/znc-2005-9-1006>.
- (145) Kawase, M.; Varu, B.; Shah, A.; Motohashi, N.; Tani, S.; Saito, S.; Debnath, S.; Mahapatra, S.; Dastidar, S.; Chakrabarty, A. Antimicrobial Activity of New

- Coumarin Derivatives. *Arzneimittelforschung* **2011**, *51* (01), 67–71. <https://doi.org/10.1055/s-0031-1300004>.
- (146) Smyth, T.; Ramachandran, V. N.; Smyth, W. F. A Study of the Antimicrobial Activity of Selected Naturally Occurring and Synthetic Coumarins. *Int. J. Antimicrob. Agents* **2009**, *33* (5), 421–426. <https://doi.org/10.1016/j.ijantimicag.2008.10.022>.
- (147) Borges Bubols, G.; da Rocha Vianna, D.; Medina-Remon, A.; von Poser, G.; Maria Lamuela-Raventos, R.; Lucia Eifler-Lima, V.; Cristina Garcia, S. The Antioxidant Activity of Coumarins and Flavonoids. *Mini Rev. Med. Chem.* **2013**, *13* (3), 318–334. <https://doi.org/10.2174/138955713804999775>.
- (148) Torres, R.; Faini, F.; Modak, B.; Urbina, F.; Labbé, C.; Guerrero, J. Antioxidant Activity of Coumarins and Flavonols from the Resinous Exudate of *Haplopappus Multifolius*. *Phytochemistry* **2006**, *67* (10), 984–987. <https://doi.org/10.1016/j.phytochem.2006.03.016>.
- (149) Hadjipavlou-Litina, D.; Kontogiorgis, C.; Pontiki, E.; Dakanali, M.; Akoumianaki, A.; Katerinopoulos, H. E. Anti-Inflammatory and Antioxidant Activity of Coumarins Designed as Potential Fluorescent Zinc Sensors. *J. Enzyme Inhib. Med. Chem.* **2007**, *22* (3), 287–292. <https://doi.org/10.1080/14756360601073914>.
- (150) Torres, F.; Brucker, N.; Andrade, S.; Kawano, D.; Garcia, S.; Poser, G.; Eifler-Lima, V. New Insights into the Chemistry and Antioxidant Activity of Coumarins. *Curr. Top. Med. Chem.* **2014**, *14* (22), 2600–2623. <https://doi.org/10.2174/1568026614666141203144551>.
- (151) Murray, R. D. H. *Fortschritte Der Chemie Organischer Naturstoffe / Progress in the Chemistry of Organic Natural Products*; Herz, W., Falk, H., Kirby, G. W., Moore, R. E., Eds.; Fortschritte der Chemie organischer Naturstoffe / Progress in the Chemistry of Organic Natural Products; Springer Vienna: Vienna, 2002; Vol. 83. <https://doi.org/10.1007/978-3-7091-6172-2>.
- (152) Venugopala, K. N.; Rashmi, V.; Odhav, B. Review on Natural Coumarin Lead Compounds for Their Pharmacological Activity. *Biomed Res. Int.* **2013**, *2013*, 1–14. <https://doi.org/10.1155/2013/963248>.
- (153) Uchiumi, F.; Hatano, T.; Ito, H.; Yoshida, T.; Tanuma, S. Transcriptional Suppression of the HIV Promoter by Natural Compounds. *Antiviral Res.* **2003**, *58* (1), 89–98. [https://doi.org/10.1016/S0166-3542\(02\)00186-9](https://doi.org/10.1016/S0166-3542(02)00186-9).

- (154) Ong, E. B. B.; Watanabe, N.; Saito, A.; Futamura, Y.; Abd El Galil, K. H.; Koito, A.; Najimudin, N.; Osada, H. Vipirinin, a Coumarin-Based HIV-1 Vpr Inhibitor, Interacts with a Hydrophobic Region of VPR. *J. Biol. Chem.* **2011**, *286* (16), 14049–14056. <https://doi.org/10.1074/jbc.M110.185397>.
- (155) You, L.; An, R.; Wang, X.; Li, Y. Discovery of Novel Osthole Derivatives as Potential Anti-Breast Cancer Treatment. *Bioorg. Med. Chem. Lett.* **2010**, *20* (24), 7426–7428. <https://doi.org/10.1016/j.bmcl.2010.10.027>.
- (156) Liu, Z.; Li, D.; Jiang, D.; Xiao, C.; Song, Z.; Jin, Y. Design, Synthesis and Antitumor Activity in Vitro of a Series of 3-Arylcoumarins. *Chem. Res. Chinese Univ.* **2013**, *29* (6), 1125–1128. <https://doi.org/10.1007/s40242-013-3107-6>.
- (157) Musa, M. A.; Latinwo, L. M.; Virgile, C.; Badisa, V. L. D.; Gbadebo, A. J. Synthesis and in Vitro Evaluation of 3-(4-Nitrophenyl)Coumarin Derivatives in Tumor Cell Lines. *Bioorg. Chem.* **2015**, *58*, 96–103. <https://doi.org/10.1016/j.bioorg.2014.11.009>.
- (158) Musa, M. A.; Badisa, V. L. D.; Latinwo, L. M.; Ntantie, E. 7,8-Dihydroxy-3-Arylcoumarin Induces Cell Death Through S-Phase Arrest in MDA-MB-231 Breast Cancer Cells. *Anticancer Res.* **2018**, *38* (11), 6091–6098. <https://doi.org/10.21873/anticancer.12959>.
- (159) Musa, M. A.; Gbadebo, A. J.; Latinwo, L. M.; Badisa, V. L. 7,8-Dihydroxy-3-(4-nitrophenyl)Coumarin Induces Cell Death via Reactive Oxygen Species–Independent S-phase Cell Arrest. *J. Biochem. Mol. Toxicol.* **2018**, *32* (12), e22203. <https://doi.org/10.1002/jbt.22203>.
- (160) Kavetsou, E.; Katopodi, A.; Argyri, L.; Chainoglou, E.; Pontiki, E.; Hadjipavlou-Litina, D.; Chroni, A.; Detsi, A. Novel 3-aryl-5-substituted-coumarin Analogues: Synthesis and Bioactivity Profile. *Drug Dev. Res.* **2020**, ddr.21639. <https://doi.org/10.1002/ddr.21639>.
- (161) Medjakovic, S.; Mueller, M.; Jungbauer, A. Potential Health-Modulating Effects of Isoflavones and Metabolites via Activation of PPAR and AhR. *Nutrients* **2010**, *2* (3), 241–279. <https://doi.org/10.3390/nu2030241>.
- (162) Patel, R. P.; Barnes, S. Isoflavones and PPAR Signaling: A Critical Target in Cardiovascular, Metastatic, and Metabolic Disease. *PPAR Res.* **2010**, *2010*, 1–10. <https://doi.org/10.1155/2010/153252>.
- (163) Hu, Y.; Wang, B.; Yang, J.; Liu, T.; Sun, J.; Wang, X. Synthesis and Biological Evaluation of 3-Arylcoumarin Derivatives as Potential Anti-Diabetic Agents. *J.*

- Enzyme Inhib. Med. Chem.* **2019**, *34* (1), 15–30.
<https://doi.org/10.1080/14756366.2018.1518958>.
- (164) Matos, M. J.; Vilar, S.; García-Morales, V.; Tatonetti, N. P.; Uriarte, E.; Santana, L.; Viña, D. Insight into the Functional and Structural Properties of 3-Arylcoumarin as an Interesting Scaffold in Monoamine Oxidase B Inhibition. *ChemMedChem* **2014**, *9* (7), 1488–1500.
<https://doi.org/10.1002/cmdc.201300533>.
- (165) Orhan, I.; Gulcan, H. Coumarins: Auspicious Cholinesterase and Monoamine Oxidase Inhibitors. *Curr. Top. Med. Chem.* **2015**, *15* (17), 1673–1682.
<https://doi.org/10.2174/1568026615666150427113103>.
- (166) Wang, Z.-M.; Li, X.-M.; Xue, G.-M.; Xu, W.; Wang, X.-B.; Kong, L.-Y. Synthesis and Evaluation of 6-Substituted 3-Arylcoumarin Derivatives as Multifunctional Acetylcholinesterase/Monoamine Oxidase B Dual Inhibitors for the Treatment of Alzheimer's Disease. *RSC Adv.* **2015**, *5* (126), 104122–104137.
<https://doi.org/10.1039/C5RA22296F>.
- (167) Yang, J.; Zhang, P.; Hu, Y.; Liu, T.; Sun, J.; Wang, X. Synthesis and Biological Evaluation of 3-Arylcoumarins as Potential Anti-Alzheimer's Disease Agents. *J. Enzyme Inhib. Med. Chem.* **2019**, *34* (1), 651–656.
<https://doi.org/10.1080/14756366.2019.1574297>.
- (168) Alipour, M.; Khoobi, M.; Nadri, H.; Sakhteman, A.; Moradi, A.; Ghandi, M.; Foroumadi, A.; Shafiee, A. Synthesis of Some New 3-Coumaranone and Coumarin Derivatives as Dual Inhibitors of Acetyl- and Butyrylcholinesterase. *Arch. Pharm. (Weinheim)*. **2013**, *346* (8), 577–587.
<https://doi.org/10.1002/ardp.201300080>.
- (169) Brühlmann, C.; Ooms, F.; Carrupt, P.-A.; Testa, B.; Catto, M.; Leonetti, F.; Altomare, C.; Carotti, A. Coumarins Derivatives as Dual Inhibitors of Acetylcholinesterase and Monoamine Oxidase. *J. Med. Chem.* **2001**, *44* (19), 3195–3198. <https://doi.org/10.1021/jm010894d>.
- (170) Melo, P. A.; Do Nascimento, M. C.; Mors, W. B.; Suarez-Kurtz, G. Inhibition of the Myotoxic and Hemorrhagic Activities of Crotalid Venoms by *Eclipta Prostrata* (Asteraceae) Extracts and Constituents. *Toxicon* **1994**, *32* (5), 595–603. [https://doi.org/10.1016/0041-0101\(94\)90207-0](https://doi.org/10.1016/0041-0101(94)90207-0).
- (171) Melo, P. A.; Ownby, C. L. Ability of Wedelolactone, Heparin, and Para-Bromophenacyl Bromide to Antagonize the Myotoxic Effects of Two Crotaline

- Venoms and Their PLA2 Myotoxins. *Toxicon* **1999**, 37 (1), 199–215. [https://doi.org/10.1016/S0041-0101\(98\)00183-4](https://doi.org/10.1016/S0041-0101(98)00183-4).
- (172) Melo, P. A.; Pinheiro, D. A.; Ricardo, H. D.; Fernandes, F. F. A.; Tomaz, M. A.; El-Kik, C. Z.; Strauch, M. A.; da Fonseca, T. F.; Sifuentes, D. N.; Calil-Elias, S.; et al. Ability of a Synthetic Coumestan to Antagonize Bothrops Snake Venom Activities. *Toxicon* **2010**, 55 (2–3), 488–496. <https://doi.org/10.1016/j.toxicon.2009.09.021>.
- (173) Harris, D. M.; Besselink, E.; Henning, S. M.; Go, V. L. W.; Heber, D. Phytoestrogens Induce Differential Estrogen Receptor Alpha- or Beta-Mediated Responses in Transfected Breast Cancer Cells. *Exp. Biol. Med.* **2005**, 230 (8), 558–568. <https://doi.org/10.1177/153537020523000807>.
- (174) Wang, C.; Kurzer, M. S. Phytoestrogen Concentration Determines Effects on DNA Synthesis in Human Breast Cancer Cells. *Nutr. Cancer* **1997**, 28 (3), 236–247. <https://doi.org/10.1080/01635589709514582>.
- (175) Magee, P. J.; McGlynn, H.; Rowland, I. R. Differential Effects of Isoflavones and Lignans on Invasiveness of MDA-MB-231 Breast Cancer Cells in Vitro. *Cancer Lett.* **2004**, 208 (1), 35–41. <https://doi.org/10.1016/j.canlet.2003.11.012>.
- (176) Luo, G.; Tang, Z.; Li, X.; Hou, Q.; Chen, Y.; Lao, K.; Xiang, H. 3, 9-Di-O-Substituted Coumestrols Incorporating Basic Amine Side Chains Act as Novel Apoptosis Inducers with Improved Pharmacological Selectivity. *Bioorg. Chem.* **2019**, 85 (November 2018), 140–151. <https://doi.org/10.1016/j.bioorg.2018.12.024>.
- (177) Qwebani-Ogunleye, T.; Kolesnikova, N. I.; Steenkamp, P.; de Koning, C. B.; Brady, D.; Wellington, K. W. A One-Pot Laccase-Catalysed Synthesis of Coumestan Derivatives and Their Anticancer Activity. *Bioorganic Med. Chem.* **2017**, 25 (3), 1172–1182. <https://doi.org/10.1016/j.bmc.2016.12.025>.
- (178) Obiorah, I. E.; Fan, P.; Jordan, V. C. Breast Cancer Cell Apoptosis with Phytoestrogens Is Dependent on an Estrogen-Deprived State. *Cancer Prev. Res.* **2014**, 7 (9), 939–949. <https://doi.org/10.1158/1940-6207.CAPR-14-0061>.
- (179) Lim, W.; Jeong, M.; Bazer, F. W.; Song, G. Coumestrol Inhibits Proliferation and Migration of Prostate Cancer Cells by Regulating AKT, ERK1/2, and JNK MAPK Cell Signaling Cascades. *J. Cell. Physiol.* **2017**, 232 (4), 862–871. <https://doi.org/10.1002/jcp.25494>.
- (180) Lee, Y. H.; Yuk, H. J.; Park, K. H.; Bae, Y. S. Coumestrol Induces Senescence

- through Protein Kinase CKII Inhibition-Mediated Reactive Oxygen Species Production in Human Breast Cancer and Colon Cancer Cells. *Food Chem.* **2013**, *141* (1), 381–388. <https://doi.org/10.1016/j.foodchem.2013.03.053>.
- (181) Cho, S. Y.; Cho, S.; Park, E.; Kim, B.; Sohn, E. J.; Oh, B.; Lee, E. O.; Lee, H. J.; Kim, S. H. Coumestrol Suppresses Hypoxia Inducible Factor 1 α by Inhibiting ROS Mediated Sphingosine Kinase 1 in Hypoxic PC-3 Prostate Cancer Cells. *Bioorganic Med. Chem. Lett.* **2014**, *24* (11), 2560–2564. <https://doi.org/10.1016/j.bmcl.2014.03.084>.
- (182) Diel, P.; Olf, S.; Schmidt, S.; Michna, H. Effects of the Environmental Estrogens Bisphenol A, o, P'-DDT, p-Tert-Octylphenol and Coumestrol on Apoptosis Induction, Cell Proliferation and the Expression of Estrogen Sensitive Molecular Parameters in the Human Breast Cancer Cell Line MCF-7. *J. Steroid Biochem. Mol. Biol.* **2002**, *80* (1), 61–70. [https://doi.org/10.1016/S0960-0760\(01\)00173-X](https://doi.org/10.1016/S0960-0760(01)00173-X).
- (183) Kaushik-Basu, N.; Bopda-Waffo, A.; Talele, T. T.; Basu, A.; Costa, P. R. R.; Da Silva, A. J. M.; Sarafianos, S. G.; Noël, F. Identification and Characterization of Coumestans as Novel HCV NS5B Polymerase Inhibitors. *Nucleic Acids Res.* **2008**, *36* (5), 1482–1496. <https://doi.org/10.1093/nar/gkm1178>.
- (184) Zhang, W.; Lun, S.; Wang, S. H.; Jiang, X. W.; Yang, F.; Tang, J.; Manson, A. L.; Earl, A. M.; Gunosewoyo, H.; Bishai, W. R.; et al. Identification of Novel Coumestan Derivatives as Polyketide Synthase 13 Inhibitors against Mycobacterium Tuberculosis. *J. Med. Chem.* **2018**, *61* (3), 791–803. <https://doi.org/10.1021/acs.jmedchem.7b01319>.
- (185) Zhang, W.; Lun, S.; Liu, L. L.; Xiao, S.; Duan, G.; Gunosewoyo, H.; Yang, F.; Tang, J.; Bishai, W. R.; Yu, L. F. Identification of Novel Coumestan Derivatives as Polyketide Synthase 13 Inhibitors against Mycobacterium Tuberculosis. Part II. *J. Med. Chem.* **2019**, *62* (7), 3575–3589. <https://doi.org/10.1021/acs.jmedchem.9b00010>.
- (186) Cao, H. Juan; Li, C. rong; Wang, L. ying; Ziadlou, R.; Grad, S.; Zhang, Y.; Cheng, Y.; Lai, Y. xiao; Yao, X. sheng; Alini, M.; et al. Effect and Mechanism of Psoralidin on Promoting Osteogenesis and Inhibiting Adipogenesis. *Phytomedicine* **2019**, *61* (January), 152860. <https://doi.org/10.1016/j.phymed.2019.152860>.
- (187) Kong, L.; Ma, R.; Yang, X.; Zhu, Z.; Guo, H.; He, B.; Wang, B.; Hao, D.

- Psoralidin Suppresses Osteoclastogenesis in BMMs and Attenuates LPS-Mediated Osteolysis by Inhibiting Inflammatory Cytokines. *Int. Immunopharmacol.* **2017**, *51* (April), 31–39. <https://doi.org/10.1016/j.intimp.2017.07.003>.
- (188) Nguyen, P. H.; Nguyen, T. N. A.; Dao, T. T.; Kang, H. W.; Ndinteh, D. T.; Mbafor, J. T.; Oh, W. K. AMP-Activated Protein Kinase (AMPK) Activation by Benzofurans and Coumestans Isolated from *Erythrina Abyssinica*. *J. Nat. Prod.* **2010**, *73* (4), 598–602. <https://doi.org/10.1021/np900745g>.
- (189) Dakshanamurthy, S.; Kim, M.; Brown, M. L.; Byers, S. W. In-Silico Fragment-Based Identification of Novel Angiogenesis Inhibitors. *Bioorganic Med. Chem. Lett.* **2007**, *17* (16), 4551–4556. <https://doi.org/10.1016/j.bmcl.2007.05.104>.
- (190) Ji, Q.; Yang, C.; Wang, M.; Xie, Y. CN1966507A, 2005.
- (191) Wang, W. CN102321090, 2012.
- (192) Iwao, M.; Ishibashi, F.; Fukuda, T.; Hasegawa, H. WO 2012099129, 2012.
- (193) Buarque, C. D.; Salustiano, E. J.; Fraga, K. C.; Alves, B. R. M.; Costa, P. R. R. 11a-N-Tosyl-5-Deoxy-Pterocarpan (LQB-223), a Promising Prototype for Targeting MDR Leukemia Cell Lines. *Eur. J. Med. Chem.* **2014**, *78*, 190–197. <https://doi.org/10.1016/j.ejmech.2014.03.039>.
- (194) Tuskaev, V. A. Synthesis and Biological Activity of Coumestan Derivatives (Review). *Pharm. Chem. J.* **2013**, *47* (1), 1–11. <https://doi.org/10.1007/s11094-013-0886-5>.
- (195) Mackey, K.; Pardo, L. M.; Prendergast, A. M.; Nolan, M.-T.; Bateman, L. M.; McGlacken, G. P. Cyclization of 4-Phenoxy-2-Coumarins and 2-Pyrones via a Double C–H Activation. *Org. Lett.* **2016**, *18* (11), 2540–2543. <https://doi.org/10.1021/acs.orglett.6b00751>.
- (196) Nolan, M.-T.; Pardo, L. M.; Prendergast, A. M.; McGlacken, G. P. Intramolecular Direct Arylation of 3-Halo-2-Pyrones and 2-Coumarins. *J. Org. Chem.* **2015**, *80* (21), 10904–10913. <https://doi.org/10.1021/acs.joc.5b02027>.
- (197) Kapdi, A. R.; Karbelkar, A.; Naik, M.; Pednekar, S.; Fischer, C.; Schulzke, C.; Tromp, M. Efficient Synthesis of Coumarin-Based Tetra and Pentacyclic Rings Using Phospha-Palladacycles. *RSC Adv.* **2013**, *3* (43), 20905. <https://doi.org/10.1039/c3ra43821j>.
- (198) Angeleska, S.; Kefalas, P.; Detsi, A. Crude Peroxidase from Onion Solid Waste as a Tool for Organic Synthesis. Part III: Synthesis of Tetracyclic Heterocycles

- (Coumestans and Benzofuroquinolinones). *Tetrahedron Lett.* **2013**, *54* (19), 2325–2328. <https://doi.org/10.1016/j.tetlet.2013.02.081>.
- (199) Chang, C.-P.; Pradiuldi, S. V.; Hong, F.-E. Synthesis of Coumarin Derivatives by Palladium Complex Catalyzed Intramolecular Heck Reaction: Preparation of a 1,2-Cyclobutadiene-Substituted CpCoCb Diphosphine Chelated Palladium Complex. *Inorg. Chem. Commun.* **2009**, *12* (7), 596–598. <https://doi.org/10.1016/j.inoche.2009.04.031>.
- (200) Cheng, C.; Chen, W.-W.; Xu, B.; Xu, M.-H. Access to Indole-Fused Polyheterocycles via Pd-Catalyzed Base-Free Intramolecular Cross Dehydrogenative Coupling. *J. Org. Chem.* **2016**, *81* (22), 11501–11507. <https://doi.org/10.1021/acs.joc.6b02160>.
- (201) Stadlbauer, W.; Laschober, R.; Kappe, T. Potential Non-Steroidal Estrogens and Antiestrogens, IV Organic Azides in Heterocyclic Synthesis, Part 13: Synthesis of Aza- and Diazacoumestrols via Azido Derivatives. *Monatshefte für Chemie - Chem. Mon.* **1991**, *122* (10), 853–861. <https://doi.org/10.1007/BF00815924>.
- (202) Baumgarten, P.; Kärgel, W. Über Eine Synthese von 2.4-Dioxy-Chinolinen. *Berichte der Dtsch. Chem. Gesellschaft (A B Ser.)* **1927**, *60* (4), 832–842. <https://doi.org/10.1002/cber.19270600403>.
- (203) Irgashev, R. A.; Karmatsky, A. A.; Slepukhin, P. A.; Rusinov, G. L.; Charushin, V. N. A Convenient Approach to the Design and Synthesis of Indolo[3,2-c]Coumarins via the Microwave-Assisted Cadogan Reaction. *Tetrahedron Lett.* **2013**, *54* (42), 5734–5738. <https://doi.org/10.1016/j.tetlet.2013.08.030>.
- (204) Rahmani-Nezhad, S.; Khosravani, L.; Saeedi, M.; Divsalar, K.; Firoozpour, L.; Pourshojaei, Y.; Sarrafi, Y.; Nadri, H.; Moradi, A.; Mahdavi, M.; et al. Synthesis and Evaluation of Coumarin–Resveratrol Hybrids as 15-Lipoxygenase Inhibitors. *Synth. Commun.* **2015**, *45* (6), 741–749. <https://doi.org/10.1080/00397911.2014.979947>.
- (205) Reddy, Y. T.; Sonar, V. N.; Crooks, P. A.; Dasari, P. K.; Reddy, P. N.; Rajitha, B. Ceric Ammonium Nitrate (CAN): An Efficient Catalyst for the Coumarin Synthesis via Pechmann Condensation Using Conventional Heating and Microwave Irradiation. *Synth. Commun.* **2008**, *38* (13), 2082–2088. <https://doi.org/10.1080/00397910802029091>.
- (206) Pu, W.; Lin, Y.; Zhang, J.; Wang, F.; Wang, C.; Zhang, G. 3-Arylcoumarins:

- Synthesis and Potent Anti-Inflammatory Activity. *Bioorg. Med. Chem. Lett.* **2014**, *24* (23), 5432–5434. <https://doi.org/10.1016/j.bmcl.2014.10.033>.
- (207) Xiao, C.-F.; Zou, Y.; Du, J.-L.; Sun, H.-Y.; Liu, X.-K. Hydroxyl Substitutional Effect on Selective Synthesis of Cis, Trans Stilbenes and 3-Arylcoumarins Through Perkin Condensation. *Synth. Commun.* **2012**, *42* (9), 1243–1258. <https://doi.org/10.1080/00397911.2010.538889>.
- (208) Viña, D.; Matos, M. J.; Yáñez, M.; Santana, L.; Uriarte, E. 3-Substituted Coumarins as Dual Inhibitors of AChE and MAO for the Treatment of Alzheimer's Disease. *Med. Chem. Commun.* **2012**, *3* (2), 213–218. <https://doi.org/10.1039/C1MD00221J>.
- (209) Matos, M. J.; Pérez-Cruz, F.; Vazquez-Rodriguez, S.; Uriarte, E.; Santana, L.; Borges, F.; Olea-Azar, C. Remarkable Antioxidant Properties of a Series of Hydroxy-3-Arylcoumarins. *Bioorg. Med. Chem.* **2013**, *21* (13), 3900–3906. <https://doi.org/10.1016/j.bmc.2013.04.015>.
- (210) Matos, M. J.; Janeiro, P.; Santana, L.; Uriarte, E.; Oliveira-Brett, A. M. Synthesis and Electrochemical Study of New 3-(Hydroxyphenyl)Benzo[f]Coumarins. *J. Electroanal. Chem.* **2014**, *726*, 62–70. <https://doi.org/10.1016/j.jelechem.2014.05.003>.
- (211) Bogdał, D. Coumarins: Fast Synthesis by Knoevenagel Condensation under Microwave Irradiation. *J. Chem. Res.* **1998**, No. 8, 468–469. <https://doi.org/10.1039/a801724g>.
- (212) Mali, R. S.; Tilve, S. G. Useful Synthesis of Coumestans. *Synth. Commun.* **1990**, *20* (12), 1781–1791. <https://doi.org/10.1080/00397919008053103>.
- (213) Zhu, F.; Li, Y.; Wang, Z.; Wu, X.-F. Iridium-Catalyzed Carbonylative Synthesis of Chromenones from Simple Phenols and Internal Alkynes at Atmospheric Pressure. *Angew. Chemie Int. Ed.* **2016**, *55* (45), 14151–14154. <https://doi.org/10.1002/anie.201608715>.
- (214) Sashidhara, K.; Palnati, G.; Avula, S.; Kumar, A. Efficient and General Synthesis of 3-Aryl Coumarins Using Cyanuric Chloride¹. *Synlett* **2012**, *23* (04), 611–621. <https://doi.org/10.1055/s-0031-1290344>.
- (215) Matos, M. J.; Vazquez-Rodriguez, S.; Borges, F.; Santana, L.; Uriarte, E. Synthesis of 3-Arylcoumarins via Suzuki-Cross-Coupling Reactions of 3-Chlorocoumarin. *Tetrahedron Lett.* **2011**, *52* (11), 1225–1227. <https://doi.org/10.1016/j.tetlet.2011.01.048>.

- (216) Jafarpour, F.; Zarei, S.; Barzegar Amiri Olia, M.; Jalalimanesh, N.; Rahiminejadan, S. Palladium-Catalyzed Decarboxylative Cross-Coupling Reactions: A Route for Regioselective Functionalization of Coumarins. *J. Org. Chem.* **2013**, *78* (7), 2957–2964. <https://doi.org/10.1021/jo302778d>.
- (217) Jafarpour, F.; Olia, M. B. A.; Hazrati, H. Highly Regioselective α -Arylation of Coumarins via Palladium-Catalyzed C–H Activation/Desulfative Coupling. *Adv. Synth. Catal.* **2013**, *355* (17), 3407–3412. <https://doi.org/10.1002/adsc.201300707>.
- (218) Jafarpour, F.; Hazrati, H.; Mohasselyazdi, N.; Khoobi, M.; Shafiee, A. Palladium Catalyzed Dehydrogenative Arylation of Coumarins: An Unexpected Switch in Regioselectivity. *Chem. Commun.* **2013**, *49* (93), 10935. <https://doi.org/10.1039/c3cc46959j>.
- (219) Yuan, J.-W.; Yang, L.-R.; Yin, Q.-Y.; Mao, P.; Qu, L.-B. KMnO₄/AcOH-Mediated C3-Selective Direct Arylation of Coumarins with Arylboronic Acids. *RSC Adv.* **2016**, *6* (42), 35936–35944. <https://doi.org/10.1039/C6RA04787D>.
- (220) Domingo, L. R.; Aurell, M. J.; Pérez, P.; Contreras, R. Quantitative Characterization of the Global Electrophilicity Power of Common Diene/Dienophile Pairs in Diels–Alder Reactions. *Tetrahedron* **2002**, *58* (22), 4417–4423. [https://doi.org/10.1016/S0040-4020\(02\)00410-6](https://doi.org/10.1016/S0040-4020(02)00410-6).
- (221) Zollinger, H. *Diazo Chemistry II*; Wiley, 1995. <https://doi.org/10.1002/3527601732>.
- (222) Chen, J.-R.; Hu, X.-Q.; Lu, L.-Q.; Xiao, W.-J. Visible Light Photoredox-Controlled Reactions of N-Radicals and Radical Ions. *Chem. Soc. Rev.* **2016**, *45* (8), 2044–2056. <https://doi.org/10.1039/C5CS00655D>.
- (223) Kärkäs, M. D. Photochemical Generation of Nitrogen-Centered Amidyl, Hydrazonyl, and Imidyl Radicals: Methodology Developments and Catalytic Applications. *ACS Catal.* **2017**, *7* (8), 4999–5022. <https://doi.org/10.1021/acscatal.7b01385>.
- (224) Du, Y.; Liu, R.; Linn, G.; Zhao, K. Synthesis of N-Substituted Indole Derivatives via PIFA-Mediated Intramolecular Cyclization. *Org. Lett.* **2006**, *8* (26), 5919–5922. <https://doi.org/10.1021/ol062288o>.
- (225) Colomer, I.; Batchelor-McAuley, C.; Odell, B.; Donohoe, T. J.; Compton, R. G. Hydrogen Bonding to Hexafluoroisopropanol Controls the Oxidative Strength of Hypervalent Iodine Reagents. *J. Am. Chem. Soc.* **2016**, *138* (28), 8855–8861.

<https://doi.org/10.1021/jacs.6b04057>.

- (226) Soto, J.; Soto, P. Miltefosine: Oral Treatment of Leishmaniasis. *Expert Rev. Anti. Infect. Ther.* **2006**, *4* (2), 177–185. <https://doi.org/10.1586/14787210.4.2.177>.
- (227) Rosa, I. A.; de Almeida, L.; Alves, K. F.; Marques, M. J.; Fregnan, A. M.; Silva, C. A.; Giacoppo, J. O. S.; Ramalho, T. C.; Carvalho, D. T.; dos Santos, M. H. Synthesis and in Vitro Evaluation of Leishmanicidal Activity of 7-Hydroxy-4-Phenylcoumarin Derivatives. *Med. Chem. Res.* **2017**, *26* (1), 131–139. <https://doi.org/10.1007/s00044-016-1729-1>.
- (228) Mandlik, V.; Patil, S.; Bopanna, R.; Basu, S.; Singh, S. Biological Activity of Coumarin Derivatives as Anti-Leishmanial Agents. *PLoS One* **2016**, *11* (10), e0164585. <https://doi.org/10.1371/journal.pone.0164585>.
- (229) Vedani, A.; Dobler, M.; Hu, Z.; Smieško, M. OpenVirtualToxLab—A Platform for Generating and Exchanging in Silico Toxicity Data. *Toxicol. Lett.* **2015**, *232* (2), 519–532. <https://doi.org/10.1016/j.toxlet.2014.09.004>.
- (230) Ruiz-Rodríguez, M. A.; Vedani, A.; Flores-Mireles, A. L.; Cháirez-Ramírez, M. H.; Gallegos-Infante, J. A.; González-Laredo, R. F. In Silico Prediction of the Toxic Potential of Lupeol. *Chem. Res. Toxicol.* **2017**, *30* (8), 1562–1571. <https://doi.org/10.1021/acs.chemrestox.7b00070>.
- (231) Hua, C.; Zhang, K.; Xin, M.; Ying, T.; Gao, J.; Jia, J.; Li, Y. High Quantum Yield and PH Sensitive Fluorescence Dyes Based on Coumarin Derivatives: Fluorescence Characteristics and Theoretical Study. *RSC Adv.* **2016**, *6* (54), 49221–49227. <https://doi.org/10.1039/C6RA05996A>.
- (232) Frisch, M. J.; Trucks, G. W.; Schlegel, H. B.; Scuseria, G. E.; Robb, M. A.; Cheeseman, J. R.; Montgomery, Jr., J. A.; Vreven, T.; Kudin, K. N.; Burant, J. C.; Millam, J. M.; Iyengar, S. S.; Tomasi, J.; Barone, V.; Mennucci, B.; Cossi, M.; Scalmani, G.; R, J. A. Gaussian 03. Gaussian, Inc.: Wallingford CT 2004.
- (233) Ruiz Espelt, L.; Wiensch, E. M.; Yoon, T. P. Brønsted Acid Cocatalysts in Photocatalytic Radical Addition of α -Amino C-H Bonds across Michael Acceptors. *J. Org. Chem.* **2013**, *78* (8), 4107–4114. <https://doi.org/10.1021/jo400428m>.
- (234) Chen, H.; Fan, W.; Yuan, X. A.; Yu, S. Site-Selective Remote C(Sp³)-H Heteroarylation of Amides via Organic Photoredox Catalysis. *Nat. Commun.* **2019**, *10* (1), 1–9. <https://doi.org/10.1038/s41467-019-12722-4>.

- (235) Moon, Y.; Park, B.; Kim, I.; Kang, G.; Shin, S.; Kang, D.; Baik, M. H.; Hong, S. Visible Light Induced Alkene Aminopyridylation Using N-Aminopyridinium Salts as Bifunctional Reagents. *Nat. Commun.* **2019**, *10* (1), 1–9. <https://doi.org/10.1038/s41467-019-12216-3>.
- (236) Bock, C. R.; Connor, J. A.; Gutierrez, A. R.; Meyer, T. J.; Whitten, D. G.; Sullivan, B. P.; Nagle, J. K. Estimation of Excited-State Redox Potentials by Electron-Transfer Quenching. Application of Electron-Transfer Theory to Excited-State Redox Processes. *J. Am. Chem. Soc.* **1979**, *101* (17), 4815–4824. <https://doi.org/10.1021/ja00511a007>.
- (237) Baffert, C.; Dumas, S.; Chauvin, J.; Leprête, J. C.; Collomb, M. N.; Deronzier, A. Photoinduced Oxidation of $[Mn(L)3]^{2+}$ and $[Mn 2O2(L)4]^{3+}$ (L = 2,2'-Bipyridine and 4,4'-Dimethyl-2,2'-Bipyridine) with the $[Ru(Bpy) 3]^{2+}$ /-Aryl Diazonium Salt System. *Phys. Chem. Chem. Phys.* **2005**, *7* (1), 202–210. <https://doi.org/10.1039/b411365a>.
- (238) Martinez, O.; Crabtree, K. N.; Gottlieb, C. A.; Stanton, J. F.; McCarthy, M. C. An Accurate Molecular Structure of Phenyl, the Simplest Aryl Radical. *Angew. Chemie - Int. Ed.* **2015**, *54* (6), 1808–1811. <https://doi.org/10.1002/anie.201409896>.
- (239) Kyne, S. H.; Schiesser, C. H.; Matsubara, H. An Ab Initio and DFT Study of Radical Addition Reactions of Imidoyl and Thieryl Radicals to Methanimine. *Org. Biomol. Chem.* **2011**, *9* (9), 3217–3224. <https://doi.org/10.1039/c1ob05105a>.
- (240) Matsubara, H.; Falzon, C. T.; Ryu, I.; Schiesser, C. H. Radicals Masquerading as Electrophiles: A Computational Study of the Intramolecular Addition Reactions of Acyl Radicals to Imines. *Org. Biomol. Chem.* **2006**, *4* (10), 1920–1926. <https://doi.org/10.1039/b603024f>.
- (241) Falzon, C. T.; Ryu, I.; Schiesser, C. H. 5-Azahexenoyl Radicals Cyclize via Nucleophilic Addition to the Acyl Carbon Rather than 5-Exo Homolytic Addition at the Imine. *Chem. Commun.* **2002**, *20*, 2338–2339. <https://doi.org/10.1039/b207729a>.
- (242) Glendening, E. D.; Reed, A. E.; Carpenter, J. E.; Weinhold, F. NBO Version 3.1.
- (243) Anslyn, E. V.; Dougherty, D. A. *Modern Physical Organic Chemistry*; University Science Books: Herndon, VA, 2006.
- (244) Lalevée, J.; Allonas, X.; Genet, S.; Fouassier, J.-P. Role of Charge-Transfer Configurations on the Addition Reaction of Aminoalkyl Radicals onto Acrylate

- Double Bonds. *J. Am. Chem. Soc.* **2003**, *125* (31), 9377–9380. <https://doi.org/10.1021/ja034750v>.
- (245) Salem, L. Intermolecular Orbital Theory of the Interaction between Conjugated Systems. I. General Theory. *J. Am. Chem. Soc.* **1968**, *90* (3), 543–552.
- (246) Creary, X.; Mehrsheikh-mohammadi, M. E.; Mcdonald, S. Methylene cyclopropane Rearrangement as a Probe for Free Radical Substituent Effects. Σ Values for Commonly Encountered Conjugating and Organometallic Groups. *J. Org. Chem.* **1987**, *52* (15), 3254–3263. <https://doi.org/10.1021/jo00391a015>.
- (247) Swain, C. G.; Unger, S. H.; Rosenquist, N. R.; Swain, M. S. Substituent Effects on Chemical Reactivity. Improved Evaluation of Field and Resonance Components. *J. Am. Chem. Soc.* **1983**, *105* (3), 492–502. <https://doi.org/10.1021/ja00341a032>.
- (248) Hu, H.; Lu, Z.; Yang, W. Fitting Molecular Electrostatic Potentials from Quantum Mechanical Calculations. *J. Chem. Theory Comput.* **2007**, *3* (3), 1004–1013. <https://doi.org/10.1021/ct600295n>.
- (249) Taft, R. W. Linear Steric Energy Relationships. *J. Am. Chem. Soc.* **1953**, *75* (18), 4538–4539. <https://doi.org/10.1021/ja01114a044>.
- (250) Taft, R. W. Linear Free Energy Relationships from Rates of Esterification and Hydrolysis of Aliphatic and Ortho-Substituted Benzoate Esters. *J. Am. Chem. Soc.* **1952**, *74* (11), 2729–2732. <https://doi.org/10.1021/ja01131a010>.
- (251) Taft, R. W. Polar and Steric Substituent Constants for Aliphatic and o-Benzoate Groups from Rates of Esterification and Hydrolysis of Esters. *J. Am. Chem. Soc.* **1952**, *74* (12), 3120–3128. <https://doi.org/10.1021/ja01132a049>.
- (252) Charton, M. Steric Effects. I. Esterification and Acid-Catalyzed Hydrolysis of Esters. *J. Am. Chem. Soc.* **1975**, *97* (6), 1552–1556. <https://doi.org/10.1021/ja00839a047>.
- (253) Charton, M. Steric Effects. II. Base-Catalyzed Ester Hydrolysis. *J. Am. Chem. Soc.* **1975**, *97* (13), 3691–3693. <https://doi.org/10.1021/ja00846a022>.
- (254) Charton, M. Steric Effects. 7. Additional ρ Constants. *J. Org. Chem.* **1976**, *41* (12), 2217–2220. <https://doi.org/10.1021/jo00874a035>.
- (255) Frisch, M. J.; Trucks, G. W.; Schlegel, H. B.; Scuseria, G. E.; Robb, M. A.; Cheeseman, J. R.; Scalmani, G.; Barone, V.; Petersson, G. A.; Nakatsuji, H.; et al. Gaussian 16. Gaussian, Inc.: Wallingford CT 2016.

- (256) Becke, A. D. A New Mixing of Hartree-Fock and Local Density-Functional Theories. *J. Chem. Phys.* **1993**, *98* (2), 1372–1377. <https://doi.org/10.1063/1.464304>.
- (257) Buarque, C.; Domingos, J.; Netto, C.; Costa, P. Palladium-Catalyzed Oxyarylation, Azaarylation and α -Arylation Reactions in the Synthesis of Bioactive Isoflavonoid Analogues. *Curr. Org. Synth.* **2015**, *12* (6), 772–794. <https://doi.org/10.2174/157017941206150828112502>.
- (258) Almabruk, K. H.; Chang, J. H.; Mahmud, T. Total Synthesis of (\pm)-Isoperbergins and Correction of the Chemical Structure of Perbergin. *J. Nat. Prod.* **2016**, *79* (9), 2391–2396. <https://doi.org/10.1021/acs.jnatprod.6b00621>.
- (259) Umehara, K.; Nemoto, K.; Matsushita, A.; Terada, E.; Monthakantirat, O.; De-Eknamkul, W.; Miyase, T.; Warashina, T.; Degawa, M.; Noguchi, H. Flavonoids from the Heartwood of the Thai Medicinal Plant *Dalbergia Parviflora* and Their Effects on Estrogenic-Responsive Human Breast Cancer Cells. *J. Nat. Prod.* **2009**, *72* (12), 2163–2168. <https://doi.org/10.1021/np900676y>.
- (260) Zhang, G.-P.; Xiao, Z.-Y.; Rafique, J.; Arfan, M.; Smith, P. J.; Lategan, C. A.; Hu, L.-H. Antiplasmodial Isoflavanones from the Roots of *Sophora Mollis*. *J. Nat. Prod.* **2009**, *72* (7), 1265–1268. <https://doi.org/10.1021/np900144c>.
- (261) Luo, M.; Liu, X.; Zu, Y.; Fu, Y.; Zhang, S.; Yao, L.; Efferth, T. Cajanol, a Novel Anticancer Agent from *Pigeonpea* [*Cajanus Cajan* (L.) Millsp.] Roots, Induces Apoptosis in Human Breast Cancer Cells through a ROS-Mediated Mitochondrial Pathway. *Chem. Biol. Interact.* **2010**, *188* (1), 151–160. <https://doi.org/10.1016/j.cbi.2010.07.009>.
- (262) Zhao, X.; Mei, W.; Gong, M.; Zuo, W.; Bai, H.; Dai, H. Antibacterial Activity of the Flavonoids from *Dalbergia Odorifera* on *Ralstonia Solanacearum*. *Molecules* **2011**, *16* (12), 9775–9782. <https://doi.org/10.3390/molecules16129775>.
- (263) Thien, D. D.; Thuy, T. T.; Anh, N. T. H.; Thang, L. Q.; Dai, T. D.; Sa, N. H.; Tam, N. T. A New Isoflavanone from *Uria Crinita*. *Nat. Prod. Res.* **2019**, 1–7. <https://doi.org/10.1080/14786419.2019.1667352>.
- (264) Boonyaketguson, S.; Trisuwan, K.; Bussaban, B.; Rukachaisirikul, V.; Phongpaichit, S. Isoflavanone and Xanthone Derivatives from *Dothideomyces Fungus* CMU-99. *Tetrahedron Lett.* **2015**, *56* (9), 1057–1059. <https://doi.org/10.1016/j.tetlet.2015.01.088>.

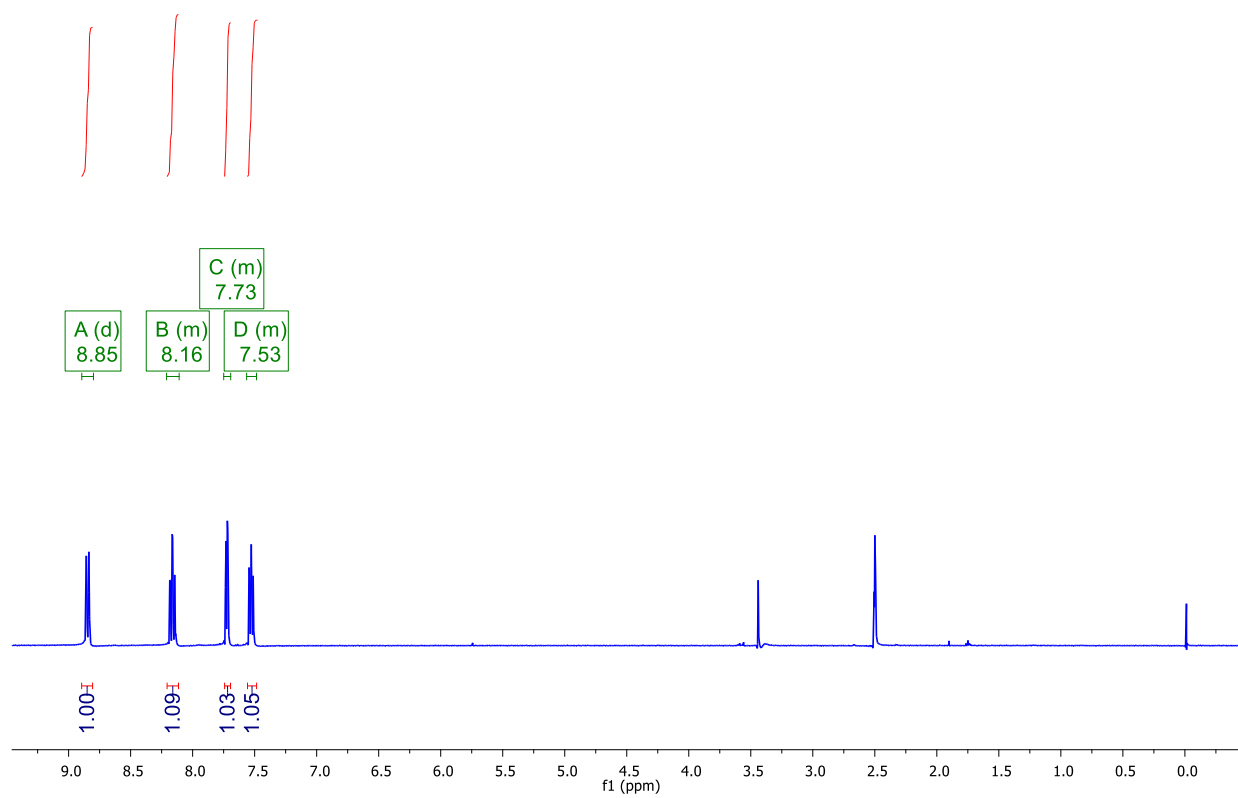
- (265) Da-Cunha, E. V. L.; Dias, C.; Barbosa-Filho, J.; Gray, A. I. Eryvellutinone, an Isoflavanone from the Stem Bark of *Erythrina Vellutina*. *Phytochemistry* **1996**, *43* (6), 1371–1373. [https://doi.org/10.1016/S0031-9422\(96\)00529-8](https://doi.org/10.1016/S0031-9422(96)00529-8).
- (266) Zhou, S.-Y.; Wang, R.; Deng, L.-Q.; Zhang, X.-L.; Chen, M. A New Isoflavanone from *Ficus Tikoua* Bur. *Nat. Prod. Res.* **2018**, *32* (21), 2516–2522. <https://doi.org/10.1080/14786419.2017.1423307>.
- (267) Mutai, P.; Heydenreich, M.; Thoithi, G.; Mugumbate, G.; Chibale, K.; Yenesew, A. 3-Hydroxyisoflavanones from the Stem Bark of *Dalbergia Melanoxylon*: Isolation, Antimycobacterial Evaluation and Molecular Docking Studies. *Phytochem. Lett.* **2013**, *6* (4), 671–675. <https://doi.org/10.1016/j.phytol.2013.08.018>.
- (268) Manvar, D.; Fernandes, T. de A.; Domingos, J. L. O.; Baljinnyam, E.; Basu, A.; Junior, E. F. T.; Costa, P. R. R.; Kaushik-Basu, N. Synthesis and Biological Evaluation of α -Aryl- α -Tetralone Derivatives as Hepatitis C Virus Inhibitors. *Eur. J. Med. Chem.* **2015**, *93*, 51–54. <https://doi.org/10.1016/j.ejmech.2015.01.057>.
- (269) Chen, H.; Zhao, S.; Cheng, S.; Dai, X.; Xu, X.; Yuan, W.; Zhang, X. Synthesis of Novel Pterocarpene Analogues via [3 + 2] Coupling-Elimination Cascade of α , α -Dicyanoolefins with Quinone Monoimines. *J. Heterocycl. Chem.* **2019**, *56* (5), 1672–1683. <https://doi.org/10.1002/jhet.3543>.
- (270) Semmelhack, M. F.; Chong, B. P.; Stauffer, R. D.; Rogerson, T. D.; Chong, A.; Jones, L. D. Total Synthesis of the Cephalotaxus Alkaloids. Problem in Nucleophilic Aromatic Substitution. *J. Am. Chem. Soc.* **1975**, *97* (9), 2507–2516. <https://doi.org/10.1021/ja00842a031>.
- (271) Kosugi, M.; Hagiwara, I.; Sumiya, T.; Migita, T. Arylation and 1-Alkenylation on α -Position of Ketones via Tributyltin Enolates Catalyzed by Palladium Complex. *Bull. Chem. Soc. Jpn.* **1984**, *57* (1), 242–246. <https://doi.org/10.1246/bcsj.57.242>.
- (272) Palucki, M.; Buchwald, S. L. Palladium-Catalyzed α -Arylation of Ketones. *J. Am. Chem. Soc.* **1997**, *119* (45), 11108–11109. <https://doi.org/10.1021/ja972593s>.
- (273) Xu, Y.; Su, T.; Huang, Z.; Dong, G. Practical Direct α -Arylation of Cyclopentanones by Palladium/Enamine Cooperative Catalysis. *Angew. Chemie* **2016**, *128* (7), 2605–2609. <https://doi.org/10.1002/ange.201510638>.
- (274) Marelli, E.; Corpet, M.; Davies, S. R.; Nolan, S. P. Palladium-Catalyzed α -Arylation of Arylketones at Low Catalyst Loadings. *Chem. - A Eur. J.* **2014**, *20*

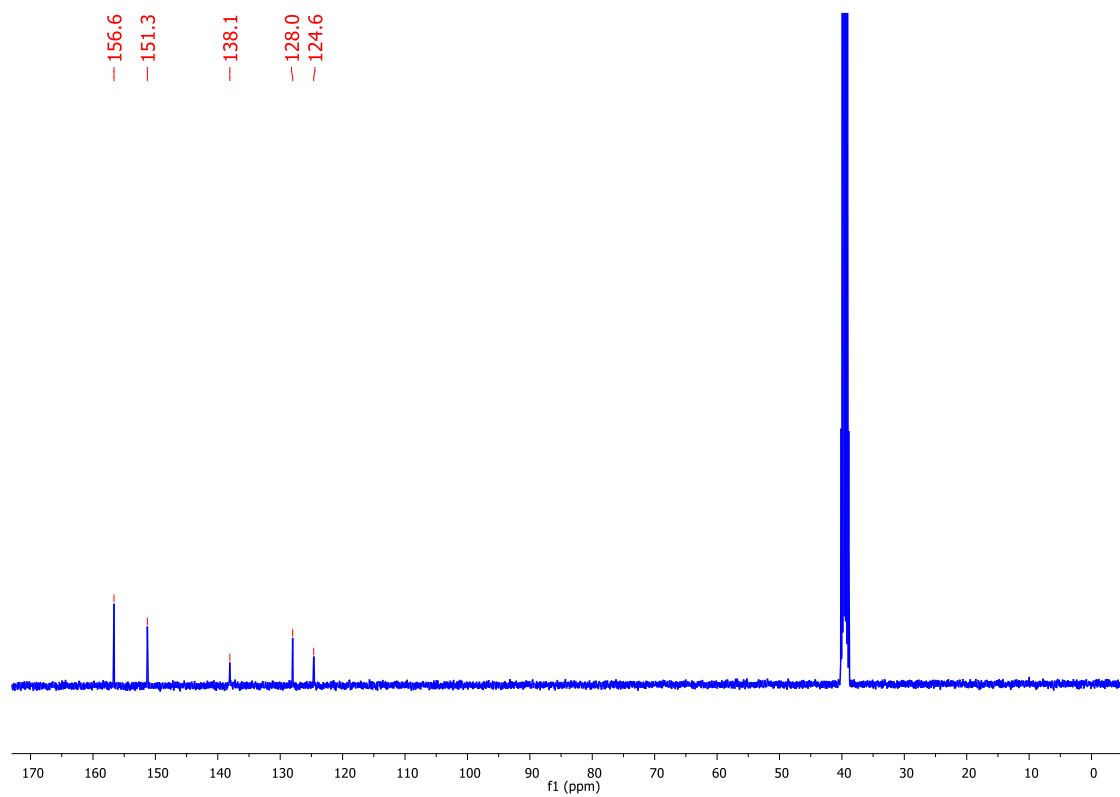
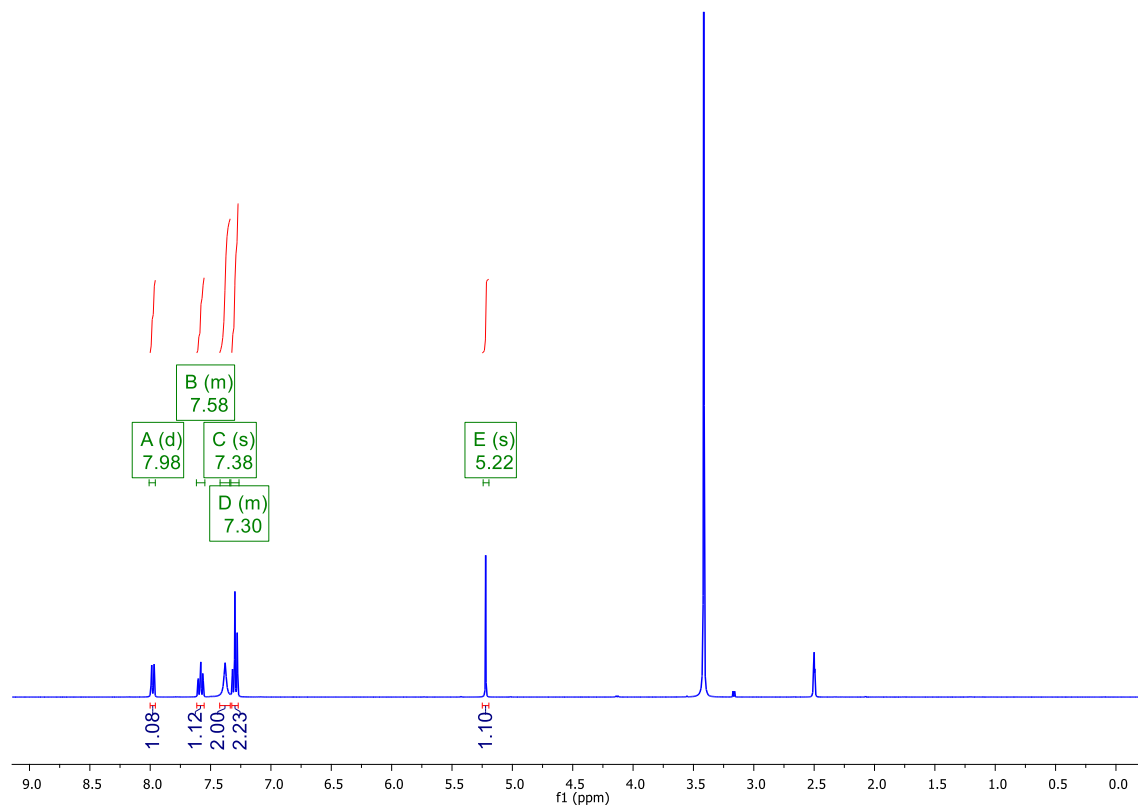
- (52), 17272–17276. <https://doi.org/10.1002/chem.201404900>.
- (275) Li, J.; Wang, Z.-X. Nickel Catalyzed α -Arylation of Ketones with Aryltrimethylammonium Triflates. *Org. Biomol. Chem.* **2016**, *14* (31), 7579–7584. <https://doi.org/10.1039/C6OB01299J>.
- (276) Xu, Q.-L.; Gao, H.; Yousufuddin, M.; Ess, D. H.; Kürti, L. Aerobic, Transition-Metal-Free, Direct, and Regiospecific Mono- α -Arylation of Ketones: Synthesis and Mechanism by DFT Calculations. *J. Am. Chem. Soc.* **2013**, *135* (38), 14048–14051. <https://doi.org/10.1021/ja4074563>.
- (277) Cook, G. *Enamines: Synthesis, Structure, and Reactions*; CRC Press: New York, 1987.
- (278) Pousse, G.; Cavelier, F. Le; Humphreys, L.; Rouden, J.; Blanchet, J. Brønsted Acid Catalyzed Asymmetric Aldol Reaction: A Complementary Approach to Enamine Catalysis. *Org. Lett.* **2010**, *12* (16), 3582–3585. <https://doi.org/10.1021/ol101176j>.
- (279) Bardagi, J. I.; Ghosh, I.; Schmalzbauer, M.; Ghosh, T.; König, B. Anthraquinones as Photoredox Catalysts for the Reductive Activation of Aryl Halides. *European J. Org. Chem.* **2018**, *2018* (1), 34–40. <https://doi.org/10.1002/ejoc.201701461>.
- (280) van der Vlugt, F. A.; Verhoeven, J. W.; Pandit, U. K. Functionalized Enamines. Part XI. Steric Effects in α -Tetralone Enamines. *Recl. des Trav. Chim. des Pays-Bas* **2010**, *89* (12), 1258–1266. <https://doi.org/10.1002/recl.19700891205>.
- (281) Sollenberger, P. Y.; Martin, R. B. Mechanism of Enamine Hydrolysis. *J. Am. Chem. Soc.* **1970**, *92* (14), 4261–4270. <https://doi.org/10.1021/ja00717a021>.
- (282) Rohe, S.; McCallum, T.; Morris, A. O.; Barriault, L. Transformations of Isonitriles with Bromoalkanes Using Photoredox Gold Catalysis. *J. Org. Chem.* **2018**, *83* (17), 10015–10024. <https://doi.org/10.1021/acs.joc.8b01380>.
- (283) Zhu, Z.-F.; Zhang, M.-M.; Liu, F. Radical Alkylation of Isocyanides with Amino Acid-/Peptide-Derived Katritzky Salts via Photoredox Catalysis. *Org. Biomol. Chem.* **2019**, *17* (6), 1531–1534. <https://doi.org/10.1039/C8OB02786B>.
- (284) Pelliccia, S.; Alfano, A. I.; Luciano, P.; Novellino, E.; Massarotti, A.; Tron, G. C.; Ravelli, D.; Giustiniano, M. Photocatalytic Isocyanide-Based Multicomponent Domino Cascade toward the Stereoselective Formation of Iminofurans. *J. Org. Chem.* **2020**, *85* (4), 1981–1990. <https://doi.org/10.1021/acs.joc.9b02709>.

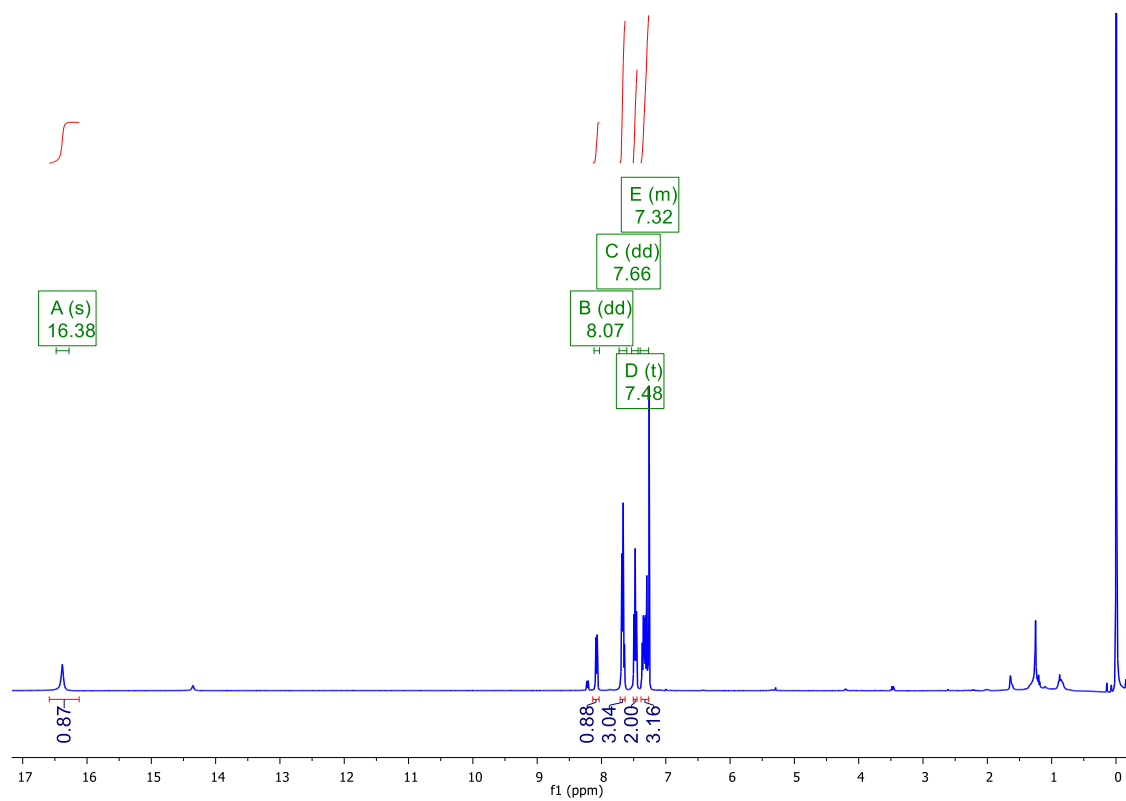
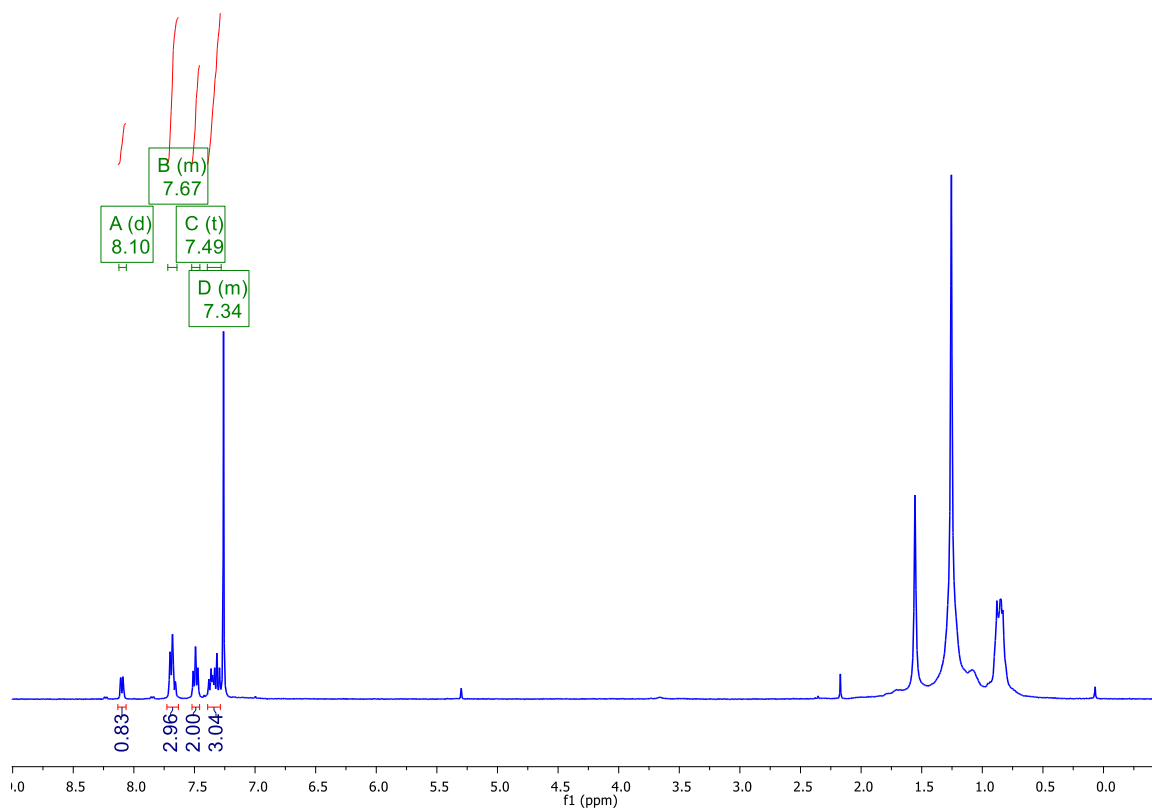
- (285) Zhang, Z.; Tang, X.; Dolbier, W. R. Photoredox-Catalyzed Tandem Insertion/Cyclization Reactions of Difluoromethyl and 1,1-Difluoroalkyl Radicals with Biphenyl Isocyanides. *Org. Lett.* **2015**, *17* (18), 4401–4403. <https://doi.org/10.1021/acs.orglett.5b02061>.
- (286) Rong, J.; Deng, L.; Tan, P.; Ni, C.; Gu, Y.; Hu, J. Radical Fluoroalkylation of Isocyanides with Fluorinated Sulfones by Visible-Light Photoredox Catalysis. *Angew. Chemie* **2016**, *128* (8), 2793–2797. <https://doi.org/10.1002/ange.201510533>.
- (287) Isse, A. A. .; Gennaro, A. Electrochemical Reduction of Benzyl Bromide in the Presence of Carbon Dioxide. *Indian J Chem A* **2003**, *42* (4), 751–757.
- (288) Lujan-Montelongo, J. A.; Estevez, A. O.; Fleming, F. F. Alkyl Sulfinates: Formal Nucleophiles for Synthesizing TosMIC Analogs. *European J. Org. Chem.* **2015**, *2015* (7), 1602–1605. <https://doi.org/10.1002/ejoc.201403615>.
- (289) Xu, C.; Guo, W.-H.; He, X.; Guo, Y.-L.; Zhang, X.-Y.; Zhang, X. Difluoromethylation of (Hetero)Aryl Chlorides with Chlorodifluoromethane Catalyzed by Nickel. *Nat. Commun.* **2018**, *9* (1), 1170. <https://doi.org/10.1038/s41467-018-03532-1>.
- (290) Mishra, S.; Halpani, C. G.; Patel, S. Nickel-Catalyzed Heck Reaction of Aryl Halides and Terminal Olefins Using Zinc/Triflate Ligand/DMA/TBAB. *ChemistrySelect* **2019**, *4* (23), 6913–6916. <https://doi.org/10.1002/slct.201901131>.
- (291) Taniguchi, N. Alkyl- or Arylthiolation of Aryl Iodide via Cleavage of the S–S Bond of Disulfide Compound by Nickel Catalyst and Zinc. *J. Org. Chem.* **2004**, *69* (20), 6904–6906. <https://doi.org/10.1021/jo040184q>.
- (292) Krasovskiy, A.; Knochel, P. Convenient Titration Method for Organometallic Zinc, Magnesium, and Lanthanide- Reagents. *Synthesis (Stuttg)*. **2006**, *2006* (05), 0890–0891. <https://doi.org/10.1055/s-2006-926345>.

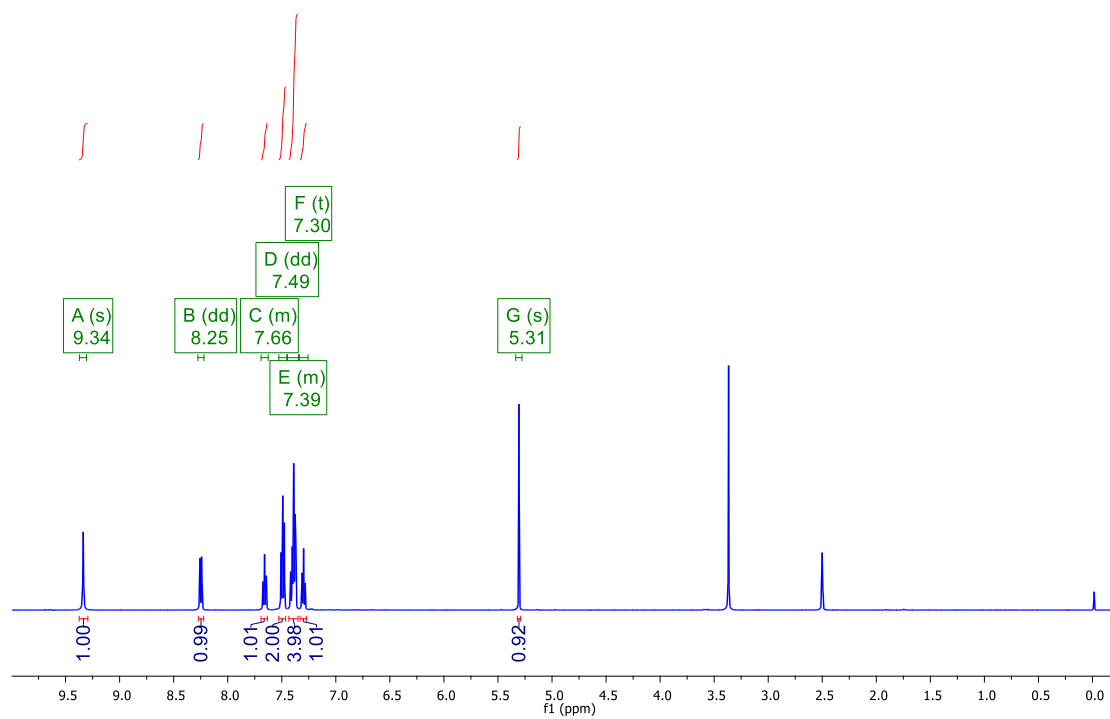
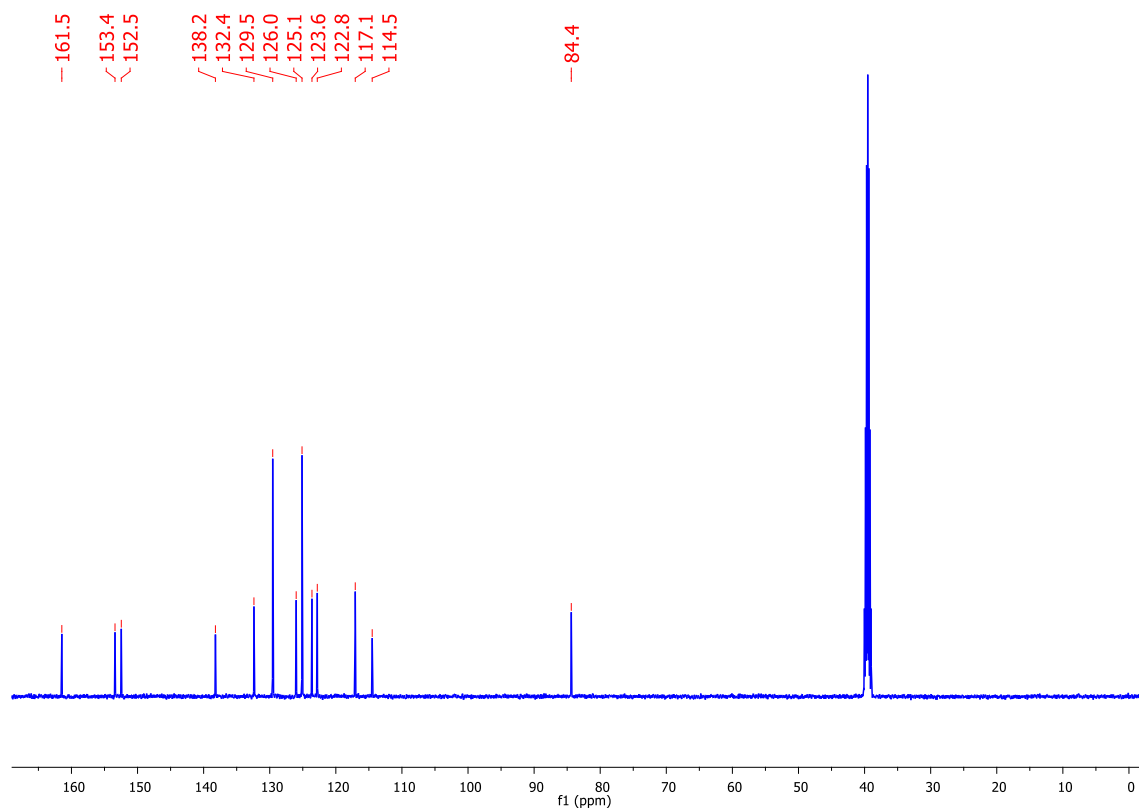
Appendix 1 – NMR spectra

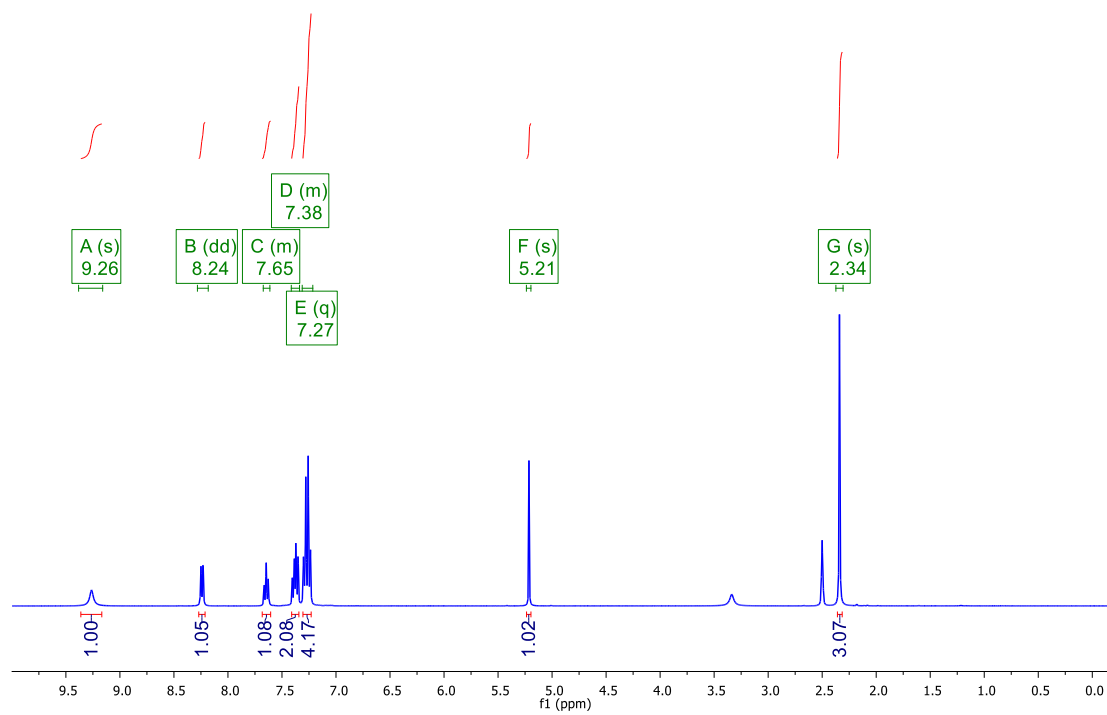
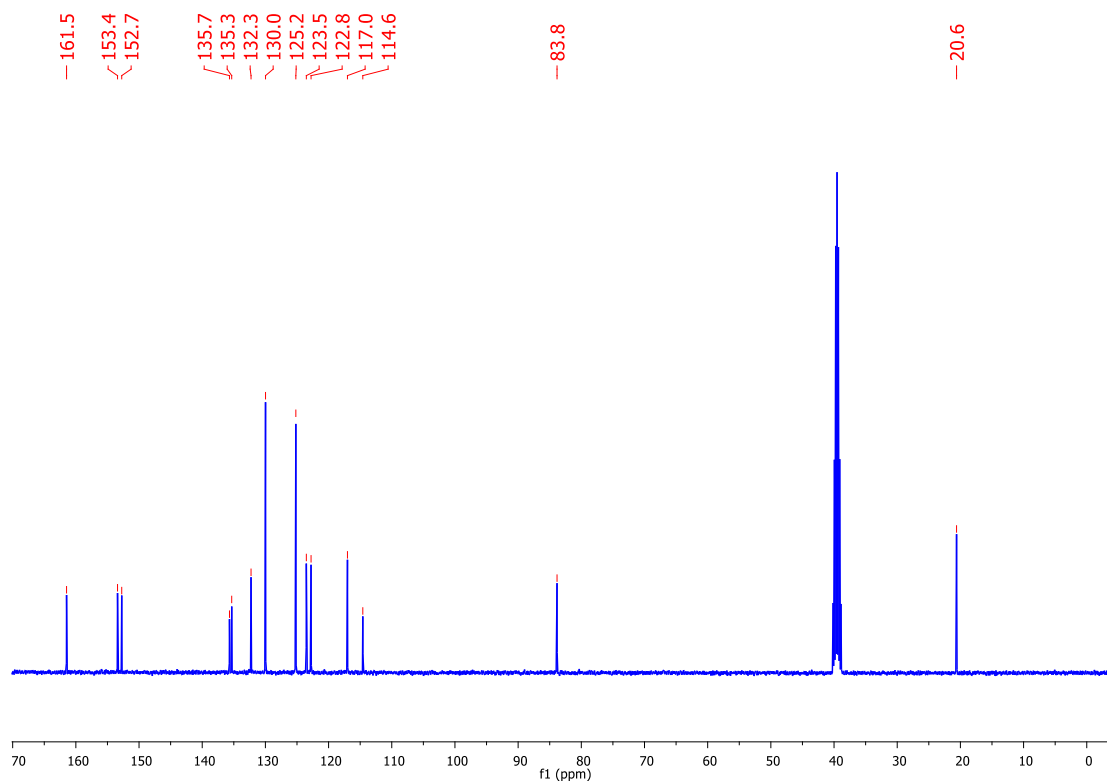
[Ru(bpy)₃]Cl₂ – ¹H NMR

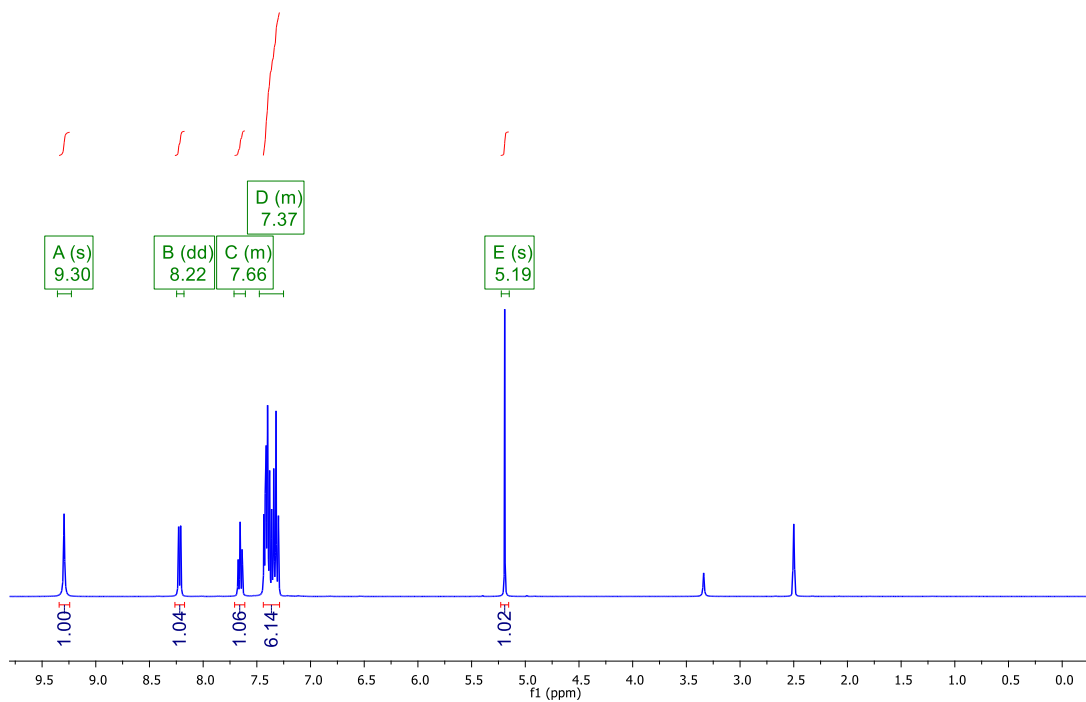
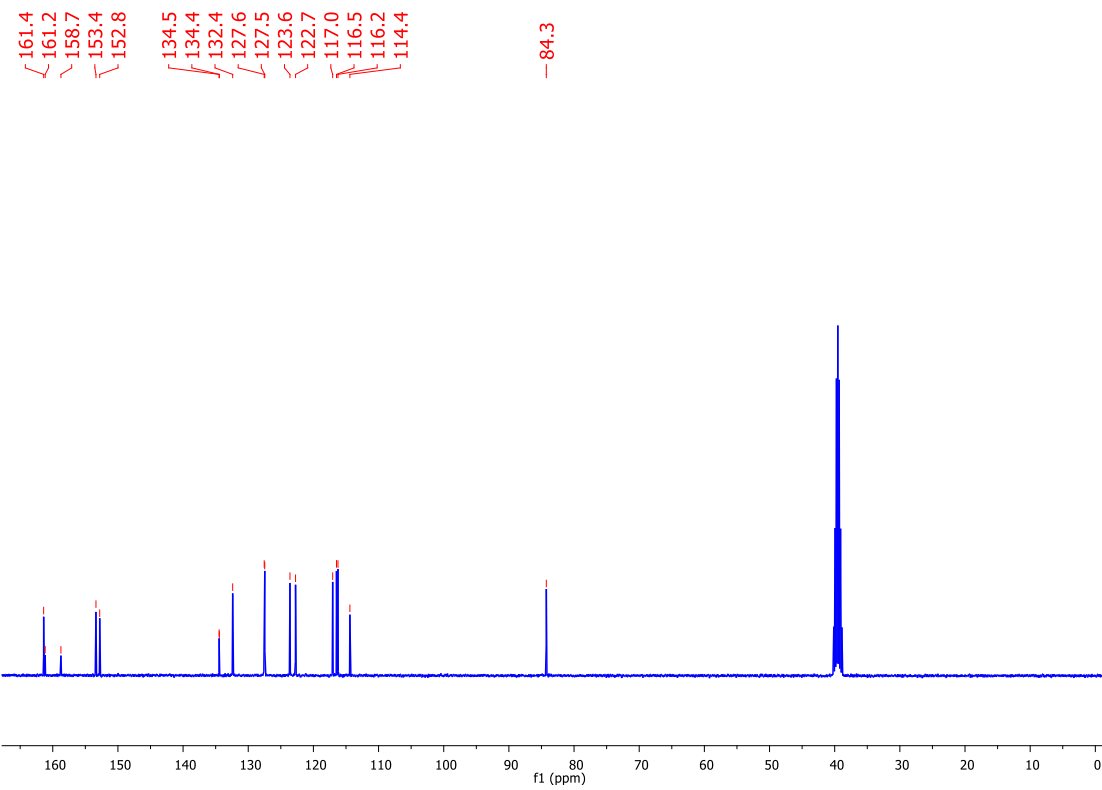


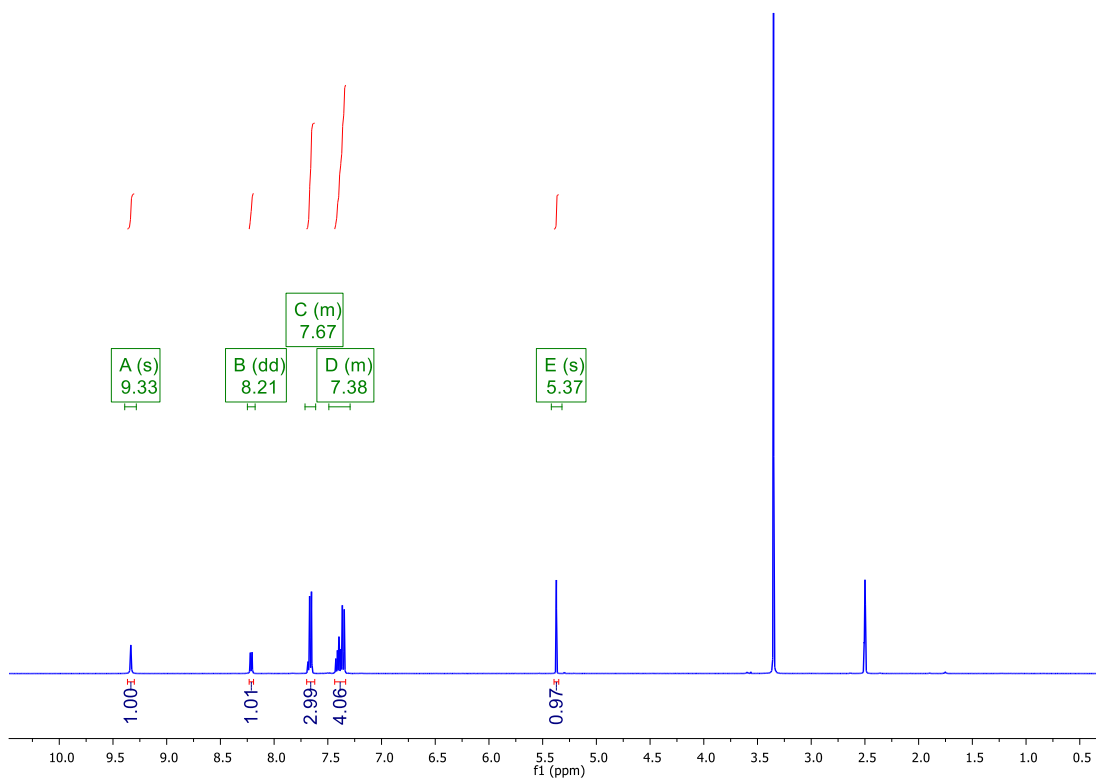
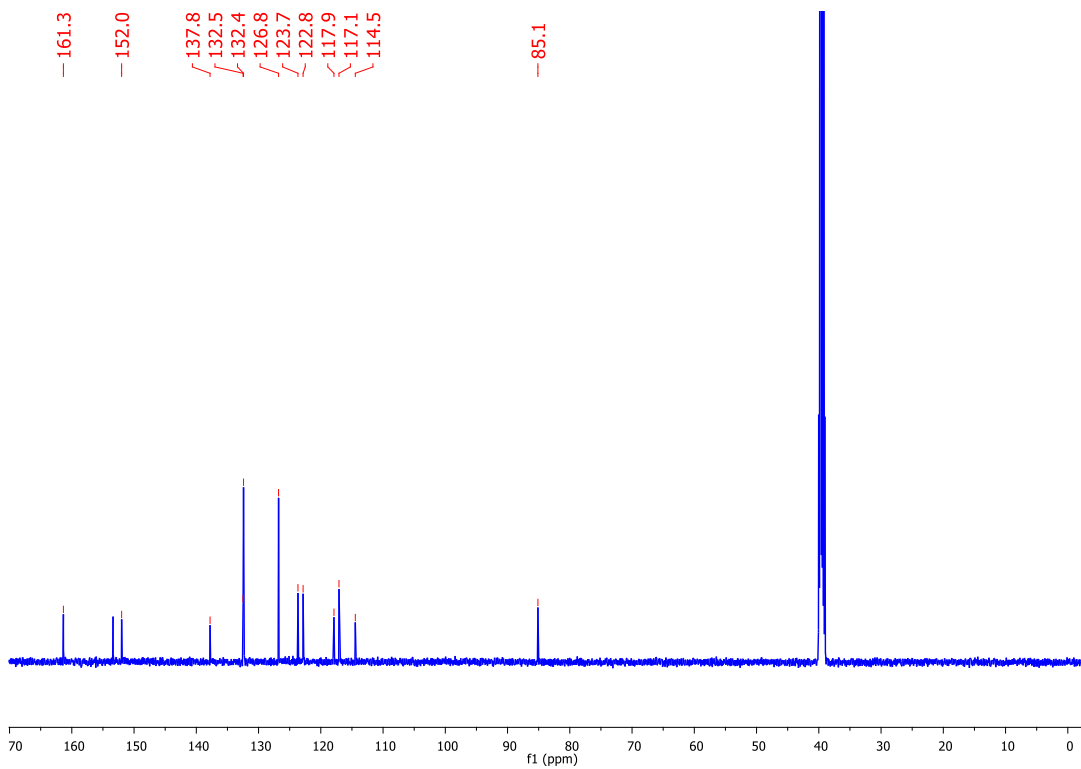
$[\text{Ru}(\text{bpy})_3]\text{Cl}_2 - ^{13}\text{C NMR}$ Compound **356** – $^1\text{H NMR}$ 

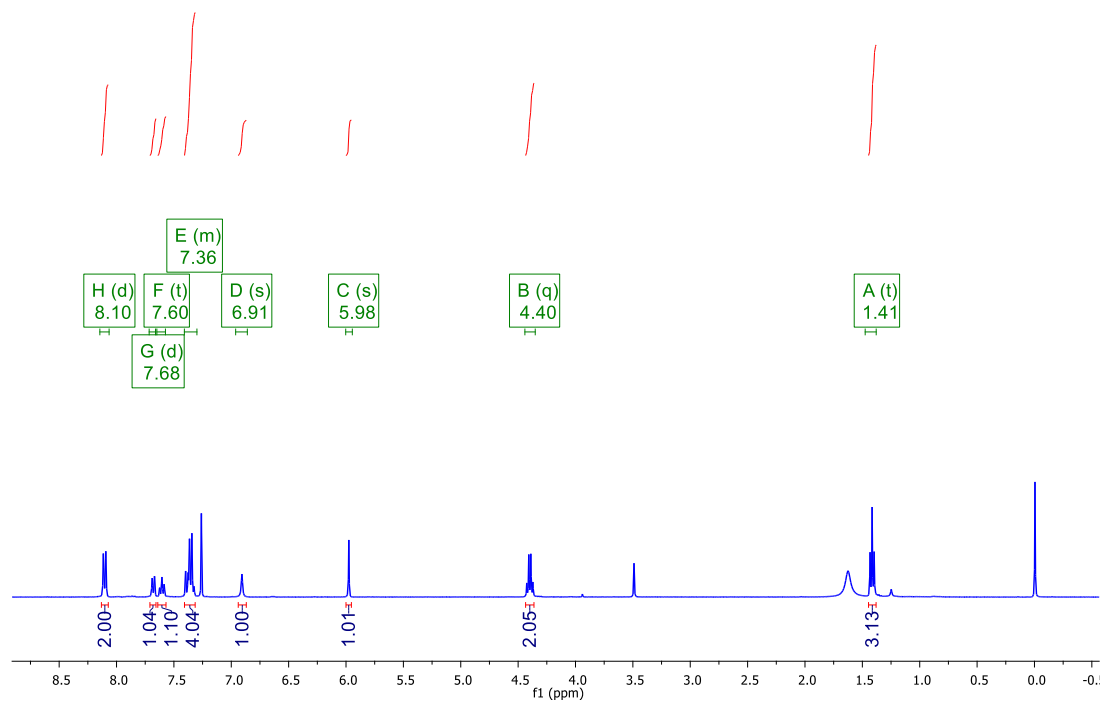
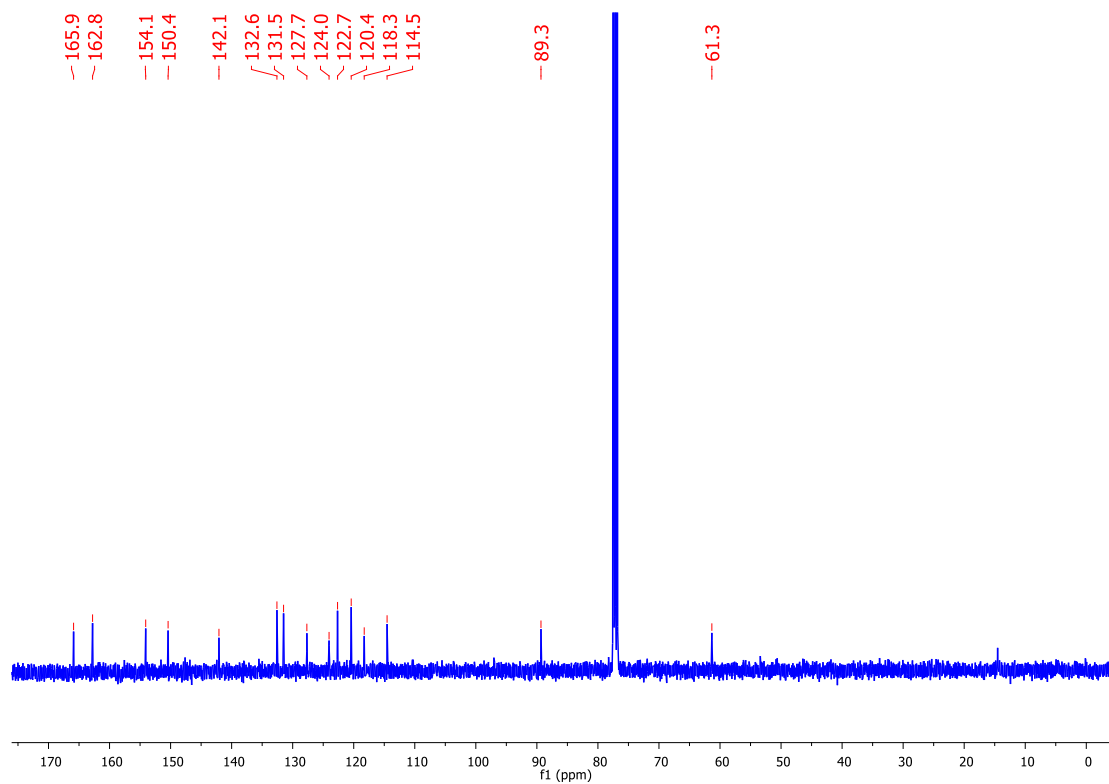
Compound 357 – ^1H NMRCompound 358 – ^1H NMR

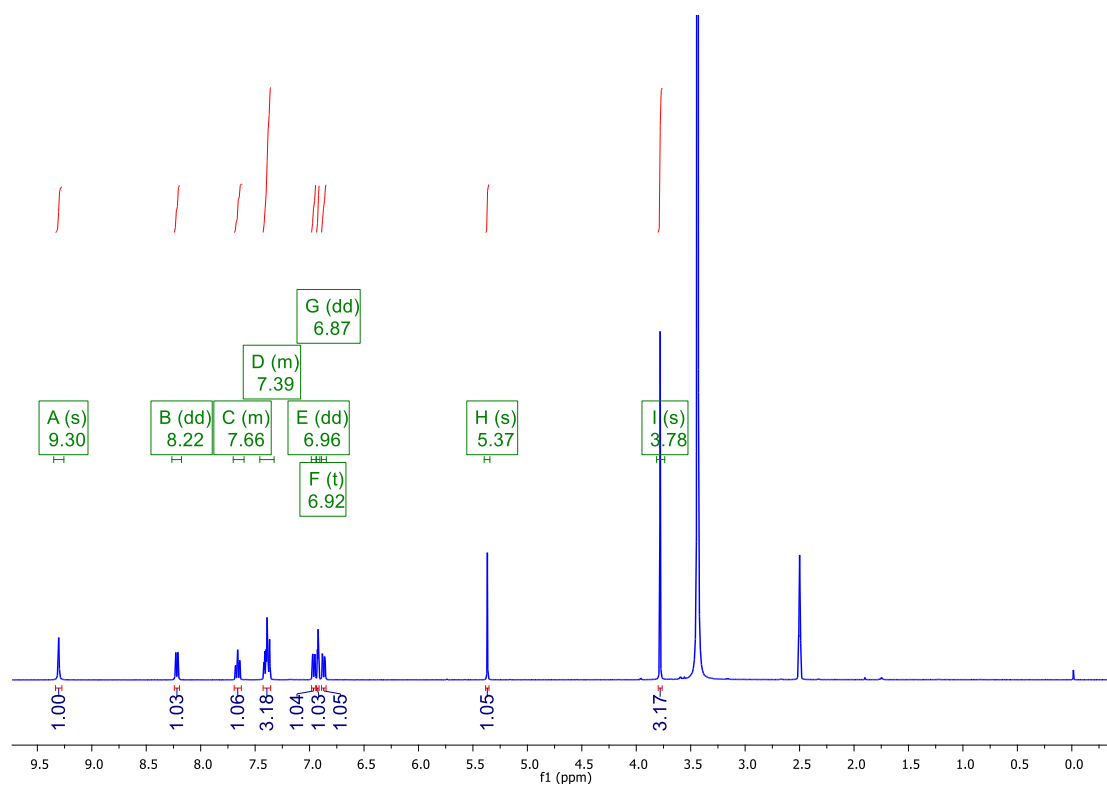
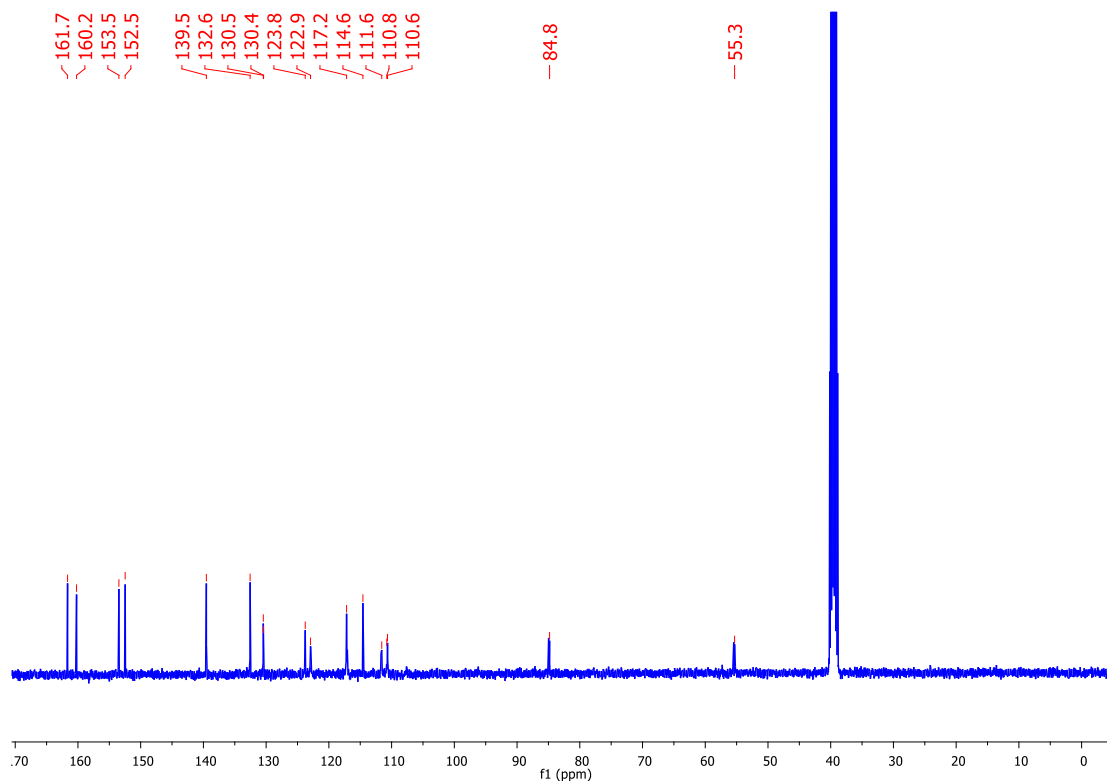
Compound **353a** – ^1H NMRCompound **353a** – ^{13}C NMR

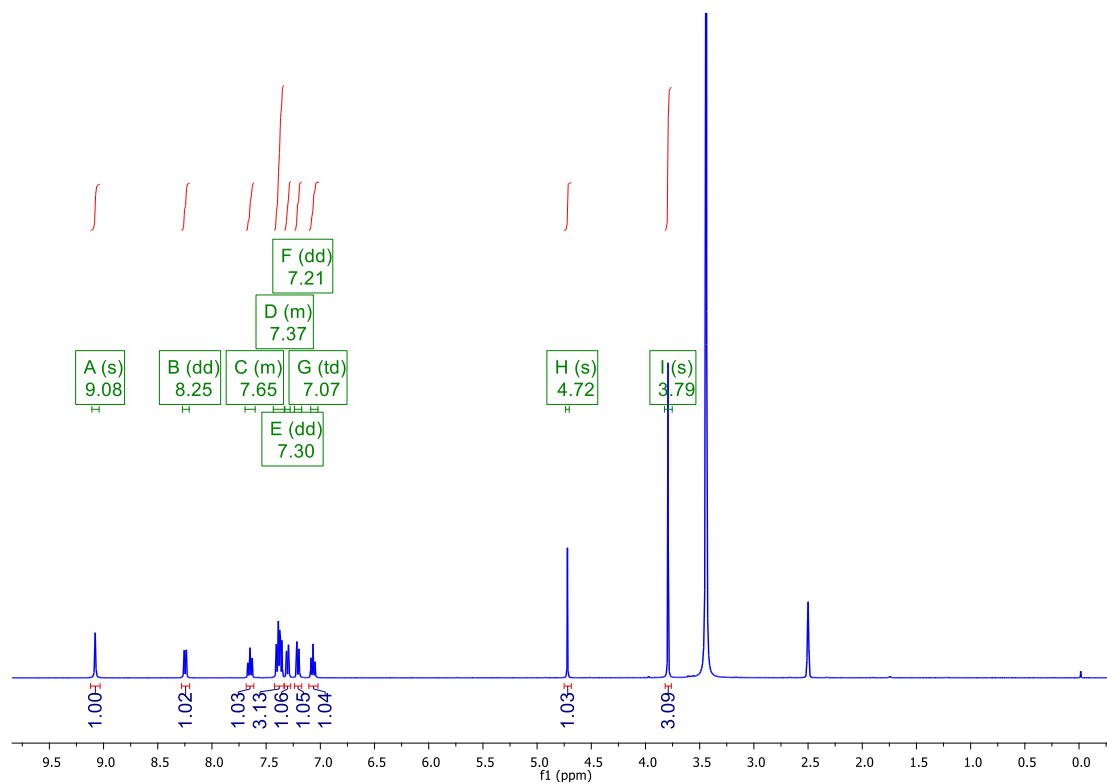
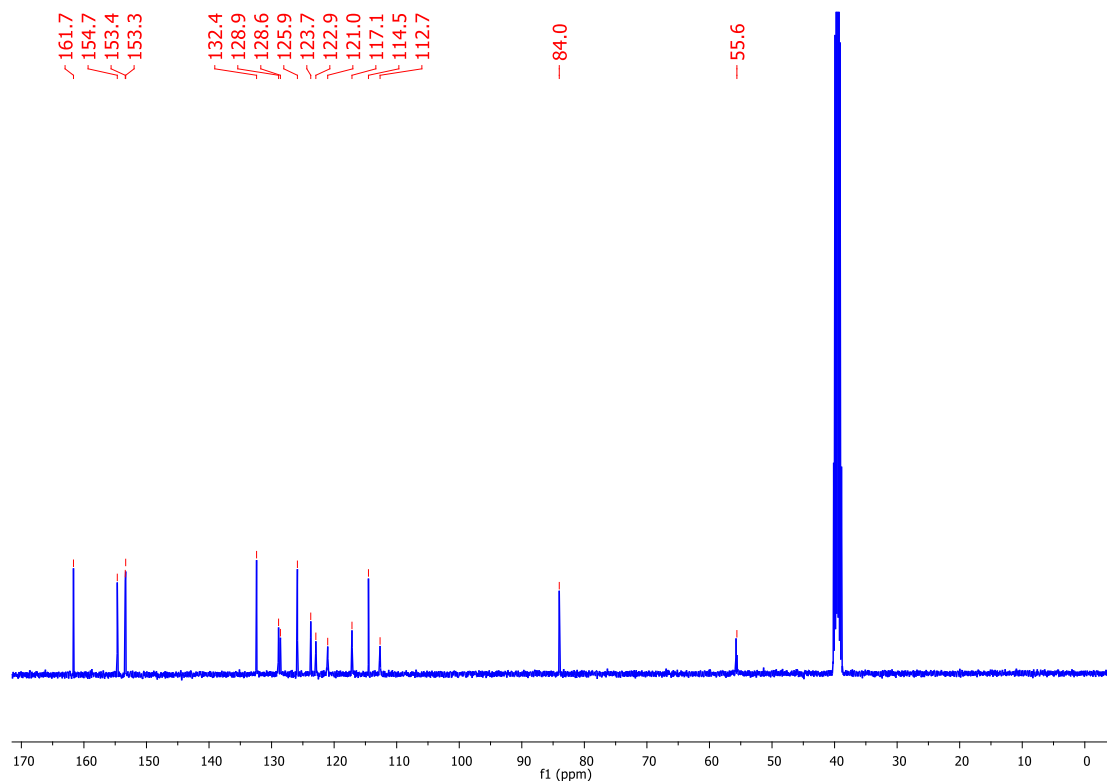
Compound **353c** – ^1H NMRCompound **353c** – ^{13}C NMR

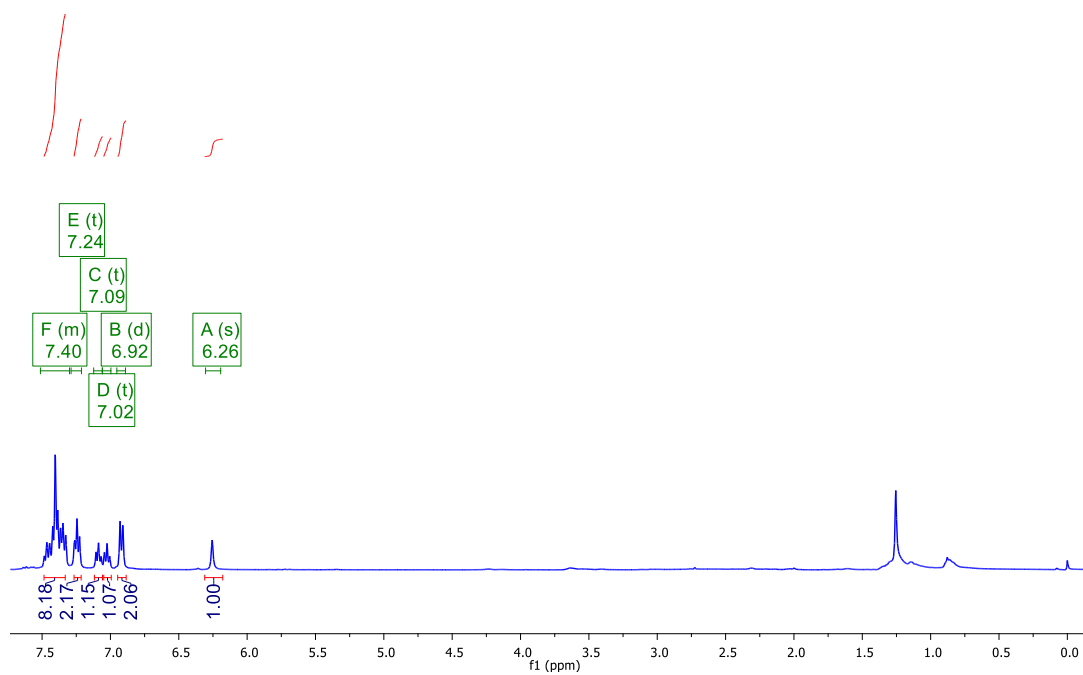
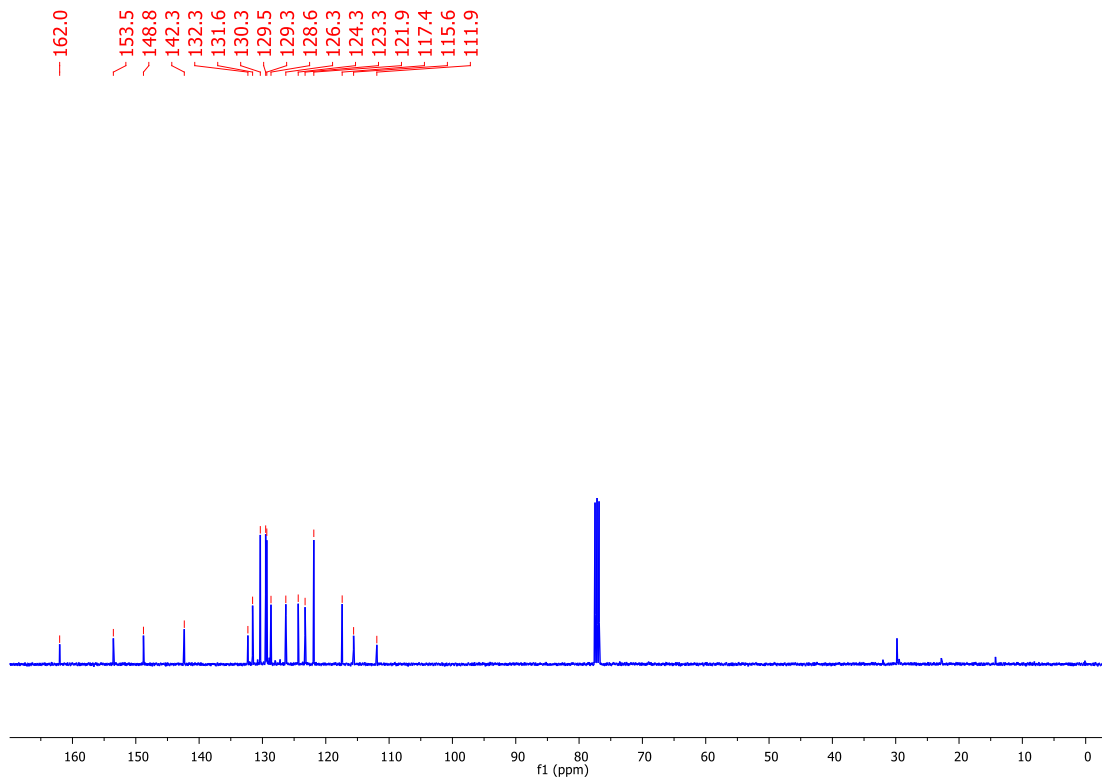
Compound **353d** – ^1H NMRCompound **353d** – ^{13}C NMR

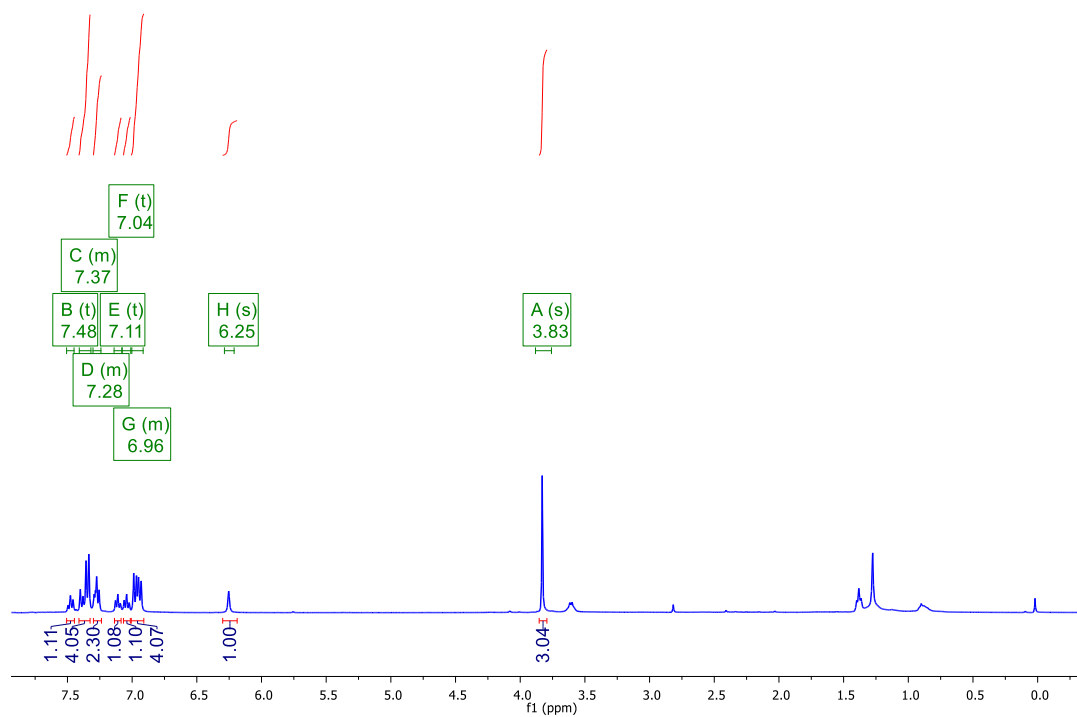
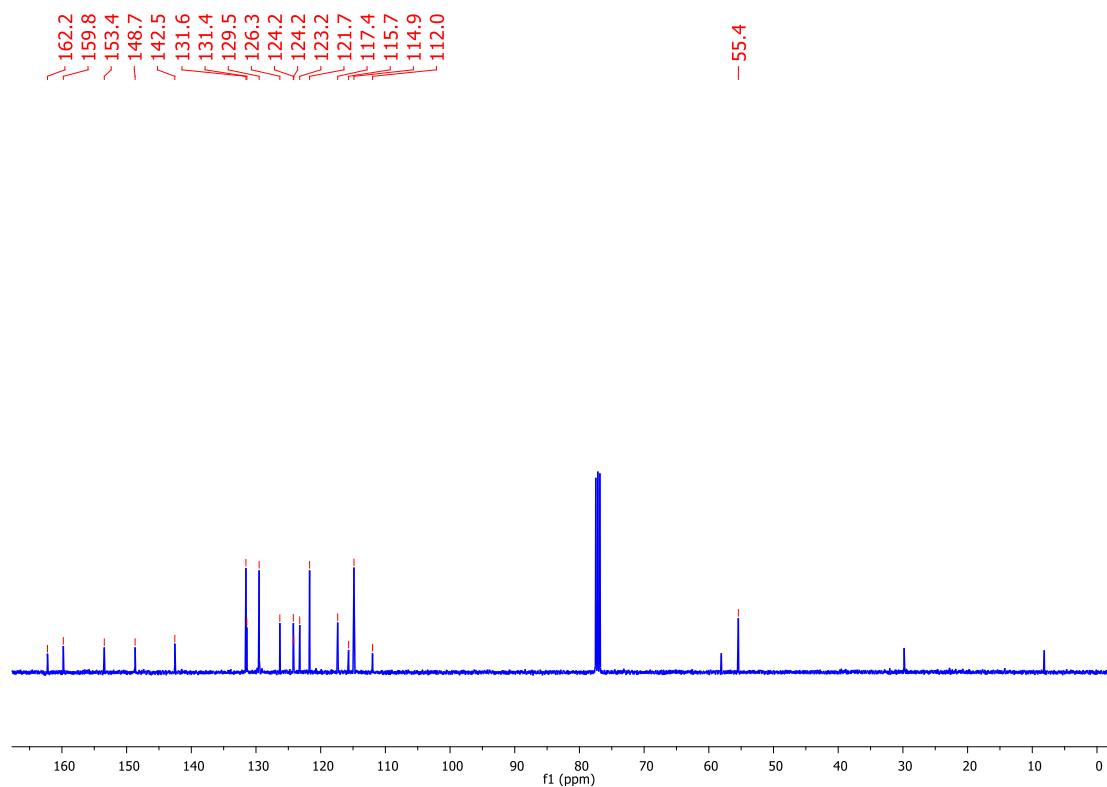
Compound **353e** – ^1H NMRCompound **353e** – ^{13}C NMR

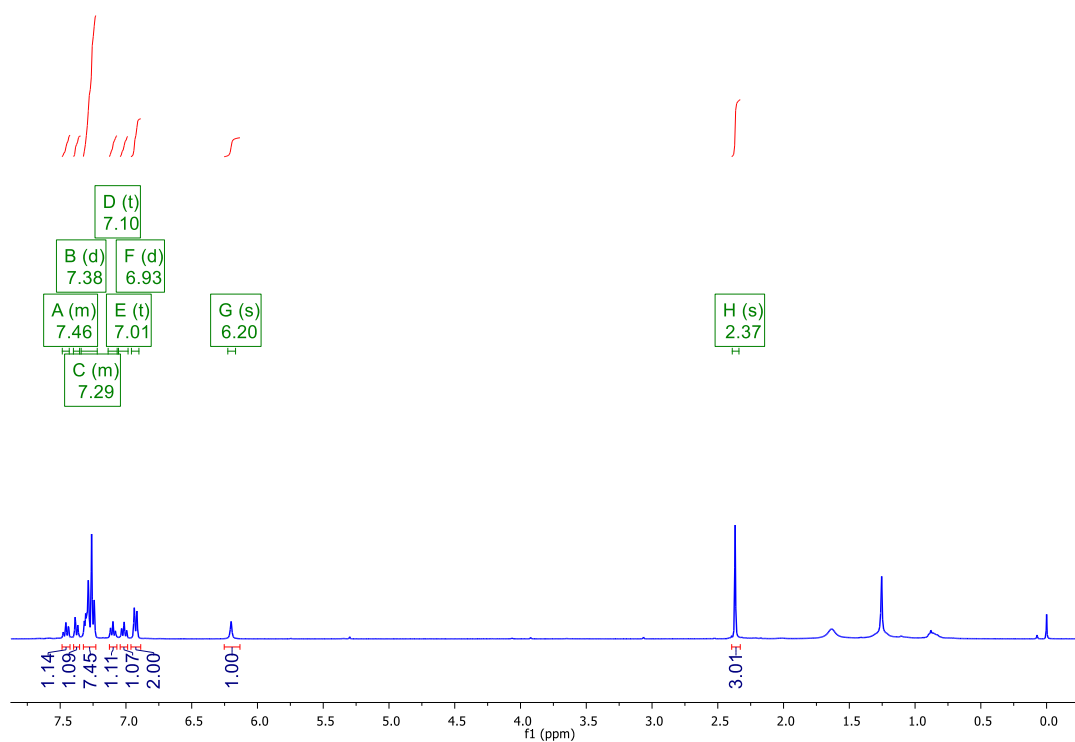
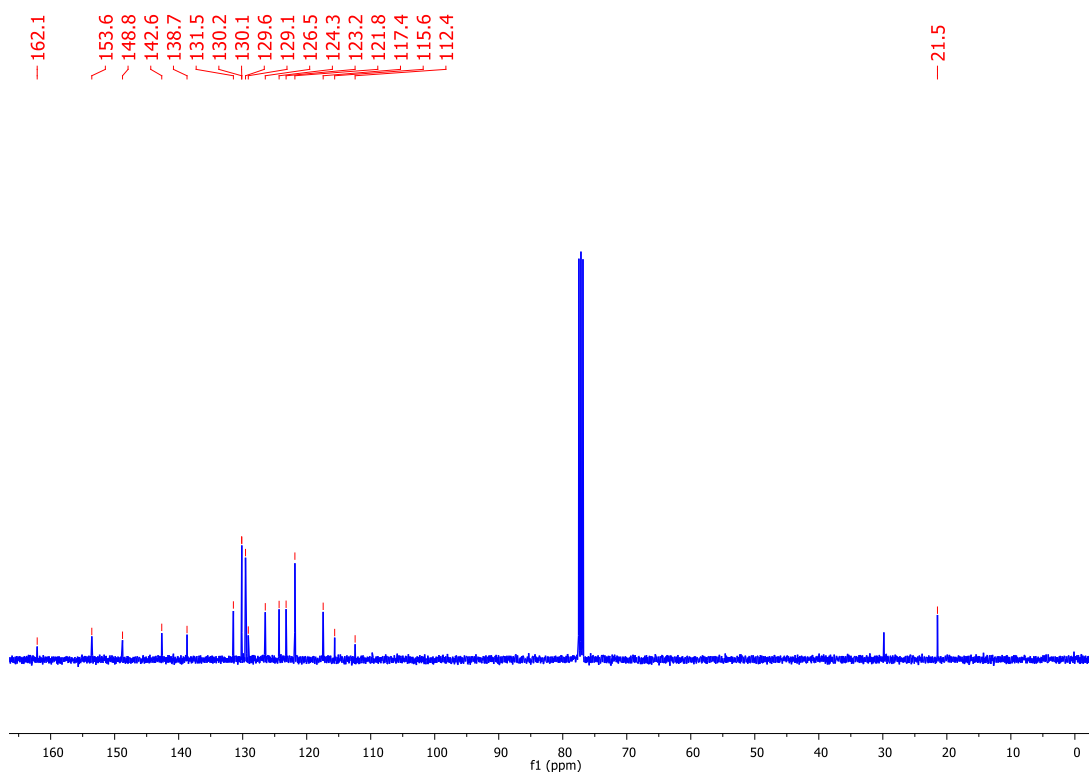
Compound **353f** – ^1H NMRCompound **353f** – ^{13}C NMR

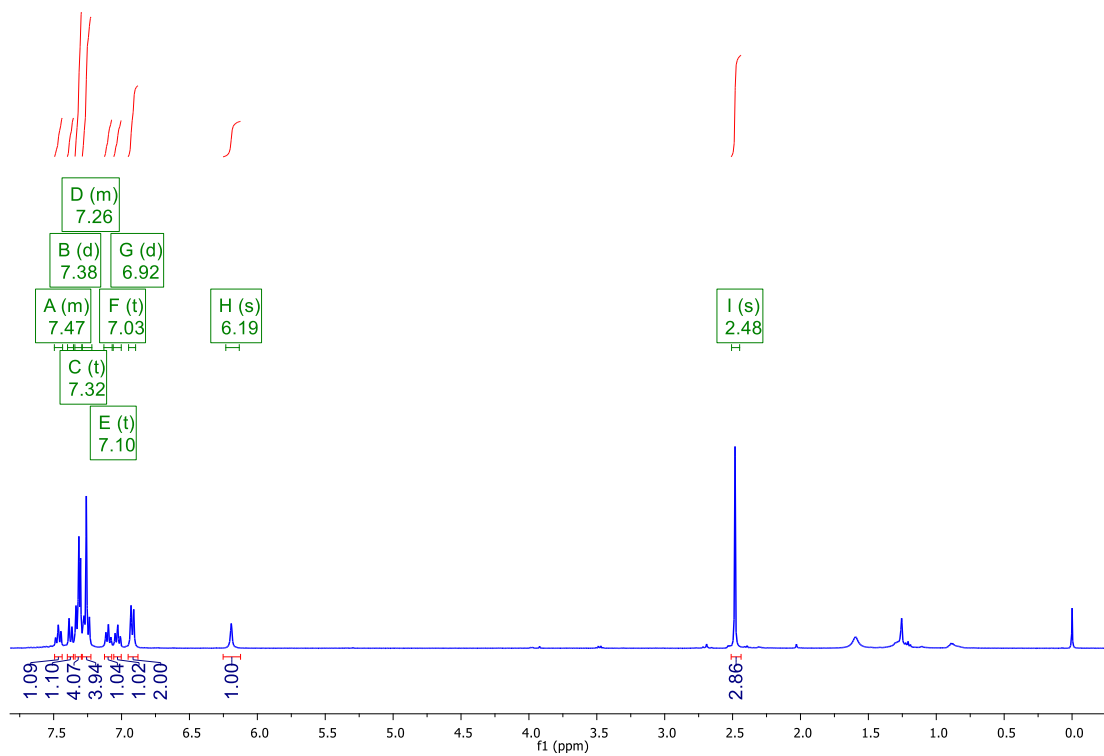
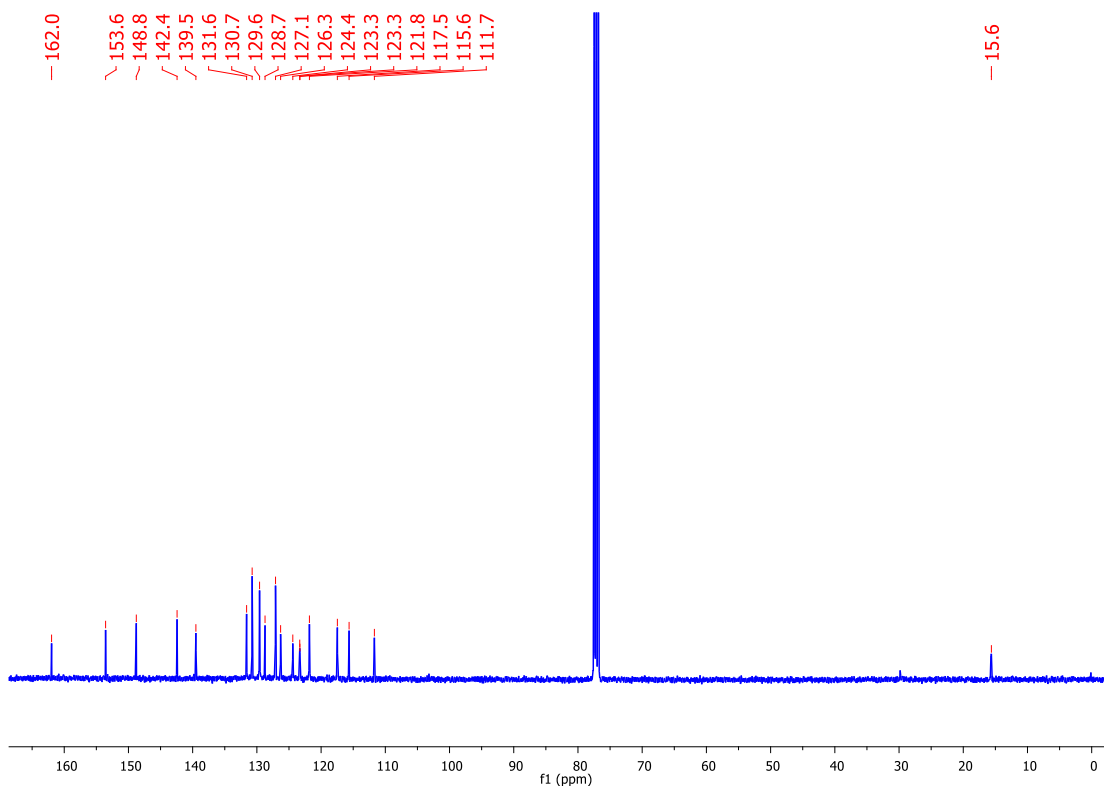
Compound **353h** – ^1H NMRCompound **353h** – ^{13}C NMR

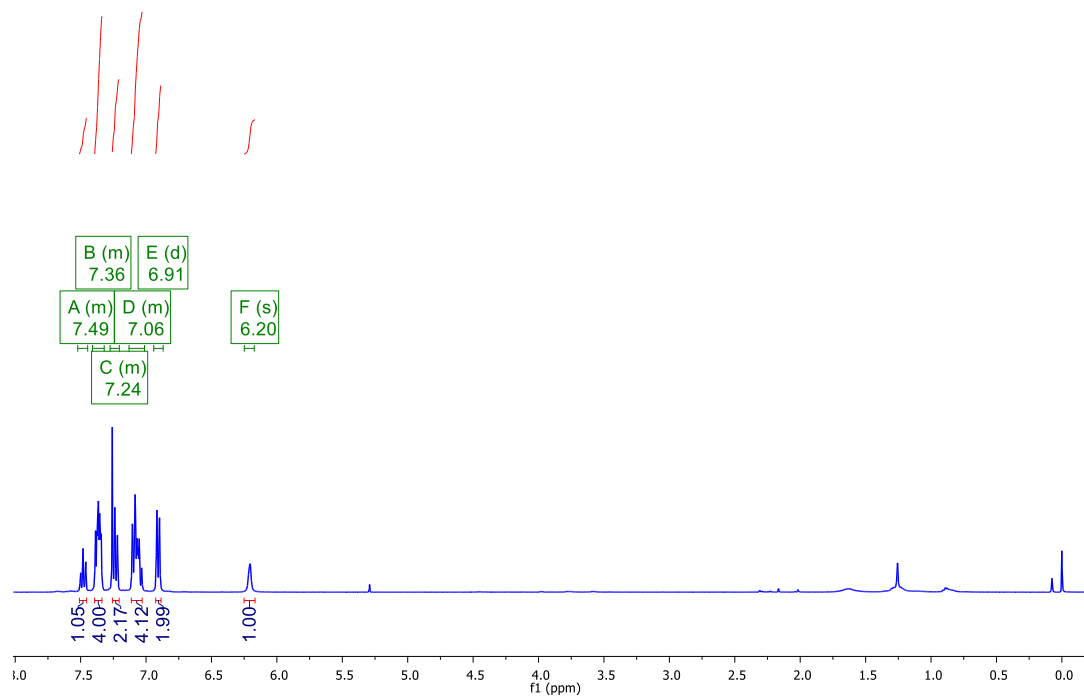
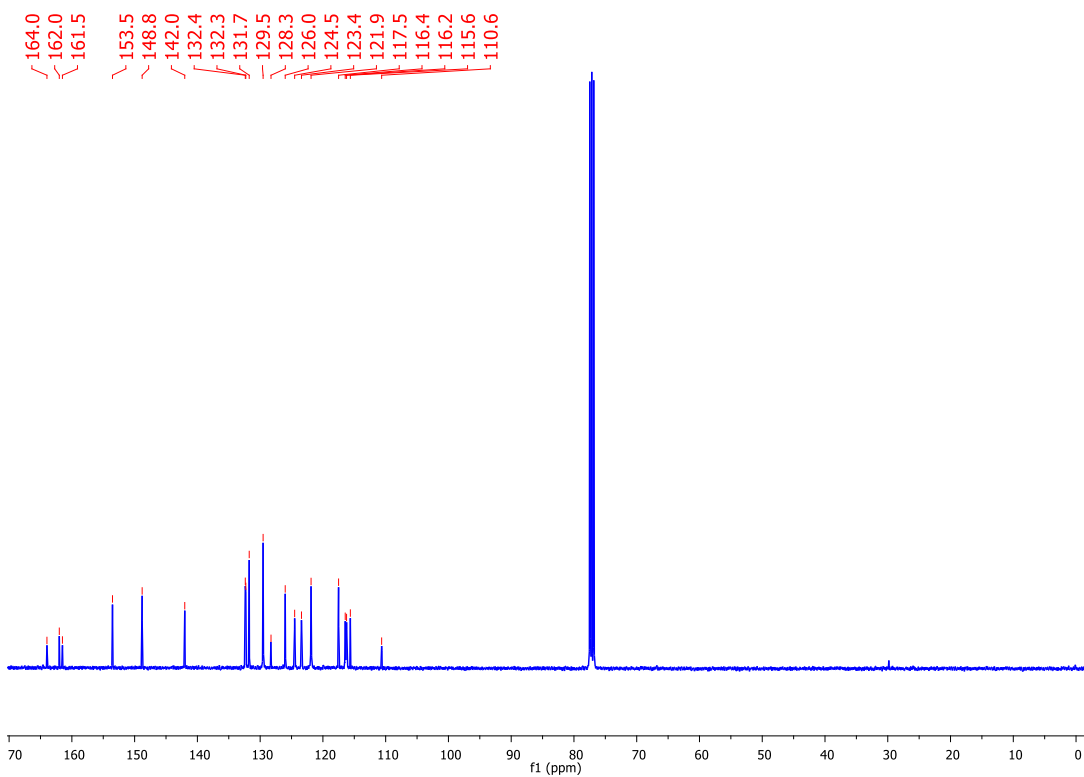
Compound **353i** – ^1H NMRCompound **353i** – ^{13}C NMR

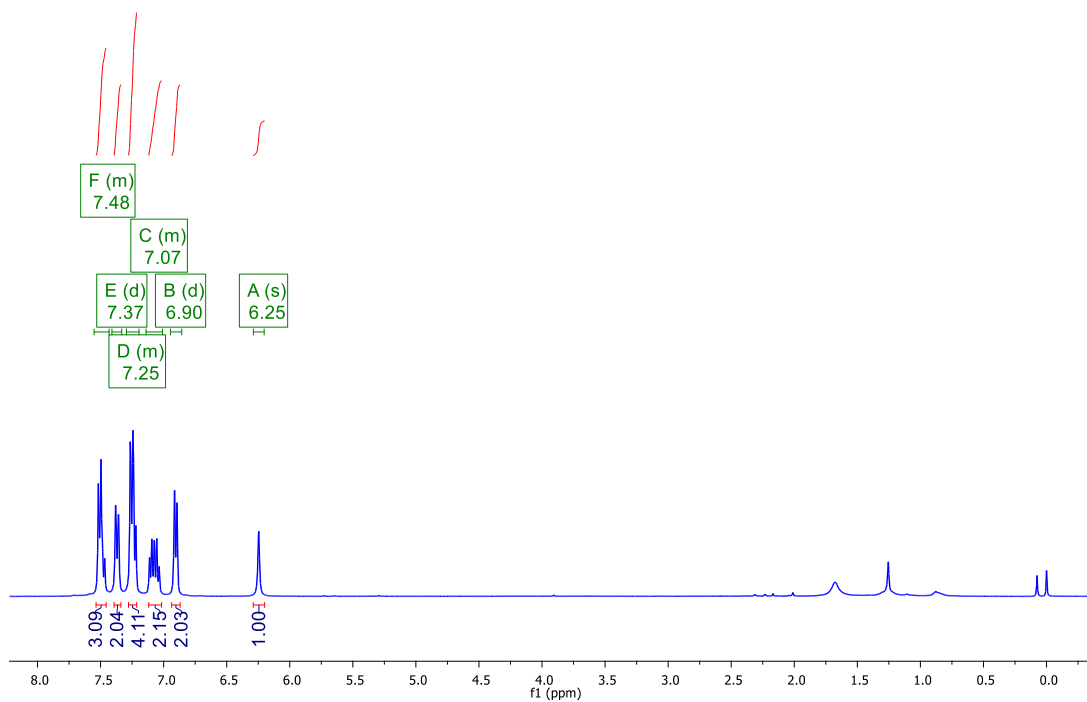
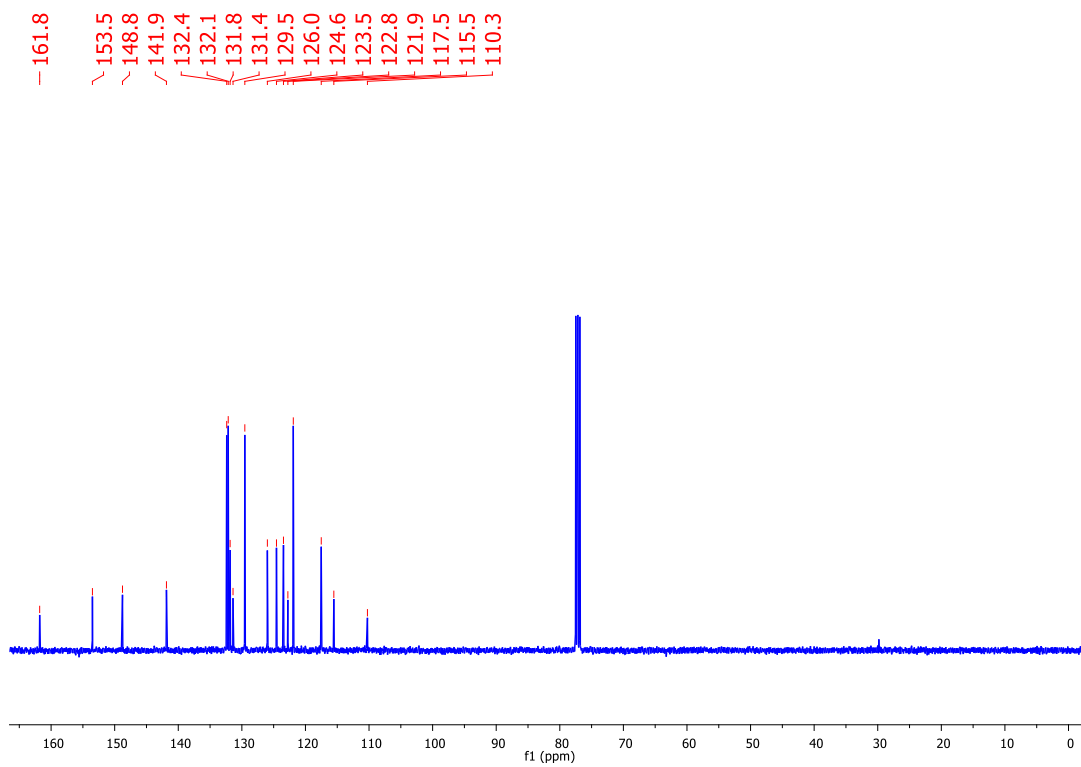
Compound **354a** – ^1H NMRCompound **354a** – ^{13}C NMR

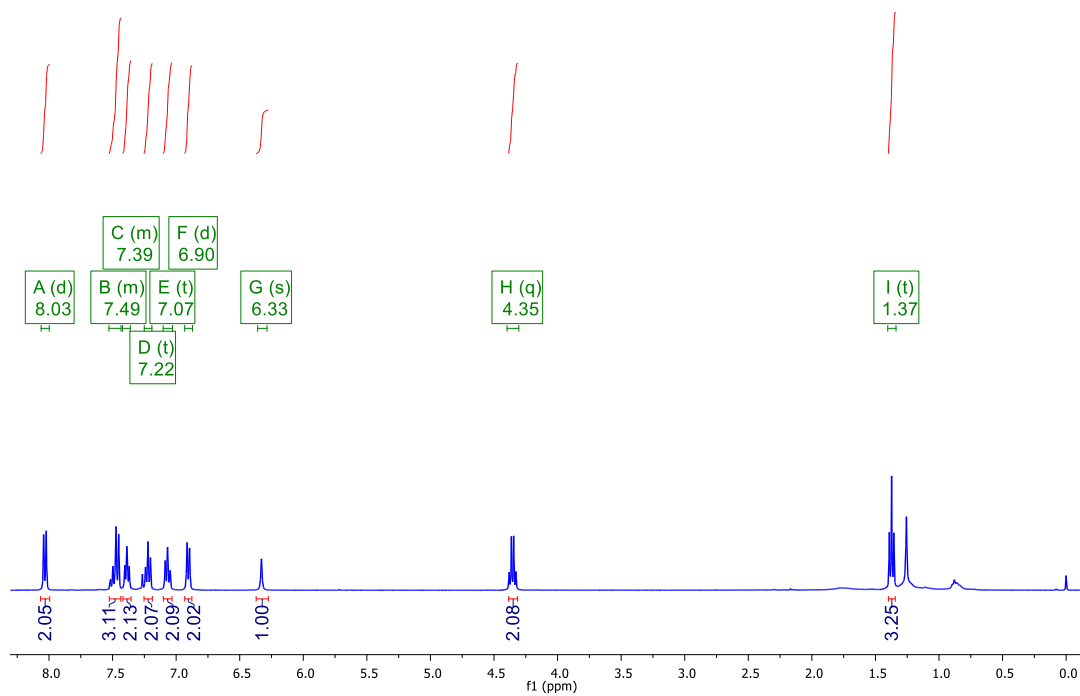
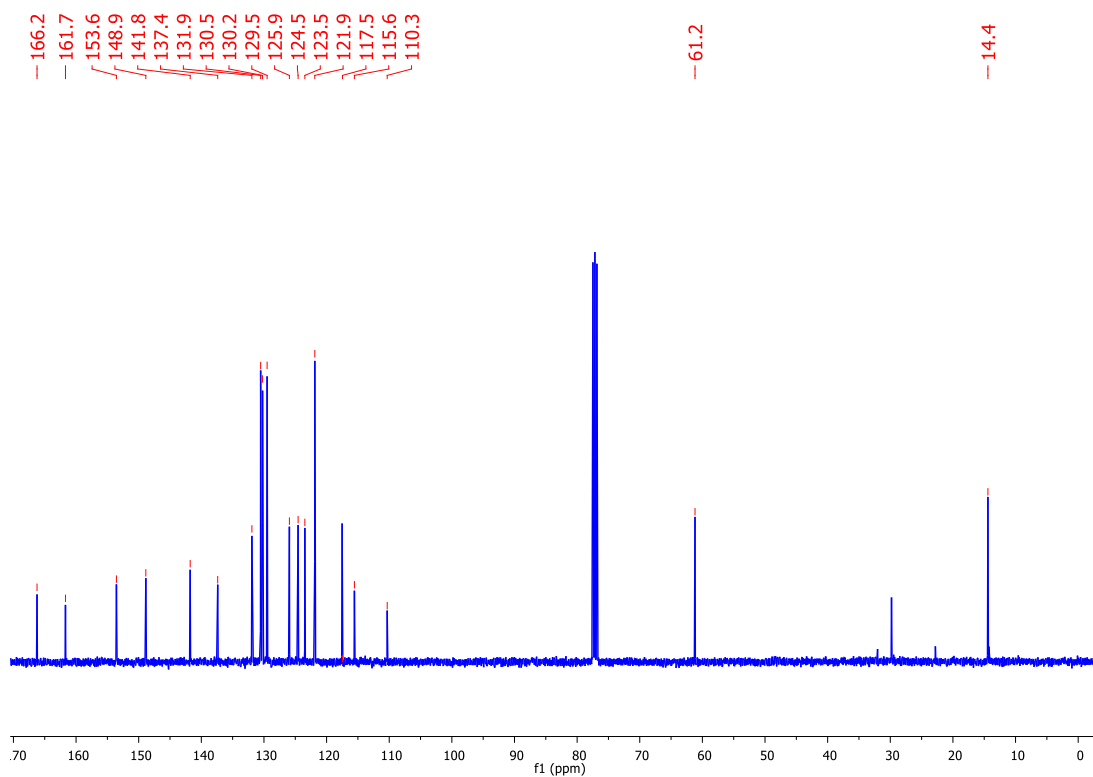
Compound **354b** – ^1H NMRCompound **354b** – ^{13}C NMR

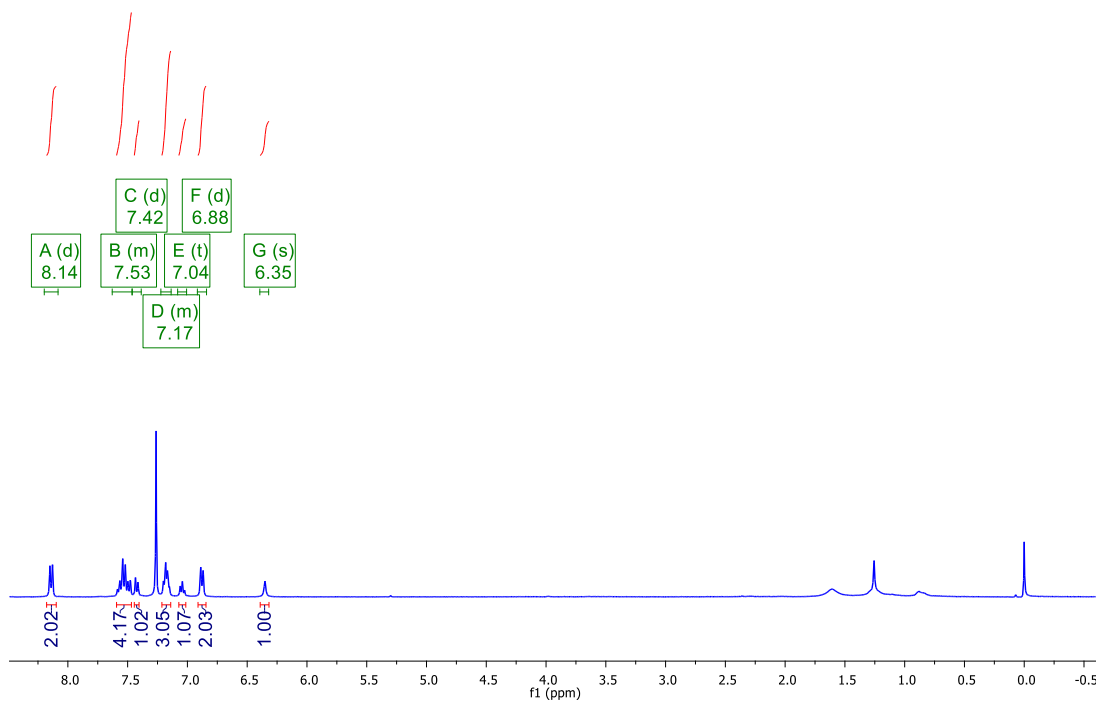
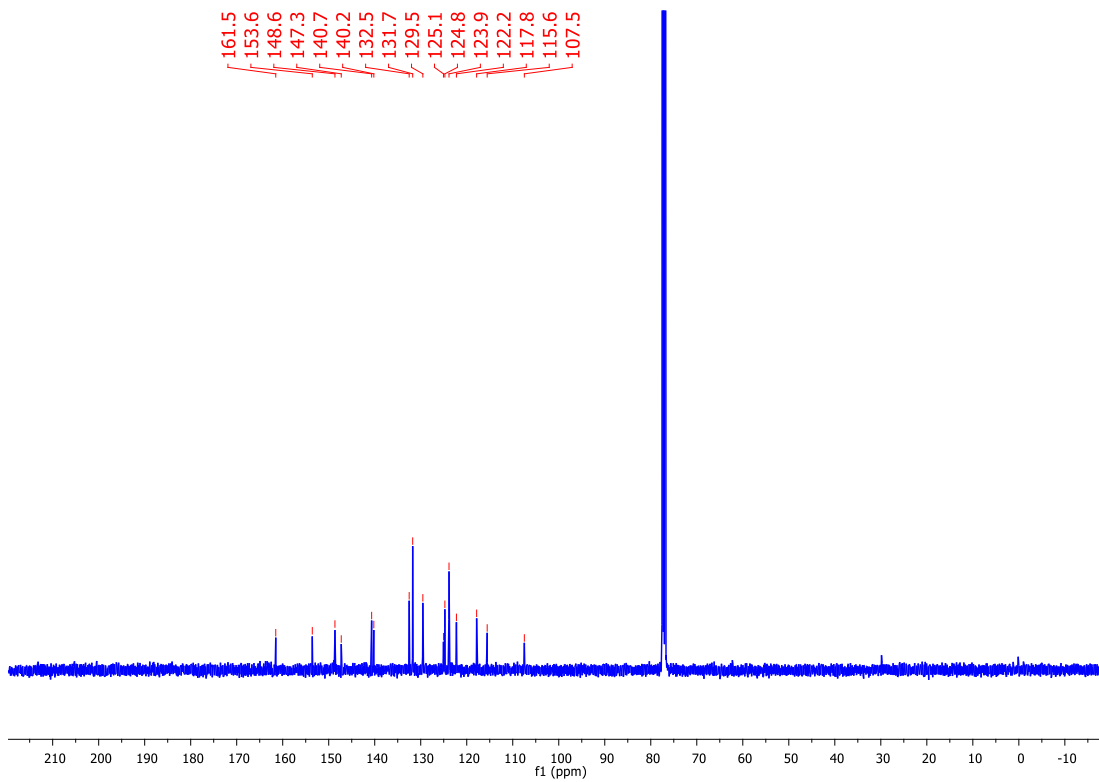
Compound **354c** – ^1H NMRCompound **354c** – ^{13}C NMR

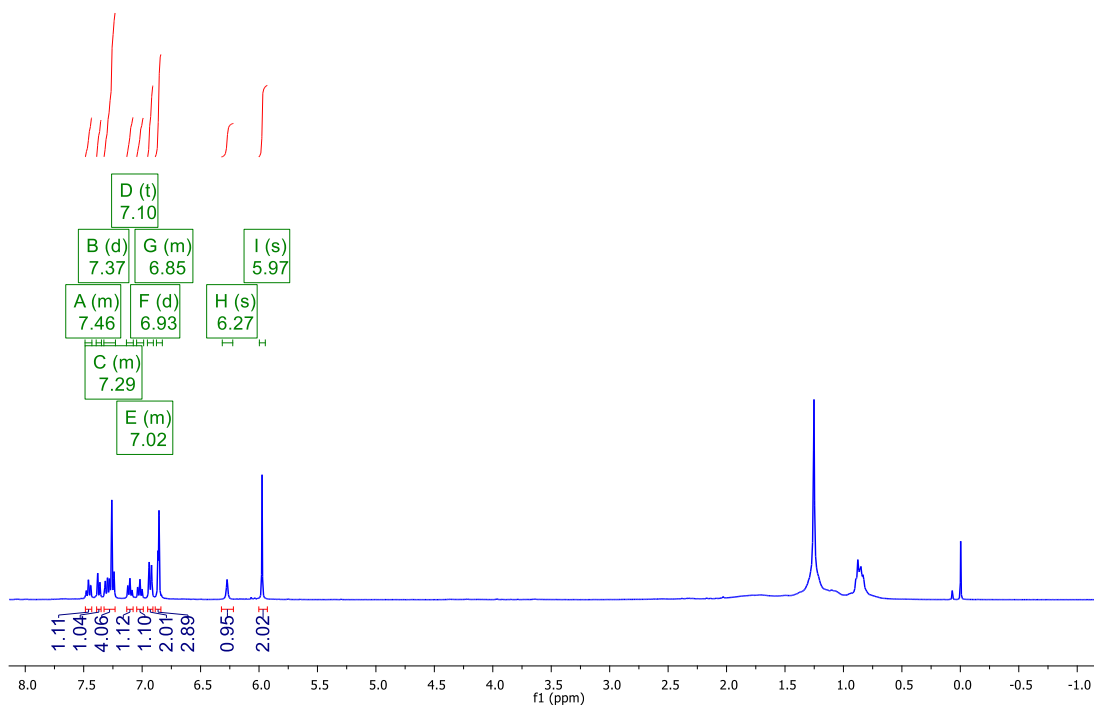
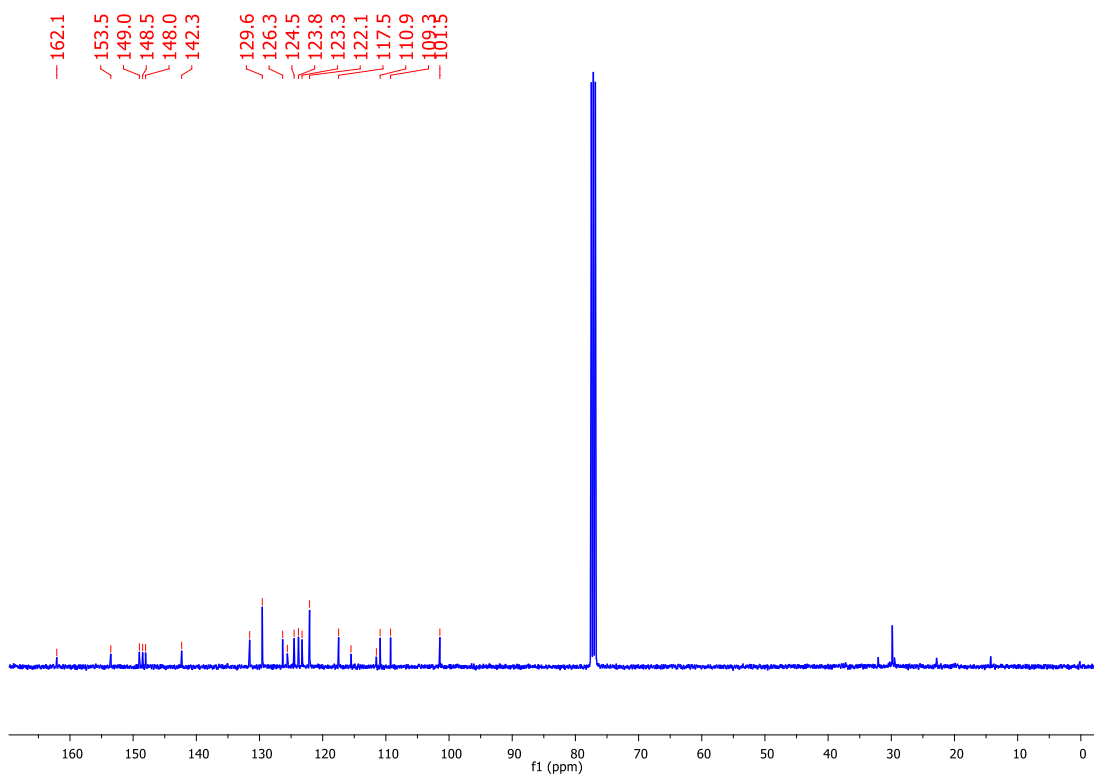
Compound **354d** – ^1H NMRCompound **354d** – ^{13}C NMR

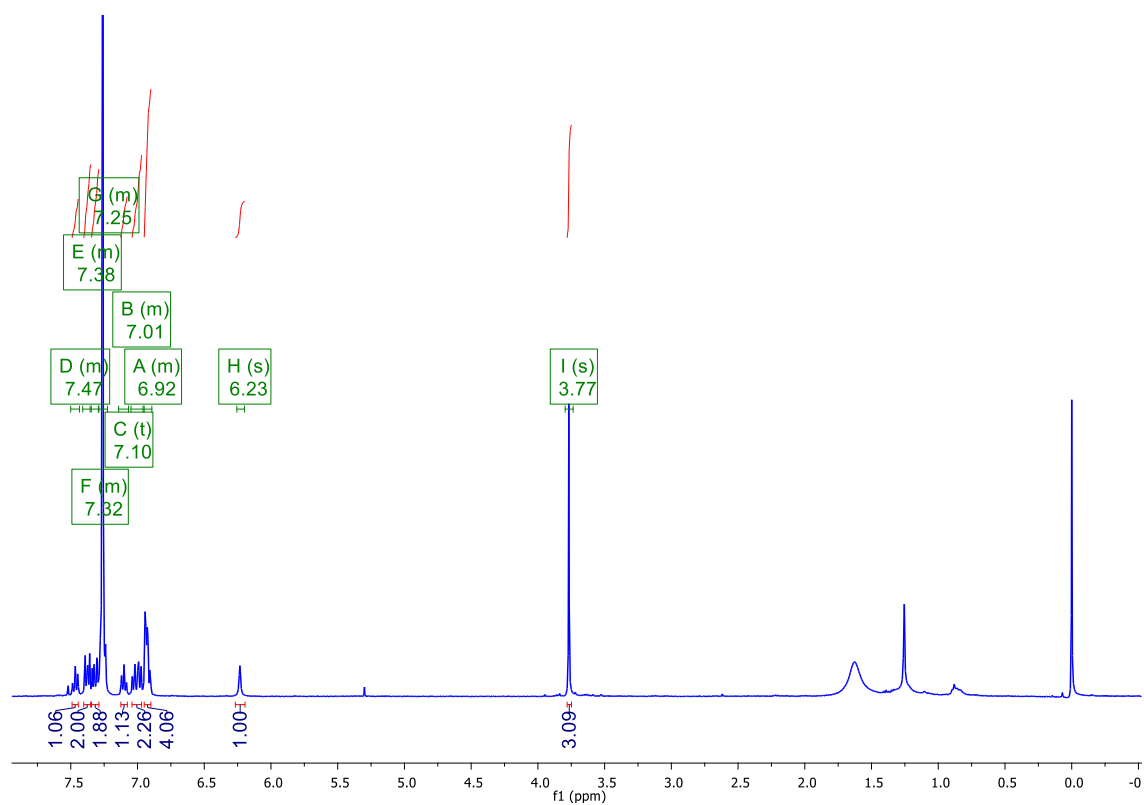
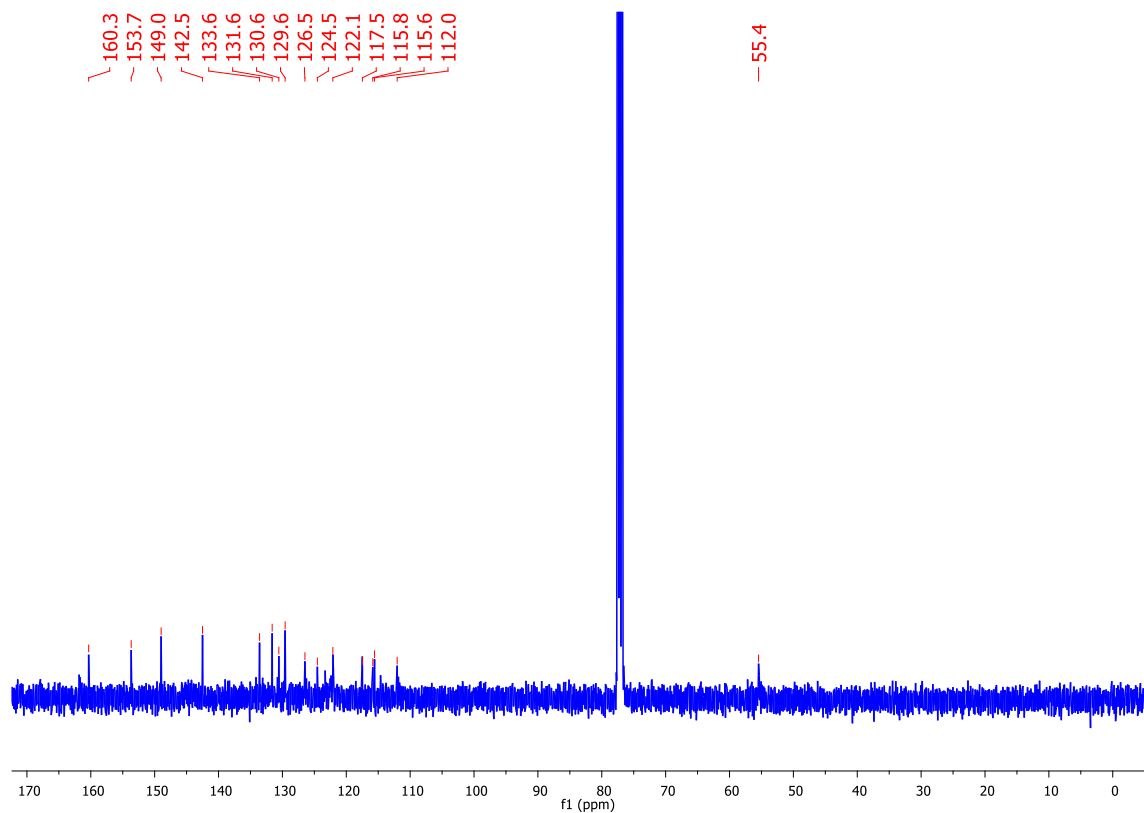
Compound **354e** – ^1H NMRCompound **354e** – ^{13}C NMR

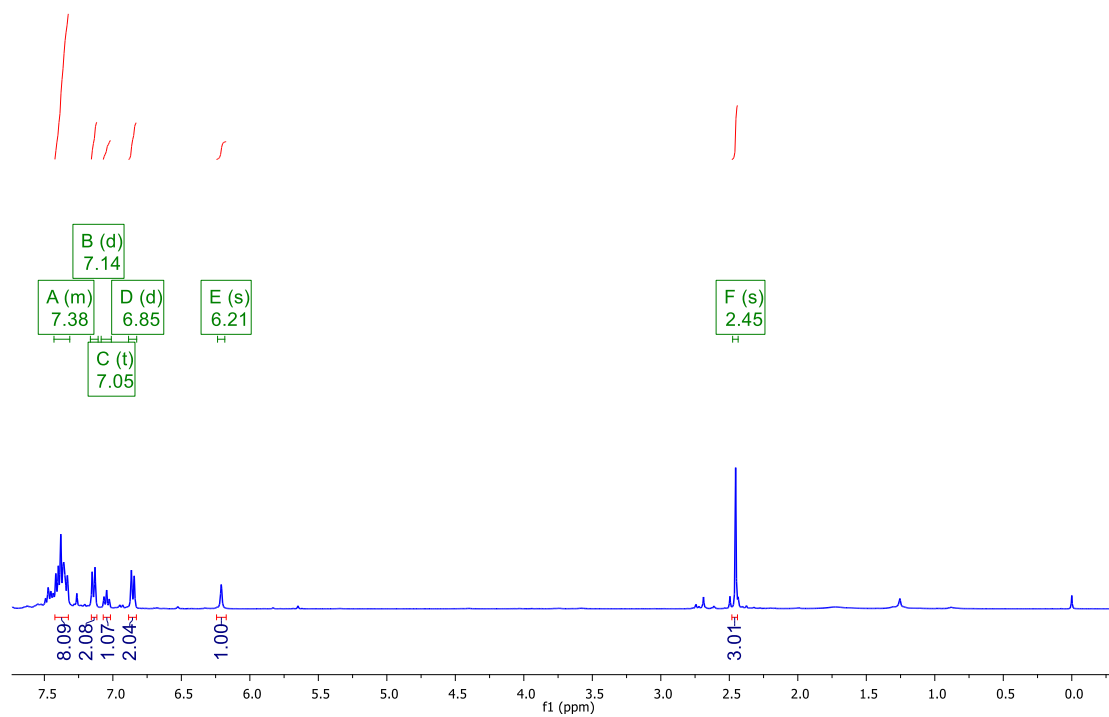
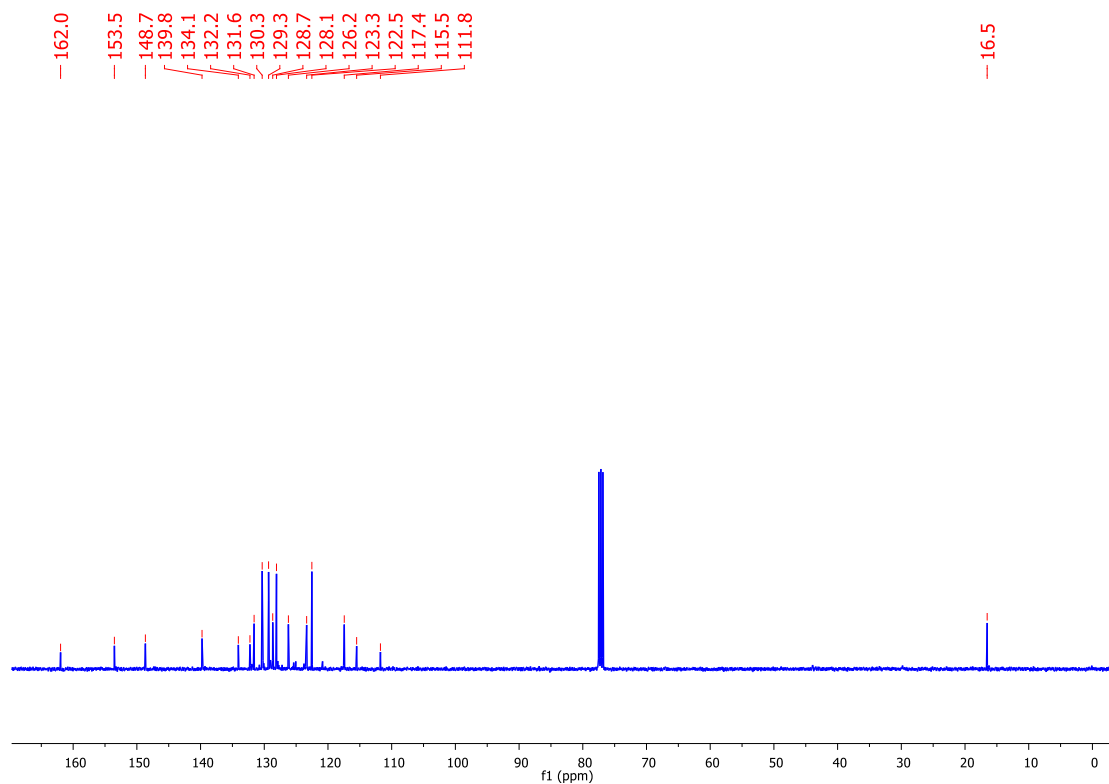
Compound **354f** – ^1H NMRCompound **354f** – ^{13}C NMR

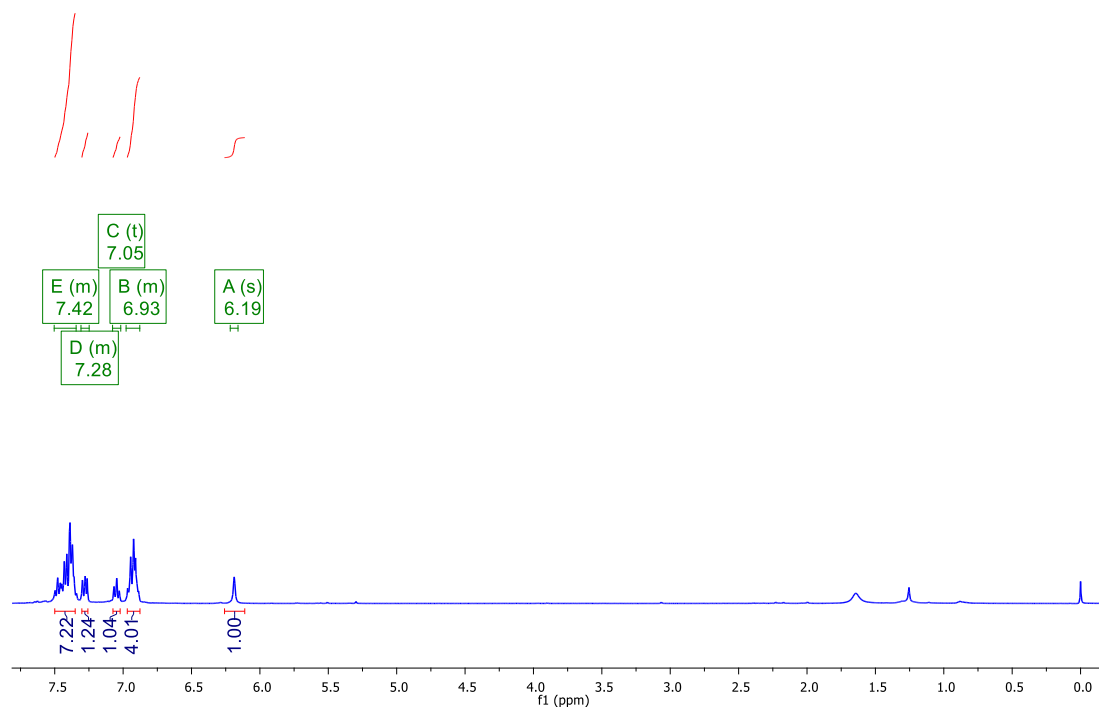
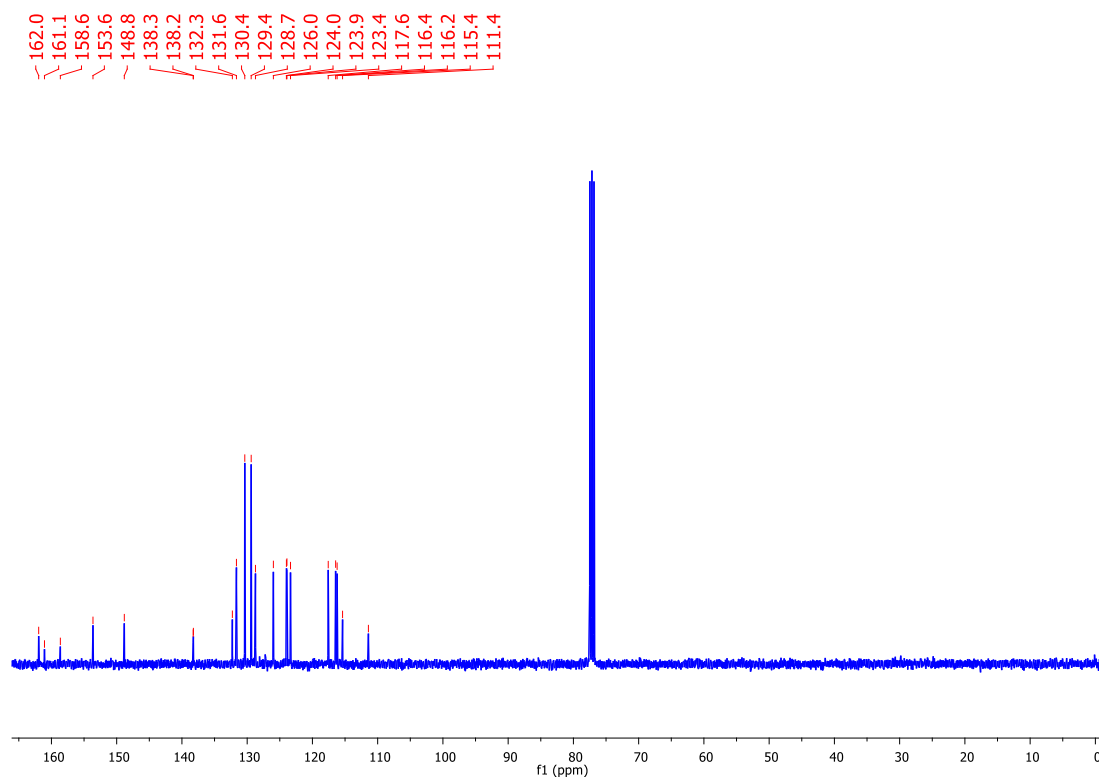
Compound **354g** – ^1H NMRCompound **354g** – ^{13}C NMR

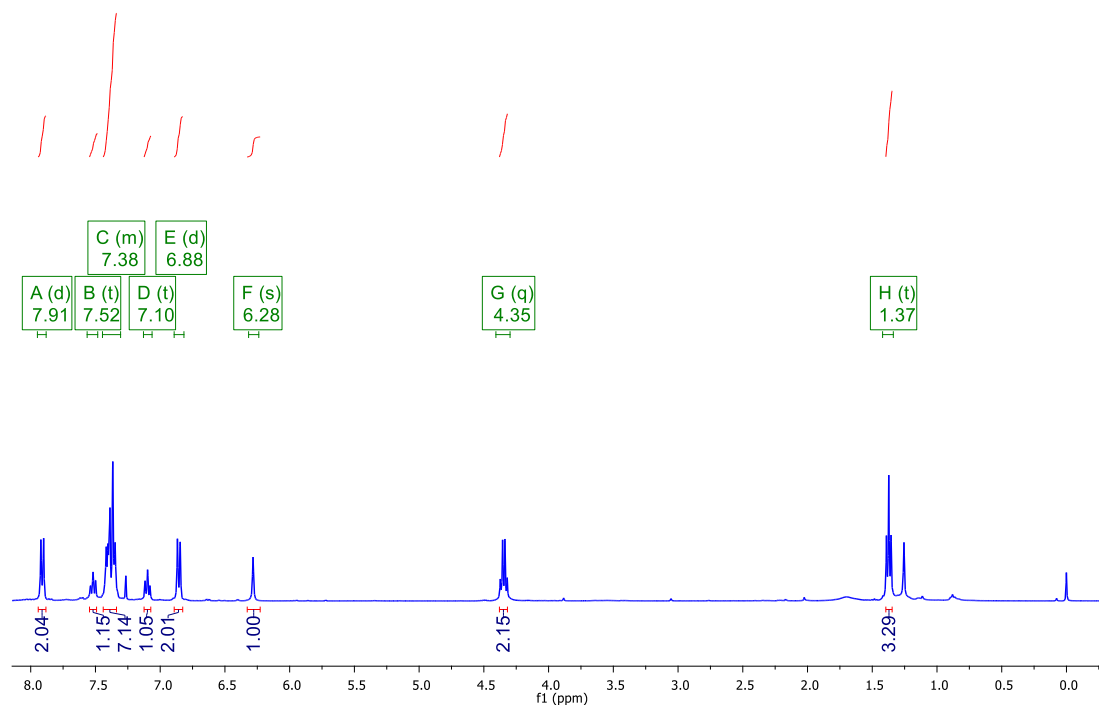
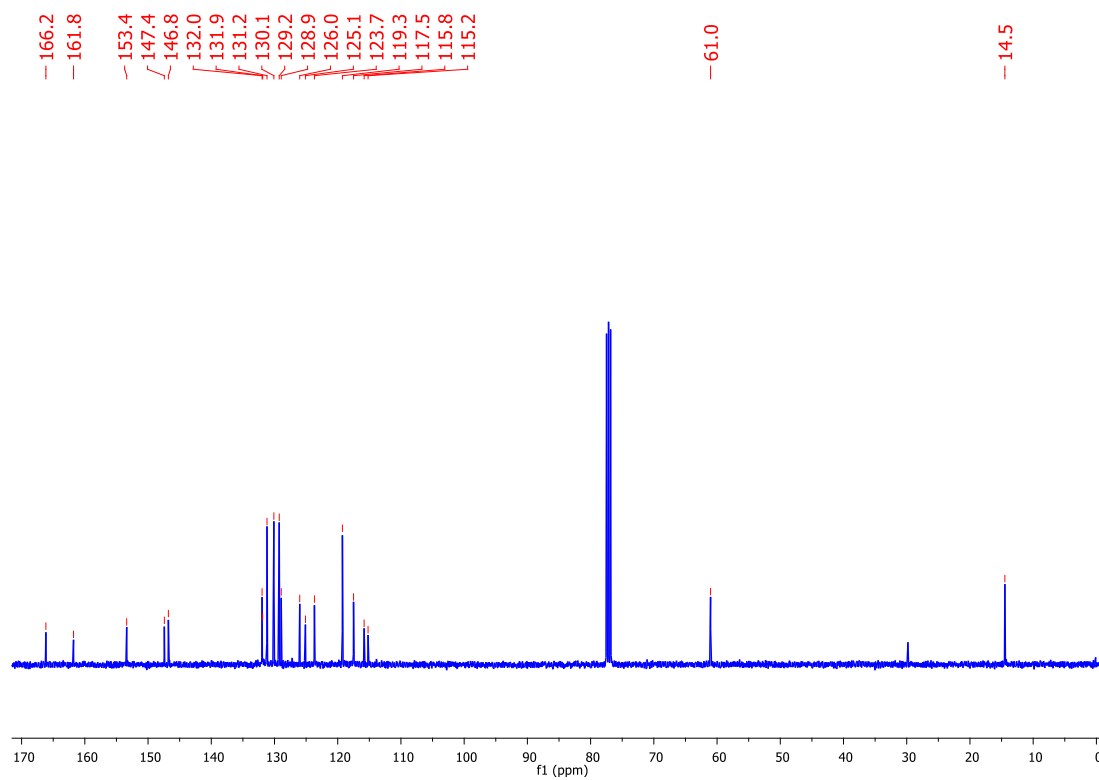
Compound **354h** – ^1H NMRCompound **354h** – ^{13}C NMR

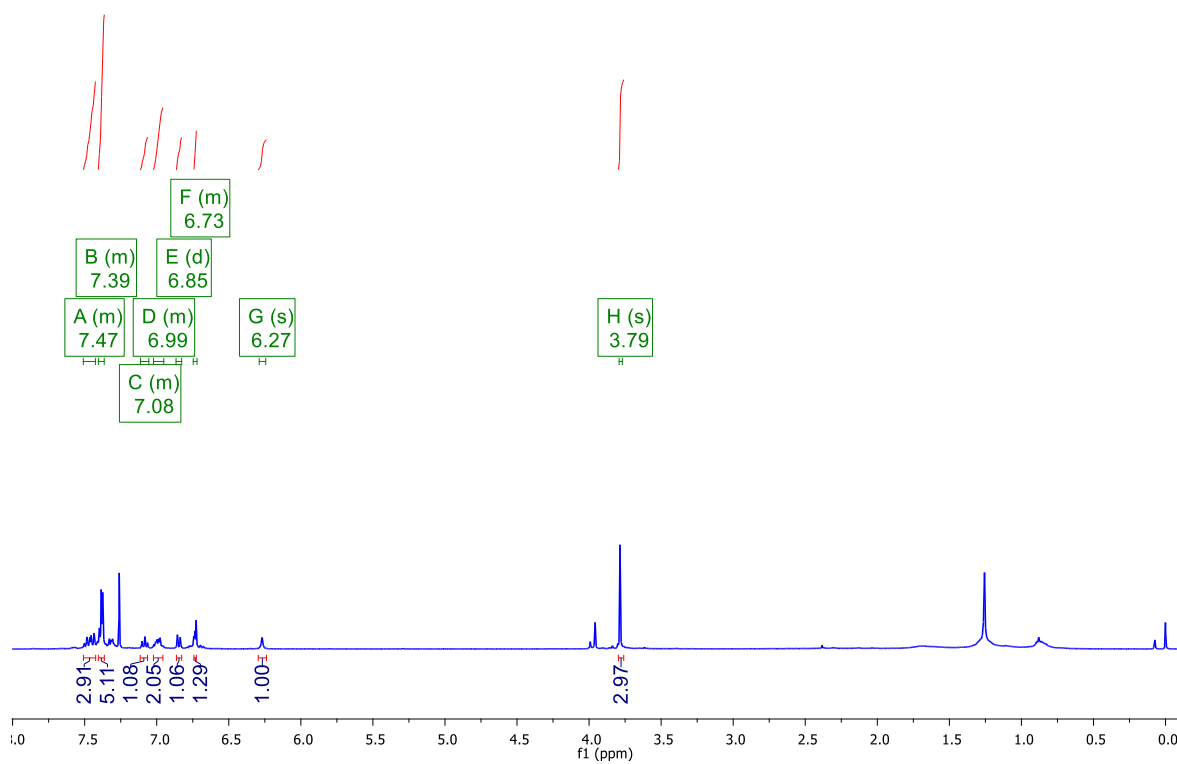
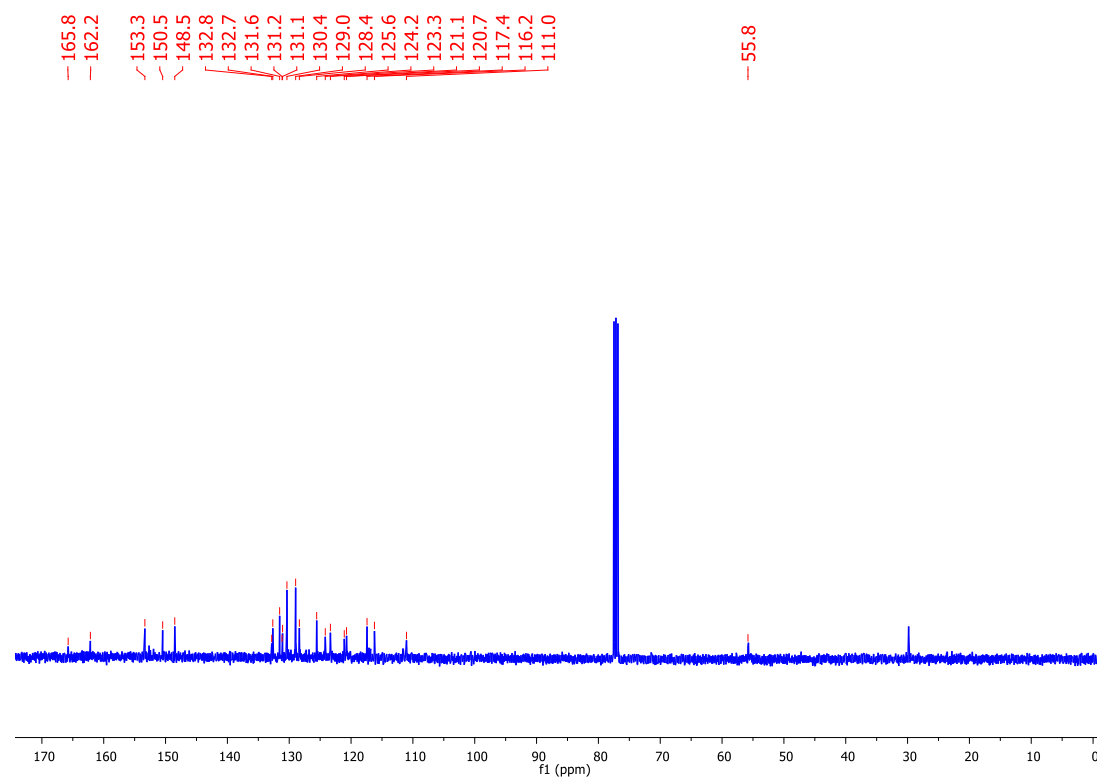
Compound **354i** – ^1H NMRCompound **354i** – ^{13}C NMR

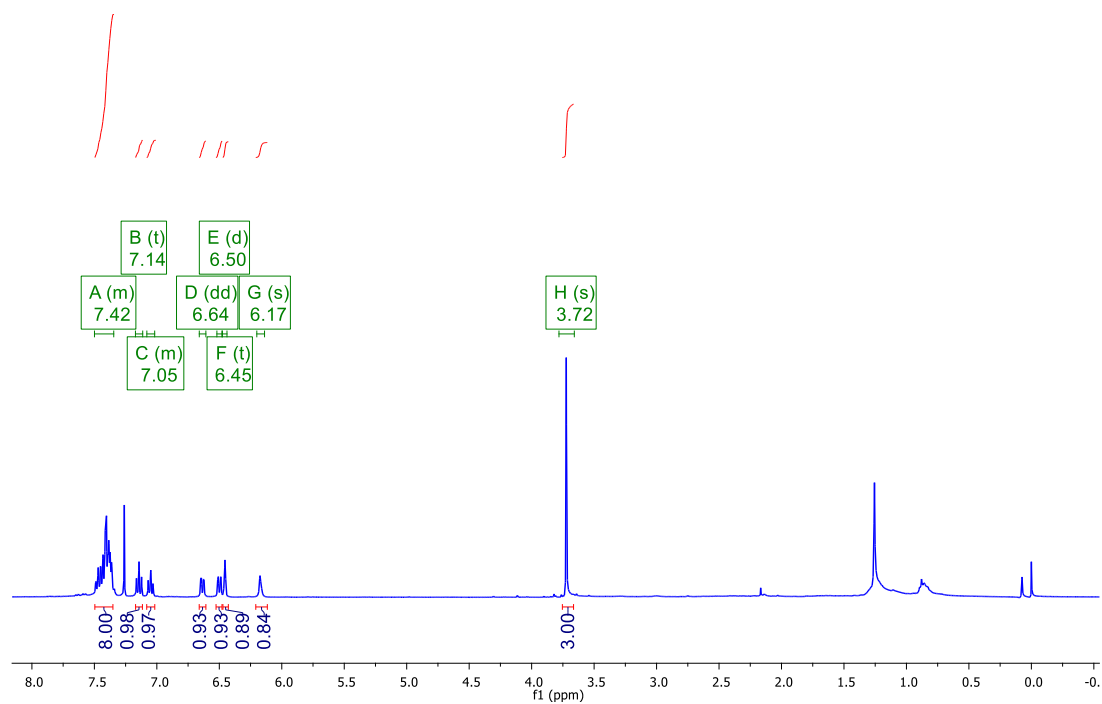
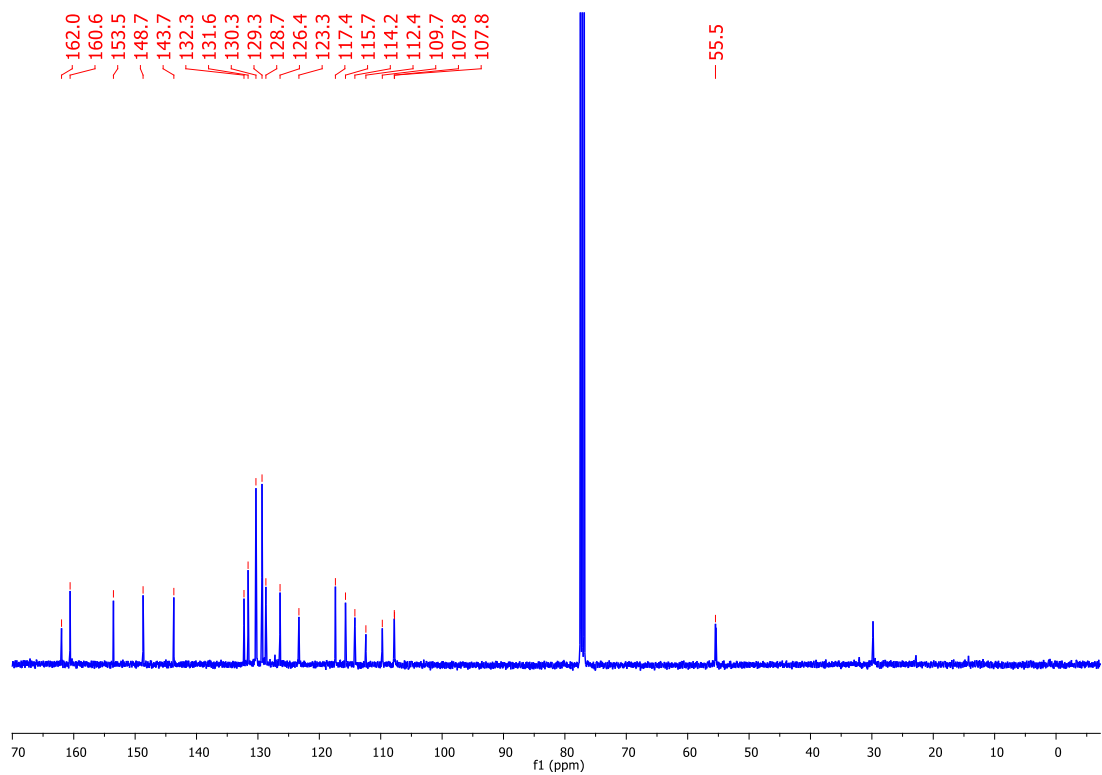
Compound **354j** – ^1H NMRCompound **354j** – ^{13}C NMR

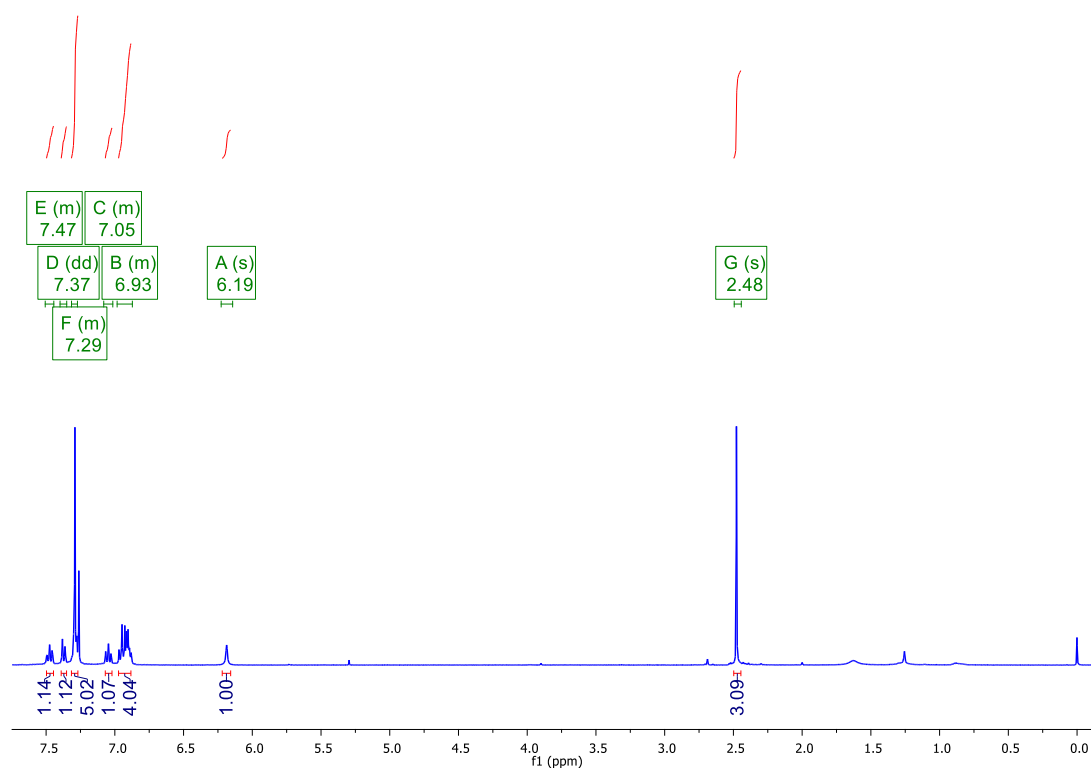
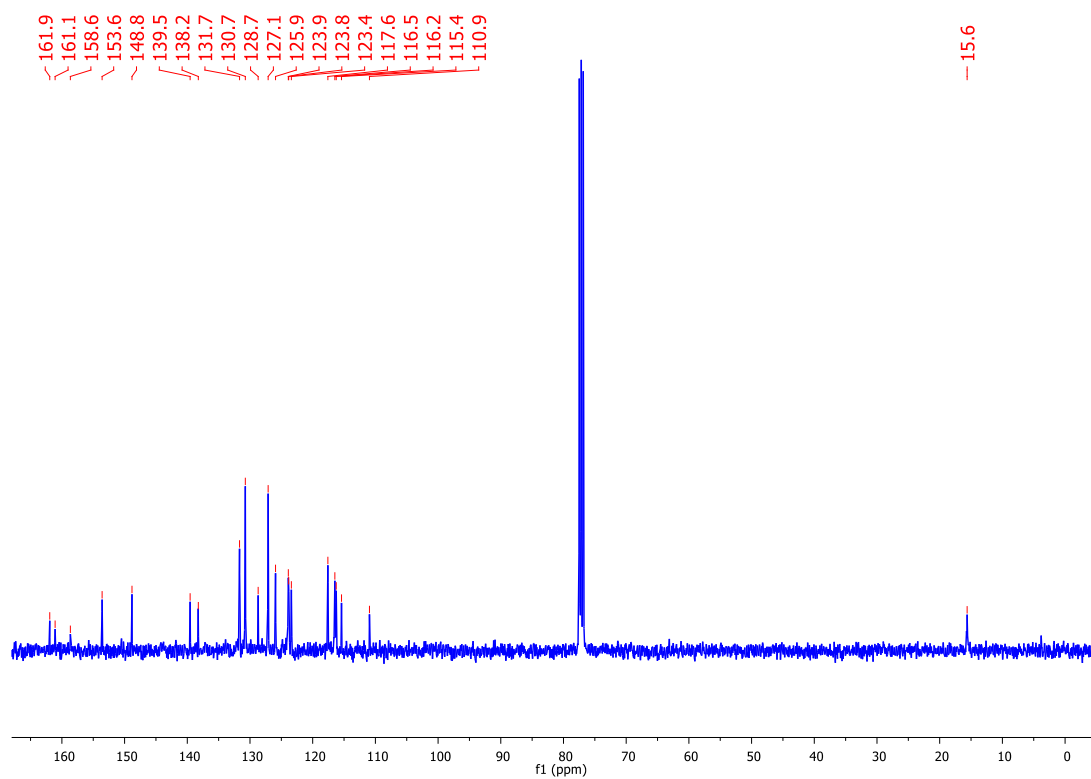
Compound **354q** – ^1H NMRCompound **#q** – ^{13}C NMR

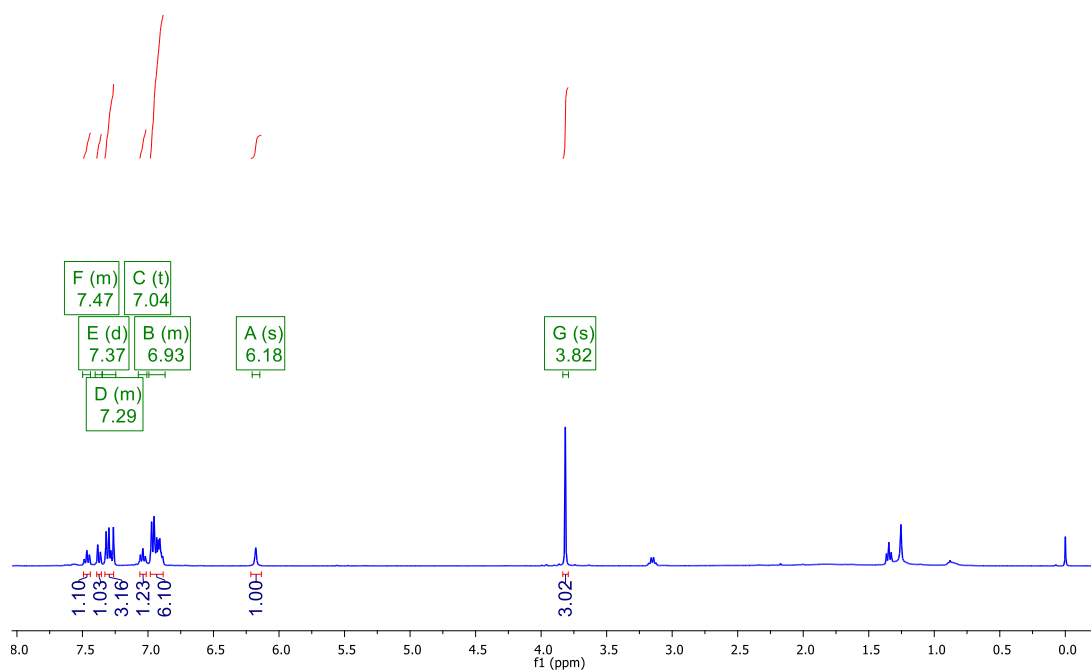
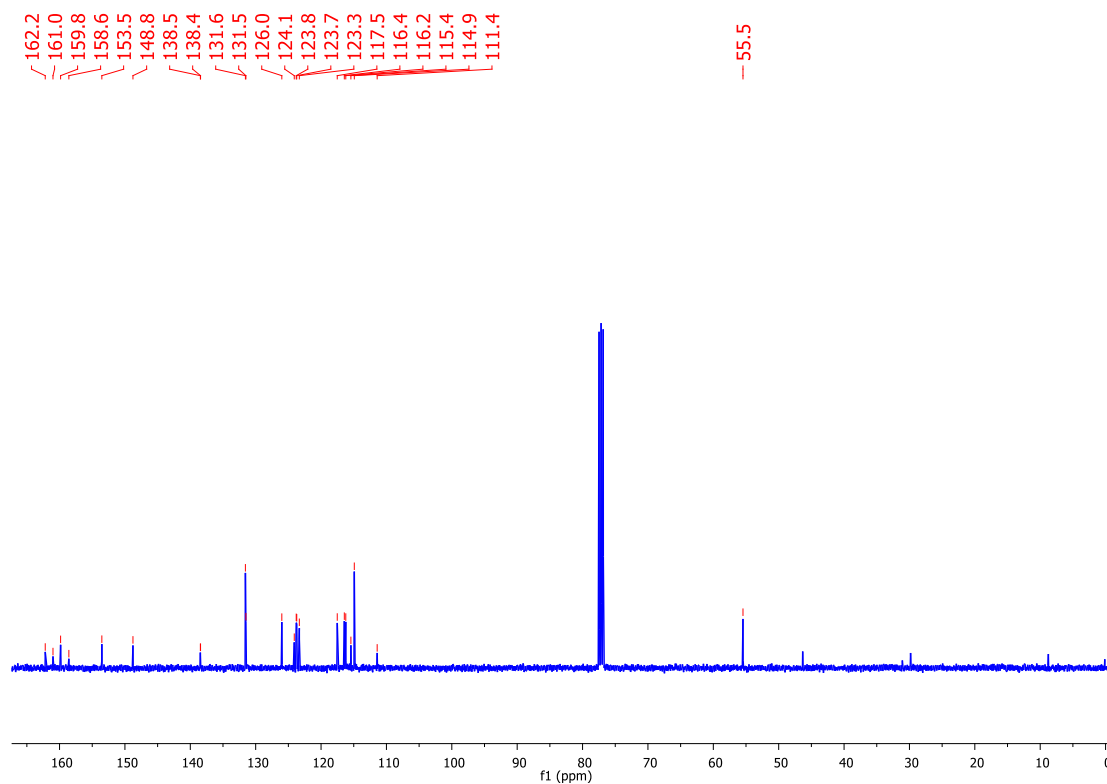
Compound #r – ^1H NMRCompound #r – ^{13}C NMR

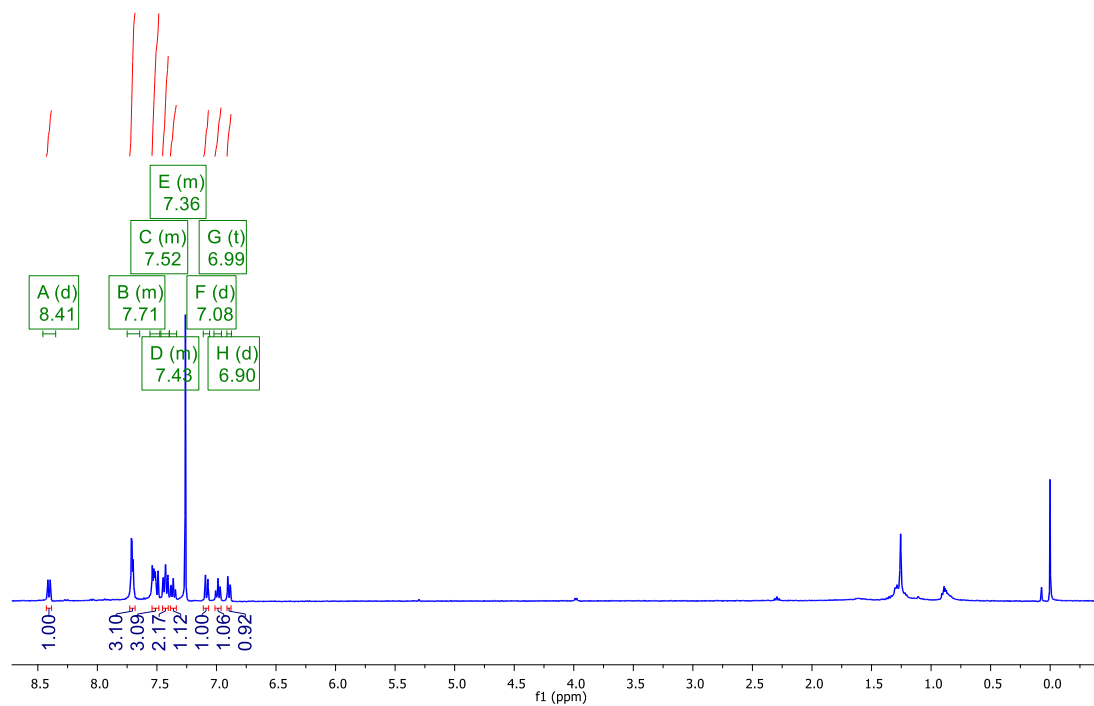
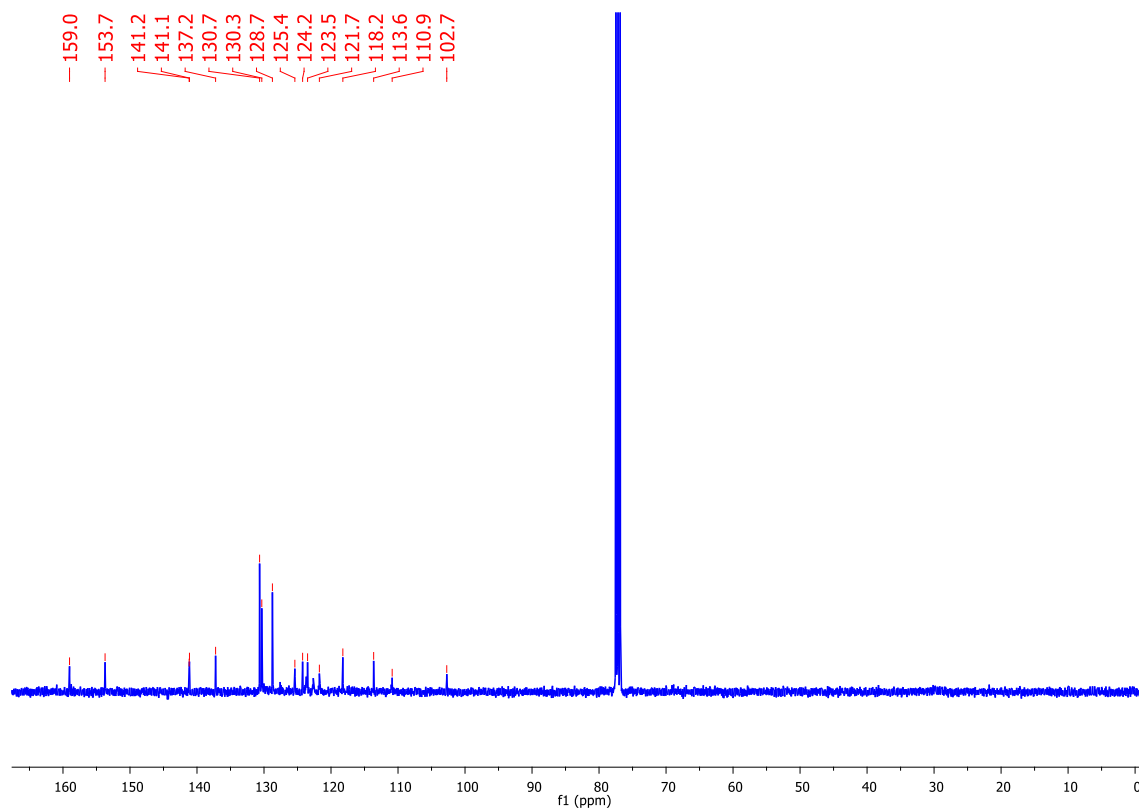
Compound #t – ^1H NMRCompound #t – ^{13}C NMR

Compound #u – ^1H NMRCompound #u – ^{13}C NMR

Compound #v – ^1H NMRCompound #v – ^{13}C NMR

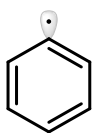
Compound #w – ^1H NMRCompound #w – ^{13}C NMR

Compound #x – ^1H NMRCompound #x – ^{13}C NMR

Compound 355 – ^1H NMRCompound 355 – ^{13}C NMR

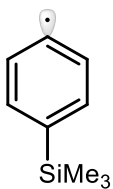
Appendix 2 – Cartesian coordinates of the optimized structures

Cartesian coordinates and energies for all optimized structures at UBHandHLYP/6-311G** level of theory.



Nimag=0
Zero-point correction= 0.090233 (Hartree/Particle)
Thermal correction to Energy= 0.094463
Thermal correction to Enthalpy= 0.095408
Thermal correction to Gibbs Free Energy= 0.062275
Sum of electronic and zero-point Energies= -231.380821
Sum of electronic and thermal Energies= -231.376590
Sum of electronic and thermal Enthalpies= -231.375646
Sum of electronic and thermal Free Energies= -231.408779

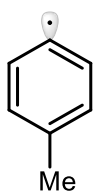
6	1.216546000	-0.764427000	0.000001000
6	1.203817000	0.626720000	0.000000000
6	0.000000000	1.313073000	-0.000001000
6	-1.203819000	0.626717000	-0.000001000
6	-1.216547000	-0.764426000	-0.000001000
6	0.000002000	-1.387991000	0.000001000
1	-2.134416000	1.168910000	-0.000002000
1	-2.142658000	-1.312544000	-0.000001000
1	2.134416000	1.168909000	0.000000000
1	2.142662000	-1.312537000	0.000002000
1	-0.000003000	2.389271000	-0.000001000



Nimag=0

Zero-point correction=	0.194262 (Hartree/Particle)
Thermal correction to Energy=	0.206149
Thermal correction to Enthalpy=	0.207093
Thermal correction to Gibbs Free Energy=	0.155482
Sum of electronic and zero-point Energies=	-639.909298
Sum of electronic and thermal Energies=	-639.897411
Sum of electronic and thermal Enthalpies=	-639.896467
Sum of electronic and thermal Free Energies=	-639.948078

6	-3.222264000	-0.009661000	-0.000157000
6	-2.582730000	-1.218172000	-0.000102000
6	-2.607247000	1.209080000	-0.000047000
6	-1.193469000	-1.186292000	0.000079000
1	-3.117946000	-2.152144000	-0.000165000
6	-1.214852000	1.206033000	0.000109000
6	-0.485247000	0.017750000	0.000160000
1	-0.661485000	-2.125273000	0.000170000
1	-0.701395000	2.153696000	0.000309000
1	-3.160294000	2.132646000	-0.000025000
6	2.013642000	-0.890700000	-1.531297000
1	3.100110000	-0.932276000	-1.549299000
1	1.645513000	-1.912719000	-1.568682000
1	1.683319000	-0.390340000	-2.437463000
6	2.046827000	1.765608000	0.001292000
1	1.722006000	2.316605000	-0.877304000
1	1.722157000	2.315161000	0.880857000
1	3.133993000	1.763959000	0.001168000
6	2.013413000	-0.893049000	1.530024000
1	3.099881000	-0.933922000	1.548844000
1	1.682202000	-0.393952000	2.436590000
1	1.645659000	-1.915231000	1.565902000
14	1.399846000	0.005015000	-0.000091000

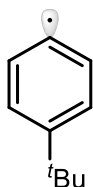


Nimag=0

Zero-point correction=	0.118368 (Hartree/Particle)
Thermal correction to Energy=	0.124414
Thermal correction to Enthalpy=	0.125358
Thermal correction to Gibbs Free Energy=	0.086861
Sum of electronic and zero-point Energies=	-270.652294
Sum of electronic and thermal Energies=	-270.646249
Sum of electronic and thermal Enthalpies=	-270.645304
Sum of electronic and thermal Free Energies=	-270.683802

6	-1.892004000	-0.001381000	0.009010000
6	-1.260487000	-1.213553000	0.002562000

6	-1.263738000	1.211230000	0.002771000
6	0.129439000	-1.195931000	-0.007997000
1	-1.802703000	-2.142985000	0.002442000
6	0.126963000	1.197253000	-0.008053000
6	0.835331000	0.001539000	-0.010873000
1	0.669151000	-2.129494000	-0.016458000
1	0.664046000	2.131993000	-0.016786000
1	-1.807766000	2.139879000	0.002326000
6	2.338434000	0.000826000	0.008478000
1	2.738424000	0.905926000	-0.435722000
1	2.715627000	-0.058929000	1.026868000
1	2.739600000	-0.846289000	-0.538060000

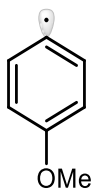


Nimag=0

Zero-point correction=	0.206005 (Hartree/Particle)
Thermal correction to Energy=	0.215442
Thermal correction to Enthalpy=	0.216386
Thermal correction to Gibbs Free Energy=	0.171271
Sum of electronic and zero-point Energies=	-388.452577
Sum of electronic and thermal Energies=	-388.443141
Sum of electronic and thermal Enthalpies=	-388.442196
Sum of electronic and thermal Free Energies=	-388.487311

6	-2.881375000	-0.006438000	0.000026000
6	-2.231662000	-1.210086000	0.000016000
6	-2.263309000	1.208519000	-0.000036000
6	-0.844845000	-1.174889000	-0.000020000
1	-2.759366000	-2.148201000	0.000024000
6	-0.869939000	1.211709000	-0.000049000
6	-0.139372000	0.029166000	-0.000077000
1	-0.310225000	-2.109514000	-0.000031000
1	-0.366032000	2.160785000	-0.000050000
1	-2.813410000	2.133748000	0.000036000
6	1.390862000	0.005565000	-0.000010000
6	1.892308000	-0.726968000	-1.252087000
1	2.978994000	-0.749834000	-1.265449000
1	1.539464000	-1.752335000	-1.288230000
1	1.553020000	-0.227013000	-2.154478000
6	1.993056000	1.410859000	-0.000381000
1	1.701035000	1.975196000	-0.881073000
1	1.701294000	1.975524000	0.880188000
1	3.076610000	1.340657000	-0.000521000
6	1.892201000	-0.726220000	1.252559000
1	2.978882000	-0.748917000	1.266073000
1	1.552713000	-0.225791000	2.154618000

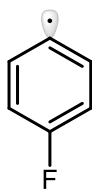
1 1.539476000 -1.751606000 1.289249000



Nimag=0

Zero-point correction= 0.123350 (Hartree/Particle)
 Thermal correction to Energy= 0.130321
 Thermal correction to Enthalpy= 0.131265
 Thermal correction to Gibbs Free Energy= 0.090047
 Sum of electronic and zero-point Energies= -345.832321
 Sum of electronic and thermal Energies= -345.825351
 Sum of electronic and thermal Enthalpies= -345.824406
 Sum of electronic and thermal Free Energies= -345.865625

6 -1.637512000 1.214874000 0.108550000
 6 -0.273105000 1.205495000 -0.155741000
 6 0.398758000 -0.000126000 -0.285047000
 6 -0.273340000 -1.205599000 -0.155599000
 6 -1.637754000 -1.214681000 0.108665000
 6 -2.253239000 0.000164000 0.231450000
 1 0.273409000 -2.124832000 -0.279588000
 1 -2.175253000 -2.142046000 0.204853000
 1 0.273806000 2.124616000 -0.279848000
 1 -2.174831000 2.142354000 0.204632000
 6 2.588983000 0.000137000 0.538345000
 1 3.602129000 -0.000029000 0.158083000
 1 2.434817000 0.885856000 1.151575000
 1 2.434783000 -0.885093000 1.152273000
 8 1.731799000 -0.000300000 -0.581964000

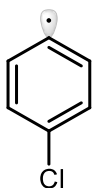


Nimag=0

Zero-point correction= 0.081974 (Hartree/Particle)
 Thermal correction to Energy= 0.086913
 Thermal correction to Enthalpy= 0.087857
 Thermal correction to Gibbs Free Energy= 0.052688
 Sum of electronic and zero-point Energies= -330.618132
 Sum of electronic and thermal Energies= -330.613194
 Sum of electronic and thermal Enthalpies= -330.612250
 Sum of electronic and thermal Free Energies= -330.647419

6 1.821348000 -0.000055000 -0.000043000
 6 1.194124000 -1.215234000 0.000026000

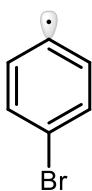
6	1.194517000	1.215019000	0.000081000
6	-0.195757000	-1.210461000	0.000066000
1	1.740362000	-2.142092000	-0.000245000
6	-0.195696000	1.210452000	0.000009000
6	-0.855696000	0.000153000	-0.000073000
1	-0.764395000	-2.123472000	0.000069000
1	-0.763923000	2.123716000	-0.000028000
1	1.740445000	2.142022000	-0.000143000
9	-2.192169000	0.000064000	-0.000006000



Nimag=0

Zero-point correction=	0.080562 (Hartree/Particle)
Thermal correction to Energy=	0.085857
Thermal correction to Enthalpy=	0.086801
Thermal correction to Gibbs Free Energy=	0.050323
Sum of electronic and zero-point Energies=	-690.998152
Sum of electronic and thermal Energies=	-690.992857
Sum of electronic and thermal Enthalpies=	-690.991913
Sum of electronic and thermal Free Energies=	-691.028391

6	-1.627963000	-1.214432000	0.000002000
6	-0.237990000	-1.208789000	0.000001000
6	0.433950000	-0.000003000	0.000000000
6	-0.237990000	1.208789000	0.000000000
6	-1.627957000	1.214435000	0.000000000
6	-2.254607000	0.000001000	0.000001000
1	0.314081000	2.131293000	-0.000001000
1	-2.171409000	2.142789000	-0.000001000
1	0.314074000	-2.131297000	0.000001000
1	-2.171410000	-2.142789000	0.000002000
17	2.178235000	0.000000000	-0.000001000

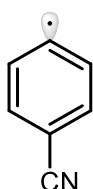


Nimag=0

Zero-point correction=	0.079950 (Hartree/Particle)
Thermal correction to Energy=	0.085473
Thermal correction to Enthalpy=	0.086417
Thermal correction to Gibbs Free Energy=	0.048600
Sum of electronic and zero-point Energies=	-2804.893572
Sum of electronic and thermal Energies=	-2804.888048
Sum of electronic and thermal Enthalpies=	-2804.887104

Sum of electronic and thermal Free Energies= -2804.924921

6	2.850644000	-0.000105000	0.000250000
6	2.223387000	-1.214414000	0.000301000
6	2.223882000	1.214140000	0.000313000
6	0.833405000	-1.209177000	-0.000505000
1	2.766135000	-2.143188000	0.000640000
6	0.833648000	1.209183000	-0.000567000
6	0.160579000	0.000148000	-0.000901000
1	0.285430000	-2.134221000	-0.000287000
1	0.286155000	2.134475000	-0.000272000
1	2.766772000	2.142931000	0.000795000
35	-1.738793000	0.000039000	0.000165000



Nimag=0

Zero-point correction= 0.089110 (Hartree/Particle)

Thermal correction to Energy= 0.094976

Thermal correction to Enthalpy= 0.095920

Thermal correction to Gibbs Free Energy= 0.058430

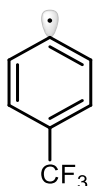
Sum of electronic and zero-point Energies= -323.594341

Sum of electronic and thermal Energies= -323.588475

Sum of electronic and thermal Enthalpies= -323.587531

Sum of electronic and thermal Free Energies= -323.625021

6	2.161120000	0.000139000	0.000168000
6	1.540965000	-1.218511000	-0.000046000
6	1.540839000	1.218625000	-0.000006000
6	0.154323000	-1.211515000	-0.000064000
1	2.089777000	-2.143606000	0.000199000
6	0.154102000	1.211420000	-0.000084000
6	-0.532821000	-0.000056000	-0.000156000
1	-0.395891000	-2.135873000	-0.000005000
1	-0.396154000	2.135754000	-0.000069000
1	2.089428000	2.143853000	0.000197000
6	-1.962375000	-0.000291000	-0.000060000
7	-3.103438000	0.000143000	0.000167000



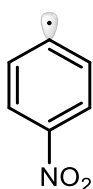
Nimag=0

Zero-point correction= 0.095691 (Hartree/Particle)

Thermal correction to Energy= 0.103277

Thermal correction to Enthalpy= 0.104221
 Thermal correction to Gibbs Free Energy= 0.060865
 Sum of electronic and zero-point Energies= -568.389850
 Sum of electronic and thermal Energies= -568.382264
 Sum of electronic and thermal Enthalpies= -568.381320
 Sum of electronic and thermal Free Energies= -568.424676

6	-2.803055000	0.000004000	0.015210000
6	-2.181030000	1.217077000	0.003973000
6	-2.181045000	-1.217069000	0.003959000
6	-0.792825000	1.207022000	-0.018404000
1	-2.728080000	2.143236000	0.008637000
6	-0.792832000	-1.207023000	-0.018413000
6	-0.110731000	-0.000007000	-0.029861000
1	-0.245245000	2.132652000	-0.035908000
1	-0.245265000	-2.132661000	-0.035924000
1	-2.728098000	-2.143226000	0.008615000
6	1.384486000	-0.000001000	-0.002558000
9	1.857305000	0.000210000	1.245080000
9	1.894060000	-1.072934000	-0.603948000
9	1.894066000	1.072722000	-0.604337000



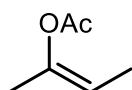
Nimag=0
 Zero-point correction= 0.093586 (Hartree/Particle)
 Thermal correction to Energy= 0.100136
 Thermal correction to Enthalpy= 0.101081
 Thermal correction to Gibbs Free Energy= 0.061227
 Sum of electronic and zero-point Energies= -435.818497
 Sum of electronic and thermal Energies= -435.811947
 Sum of electronic and thermal Enthalpies= -435.811002
 Sum of electronic and thermal Free Energies= -435.850856

6	1.868364000	-1.219942000	-0.000324000
6	0.481318000	-1.215333000	-0.000123000
6	-0.179255000	0.000000000	0.000002000
6	0.481322000	1.215334000	0.000103000
6	1.868365000	1.219941000	0.000323000
6	2.487600000	-0.000002000	0.000009000
1	-0.086772000	2.126300000	0.000237000
1	2.417689000	2.144415000	0.000484000
1	-0.086775000	-2.126298000	-0.000253000
1	2.417682000	-2.144419000	-0.000460000
7	-1.643580000	0.000001000	-0.000003000
8	-2.200190000	1.066422000	-0.000549000
8	-2.200192000	-1.066421000	0.000558000



Nimag=0
 Zero-point correction= 0.126283 (Hartree/Particle)
 Thermal correction to Energy= 0.134272
 Thermal correction to Enthalpy= 0.135216
 Thermal correction to Gibbs Free Energy= 0.093180
 Sum of electronic and zero-point Energies= -345.551659
 Sum of electronic and thermal Energies= -345.543670
 Sum of electronic and thermal Enthalpies= -345.542726
 Sum of electronic and thermal Free Energies= -345.584762

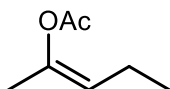
6	-1.482918000	1.332606000	0.000222000
1	-2.516664000	1.627230000	0.000238000
1	-0.728153000	2.089037000	0.000313000
6	-1.213406000	0.040884000	0.000051000
6	-2.228783000	-1.049569000	-0.000118000
1	-3.230487000	-0.639921000	-0.000053000
1	-2.105219000	-1.680394000	-0.875914000
1	-2.105218000	-1.680672000	0.875478000
6	1.215243000	0.121456000	-0.000224000
6	2.346501000	-0.860486000	0.000121000
1	2.278923000	-1.497793000	-0.874831000
1	3.284736000	-0.324986000	0.000265000
1	2.278564000	-1.497644000	0.875155000
8	1.334385000	1.302395000	-0.000138000
8	0.043577000	-0.540421000	0.000017000



Nimag=0
 Zero-point correction= 0.155022 (Hartree/Particle)
 Thermal correction to Energy= 0.164777
 Thermal correction to Enthalpy= 0.165721
 Thermal correction to Gibbs Free Energy= 0.118705
 Sum of electronic and zero-point Energies= -384.820216
 Sum of electronic and thermal Energies= -384.810461
 Sum of electronic and thermal Enthalpies= -384.809516
 Sum of electronic and thermal Free Energies= -384.856532

6	1.362013000	-0.722966000	-0.000475000
1	0.757929000	-1.608243000	-0.001049000
6	0.750694000	0.449884000	-0.000238000
6	-1.574756000	-0.320003000	-0.000141000
6	-2.932021000	0.316775000	0.000044000
1	-3.039772000	0.951969000	-0.872445000
1	-3.688754000	-0.454355000	-0.003941000
1	-3.042288000	0.944629000	0.877598000

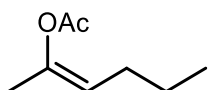
8	-1.376081000	-1.492351000	0.000658000
8	-0.632055000	0.633045000	-0.000927000
6	1.363462000	1.809362000	0.000549000
1	1.036576000	2.364205000	-0.874592000
1	2.442773000	1.770690000	0.001175000
6	2.842042000	-0.935530000	0.000102000
1	3.415473000	-0.017554000	0.000691000
1	3.139121000	-1.513169000	0.872497000
1	1.035532000	2.363681000	0.875630000
1	3.139893000	-1.512526000	-0.872456000



Nimag=0

Zero-point correction=	0.184580 (Hartree/Particle)
Thermal correction to Energy=	0.195556
Thermal correction to Enthalpy=	0.196501
Thermal correction to Gibbs Free Energy=	0.145989
Sum of electronic and zero-point Energies=	-424.087669
Sum of electronic and thermal Energies=	-424.076693
Sum of electronic and thermal Enthalpies=	-424.075748
Sum of electronic and thermal Free Energies=	-424.126260

6	-1.031965000	-0.283457000	-0.330215000
1	-0.612201000	-1.267356000	-0.409149000
6	-0.213915000	0.727956000	-0.089215000
6	1.907729000	-0.493934000	-0.003455000
6	3.351854000	-0.153013000	0.210789000
1	3.476718000	0.328100000	1.174746000
1	3.943094000	-1.056131000	0.164794000
1	3.679587000	0.547648000	-0.549591000
8	1.492262000	-1.590199000	-0.201660000
8	1.168578000	0.622696000	0.063060000
6	-0.552719000	2.171725000	0.069568000
1	-0.209154000	2.526967000	1.037057000
1	-1.614671000	2.352559000	-0.007348000
6	-2.518267000	-0.191952000	-0.490954000
1	-2.861117000	0.836465000	-0.496987000
1	-2.782401000	-0.605460000	-1.463401000
1	-0.043888000	2.759573000	-0.689582000
6	-3.261855000	-0.971908000	0.591248000
1	-2.952917000	-2.013228000	0.602312000
1	-3.060142000	-0.558003000	1.574713000
1	-4.334796000	-0.943614000	0.424629000

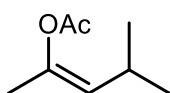


Nimag=0

Zero-point correction=	0.213866 (Hartree/Particle)
------------------------	-----------------------------

Thermal correction to Energy= 0.226173
 Thermal correction to Enthalpy= 0.227117
 Thermal correction to Gibbs Free Energy= 0.173131
 Sum of electronic and zero-point Energies= -463.355830
 Sum of electronic and thermal Energies= -463.343523
 Sum of electronic and thermal Enthalpies= -463.342579
 Sum of electronic and thermal Free Energies= -463.396566

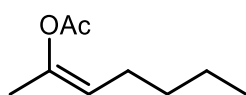
6	0.524112000	-0.140949000	0.393192000
1	0.181092000	-1.152982000	0.484576000
6	-0.364549000	0.796339000	0.106702000
6	-2.377844000	-0.594203000	-0.016224000
6	-3.838921000	-0.373396000	-0.269616000
1	-3.977811000	0.087276000	-1.241602000
1	-4.356288000	-1.320978000	-0.228077000
1	-4.241294000	0.305281000	0.474707000
8	-1.880406000	-1.651397000	0.204318000
8	-1.729924000	0.577964000	-0.076986000
6	-0.136873000	2.258617000	-0.078157000
1	-0.478140000	2.563411000	-1.063523000
1	0.904662000	2.525281000	0.024097000
6	1.992972000	0.073351000	0.588528000
1	2.252151000	1.127030000	0.600299000
1	2.269463000	-0.317213000	1.568149000
1	-0.713430000	2.820811000	0.651434000
6	2.833065000	-0.640281000	-0.470956000
1	2.561883000	-1.693952000	-0.490428000
1	2.577431000	-0.243111000	-1.451037000
6	4.327987000	-0.500158000	-0.228912000
1	4.610118000	-0.919681000	0.733479000
1	4.902066000	-1.013654000	-0.994232000
1	4.631044000	0.544020000	-0.233833000



Nimag=0
 Zero-point correction= 0.213831 (Hartree/Particle)
 Thermal correction to Energy= 0.225858
 Thermal correction to Enthalpy= 0.226803
 Thermal correction to Gibbs Free Energy= 0.174889
 Sum of electronic and zero-point Energies= -463.352514
 Sum of electronic and thermal Energies= -463.340486
 Sum of electronic and thermal Enthalpies= -463.339542
 Sum of electronic and thermal Free Energies= -463.391456

6	-0.856582000	-0.578864000	-0.198485000
1	-0.518677000	-1.568549000	-0.469689000
6	0.078116000	0.173352000	0.351526000
6	2.355158000	-0.075346000	-0.234997000
6	3.590348000	-0.839986000	0.127601000

1	3.408976000	-1.903231000	0.014124000
1	4.405941000	-0.529642000	-0.509353000
1	3.838240000	-0.660734000	1.168277000
8	2.279333000	0.752912000	-1.084848000
8	1.324116000	-0.453249000	0.536727000
6	0.064347000	1.555146000	0.906044000
1	0.407902000	1.528326000	1.937207000
1	-0.916548000	1.999585000	0.883246000
6	-2.310330000	-0.351731000	-0.512511000
1	-2.416682000	-0.630554000	-1.561828000
1	0.746616000	2.183182000	0.342659000
6	-2.857415000	1.063057000	-0.379467000
1	-2.262908000	1.781778000	-0.933269000
1	-3.868602000	1.095446000	-0.774523000
1	-2.908612000	1.380469000	0.657788000
6	-3.163888000	-1.334102000	0.294758000
1	-4.205671000	-1.278124000	-0.008515000
1	-2.829075000	-2.357767000	0.156135000
1	-3.107017000	-1.106646000	1.355900000

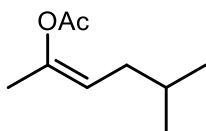


Nimag=0

Zero-point correction=	0.243166 (Hartree/Particle)
Thermal correction to Energy=	0.256802
Thermal correction to Enthalpy=	0.257746
Thermal correction to Gibbs Free Energy=	0.200128
Sum of electronic and zero-point Energies=	-502.623743
Sum of electronic and thermal Energies=	-502.610107
Sum of electronic and thermal Enthalpies=	-502.609163
Sum of electronic and thermal Free Energies=	-502.666781

6	0.006846000	0.039924000	-0.526190000
1	0.270583000	-0.983886000	-0.706308000
6	0.944365000	0.856280000	-0.073551000
6	2.819286000	-0.717150000	0.032502000
6	4.267883000	-0.659440000	0.414568000
1	4.363951000	-0.323149000	1.441196000
1	4.707238000	-1.639841000	0.300154000
1	4.784391000	0.057596000	-0.214385000
8	2.256083000	-1.694349000	-0.343865000
8	2.267607000	0.495668000	0.181160000
6	0.824742000	2.305392000	0.258223000
1	1.109144000	2.471553000	1.293515000
1	-0.179359000	2.675383000	0.112515000
6	-1.418543000	0.407537000	-0.800429000
1	-1.586182000	1.475920000	-0.712572000
1	-1.645751000	0.149351000	-1.834898000
1	1.503143000	2.886761000	-0.360307000
6	-2.396864000	-0.333871000	0.110263000

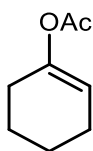
1	-2.217092000	-1.405392000	0.032620000
1	-2.190857000	-0.066686000	1.145728000
6	-3.855003000	-0.040800000	-0.213145000
1	-4.053043000	-0.309509000	-1.249854000
1	-4.031453000	1.031599000	-0.139206000
6	-4.825956000	-0.778046000	0.696752000
1	-5.857405000	-0.551193000	0.443837000
1	-4.694992000	-1.854234000	0.618306000
1	-4.672369000	-0.503785000	1.737335000



Nimag=0

Zero-point correction=	0.242712 (Hartree/Particle)
Thermal correction to Energy=	0.256177
Thermal correction to Enthalpy=	0.257121
Thermal correction to Gibbs Free Energy=	0.201125
Sum of electronic and zero-point Energies=	-502.626907
Sum of electronic and thermal Energies=	-502.613442
Sum of electronic and thermal Enthalpies=	-502.612497
Sum of electronic and thermal Free Energies=	-502.668494

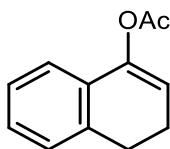
6	0.392319000	0.122828000	0.867399000
1	0.203957000	-0.782058000	1.422704000
6	-0.668424000	0.740339000	0.384996000
6	-2.636950000	-0.386384000	-0.266543000
6	-3.945273000	-0.877946000	0.269321000
1	-4.507764000	-0.045771000	0.678746000
1	-4.504124000	-1.352343000	-0.524259000
1	-3.768817000	-1.580675000	1.076357000
8	-2.265441000	-0.491358000	-1.391023000
8	-1.919332000	0.198755000	0.706551000
6	-0.750902000	2.002725000	-0.398396000
1	-1.173730000	1.805716000	-1.377761000
1	0.222938000	2.454695000	-0.528488000
6	1.818875000	0.544585000	0.710761000
1	1.876323000	1.592972000	0.435165000
1	2.317755000	0.456361000	1.676282000
1	-1.397228000	2.712360000	0.112158000
6	2.609984000	-0.276703000	-0.318871000
1	2.097542000	-0.176373000	-1.274888000
6	4.018132000	0.285825000	-0.468399000
1	4.567021000	0.210502000	0.468251000
1	4.578585000	-0.257876000	-1.223518000
1	3.999177000	1.333068000	-0.758024000
6	2.654166000	-1.757698000	0.037738000
1	3.123052000	-1.907925000	1.008726000
1	1.661151000	-2.193673000	0.072250000
1	3.230790000	-2.313582000	-0.695957000



Nimag=0

Zero-point correction=	0.194507 (Hartree/Particle)
Thermal correction to Energy=	0.204324
Thermal correction to Enthalpy=	0.205268
Thermal correction to Gibbs Free Energy=	0.158098
Sum of electronic and zero-point Energies=	-462.177531
Sum of electronic and thermal Energies=	-462.167714
Sum of electronic and thermal Enthalpies=	-462.166770
Sum of electronic and thermal Free Energies=	-462.213939

6	2.043737000	1.377829000	0.088103000
6	2.905696000	0.213240000	-0.381611000
6	2.467657000	-1.079223000	0.290962000
6	1.020895000	-1.403293000	-0.058304000
6	0.142097000	-0.194840000	0.027695000
6	0.577280000	1.050867000	0.109435000
1	3.110747000	-1.905299000	0.001699000
1	2.807406000	0.104853000	-1.460715000
1	3.953407000	0.416266000	-0.178476000
1	2.354036000	1.691425000	1.085820000
1	0.952224000	-1.816913000	-1.064434000
1	0.623861000	-2.164266000	0.608504000
1	2.560165000	-0.969198000	1.370075000
8	-1.182624000	-0.610631000	0.007979000
6	-2.261798000	0.186607000	-0.009289000
8	-2.240792000	1.374746000	0.013825000
6	-3.504772000	-0.649349000	-0.059681000
1	-3.490833000	-1.274950000	-0.945575000
1	-3.540499000	-1.305214000	0.803476000
1	-4.370411000	-0.003004000	-0.072725000
1	2.202010000	2.241800000	-0.553436000
1	-0.119531000	1.860555000	0.187491000

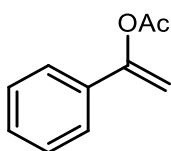


Nimag=0

Zero-point correction=	0.219035 (Hartree/Particle)
Thermal correction to Energy=	0.230826
Thermal correction to Enthalpy=	0.231770
Thermal correction to Gibbs Free Energy=	0.179606
Sum of electronic and zero-point Energies=	-614.524991
Sum of electronic and thermal Energies=	-614.513200

Sum of electronic and thermal Enthalpies= -614.512256
 Sum of electronic and thermal Free Energies= -614.564420

6	-3.266089000	-1.425146000	0.017133000
6	-3.118104000	-0.059726000	-0.161190000
6	-1.865667000	0.526042000	-0.162971000
6	-0.736396000	-0.277547000	0.023843000
6	-0.888945000	-1.647192000	0.194547000
6	-2.148284000	-2.218734000	0.192232000
1	-1.479802000	2.133531000	-1.484756000
1	-4.248980000	-1.864132000	0.017874000
1	-3.988287000	0.559394000	-0.304924000
6	-1.671288000	1.994198000	-0.419923000
6	0.582921000	0.371298000	0.054933000
1	-0.018223000	-2.260586000	0.332899000
1	-2.253860000	-3.281055000	0.329715000
6	0.725533000	1.680741000	0.217575000
6	-0.491227000	2.548369000	0.363261000
1	-0.749316000	2.630168000	1.420843000
8	1.598083000	-0.562102000	-0.052337000
6	2.914733000	-0.296017000	-0.057858000
8	3.396179000	0.786251000	0.031431000
6	3.685513000	-1.573301000	-0.193837000
1	3.470966000	-2.221373000	0.649365000
1	3.380447000	-2.094006000	-1.094795000
1	4.741955000	-1.350255000	-0.229533000
1	-2.579708000	2.540874000	-0.187559000
1	-0.263498000	3.554687000	0.025826000
1	1.698012000	2.121650000	0.285832000

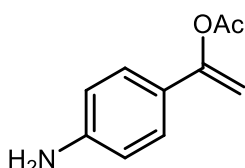


Nimag=0

Zero-point correction= 0.181431 (Hartree/Particle)
 Thermal correction to Energy= 0.192223
 Thermal correction to Enthalpy= 0.193167
 Thermal correction to Gibbs Free Energy= 0.142964
 Sum of electronic and zero-point Energies= -537.158888
 Sum of electronic and thermal Energies= -537.148097
 Sum of electronic and thermal Enthalpies= -537.147153
 Sum of electronic and thermal Free Energies= -537.197356

6	-0.831409000	2.006569000	-0.373995000
1	-0.050721000	2.718129000	-0.566017000
1	-1.848232000	2.331500000	-0.412580000
6	-0.487522000	0.754485000	-0.117469000
6	-2.705960000	-0.223322000	0.079550000
6	-3.283676000	-1.583113000	0.325049000

1	-2.896088000	-1.986791000	1.253686000
1	-4.360767000	-1.510587000	0.366696000
1	-2.988312000	-2.254871000	-0.474197000
8	-3.336380000	0.766337000	-0.098514000
8	-1.361467000	-0.296801000	0.093787000
6	0.904642000	0.264436000	-0.043018000
6	1.210424000	-1.054122000	-0.362487000
6	1.938169000	1.113029000	0.341688000
6	2.517414000	-1.503340000	-0.323704000
1	0.420938000	-1.724776000	-0.646584000
6	3.243179000	0.662541000	0.380068000
1	1.717326000	2.124016000	0.634361000
6	3.539353000	-0.647382000	0.044456000
1	2.736302000	-2.525235000	-0.581921000
1	4.028532000	1.332468000	0.685223000
1	4.556107000	-0.998833000	0.078311000

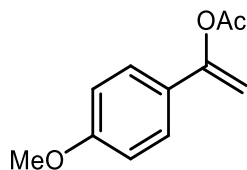


Nimag=0

Zero-point correction=	0.198498 (Hartree/Particle)
Thermal correction to Energy=	0.210770
Thermal correction to Enthalpy=	0.211714
Thermal correction to Gibbs Free Energy=	0.158401
Sum of electronic and zero-point Energies=	-592.482654
Sum of electronic and thermal Energies=	-592.470381
Sum of electronic and thermal Enthalpies=	-592.469437
Sum of electronic and thermal Free Energies=	-592.522751

6	1.419140000	2.013166000	-0.361951000
1	0.698272000	2.784592000	-0.557136000
1	2.458117000	2.259543000	-0.382719000
6	0.975710000	0.788997000	-0.119841000
6	3.115857000	-0.354796000	0.083458000
6	3.586993000	-1.759514000	0.307025000
1	3.160302000	-2.150579000	1.223859000
1	3.250290000	-2.391528000	-0.508156000
1	4.666019000	-1.769654000	0.359959000
8	3.824147000	0.585776000	-0.068845000
8	1.771452000	-0.326955000	0.085074000
6	-0.444241000	0.400229000	-0.049795000
6	-1.426454000	1.317065000	0.311523000
6	-0.853385000	-0.894786000	-0.349310000
6	-2.758124000	0.967658000	0.347221000
1	-1.145149000	2.317096000	0.590827000
6	-2.184211000	-1.253430000	-0.317085000
1	-0.117965000	-1.630620000	-0.617803000
6	-3.163520000	-0.326328000	0.027230000

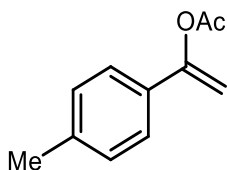
1	-3.493916000	1.696489000	0.644605000
1	-2.470763000	-2.264209000	-0.556795000
7	-4.495180000	-0.694881000	0.114137000
1	-5.155194000	0.051117000	0.025371000
1	-4.755137000	-1.498216000	-0.421649000



Nimag=0

Zero-point correction=	0.215059 (Hartree/Particle)
Thermal correction to Energy=	0.228402
Thermal correction to Enthalpy=	0.229346
Thermal correction to Gibbs Free Energy=	0.173177
Sum of electronic and zero-point Energies=	-651.615423
Sum of electronic and thermal Energies=	-651.602080
Sum of electronic and thermal Enthalpies=	-651.601136
Sum of electronic and thermal Free Energies=	-651.657305

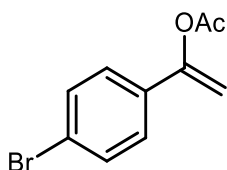
6	1.828477000	2.011768000	-0.384688000
1	1.099592000	2.768632000	-0.605744000
1	2.863913000	2.273844000	-0.388090000
6	1.398841000	0.784610000	-0.135311000
6	3.547054000	-0.328589000	0.127528000
6	4.032157000	-1.723935000	0.375873000
1	3.728665000	-2.366555000	-0.444096000
1	5.109256000	-1.717407000	0.459380000
1	3.584957000	-2.115128000	1.282739000
8	4.243840000	0.620808000	-0.021282000
8	2.201593000	-0.318625000	0.101322000
6	-0.018940000	0.379263000	-0.092006000
6	-1.010509000	1.275957000	0.273909000
6	-0.405732000	-0.918893000	-0.424311000
6	-2.346915000	0.915088000	0.286711000
1	-0.742281000	2.272465000	0.577155000
6	-1.729219000	-1.290726000	-0.415634000
1	0.343325000	-1.639136000	-0.696815000
6	-2.714312000	-0.375337000	-0.063259000
1	-3.081528000	1.639854000	0.583519000
1	-2.029937000	-2.289123000	-0.679067000
6	-5.023398000	0.044408000	0.263427000
1	-5.937703000	-0.525047000	0.172627000
1	-4.923300000	0.398216000	1.287076000
1	-5.065150000	0.897374000	-0.410166000
8	-3.982287000	-0.832142000	-0.081534000



Nimag=0

Zero-point correction= 0.209412 (Hartree/Particle)
 Thermal correction to Energy= 0.222126
 Thermal correction to Enthalpy= 0.223070
 Thermal correction to Gibbs Free Energy= 0.167279
 Sum of electronic and zero-point Energies= -576.431318
 Sum of electronic and thermal Energies= -576.418604
 Sum of electronic and thermal Enthalpies= -576.417660
 Sum of electronic and thermal Free Energies= -576.473451

6	1.438860000	2.010546000	-0.348075000
1	0.718977000	2.784140000	-0.537658000
1	2.478477000	2.254335000	-0.373488000
6	0.994399000	0.786504000	-0.110525000
6	3.128475000	-0.365808000	0.084364000
6	3.595337000	-1.770336000	0.314613000
1	3.169404000	-2.155267000	1.234337000
1	3.254777000	-2.405378000	-0.496611000
1	4.674425000	-1.783637000	0.364889000
8	3.837265000	0.572005000	-0.079892000
8	1.782940000	-0.332317000	0.094093000
6	-0.430811000	0.404807000	-0.050485000
6	-1.405316000	1.327556000	0.317418000
6	-0.839403000	-0.883916000	-0.369196000
6	-2.738966000	0.976977000	0.340399000
1	-1.117137000	2.322460000	0.607234000
6	-2.178147000	-1.228446000	-0.344434000
1	-0.105502000	-1.617989000	-0.645910000
6	-3.152517000	-0.307808000	0.009078000
1	-3.471585000	1.711633000	0.631944000
1	-2.467748000	-2.232574000	-0.606891000
6	-4.603308000	-0.688788000	0.065612000
1	-4.917273000	-0.873640000	1.090438000
1	-5.233887000	0.101369000	-0.329715000
1	-4.796189000	-1.590685000	-0.504788000

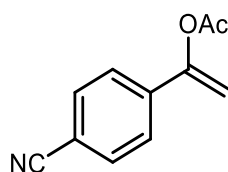


Nimag=0

Zero-point correction= 0.170946 (Hartree/Particle)
 Thermal correction to Energy= 0.183200
 Thermal correction to Enthalpy= 0.184145
 Thermal correction to Gibbs Free Energy= 0.129283

Sum of electronic and zero-point Energies= -3110.672727
 Sum of electronic and thermal Energies= -3110.660473
 Sum of electronic and thermal Enthalpies= -3110.659528
 Sum of electronic and thermal Free Energies= -3110.714390

6	2.680609000	-1.989081000	-0.347271000
1	2.020343000	-2.814418000	-0.535660000
1	3.735374000	-2.155959000	-0.371982000
6	2.148755000	-0.799954000	-0.113254000
6	4.189390000	0.506906000	0.091427000
6	4.550934000	1.941834000	0.318771000
1	4.092248000	2.298026000	1.234321000
1	5.625789000	2.033424000	0.376126000
1	4.171041000	2.547671000	-0.497290000
8	4.962324000	-0.379861000	-0.061786000
8	2.847317000	0.375363000	0.088825000
6	0.697830000	-0.527343000	-0.059316000
6	0.198611000	0.729070000	-0.382931000
6	-0.202730000	-1.520109000	0.311906000
6	-1.159681000	0.983484000	-0.364079000
1	0.877740000	1.514404000	-0.657194000
6	-1.561883000	-1.278790000	0.334785000
1	0.158108000	-2.488292000	0.609125000
6	-2.032095000	-0.025382000	-0.007928000
1	-1.533334000	1.956789000	-0.624392000
1	-2.246051000	-2.053319000	0.629052000
35	-3.898195000	0.316395000	0.026540000

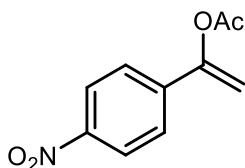


Nimag=0

Zero-point correction= 0.180191 (Hartree/Particle)
 Thermal correction to Energy= 0.192741
 Thermal correction to Enthalpy= 0.193685
 Thermal correction to Gibbs Free Energy= 0.139136
 Sum of electronic and zero-point Energies= -629.373043
 Sum of electronic and thermal Energies= -629.360494
 Sum of electronic and thermal Enthalpies= -629.359550
 Sum of electronic and thermal Free Energies= -629.414098

6	1.740129000	1.996586000	-0.339038000
1	1.044967000	2.794398000	-0.519650000
1	2.786743000	2.207713000	-0.373119000
6	1.262279000	0.784539000	-0.105217000
6	3.356617000	-0.434746000	0.083250000
6	3.780935000	-1.851625000	0.311194000
1	3.340919000	-2.226958000	1.228209000
1	3.426301000	-2.474182000	-0.503699000

1	4.858891000	-1.895693000	0.365435000
8	4.086859000	0.485275000	-0.079266000
8	2.008237000	-0.360185000	0.090742000
6	-0.176602000	0.453259000	-0.049579000
6	-1.117168000	1.414777000	0.310032000
6	-0.618893000	-0.829243000	-0.359026000
6	-2.461207000	1.115080000	0.333951000
1	-0.795303000	2.399446000	0.595855000
6	-1.962701000	-1.137428000	-0.338133000
1	0.095881000	-1.585540000	-0.622087000
6	-2.893342000	-0.165303000	0.005990000
1	-3.178853000	1.863591000	0.617952000
1	-2.295527000	-2.128967000	-0.587444000
6	-4.285853000	-0.481738000	0.033543000
7	-5.398565000	-0.734211000	0.054990000



Nimag=0

Zero-point correction= 0.184609 (Hartree/Particle)

Thermal correction to Energy= 0.197884

Thermal correction to Enthalpy= 0.198828

Thermal correction to Gibbs Free Energy= 0.141951

Sum of electronic and zero-point Energies= -741.597492

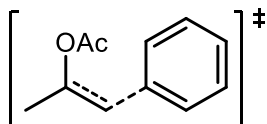
Sum of electronic and thermal Energies= -741.584217

Sum of electronic and thermal Enthalpies= -741.583273

Sum of electronic and thermal Free Energies= -741.640150

6	2.180568000	1.992515000	-0.400093000
1	1.499726000	2.796398000	-0.606240000
1	3.230779000	2.183972000	-0.440142000
6	1.681889000	0.796756000	-0.128722000
6	3.754070000	-0.452240000	0.101540000
6	4.153273000	-1.867184000	0.379831000
1	3.715519000	-2.197498000	1.315149000
1	3.778255000	-2.514126000	-0.406331000
1	5.230642000	-1.930123000	0.426197000
8	4.499349000	0.449207000	-0.092516000
8	2.406486000	-0.353821000	0.105485000
6	0.236987000	0.493453000	-0.067464000
6	-0.686238000	1.485069000	0.256873000
6	-0.225037000	-0.792068000	-0.335701000
6	-2.036338000	1.212365000	0.286665000
1	-0.347154000	2.472380000	0.510858000
6	-1.574253000	-1.078261000	-0.309562000
1	0.477476000	-1.568470000	-0.570592000
6	-2.462325000	-0.069098000	-0.001349000
1	-2.756558000	1.966454000	0.539960000

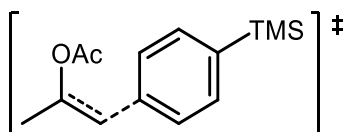
1	-1.943870000	-2.062772000	-0.523447000
7	-3.893399000	-0.366481000	0.032941000
8	-4.642444000	0.533999000	0.308774000
8	-4.234215000	-1.492971000	-0.217757000



Nimag=1 (-281 cm⁻¹)

Zero-point correction=	0.216465 (Hartree/Particle)
Thermal correction to Energy=	0.229873
Thermal correction to Enthalpy=	0.230817
Thermal correction to Gibbs Free Energy=	0.172291
Sum of electronic and zero-point Energies=	-576.936031
Sum of electronic and thermal Energies=	-576.922623
Sum of electronic and thermal Enthalpies=	-576.921679
Sum of electronic and thermal Free Energies=	-576.980204

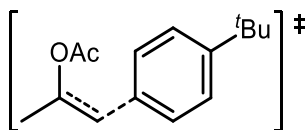
6	-0.633593000	1.112689000	1.239284000
1	-0.107207000	1.971112000	1.613351000
1	-0.698808000	0.244685000	1.857761000
6	-1.434397000	1.303709000	0.177971000
6	-1.483356000	2.544498000	-0.639296000
1	-0.856074000	3.312412000	-0.205726000
1	-1.143311000	2.344800000	-1.652857000
1	-2.501865000	2.917331000	-0.705666000
6	-2.476068000	-0.891955000	0.043450000
6	-3.438705000	-1.594056000	-0.858923000
1	-3.027549000	-1.641102000	-1.861469000
1	-3.622603000	-2.591394000	-0.486966000
1	-4.367189000	-1.036362000	-0.909181000
8	-1.966056000	-1.368771000	1.010886000
8	-2.264658000	0.357988000	-0.395487000
6	1.401946000	0.243766000	0.426954000
6	1.500094000	-1.121890000	0.318665000
6	2.411687000	1.109551000	0.085469000
6	2.695550000	-1.650899000	-0.156240000
1	0.679874000	-1.764621000	0.591052000
6	3.601331000	0.566170000	-0.388523000
6	3.739813000	-0.808477000	-0.507509000
1	2.809195000	-2.718021000	-0.252002000
1	4.415653000	1.215720000	-0.663671000
1	4.662333000	-1.223665000	-0.875464000
1	2.297462000	2.176731000	0.179835000



Nimag=1 (-278 cm⁻¹)

Zero-point correction=	0.320813 (Hartree/Particle)
Thermal correction to Energy=	0.341933
Thermal correction to Enthalpy=	0.342878
Thermal correction to Gibbs Free Energy=	0.266433
Sum of electronic and zero-point Energies=	-985.456761
Sum of electronic and thermal Energies=	-985.435640
Sum of electronic and thermal Enthalpies=	-985.434696
Sum of electronic and thermal Free Energies=	-985.511141

6	2.844270000	1.208241000	-1.153002000
1	2.561016000	2.188750000	-1.488109000
1	2.809030000	0.402507000	-1.853239000
6	3.519477000	1.129469000	0.004833000
6	3.712680000	2.254116000	0.957894000
1	3.337866000	3.179148000	0.538716000
1	3.189250000	2.055470000	1.890412000
1	4.765882000	2.377138000	1.195585000
6	3.997569000	-1.253268000	0.030941000
6	4.688382000	-2.222787000	0.939224000
1	4.662722000	-3.208169000	0.497120000
1	5.713910000	-1.909557000	1.101010000
1	4.192798000	-2.233451000	1.904124000
8	3.472921000	-1.535036000	-0.998329000
8	4.057358000	-0.018526000	0.556713000
6	0.587436000	0.737693000	-0.676236000
6	0.186749000	-0.565862000	-0.811375000
6	-0.252905000	1.751222000	-0.289633000
6	-1.146352000	-0.862298000	-0.548740000
1	0.878768000	-1.335266000	-1.109821000
6	-1.578713000	1.430197000	-0.031978000
6	-2.052822000	0.122295000	-0.155723000
1	-1.475662000	-1.883437000	-0.655312000
1	-2.249499000	2.220382000	0.270118000
1	0.092475000	2.767185000	-0.189086000
6	-4.255108000	0.181543000	1.982782000
6	-4.955789000	0.739024000	-0.941829000
6	-4.184569000	-2.096173000	-0.067406000
1	-3.647857000	-0.393893000	2.676260000
1	-4.066305000	1.234081000	2.177722000
1	-5.300126000	-0.013264000	2.212176000
1	-4.763779000	0.494625000	-1.983027000
1	-6.007802000	0.549235000	-0.742132000
1	-4.785069000	1.805428000	-0.819067000
1	-5.227898000	-2.324800000	0.135730000
1	-3.978013000	-2.395693000	-1.091419000
1	-3.580687000	-2.715476000	0.590494000
14	-3.858936000	-0.268066000	0.202583000



Nimag=1 (-274 cm⁻¹)

Zero-point correction= 0.332525 (Hartree/Particle)

Thermal correction to Energy= 0.351199

Thermal correction to Enthalpy= 0.352143

Thermal correction to Gibbs Free Energy= 0.282276

Sum of electronic and zero-point Energies= -734.000062

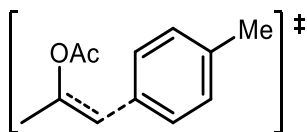
Sum of electronic and thermal Energies= -733.981388

Sum of electronic and thermal Enthalpies= -733.980444

Sum of electronic and thermal Free Energies= -734.050311

6	2.453546000	1.203225000	-1.174237000
1	2.140666000	2.171975000	-1.517027000
1	2.419024000	0.385994000	-1.860980000
6	3.154244000	1.156278000	-0.030371000
6	3.343546000	2.298852000	0.901950000
1	2.940559000	3.209422000	0.477260000
1	2.843785000	2.103409000	1.848039000
1	4.398612000	2.447463000	1.115635000
6	3.683251000	-1.215261000	0.020863000
6	4.408413000	-2.157315000	0.931489000
1	4.400629000	-3.148261000	0.501275000
1	5.428005000	-1.818036000	1.077199000
1	3.924668000	-2.168401000	1.902420000
8	3.147134000	-1.523266000	-0.994920000
8	3.727340000	0.027920000	0.527276000
6	0.215191000	0.688305000	-0.642830000
6	-0.163784000	-0.621574000	-0.754702000
6	-0.648859000	1.682984000	-0.258730000
6	-1.487550000	-0.947368000	-0.473135000
1	0.537410000	-1.383272000	-1.051358000
6	-1.962238000	1.336088000	0.017792000
6	-2.408483000	0.018285000	-0.083695000
1	-1.787389000	-1.975577000	-0.564381000
1	-2.646694000	2.112074000	0.317110000
1	-0.330792000	2.709095000	-0.173191000
6	-3.869266000	-0.310985000	0.231418000
6	-4.183380000	0.081734000	1.681562000
6	-4.788010000	0.471914000	-0.716646000
6	-4.177694000	-1.799403000	0.066907000
1	-3.548390000	-0.461931000	2.374942000
1	-4.030863000	1.142075000	1.853788000
1	-5.219217000	-0.147537000	1.919259000
1	-4.588311000	0.209833000	-1.751455000
1	-5.830231000	0.246420000	-0.504622000
1	-4.653451000	1.543650000	-0.614166000
1	-5.222532000	-1.981535000	0.300517000
1	-4.004862000	-2.137028000	-0.950613000

1 -3.579986000 -2.411613000 0.735689000



Nimag=1 (-277 cm⁻¹)

Zero-point correction= 0.244992 (Hartree/Particle)

Thermal correction to Energy= 0.260185

Thermal correction to Enthalpy= 0.261129

Thermal correction to Gibbs Free Energy= 0.198153

Sum of electronic and zero-point Energies= -616.199711

Sum of electronic and thermal Energies= -616.184518

Sum of electronic and thermal Enthalpies= -616.183574

Sum of electronic and thermal Free Energies= -616.246550

6 -1.245472000 1.165579000 1.221392000

1 -0.831065000 2.086953000 1.586331000

1 -1.244205000 0.316449000 1.869193000

6 -2.010385000 1.232742000 0.120432000

6 -2.151030000 2.430390000 -0.749242000

1 -1.647987000 3.282579000 -0.310359000

1 -1.722773000 2.239034000 -1.730575000

1 -3.199414000 2.677110000 -0.893901000

6 -2.744944000 -1.080763000 -0.001577000

6 -3.599877000 -1.913351000 -0.906241000

1 -3.654000000 -2.920974000 -0.520381000

1 -4.592663000 -1.482622000 -0.975145000

1 -3.174740000 -1.918504000 -1.904278000

8 -2.180323000 -1.481637000 0.965235000

8 -2.709812000 0.184737000 -0.449849000

6 0.906200000 0.492861000 0.534076000

6 1.172214000 -0.852957000 0.563155000

6 1.823454000 1.431399000 0.138956000

6 2.439683000 -1.271144000 0.181270000

1 0.422668000 -1.563594000 0.867904000

6 3.086050000 0.991019000 -0.239969000

6 3.409755000 -0.359499000 -0.221037000

1 2.676304000 -2.323491000 0.194560000

1 3.826191000 1.709165000 -0.555635000

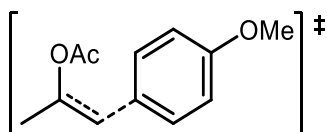
1 1.586213000 2.482393000 0.117316000

6 4.786543000 -0.826505000 -0.603055000

1 5.280472000 -0.110025000 -1.250794000

1 5.412735000 -0.959237000 0.276444000

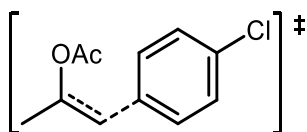
1 4.750200000 -1.778666000 -1.122728000



Nimag=1 (-271 cm⁻¹)

Zero-point correction=	0.250653 (Hartree/Particle)
Thermal correction to Energy=	0.266478
Thermal correction to Enthalpy=	0.267422
Thermal correction to Gibbs Free Energy=	0.203714
Sum of electronic and zero-point Energies=	-691.382843
Sum of electronic and thermal Energies=	-691.367019
Sum of electronic and thermal Enthalpies=	-691.366074
Sum of electronic and thermal Free Energies=	-691.429782

6	-1.754877000	1.180504000	1.178234000
1	-1.445113000	2.153118000	1.512632000
1	-1.667680000	0.359360000	1.855531000
6	-2.507979000	1.125837000	0.069100000
6	-2.766489000	2.269786000	-0.844696000
1	-2.363156000	3.186261000	-0.433255000
1	-2.308655000	2.091106000	-1.814983000
1	-3.833549000	2.396691000	-1.006422000
6	-2.977376000	-1.258320000	0.017287000
6	-3.737799000	-2.207210000	-0.856822000
1	-3.674309000	-3.203558000	-0.444037000
1	-4.773684000	-1.894215000	-0.926972000
1	-3.322008000	-2.191052000	-1.858649000
8	-2.367182000	-1.565699000	0.990776000
8	-3.086200000	-0.010681000	-0.466879000
6	0.470238000	0.719054000	0.535108000
6	0.883797000	-0.581001000	0.628793000
6	1.297643000	1.737930000	0.123842000
6	2.203449000	-0.887291000	0.302321000
1	0.209742000	-1.358369000	0.946531000
6	2.606686000	1.432857000	-0.200854000
6	3.062030000	0.120757000	-0.111539000
1	2.540050000	-1.905134000	0.375995000
1	3.297510000	2.191601000	-0.525527000
1	0.950246000	2.755490000	0.053854000
6	4.888695000	-1.367977000	-0.377813000
1	5.922576000	-1.288599000	-0.684649000
1	4.847068000	-1.760798000	0.636077000
1	4.370021000	-2.051216000	-1.047385000
8	4.358736000	-0.072399000	-0.450960000

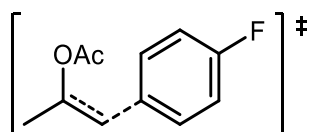


Nimag=1 (-264 cm⁻¹)

Zero-point correction=	0.207215 (Hartree/Particle)
Thermal correction to Energy=	0.221681
Thermal correction to Enthalpy=	0.222625
Thermal correction to Gibbs Free Energy=	0.161662
Sum of electronic and zero-point Energies=	-1036.546967
Sum of electronic and thermal Energies=	-1036.532500

Sum of electronic and thermal Enthalpies= -1036.531556
 Sum of electronic and thermal Free Energies= -1036.592520

6	-1.701463000	1.192203000	1.191607000
1	-1.335208000	2.140942000	1.537429000
1	-1.681651000	0.364025000	1.865958000
6	-2.436346000	1.192574000	0.068485000
6	-2.603567000	2.356928000	-0.840792000
1	-2.141602000	3.240907000	-0.420157000
1	-2.150019000	2.150859000	-1.807536000
1	-3.657393000	2.558533000	-1.012209000
6	-3.050246000	-1.157206000	-0.013178000
6	-3.893895000	-2.040272000	-0.878546000
1	-3.515099000	-2.023926000	-1.894828000
1	-3.873583000	-3.047867000	-0.489535000
1	-4.911874000	-1.667076000	-0.902377000
8	-2.435147000	-1.516176000	0.939068000
8	-3.088241000	0.103761000	-0.477555000
6	0.503343000	0.595649000	0.579891000
6	0.822187000	-0.737573000	0.641020000
6	1.393447000	1.569755000	0.206004000
6	2.117363000	-1.116616000	0.313792000
1	0.092347000	-1.473327000	0.931923000
6	2.688352000	1.188980000	-0.122147000
6	3.030133000	-0.148790000	-0.062909000
1	2.415038000	-2.149418000	0.350056000
1	3.420807000	1.918389000	-0.418753000
1	1.113945000	2.609204000	0.164890000
17	4.658562000	-0.629159000	-0.476254000

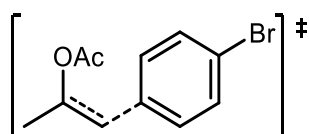


Nimag=1 (-266 cm⁻¹)

Zero-point correction= 0.208636 (Hartree/Particle)
 Thermal correction to Energy= 0.222721
 Thermal correction to Enthalpy= 0.223666
 Thermal correction to Gibbs Free Energy= 0.163969
 Sum of electronic and zero-point Energies= -676.166693
 Sum of electronic and thermal Energies= -676.152607
 Sum of electronic and thermal Enthalpies= -676.151663
 Sum of electronic and thermal Free Energies= -676.211360

6	-1.194235000	1.164035000	1.229195000
1	-0.760996000	2.077400000	1.592330000
1	-1.196055000	0.311942000	1.873262000
6	-1.969830000	1.246453000	0.137100000
6	-2.104079000	2.450347000	-0.724932000
1	-1.578587000	3.291845000	-0.291865000
1	-1.697288000	2.255137000	-1.714499000

1	-3.150370000	2.715581000	-0.849717000
6	-2.722777000	-1.060121000	0.001411000
6	-3.639109000	-1.864902000	-0.866720000
1	-3.285290000	-1.839414000	-1.891805000
1	-3.668964000	-2.883582000	-0.508361000
1	-4.633366000	-1.432083000	-0.852518000
8	-2.103997000	-1.485433000	0.923552000
8	-2.701071000	0.215313000	-0.421415000
6	0.947361000	0.465859000	0.510909000
6	1.191226000	-0.885148000	0.522037000
6	1.878679000	1.400543000	0.134827000
6	2.451258000	-1.326381000	0.138871000
1	0.429499000	-1.585966000	0.817217000
6	3.138800000	0.958630000	-0.249372000
6	3.394815000	-0.395013000	-0.237768000
1	2.707117000	-2.371497000	0.128714000
1	3.913041000	1.641445000	-0.552703000
1	1.655567000	2.454280000	0.134371000
9	4.608176000	-0.822215000	-0.608318000

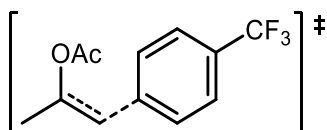


Nimag=1 (-263 cm⁻¹)

Zero-point correction=	0.206571 (Hartree/Particle)
Thermal correction to Energy=	0.221292
Thermal correction to Enthalpy=	0.222236
Thermal correction to Gibbs Free Energy=	0.159920
Sum of electronic and zero-point Energies=	-3150.442377
Sum of electronic and thermal Energies=	-3150.427656
Sum of electronic and thermal Enthalpies=	-3150.426712
Sum of electronic and thermal Free Energies=	-3150.489028

6	-2.489086000	1.206680000	1.157045000
1	-2.179781000	2.180691000	1.487921000
1	-2.452765000	0.398430000	1.854514000
6	-3.185699000	1.142340000	0.011514000
6	-3.377310000	2.273113000	-0.934585000
1	-2.971588000	3.188932000	-0.524187000
1	-2.882848000	2.063746000	-1.880334000
1	-4.433208000	2.419431000	-1.144943000
6	-3.685988000	-1.235354000	-0.023901000
6	-4.458055000	-2.180218000	-0.890813000
1	-4.046659000	-2.172821000	-1.894447000
1	-4.403707000	-3.175027000	-0.473213000
1	-5.490990000	-1.856678000	-0.957831000
8	-3.086971000	-1.539208000	0.957322000
8	-3.767273000	0.009636000	-0.524491000
6	-0.240099000	0.701771000	0.632627000
6	0.139305000	-0.612479000	0.738819000

6	0.614141000	1.708048000	0.260687000
6	1.461249000	-0.937317000	0.461823000
1	-0.563689000	-1.375259000	1.026490000
6	1.936111000	1.382505000	-0.017406000
6	2.339117000	0.064123000	0.087811000
1	1.801341000	-1.954751000	0.536022000
1	2.638381000	2.142367000	-0.310112000
1	0.287184000	2.731554000	0.183409000
35	4.148862000	-0.383809000	-0.293362000



Nimag=1 (-2228 cm⁻¹)

Zero-point correction= 0.221966 (Hartree/Particle)

Thermal correction to Energy= 0.238939

Thermal correction to Enthalpy= 0.239883

Thermal correction to Gibbs Free Energy= 0.170243

Sum of electronic and zero-point Energies= -913.937748

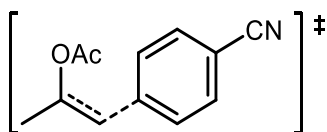
Sum of electronic and thermal Energies= -913.920775

Sum of electronic and thermal Enthalpies= -913.919831

Sum of electronic and thermal Free Energies= -913.989471

6	-2.384293000	-1.494658000	-0.668890000
1	-2.068329000	-2.521226000	-0.669844000
1	-2.382962000	-0.959068000	-1.594102000
6	-3.031149000	-1.046988000	0.415251000
6	-3.184731000	-1.793134000	1.691774000
1	-2.755637000	-2.783496000	1.610614000
1	-2.693258000	-1.265217000	2.505445000
1	-4.235651000	-1.884467000	1.953669000
6	-3.927001000	1.029139000	-0.454699000
6	-4.414566000	2.335521000	0.088697000
1	-3.605061000	2.838248000	0.607510000
1	-4.769656000	2.950561000	-0.725316000
1	-5.208245000	2.164538000	0.807279000
8	-3.886772000	0.730780000	-1.601649000
8	-3.538986000	0.229554000	0.563549000
6	-0.097791000	-0.829132000	-0.364899000
6	0.177815000	0.109146000	0.596495000
6	0.856589000	-1.401620000	-1.166908000
6	1.497836000	0.499863000	0.764552000
1	-0.600531000	0.534051000	1.207132000
6	2.174475000	-1.005333000	-0.992021000
6	2.487879000	-0.059560000	-0.028294000
1	1.759103000	1.227767000	1.512515000
1	2.955498000	-1.434487000	-1.594734000
1	0.604770000	-2.136887000	-1.912190000
6	3.901173000	0.401456000	0.122405000
9	4.174387000	0.776425000	1.371395000

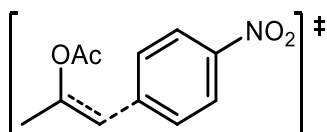
9	4.775466000	-0.548315000	-0.205873000
9	4.168882000	1.451759000	-0.657074000



Nimag=1 (-223 cm⁻¹)

Zero-point correction=	0.215470 (Hartree/Particle)
Thermal correction to Energy=	0.230686
Thermal correction to Enthalpy=	0.231630
Thermal correction to Gibbs Free Energy=	0.167836
Sum of electronic and zero-point Energies=	-669.142604
Sum of electronic and thermal Energies=	-669.127388
Sum of electronic and thermal Enthalpies=	-669.126443
Sum of electronic and thermal Free Energies=	-669.190238

6	1.517483000	-1.468202000	0.707613000
1	1.144012000	-2.475065000	0.730616000
1	1.532936000	-0.907142000	1.617373000
6	2.201690000	-1.087646000	-0.379327000
6	2.331165000	-1.879760000	-1.630762000
1	1.844279000	-2.840940000	-1.528270000
1	1.884454000	-1.348955000	-2.467955000
1	3.379000000	-2.039008000	-1.871377000
6	3.181132000	0.972027000	0.441819000
6	3.770617000	2.220021000	-0.136141000
1	3.020630000	2.739495000	-0.723249000
1	4.118076000	2.855155000	0.665606000
1	4.590003000	1.968299000	-0.800161000
8	3.075488000	0.729215000	1.597558000
8	2.786192000	0.150775000	-0.557243000
6	-0.727320000	-0.681079000	0.350561000
6	-0.940828000	0.229702000	-0.653138000
6	-1.717193000	-1.160535000	1.171725000
6	-2.232032000	0.690543000	-0.850178000
1	-0.134148000	0.582989000	-1.272475000
6	-3.007719000	-0.698145000	0.971998000
6	-3.263151000	0.225411000	-0.038267000
1	-2.447789000	1.405389000	-1.625007000
1	-3.816414000	-1.045455000	1.591078000
1	-1.510507000	-1.872403000	1.952651000
6	-4.595072000	0.700536000	-0.243804000
7	-5.658657000	1.080071000	-0.409136000

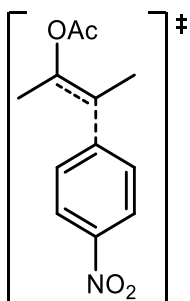


Nimag=1 (-216 cm⁻¹)

Zero-point correction=	0.219936 (Hartree/Particle)
------------------------	-----------------------------

Thermal correction to Energy= 0.235861
 Thermal correction to Enthalpy= 0.236805
 Thermal correction to Gibbs Free Energy= 0.170611
 Sum of electronic and zero-point Energies= -781.367135
 Sum of electronic and thermal Energies= -781.351210
 Sum of electronic and thermal Enthalpies= -781.350266
 Sum of electronic and thermal Free Energies= -781.416460

6	1.968645000	1.572176000	-0.499036000
1	1.622763000	2.581612000	-0.375561000
1	1.972971000	1.148497000	-1.480410000
6	2.633455000	1.017743000	0.523078000
6	2.777063000	1.616857000	1.876209000
1	2.318392000	2.596486000	1.912711000
1	2.310300000	0.983628000	2.626725000
1	3.827441000	1.709084000	2.139486000
6	3.548374000	-0.935526000	-0.584550000
6	4.108940000	-2.265081000	-0.188675000
1	3.351552000	-2.839262000	0.334452000
1	4.429634000	-2.795000000	-1.073684000
1	4.942520000	-2.126661000	0.490813000
8	3.439535000	-0.534567000	-1.694999000
8	3.183671000	-0.248257000	0.521889000
6	-0.303031000	0.800636000	-0.262589000
6	-0.544215000	-0.240010000	0.599635000
6	-1.275486000	1.420818000	-1.008096000
6	-1.847524000	-0.692009000	0.728354000
1	0.249899000	-0.699761000	1.162239000
6	-2.579843000	0.970653000	-0.880530000
6	-2.838418000	-0.076031000	-0.014226000
1	-2.105889000	-1.501751000	1.384425000
1	-3.388209000	1.410508000	-1.433675000
1	-1.045846000	2.231831000	-1.677581000
7	-4.215120000	-0.551116000	0.121810000
8	-4.418449000	-1.464431000	0.879121000
8	-5.063190000	-0.000589000	-0.531020000

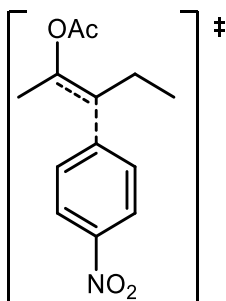


Nimag=1 (-275 cm⁻¹)
 Zero-point correction= 0.248993 (Hartree/Particle)
 Thermal correction to Energy= 0.266436
 Thermal correction to Enthalpy= 0.267380
 Thermal correction to Gibbs Free Energy= 0.199471

Sum of electronic and zero-point Energies= -820.635623
 Sum of electronic and thermal Energies= -820.618180
 Sum of electronic and thermal Enthalpies= -820.617236
 Sum of electronic and thermal Free Energies= -820.685145

6	2.073987000	-1.145368000	0.845442000
1	2.019592000	-0.393675000	1.605346000
6	2.633100000	-0.807176000	-0.334717000
6	2.846292000	1.602845000	0.012204000
6	3.247783000	2.787049000	-0.810691000
1	2.564045000	2.896137000	-1.645894000
1	3.226147000	3.674603000	-0.195232000
1	4.241018000	2.634691000	-1.218010000
8	2.508291000	1.646675000	1.152475000
8	2.920944000	0.487995000	-0.732547000
6	-0.201010000	-0.618110000	0.451862000
6	-0.652105000	0.592639000	0.921976000
6	-0.987760000	-1.507020000	-0.240930000
6	-1.976972000	0.929273000	0.693582000
1	0.001114000	1.265891000	1.449091000
6	-2.311804000	-1.171771000	-0.471971000
6	-2.779381000	0.040863000	0.001120000
1	-2.392364000	1.857532000	1.038274000
1	-2.978385000	-1.823837000	-1.004288000
1	-0.600849000	-2.446289000	-0.597430000
6	2.941100000	-1.712060000	-1.474268000
7	-4.176313000	0.397559000	-0.243167000
8	-4.563694000	1.458690000	0.172623000
8	-4.857416000	-0.390835000	-0.846727000
1	2.329219000	-1.453636000	-2.335695000
1	2.771743000	-2.749368000	-1.224114000
6	1.903780000	-2.567969000	1.297310000
1	1.149579000	-2.623815000	2.072967000
1	1.603960000	-3.236769000	0.499184000
1	2.832507000	-2.948917000	1.716785000
1	3.979814000	-1.594838000	-1.770925000

PUC-Rio - Certificação Digital N° 1613320/CA



Nimag=1 (-258 cm⁻¹)

Zero-point correction= 0.278307 (Hartree/Particle)

Thermal correction to Energy= 0.297042

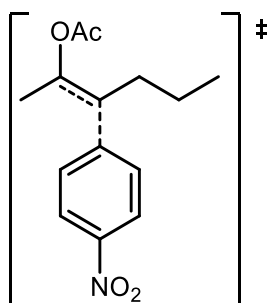
Thermal correction to Enthalpy= 0.297987

Thermal correction to Gibbs Free Energy= 0.227051

Sum of electronic and zero-point Energies= -859.902684
 Sum of electronic and thermal Energies= -859.883948
 Sum of electronic and thermal Enthalpies= -859.883004
 Sum of electronic and thermal Free Energies= -859.953939

6	2.111029000	1.009399000	-0.333458000
1	2.049170000	0.512503000	-1.280215000
6	2.542108000	0.300547000	0.729612000
6	2.586873000	-1.927269000	-0.266343000
6	2.802246000	-3.328995000	0.212386000
1	2.028554000	-3.589875000	0.926810000
1	2.771177000	-4.003990000	-0.630482000
1	3.756846000	-3.403967000	0.720991000
8	2.360330000	-1.616770000	-1.392497000
8	2.683264000	-1.075658000	0.767917000
6	-0.228664000	0.577653000	-0.195970000
6	-0.730581000	-0.405223000	-1.016332000
6	-0.982360000	1.244686000	0.740045000
6	-2.072746000	-0.730788000	-0.901212000
1	-0.102873000	-0.915563000	-1.725738000
6	-2.323923000	0.920185000	0.858100000
6	-2.841905000	-0.061894000	0.033510000
1	-2.526491000	-1.485710000	-1.515426000
1	-2.965921000	1.407310000	1.567634000
1	-0.556742000	2.006324000	1.370986000
6	2.832091000	0.834549000	2.086698000
7	-4.257190000	-0.407793000	0.157849000
8	-4.688235000	-1.268666000	-0.564682000
8	-4.908657000	0.188246000	0.976429000
1	2.128399000	0.427984000	2.809880000
1	2.773501000	1.913574000	2.112422000
6	2.100218000	2.518750000	-0.355322000
1	1.519072000	2.912990000	0.473954000
1	3.116235000	2.882520000	-0.208749000
1	3.827509000	0.533663000	2.402048000
6	1.560938000	3.077854000	-1.663540000
1	1.586208000	4.162866000	-1.659627000
1	2.154875000	2.734698000	-2.505902000
1	0.535250000	2.765279000	-1.829913000

PUC-Rio - Certificação Digital N° 1613320/CA

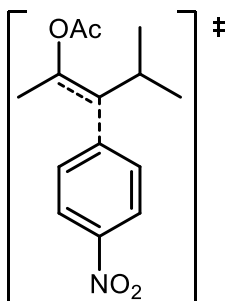


Nimag=1 (-259 cm⁻¹)
 Zero-point correction=

0.307550 (Hartree/Particle)

Thermal correction to Energy= 0.327652
 Thermal correction to Enthalpy= 0.328596
 Thermal correction to Gibbs Free Energy= 0.254203
 Sum of electronic and zero-point Energies= -899.170817
 Sum of electronic and thermal Energies= -899.150715
 Sum of electronic and thermal Enthalpies= -899.149771
 Sum of electronic and thermal Free Energies= -899.224163

6	2.091050000	0.533035000	-0.092011000
1	2.001697000	0.198984000	-1.105647000
6	2.415138000	-0.375979000	0.850004000
6	2.246838000	-2.412652000	-0.484322000
6	2.294869000	-3.886993000	-0.230439000
1	1.476473000	-4.167891000	0.424081000
1	2.216060000	-4.414834000	-1.169687000
1	3.220103000	-4.146292000	0.271814000
8	2.088279000	-1.907442000	-1.549994000
8	2.404640000	-1.748512000	0.672449000
6	-0.281245000	0.346192000	-0.048532000
6	-0.863357000	-0.430406000	-1.022775000
6	-0.985410000	0.937930000	0.972871000
6	-2.236234000	-0.614441000	-0.979154000
1	-0.274258000	-0.890249000	-1.796897000
6	-2.357697000	0.754448000	1.019650000
6	-2.955390000	-0.018558000	0.040888000
1	-2.751441000	-1.205526000	-1.712793000
1	-2.963566000	1.192955000	1.790062000
1	-0.497843000	1.535662000	1.724099000
6	2.724573000	-0.094724000	2.276863000
7	-4.403500000	-0.215294000	0.089126000
8	-4.904508000	-0.895527000	-0.768342000
8	-5.010252000	0.314112000	0.984310000
1	1.961935000	-0.528177000	2.920289000
1	2.781585000	0.967104000	2.471044000
6	2.244494000	2.018498000	0.124283000
1	1.668513000	2.347674000	0.986300000
1	3.285644000	2.241296000	0.357620000
1	3.672919000	-0.549146000	2.550749000
6	1.833778000	2.835372000	-1.093970000
1	2.428683000	2.519298000	-1.948841000
1	0.798923000	2.613119000	-1.341562000
6	2.001788000	4.331157000	-0.880051000
1	3.034930000	4.583868000	-0.654823000
1	1.710694000	4.889945000	-1.763922000
1	1.389006000	4.680958000	-0.052982000



Nimag=1 (-259 cm⁻¹)

Zero-point correction= 0.307024 (Hartree/Particle)

Thermal correction to Energy= 0.327037

Thermal correction to Enthalpy= 0.327981

Thermal correction to Gibbs Free Energy= 0.253846

Sum of electronic and zero-point Energies= -899.167096

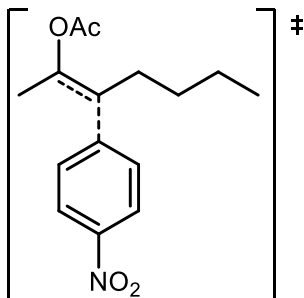
Sum of electronic and thermal Energies= -899.147082

Sum of electronic and thermal Enthalpies= -899.146138

Sum of electronic and thermal Free Energies= -899.220273

6	1.751640000	0.923769000	-0.324239000
1	1.510752000	0.633120000	-1.332841000
6	2.286662000	-0.048562000	0.443300000
6	3.205263000	-2.061617000	-0.376735000
6	2.814633000	-3.446439000	-0.783145000
1	2.353340000	-3.955217000	0.056578000
1	2.080155000	-3.401476000	-1.579617000
1	3.691377000	-3.986273000	-1.109962000
8	4.307341000	-1.618301000	-0.374152000
8	2.119407000	-1.354852000	-0.003744000
6	-0.541983000	0.484789000	-0.107547000
6	-1.312189000	0.650587000	-1.234247000
6	-1.027083000	-0.042302000	1.065675000
6	-2.647557000	0.283567000	-1.182216000
1	-0.902922000	1.054650000	-2.144354000
6	-2.360216000	-0.410888000	1.122758000
6	-3.144850000	-0.239395000	-0.003542000
1	-3.299010000	0.392509000	-2.028782000
1	-2.796857000	-0.825015000	2.012006000
1	-0.395058000	-0.169862000	1.926983000
6	2.906684000	0.072387000	1.787309000
7	-4.552773000	-0.629869000	0.053871000
8	-5.216948000	-0.473677000	-0.937834000
8	-4.964620000	-1.084570000	1.089564000
1	3.905164000	-0.352545000	1.772067000
1	2.324272000	-0.474809000	2.526568000
6	1.932181000	2.408125000	-0.060626000
1	2.961384000	2.543652000	0.268256000
1	2.976799000	1.104955000	2.100424000
6	1.027869000	2.982083000	1.029059000
1	1.092344000	2.417743000	1.953422000
1	1.312996000	4.008101000	1.244840000

1	-0.010127000	2.979956000	0.714440000
6	1.765884000	3.193789000	-1.357512000
1	1.964173000	4.248825000	-1.195989000
1	2.446839000	2.839107000	-2.125453000
1	0.750727000	3.103503000	-1.736109000

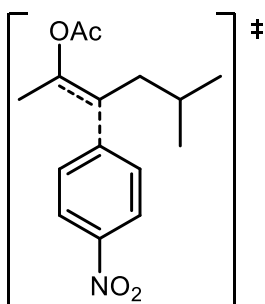


Nimag=1 (-296 cm⁻¹)

Zero-point correction=	0.336845 (Hartree/Particle)
Thermal correction to Energy=	0.358291
Thermal correction to Enthalpy=	0.359235
Thermal correction to Gibbs Free Energy=	0.281375
Sum of electronic and zero-point Energies=	-938.438756
Sum of electronic and thermal Energies=	-938.417310
Sum of electronic and thermal Enthalpies=	-938.416366
Sum of electronic and thermal Free Energies=	-938.494226

6	2.017585000	-0.134004000	0.105508000
1	1.917636000	-0.292382000	-0.948959000
6	2.125759000	-1.216206000	0.902922000
6	1.654293000	-2.966697000	-0.731281000
6	1.422140000	-4.445196000	-0.705831000
1	0.536842000	-4.662064000	-0.117383000
1	1.292713000	-4.804760000	-1.716269000
1	2.260638000	-4.943535000	-0.232394000
8	1.640746000	-2.289552000	-1.709708000
8	1.874808000	-2.521317000	0.516514000
6	-0.348954000	0.120096000	0.074173000
6	-1.016150000	-0.383052000	-1.017990000
6	-0.981073000	0.675652000	1.160943000
6	-2.400209000	-0.313424000	-1.028252000
1	-0.484686000	-0.825291000	-1.842444000
6	-2.364584000	0.745274000	1.153886000
6	-3.046235000	0.249055000	0.057580000
1	-2.979271000	-0.684239000	-1.853014000
1	-2.916204000	1.170511000	1.971070000
1	-0.428780000	1.055449000	2.003607000
6	2.412174000	-1.211006000	2.361933000
7	-4.506694000	0.319605000	0.048607000
8	-5.082266000	-0.122667000	-0.911654000
8	-5.048479000	0.815432000	1.002768000
1	1.553334000	-1.584050000	2.915778000
1	2.651953000	-0.218970000	2.718012000

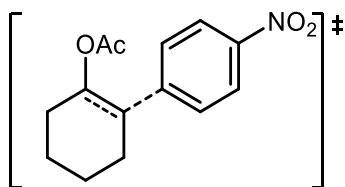
6	2.427178000	1.248431000	0.551063000
1	1.879658000	1.547103000	1.442105000
1	3.478904000	1.235330000	0.836564000
1	3.247745000	-1.870112000	2.581641000
6	2.229800000	2.297827000	-0.534620000
1	2.800206000	2.009067000	-1.416776000
1	1.184645000	2.310962000	-0.836916000
6	2.649635000	3.693588000	-0.097531000
1	3.693511000	3.675846000	0.213156000
1	2.076026000	3.981907000	0.782436000
6	2.462509000	4.737851000	-1.187770000
1	1.421907000	4.800448000	-1.494878000
1	2.767344000	5.723298000	-0.848971000
1	3.051072000	4.493935000	-2.068357000



Nimag=1 (-259 cm ⁻¹)	
Zero-point correction=	0.336410 (Hartree/Particle)
Thermal correction to Energy=	0.357782
Thermal correction to Enthalpy=	0.358727
Thermal correction to Gibbs Free Energy=	0.281467
Sum of electronic and zero-point Energies=	-938.439133
Sum of electronic and thermal Energies=	-938.417760
Sum of electronic and thermal Enthalpies=	-938.416816
Sum of electronic and thermal Free Energies=	-938.494076

6	-1.956166000	-0.179813000	0.156548000
1	-1.875586000	0.054489000	-0.884169000
6	-2.145579000	0.840746000	1.018046000
6	-1.842097000	2.716464000	-0.512839000
6	-1.708450000	4.203051000	-0.400953000
1	-0.820158000	4.443549000	0.173693000
1	-1.637068000	4.631680000	-1.389994000
1	-2.561733000	4.612972000	0.127604000
8	-1.812536000	2.102635000	-1.532106000
8	-1.994966000	2.181868000	0.709545000
6	0.414461000	-0.237139000	0.076745000
6	1.014579000	0.379257000	-0.996275000
6	1.114292000	-0.803856000	1.115238000
6	2.399231000	0.418278000	-1.038771000
1	0.431182000	0.826243000	-1.782261000
6	2.498429000	-0.764893000	1.076290000
6	3.112944000	-0.154438000	-0.001888000

1	2.927592000	0.880341000	-1.851406000
1	3.100924000	-1.192516000	1.855415000
1	0.614024000	-1.273650000	1.944905000
6	-2.422358000	0.726427000	2.474282000
7	4.573888000	-0.110705000	-0.044539000
8	5.090031000	0.429679000	-0.988231000
8	5.175311000	-0.617234000	0.867294000
1	-1.593865000	1.135985000	3.048185000
1	-2.576519000	-0.301457000	2.771274000
6	-2.243622000	-1.615243000	0.524808000
1	-1.614491000	-1.925175000	1.355438000
1	-3.271345000	-1.702327000	0.879216000
1	-3.308170000	1.299943000	2.733922000
6	-2.052086000	-2.594744000	-0.634756000
1	-1.064054000	-2.418025000	-1.057272000
6	-2.098161000	-4.030687000	-0.127069000
1	-3.058913000	-4.248307000	0.335573000
1	-1.957247000	-4.737302000	-0.939598000
1	-1.323276000	-4.215423000	0.611835000
6	-3.088173000	-2.381726000	-1.733587000
1	-4.090848000	-2.574298000	-1.356731000
1	-3.071215000	-1.369701000	-2.125519000
1	-2.912650000	-3.057780000	-2.565274000

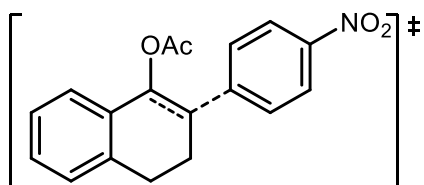


Nimag=1 (-262 cm⁻¹)

Zero-point correction=	0.288212 (Hartree/Particle)
Thermal correction to Energy=	0.305878
Thermal correction to Enthalpy=	0.306822
Thermal correction to Gibbs Free Energy=	0.237421
Sum of electronic and zero-point Energies=	-897.992189
Sum of electronic and thermal Energies=	-897.974524
Sum of electronic and thermal Enthalpies=	-897.973580
Sum of electronic and thermal Free Energies=	-898.042981

6	-1.928856000	-2.140177000	1.044750000
6	-2.037669000	-2.898061000	-0.270827000
6	-3.122197000	-2.291796000	-1.150236000
6	-2.819299000	-0.831126000	-1.466289000
6	-2.362307000	-0.081776000	-0.259401000
6	-1.850696000	-0.650041000	0.848943000
1	-3.227467000	-2.851821000	-2.074478000
1	-1.082165000	-2.854795000	-0.790423000
1	-2.247493000	-3.946233000	-0.078599000
1	-2.795656000	-2.357231000	1.669622000
1	-2.050649000	-0.761911000	-2.237943000

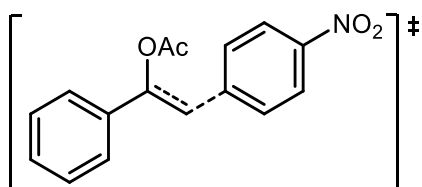
1	-3.696117000	-0.332310000	-1.871007000
1	-4.077612000	-2.354907000	-0.632691000
8	-2.357581000	1.279013000	-0.500648000
6	-2.556654000	2.216456000	0.453368000
8	-2.786542000	1.977556000	1.592021000
6	-2.444185000	3.582416000	-0.146285000
1	-1.423115000	3.746739000	-0.475630000
1	-3.087300000	3.664137000	-1.014842000
1	-2.712129000	4.321101000	0.595074000
1	-1.065079000	-2.481733000	1.606309000
6	0.476203000	-0.379011000	0.405288000
6	1.367242000	-0.926226000	1.297745000
6	0.858847000	0.361762000	-0.687554000
6	2.721620000	-0.731198000	1.080351000
1	1.037863000	-1.492670000	2.151983000
6	2.212284000	0.558189000	-0.909306000
1	0.132360000	0.787138000	-1.357699000
6	3.116515000	0.005955000	-0.020890000
1	3.465774000	-1.133832000	1.741441000
1	2.573907000	1.124429000	-1.746890000
7	4.545641000	0.212149000	-0.253085000
8	5.315759000	-0.280176000	0.530012000
8	4.867445000	0.861958000	-1.213989000
1	-1.662352000	-0.040139000	1.710248000



Nimag=1 (-237 cm ⁻¹)	
Zero-point correction=	0.312817 (Hartree/Particle)
Thermal correction to Energy=	0.332459
Thermal correction to Enthalpy=	0.333403
Thermal correction to Gibbs Free Energy=	0.259797
Sum of electronic and zero-point Energies=	-1050.341363
Sum of electronic and thermal Energies=	-1050.321721
Sum of electronic and thermal Enthalpies=	-1050.320777
Sum of electronic and thermal Free Energies=	-1050.394382

6	4.189719000	-2.266845000	1.266749000
6	3.946767000	-2.172411000	-0.094305000
6	3.139018000	-1.173493000	-0.603663000
6	2.555528000	-0.251747000	0.275952000
6	2.811578000	-0.344542000	1.640756000
6	3.623436000	-1.348641000	2.132680000
1	3.613176000	-0.251185000	-2.449772000
1	4.820269000	-3.052115000	1.646535000

1	4.397255000	-2.881050000	-0.769362000
6	2.909565000	-0.996615000	-2.077991000
6	1.688927000	0.778838000	-0.285411000
1	2.366454000	0.368516000	2.309473000
1	3.810462000	-1.415477000	3.190415000
6	1.104722000	0.645031000	-1.497358000
6	1.490143000	-0.527922000	-2.365051000
1	0.796155000	-1.350498000	-2.206056000
8	1.449273000	1.794931000	0.612628000
6	0.798158000	2.942920000	0.350589000
8	0.361992000	3.252370000	-0.711052000
6	0.706944000	3.766849000	1.596036000
1	0.111696000	3.239494000	2.334313000
1	1.695297000	3.917219000	2.015360000
1	0.247953000	4.716576000	1.363119000
6	-1.106843000	0.048006000	-0.761291000
6	-1.275502000	-1.178525000	-0.166966000
6	-2.121420000	0.952716000	-0.959210000
6	-2.549900000	-1.534471000	0.243494000
1	-0.448230000	-1.850817000	-0.014909000
6	-3.397238000	0.597210000	-0.549932000
1	-1.938432000	1.913518000	-1.408025000
6	-3.584905000	-0.639121000	0.040845000
1	-2.752052000	-2.478728000	0.712905000
1	-4.236683000	1.254451000	-0.677769000
7	-4.930733000	-1.013193000	0.474568000
8	-5.073443000	-2.094506000	0.984162000
8	-5.816742000	-0.217918000	0.297094000
1	3.119162000	-1.920962000	-2.606520000
1	1.394728000	-0.245305000	-3.408251000
1	0.577108000	1.466273000	-1.931632000

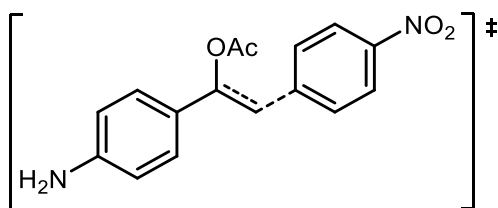


Nimag=1 (185 cm⁻¹)

Zero-point correction=	0.275339 (Hartree/Particle)
Thermal correction to Energy=	0.293998
Thermal correction to Enthalpy=	0.294942
Thermal correction to Gibbs Free Energy=	0.222193
Sum of electronic and zero-point Energies=	-972.977595
Sum of electronic and thermal Energies=	-972.958937
Sum of electronic and thermal Enthalpies=	-972.957992
Sum of electronic and thermal Free Energies=	-973.030741

6	-1.173641000	0.647502000	-1.729762000
1	-1.102043000	-0.226418000	-2.347101000
1	-0.741826000	1.556657000	-2.085603000

6	-1.986135000	0.607647000	-0.662497000
6	-1.576597000	2.852834000	0.181989000
6	-2.088260000	3.708675000	1.297675000
1	-3.168583000	3.780519000	1.244356000
1	-1.834850000	3.253086000	2.249421000
1	-1.640550000	4.689389000	1.229364000
8	-0.739798000	3.172742000	-0.598941000
8	-2.206239000	1.662970000	0.199178000
6	1.063035000	0.114379000	-0.849578000
6	1.918872000	1.168477000	-0.647901000
6	1.382829000	-1.201788000	-0.628731000
6	3.199054000	0.879550000	-0.201918000
1	1.607500000	2.183789000	-0.818881000
6	2.663114000	-1.488709000	-0.182159000
6	3.544174000	-0.441700000	0.019921000
1	3.923737000	1.651550000	-0.023724000
1	2.984563000	-2.494854000	0.010450000
1	0.671591000	-1.993466000	-0.788624000
6	-2.706677000	-0.587879000	-0.202207000
6	-3.018734000	-1.620923000	-1.085312000
6	-3.089358000	-0.717861000	1.130706000
6	-3.669744000	-2.754920000	-0.643547000
1	-2.775002000	-1.528445000	-2.128479000
6	-3.741098000	-1.854831000	1.569815000
1	-2.867656000	0.072758000	1.822433000
6	-4.031661000	-2.879433000	0.687525000
1	-3.906825000	-3.538019000	-1.342855000
1	-4.021482000	-1.939339000	2.605573000
1	-4.542167000	-3.762701000	1.030014000
7	4.895005000	-0.744464000	0.492418000
8	5.176741000	-1.900203000	0.677583000
8	5.645986000	0.179570000	0.668756000

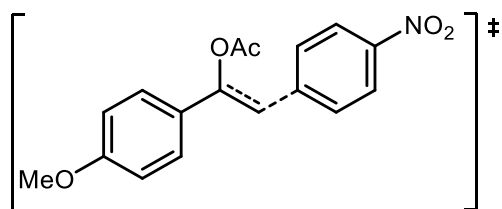


Nimag=1 (-173 cm⁻¹)

Zero-point correction=	0.292379 (Hartree/Particle)
Thermal correction to Energy=	0.312547
Thermal correction to Enthalpy=	0.313491
Thermal correction to Gibbs Free Energy=	0.237394
Sum of electronic and zero-point Energies=	-1028.302162
Sum of electronic and thermal Energies=	-1028.281994
Sum of electronic and thermal Enthalpies=	-1028.281050
Sum of electronic and thermal Free Energies=	-1028.357148

6	0.745571000	1.096450000	1.764408000
1	0.786350000	0.261704000	2.436545000

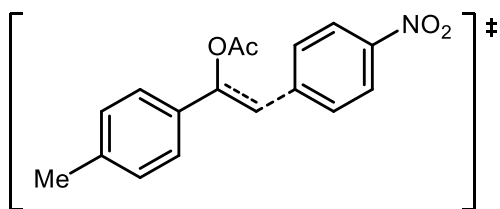
1	0.178041000	1.952885000	2.053841000
6	1.579923000	1.108130000	0.713326000
6	0.854829000	3.208486000	-0.284825000
6	1.254394000	4.055149000	-1.452956000
1	2.310828000	4.291320000	-1.395737000
1	1.089152000	3.504122000	-2.373134000
1	0.664571000	4.960190000	-1.456367000
8	-0.037193000	3.452476000	0.462121000
8	1.656470000	2.131203000	-0.213125000
6	-1.376846000	0.180302000	0.876612000
6	-2.372591000	1.079733000	0.585435000
6	-1.491945000	-1.179457000	0.727850000
6	-3.578669000	0.577747000	0.122372000
1	-2.221255000	2.138440000	0.701451000
6	-2.697909000	-1.680522000	0.264188000
1	-0.677524000	-1.845047000	0.956037000
6	-3.716435000	-0.790873000	-0.027168000
1	-4.402425000	1.221094000	-0.123557000
1	-2.859760000	-2.732793000	0.125210000
7	-4.988418000	-1.319132000	-0.518233000
8	-5.088758000	-2.512852000	-0.641193000
8	-5.861859000	-0.530392000	-0.771744000
6	2.487327000	0.018999000	0.342799000
6	2.918370000	-0.919121000	1.280296000
6	2.949549000	-0.124046000	-0.963724000
6	3.746896000	-1.959631000	0.928942000
1	2.621503000	-0.824725000	2.309767000
6	3.779061000	-1.163228000	-1.323745000
1	2.646787000	0.586661000	-1.709760000
6	4.190894000	-2.105949000	-0.385180000
1	4.073404000	-2.659160000	1.680472000
1	4.116641000	-1.247158000	-2.343494000
7	5.064240000	-3.118775000	-0.728897000
1	5.061731000	-3.921090000	-0.132523000
1	5.097395000	-3.357598000	-1.699091000



Nimag=1 (-179 cm⁻¹)

Zero-point correction=	0.308971 (Hartree/Particle)
Thermal correction to Energy=	0.330199
Thermal correction to Enthalpy=	0.331143
Thermal correction to Gibbs Free Energy=	0.252416
Sum of electronic and zero-point Energies=	-1087.434399
Sum of electronic and thermal Energies=	-1087.413171
Sum of electronic and thermal Enthalpies=	-1087.412227
Sum of electronic and thermal Free Energies=	-1087.490954

6	-0.294278000	1.319510000	-1.754077000
1	-0.461445000	0.491039000	-2.414522000
1	0.390615000	2.080073000	-2.057242000
6	-1.114484000	1.468025000	-0.702217000
6	-0.090930000	3.452515000	0.268038000
6	-0.348977000	4.352167000	1.435895000
1	-0.244888000	3.788311000	2.357257000
1	0.360139000	5.166989000	1.422417000
1	-1.363578000	4.731592000	1.395005000
8	0.813191000	3.564148000	-0.495390000
8	-1.036854000	2.496740000	0.216117000
6	1.670950000	0.126022000	-0.864357000
6	2.790767000	0.877598000	-0.607227000
6	1.590612000	-1.232942000	-0.689058000
6	3.919836000	0.214945000	-0.152048000
1	2.792109000	1.944730000	-0.743069000
6	2.719930000	-1.894397000	-0.233294000
6	3.861199000	-1.156150000	0.023644000
1	4.832104000	0.736761000	0.067963000
1	2.730539000	-2.956232000	-0.074651000
1	0.684779000	-1.777936000	-0.890882000
6	-2.171426000	0.525062000	-0.319824000
6	-2.764024000	-0.313880000	-1.255126000
6	-2.614325000	0.436928000	1.002107000
6	-3.740654000	-1.225649000	-0.897792000
1	-2.482490000	-0.246477000	-2.290886000
6	-3.584132000	-0.464387000	1.369310000
1	-2.184093000	1.080455000	1.746304000
6	-4.155840000	-1.308766000	0.423763000
1	-4.176537000	-1.848769000	-1.655860000
1	-3.919273000	-0.537592000	2.388507000
7	5.052888000	-1.853857000	0.505304000
8	4.982841000	-3.047275000	0.648759000
8	6.034609000	-1.194593000	0.730468000
8	-5.097783000	-2.155703000	0.877772000
6	-5.713988000	-3.036826000	-0.026662000
1	-4.989873000	-3.706896000	-0.484153000
1	-6.418210000	-3.616664000	0.552896000
1	-6.249547000	-2.497567000	-0.804474000



Nimag=1 (-182 cm⁻¹)

Zero-point correction=

Thermal correction to Energy=

Thermal correction to Enthalpy=

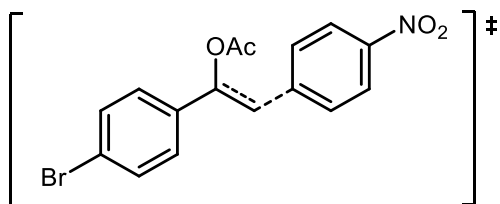
0.303303 (Hartree/Particle)

0.323898

0.324842

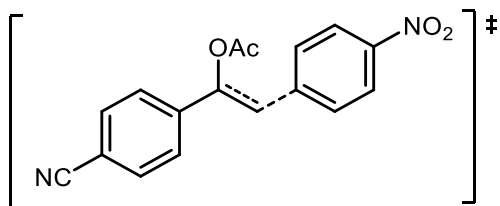
Thermal correction to Gibbs Free Energy= 0.246509
 Sum of electronic and zero-point Energies= -1012.250264
 Sum of electronic and thermal Energies= -1012.229670
 Sum of electronic and thermal Enthalpies= -1012.228726
 Sum of electronic and thermal Free Energies= -1012.307058

6	0.724361000	1.110129000	1.755037000
1	0.766687000	0.275371000	2.426869000
1	0.147309000	1.961741000	2.040261000
6	1.567301000	1.130109000	0.711125000
6	0.843301000	3.227532000	-0.289451000
6	1.254216000	4.082711000	-1.446780000
1	2.307718000	4.326870000	-1.371742000
1	1.107968000	3.534871000	-2.372032000
1	0.657378000	4.983073000	-1.455021000
8	-0.060405000	3.459893000	0.446764000
8	1.650768000	2.153736000	-0.211633000
6	-1.378537000	0.182089000	0.859728000
6	-2.379273000	1.075780000	0.569392000
6	-1.485151000	-1.178799000	0.717811000
6	-3.584348000	0.564789000	0.113465000
1	-2.233225000	2.135679000	0.680536000
6	-2.690495000	-1.688083000	0.261159000
1	-0.666198000	-1.838875000	0.945478000
6	-3.714878000	-0.805129000	-0.029511000
1	-4.412697000	1.202441000	-0.131783000
1	-2.846980000	-2.741806000	0.127226000
7	-4.986514000	-1.342459000	-0.512707000
8	-5.080993000	-2.537120000	-0.628730000
8	-5.864541000	-0.559107000	-0.766550000
6	2.477870000	0.037383000	0.346043000
6	2.902598000	-0.895272000	1.292181000
6	2.943141000	-0.101914000	-0.957420000
6	3.736315000	-1.933721000	0.938299000
1	2.602439000	-0.794642000	2.319931000
6	3.779189000	-1.146675000	-1.303916000
1	2.644555000	0.609724000	-1.704000000
6	4.188088000	-2.084640000	-0.368566000
1	4.055043000	-2.633031000	1.693690000
1	4.119225000	-1.231032000	-2.322697000
6	5.078761000	-3.231216000	-0.747364000
1	5.848200000	-3.395778000	0.000506000
1	4.508386000	-4.153061000	-0.835111000
1	5.566410000	-3.053990000	-1.699351000



Nimag=1 (-258 cm⁻¹)
 Zero-point correction= 0.264800 (Hartree/Particle)
 Thermal correction to Energy= 0.284945
 Thermal correction to Enthalpy= 0.285889
 Thermal correction to Gibbs Free Energy= 0.208436
 Sum of electronic and zero-point Energies= -3546.490982
 Sum of electronic and thermal Energies= -3546.470837
 Sum of electronic and thermal Enthalpies= -3546.469893
 Sum of electronic and thermal Free Energies= -3546.547346

6	-0.561412000	1.614917000	1.757120000
1	-0.331114000	0.857811000	2.480846000
1	-1.360474000	2.290571000	1.968104000
6	0.299070000	1.814688000	0.746691000
6	-0.901622000	3.591694000	-0.403017000
6	-0.677838000	4.463696000	-1.597721000
1	0.270313000	4.981245000	-1.506702000
1	-0.634290000	3.850018000	-2.491648000
1	-1.488707000	5.172765000	-1.678573000
8	-1.863795000	3.614271000	0.293506000
8	0.154542000	2.771168000	-0.236577000
6	-2.294426000	0.120562000	0.851761000
6	-3.476078000	0.708279000	0.474736000
6	-2.040924000	-1.226873000	0.796191000
6	-4.487297000	-0.121810000	0.016712000
1	-3.613007000	1.774096000	0.522371000
6	-3.053286000	-2.054922000	0.337203000
1	-1.092282000	-1.640038000	1.091981000
6	-4.255081000	-1.484321000	-0.041018000
1	-5.439479000	0.265135000	-0.293953000
1	-2.927906000	-3.118975000	0.267649000
7	-5.323335000	-2.358359000	-0.526410000
8	-5.102817000	-3.541018000	-0.566072000
8	-6.359454000	-1.843278000	-0.857639000
6	1.489618000	0.994162000	0.487440000
6	2.100021000	0.267891000	1.508677000
6	2.038928000	0.919710000	-0.789824000
6	3.202978000	-0.523156000	1.262406000
1	1.730170000	0.335697000	2.515750000
6	3.143225000	0.130649000	-1.047754000
1	1.594242000	1.479110000	-1.590798000
6	3.717579000	-0.590022000	-0.019516000
1	3.666302000	-1.071705000	2.061787000
1	3.550746000	0.077127000	-2.040588000
35	5.235723000	-1.671553000	-0.363646000



Nimag=1 (-186 cm⁻¹)

Zero-point correction= 0.274027 (Hartree/Particle)

Thermal correction to Energy= 0.294457

Thermal correction to Enthalpy= 0.295401

Thermal correction to Gibbs Free Energy= 0.218293

Sum of electronic and zero-point Energies= -1065.190841

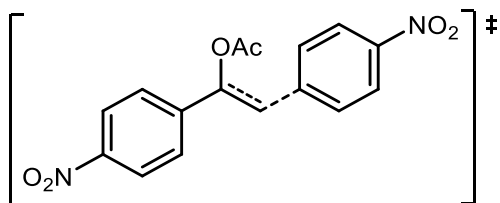
Sum of electronic and thermal Energies= -1065.170410

Sum of electronic and thermal Enthalpies= -1065.169466

Sum of electronic and thermal Free Energies= -1065.246574

6	0.435166000	1.268129000	1.746692000
1	0.534986000	0.452306000	2.435254000
1	-0.226811000	2.065994000	2.001212000
6	1.298395000	1.352701000	0.722359000
6	0.422038000	3.366286000	-0.324854000
6	0.785684000	4.240877000	-1.482015000
1	1.810168000	4.580924000	-1.381878000
1	0.715105000	3.672210000	-2.403514000
1	0.110645000	5.083344000	-1.517872000
8	-0.511413000	3.524841000	0.392057000
8	1.315814000	2.361136000	-0.216800000
6	-1.566682000	0.150655000	0.834111000
6	-2.623326000	0.963643000	0.509576000
6	-1.572190000	-1.217554000	0.734787000
6	-3.783645000	0.353613000	0.058713000
1	-2.555349000	2.033889000	0.591646000
6	-2.733761000	-1.824449000	0.283012000
1	-0.712493000	-1.811657000	0.991594000
6	-3.814265000	-1.025487000	-0.043650000
1	-4.652740000	0.922746000	-0.212660000
1	-2.813673000	-2.890234000	0.180622000
7	-5.040137000	-1.666599000	-0.521506000
8	-5.047925000	-2.867502000	-0.599147000
8	-5.966808000	-0.954565000	-0.808421000
6	2.312442000	0.339740000	0.401542000
6	2.774210000	-0.549488000	1.373035000
6	2.837788000	0.245458000	-0.886017000
6	3.707690000	-1.512631000	1.065620000
1	2.421852000	-0.474749000	2.385305000
6	3.772540000	-0.717414000	-1.200846000
1	2.504660000	0.928174000	-1.643650000
6	4.212415000	-1.605901000	-0.227790000
1	4.059841000	-2.187563000	1.824856000
1	4.163906000	-0.785324000	-2.199989000
6	5.183552000	-2.602007000	-0.548883000

7 5.959314000 -3.398883000 -0.804894000



Nimag=1 (-185 cm⁻¹)

Zero-point correction= 0.278442 (Hartree/Particle)

Thermal correction to Energy= 0.299601

Thermal correction to Enthalpy= 0.300545

Thermal correction to Gibbs Free Energy= 0.221140

Sum of electronic and zero-point Energies= -1177.415165

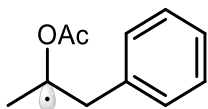
Sum of electronic and thermal Energies= -1177.394006

Sum of electronic and thermal Enthalpies= -1177.393062

Sum of electronic and thermal Free Energies= -1177.472467

6	-0.031837000	1.445571000	1.768314000
1	0.133264000	0.648443000	2.466020000
1	-0.769932000	2.179526000	2.005336000
6	0.834616000	1.602885000	0.755321000
6	-0.208776000	3.518929000	-0.321010000
6	0.091509000	4.417716000	-1.477553000
1	1.077940000	4.852427000	-1.362670000
1	0.090102000	3.840329000	-2.396329000
1	-0.658465000	5.193259000	-1.530136000
8	-1.164918000	3.592284000	0.379409000
8	0.773288000	2.601886000	-0.191315000
6	-1.906026000	0.135572000	0.840281000
6	-3.026350000	0.843541000	0.485188000
6	-1.783215000	-1.228382000	0.761968000
6	-4.116751000	0.122826000	0.023155000
1	-3.058849000	1.916444000	0.552663000
6	-2.875260000	-1.945821000	0.298820000
1	-0.877802000	-1.737266000	1.043398000
6	-4.018189000	-1.254399000	-0.059023000
1	-5.029292000	0.605564000	-0.271980000
1	-2.854799000	-3.015717000	0.211261000
7	-5.170602000	-2.012356000	-0.548880000
8	-5.065890000	-3.209643000	-0.609151000
8	-6.153373000	-1.392746000	-0.862145000
6	1.942425000	0.685271000	0.457613000
6	2.463811000	-0.155586000	1.443035000
6	2.497052000	0.638299000	-0.820931000
6	3.487200000	-1.031337000	1.158895000
1	2.086921000	-0.110571000	2.447893000
6	3.522535000	-0.235023000	-1.116994000
1	2.116632000	1.286202000	-1.586426000
6	4.002208000	-1.061697000	-0.122746000
1	3.898478000	-1.677123000	1.910832000

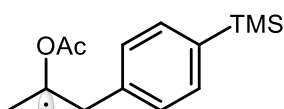
1	3.950503000	-0.284755000	-2.099894000
7	5.091499000	-1.986862000	-0.428984000
8	5.484455000	-2.696191000	0.460081000
8	5.526352000	-1.982144000	-1.550745000



Nimag=0

Zero-point correction=	0.220820 (Hartree/Particle)
Thermal correction to Energy=	0.233644
Thermal correction to Enthalpy=	0.234588
Thermal correction to Gibbs Free Energy=	0.179028
Sum of electronic and zero-point Energies=	-576.991602
Sum of electronic and thermal Energies=	-576.978779
Sum of electronic and thermal Enthalpies=	-576.977834
Sum of electronic and thermal Free Energies=	-577.033394

6	-0.185565000	1.024067000	1.193620000
1	0.105398000	1.966876000	1.646712000
1	-0.600930000	0.399910000	1.975051000
6	-1.245072000	1.327669000	0.177518000
6	-1.259710000	2.594117000	-0.594481000
1	-1.030925000	3.435933000	0.049890000
1	-0.525253000	2.579107000	-1.403825000
1	-2.233860000	2.755052000	-1.045245000
6	-2.222952000	-0.838958000	-0.034690000
6	-2.612691000	-1.816775000	-1.098209000
1	-1.722593000	-2.138539000	-1.629355000
1	-3.098470000	-2.668117000	-0.643673000
1	-3.270704000	-1.342827000	-1.817497000
8	-2.315476000	-1.020332000	1.137743000
8	-1.742789000	0.285261000	-0.589025000
6	1.033107000	0.346670000	0.603125000
6	1.190516000	-1.029455000	0.698662000
6	2.007541000	1.081229000	-0.061529000
6	2.290149000	-1.657187000	0.138050000
1	0.448943000	-1.609317000	1.222420000
6	3.107366000	0.457300000	-0.621614000
1	1.910094000	2.152207000	-0.133056000
6	3.251106000	-0.916283000	-0.525642000
1	2.398365000	-2.724877000	0.226631000
1	3.855170000	1.043604000	-1.128019000
1	4.108117000	-1.402796000	-0.958630000

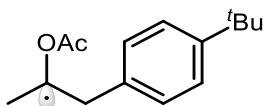


Nimag=0

Zero-point correction=	0.324681 (Hartree/Particle)
------------------------	-----------------------------

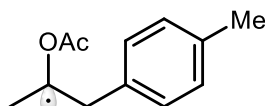
Thermal correction to Energy=	0.345334
Thermal correction to Enthalpy=	0.346278
Thermal correction to Gibbs Free Energy=	0.272060
Sum of electronic and zero-point Energies=	-985.520274
Sum of electronic and thermal Energies=	-985.499621
Sum of electronic and thermal Enthalpies=	-985.498676
Sum of electronic and thermal Free Energies=	-985.572894

6	2.371495000	1.189268000	-1.093769000
1	2.450146000	2.219086000	-1.428582000
1	2.728128000	0.555339000	-1.896131000
6	3.266799000	1.040250000	0.099446000
6	3.496514000	2.148877000	1.057648000
1	3.640577000	3.085187000	0.529647000
1	2.650616000	2.272295000	1.738740000
1	4.374465000	1.952562000	1.664850000
6	3.535525000	-1.330993000	0.101025000
6	3.426774000	-2.492043000	1.038672000
1	3.729646000	-3.395481000	0.529330000
1	4.043901000	-2.323807000	1.913783000
1	2.398670000	-2.583284000	1.374250000
8	3.790875000	-1.401465000	-1.059043000
8	3.297248000	-0.181987000	0.752983000
6	0.923998000	0.860881000	-0.797694000
6	0.399518000	-0.383350000	-1.122037000
6	0.090644000	1.781670000	-0.178699000
6	-0.915533000	-0.694045000	-0.827711000
1	1.026267000	-1.108039000	-1.615131000
6	-1.224779000	1.465991000	0.112628000
6	-1.762956000	0.219554000	-0.201472000
1	-1.284157000	-1.670462000	-1.101361000
1	-1.839208000	2.211839000	0.589444000
1	0.469280000	2.759885000	0.070427000
6	-3.583501000	-1.736303000	1.305132000
6	-4.404286000	1.205641000	1.026952000
6	-4.444295000	-0.642743000	-1.420357000
1	-3.083902000	-2.586315000	0.847619000
1	-3.083994000	-1.530678000	2.247982000
1	-4.605111000	-2.035936000	1.526595000
1	-4.418497000	2.092863000	0.399483000
1	-5.436473000	0.949178000	1.252257000
1	-3.920768000	1.466372000	1.964681000
1	-5.475582000	-0.929932000	-1.229239000
1	-4.454311000	0.210747000	-2.092749000
1	-3.965262000	-1.466153000	-1.943687000
14	-3.550350000	-0.233828000	0.179121000



Nimag=0
 Zero-point correction= 0.336343 (Hartree/Particle)
 Thermal correction to Energy= 0.354564
 Thermal correction to Enthalpy= 0.355508
 Thermal correction to Gibbs Free Energy= 0.287855
 Sum of electronic and zero-point Energies= -734.064195
 Sum of electronic and thermal Energies= -734.045974
 Sum of electronic and thermal Enthalpies= -734.045030
 Sum of electronic and thermal Free Energies= -734.112682

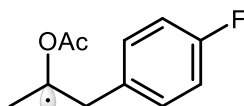
6	1.994030000	1.192144000	-1.107271000
1	2.042288000	2.220033000	-1.453756000
1	2.349402000	0.559318000	-1.911130000
6	2.917575000	1.076236000	0.067893000
6	3.136740000	2.198873000	1.012244000
1	3.249615000	3.133323000	0.473417000
1	2.299192000	2.308650000	1.705931000
1	4.028959000	2.029326000	1.606577000
6	3.241822000	-1.287997000	0.086865000
6	3.178391000	-2.442017000	1.037519000
1	3.492726000	-3.343170000	0.531043000
1	3.807844000	-2.250757000	1.899018000
1	2.159238000	-2.553919000	1.393532000
8	3.475505000	-1.364983000	-1.077446000
8	2.990632000	-0.138728000	0.732460000
6	0.560801000	0.832791000	-0.779616000
6	0.057084000	-0.427507000	-1.073593000
6	-0.288021000	1.735674000	-0.161357000
6	-1.242738000	-0.766383000	-0.752131000
1	0.689066000	-1.147343000	-1.567016000
6	-1.591839000	1.393753000	0.158863000
6	-2.101299000	0.133784000	-0.125888000
1	-1.591761000	-1.753240000	-1.003848000
1	-2.210022000	2.133614000	0.633027000
1	0.064425000	2.728210000	0.068655000
6	-3.533885000	-0.281498000	0.208774000
6	-3.508555000	-1.489992000	1.154662000
6	-4.317598000	0.839676000	0.891283000
6	-4.271858000	-0.662638000	-1.081910000
1	-3.003467000	-2.340038000	0.707962000
1	-2.994584000	-1.246075000	2.079827000
1	-4.521668000	-1.797810000	1.400865000
1	-4.400253000	1.717671000	0.257522000
1	-5.324560000	0.497577000	1.110820000
1	-3.860084000	1.137951000	1.829998000
1	-5.293162000	-0.960752000	-0.858594000
1	-4.306800000	0.177216000	-1.769517000
1	-3.789399000	-1.489490000	-1.592468000



Nimag=0

Zero-point correction= 0.248820 (Hartree/Particle)
 Thermal correction to Energy= 0.263544
 Thermal correction to Enthalpy= 0.264488
 Thermal correction to Gibbs Free Energy= 0.203608
 Sum of electronic and zero-point Energies= -616.263614
 Sum of electronic and thermal Energies= -616.248889
 Sum of electronic and thermal Enthalpies= -616.247945
 Sum of electronic and thermal Free Energies= -616.308825

6	-0.823039000	1.133987000	1.156055000
1	-0.718312000	2.137581000	1.557235000
1	-1.200124000	0.502477000	1.950977000
6	-1.831295000	1.201694000	0.048798000
6	-1.979199000	2.399379000	-0.813654000
1	-1.935590000	3.305071000	-0.218634000
1	-1.188521000	2.451782000	-1.566541000
1	-2.927078000	2.374897000	-1.341917000
6	-2.440041000	-1.102443000	-0.072410000
6	-2.580381000	-2.194963000	-1.085414000
1	-2.966931000	-3.082728000	-0.605990000
1	-3.238055000	-1.878537000	-1.886845000
1	-1.608254000	-2.403153000	-1.520812000
8	-2.601773000	-1.223612000	1.100326000
8	-2.097325000	0.047811000	-0.672669000
6	0.528844000	0.622193000	0.706416000
6	0.892895000	-0.699417000	0.914477000
6	1.432359000	1.452091000	0.054182000
6	2.117926000	-1.177016000	0.479528000
1	0.212585000	-1.360387000	1.425483000
6	2.654206000	0.973941000	-0.377814000
6	3.019949000	-0.350878000	-0.172958000
1	2.375831000	-2.208473000	0.656575000
1	3.337002000	1.640909000	-0.878925000
1	1.180986000	2.487011000	-0.112390000
6	4.361867000	-0.857860000	-0.618081000
1	4.637810000	-0.447967000	-1.584659000
1	5.139518000	-0.576826000	0.088552000
1	4.367377000	-1.939504000	-0.698109000

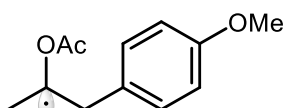


Nimag=0

Zero-point correction= 0.212031 (Hartree/Particle)
 Thermal correction to Energy= 0.225776
 Thermal correction to Enthalpy= 0.226721

Thermal correction to Gibbs Free Energy= 0.168863
 Sum of electronic and zero-point Energies= -676.231727
 Sum of electronic and thermal Energies= -676.217982
 Sum of electronic and thermal Enthalpies= -676.217037
 Sum of electronic and thermal Free Energies= -676.274895

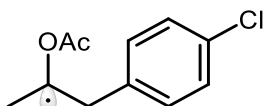
6	-0.571427000	0.704847000	0.910145000
1	-0.549749000	1.625513000	1.499418000
1	-0.998495000	-0.063161000	1.544981000
6	-1.448592000	0.896119000	-0.285591000
6	-1.239055000	2.007374000	-1.240990000
1	-0.179809000	2.158481000	-1.415339000
1	-1.722504000	1.799910000	-2.190407000
1	-1.655582000	2.943301000	-0.858329000
6	-3.138418000	-0.718425000	0.030848000
6	-4.618972000	-0.847079000	0.201053000
1	-5.126148000	-0.404193000	-0.648968000
1	-4.881370000	-1.890908000	0.293488000
1	-4.931725000	-0.304367000	1.086963000
8	-2.358934000	-1.617569000	0.046218000
8	-2.790960000	0.567632000	-0.145571000
6	0.839817000	0.317805000	0.540831000
6	1.078155000	-0.895522000	-0.097169000
6	1.916733000	1.140080000	0.829282000
6	2.360868000	-1.277696000	-0.437017000
1	0.244965000	-1.539105000	-0.322378000
6	3.210148000	0.772195000	0.493717000
6	3.407391000	-0.433310000	-0.134810000
1	2.559971000	-2.214076000	-0.927002000
1	4.053149000	1.402604000	0.713202000
1	1.751137000	2.081830000	1.325519000
9	4.650604000	-0.799407000	-0.463125000



Nimag=0
 Zero-point correction= 0.254462 (Hartree/Particle)
 Thermal correction to Energy= 0.269822
 Thermal correction to Enthalpy= 0.270766
 Thermal correction to Gibbs Free Energy= 0.209225
 Sum of electronic and zero-point Energies= -691.447177
 Sum of electronic and thermal Energies= -691.431818
 Sum of electronic and thermal Enthalpies= -691.430873
 Sum of electronic and thermal Free Energies= -691.492415

6	-1.257296000	1.142962000	1.158298000
1	-1.175197000	2.147797000	1.561670000
1	-1.688192000	0.517637000	1.930541000
6	-2.192648000	1.210509000	-0.011503000

6	-2.274745000	2.405771000	-0.886181000
1	-2.271486000	3.313284000	-0.292253000
1	-1.431430000	2.453615000	-1.580085000
1	-3.181979000	2.382270000	-1.481500000
6	-2.799321000	-1.092176000	-0.167726000
6	-2.879999000	-2.186007000	-1.185811000
1	-1.882487000	-2.402227000	-1.554968000
1	-3.303455000	-3.070040000	-0.731300000
1	-3.480599000	-1.867122000	-2.029892000
8	-3.033773000	-1.211110000	0.992988000
8	-2.415448000	0.055801000	-0.746716000
6	0.118487000	0.622490000	0.800374000
6	0.456680000	-0.709449000	1.022384000
6	1.074567000	1.441990000	0.226484000
6	1.696409000	-1.200522000	0.676216000
1	-0.263391000	-1.366912000	1.480434000
6	2.328320000	0.965618000	-0.126933000
1	0.850714000	2.482219000	0.054342000
6	2.643002000	-0.365658000	0.095512000
1	1.960590000	-2.228215000	0.853019000
1	3.042257000	1.638496000	-0.564141000
8	3.830385000	-0.934714000	-0.208222000
6	4.830119000	-0.140655000	-0.788849000
1	5.679398000	-0.791422000	-0.944263000
1	4.511925000	0.265130000	-1.746924000
1	5.122568000	0.676432000	-0.132680000

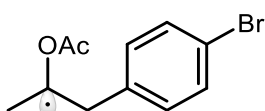


Nimag=0

Zero-point correction=	0.211006 (Hartree/Particle)
Thermal correction to Energy=	0.225028
Thermal correction to Enthalpy=	0.225973
Thermal correction to Gibbs Free Energy=	0.167047
Sum of electronic and zero-point Energies=	-1036.610427
Sum of electronic and thermal Energies=	-1036.596405
Sum of electronic and thermal Enthalpies=	-1036.595461
Sum of electronic and thermal Free Energies=	-1036.654386

6	-1.273329000	1.165804000	1.131537000
1	-1.245691000	2.187501000	1.497530000
1	-1.633150000	0.539006000	1.937789000
6	-2.247195000	1.128643000	-0.007862000
6	-2.464559000	2.292785000	-0.900917000
1	-2.504342000	3.211930000	-0.326740000
1	-1.663515000	2.389272000	-1.638423000
1	-3.394943000	2.184261000	-1.449099000
6	-2.666129000	-1.221138000	-0.088355000
6	-2.731950000	-2.334844000	-1.085007000

1	-1.756532000	-2.464068000	-1.542799000
1	-3.029765000	-3.246099000	-0.586876000
1	-3.433554000	-2.086847000	-1.873322000
8	-2.814322000	-1.334956000	1.086936000
8	-2.408395000	-0.057019000	-0.706370000
6	0.122935000	0.729170000	0.743408000
6	0.566170000	-0.555531000	1.024649000
6	0.986762000	1.593654000	0.083152000
6	1.832201000	-0.973835000	0.653769000
1	-0.084760000	-1.237730000	1.544625000
6	2.254462000	1.192260000	-0.293490000
1	0.672401000	2.600830000	-0.134580000
6	2.665707000	-0.094332000	-0.005630000
1	2.169999000	-1.969004000	0.879499000
1	2.918876000	1.868980000	-0.799337000
17	4.264486000	-0.610474000	-0.475548000

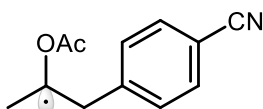


Nimag=0

Zero-point correction=	0.209964 (Hartree/Particle)
Thermal correction to Energy=	0.224363
Thermal correction to Enthalpy=	0.225307
Thermal correction to Gibbs Free Energy=	0.164796
Sum of electronic and zero-point Energies=	-3150.507103
Sum of electronic and thermal Energies=	-3150.492704
Sum of electronic and thermal Enthalpies=	-3150.491760
Sum of electronic and thermal Free Energies=	-3150.552271

6	-1.781303000	0.830259000	0.891890000
1	-1.871388000	1.789663000	1.408016000
1	-2.170743000	0.073906000	1.563739000
6	-2.606367000	0.851223000	-0.355280000
6	-2.446051000	1.905479000	-1.382128000
1	-1.396725000	2.140613000	-1.519847000
1	-2.859340000	1.586453000	-2.333663000
1	-2.962829000	2.824254000	-1.091311000
6	-4.157799000	-0.887654000	0.008087000
6	-5.627741000	-1.142856000	0.113794000
1	-6.122802000	-0.818297000	-0.794775000
1	-5.799174000	-2.196455000	0.279576000
1	-6.039331000	-0.564524000	0.934331000
8	-3.301713000	-1.704469000	0.134955000
8	-3.918622000	0.408826000	-0.254128000
6	-0.324755000	0.546547000	0.619273000
6	0.051654000	-0.681995000	0.087703000
6	0.659954000	1.480860000	0.893257000
6	1.379011000	-0.969833000	-0.162610000
1	-0.708097000	-1.414350000	-0.126457000

6	1.996174000	1.208375000	0.646446000
6	2.342254000	-0.017790000	0.119487000
1	1.662830000	-1.922965000	-0.570088000
1	2.752360000	1.940649000	0.862887000
1	0.389112000	2.437620000	1.308142000
35	4.170818000	-0.407060000	-0.224191000



Nimag=0

Zero-point correction= 0.219200 (Hartree/Particle)

Thermal correction to Energy= 0.233972

Thermal correction to Enthalpy= 0.234916

Thermal correction to Gibbs Free Energy= 0.173488

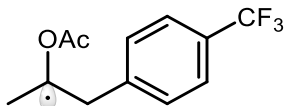
Sum of electronic and zero-point Energies= -669.205943

Sum of electronic and thermal Energies= -669.191171

Sum of electronic and thermal Enthalpies= -669.190227

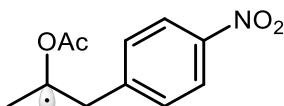
Sum of electronic and thermal Free Energies= -669.251655

6	-0.904606000	-1.129720000	-0.725928000
1	-0.858696000	-2.182466000	-0.989709000
1	-1.337823000	-0.619158000	-1.578943000
6	-1.814226000	-0.984363000	0.451003000
6	-1.552917000	-1.667410000	1.739258000
1	-1.168035000	-2.666734000	1.566029000
1	-0.818038000	-1.128310000	2.341136000
1	-2.463870000	-1.741499000	2.324837000
6	-3.370412000	0.646427000	-0.275075000
6	-3.918468000	1.985466000	0.104482000
1	-3.137870000	2.734816000	0.017172000
1	-4.737750000	2.236236000	-0.553566000
1	-4.248425000	1.974698000	1.136763000
8	-3.676907000	0.015482000	-1.233462000
8	-2.454091000	0.235931000	0.626327000
6	0.503182000	-0.626950000	-0.480736000
6	0.729851000	0.669840000	-0.029218000
6	1.597963000	-1.449488000	-0.707977000
6	2.010140000	1.133310000	0.183781000
1	-0.105981000	1.318806000	0.165183000
6	2.886229000	-0.997447000	-0.500401000
6	3.098655000	0.299645000	-0.052805000
1	2.175421000	2.137359000	0.531843000
1	3.726664000	-1.643417000	-0.681822000
1	1.442626000	-2.456858000	-1.055178000
6	4.427528000	0.775621000	0.166413000
7	5.488892000	1.156517000	0.342363000



Nimag=0
 Zero-point correction= 0.226102 (Hartree/Particle)
 Thermal correction to Energy= 0.242458
 Thermal correction to Enthalpy= 0.243402
 Thermal correction to Gibbs Free Energy= 0.177644
 Sum of electronic and zero-point Energies= -914.002016
 Sum of electronic and thermal Energies= -913.985660
 Sum of electronic and thermal Enthalpies= -913.984716
 Sum of electronic and thermal Free Energies= -914.050474

6	1.951687000	-1.190329000	1.112628000
1	1.990211000	-2.220538000	1.452416000
1	2.313462000	-0.564005000	1.918228000
6	2.870914000	-1.076108000	-0.066629000
6	3.105214000	-2.205601000	-0.998896000
1	3.214179000	-3.135658000	-0.451933000
1	2.278886000	-2.323185000	-1.704684000
1	4.004761000	-2.037384000	-1.582242000
6	3.176914000	1.292593000	-0.097951000
6	3.155529000	2.432568000	-1.066091000
1	2.160588000	2.525439000	-1.489299000
1	3.425949000	3.344504000	-0.553837000
1	3.841838000	2.238752000	-1.882585000
8	3.365438000	1.382191000	1.073496000
8	2.945862000	0.133395000	-0.737073000
6	0.520687000	-0.817674000	0.791700000
6	-0.324134000	-1.715343000	0.149735000
6	0.028245000	0.437928000	1.120624000
6	-1.622681000	-1.367989000	-0.164239000
1	0.032752000	-2.701122000	-0.097086000
6	-1.270961000	0.793850000	0.808939000
6	-2.096771000	-0.108829000	0.163925000
1	-2.271026000	-2.075237000	-0.649881000
1	-1.645409000	1.765054000	1.078862000
1	0.666408000	1.138453000	1.631451000
6	-3.485066000	0.286823000	-0.219810000
9	-4.319321000	-0.751561000	-0.216367000
9	-3.989703000	1.204641000	0.602179000
9	-3.531028000	0.807909000	-1.448524000

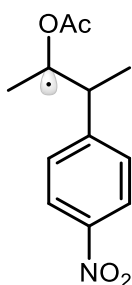


Nimag=0
 Zero-point correction= 0.223693 (Hartree/Particle)
 Thermal correction to Energy= 0.239098
 Thermal correction to Enthalpy= 0.240042

Thermal correction to Gibbs Free Energy= 0.177719
 Sum of electronic and zero-point Energies= -781.432808
 Sum of electronic and thermal Energies= -781.417403
 Sum of electronic and thermal Enthalpies= -781.416459
 Sum of electronic and thermal Free Energies= -781.478782

6	0.973852000	0.618514000	-0.767443000
1	0.704718000	1.560450000	-1.250754000
1	1.487761000	0.018517000	-1.509376000
6	1.897292000	0.885271000	0.379201000
6	1.571142000	1.876036000	1.429702000
1	0.518838000	1.823395000	1.685737000
1	2.156638000	1.698371000	2.326040000
1	1.784872000	2.894235000	1.093966000
6	3.807779000	-0.376374000	-0.186763000
6	5.271490000	-0.229243000	-0.453334000
1	5.757388000	0.218800000	0.406373000
1	5.698496000	-1.198953000	-0.663513000
1	5.422656000	0.435893000	-1.297029000
8	3.191339000	-1.393367000	-0.240273000
8	3.259664000	0.809877000	0.128709000
6	-0.284397000	-0.098043000	-0.342085000
6	-0.205919000	-1.389561000	0.173207000
6	-1.524732000	0.500395000	-0.460122000
6	-1.345659000	-2.069287000	0.559364000
1	0.762446000	-1.851440000	0.263100000
6	-2.652290000	-0.196189000	-0.065269000
6	-2.589700000	-1.475116000	0.443719000
1	-1.267745000	-3.068022000	0.951333000
1	-1.634481000	1.493609000	-0.853689000
1	-3.491938000	-1.977388000	0.735209000
7	-3.958694000	0.451368000	-0.194416000
8	-3.985602000	1.571887000	-0.634029000
8	-4.928144000	-0.174080000	0.147150000

PUC-Rio - Certificação Digital N° 1613320/CA

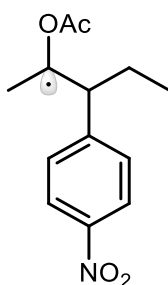


Nimag=0
 Zero-point correction= 0.252972 (Hartree/Particle)
 Thermal correction to Energy= 0.269722
 Thermal correction to Enthalpy= 0.270666
 Thermal correction to Gibbs Free Energy= 0.205134
 Sum of electronic and zero-point Energies= -820.697326
 Sum of electronic and thermal Energies= -820.680575

Sum of electronic and thermal Enthalpies= -820.679631
 Sum of electronic and thermal Free Energies= -820.745163

6	1.550048000	-1.056361000	0.811860000
1	1.886013000	-0.412685000	1.615676000
6	2.418019000	-0.742854000	-0.378445000
6	2.673842000	1.615881000	-0.067632000
6	2.532437000	2.888563000	-0.840551000
1	1.502005000	3.003824000	-1.160348000
1	2.822251000	3.721861000	-0.217103000
1	3.149033000	2.850323000	-1.731504000
8	2.983643000	1.532034000	1.077836000
8	2.397644000	0.559991000	-0.853701000
6	0.098857000	-0.698055000	0.538612000
6	-0.470425000	0.403423000	1.166556000
6	-0.681319000	-1.437639000	-0.346190000
6	-1.782197000	0.764545000	0.926394000
1	0.122044000	0.984748000	1.852030000
6	-1.992161000	-1.092595000	-0.598709000
6	-2.524551000	0.008418000	0.043858000
1	-2.232366000	1.610975000	1.409070000
1	-2.603898000	-1.656147000	-1.276998000
1	-0.265671000	-2.295890000	-0.843910000
6	2.703435000	-1.687984000	-1.486147000
7	-3.913287000	0.380774000	-0.218650000
8	-4.348401000	1.348683000	0.349151000
8	-4.538013000	-0.302467000	-0.987984000
1	1.874570000	-1.739766000	-2.196653000
1	2.893740000	-2.687505000	-1.116142000
6	1.714125000	-2.500136000	1.282779000
1	1.153838000	-2.653152000	2.198559000
1	1.357784000	-3.220397000	0.554236000
1	2.758480000	-2.714221000	1.486223000
1	3.575532000	-1.354536000	-2.039313000

PUC-Rio - Certificação Digital N° 1613320/CA

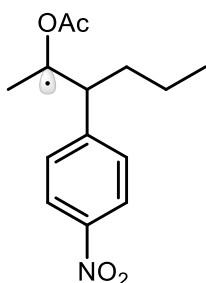


Nimag=0
 Zero-point correction= 0.282249 (Hartree/Particle)
 Thermal correction to Energy= 0.300388
 Thermal correction to Enthalpy= 0.301333
 Thermal correction to Gibbs Free Energy= 0.232536
 Sum of electronic and zero-point Energies= -859.964837
 Sum of electronic and thermal Energies= -859.946698

Sum of electronic and thermal Enthalpies= -859.945753
 Sum of electronic and thermal Free Energies= -860.014550

6	-1.536543000	-0.969826000	-0.316269000
1	-1.881931000	-0.571463000	-1.263428000
6	-2.336113000	-0.276959000	0.756021000
6	-2.569257000	1.881957000	-0.249103000
6	-2.362286000	3.324344000	0.088603000
1	-1.314380000	3.496461000	0.311208000
1	-2.669493000	3.936785000	-0.746629000
1	-2.931227000	3.581231000	0.975088000
8	-2.947841000	1.463554000	-1.296331000
8	-2.263799000	1.107612000	0.807245000
6	-0.062954000	-0.617320000	-0.198700000
6	0.520540000	0.236527000	-1.127330000
6	0.724048000	-1.108886000	0.839536000
6	1.851104000	0.596064000	-1.032156000
1	-0.075853000	0.623296000	-1.935758000
6	2.054014000	-0.762258000	0.950737000
6	2.599310000	0.089544000	0.009666000
1	2.311493000	1.251851000	-1.746349000
1	2.670660000	-1.136748000	1.745361000
1	0.298416000	-1.773394000	1.570531000
6	-2.576000000	-0.826147000	2.113608000
7	4.008044000	0.462263000	0.121038000
8	4.454274000	1.211644000	-0.708376000
8	4.637098000	-0.001908000	1.036383000
1	-1.713731000	-0.673694000	2.767450000
1	-2.791699000	-1.886553000	2.080385000
6	-1.793507000	-2.480590000	-0.342001000
1	-1.399364000	-2.950319000	0.555433000
1	-2.869129000	-2.637989000	-0.324631000
1	-3.417468000	-0.318156000	2.573852000
6	-1.203427000	-3.157413000	-1.569799000
1	-1.427635000	-4.219356000	-1.569040000
1	-1.612288000	-2.732536000	-2.482367000
1	-0.124107000	-3.046701000	-1.606606000

PUC-Rio - Certificação Digital N° 1613320/CA



Nimag=0

Zero-point correction=

0.311478 (Hartree/Particle)

Thermal correction to Energy=

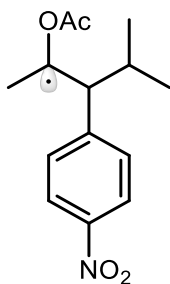
0.331007

Thermal correction to Enthalpy=

0.331951

Thermal correction to Gibbs Free Energy= 0.259586
 Sum of electronic and zero-point Energies= -899.232836
 Sum of electronic and thermal Energies= -899.213307
 Sum of electronic and thermal Enthalpies= -899.212363
 Sum of electronic and thermal Free Energies= -899.284728

6	1.538074000	0.498994000	-0.094425000
1	1.856917000	0.200094000	-1.086344000
6	2.188788000	-0.458837000	0.869254000
6	2.154024000	-2.450274000	-0.456775000
6	1.730976000	-3.881256000	-0.352755000
1	0.661327000	-3.929990000	-0.177413000
1	1.980793000	-4.397514000	-1.268250000
1	2.222314000	-4.350816000	0.492031000
8	2.630998000	-1.937503000	-1.418354000
8	1.918146000	-1.809333000	0.701757000
6	0.025693000	0.354932000	-0.053139000
6	-0.640367000	-0.254266000	-1.110117000
6	-0.719695000	0.795202000	1.037524000
6	-2.011343000	-0.423577000	-1.090035000
1	-0.076831000	-0.598731000	-1.960187000
6	-2.088805000	0.635958000	1.075449000
6	-2.716407000	0.025462000	0.006810000
1	-2.534909000	-0.889347000	-1.903073000
1	-2.673648000	0.973385000	1.909734000
1	-0.229659000	1.271804000	1.868037000
6	2.450046000	-0.164398000	2.300060000
7	-4.167148000	-0.147436000	0.039747000
8	-4.686175000	-0.689011000	-0.901518000
8	-4.755786000	0.261414000	1.006919000
1	1.550560000	-0.291559000	2.907488000
1	2.810666000	0.847095000	2.437436000
6	2.012391000	1.940396000	0.117811000
1	1.647666000	2.329257000	1.066179000
1	3.098413000	1.932114000	0.186736000
1	3.195299000	-0.851301000	2.688375000
6	1.591954000	2.880275000	-1.004042000
1	1.970004000	2.495820000	-1.949669000
1	0.507768000	2.887186000	-1.088635000
6	2.093841000	4.300802000	-0.794441000
1	3.178901000	4.330030000	-0.736968000
1	1.788749000	4.950133000	-1.609069000
1	1.703211000	4.723383000	0.127845000



Nimag=0

Zero-point correction= 0.310957 (Hartree/Particle)

Thermal correction to Energy= 0.330378

Thermal correction to Enthalpy= 0.331322

Thermal correction to Gibbs Free Energy= 0.260242

Sum of electronic and zero-point Energies= -899.228227

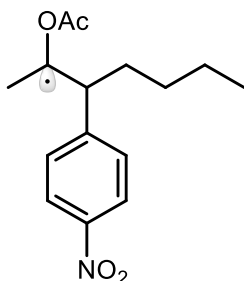
Sum of electronic and thermal Energies= -899.208805

Sum of electronic and thermal Enthalpies= -899.207861

Sum of electronic and thermal Free Energies= -899.278941

6	1.585770000	-0.632533000	0.374562000
1	1.815541000	-0.290398000	1.379989000
6	2.393917000	0.246462000	-0.540700000
6	1.884321000	2.364140000	0.428630000
6	1.348312000	3.704858000	0.039763000
1	1.931007000	4.116549000	-0.776278000
1	0.326670000	3.594138000	-0.309171000
1	1.374718000	4.364309000	0.895033000
8	2.177608000	2.026749000	1.530427000
8	1.992635000	1.569942000	-0.653421000
6	0.090370000	-0.423332000	0.201389000
6	-0.720025000	-0.280190000	1.321926000
6	-0.503104000	-0.359537000	-1.056535000
6	-2.085073000	-0.105183000	1.203466000
1	-0.274433000	-0.294988000	2.301167000
6	-1.863522000	-0.183112000	-1.196738000
6	-2.637805000	-0.062748000	-0.059267000
1	-2.716930000	0.004492000	2.064073000
1	-2.329778000	-0.134626000	-2.162195000
1	0.104576000	-0.441412000	-1.939816000
6	3.235971000	-0.148103000	-1.695315000
7	-4.080335000	0.126899000	-0.198871000
8	-4.729909000	0.229938000	0.809050000
8	-4.532208000	0.168210000	-1.313929000
1	4.021406000	0.587991000	-1.839641000
1	2.666565000	-0.189089000	-2.627889000
6	2.006796000	-2.124788000	0.333254000
1	3.095059000	-2.122101000	0.325352000
1	3.698927000	-1.114256000	-1.545778000
6	1.522422000	-2.900734000	-0.887996000
1	1.789460000	-2.424544000	-1.824859000
1	1.961048000	-3.894341000	-0.890255000

1	0.443648000	-3.020817000	-0.872647000
6	1.574100000	-2.843279000	1.607665000
1	1.936777000	-3.866867000	1.606220000
1	1.966632000	-2.352414000	2.493393000
1	0.491745000	-2.880158000	1.693752000

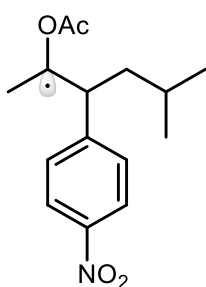


Nimag=0

Zero-point correction=	0.340768 (Hartree/Particle)
Thermal correction to Energy=	0.361651
Thermal correction to Enthalpy=	0.362595
Thermal correction to Gibbs Free Energy=	0.286731
Sum of electronic and zero-point Energies=	-938.500806
Sum of electronic and thermal Energies=	-938.479923
Sum of electronic and thermal Enthalpies=	-938.478979
Sum of electronic and thermal Free Energies=	-938.554843

6	1.444101000	-0.247772000	0.077115000
1	1.720773000	-0.498436000	-0.940472000
6	1.713341000	-1.475802000	0.907214000
6	1.163739000	-3.170212000	-0.690307000
6	0.321807000	-4.401597000	-0.801392000
1	-0.721555000	-4.139763000	-0.659558000
1	0.463327000	-4.847263000	-1.775266000
1	0.591333000	-5.104648000	-0.021254000
8	1.834059000	-2.709338000	-1.558282000
8	1.059007000	-2.643849000	0.542786000
6	-0.041027000	0.074656000	0.065906000
6	-0.791384000	-0.160312000	-1.080271000
6	-0.686888000	0.578181000	1.192104000
6	-2.148284000	0.097303000	-1.112964000
1	-0.304946000	-0.548538000	-1.958625000
6	-2.040128000	0.842370000	1.178556000
6	-2.753518000	0.595947000	0.021440000
1	-2.735280000	-0.077250000	-1.994473000
1	-2.547930000	1.232621000	2.039819000
1	-0.129644000	0.771052000	2.091718000
6	1.959991000	-1.464306000	2.370474000
7	-4.188208000	0.872973000	-0.000719000
8	-4.785642000	0.641680000	-1.019670000
8	-4.686530000	1.315032000	1.001958000
1	1.027498000	-1.385500000	2.934805000
1	2.600118000	-0.640050000	2.658351000

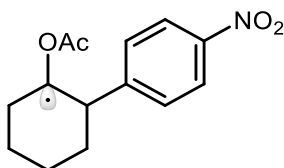
6	2.315651000	0.938179000	0.503731000
1	2.025074000	1.292255000	1.490421000
1	3.341793000	0.587414000	0.593174000
1	2.436379000	-2.391753000	2.672003000
6	2.268917000	2.098699000	-0.480385000
1	2.574961000	1.745015000	-1.464505000
1	1.243989000	2.449364000	-0.587756000
6	3.156484000	3.264466000	-0.066672000
1	4.181683000	2.914171000	0.044170000
1	2.848736000	3.618821000	0.916215000
6	3.118899000	4.419232000	-1.056077000
1	2.110758000	4.811334000	-1.162308000
1	3.759179000	5.235699000	-0.736281000
1	3.453850000	4.102246000	-2.040309000



Nimag=0	
Zero-point correction=	0.340333 (Hartree/Particle)
Thermal correction to Energy=	0.361174
Thermal correction to Enthalpy=	0.362118
Thermal correction to Gibbs Free Energy=	0.286653
Sum of electronic and zero-point Energies=	-938.500683
Sum of electronic and thermal Energies=	-938.479842
Sum of electronic and thermal Enthalpies=	-938.478898
Sum of electronic and thermal Free Energies=	-938.554363

6	-1.462333000	-0.183315000	0.104903000
1	-1.793438000	0.072813000	-0.892919000
6	-1.952504000	0.923173000	1.003335000
6	-1.734731000	2.777042000	-0.496724000
6	-1.147695000	4.152538000	-0.528541000
1	-0.074154000	4.090562000	-0.383815000
1	-1.367764000	4.615468000	-1.479509000
1	-1.553252000	4.745764000	0.283350000
8	-2.299274000	2.245003000	-1.398835000
8	-1.534398000	2.212967000	0.707053000
6	0.056972000	-0.212891000	0.074469000
6	0.733975000	0.233404000	-1.054654000
6	0.802083000	-0.651227000	1.166229000
6	2.114612000	0.244297000	-1.104416000
1	0.171351000	0.576889000	-1.905739000
6	2.180564000	-0.648329000	1.135306000
6	2.818692000	-0.198157000	-0.004337000

1	2.645839000	0.583455000	-1.973248000
1	2.764735000	-0.985892000	1.970014000
1	0.304094000	-1.003373000	2.052182000
6	-2.180759000	0.786524000	2.463450000
7	4.279486000	-0.191970000	-0.044739000
8	4.808370000	0.212319000	-1.047495000
8	4.866083000	-0.590747000	0.927856000
1	-1.244049000	0.837916000	3.024112000
1	-2.667302000	-0.150166000	2.703689000
6	-2.083172000	-1.534793000	0.476098000
1	-1.736695000	-1.844655000	1.458999000
1	-3.160835000	-1.400619000	0.560306000
1	-2.807005000	1.599839000	2.815687000
6	-1.804884000	-2.667307000	-0.514912000
1	-0.725978000	-2.751756000	-0.638971000
6	-2.312075000	-3.987921000	0.054506000
1	-3.388903000	-3.956002000	0.207734000
1	-2.099987000	-4.811784000	-0.620519000
1	-1.847056000	-4.213372000	1.010349000
6	-2.420721000	-2.408243000	-1.885851000
1	-3.499398000	-2.288638000	-1.808002000
1	-2.022787000	-1.515878000	-2.357469000
1	-2.228220000	-3.241878000	-2.554852000

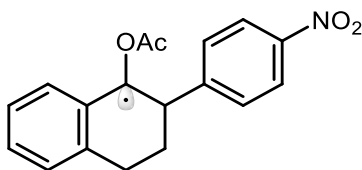


Nimag=0

Zero-point correction=	0.292054 (Hartree/Particle)
Thermal correction to Energy=	0.309149
Thermal correction to Enthalpy=	0.310093
Thermal correction to Gibbs Free Energy=	0.243205
Sum of electronic and zero-point Energies=	-898.051657
Sum of electronic and thermal Energies=	-898.034563
Sum of electronic and thermal Enthalpies=	-898.033618
Sum of electronic and thermal Free Energies=	-898.100506

6	-1.599707000	1.983739000	-1.219386000
6	-1.813895000	2.890118000	-0.015913000
6	-2.994681000	2.398624000	0.810437000
6	-2.769507000	0.973093000	1.306145000
6	-2.254009000	0.075598000	0.237111000
6	-1.300757000	0.521404000	-0.829075000
1	-3.173017000	3.053140000	1.658311000
1	-0.914574000	2.917814000	0.598166000
1	-1.991561000	3.907592000	-0.352647000
1	-2.501697000	1.991325000	-1.827546000
1	-2.066192000	0.991322000	2.145700000
1	-3.688260000	0.550845000	1.705945000

1	-3.891923000	2.428222000	0.195278000
8	-2.186673000	-1.240307000	0.661909000
6	-2.358803000	-2.260938000	-0.202147000
8	-2.626635000	-2.116442000	-1.350671000
6	-2.166884000	-3.570599000	0.493669000
1	-1.139548000	-3.651126000	0.833709000
1	-2.806493000	-3.623078000	1.367437000
1	-2.393266000	-4.376420000	-0.189261000
1	-0.794696000	2.355762000	-1.844970000
6	0.168403000	0.325632000	-0.480686000
6	1.088496000	0.246235000	-1.523939000
6	0.640238000	0.230673000	0.822731000
6	2.437046000	0.097421000	-1.283644000
1	0.738887000	0.297341000	-2.541233000
6	1.988838000	0.079060000	1.084589000
1	-0.045246000	0.259643000	1.648763000
6	2.869617000	0.018751000	0.026122000
1	3.150494000	0.035440000	-2.083067000
1	2.361729000	0.005803000	2.088366000
7	4.296535000	-0.142278000	0.296028000
8	5.040536000	-0.192283000	-0.648798000
8	4.642598000	-0.214528000	1.446760000
1	-1.485371000	-0.092061000	-1.704829000



Nimag=0

Zero-point correction=	0.316024 (Hartree/Particle)
Thermal correction to Energy=	0.335200
Thermal correction to Enthalpy=	0.336144
Thermal correction to Gibbs Free Energy=	0.264999
Sum of electronic and zero-point Energies=	-1050.417025
Sum of electronic and thermal Energies=	-1050.397849
Sum of electronic and thermal Enthalpies=	-1050.396905
Sum of electronic and thermal Free Energies=	-1050.468049

6	5.302822000	-0.643606000	1.011114000
6	4.579383000	-1.489942000	0.179869000
6	3.298572000	-1.179063000	-0.222525000
6	2.700403000	0.025180000	0.233167000
6	3.451575000	0.879380000	1.070681000
6	4.729551000	0.544503000	1.449370000
1	2.704680000	-1.727298000	-2.189739000
1	6.301580000	-0.907774000	1.311596000
1	5.027907000	-2.406925000	-0.165720000
6	2.528592000	-2.058047000	-1.165510000
6	1.390333000	0.340016000	-0.163297000
1	3.003845000	1.792253000	1.417144000

1	5.285776000	1.205062000	2.092059000
6	0.502009000	-0.573861000	-0.953082000
6	1.036307000	-2.010916000	-0.874948000
1	0.849356000	-2.412007000	0.118041000
8	0.878701000	1.542997000	0.274244000
6	0.380881000	2.424391000	-0.621460000
8	0.412323000	2.249032000	-1.795516000
6	-0.199961000	3.609242000	0.078709000
1	-1.025705000	3.287961000	0.704673000
1	0.545321000	4.060746000	0.724083000
1	-0.545430000	4.324563000	-0.653206000
6	-0.943708000	-0.514336000	-0.511158000
6	-1.291652000	-0.687942000	0.825276000
6	-1.951722000	-0.317179000	-1.444868000
6	-2.611814000	-0.677864000	1.221856000
1	-0.520762000	-0.825775000	1.563709000
6	-3.280823000	-0.307053000	-1.067208000
1	-1.693613000	-0.160023000	-2.477590000
6	-3.590063000	-0.489227000	0.264146000
1	-2.894392000	-0.810913000	2.248629000
1	-4.069171000	-0.157046000	-1.779827000
7	-4.992885000	-0.476461000	0.676080000
8	-5.231722000	-0.627887000	1.846100000
8	-5.824212000	-0.314949000	-0.178971000
1	2.892783000	-3.078761000	-1.101963000
1	0.488454000	-2.629735000	-1.578637000
1	0.534732000	-0.254695000	-1.993462000